AUSTRALIA

AGSO JOURNAL
OF AUSTRALIAN GEOLOGY & GEOPHYSICS

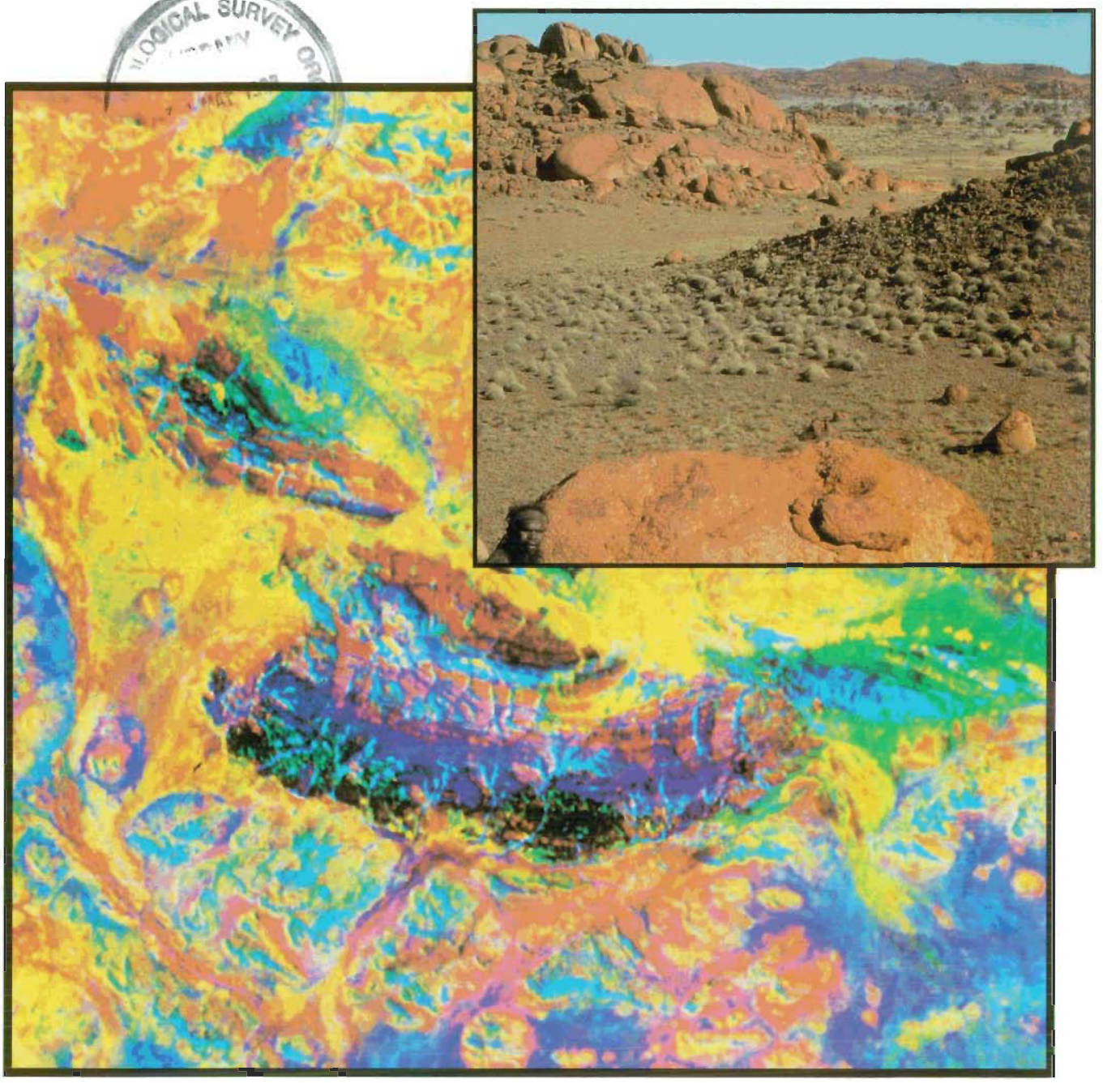

VOLUME 16, NUMBERS 1 & 2
1995

AGSO Journal of Australian Geology & Geophysics

Policy

The *AGSO Journal of Australian Geology & Geophysics* is a quarterly journal of geoscientific research results relating to the program and interests of the Australian Geological Survey Organisation (AGSO). It complements other earth science journals by focusing on Australia, and includes papers covering the broader Australasian and SW Pacific region.

The *Journal*'s target audience is the world-wide geoscientific community, catering for the interests of the resource, exploration and environmental industries, as well as those of researchers in universities and State and Federal agencies.

The Editorial Board is responsible for the scientific policies and standards of the *Journal*, which will publish papers on fundamental research, applied research and review topics. Contributions are invited from anyone. Scientific excellence and relevance to the broad aims of AGSO are the main criteria for acceptance of manuscripts for publication. Peer review and editorial and production standards are similar to those of leading international journals.

Guide for contributors

Submission of a paper to the *Journal* implies that the paper is original and unpublished, and is not being considered for publication elsewhere. Papers published in the *AGSO Journal of Australian Geology & Geophysics* become Commonwealth copyright. Authors are responsible for obtaining permission to reproduce any material, especially a figure, that has been published previously.

All submissions will be peer-reviewed. Submissions by AGSO authors will normally be reviewed by non-AGSO referees; those by non-AGSO authors, by at least one AGSO referee.

When your paper has been accepted you will be asked to supply a copy on an IBM-compatible diskette. Do not send this until it is requested.

Submission of manuscripts

- Three copies of the complete manuscript should be sent to the Editor.
- Your manuscript should be double-spaced, with margins of at least 25 mm, on one side only of A4 paper, with all pages numbered. Single-spaced copies are not suitable for refereeing or editing and will not be accepted.
- Use a straightforward print-out in Times or Courier font. Do not use desktop publishing software to prepare your manuscript.
- Photocopies of draft figures are acceptable when the manuscript is first submitted, as long as they are clear enough for the reviewers. Final versions of figures must be supplied when the final version of the manuscript is accepted for publication.
- Photographs should be supplied as glossy prints.

Style

Contributions should be written in English, and spelling should follow the latest edition of *The Macquarie Dictionary*. Refer to a recent issue of the *Journal* for further guidance on general style. But note that a revised style for references is being introduced with these instructions. Heading hierarchy should be indicated in the margin by ringed capital letters; A for main headings, B for second level headings, etc.

Abstract and key words

An abstract is required at the beginning of the manuscript. It should provide an informative summary of the main results and conclusions contained in the manuscript. It should not exceed 300 words. (An abstract is not adequate if it states that certain work was done, but fails to summarise the outcomes.) Up to 10 key words or short phrases should be supplied to assist indexing of your paper.

References

The Journal does not cite 'in prep' references. References 'in press' are acceptable only if the journal and issue can be supplied. References to unpublished data, if necessary, should be quoted as personal communications, giving the affiliation of the person being quoted and the date of communication. References should be cited in the text by author(s) and year in the normal Harvard style. For example: 'Ernest (1976, p. 312) showed that ..' or as described by earlier workers (Zagreb 1931; Ernest 1976; Melway & Murray 1977; Melway et al. 1978). References should be listed at the end of the text, in alphabetical order and in the style shown below. Please note that all journal titles are spelt out in full.

Continued inside back cover

AGSO JOURNAL

OF AUSTRALIAN GEOLOGY & GEOPHYSICS

VOLUME 16, NUMBERS 1 & 2, 1995

CONTENTS

Thematic issue: The Giles mafic–ultramafic complex and environs, western Musgrave Block, central Australia

ISSN 1320–1271

Subscriptions to the AGSO Journal are available through the Australian Geological Survey Organisation (GPO Box 378, Canberra ACT 2601; tel. 06 249 9642, fax 06 249 9982).

Other matters concerning the Journal should be sent to the Editor, AGSO Journal

Editors, AGSO Journal: Dr. Karl H. Wolf, Mr Ian Hodgson
Cover design and figures prepared by AGSO Cartographic Services Unit unless otherwise indicated
Prepared for publication by Lin Kay

Printed in Australia by National Capital Printing, Fyshwick, A.C.T. 2609

AUSTRALIAN GOVERNMENT PUBLISHING SERVICE CANBERRA 1995

Month of issue, April 1995

***Front-cover illustration*:**

A Landsat-5 Thematic Mapper RGB pc2 (4/3 ; 5/7) : 5/4 : 4/3 : showing the Mount Davies, Gosse Pile and Kalka layered mafic-ultramafic intrusions of the Giles Complex and associated felsic granulites. For geological explanation see Fig. 3 in Glikson and Creasey (1995—this issue). Inset – a view in the Musgrave Block, showing tors of granite gneiss and mafic granulites.

AGSO Journal of Australian Geology & Geophysics, 16 (1/2), 1–2

The Giles mafic–ultramafic complex and environs, western Musgrave Block, central Australia

Preface

The Giles Complex comprises a series of over twenty layered mafic–ultramafic intrusions and faulted segments emplaced within the southern granulite terrane of the Musgrave Block, central Australia, over an east–west strike length of some 500 km—constituting the largest mafic–ultramafic intrusive suite on the Australian continent. Earlier documentation of this suite during the 1960s included 1:250 000 mapping by the Geological Survey of Western Australia and the South Australia Department of Mines, and local detailed studies by staff and students of the University of Adelaide. The papers presented in this issue report some of the principal results of AGSO's Musgrave project, initiated in 1987 as a specialised study of the layered mafic–ultramafic intrusions of the Giles Complex and continued in 1990 within the framework of the National Geoscience Mapping Accord. Field work in the western Musgrave Block concentrated in the Tomkinson Ranges–Blackstone Range–Jameson Range region of Western Australia and South Australia. Geological mapping was accompanied by multidisciplinary investigations, comprising detailed field mapping of surface deposits and vegetation patterns, structural studies, comprehensive petrological studies based on electron-probe analyses, pressure–temperature studies, U–Pb and Sm–Nd isotopic analyses, whole-rock geochemistry, and remotely sensed studies using Landsat-5 TM and Geoscan Mk I. A list of reports, publications and maps released by the Musgrave project follows. Geological and environmental maps on the scales of 1:100 000 and 1:50 000 will be released separately from this issue.

In view of the broad contemporaneity of the western Musgrave Block and the ~1.3–1.0 Ga Grenville belt in North America, Tony Davidson, an authority on the Grenville system, was invited to write a review of this terrane. Geoff Clarke was invited to review Grenville-age belts in Australia and Antarctica, on the basis of his personal experience in the Albany–Fraser, Musgrave, Arunta, Rudall and Antarctic terranes. Other papers are organised according to a thematic sequence, including the geological framework and petrology of the Giles Complex, pre-Giles Complex granulite facies gneisses in the type area of Mount Aloysius, geochemical studies, structural and palaeo-pressure/temperature evolution of host rocks of the Giles Complex, boundary thrust faults of the western Musgrave Block, and multispectral, remotely sensed studies of the Giles Complex and associated granulites. Papers on the isotopic ages of key units in the Musgrave Block will appear in a future issue of the *AGSO Journal*, reporting a probable ~1.08 Ga age for the Giles Complex and Tollu Group volcanics (Sun et al. in press).

Some of the principal conclusions arising from the project and reported in this issue include (1) recognition of vertical crustal zonation pattern in the western Musgrave Block, ranging from ultramafic-dominated bodies at deep crustal levels along the Woodroffe Thrust, to layered gabbro–pyroxenite intrusions, crystallised at ~6 kb, to silica-undersaturated troctolite intrusions at shallower crustal levels (< 4 kb) to the west and south; and to supracrustal levels, where the probably coeval volcanics of the Tollu Group (~1.08 Ga) were extruded in the southwest; (2) identification of the western extension of the Woodroffe Thrust north of the Tomkinson Ranges; (3) documentation of original magma fractionation trends, which define mafic–ultramafic bodies as originally separate intrusions, rather than fault segments of an original lopolith; (4) recognition of multiple intrusion of magma batches, including injection of late ultramafic increments into resident gabbro magma chambers and of late doleritic sills into chambers of above-solidus gabbroic magma; (5) interpretation of silica-undersaturated iron-rich fayalitic olivine–plagioclase–magnetite troctolite suites in terms of high-pressure (> 10 kb) fractionation of orthopyroxene from parent magma and emplacement of the fractionated liquids under low-pressure (< 4 kb), high-oxygen fugacity conditions; (6) isobaric cooling of mafic–ultramafic magmas; (7) resolution of seven deformation stages and multiple high-pressure events in the western Musgrave Block, including identification of ~550 Ma sub-ecologite facies rocks (~14 kb) above the Woodroffe Thrust; (8) extensive recrystallization of Giles Complex mafic rocks into mafic granulites in conjunction with intrusion of granitic veins; (9) geochemical characterisation of several granite magma types and at least four geochemically distinct mafic dyke swarms; (10) recognition of partial melting features in pre-Giles Complex granulites induced by high temperature emplacement of the mafic–ultramafic intrusions; (11) chemical characterisation of pre-Giles Complex orthogneisses and paragneisses, which include quartzite and minor pelitic and calc-silicate gneisses; and (12) correlations of remotely sensed multispectral data with a range of bedrock and surface deposit types.

The Musgrave project has not been an easy one to pursue, from the logistic point of view, owing to limitations on access into Aboriginal reserve land, as well as the geological complexities inherent in the study of multiply deformed high-grade metamorphic terranes. However, the project enjoyed the goodwill of a dedicated team, most of whom worked beyond the call of duty. I am grateful to my colleagues Chris Ballhaus, Geoff Clarke, John Creasey, Erwin Feeken, Alastair Stewart, John Sheraton, Shen-Su Sun, and John Vickers for their efforts and achievements. I thank members and field guides of the Ngganyatjarra and Pitjantjatjarra Aboriginal tribes and community coordinators, Ruth Raintree, Murray Wells, Diana James, and, in particular, Rob Shelton—without whose support and friendship, field work may not have been possible.

Andrew Glikson
March 1995

Reports, publications and maps released by the Musgrave Project (excepting papers of this issue)

Ballhaus, C.G., 1992. Petrology of the Giles Complex, Musgrave Block, central Australia: the Jameson, Blackstone, Bell Rock, Murray, The Wart, Latitude Hill and Hinckley intrusions. Australian Geological Survey Organisation, Record 1992/73.

Ballhaus, C.G. & Glikson, A.Y., 1989. Magma mixing and intraplutonic quenching in the Giles Complex, central Australia. Journal of Petrology, 30, 1443–1469.

Ballhaus, C.G. & Berry, R.F., 1991. Crystallization pressure and cooling history of the Giles layered igneous complex, central Australia. Journal of Petrology, 32, 1–28.

Ballhaus, C.G., Glikson, A.Y. & Keays, R.R., 1992. Magmatic and metamorphic evolution and economic potential of the mafic/ultramafic Giles Complex, western Musgrave Block, W.A. BMR Research Newsletter, 16, 6–9.

Clarke, G.L., 1992. Field relations and tectonic history of the Hinckley Gabbro, felsic to mafic granulites and ganitoids, western Hinckley Range and Champ de Mars areas, Tomkinson Ranges, Musgrave Block, Western Australia. Bureau of Mineral Resources, Australia, Record 1992/33.

Clarke, G.L., Buick, I.S. & Glikson, A.Y., 1992. Contact relationships and structure of the Hinckley Gabbro and host rocks, Giles Complex, western Musgrave Block, W.A. AGSO Research Newsletter, 17, 6–8.

Clarke, G.L, Stewart, A.J. & Glikson, A.Y., 1993. High-pressure eclogite-facies metamorphism in the western Musgrave Block, central Australia. AGSO Research Newsletter, 1, 6–7.

Feeken, E., 1991. Environmental mapping in BMR: Cainozoic deposits, landforms and vegetation in the Tomkinson Ranges. BMR Research Newsletter, 14, 7–8.

Feeken, E., 1992. Notes on the 1:100 000 environmental map of the Tomkinson Ranges, Western Musgrave Block, central Australia. Australian Geological Survey Organisation, Record 1992/34.

Glikson, A.Y. & Ballhaus, C.G., 1989. Significance of ultrabasic components of the Giles Complex, central Australia. BMR Research Newsletter, 10, 4–6.

Glikson, A.Y. & Stewart, A.J., 1992. Mapping in high grade terranes: use of remotely sensed data and airborne geophysics. BMR Research Newsletter, 16, 22–23

Glikson, A.Y., 1993. Landsat-5 Thematic Mapper image correlations: application to NGMA mapping of the western Musgrave Block, central Australia. 7th Australasian Remote Sensing Conference, Melbourne, 6 pp.

Glikson, A.Y., 1994. Landsat-5 Thematic Mapper image correlations: application to NGMA mapping of the western Musgrave Block, central Australia. Australian Geological Survey Organisation, Record 1994/17.

Glikson, A.Y. & Mernagh, T.P., 1990. Significance of pseudotachylite vein systems, Giles basic/ultrabasic complex, Tomkinson Ranges, western Musgrave Block, central Australia. BMR Journal of Australia Geology & Geophysics, 11, 509–519.

Glikson, A.Y., Ballhaus, C.G., Goleby, B.R. & Shaw, R.D., 1990. Major thrust faults and crustal zonation of the middle to upper Proterozoic crust in central Australia. NATO Advanced Study Institute on Exposed cross sections through the continental crust. Kluwer Academic Publishers, Netherlands, 285–304.

Glikson, A.Y., Ballhaus, C.G. & Pharaoh, T., 1990. The Giles Complex, central Australia: new insights into tectonics and metamorphism. BMR Research Newsletter, 12, 18–20

Glikson, A.Y., Stewart, A.J. & Feeken, E., 1995. 1:100 000 Geological map of the Giles Complex and environs, western Musgrave Block, central Australia (3 plates), in press.

Pharaoh, T.C., 1990. Aspects of structural geology of the Giles layered mafic/ultrmafic complex, Tomkinson Range, Musgrave Block, central Australia. Bureau of Mineral Resources, Australia, Record 1990/6.

Stewart, A.J., 1993. Extension of the Woodroffe Thrust into, Musgrave Block, Western Australia. AGSO Research Newsletter, 18, 5–6.

Stewart, A.J., in press. Bates 1:100 000, Western Australia, Explanatory Notes. Australian Geological Survey Organisation, Record.

Stewart, A.J. & Glikson, A.Y., 1991. The felsic metamorphic/igneous core complexes hosting the Giles Complex. BMR Research Newsletter, 14, 6–7.

Sun, S.S. & Sheraton, J.W., 1992. Zircon u/Pb chronology, tectono-thermal and crust-forming events in the Tomkinson Ranges, Musgrave Block, central Australia. AGSO Research Newsletter, 17, 9–10.

AGSO Journal of Australian Geology & Geophysics, 16 (1/2), 3–24

A review of the Grenville orogen in its North American type area

A. Davidson[1]

In a reconstructed supercontinent assembly at ~0.9 Ga, the Grenville orogen extends from Scandinavia through North America and Antarctica to Australia. Part of it, the 2000 km long Grenville Province, exposed in the southeastern Canadian Shield, is large enough to allow a comprehensive view of its tectonic character. It has an orogen-parallel zonation: older, reworked crust, representing Archaean and Palaeoproterozoic orogens exposed in adjacent parts of the shield, is restricted to its northwest side; supracrustal and plutonic rocks of Grenvillian age (~1.3–0.95 Ga) are limited to the southeastern half. The latter lie on or within late Palaeoproterozoic and earlier Mesoproterozoic crust, which is the deformed, temporal equivalent of terranes that form a substantial part of the buried North American craton south of the shield. A pre-Grenvillian period of quiescence at ~1.5 Ga may have followed an earlier continental assembly. Grenvillian calc-alkaline igneous rocks, limited in volume and distribution, represent arc accretion that terminated with ocean closure by ~1.2 Ga. New crust was added after continent–continent collision and attendant crustal thickening by emplacement of large gabbro–anorthosite massifs of mantle origin, associated with, and in part responsible for, granitoid magma derived from the lower crust. This magmatism, beginning at ~1.18 Ga, was accompanied or followed by high-grade metamorphism, except in parts of the Grenvillian supracrustal terranes, and by low-angle, thrust-sense, ductile deformation directed toward the north and northwest. Ductile followed by brittle extensional deformation between 1.05 and 1.0 Ga, along with terminal thrust-uplift along the northwest margin of the orogen, represent the closing stages of tectonic activity, leading to unroofing and cooling by ~0.9 Ga. There is little evidence in the Grenville Province for supercontinent break-up until ~600 Ma.

Introduction

According to recently published reconstructions (Moores 1991; Dalziel 1991; Hoffman 1991; Borg & DePaolo 1994), plate interactions during Neoproterozoic supercontinent assembly[1] produced an interconnected, global orogenic system (Fig. 1). Part of this system, the Grenville Province of the Canadian Shield, has given its name to this worldwide orogeny, active between ~1.3 and 0.95 Ga. The Grenvillian orogeny occurred between two relatively quiescent periods of Earth history, namely at ~1.5 and 0.8 Ga; the older of these was preceded by major orogeny in various parts of the world, between 1.9 and 1.6 Ga (Penokean, Hudsonian, Yavapai–Mazatzal, Ketilidian, Labradorian, Svecofennian, etc.), and the younger was succeeded by latest Proterozoic to early Phanerozoic events (Pan-African, Avalonian, Caledonian–Appalachian, etc.).

The purpose of this paper is to provide an up-to-date review of the Grenville orogen in its type area, the Canadian Shield, so that others may compare it with crust of similar age exposed in the Musgrave Block of central Australia, at the other end of the reconstructed Grenvillian orogen. The Grenville Province (Gill 1948) is defined as that part of the Grenville orogen which is exposed in the southeastern Canadian Shield. In North America, the Grenville orogen is known to extend, mainly in the subsurface, southwestward from the Shield to Texas and Mexico (Ruiz et al. 1988; Rankin et al. 1993) (Fig. 2). Precambrian rocks affected by Grenvillian orogeny occur as basement windows and slices throughout the Appalachian orogenic system, emerging in the foreland of this Palaeozoic belt in Texas (notably in the Llano uplift). In eastern Mexico, however, Grenvillian rocks may lie within or on the opposite side of the southward continuation of the Appalachian–Ouachita orogenic system (Ruiz et al. 1988). The Sveconorwegian Province in southwest Scandinavia is the trans-Atlantic counterpart, east of the Caledonides (Gower 1985, 1990), and must continue in the subsurface south of the Baltic Sea. Grenvillian remnants have also been recognised in Scotland and northern Ireland. Other orogenic belts of Grenvillian age can be fitted into reconstructions of continental plate configurations at ~0.8 Ga (e.g. Hoffman 1991). Such reconstructions show a Grenvillian connection with the Albany–Fraser Belt in southwest Australia via Antarctica, also incorporating Madagascar and eastern India (Fig. 1). It is curious that reconstructions (e.g. Moores 1991) show the northeast extension of the Albany–Fraser Belt to pass south of the central Australian Musgrave Block, in which metamorphism, deformation and plutonism in the Grenvillian range have been identified. Sun & Sheraton (1992) noted that the Musgrave Block and Albany–Fraser Belt appear to show contrasting tectonic styles (intraplate vs collisional, respectively), although tectonic activity was similar in age; they inferred (op. cit., p. 11) that central and western Australia may have undergone a more complex Grenvillian evolution than is usually portrayed. The Musgrave Block is therefore included in the Grenvillian system in Figure 1.

The volume of literature on the Grenville Province and related topics has increased several fold in the last decade, and a fully comprehensive bibliography would run to many hundred references. In the following review, much information has been drawn from summary volumes and key papers, such as Moore et al. (1986), Rivers et al. (1989), Gower et al. (1990), Rankin et al. (1993) and, in particular, Hoffman (1989a). Many references are to recent papers reporting results of tracer isotope and geochronological studies linked to assessment of both specific and regional field relationships, without which understanding of the Grenville Province might

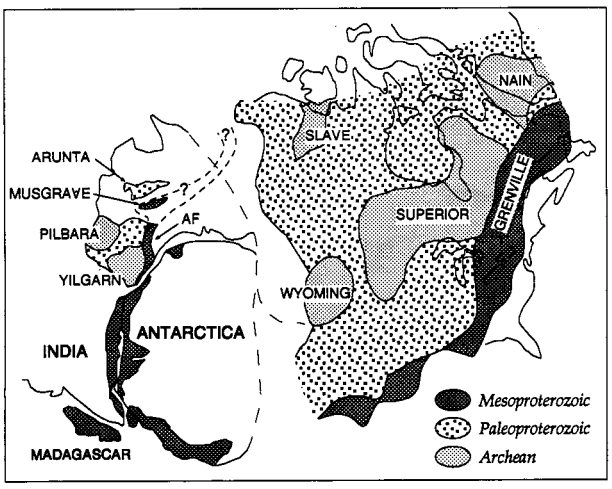

Figure 1. Distribution of Mesoproterozoic Grenvillian belts in post-Grenvillian supercontinent reconstruction, after Moores (1991). AF is Albany–Fraser belt. Palaeoproterozoic in North America includes reworked Archaean blocks.

[1] *McMenamin & McMenamin (1990, p. 95) proposed the name 'Rodinia' for this supercontinent, but their reconstruction differs from that shown in Figure 1.*

1 Geological Survey of Canada, 601 Booth Street, Ottawa, Canada K1A 0E8

not be much further ahead than it was at the time of the first attempt to synthesise its geology and tectonic history as a whole (Wynne-Edwards 1972).

Before the Grenville Province and its component parts are described, two terms require clarification. The first is *Grenvillian*, used in the chronological sense. Traditionally, the Grenvillian orogeny is considered to have culminated by ~1.0 Ga, but a record of earlier events has been recognised for some time. Moreover, pre-1.0 Ga deformation has affected <1.3 Ga supracrustal rocks restricted to the Grenville orogen; these rocks therefore carry a tectonic signature which is not recognised in Shield orogens outside the Grenville Province. On this basis, Moore & Thompson (1980) suggested the terms Elzevirian and Ottawan orogenies for older and younger events in Ontario; they combined these in their term 'Grenvillian orogenic cycle', alluding to the Wilson cycle concept for development of the Grenville orogen. Modern geochronological studies, though far from complete, have provided a firm basis for assigning ages to various events in different parts of the province. As will be described later below, calc-alkaline

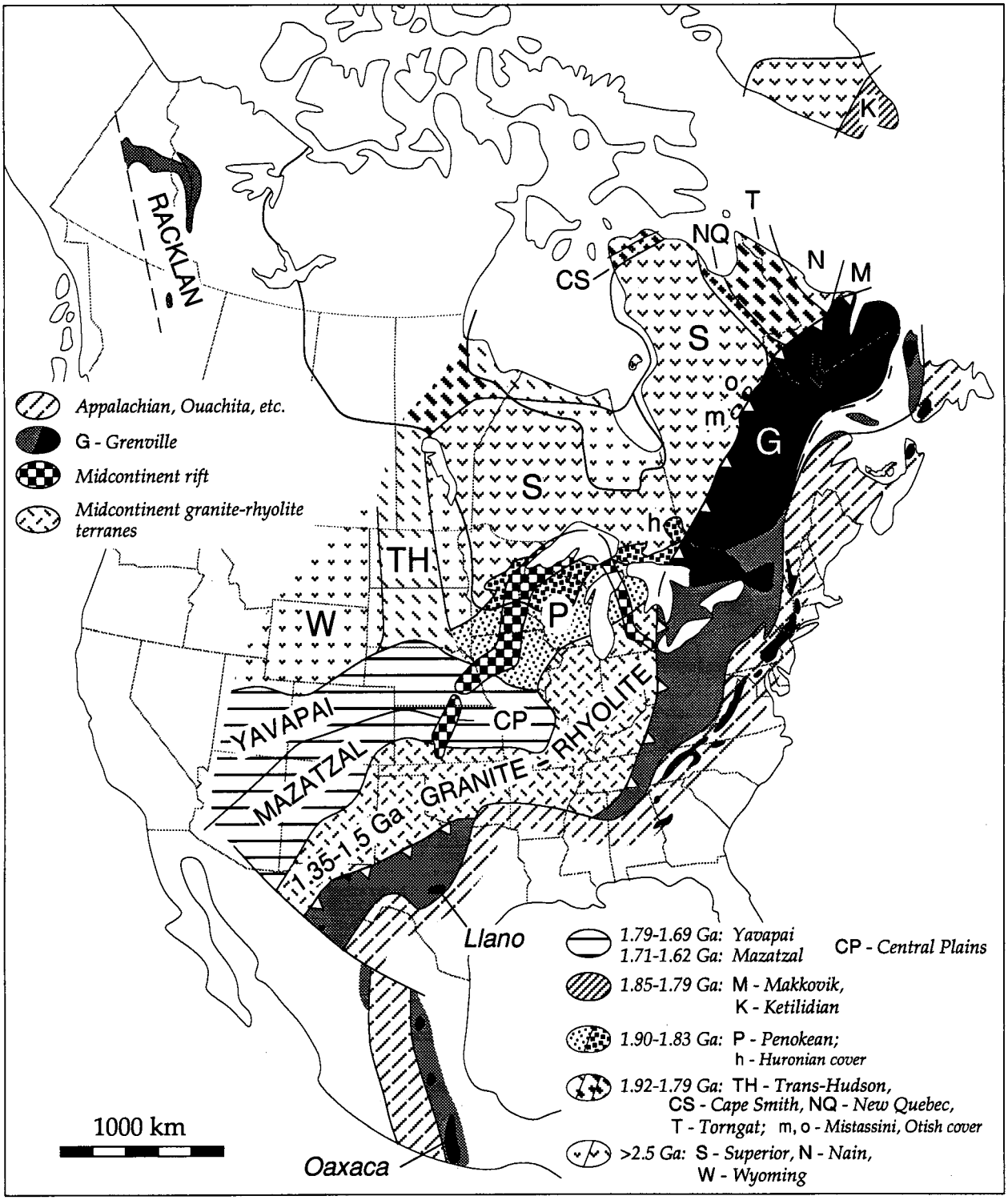

Figure 2. The Grenville orogen in North America. Parts of Superior, Wyoming, Trans-Hudson and Penokean provinces identified by smaller patterns, and grey part of the Grenville orogen, are covered by Phanerozoic rocks. The Grenville Front is marked with white teeth. The Racklan orogen is also Grenvillian in age. Data abstracted principally from Hoffman (1989a), Ruiz et al. (1988), and Van Schmus et al. (1992).

volcanic and plutonic rocks in the type area of the Elzevirian orogeny, considered to represent arc accretion (Windley 1986) and dated between 1.29 and 1.23 Ga, are an early manifestation of the Grenvillian orogenic cycle. There is evidence, however, for somewhat earlier, juvenile, calc-alkaline plutonic activity (1.35–1.30 Ga) in the Adirondack region of New York (McLelland & Chiarenzelli 1990) and inliers of the northern Appalachians (Ratcliffe et al. 1991), and of an even earlier volcanic arc (1.45–1.39 Ga) in central Quebec (Nadeau & van Breemen 1994), but their relationships to the Grenvillian orogenic cycle are at present uncertain. At the younger end of the Grenvillian time span, plutonism continued until ~1.06 Ga in the southwest part of the province, and until ~0.95 Ga in the east. High-grade metamorphism is recorded at ~1.05 - 1.02 Ga in several parts of the province. The Grenville Front was terminally active at ~1.0 Ga; cooling ages (U-Pb titanite, rutile, and $^{40}Ar/^{39}Ar$ hornblende) are of the same order or somewhat younger, with some exceptions of earlier cooling, noted below. In this paper, therefore, the term *Grenvillian* is used for rocks and events within the range ~1.3–0.95 Ga, with the proviso that this may be expanded in the future to include somewhat earlier events.

The second involves the term *terrane*, employed widely in the last decade for convenient description of segments of crust in the Grenville Province which, on the basis of lithology, structure, metamorphism, age of events and geophysical signature, are sufficiently distinct to set them apart from adjacent segments. The term *domain* has been used in the same sense (e.g. Davidson et al. 1982). Such distinctive segments are usually separated by continuous zones of high strain, in places amounting to well-defined ductile shear zones or faults. Rivers et al. (1989) suggested a non-genetic terminological hierarchy in which continuous *belts* within the Grenville Province may contain several terranes, themselves divisible into domains where appropriate. If the term *terrane* is considered in the narrower plate tectonic sense to define an out-of-place segment of crust bounded by sutures (e.g. Coney et al. 1980), then there are few viable candidates within the Grenville Province; discrete sutures have not been identified with certainty in the field, although some have been inferred on the basis of indirect evidence such as crust-formation ages (e.g. Dickin & McNutt 1989). It would be surprising indeed if terranes, in the plate tectonic sense, do not exist in an orogen such as the Grenville. Moreover, since much of the province is underlain by rocks of older orogens reworked during the Grenvillian orogeny, it is probable that pre-Grenvillian sutures are present as well. In deep crust such as characterises the exhumed Grenville orogen, however, terrane-bounding sutures are likely to be both cryptic and deformed, rendering their identification difficult and subject to circumstantial evidence. Nevertheless, it is quite clear that many of the named terranes within the Grenville Province are *not* bounded by sutures. The term *terrane* will therefore be used here in the non-genetic sense to avoid confusion with published nomenclature.

The Grenville Province

The Grenville Province, as defined above, underlies a belt, about 400 km wide, extending from the Atlantic coast of Labrador 2000 km southwestward to Lake Huron, beyond which rocks affected by the Grenvillian orogeny are covered by Phanerozoic platform sediments (Michigan Basin) of the continental cratonic interior (Fig. 2). The original width of the Grenville orogen is not known. The southeast margin of the Grenville Province is mostly covered by a narrow strip of unmetamorphosed and little-disturbed Early Palaeozoic sediments, but it abuts the Appalachian front along the east side of the Adirondack Mountains of New York, the southern part of which is nearly 600 km southeast of the Grenville Front. Throughout the Appalachian system of Canada and the eastern United States, Grenvillian rocks in tectonic windows and thrust slices attest to a considerably wider orogen than is now preserved in the Grenville Province itself.

In contrast, its northwest margin, the Grenville Front, is a remarkably sharp tectonic lineament. It cuts across several cratonic provinces, truncating their boundaries and internal structures, a feature that is expressed convincingly on regional aeromagnetic maps (see Fig. 2 *in* Rivers et al. 1989). It is the locus of moderately to steeply southeast-dipping thrust faults and mylonite zones, whose hanging walls generally carry uplifted and reworked rocks that represent deeper levels of the adjoining older Shield provinces; for this reason, the Grenville Front itself cannot be a suture.

Mid to deep crustal levels are exposed throughout most of the Grenville Province, as shown by the prevalence of granulite or upper amphibolite-facies gneiss and migmatite, and by the ductile style of deformation. Exceptions are restricted to the southeast part of the province in terranes containing supracrustal rocks of Grenvillian age. In the past, it was tacitly assumed that an overwhelming proportion of the structure and metamorphism within the province resulted from Grenvillian orogeny. However, it is obvious that rocks of older shield orogens, where recognised southeast of the Grenville Front, must have been previously deformed and metamorphosed. Although this was realised thirty years ago by Stockwell (1964), thanks to modern geochronology the full extent and significance of preserved pre-Grenvillian high-grade rocks and structures is only now beginning to be appreciated fully. In some parts of the province, Grenvillian remobilisation has effectively obscured or erased the record of earlier metamorphism and deformation. In other parts, however, interpretation of Grenvillian tectonic history as a whole is complicated by large tracts of crystalline crust in which an earlier orogenic record is the dominant one preserved and, at present, by uncertainty about the distribution of such tracts in poorly exposed or less well mapped parts.

Before the more specific geologic attributes of the Grenville Province and its component parts are discussed, the nature of the foreland immediately northwest of the Grenville Front is reviewed briefly. This is important with respect to recognition of older Laurentian rocks within the Grenville orogen.

The Grenville foreland

Along two-thirds of the exposed Grenville Front (Fig. 3), the Grenville Province abuts late Archaean rocks of the Superior Province, comprising east-trending, alternating metavolcanic (greenstone) and metasedimentary belts, each with its complement of granitoid rocks, and, in the northeast, granulite-facies rocks of the Ashuanipi complex (Card 1990). To the northeast, mid-Palaeoproterozoic sedimentary rocks (Kaniapiskau Supergroup) overlying the Superior craton are thrust westward in the fold-thrust belt (Labrador Trough) of the New Quebec orogen (Hoffman 1988); probable correlatives of these rocks (Otish and Mistassini groups) unconformably overlie Archaean rocks southwest of this orogen, and are undisturbed except where folded and faulted adjacent to the Grenville Front. Farther east, the hinterland of the New Quebec orogen (Rae Province), comprising reworked Archaean rocks, Palaeoproterozoic supracrustal rocks and ~1.83 Ga granites, and the adjacent Archaean Nain Province to the east are cut by voluminous, anorogenic plutons of anorthosite, gabbro and granitoid rocks of two age groups (~1.45 and ~1.3 Ga). Plutons of the older group are overlain by red beds and basalts of the Seal Lake Group (~1.25 Ga), which are preserved in a north-directed fold-thrust belt, probably late Grenvillian in age, adjacent to the Grenville Front. Farther east again, mid-Archaean granulites of the Nain Province are succeeded by late Palaeoproterozoic volcanic rocks (Aillik, Bruce River

groups) and granites of the Makkovik Province, ranging in age and younging southeastward from ~1.9 (Ketilidian) to 1.65 Ga (Labradorian) (Kerr et al. 1992).

Adjoining the southwest part of the Grenville Province, Archaean rocks of the Superior Province are overlain unconformably by the early Palaeoproterozoic Huron Supergroup (<2.48 to >2.22 Ga). This thick succession (~12 km) is folded and metamorphosed in the Southern Province of Ontario, tectonism being ascribed to the Penokean orogeny (1.90–1.83 Ga). Granitoid rocks of two ages, ~1.74 and ~1.47 Ga, intrude the Huron Supergroup (van Breemen & Davidson 1988a; Davidson & van Breemen 1994). The former are age-correlative with Yavapai plutonism in the western mid-continent, also represented in the Central Plains orogen (Sims & Peterman 1986); the latter lie within the age range of the older of two groups of Mesoproterozoic anorogenic plutons (~1.45 and ~1.37 Ga; Bickford et al. 1986) (Fig. 2). It is interesting that Proterozoic plutonic suites, both orogenic (late Palaeoproterozoic) and anorogenic (early Mesoproterozoic), occur at both ends of the exposed Grenville Front. This has important implications for the derivation of deformed and metamorphosed plutonic suites within the Grenville Province.

Interior of the Grenville Province

Following the early attempt by Stockwell (1964) to identify the distribution of superposed orogenic events within the Grenville Province using the geochronologic data available at that time, Wynne-Edwards (1972) divided the Grenville Province into subprovinces on the basis of lithologic assemblage and character of metamorphism, although boundaries between these were poorly defined. More recent structural studies and a burgeoning database of more sophisticated geochronology (see Moore et al. 1986; Hoffman 1989a) have prompted reassessment of Wynne-Edwards' scheme. It is now considered more convenient to view the Grenville Province in terms of three orogen-parallel belts in the manner of Rivers et al. (1989), namely (1) a northwestern parautochthonous belt, closest to the front, in which rocks can be reasonably correlated with those in the adjacent foreland: (2) a central allochthonous belt of rocks that have undergone pre-Grenvillian orogeny, but which do not appear to directly correlate with those in the parautochthon or foreland: and (3) a southeastern, discontinuous allochthonous belt of supracrustal and associated plutonic rocks that have undergone only the Grenvillian orogenic cycle (Figs 3 and 4).

Plutonic rocks of Grenvillian age are present in parts of the central, allochthonous polycyclic belt, but are extremely rare in the parautochthon. The three belts are delimited by moderately to shallowly southeast to south-dipping ductile shear zones. For the most part these exhibit northwest to north-directed thrust sense (Rivers & Chown 1986; Wardle et al. 1986, 1990; Hanmer 1988), but extensional tectonics have been documented for part of the southeastern belt (Rivers et al. 1989), and recognised as succeeding or overprinting earlier ductile thrusting elsewhere (van der Pluijm & Carlson 1989; Carlson et al. 1990; Culshaw et al. 1994).

Although useful as a first approach, this division is,

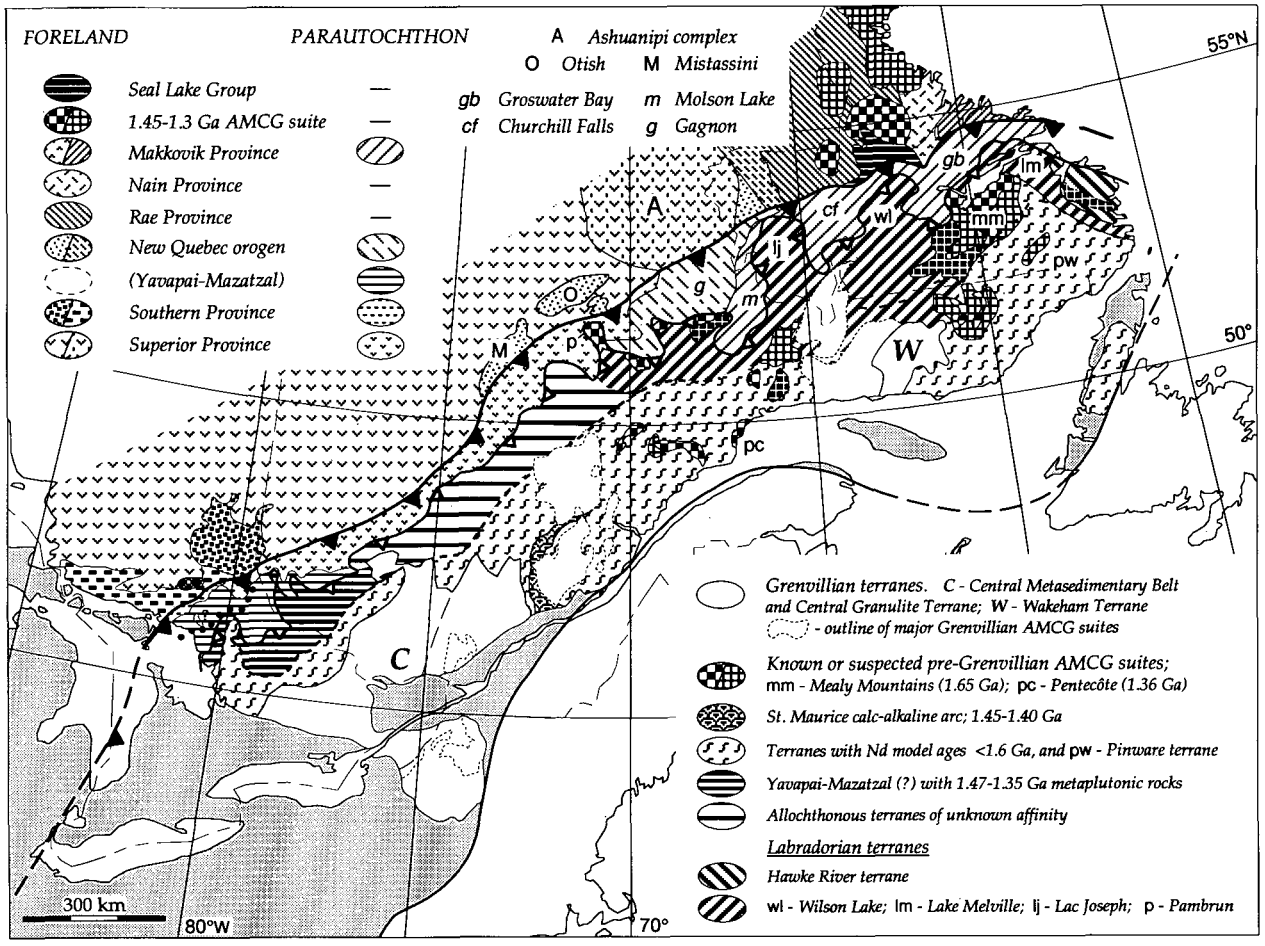

Figure 3. Principal tectonic elements of the Grenville Province. Solid toothed line is the Grenville Front, open teeth mark the internal allochthon boundary thrust system (modified after Rivers et al., 1989); dotted line in the southwest is proposed Penokean suture of Dickin & McNutt (1989). The diagram shows the distribution of reworked foreland provinces within the northwestern parautochthonous belt, and of Palaeoproterozoic units in the central allochthonous belt, including pre-Grenvillian AMCG suites. Grenvillian terranes and the main Grenvillian AMCG suites are unpatterned.

admittedly, simplistic; it is complicated by changes in pre- and syn-Grenvillian lithology and apparent differences in age and succession of events along the length of the belts, and also by recent recognition of major boundaries within each of the belts. A further concern is that much of the central belt may indeed have foreland correlatives beyond the confines of the exposed Shield (e.g. in the buried mid-continent) and, thus, that some boundaries within the province may be pre-Grenvillian in origin, though reactivated in Grenvillian time.

The northwestern parautochthonous belt

There is little doubt about the correlation across the Grenville Front of at least three major rock associations: namely, Archaean rocks of the Superior Province, Proterozoic supracrustal rocks of the Kaniapiskau Supergroup, and Proterozoic plutonic rocks in the northeast (~1.65 Ga Trans-Labrador batholith) and southwest (1.75 and 1.45 Ga granites) (Fig. 3). In addition, metamorphosed and deformed equivalents of Proterozoic mafic rocks and dyke swarms in the foreland (e.g. 1.46 Ga Shabogamo and 1.43 Ga Michael gabbro in Labrador, 1.24 Ga Sudbury diabase dykes in Ontario) have also been recognised in the Grenville Province.

Tracking these units southeast of the front to where they are tectonically buried beneath allochthonous rocks gives at least a minimum estimate of how much of the Grenville Province was derived from pre-Grenvillian Laurentia. U–Pb geochronology has been the key to correlation in many cases, as the foreland rocks are commonly deformed and metamorphosed southeast of the front to the extent that their protoliths are physically unrecognisable. This is not true, however, for the Kaniapiskau Supergroup in Labrador and eastern Quebec, where a particularly diagnostic stratigraphic succession of dolostone, orthoquartzite and iron formation (Denault, Wishart, and Sokoman formations) is recognisable within the Grenville Province for well over 100 km south of the front (Rivers & Chown 1986). In contrast, it is surprising that the Huron Supergroup in the east-trending Southern Province fold belt, characterised by thick quartzite formations, cannot likewise be traced across the front with confidence (e.g. Frarey 1985). However, the absence immediately southeast of the front of pre-Grenvillian cratonic cover (Seal Lake, Otish and Mistassini groups, and northeastern part of the Huron Supergroup; Fig. 3) can be accounted for by relatively deep exhumation of the frontal hanging wall; there is no evidence for large-scale lateral offset. It is of interest that there are no known occurrences of large plutons belonging to the 1.45 and 1.3 Ga anorogenic suites of the Rae and Nain Provinces within the adjacent parautochthonous belt in Labrador, although it is possible that the Shabogamo and Michael gabbro intrusions are related to the older suite, with which they are coeval (Gower 1990).

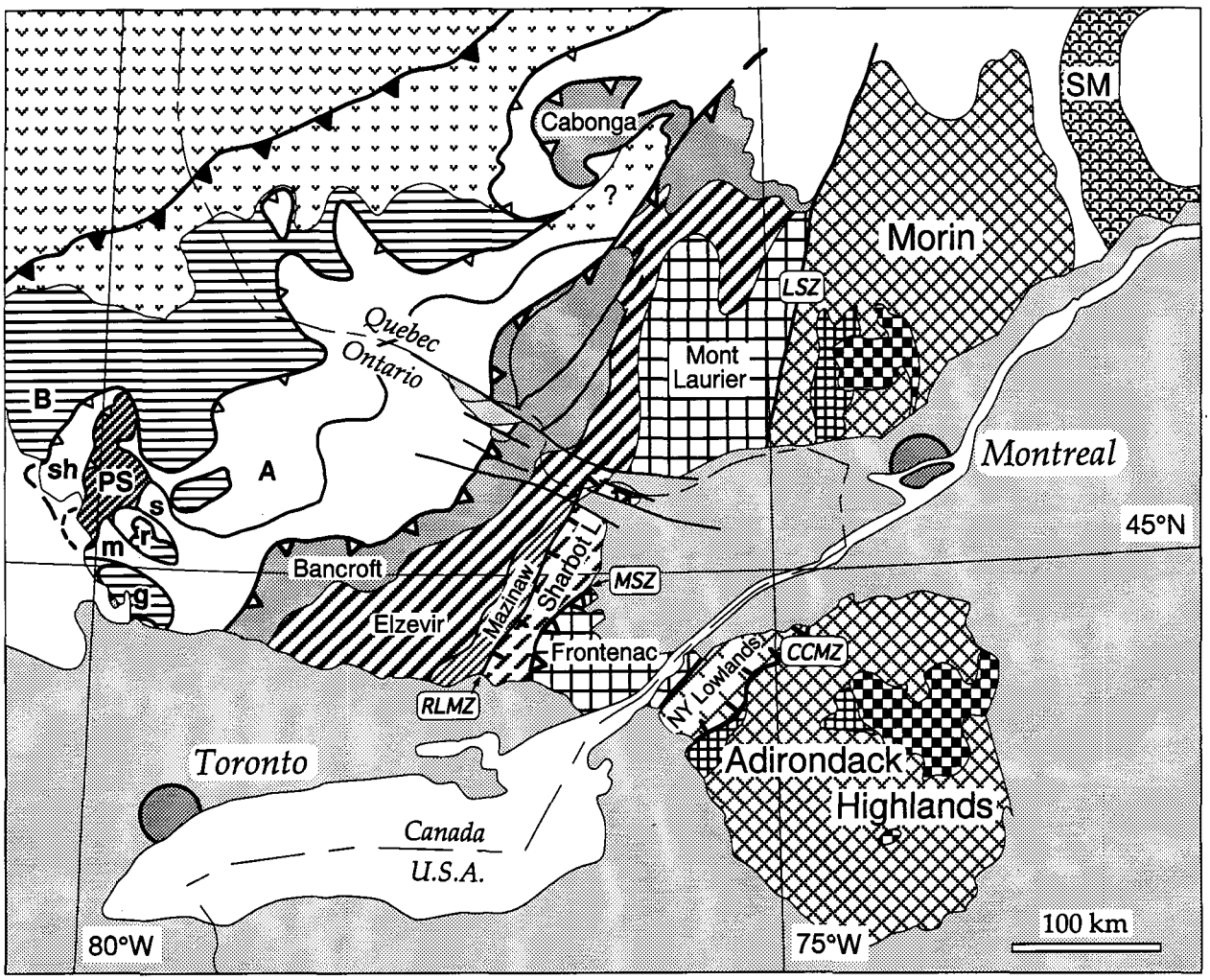

Figure 4. Detail of terranes in the southwestern Grenville Province. B—Britt, sh—Shawanaga, PS—Parry Sound, A—Algonquin, g—Go Home, m—Moon River, r—Rosseau, s—Seguin, SM—St. Maurice. Morin and Adirondack Highlands terranes, with Grenvillian AMCG suites, comprise the Central Granulite Terrane of Wynne-Edwards (1972). Patterned terranes immediately to the west make up the Central Metasedimentary Belt, within which labelled terrane boundaries are: *RLMZ*—Robertson Lake mylonite zone, *MSZ*—Maberly shear zone, *CCMZ*—Carthage–Colton mylonite zone, and *LSZ*—Labelle shear zone. The northwest boundary of Bancroft terrane (Central Metasedimentary Belt boundary thrust zone of Hanmer & McEachern, 1992) passes into a zone of oblique shear to the north in Quebec (Hanmer & Ciesielski, 1984), almost isolating the Cabonga allochthon (Martignole & Pouget, 1993).

Many of the metamorphosed plutonic rocks in Wynne-Edwards' (1972) 'Central Gneiss Belt' in Ontario are now known to have primary ages of ~1.46 Ga and to lie within gneisses among which older granitoid rocks give ages of ~1.7 Ga (van Breemen et al. 1986; Davidson et al. 1992; Corrigan et al. 1994a). In the southeastern part of the extent of these rocks, the enveloping gneisses have Nd depleted mantle model ages (DePaolo 1981) that are too young (≤1.98–~1.7 Ga; Dickin & McNutt 1989, 1990) for them to correlate with rocks of either the Superior or Southern provinces in the adjacent foreland. Similar crust-formation ages, however, are recorded for plutonic rocks within the Yavapai and Mazatzal orogens in the United States mid-continent southwest of the shield, and also for younger granites of the granite–rhyolite terranes farther south (Nelson & DePaolo 1985; Patchett & Arndt 1986). It is, therefore, reasonable that much of this gneiss terrane in Ontario correlates with terranes beyond the Grenville Front which are mainly buried south of the shield, but which form part of the pre-Grenvillian Laurentian craton.

Significant boundaries are now being recognised, by observation or by inference, within the northwestern parautochthonous belt. Two major terranes have been defined within the parautochthon in west-central Labrador (Fig. 3). The structurally lower one (Gagnon terrane; Rivers et al. 1989) corresponds to the foreland of the New Quebec orogen, namely the Palaeoproterozoic Kaniapiskau Supergroup and its Archaean basement; the effect of Grenvillian orogeny has been to produce a fold-thrust belt involving the previously undeformed foreland cover, in which Grenvillian metamorphic facies increase rapidly southeast of the Grenville Front (Rivers 1983; Brown et al. 1992). The Gagnon terrane is structurally overlain by younger rocks (Molson Lake terrane; Connelly et al. 1989, 1993), comprising mostly granitoids of Labradorian age (~1.65 Ga). Shabogamo metagabbro occurs within both terranes, suggesting that they had been together before ~1.46 Ga. High-pressure metamorphism of Shabogamo gabbro, approaching eclogite facies (Indares 1993) in the lower level of the Molson Lake terrane, attests to extensive Grenvillian uplift along the boundary between the two terranes. In this area, it is implied that the Molson Lake thrust plate has overstepped the whole of the hinterland (Rae Province) of the New Quebec orogen, as well as the Archaean rocks of the Nain Province on its eastern flank, a distance of several hundred kilometres; the relative amounts of displacement due to Labradorian and Grenvillian orogeny (respectively, lateral vs orthogonal with respect to the Grenville Front) are unknown.

A pre-Grenvillian crustal boundary is inferred from Nd model ages in the southwestern Grenville Province (Dickin & McNutt 1989, 1990) (dotted line in Fig. 3). It corresponds to an abrupt change in model ages from Archaean and early Palaeoproterozoic (≥2.2 Ga) to ≤1.98–1.7 Ga, and has been equated with the eastward projection into the Grenville Province of the Niagara fault, a suture within the Penokean orogen south of Lake Superior (Van Schmus et al. 1993). Its trace has not been identified on the ground, however, and its projection to the northeast appears to coincide with a boundary between post-Penokean metasedimentary rocks (~1685 Ma detrital zircons; Krogh 1989) and reworked Archaean basement. At present, it is uncertain if part of this boundary is in fact the allochthon boundary thrust.

In the same region (Fig. 3), the boundary in the foreland between folded and metamorphosed Huron Supergroup of the Southern Province and its Archaean ramp to the north (Superior Province and undeformed Huronian cover) has yet to be identified in the Grenville parautochthon. Reworked Archaean rocks in the frontal hanging wall give way southward to gneisses in which the metasedimentary component has Nd model ages too young (2.4–2.15 Ga) for them to have been derived from the Huron Supergroup (model age >2.5 Ga). Metaplutonic rocks in this region are dated at ≤1.75 or ~1.47 Ga, the same ages as post-Penokean plutonic suites west of the Grenville front. This region is interpreted in Figure 3 as being equivalent to Yavapai–Mazatzal crust (Fig. 2) with the addition of early Mesoproterozoic plutonic rocks equivalent to those of the midcontinental granite-rhyolite terranes; it also carries evidence for ~1.45 Ga metamorphism (Ketchum et al. 1994; Dudàs et al. 1994). If this is correct, any former eastward continuation of the Southern Province (Penokean orogen) into the Grenville Province would appear to have been occluded by northwestward translation of post-Penokean rocks.

The foregoing serves to illustrate the complexity of the history of shield rocks that have been 'caught up' (telescoped) in the marginal zone of the Grenville orogen, particularly at its northeast and southwest ends. If the southeastern Superior Province was flanked by early to mid-Palaeoproterozoic orogens (southern extension of the New Quebec orogen and its reworked Archaean hinterland; eastern extension of the Penokean orogen), they were either rifted away before or overridden by younger rocks during late Palaeoproterozoic orogeny (Yavapai-Mazatzal and Labradorian), Mesoproterozoic Grenvillian shortening, or both.

The central, polycyclic allochthonous belt

The central belt, comprising metamorphosed sedimentary and plutonic rocks, underlies most of the Grenville Province. Its northwestern 'leading edge' against the parautochthon describes a sinuous trace for the whole length of the province (Fig. 3). Much of this boundary (central Labrador to western Quebec) is marked by an abrupt change in aeromagnetic signature, from relatively flat over the parautochthon to short-order, high-relief patterns. The latter reflect the prevalence of high-grade granulites in the hanging wall of the 'allochthon boundary thrust' (Rivers et al. 1989) compared to middle to upper amphibolite grade in the parautochthonous footwall. Wherever examined, the boundary itself is the locus of moderate to low-angle, generally southeast-dipping ductile mylonite and 'straight gneiss' (continuously and commonly thinly layered, fine-grained gneiss of ductile tectonic origin; Davidson 1984a; Hanmer 1988). Metamorphic inversion and shear-sense indicators accord with northerly to northwesterly directed thrust tectonics along this boundary. Large-scale undulations in its attitude account for much of its irregular trace, but in places these may be due to overlapping thrust slices. In a few places, granulite blocks are isolated, or nearly so, from their southeastern sources (e.g. the Wilson Lake terrane in central Labrador, the Pambrun lobe in Quebec, the Parry Sound allochthon in Ontario; Figs. 3 and 4), and in others, northwest-projecting lobes are known to be thin (e.g. the Lac Joseph terrane in western Labrador has a central window to underlying the Molson Lake terrane; Connelly et al. 1993).

There is no evidence for Archaean or early to mid-Palaeoproterozoic rock (i.e., >1.85 Ga, Nd model ages >2.0 Ga) in the terranes of the central polycyclic belt in the hanging wall of the allochthon boundary thrust. In Labrador, metamorphism and deformation internal to the allochthonous lobes have been found to be Labradorian in age (~1.65 Ga), with relatively minor Grenvillian thermal overprint (Connelly & Heaman 1993). This late Palaeoproterozoic tectonism is thus coeval with Labradorian magmatism in the underlying parautochthon in this area. The metasedimentary gneisses that host the parautochthonous Trans-Labrador batholith are similar to those at granulite grade in the overriding slices (both have pelitic and arenitic progenitors), but there is a distinct difference in the respective magmatic rocks: the Trans-Labrador batholith is a juvenile granodiorite–granite suite with calc-alkaline affinity, whereas plutonic rocks in the allochthons are mainly noritic gabbro, anorthosite, and associated pyroxene monzonite and granite; the suites are in part coeval at ~1.65 Ga, although calc-alkaline Trans-Labradorian magmatism began somewhat

earlier (~1.7 Ga). The recorded timing of allochthon displacement, however, is Grenvillian; thus, although both footwall and hanging wall record Labradorian orogeny, they may represent quite different parts of the Labrador orogen. Connelly & Heaman (1993) suggested that the initial juxtaposition of these disparate terranes occurred during Labradorian orogeny, the juncture being modified by Grenvillian shortening. A similar two-stage history was expressed earlier by Wardle et al. (1986), and has been confirmed along the same thrust system 400 km farther east (Philippe et al. 1993). Hoffman (1989a, p. 498) pointed out that the geochronology '... is consistent with the central zone having been contiguous with the protocraton since about 1.65 Ga ...', but, in fact, this does not preclude extensional separation following Labradorian orogeny and reamalgamation with marked overstepping during the Grenvillian.

West of the Lac Joseph allochthonous lobe (Fig. 3), the allochthon boundary thrust oversteps the Molson Lake terrane and places high-grade granulites and their attendant gabbro–anorthosite massifs (not dated) over the southwestern continuation of the Kaniapiskau Supergroup in the parautochthonous Gagnon terrane. Farther west again, the boundary thrust passes across reworked Archaean rocks and, in the Pambrun lobe, almost oversteps them as far as the Grenville Front south of the autochthonous Otish basin. Beyond this, the allochthon boundary thrust can be traced to western Quebec on the basis of aeromagnetic contrast and scattered field observations, but the position of its continuation into Ontario is not resolved. Near Georgian Bay (Lake Huron), Rivers et al. (1989) placed it at the western thrust boundary of the Parry Sound granulite allochthon (Davidson 1986), but more recent evidence suggests that it may lie at a lower structural level to the northwest along a shear zone carrying remnants of eclogite (Davidson 1991; Culshaw et al. 1994). This location would be in accord with demarcation near the Quebec–Ontario border of granulite-facies rocks that structurally overlie a Proterozoic metasedimentary assemblage (quartzite, meta-arkose, pelitic gneiss, iron formation and minor marble) which contains the 1685 Ma detrital zircons already mentioned, and which lies structurally above the Archaean parautochthon. This metasedimentary unit has no counterpart in the adjacent foreland, and may also be separated from the Archaean part of the parautochthon by a structural discontinuity. The map pattern in this region may well be complicated by windows of parautochthonous rocks to the south, not yet delineated in the field. This trace of the allochthon boundary shown in Figures 3 and 4, to date not resolved by mapping, may pass southeast of the complex region of the southwesternmost parautochthon discussed in the last section.

Rivers et al. (1989) identified a large part of the Grenville interior in Ontario as parautochthonous on the basis that it contains ~1.75 Ga and 1.47–1.34-Ga orthogneissic rocks (deformed batholiths), making it comparable in age to the substrate of the mid-continent south of the shield. Some of this terrane lies southeast of the redefined allochthon boundary thrust (Fig. 3), and the situation may be analogous to that of the Labradorian in the northeast part of the province, complicated by structural culminations that provide windows to the underlying parautochthon (Rosseau, Go Home and parts of Algonquin domains south and east of the Parry Sound allochthon; Fig. 4). Within the same region, Nd model age determination (Dickin & McNutt 1990) has identified significantly younger crust derivation within the Parry Sound allochthon and in synformal lobes that overlie it to the southeast (1.6–1.4 Ga vs 2.0–1.7 Ga to the north), conforming to the map pattern and order of stacking deduced from field studies (Davidson 1984b). Dated metaplutonic rocks in areas with the older crust-formation ages include units belonging to the ~1.45 Ga suite. The few plutonic ages available in areas with crust-formation ages of <1.6 Ga appear to be younger, ~1.35 Ga. It seems, therefore, that the central belt in Ontario may conceal a pre-Grenvillian crustal boundary. Whether or not this boundary is present in the buried mid-continent beyond the Grenville Front is uncertain; most of the Mesoproterozoic igneous rocks there (1.5–1.35 Ga) have 1.9–1.7 Ga Nd depleted mantle model ages, but there is new evidence that some in the southern mid-continent are entirely juvenile (see Van Schmus et al. 1993, p. 290, and references therein).

The same duality of crust-forming age is becoming apparent in the central and northeastern parts of the polycyclic belt. Dickin & Higgins (1992) have documented a large region in the southern part of the belt in which 'grey gneisses', tentatively interpreted in terms of subduction-related arc terranes, have Nd model ages between 1.60 and 1.46 Ga (Fig. 3); the igneous crystallisation ages of their precursors is not known, but they can be no older than their model ages, making them younger than the Labradorian rocks that lie above the allochthon boundary thrust to the north and northeast. The boundary between Labradorian and younger crust has yet to be defined in this poorly exposed and generally inaccessible part of the province, where only regional reconnaissance mapping is available. It is noted that granitic rocks with ages between 1.49 and 1.47 Ga have been identified recently in east of the Pinware terrane, just south of the Labradorian Hawke River terrane (Fig. 3) (Tucker & Gower 1994), and also that 1.40 Ga monazite in migmatite leucosome in the south of the Lac Joseph terrane suggests regional heating at that time (Connelly & Heaman 1993).

Important with respect to the younger crustal terrane in the central belt is the recent recognition of a deformed volcano-plutonic arc (St. Maurice terrane, Figs 3 and 4), for which preliminary dating indicates an age in the range 1.45–1.39 Ga (Nadeau & van Breemen 1994; Hervet et al. 1994). Supracrustal rocks (Montauban group) include pelitic gneiss and layered amphibolite that locally preserves pillow structure. Plutonic rocks (La Bostonnais complex) range from gabbro to granodiorite, have a calc-alkaline character, and Nd model ages of ~1.6 Ga (L. Nadeau, pers. comm. 1994).

Also important in this general region is the presence of pre-Grenvillian anorthosite–mangerite–charnockite–granite (AMCG) suites of two ages. In Labrador, a large massif of anorthosite, gabbro and related granitoid rocks in the Mealy Mountains terrane, the White Bear Arm suite in the Hawke River terrane, and large gabbro masses (Ossokmanuan suite) in the Lac Joseph terrane all have late Labradorian ages (1645–1625 Ma; Emslie & Hunt 1990; Gower et al. 1992; Connelly & Heaman 1993). In Quebec, Mesoproterozoic, but pre-Grenvillian, AMCG magmatism is represented by the Pentecôte anorthosite–charnockite pluton west of Sept Iles (1.35 Ga; Emslie & Hunt 1992; Martignole et al. 1993); this is the only complex so far dated that is roughly coeval with the anorogenic AMCG magmatism in Labrador north of the Grenville Front. The fact that these pre-Grenvillian AMCG rocks are as well preserved as younger Grenvillian suites of the same type, and are petrographically indistinguishable from them, means that assignation of age to the several undated plutons in this region must await isotopic analysis.

In the foregoing, emphasis has been placed on the nature and age of the plutonic rocks in the central belt, and although these may be volumetrically dominant, a large proportion of the rocks are supracrustal in origin. Supracrustal assemblages vary from place to place, and distinctive assemblages may characterise individual terranes (e.g. layered mafic granulite and marble in the Parry Sound allochthon). Recognisable mafic volcanic rocks are rare (Labradorian Hawke River terrane (Gower et al. 1991), early Mesoproterozoic Montauban group (Rondot 1986)), as are tracts of amphibolite. It is possible, however, that felsic volcanic, pyroclastic and hypabyssal rocks are unrecognised precursors of leucocratic quartzofeldspathic gneiss units. Sillimanite- and garnet-bearing paragneiss, in

places with abundant pyrite and graphite, is common in many areas, and may be associated with subordinate quartzite, impure calcareous rocks and rare metaconglomerate. Deformation and metamorphism, however, have rendered any form of stratigraphic analysis and regional correlation impossible.

In summary, the central polycyclic allochthonous belt contains several terranes bounded by shear zones, together embracing two belts of Proterozoic crust, mid to late Palaeoproterozoic to the northwest and early Mesoproterozoic to the southeast. Windows of the earlier crust appear in the southeastern part, and plutonic rocks of early Mesoproterozoic age (1.9–1.7 Nd model ages) occur in the northwestern part. The former relationship between these two units and their distribution have been modified during northwest-compressional Grenvillian tectonism. This is the setting in which the southeastern Grenvillian belt must be considered.

The southeastern Grenvillian belt

Two regions near the southeastern margin of the Grenville Province are underlain by supracrustal rocks younger than ~1.3 Ga: namely, the Wakeham Supergroup in eastern Quebec and the Grenville Supergroup in eastern Ontario and southwestern Quebec (Fig. 3). These two assemblages, at least in part coeval, are represented by entirely distinct facies, indicating different depositional regimes. Although both are deformed and exhibit a wide range in metamorphic grade, the least deformed parts, particularly in the Wakeham Supergroup, allow recognition of primary sedimentary and volcanic structures and of stratigraphic relationships.

Wakeham Supergroup. The Wakeham Supergroup underlies an area of ~15 000 km^2 in eastern Quebec near the north shore of the St. Lawrence (Fig. 3; also see Fig. 6). It has been divided into two groups, the older Aguanus Group being unconformably overlain by the Davy Group; both deposited in continental extensional environments (Martignole et al. 1987, 1994). The Aguanus Group is composed primarily of orthoquartzite and feldspathic sandstone with minor argillaceous units, intercalated with bimodal volcanic rocks (rhyolite flows and tuffs with subordinate basalt). On the basis of its peralkaline chemistry, Bourne (1986) suggested an 'anorogenic' environment for this magmatism. Rhyolite from this group has been dated at 1.27 Ga (Loveridge 1986). Associated with the felsic volcanic rocks are hypabyssal granite intrusions, two of which have been dated at ~1.24 Ga (Martignole et al. 1994). Cobbles of these granites, as well as quartzite, are present in the basal conglomerate of the Davy Group, which overlies folded Aguanus strata and is composed predominantly of cross-bedded arkose and hematite-rich siltstone. Both groups were intruded by gabbro sills (1.18 Ga; Martignole et al. 1994) before a second period of folding affected the whole assemblage. The Wakeham Supergroup has some environmental affinity with the 1.32 Ga Letitia Lake Group (peralkaline volcanic rocks) and ~1.25 Ga Seal Lake Group in the foreland of the Grenville Province 300 km to the north.

Much of the Wakeham Supergroup is only metamorphosed to greenschist facies, and in some parts, particularly in the north, is at sub-greenschist grade. West and southeast of the main exposure, however, remnants of quartzite and amphibolite within quartzofeldspathic gneisses may represent more thoroughly deformed and metamorphosed Wakeham Supergroup rocks. High-grade migmatitic gneisses, including orthogneiss of Labradorian age (Loveridge 1986), lie structurally beneath the Wakeham Supergroup along its northern margin, and although an undisturbed contact has not been observed, it is possible that it is a profound unconformity. Along the northwest flank, highly foliated rocks dipping moderately to the southeast display extensional kinematic indicators against older granite gneiss, itself intruded by younger (1.08 Ga) charnockitic rocks, part of a large AMCG plutonic mass lying to the west (Romaine River complex). The Wakeham Supergroup itself is cut by several small plutons of undeformed granite, one of which has been dated at 993 Ma (Loveridge 1986; Bourne 1991).

Grenville Supergroup. Replacing the earlier name 'Grenville series' (Logan 1863), the term Grenville Supergroup applies collectively to all the sedimentary and volcanic strata that underlie the 'Central Metasedimentary Belt' in Ontario and southwest Quebec (Wynne-Edwards 1972) (Fig. 3). A characteristic and volumetrically important rock type common to all parts of this belt is marble, by contrast rare in all other parts of the Grenville Province except the 'Central Granulite Terrane' immediately to the east (Adirondack and Morin terranes of Rivers et al. (1989), but now considered to be part of the southeastern zone). This whole region, about 135 000 km^2, consists of a number of terranes (Fig. 4), defined on the basis of differences in supracrustal assemblages, type and age of plutonic rocks, internal structure, and the nature of their mutual boundaries (Easton 1992; Easton & Davidson 1994). It seems increasingly likely that the Grenville Supergroup, as defined by Wynne-Edwards (op. cit.), includes rock groups that are not stratigraphically and perhaps not even temporally related. Although well preserved at upper greenschist grade in parts of Ontario, in most places these rocks have been intensely deformed and metamorphosed (middle amphibolite to high-temperature granulite facies; Carmichael et al. 1978; Davidson et al. 1990), rendering stratigraphic analysis and correlation from place to place extremely difficult, if not impossible, at all but local scale.

The Grenville Supergroup's original basement has not been recognised. The contact with older rocks of the central belt to the northwest is entirely tectonic, and lies within a broad, shallowly southeast-dipping ductile shear zone. This zone, at upper amphibolite facies, involves both the supergroup and the footwall gneisses of the central belt. Thrust-displacement sense has been documented along this zone in Ontario, but to the north, in Quebec, displacement appears to be oblique (Hanmer & Ciesielski 1984). Martignole & Pouget (1993; in press), however, document thrust tectonics in the Cabonga allochthon in western Quebec (Fig. 4). The marginal Bancroft and Cabonga terranes are characterised by marble tectonite, syenitic gneiss, and minor pelite and quartzite, as well as thrust slices of various kinds of metaplutonic rock (Hanmer & McEachern 1992). Thin units of nepheline-bearing gneiss associated with marble have usually been interpreted either to have had alkaline igneous protoliths or to have resulted from nephelinisation of pre-existing rocks (see Miller & Lenz 1993), but ultimate derivation from an evaporite-bearing sedimentary succession (Appleyard 1974; Haynes 1986) is not out of the question.

The Elzevir terrane (Brock & Moore 1983; Davidson 1986), southeast of the Bancroft terrane (Fig. 4), has recently been accorded superterrane status and divided into a number of smaller units (Easton 1992). Elzevir is characterised by volcanic rocks, predominantly mafic (including pillowed basalts), ranging in composition from tholeiitic to calc-alkaline (Condie & Moore 1977; Harnois & Moore 1991), and dated between 1.29 and 1.25 Ga (Davis & Bartlett 1988; Lumbers et al. 1990). They are associated with calc-alkaline plutons ranging from gabbro through tonalite to monzogranite, dated between 1.27 and 1.23 Ga. The volcanic rocks are interlayered with marble, which in less-deformed areas can be seen to have been derived from carbonate silt rhythmites, perhaps suggestive of a shelf-slope environment. Discontinuous units of fine, pyritic, siliciclastic sediments have been interpreted as submarine fans associated with local felsic volcanic sources (Easton 1986). Shallower water conditions are indicated, either locally or at certain stages, by stromatolitic dolomite marble and cross-bedded sandstone. The chemistry of the volcanic rocks suggest a palaeoenvironment of a convergent volcanic arc and a back-arc basin on stretched sialic crust (Condie &

Moore 1977; Holm et al. 1986; Harnois & Moore 1991). However, plutons of nepheline syenite and peralkaline granite, dated at ~1.24 Ga, seem out of place in this type of environment.

An apparently restricted part of the Elzevir superterrane (Mazinaw terrane; Easton 1992) includes an unconformably overlying succession of conglomerate, quartz sandstone, argillaceous sediment and carbonate (including an olistostromal facies), together constituting the Flinton Group (Moore & Thompson 1980). This group was deposited after folding of the underlying Grenville Supergroup, and after emplacement of the 1.27–1.23 Ga plutons. Detrital zircons from lower quartzose units indicate a maximum age of 1.15 Ga for sedimentation (Sager-Kinsman & Parrish 1993). The Flinton Group is preserved only in narrow synclines and was metamorphosed, along with underlying supracrustal and plutonic rocks, at ~1.03 Ga (Corfu & Easton 1994). This metamorphism (Ottawan orogeny as opposed to earlier Elzevirian orogeny, but both part of the Grenvillian orogenic cycle of Moore & Thompson 1980) is not known to be associated with plutonism of any kind. U–Pb titanite (Mezger et al. 1993) and $^{40}Ar/^{39}Ar$ amphibole cooling ages (Cosca et al. 1992) are consistent with relatively rapid uplift following this event. However, the southeasternmost part of the Elzevir superterrane (Sharbot Lake terrane) appears to have cooled several tens of million years earlier; this belt is separated from the Mazinaw terrane by the southeast-dipping Robertson Lake mylonite zone (Fig. 4), which records early ductile and later brittle deformation at low metamorphic grade and exhibits extensional kinematics. The age of regional metamorphism in the Sharbot Lake terrane is not known, but this terrane does not appear to record the 1.03 Ga amphibolite-facies metamorphism of underlying the Mazinaw terrane, as ~1.07 Ga plutons within it are neither deformed nor metamorphosed. Evidently, rocks that had cooled earlier at higher crustal level have been brought into juxtaposition with deeper level rocks.

A different geologic history is told by the neighbouring Frontenac terrane to the southeast, which also applies to most of Wynne-Edwards' (1972) 'Mont Laurier basin' in Quebec to the north. Here, the predominant supracrustal assemblage is pelite–quartzite–marble and lacks volcanic rocks. The boundary with the Elzevir superterrane is a high-strain thrust zone (Maberly shear zone), inclined to the southeast, along which granulite-facies rocks in the hanging wall contrast sharply with upper greenschist to lower amphibolite facies rock in parts of the Sharbot Lake terrane footwall. Meta-ultramafic to anorthositic rocks and monzonitic orthogneiss lenses reside in the immediate hanging wall. The monzonitic rocks are similar to less-deformed plutonic rocks farther southeast, which have been dated at ~1.17 Ma (van Breemen & Davidson 1988b; Marcantonio et al. 1990); similar ages have been obtained from monzonitic and charnockitic plutons to the north in Quebec (O. van Breemen, pers. comm. 1993). This plutonic suite ranges from noritic gabbro through pyroxene monzonite to leucogranite, and is chemically distinct from the older calc-alkaline suite in the Elzevir superterrane. Northwest-trending, undeformed olivine diabase dykes (Kingston swarm) cut these plutons in the southeast of the Frontenac terrane; they have been dated at 1160 Ma (U–Pb baddeleyite ages; S. Kamo, S. Pehrsson, pers. comm 1993).

Regional metamorphic mineral assemblages in the Frontenac terrane, uniformly at granulite grade, record higher pressure in the northwest (orthopyroxene–sillimanite assemblages, >7 kbar) than in the southeast (orthopyroxene–garnet–cordierite, <7 kbar). Metamorphism appears to pre-date the 1.17 Ga plutonic rocks; U–Pb ages of titanite in calc-silicate rocks record cooling through its blocking temperature between 1178 and 1157 Ma (Mezger et al. 1993), spanning this plutonism, with hornblende $^{40}Ar/^{39}Ar$ ages being somewhat younger (~1115 Ma; Cosca et al. 1992). The youngest plutons (~1075 Ma; Marcantonio et al. 1990) thus post-date regional cooling. There is no evidence for magmatism of Elzevirian age in the Frontenac terrane in Ontario. An older age (1415 Ma; McLelland et al. 1988) obtained for one granite that intrudes quartzite and is itself cut by 1.17 Ga granite dykes, is in conflict with single detrital zircon ages obtained from the quartzite (youngest 1306 Ma; Sager-Kinsman & Parrish 1993), and may be an artifact of inherited zircon.

Just south of the International Boundary, the Black Lake lineament, parallel to the St. Lawrence River, appears to separate rock associations typical of the Frontenac terrane from carbonate–pelite-dominated supracrustal rocks in the New York Lowlands terrane, and is associated with a southeastward drop in metamorphic grade. Diabase dykes of the Kingston swarm have not been observed in the New York Lowlands terrane. Leucogranites record ages between 1230 and 1285 Ma (McLelland & Chiarenzelli 1990), but U–Pb titanite cooling ages are similar to those in the Frontenac terrane (Mezger et al. 1993). Similarly, granodiorite orthogneiss in Quebec along the east side of the Central Metasedimentary Belt is dated at 1285 Ma (Machado et al. 1991). Along the southeast boundary of the New York Lowlands terrane, an apparently younger, unnamed succession of mainly carbonate rocks, including stromatolitic marble and hosting stratiform zinc deposits, occupies what may be a recumbent nappe, derived from the southeast and overriding more highly deformed metasedimentary rocks (Gouverneur marble, Popple Hill gneiss).

The Elzevir and Frontenac terranes in Ontario and their counterparts in Quebec are stitched by a potassic plutonic suite, comprising stocks of undeformed syenite and granite, dated at ~1.08 Ga (Corriveau et al. 1990). This suite has not been identified in the New York Lowlands terrane, nor in the Adirondack Highlands and Morin terranes to the east (Fig. 4); neither does it penetrate the northwestern boundary thrust zone in the central polycyclic zone. It is, however, coeval with younger components of Grenvillian AMCG plutonic suites farther east (dealt with in the next section).

The Adirondack Highlands and Morin terranes (presumably linked beneath Palaeozoic cover) contain highly deformed marble, pelitic and arenitic gneiss, and leucocratic gneiss possibly derived from felsic volcanic rocks. These host an early suite of tonalitic intrusions (1.35–1.30 Ga), superseded by massive intrusions of anorthosite and charnockitic granitoids, dated between 1.17 and 1.12 Ga (McLelland et al. 1988; Emslie & Hunt 1990; Chiarenzelli & McLelland 1993). Younger ages obtained from the AMCG suite and other plutonic rocks in the Adirondack Highlands terrane have been interpreted as the result of thermal disturbance of zircon U–Pb systematics (Chiarenzelli & McLelland 1993). Regional metamorphism is everywhere at medium-pressure granulite facies (≤8 kbar; Bohlen et al. 1985). Absolute age of metamorphism is uncertain, but mineral cooling ages in the Adirondacks are around 1.03 Ga (Mezger et al. 1991), at least 100 m.y. younger than in New York Lowlands and Frontenac terranes to the northwest, but coeval with most of the Elzevir terrane. The Adirondack Highlands and New York Lowlands terranes are separated by the Carthage–Colton mylonite zone, characterised by early ductile fabric, inclined to the northwest, and later brittle fabric, more steeply inclined, both indicating top-side-down displacement to the northwest (Heyn 1990). The brittle phase may reflect late extensional collapse off the Adirondack Highland core, but the early ductile phase could equally well represent nappe emplacement originating from the southeast. The equivalent boundary in Quebec (Labelle shear zone west of the Morin terrane; Indares & Martignole 1990a) is a steep ductile shear zone with shallow southeast-plunging stretching lineation; its kinematic significance is equivocal at present.

Plutonic rocks

Plutonic rocks within the Grenville Province are divisible into

three main groups with respect to time:

(1) integral plutonic components of pre-Grenvillian orogens, i.e. deformed Archaean granitoids in the parautochthonous belt, and Palaeoproterozoic suites, including 1.65 Ga Labradorian suites in the northeast part of the province and ~1.7 Ga age-equivalents of Yavapai and Mazatzal granites in the southwest;

(2) early Mesoproterozoic suites (1.5–1.35 Ga) within both the northwestwern parautochthonous and central polycyclic belts;

(3) Grenvillian suites (~1.3–0.95 Ga) concentrated predominantly in the southeastern part of the province.

Plutonic rocks of the first group are not related to the development of the Grenville orogen, and are not considered further. Those of the second group, however, may possibly presage the Grenvillian orogeny (cf. Windley 1989, 1993), and their distribution and ages are therefore summarised along with those of Grenvillian plutonic rocks in Figure 5.

The plutonic rocks of the second group have been described briefly in preceding sections. In summary, early Mesoproterozoic metaplutonic rocks in the parautochthonous and polycyclic belts in Ontario (Fig. 3) are coeval with 'anorogenic' igneous activity in the granite–rhyolite terranes of the United States midcontinent (Fig. 2), and may in part be their deformed and metamorphosed correlatives. Granitoid rocks of similar age occur in the Pinware terrane at the other end of the province, but have not yet been identified in the intervening region where the only dated igneous rocks in this age group are the calc-alkaline rocks of the St. Maurice terrane and the somewhat younger AMCG Pentecôte suite. Anorthositic rocks dated at ~1.35 Ga are also present in the Parry Sound domain and in the footwall of the Cabonga allochthon (Fig. 4), but are not associated with charnockite or granite and appear to have a more primitive chemistry (more calcic and magnesian) than anorthosite typical of AMCG suites.

Grenvillian igneous suites

The presently known distribution of Grenvillian plutonic rocks is shown in Figure 6. With the exception of scattered occurrences in the range 1.31–1.24 Ga near the Grenville

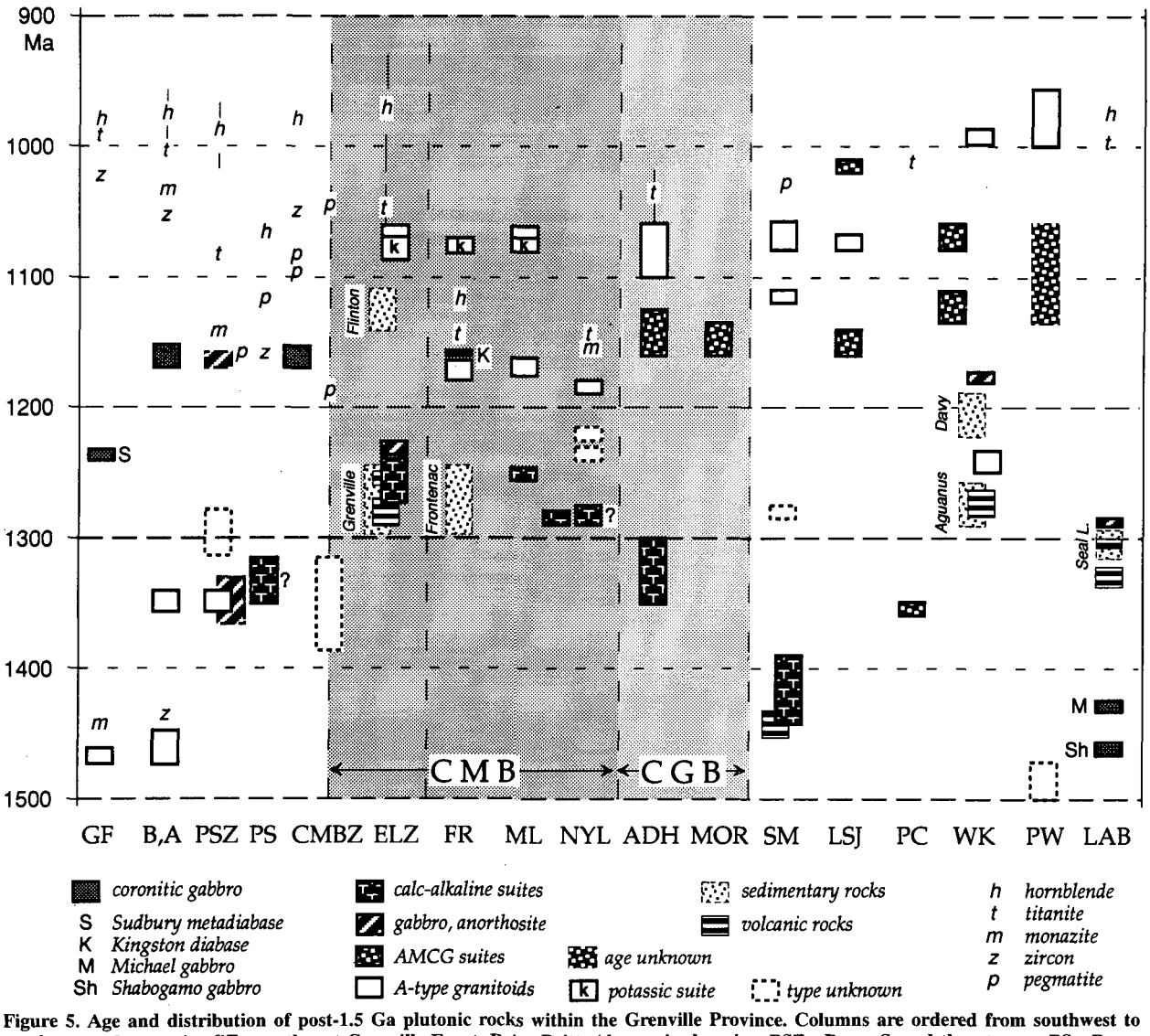

Figure 5. Age and distribution of post-1.5 Ga plutonic rocks within the Grenville Province. Columns are ordered from southwest to northeast and comprise GF—southwest Grenville Front, B,A—Britt, Algonquin domains, PSZ—Parry Sound thrust zone, PS—Parry Sound domain, CMBZ—Central Metasedimentary Belt boundary thrust zone, ELZ—Elzevir terrane, FR—Frontenac, ML—Mont Laurier, NYL—New York Lowlands, ADH—Adirondack Highlands, MOR—Morin, SM—St. Maurice, LSJ—Lac St. Jean area, PC—Pentecôte, WK—Wakeham terrane, PW—Pinware terrane, and LAB—Grenville Front region in Labrador. CMB and CGB are Central Metasedimentary Belt and Central Granulite Terrane of Wynne-Edwards (1972). Age ranges are shown for the principal, named Grenvillian supracrustal units; metasedimentary rocks similar in age to or somewhat older that the Grenville Supergroup are present in the other CMB and CGB terranes. Ages of metamorphism (*z, m*) and cooling (*t, h*) are U-Pb ages except hornblende, which is $^{40}Ar/^{39}Ar$. Zircon ages obtained from syn-deformation pegmatites are shown by *p*.

Front, they are restricted to the southeastern half of the province, and span the whole range (~1.3–0.95 Ga) accorded to the Grenvillian orogenic cycle. It is becoming apparent, however, that 1.3 Ga may not be an appropriate older age limit for 'Grenvillian' activity, that there may be a time gap of ~50 m.y. between early calc-alkaline igneous activity (>1.23 Ga) and younger anorthosite–mangerite–charnockite–granite (AMCG) suite plutons (<1.18 Ga), and that AMCG and A-type granite–syenite magmatism is volumetrically the most important. Within any one area, igneous rocks usually display episodic intrusion without temporal overlap of different types, and certain types are restricted to specific parts of the province.

Several of the Grenvillian igneous suites have been mentioned in the context of the Wakeham and Grenville supergroups. Calc-alkaline plutonic rocks (tonalite, trondhjemite and granodiorite) are present in the area underlain by the Grenville Supergroup in the southwest part of the province, where they are associated with volcanic rocks; this igneous activity spanned ~60 m.y., from 1.29–1.23 Ga, perhaps in two pulses (Easton 1992). Somewhat earlier calc-alkaline plutonic rocks (1.35–1.30 Ga) occur in the Adirondack Highlands of New York (McLelland & Chiarenzelli 1990) and in basement windows in the nearby northern Appalachians (Ratcliffe et al. 1991), raising the possibility that arc magmatism began earlier east of the Elzevir superterrane. The relationship between this and the even earlier calc-alkaline St. Maurice arc (1.45–1.39 Ga) farther northeast is not known, but it is tempting to postulate a westward-younging progression of successive arcs.

Of particular interest is the fact that volcanic rocks (rhyolite and tuff with subordinate tholeiitic basalt) and associated high-level granite plutons (1.27–1.24 Ga) of the Wakeham Supergroup in eastern Quebec, although coeval with Elzevirian calc-alkaline activity, are fundamentally different in character, being of continental rift type. A similar setting is reflected by peralkaline igneous rocks of the Letitia Lake Group and the overlying red-bed and basalt succession of the Seal Lake Group adjacent to the Grenville Front to the north (Fig. 3). Northeastern and southwestern parts of the Grenvillian Province thus record different tectonic environments early in the Grenvillian orogenic cycle; how far removed from one another they may have been at the time, however, is conjectural.

By far the most voluminous Grenvillian plutonism, that of the AMCG suite, gave rise to the well-known anorthosite–charnockite massifs in the central and eastern parts of the province (Fig. 6), as well as numerous, smaller satellite plutons. Known ages range between 1.16 and 1.01 Ga (Emslie & Hunt 1990; Doig 1990; Higgins & van Breemen 1992; van Breemen & Higgins 1993; Owens et al. 1994; Corrigan et al. 1994b). Individual massifs appear to have restricted ranges of age within this lengthy period. In the Frontenac terrane (Fig. 4), which is apparently devoid of the calc-alkaline magmatism of the Elzevir superterrane, A-type monzonite, syenite and granite plutons (Lumbers et al. 1990), dated between 1.18 and 1.16 Ga (van Breemen & Davidson 1988b; Marcantonio et

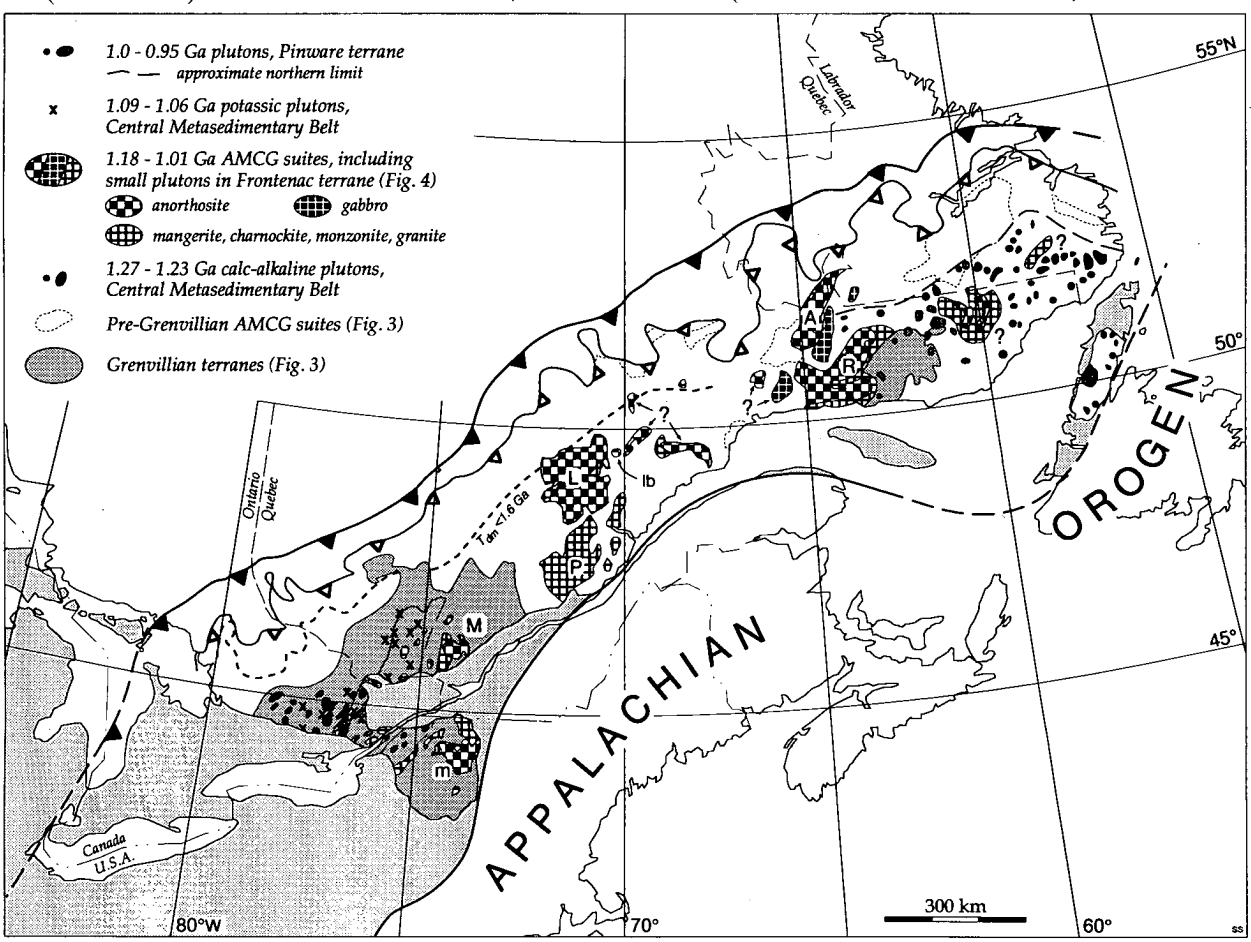

Figure 6. Known distribution of plutonic rocks of Grenvillian age (<1.3 Ga). Many small plutons in the central part of the province have not been dated and are not shown. Northwest limit of <1.6 Ga Nd model ages is based on the work of Dickin & McNutt (1990) and Dickin & Higgins (1992). Dated AMCG suites are M—Morin (1160–1135 Ma), m—Marcy (1160–1125 Ma), L—Lac St. Jean (1160–1140 Ma, 1075 Ma), P—Parc des Laurentides (~1080 Ma), lb—Labrieville (1020–1010 Ma), A—Atikonak (1135–1110 Ma), and R—Romaine River (1080 Ma), Magpie River (1125 Ma, 1060 Ma) and Lac Allard; ? indicates undated AMCG suites which may be older (see Figure 3). Small monzonitic plutons in Frontenac terrane are between 1180 and 1160 Ma. (See text for references to geochronology.)

al. 1990), are similar in age to AMCG suites in the Adirondack and Morin terranes, where older calc-alkaline rocks are again present. Monzonitic rocks of ~1.17 Ga age are also present in the Mont Laurier region of the Central Metasedimentary Belt in Quebec, but do not occur in the Elzevir superterrane in Ontario, with the possible exception of the Sharbot Lake terrane. However, small plutons of potassic syenite and granite with ages in the range 1.09–1.06 Ga (Corriveau et al. 1990) are present throughout the Central Metasedimentary Belt, though not in the central polycyclic belt to the northwest (Fig. 6).

Along the eastern side of the Wakeham terrane in the northeastern part of the province, the Davy Group is intruded by monzonite (1.08 Ga; Loveridge 1986) that is probably related to the neighbouring Havre St. Pierre AMCG complex, dated at ~1.06 Ga (van Breemen & Higgins 1993). An AMCG complex farther east in the Pinware terrane has not been dated. The Wakeham and Pinware terranes and the Long Range inlier in Newfoundland (Fig. 6) host numerous younger granite and syenite plutons dated between 1.01 and 0.95 Ga (Loveridge 1986; Gower et al. 1991; Owen & Erdmer 1990).

By way of contrast, igneous rocks of the time period 1.18–0.95 Ga are virtually absent from the central belt in Ontario and Quebec, the main exception being small amounts of coronitic olivine gabbro, which occurs almost invariably as small masses tectonically enclosed in ductile gneiss (Davidson 1991). Its crystallisation age is well established from primary baddeleyite at 1.17–1.15 Ga and it records metamorphism at 1.05 Ga (Davidson & van Breemen 1988; Heaman & LeCheminant 1993). Similar ages (~1.16 Ga) have been determined for zircon in meta-anorthosite and dykes of amphibolite in the footwall of the Parry Sound allochthon (Wodicka et al. 1994), ages that coincide closely with granulite-facies metamorphism in the allochthon and with syn-deformational pegmatite in the bounding shear zone (van Breemen et al. 1986). An earlier, isolated, deformed granite orthogneiss pluton dated at 1.24 Ga (Lumbers et al. 1991) occurs some 25 km south of the Grenville Front in Ontario, a region where otherwise the youngest plutonic rocks belong to the ~1.45 Ga suite. The only other dated igneous activity of comparable age in this area is that of intrusion of the 1235 Ma continental Sudbury diabase dyke swarm of the Southern and Superior provinces, deformed and metamorphosed in the parautochthonous belt (Dudàs et al. 1994).

With respect to the overall architecture of the Grenville Province, it is important to note that the limited number of Nd–Sm isotope studies made to date indicate relatively juvenile depleted mantle model ages for the calc-alkaline suite in the Adirondack Highlands (Daly & McLelland 1991), the AMCG suites (Ashwal & Wooden 1983; Emslie & Hegner 1993), and A-type and potassic suites in the Frontenac terrane (Marcantonio et al. 1990). T_{dm}s range between 1.55 and 1.20 Ga, in keeping with the fact that almost all of these igneous rocks lie southeast of the T_{dm} <1.6 Ga line shown in Figure 6. The only exception known so far is the Atikonak massif (T_{dm} >1.75 Ga; Emslie & Hegner 1993), which is the most northerly massif and known to lie within Labradorian crust.

In summary, calc-alkaline plutonic and associated volcanic rocks are spatially restricted to the central and southwest parts of the province, whereas AMCG and A-type plutons occur in the central and northeast parts, the two overlapping only in the central region. In terms of time, geochronology has shown that there is an apparent break of ~50 m.y. between the cessation of calc-alkaline igneous activity at ~1.23 Ga and the inception of AMCG and A-type plutonism at ~1.18 Ga. Earlier stages of the former overlapped AMCG and A-type plutonism in the range 1.47–1.34 Ga in other parts of the province, particularly if the St. Maurice arc is considered to have been the first manifestation of closure of a Grenvillian ocean. Grenvillian AMCG and A-type plutonism continued for ~230 m.y., a period equivalent in more familiar terms to the Mesozoic and Cainozoic eras combined; the span of time in any one area, however, may have been shorter, i.e. 1.18–1.06 Ga in the Frontenac and Mont Laurier regions of the Central Metasedimentary Belt, 1.13–1.0 Ga in eastern Quebec, extending to 0.95 Ga farther east. Although suggestive, the geochronological database is as yet insufficient to confirm whether there was a progressive younging eastward, or whether this igneous activity was episodic or relatively continuous.

It has been argued that the Grenvillian AMCG suites represent 'anorogenic' magmatism (McLelland 1986, 1989; Emslie & Hunt 1990). In terms of the Grenville Province as a whole, however, it is clear that metamorphism and contractional deformation occurred in some parts of the province at the same time as AMCG pluton emplacement in others, that the AMCG suites are themselves variously deformed and metamorphosed, and that contractional deformation (ductile thrusting) on major shear zones and along the Grenville Front continued within the period 1.05–1.0 Ga, after all but the youngest A-type plutons had been emplaced. The role of plutonic types in the overall development of the Grenville orogen will be addressed after the following summaries of metamorphism, deformation and post-Grenvillian events.

Metamorphism

Grenvillian metamorphism has affected all parts of the province, but is not everywhere easy to distinguish from the effects of earlier metamorphisms. It is clear from geochronologic studies that older crystalline rocks were not necessarily overprinted to the extent that their earlier metamorphic history is obliterated. This is particularly true where Archaean rocks extend southeast of the Grenville Front (e.g. Indares & Martignole 1989, 1990b; Gariépy et al. 1990), and also in large parts of Labrador, where granulites are now known to have formed at ~1.65 Ga (e.g. Connelly & Heaman 1993). Moreover, surprises occur, such as the recent identification of 1.45 Ga metamorphism in the gneiss terranes of Ontario (Ketchum et al. 1994; Dudàs et al. 1994). It is for this reason, as well as the pre-Grenvillian ages of certain plutonic rocks, that much of the Grenville Province is termed polycyclic. In most of the regions where pre-Grenvillian metamorphism is recognised, however, Grenvillian metamorphism accompanying ductile deformation is pervasive.

An abrupt increase in grade is evident at the Grenville Front. This is due in part to uplift of lower levels of foreland rocks with pre-Grenvillian metamorphic assemblages within the adjacent parautochthon; for example, granulite-facies gneisses in the frontal hanging wall lie within 8 km of Huronian sedimentary rocks at greenschist grade in the neighbouring Southern Province, Ontario (Bethune & Davidson 1988). In places where previously low-grade or unmetamorphosed foreland rocks can be traced across the front, such as the Kaniapiskau Supergroup in western Labrador (Gagnon terrane in Fig. 3), upper amphibolite facies Grenvillian metamorphism is attained in the parautochthon within 30 km of the front (e.g. Rivers 1983; Rivers et al. 1993).

Metamorphic grade in the northwestern and central belts, manifested in gneiss and migmatite of both supracrustal and plutonic origin, is generally in upper amphibolite to granulite facies. Maximum palaeopressure estimates are relatively high, e.g. ~11 kbar in the Parry Sound region of Ontario (Anovitz & Essene 1990), ~8.5 kbar in the Adirondack Highlands of New York (Bohlen et al. 1985), ~10 kbar in western Quebec (Indares & Martignole 1990a) and in central Labrador (Arima et al. 1986). Evidence for eclogite-facies mineral assemblages, preserved in metamorphosed mafic igneous rocks akin to those in the Caledonian Western Gneiss Region of Norway (e.g. Griffin 1987), have been reported in Ontario (Grant 1989; Davidson 1990) and in the Molson Lake terrane in Labrador

(Indares 1993). These occurrences, for which pressure estimates are 14–16 kbar at ~750°C, are located in the lower parts of crust-scale thrust slices. This suggests that rocks buried tectonically to deep crustal level have been thrust, during a later stage of Grenvillian orogeny, to a level high enough for them to be exposed by subsequent erosional unroofing of the orogen, perhaps preceded by uplift associated with late Grenvillian extension. The same is likely true for some of the granulite terranes, particularly where they are thrust over amphibolite-facies rocks along low-angle ductile shear zones (e.g. Parry Sound domain and the Labradorian allochthons), coincident with inverted metamorphic gradients and changes in palaeopressure estimates (e.g. Tucillo et al. 1992).

The grade of Grenvillian metamorphism exposed in supracrustal rocks younger than ~1.3 Ga is varied. In Ontario, it is as low as upper greenschist facies in the central part of the Central Metasedimentary Belt (e.g. Carmichael et al. 1978; Davidson 1986). In the same area, relatively low-pressure granulite-facies rocks (7–5 kbar; Schau et al. 1986; Anovitz & Essene 1990) of the Frontenac terrane abut lower amphibolite-facies rocks of the Sharbot Lake terrane along a shear zone (Fig. 4), again indicating tectonic juxtaposition. In eastern Quebec, supracrustal rocks of the Wakeham Supergroup at greenschist grade lie structurally above migmatitic rocks, suggesting either an extensional tectonic or an unconformable relationship with older metamorphic rocks.

Grenvillian plutonic rocks are also metamorphosed, with the exception of the youngest ones. For example, although undoubted igneous charnockite is present in some AMCG complexes, many of the granitoid members of this suite are represented by well-foliated charnockitic orthogneiss carrying metamorphic orthopyroxene and garnet. Anorthosite and gabbro, although inherently resistant to deformation and recrystallisation, are in places reduced to gneiss containing upper amphibolite- to granulite-facies mineral assemblages. These rocks where undeformed, particularly troctolitic members, commonly exhibit coronas of metamorphic origin (cf. Davidson & van Breemen 1988).

Except for the rapid increase in metamorphic grade across the Grenville Front, there is no throughgoing zonal arrangement of metamorphic facies parallel to the orogen. Some grade changes within the interior reflect variations in tectonic level brought about by different amounts of uplift experienced by adjacent crustal segments. Others may be due to incomplete retrogression of granulite to amphibolite facies accompanying late-stage ductile Grenvillian deformation, explaining, for example, the occurrence of small areas of granulite-facies rocks in the central belt in Ontario and western Quebec, which is dominated by amphibolite-facies migmatitic gneiss (Davidson et al. 1990). Throughout most of the province, high-grade metamorphism occurred between ~1.06 and 1.02 Ga, followed by cooling to the argon closure temperature of hornblende by ~0.97 Ga (Fig. 5). Certain terranes, for example the Parry Sound, Frontenac and New York Lowlands terranes, experienced cooling at least 100 m.y. earlier (Cosca et al. 1991; Mezger et al. 1993). The significance of different T-time paths for adjacent crustal blocks in the southwest part of the province is discussed by van der Pluijm et al. (1994).

Structural overview

As stated at the beginning of this review, the Grenville Front is a geophysically well-defined tectonic lineament represented at the surface by moderately to steeply south to southeast-dipping, thrust-sense faults and mylonite zones. This structural orientation is shared by much of the layering and foliation in the gneiss and granulite terranes of the northwest and central belts and by the bounding thrust zones between the two belts, although it is generally more shallowly inclined. Dip-parallel mineral stretching lineation is common. Northwest trends occur in eastern Labrador (Hawke River and southeastern Lake Melville terranes; Fig. 3) and in parts of western Quebec and Ontario, but in the latter are due to open folding about gently southeast-plunging axes of formerly southeasterly-inclined gneisses (e.g. Schwerdtner & van Berkel 1991). Domains with irregular structure, or with trends at a high angle to the prevalent northeast trend, are commonly found to be structurally discontinuous with surrounding domains, from which they are usually separated by narrow belts of well-layered gneiss. Formerly interpreted as paragneiss, these rocks are now recognised as ductile tectonites, equally likely to have developed from originally massive plutonic rocks by extreme attenuation as from layered supracrustal rocks (Davidson 1984a; Hanmer 1988). These ductile shear zones provide the basis for subdivision of the two belts into the lithotectonic domains or terranes outlined in preceding sections (see articles in Moore et al. 1986; Rivers et al. 1989). In some of these zones, features suggestive of severe flattening in S- and SL-tectonites point to a large component of pure shear. However, consistently oriented kinematic indicators in several shear zones imply a northwesterly directed sense of thrust displacement, although shear sense in others of similar orientation is extensional, with low-angle displacement toward the southeast (e.g. Culshaw et al. 1994).

Timing of displacement has been estimated for some of these shear zones by dating syntectonic pegmatites (Fig. 5). In the interior of the central belt in Ontario, thrust displacement took place along the western margin of the Parry Sound domain (Fig. 4) at around 1.16 Ga (van Breemen et al. 1986; Wodicka et al. 1994). Similar displacements occurred at ~1.10 Ga along the margins of the Seguin and Moon River thrust sheets (van Breemen & Davidson 1990) and at ~1.06 Ga farther east, suggesting large-scale (in terms of both time and space) out-of-sequence thrusting (break-back stacking of Nadeau & Hanmer 1992). Farther northwest, later extensional displacement occurred at ~1.03 Ga along the northwest boundary of the Shawanaga terrane (Fig. 4; Culshaw et al. 1994); this predates the last stages of thrusting along the Grenville Front to the northwest, estimated to have occurred at ~0.98 Ga (Haggart et al. 1993), only slightly older than cooling through the Ar closure temperature of amphibole farther southeast (~0.97 Ga; Culshaw et al. 1991; see Fig. 5). The timing of deformation in this part of the province is summarised by Jamieson et al. (1992). Timing is not so well constrained in other parts of the province. As stated earlier, the earliest amalgamation of terranes in the northeast part of the province may have been Labradorian (~1.6 Ga), but northward deep-crustal thrusting along both the Grenville Front, the boundary between the Gagnon and Molson Lake terranes, and the allochthon boundary thrust appears to have occurred late during the Grenvillian orogenic cycle (~0.99 Ga; Connelly & Heaman 1993; Connelly et al. 1993). In the central part of the province, the St. Maurice arc shows evidence of westerly directed thrust imbrication as early as 1.15 Ga, followed some 50 m.y. later by oblique sinistral shear (Corrigan et al. 1994b).

Turning to the Grenvillian supracrustal terranes of the southeastern belt, the northwest margin of the Central Metasedimentary Belt in Ontario (Fig. 4) is a broad ductile thrust stack inclined shallowly to the southeast (Hanmer & McEachern 1992), but in Quebec, except for the Cabonga allochthon, it is a zone of an oblique displacement (Hanmer & Ciesielski 1984). Terrane boundaries within the Central Metasedimentary Belt are also marked by high-strain zones (e.g. the thrust-sense Maberly shear zone and the extensional Robertson Lake mylonite zone; Fig. 4). Fold patterns within the various terranes differ from one another (e.g. interference folds vs linear fold belts), suggesting different histories. The southeastern boundary in New York State (Carthage–Colton mylonite zone) dips northwest and has top-side-down sense of shear to the northwest, whereas the equivalent boundary in Quebec (Labelle shear

zone) is the locus of sinistral displacement. The other Grenvillian supracrustal terrane, the Wakeham terrane, is bounded on its northwest side by southeast-dipping extensional faults (Martignole et al. 1994), but to the southeast merges with high-grade gneisses.

Northwestward thrust displacement along the Central Metasedimentary Belt boundary zone (Fig. 4) began as early as ~1.19 Ga and was succeeded by a second period of thrusting between 1.08 and 1.06 Ga (McEachern & van Breemen 1993). High-grade ductile thrusting along the Maberly shear zone has not been dated directly, but post-dated emplacement of plutonic rocks of the ~1.17 Ga suite in overriding the Frontenac terrane. Southeastward extensional displacement along narrow zones of low-temperature mylonite developed in marble in the southeast of the Bancroft terrane has been dated at ~1.0 Ga, based on comparison with cooling curves in adjacent rocks (van der Pluijm & Carlson 1989). Similar displacement on the Robertson Lake mylonite zone, also occurring at relatively low temperature, may have been of comparable age; it appears to offset rocks with middle amphibolite assemblages dated at ~1.03 Ga (Corfu & Easton 1994).

Seismic reflection profiling of Grenvillian crystalline terranes has given another dimension to regional structural analysis. Several surveys have shown a wealth of moderately to shallowly inclined reflectors, in essence confirming cross-sections constructed from ground-based observations (e.g. Davidson 1984a; Rivers et al. 1989). Notable among these is a shipboard transect across the Grenville Front in Lake Huron (Green et al. 1988). This transect showed that the front and parallel structures above it penetrate the entire crust, shallowing slightly with depth and coinciding with minor depression of the crust–mantle boundary ('reflection Moho') at ~40 km depth. Transects on land within the orogen in Ontario have been equally fruitful in delineating crustal-scale thrust structure (White et al. 1994; Forsyth et al. 1994a 1994b), an example of which is shown in Figure 7. The most recent transects in western and eastern Quebec and across the Grenville Front along the Atlantic coast of Labrador await final processing.

In summary, the Grenville orogen in its type area, the southeastern Canadian Shield, can be envisaged as an imbricate stack of crustal-scale lenses inclined toward the south and southeast and riding on a basal, crust-penetrating thrust expressed at the surface by the Grenville Front. The stack was compiled largely by thrusting at deep to mid-crustal level with displacements of unknown, but perhaps large, magnitude during continued compression directed toward the Laurentian craton in the period 1.2–1.0 Ga, following closure of a postulated Grenvillian ocean. It was modified by extensional shearing and faulting late in its orogenic history (Ga), coincident with the youngest stage of thrust-associated uplift along the Grenville Front.

Post-Grenvillian events

Most parts of the Grenville Province record uplift and cooling between 1.0 and 0.9 Ga, the time of final assembly of an early Neoproterozoic supercontinent (Hoffman 1991; Windley 1993). Evidence for its subsequent break-up, leading to opening of the Iapetus Ocean and removal of the 'other side' of the Grenville orogen, is given by both sedimentary and igneous rocks associated with rift formation within and marginal to the province (Fig. 8). In Labrador, branching rifts are filled with terrestrial sediments of local derivation (Double Mer Formation), considered to be Eocambrian in age on the basis of palaeomagnetic comparison to 615 Ma diabase dykes of the Long Range swarm (Kamo et al. 1989; Murthy et al. 1992). Thin, undisturbed, sub-Cambrian terrestrial sediments associated with minor basalt occur on the eroded orogen opposite northern Newfoundland (Gower et al. 1994), and the Long Range inlier of Newfoundland is replete with northeast-trending diabase dykes. A number of late Neoproterozoic plutons lie along the St. Lawrence, notable among which is the large Sept Iles gabbro–anorthosite intrusion; this intrusion is at least 60 km in diameter, judging by the extent of its aeromagnetic and gravity anomaly beneath the St. Lawrence estuary, and has been dated, using Rb–Sr, at ~540 Ma (Higgins & Doig 1981) and by U–Pb zircon at 565 Ma (O. van Breemen,

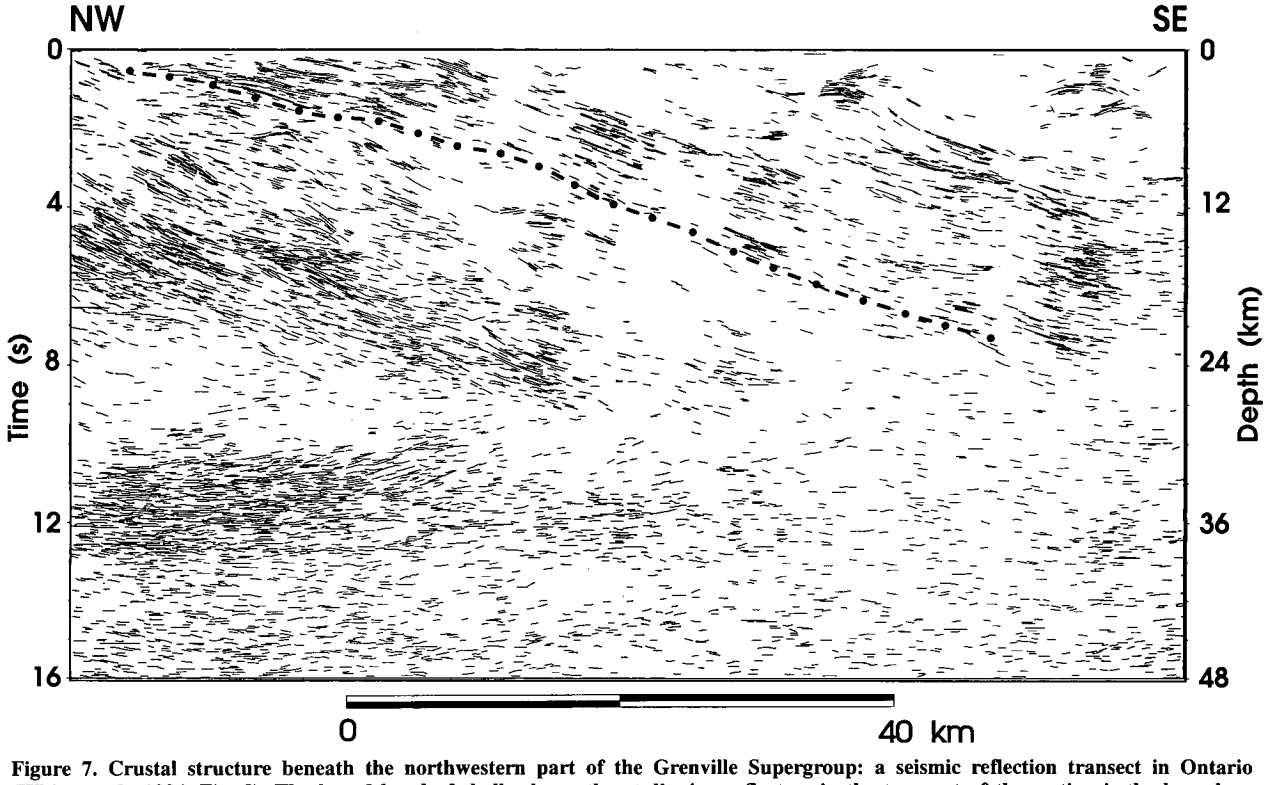

Figure 7. Crustal structure beneath the northwestern part of the Grenville Supergroup: a seismic reflection transect in Ontario (White et al., 1994, Fig. 8). The broad band of shallowly southeast-dipping reflectors in the top part of the section is the boundary thrust zone of the Central Metasedimentary Belt (see Figure 4); the reflection Moho is at ~40 km.

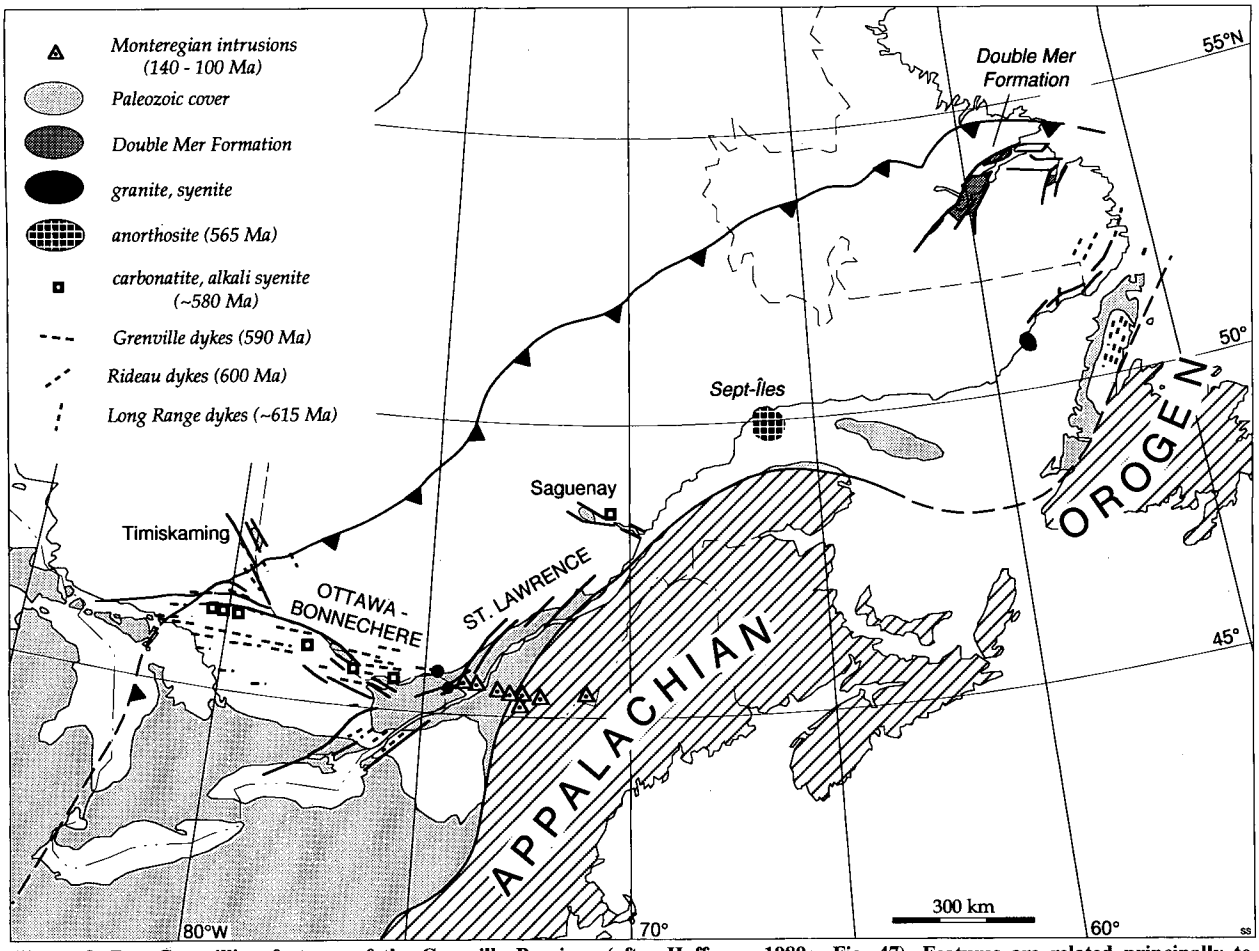

Figure 8. Post-Grenvillian features of the Grenville Province (after Hoffman, 1989a, Fig. 47). Features are related principally to continental break-up at ~600 Ma (except Monteregian intrusions). Main rift faults are shown as solid lines, diabase dykes swarms are represented by short dashes.

pers. comm. 1994). Rift faults along the St. Lawrence pass southwestward through the southern part of the Frontenac and New York Lowlands terranes, where northeast-trending diabase dykes (Rideau swarm; Fahrig & West 1986) and small occurrences of tilted conglomerate and sandstone are also present. Branches of the St. Lawrence rift system (Saguenay, Ottawa-Bonnechere, and Timiskaming graben) are associated with local alkaline igneous activity, including minor potassic volcanism and carbonatite intrusion, all Eocambrian in age. Tholeiitic diabase dykes of the Grenville swarm (Fahrig & West 1986), dated at 590 Ma (Kumarapeli et al. 1990) parallel the Ottawa–Bonnechere graben, extending over 500 km from near Montreal to beyond the Grenville Front in the Sudbury area.

As well as lack of evidence for rifting before about 600 Ma, there is also little evidence of appreciable topography at the time of early Palaeozoic sedimentation. Coarse detritus is not present in the basal part the Late Cambrian to Early Ordovician succession, which is represented by mature littoral sandstone succeeded by shallow marine carbonates. Reactivated faults of the rift system offset the Precambrian–Palaeozoic unconformity. Their renewed movement is likely related to Monteregian igneous activity (Cretaceous; Eby 1984), itself possibly linked to passage across a hot-spot (Sleep 1990).

Concluding remarks

The early manifestations of Grenvillian orogeny (*sensu lato*) are recorded by the closure of what has been referred to as the Grenvillian ocean (Windley 1989, 1993), which may have been a wedge-shaped aulacogen closing to the north (but see Gower & Tucker 1994). This activity is recorded by the calc-alkaline volcanic and plutonic rocks (perhaps in a number of westward-younging arcs?), terminating with volcanism in the Elzevir superterrane at ~1.25 Ga and plutonism extending to ~1.23 Ga, considered to have been associated with south-east-directed subduction (Windley 1986). Thrust-sense ductile deformation at least as early as 1.19 Ga along the northwest boundary of the Central Metasedimentary Belt may record final closure and obduction of the arc rocks over older Mesoproterozoic crust (central belt) and perhaps its sedimentary cover (Bancroft terrane; Fig. 4). Continued northwest-directed compression may be represented by thrust-uplift at ≤1.16 Ga of the adjacent Frontenac block, which may have 'docked' during closure at ~1.2 Ga and thus be a terrane in the plate tectonic sense. Uplift and cooling of the Frontenac terrane began at this time (Mezger et al. 1993; Cosca et al. 1992), and detritus was shed northwestward onto exhumed arc rocks of the Elzevir superterrane (Flinton Group; Moore & Thompson 1980; Sager-Kinsman & Parrish 1993). The different terranes of the Central Metasedimentary Belt are apparently 'stitched' by small plutons of potassic syenite and granite (1.09–1.06 Ga; Fig. 5). Distribution of the youngest metamorphic event (≤1.03 Ga) recorded in parts of the Elzevir superterrane has been disrupted by extensional faulting.

Grenvillian AMCG and A-type plutonism, beginning at ~1.18 Ga, is all but restricted to the region east and northeast of the closed ocean basin (Figs 5 and 6). The lengthy period of perhaps episodic pluton emplacement (to 1.06 Ga in the Central Metasedimentary Belt, ~1.0 Ga in central Quebec, and 0.95 Ga farther northeast) overlapped continued ductile thrusting at least in the southwest part of the central belt

(1.16 to 1.05 Ga), and perhaps elsewhere in this belt (at present unconstrained by dating). Grenvillian metamorphism is dated in many places between 1.08 and 1.03 Ga, with some notable exceptions (earlier in the Parry Sound and Frontenac terranes, barely recorded in some of the Labradorian thrust sheets in the northeast part of the province).

Concerning application of the term 'anorogenic' to AMCG and A-type suites in general, a clear example of anorogenic setting is given by the well-known 1.45–1.3 Ga AMCG suites in Labrador north of the Grenville Front—they are neither deformed nor metamorphosed, and do not appear to be related to regional orogeny of any kind. In terms of petrochemistry, it is perhaps a logical extension to consider that virtually identical suites within the Grenville represent anorogenic magmatism (cf. McLelland 1989; Emslie & Hunt 1990). This may be true for such rocks of pre-Grenvillian age now incorporated into the Grenville orogen (cf. Windley 1989, 1993), which may thus be termed 'pre-orogenic' with respect to the Grenvillian orogenic cycle. In comparison, those younger than 1.18 Ga might be considered 'post-orogenic' with respect to closure of the Grenvillian ocean, represented by Elzevirian orogeny (≥1.23 Ga) in the southwest part of the province. Plutonism of this type closely following orogeny would correspond to 'anorogenic plutonism' following continental assembly of Windley (1993). However, in view of the evidence in the Grenville for continued compressive tectonics and high-grade metamorphism grossly coeval with AMCG and A-type plutonism, it must be asked whether these suites are really anorogenic (e.g. Corrigan et al. 1994b). Perhaps plutonic suites of 'anorogenic character' can be generated within the broad confines of a still-active orogen, following earlier tectonic crustal thickening and development of a thermal anomaly in the underlying asthenosphere. Resulting from this, addition to the middle and upper crust of magma derived through fractionation of mantle melts (gabbro, anorthosite) and melting in the lower crust (granitoid phases) (McLelland 1989; Emslie & Hunt 1990; Windley 1993; also see Hoffman 1989b) would follow the same course as for a strictly anorogenic environment (static thermal anomaly, mantle plume). If, however, compressional or transpressional orogenic forces, resulting from continued impingement of a continental block to the southeast, were still active during episodic plutonism or resumed shortly afterwards, thermal relaxation in the mid-crust, enhanced by heat from ascending plutons, would lead to metamorphism and softening with ductile deformation. The fact that many of the Grenvillian AMCG and A-type plutonic rocks are themselves deformed and metamorphosed (e.g. Martignole & Schrijver 1970), in contrast to the AMCG suites north of the front, may be the consequence of such a process. That parts or all of some Grenvillian complexes are not deformed may be explained by their inherent tectonic hardness, their age relative to deformation, or their localisation within slices bounded by ductile shear zones. In this regard, it is interesting that the 'anorogenic' setting widely accorded to Mesoproterozoic igneous rocks in the United States midcontinent is the subject of current dispute (cf. Nyman et al. 1994).

Many major questions about development of the Grenville Province remain unanswered. For example, if the province formed ultimately by continent–continent collision, and the calc-alkaline suites and Grenville Supergroup are all that remains of the intervening ocean, where is the suture between the two continental blocks? It cannot coincide with the T_{dm} <1.6-Ga line shown in Figure 6, as this lies on the wrong side of the closed ocean basin. If the pre-Grenvillian crust containing the Grenvillian AMCG suites in the southeastern belt is all composed of reworked, but relatively young, Laurentian crust, as suggested by the model ages of these suites, then the whole of the Central Metasedimentary Belt may represent an enormous nappe structure rooted formerly southeast of the Adirondack Highlands (Davidson 1986; Hoffman 1992). Allowing this, a suture may lie in the northwestern Central Metasedimentary Belt, perhaps along the juncture between the Bancroft and Elzevir terranes (see Hanmer & McEachern 1992). The early interplay of these different crustal segments, particularly with respect to timing of displacement involving the terranes of the Central Metasedimentary Belt, remains to be worked out.

Two other aspects of Grenville geology deserve comment. One concerns the relationship between the mid-continental rift system (Fig. 2) and Grenvillian orogeny. The rift fill is exposed only in the Lake Superior region, the remainder being identified primarily on the basis of its gravity anomaly. It contains a thick fill of mainly basaltic flows, associated with mafic intrusions, that erupted during a 15 m.y. interval at ~1.10 Ga. Although occurring during the prolonged period of Grenvillian AMCG magmatism, the two do not coincide precisely; most AMCG ages are either older or younger than 1.10 Ga (see Fig. 5 and caption for Fig. 6). It does, however, coincide with a stage of thrusting within the central belt in Ontario (Moon River and Seguin terranes over the Parry Sound terrane; Fig. 4). Formation of the midcontinental rift (Gordon & Hempton 1986) and its partial closure (Cannon 1994) have been related to Grenvillian compression. Later displacement along the Grenville Front has apparently caused the southeast extension of the rift to be overridden, as its gravity anomaly dies out at the front. The volcanic fill has a thick detrital sediment cover, but it is curious that this sediment shows no evidence of a Grenvillian component.

This raises the second aspect, namely the lack of foreland basins adjacent to the front, and molasse-type deposits derived from what intuitively must have been a source of sediment, judging by the amount of uplift required by the steep metamorphic gradient parallel to the front. Related to this is the highly restricted development of fold-thrust deformation style in the frontal region. Steep, closely-spaced thrusts involving older foreland rocks are evident in some places, but only in Labrador is this style developed to any great extent, involving the Palaeoproterozoic Kaniapiskau Supergroup and, farther east, the Seal Lake Group. This scenario is attributed by Hoffman & Grotzinger (1993, following Beaumont et al. 1991) to the spatial relationship and orientation of the Grenville Province, during uplift and unroofing, to palaeolatitude and its control on prevailing wind direction, rainfall and erosion. The presence of a Grenvillian foreland thrust belt, however, has been interpreted from seismic data in the eastern U.S. midcontinent (Hauser 1993).

The prevalence of pre-Grenvillian anorogenic magmatism in two pulses (~1.7–1.6 Ga and 1.5–1.35 Ga), well documented in the Grenville Province and corresponding to igneous events beyond the front in the North American mid-continent and in Scandinavia, has been related to the final stages of assembly and subsequent break-up, respectively, of a supercontinent assembled at ~1.5 Ga (Windley 1993). Supercontinent break-up led to opening of the Grenvillian ocean. Subsequent to this, the Grenvillian orogenic cycle represents early closure of this ocean, continent–continent collision, and attendant crustal thickening during supercontinent reassembly. The latter was accompanied and followed by a long period of magmatism of 'anorogenic type' during gradual thermal relaxation, coeval on a gross scale with primarily northwestward translation and later gravitational collapse of thermally softened crust. Final cooling, bulk uplift and erosion occurred between 1.0 and 0.9 Ga. The Grenville Province remained quiescent until ~600 Ma, when break-up leading to opening of the Iapetus Ocean began. At this time it is likely that the 'other half' of the Grenville orogen, comprising the enigmatic southeastern continental mass, rifted away.

The Musgrave Block—a brief comparison

The main similarities between the Grenville Province and the Musgrave Block lie in the nature and association of magmatism and metamorphism during the Grenvillian time span, imposed on pre-Grenvillian, Proterozoic crystalline crust (felsic and mafic gneisses). In this respect the Musgrave is comparable to the central belt of the Grenville Province. Introduction of mantle-derived gabbro and anorthosite (Giles Complex) into the mid-crust took place at about 1.08 Ga, and appears to have been of fairly short duration. Metamorphism was of relatively low-pressure type (Clarke et al. 1992). The possibility exists that the mafic–ultramafic plutonic activity was contemporaneous with mafic and A-type volcanic rocks at ~1.08 Ga (Tollu volcanics; Sun & Sheraton 1992; Sun et al. in press). This requires earlier Grenvillian plutonic and metamorphic rocks to have been unroofed by this time, at least in the western part of the Musgrave Block. Although granitoid rocks of similar age are present in the southeastern part of the Grenville Province, there is no evidence for coeval volcanism or sedimentation, this being a time of ductile deformation and high-grade metamorphism throughout much of the province. Also, unlike in the Musgrave Block, there is no equivalent to the latest Proterozoic to early Cambrian deformation and high-pressure metamorphism represented by the north-directed Woodroffe Thrust system (Clarke et al. 1993). Grenvillian basement is exposed in thrust slices within the neighbouring Appalachian orogen; the frontal thrusts of this orogen are directed toward the Grenville Province, and lie at high crustal level within Lower Palaeozoic cratonic cover.

If the continental reconstruction shown in Figure 1 is correct, the known belts of Grenvillian age in Australia are considerably narrower than in North America. The equivalent of the Grenville Front, identified in Antarctica by Storey et al. (1994), should lie on the southeast side of the Albany–Fraser belt and south of the Musgrave Block, passing north of the Gawler Craton.

Acknowledgements

I thank John Sheraton, Geoffrey Clarke, John Percival and Steve Lucas for their helpful and constructive reviews, and am grateful for many discussions with 'friends of the Grenville', too numerous to name. Don White is acknowledged for permission to reproduce the seismic reflection profile in Figure 7. Susan Schaan helped prepare the diagrams. This paper is Geological Survey of Canada contribution no. 51294.

References

Anovitz, L.M. & Essene, E.J., 1990. Thermobarometry and pressure–temperature paths in the Grenville Province of Ontario. Journal of Petrology, 31, 197–241.

Appleyard, E.C., 1974. Syn-orogenic igneous alkaline rocks of eastern Ontario and northern Norway. Lithos, 7, 147–169.

Arima, M., Kerrich, R. & Thomas, A., 1986. Geobarometry, geothermometry, $^{18}O/^{16}O$ and related geochemistry of Grenville Province sapphirine bearing granulites from central Labrador. Geological Association of Canada, Program with Abstracts, 11, A42.

Ashwal, L.D. & Wooden, J.L., 1983. Sr and Nd isotope geochronology, geologic history, and origin of the Adirondack anorthosite. Geochimica et Cosmochimica Acta, 47, 1875–1885.

Beaumont, C., Fullsack, P. & Hamilton, J., 1991. Erosional control of active compressional orogens. In: McClay, K.R., (editor), Thrust tectonics. Chapman & Hall, New York, 1–18.

Bethune, K.M. & Davidson, A., 1988. Diabase dykes and the Grenville Front southwest of Sudbury, Ontario. In: Current research, Part A. Geological Survey of Canada, Paper 88-1C, 151–159.

Bickford, M.E., Van Schmus, W.R. & Zeitz, I., 1986. Proterozoic history of the midcontinent region of North America. Geology, 14, 492–496.

Bohlen, S.R., Valley, J.W. & Essene, E.J., 1985. Metamorphism in the Adirondacks. I. Petrology, pressure and temperature. Journal of Petrology, 26, 971–992.

Borg, S.G. & DePaolo, D.J., 1994. Laurentia, Australia, and Antarctica as a Late Proterozoic supercontinent: constraints from isotopic mapping. Geology, 22, 307–310.

Bourne, J.H., 1986. Geochemistry of the felsic metavolcanic rocks of the Wakeham Group: a metamorphosed peralkaline suite from the eastern Grenville Province, Quebec, Canada. Canadian Journal of Earth Sciences, 23, 978–984.

Bourne, J., 1991. The geochemistry of the La Galissonière pluton: a Middle Proterozoic late-orogenic intrusion from the eastern Grenville Province, Quebec. Canadian Journal of Earth Sciences, 28, 37–43.

Brock, B.S. & Moore, J.M., Jr., 1983. Chronology, chemistry, and tectonics of igneous rocks in terranes of the Grenville Province. Geological Society of America, Abstracts with Programs, 15, 533.

Brown, D., Rivers, T. & Calon, T., 1992. A structural analysis of a metamorphic fold-thrust belt, northeast Gagnon terrane, Grenville Province. Canadian Journal of Earth Sciences, 29, 1915–1927.

Cannon, W.F., 1994. Closing of the Midcontinent rift—a far-field effect of Grenvillian compression. Geology, 22, 155–158.

Card, K.D., 1990. A review of the Superior Province of the Canadian Shield, a product of Archean accretion. Precambrian Research, 48, 99–156,

Carlson, K.A., van der Pluijm, B.A. & Hanmer, S., 1990. Marble mylonites near Bancroft, Ontario: evidence for crustal extension in the Canadian Grenville. Geological Society of America, Bulletin, 102, 174–181.

Carmichael, D.M., Moore, J.M., Jr. & Skippen, G.B., 1978. Isograds around the Hastings metamorphic 'low'. In: Currie, A.L. & Mackasey, W.O. (editors), Toronto '78. Geological Association of Canada, Field Trips Guidebook, 325–346.

Chiarenzelli, J.R. & McLelland, J.M., 1993. Granulite facies metamorphism, palæo-isotherms and disturbance of the U-Pb systematics of zircon in anorogenic plutonic rocks from the Adirondack Highlands. Journal of Metamorphic Geology, 11, 59–70.

Clarke, G., Stewart, A. & Glikson, A, 1993. High-pressure granulite to eclogite-facies metamorphism in the western Musgrave Block, central Australia. Australian Geological Survey Organisation, Research Newsletter, 18, 6–7.

Condie, K.C. & Moore, J.M., 1977. Geochemistry of Proterozoic volcanic rocks from the Grenville Province, eastern Ontario. In: Baragar, W.R.A., Coleman, L.C. & Hall, J.M. (editors), Volcanic regimes in Canada. Geological Association of Canada, Special Paper 16, 149–168.

Coney, P.J., Jones, D.L. & Monger, J.W.H., 1980. Cordilleran suspect terranes. Nature, 288, 329–333.

Connelly, J.N. & Heaman, L.M., 1993. U–Pb geochronological constraints on the tectonic evolution of the Grenville Province, western Labrador. Precambrian Research, 63, 123–142.

Connelly, J.N., van Gool, J. & Rivers, T., 1989. Molson Lake terrane, a new terrane in the parautochthonous belt of the Grenville Province in southwestern Labrador. Geological Association of Canada, Program with Abstracts, 14, A23.

Connelly, J.N., van Gool, J., Rivers, T. & James, D.T., 1993. Field guide to the geology of the Grenville Province of western Labrador. Friends of the Grenville, 96 p.

Corfu, F. & Easton, R.M., 1994. U–Pb geochronology of the Mazinaw terrane, Central Metasedimentary Belt, Grenville Province, Ontario. Geological Association of Canada, Program with Abstracts, 19, A22.

Corrigan, D., Culshaw, N.G. & Mortensen, J.K., 1994a. Pre-Grenvillian evolution and Grenvillian overprinting of the parautochthonous belt in Key Harbour, Ontario: U–Pb and field constraints. Canadian Journal of Earth Sciences, 31, 583–596.

Corrigan, D., Hanmer, S., van Breemen, O. & Nadeau, L., 1994b. The St-Maurice region, Quebec: a new perspective on the tectonic evolution of the southwest Grenville orogen. Geological Association of Canada, Program with Abstracts, 19, A23.

Corriveau, L., Heaman, L.M., Marcantonio, F. & van Breemen, O., 1990. 1.1 Ga K-rich alkaline plutonism in the SW Grenville Province. Contributions to Mineralogy and Petrology, 105, 473–485.

Cosca, M.A., Sutter, J.F. & Essene, E.J., 1991. Cooling and inferred uplift/erosion history of the Grenville orogen, Ontario: constraints from $^{40}Ar/^{39}Ar$ thermochronology. Tectonics, 10, 959–977.

Cosca, M.A., Essene, E.J., Kunk, M.J. & Sutter, J.F., 1992. Differential unroofing within the Central Metasedimentary Belt of the Grenville Orogen: constraints from $^{40}Ar/^{39}Ar$ thermochronology. Contributions to Mineralogy and Petrology, 110, 211–225.

Culshaw, N., Reynolds, P.H. & Check, G., 1991. A $^{40}Ar/^{39}Ar$ study of post-tectonic cooling in the Britt domain of the Grenville Province, Ontario. Earth and Planetary Science Letters, 105, 405–415.

Culshaw, N.G., Ketchum, J.W.F., Wodicka, N. & Wallace, P., 1994. Deep crustal ductile extension following thrusting in the southwestern Grenville Province, Ontario. Canadian Journal of Earth Sciences, 31, 160-175.

Daly, J.S. & McLelland, J.M., 1991. Juvenile Middle Proterozoic crust in the Adirondack Highlands, Grenville Province, northeastern North America. Geology, 19, 119–122.

Dalziel, I.W.D., 1991. Pacific margins of Laurentia and East Antarctica as a conjugate rift pair: evidence and implications for an Eocambrian supercontinent. Geology, 19, 598–601.

Davidson, A., 1984a. Identification of ductile shear zones in the southwestern Grenville Province of the Canadian Shield. In: Kröner, A. & Greiling, R. (editors), Precambrian tectonics illustrated. E. Schweitzerbart'sche Verlagsbuchhandlung, Stuttgart, 263–279.

Davidson, A., 1984b. Tectonic boundaries within the Grenville Province of the Canadian Shield. Journal of Geodynamics, 1, 433–444.

Davidson, A., 1986. New interpretations in the southwest Grenville Province. In: Moore, J.M., Davidson, A. & Baer, A.J. (editors), The Grenville Province. Geological Association of Canada, Special Paper 31, 61–74.

Davidson, A., 1990. Evidence for eclogite metamorphism in the southwestern Grenville Province. In: Current research, part C. Geological Survey of Canada, Paper 90-1C, 113–118.

Davidson, A., 1991. Metamorphism and tectonic setting of gabbroic and related rocks in the Central Gneiss Belt, Grenville Province, Ontario. Geological Association of Canada, Toronto '91 Field Trip A.2 Guidebook, 60 pp.

Davidson, A. & van Breemen, O., 1988. Baddeleyite-zircon relationships in coronitic metagabbro, Grenville Province, Ontario: implications for geochronology. Contributions to Mineralogy and Petrology, 100, 291–299.

Davidson, A. & van Breemen, O., 1994. U–Pb ages of granites near the Grenville Front, Ontario. In: Radiogenic ages and isotopic studies: report 8. Geological Survey of Canada, Current research 1994-F, 107–114.

Davidson, A., Culshaw, N.G. & Nadeau, L., 1982. A tectono-metamorphic framework for part of the Grenville Province, Parry Sound region, Ontario. In: Current research, Part A. Geological Survey of Canada, Paper 82-1a, 175–190.

Davidson, A., Carmichael, D.M. & Pattison, D.R.M., 1990. Metamorphism and geodynamics of the southwestern Grenville Province, Ontario. International Union of Geological Sciences, International Geological Correlation Project 235-304, Field Trip #1 Guidebook, 123 pp.

Davidson, A., van Breemen, O. & Sullivan, R.W., 1992. Circa 1.75 Ga ages for plutonic rocks from the Southern Province and adjacent Grenville Province: what is the expression of the Penokean orogeny? In: Radiogenic age and isotopic studies: report 6. Geological Survey of Canada, Paper 92-2, 107–118.

Davis, D.W. & Bartlett, J.R., 1988. Geochronology of the Belmont Lake metavolcanic complex and implications for crustal development in the Central Metasedimentary Belt, Grenville Province, Ontario. Canadian Journal of Earth Sciences, 25, 1751–1759.

DePaolo, D.J., 1981. Neodymium isotopes in the Colorado Front Range and crust-mantle evolution in the Proterozoic. Nature, 291, 193–196.

Dickin, A.P. & Higgins, M.D., 1992. Sm/Nd evidence for a major 1.5 Ga. crust-forming event in the central Grenville Province. Geology, 20, 137–140.

Dickin, A.P. & McNutt, R.H., 1989. Nd model age mapping of the southeast margin of the Archean foreland in the Grenville Province of Ontario. Geology, 17, 299–302.

Dickin, A.P. & McNutt, R.H., 1990. Nd model-age mapping of Grenville lithotectonic domains: Mid-Proterozoic crustal evolution in Ontario. In: Gower, C.F., Rivers, T. & Ryan, A.B. (editors), Mid-Proterozoic Laurentia-Baltica. Geological Association of Canada, Special Paper 38, 79–94.

Doig, R., 1990. U–Pb zircon dates of Morin anorthosite suite rocks, Grenville Province, Quebec. Journal of Geology, 99, 729–738.

Dudàs, F.Ö., Davidson, A. & Bethune, K.M., 1994. Age of the Sudbury diabase dykes and their metamorphism in the Grenville Province. In: Radiogenic ages and isotopic studies: report 8. Geological Survey of Canada, Current Research 1994-F, 97–106.

Easton, R.M., 1986. Paleoenvironment and facies of the Apsley Formation, Peterborough County. Ontario Geological Survey, Miscellaneous Paper 132, 141–151.

Easton, R.M., 1992. The Grenville Province and the Proterozoic history of central and southern Ontario. In: Thurston, P.C., Williams, H.R., Sutcliffe, R.H. & Stott, G.M. (editors), Geology of Ontario. Ontario Geological Survey, Special Volume 4, pt. 2, 715–904.

Easton, R.M. & Davidson, A., 1994. Terrane boundaries and lithotectonic assemblages within the Grenville Province, eastern Ontario. Geological Association of Canada, Field Trip A1 Guidebook, 89 pp.

Eby, G.N., 1984. Geochronology of the Monteregian Hills alkaline igneous province, Quebec. Geology, 12, 468–470.

Emslie, R.F. & Hegner, E., 1993. Reconnaissance isotopic geochemistry of anorthosite–mangerite–charnockite–granite (AMCG) complexes, Grenville Province, Canada. Chemical Geology, 106, 279–298.

Emslie, R.F. & Hunt, P.A., 1990. Ages and petrogenetic

significance of igneous mangerite–charnockite suites associated with massif anorthosites, Grenville Province. Journal of Geology, 98, 213–231.

Fahrig, W.F. & West, T.D., 1986. Diabase dyke swarms of the Canadian Shield. Geological Survey of Canada Map 1627A.

Forsyth, D.A., Milkereit, B., Davidson, A., Hanmer, S., Hutchinson, D.R., Hinze, W.J. & Mereu, R.F., 1994a. Seismic images of a tectonic subdivision of the Grenville orogen beneath lakes Ontario and Erie. Canadian Journal of Earth Sciences, 31, 229–242.

Forsyth, D.A., Milkereit, B., Zelt, C.A., White, D.J., Easton, R.M. & Hutchinson, D.R., 1994b. Deep structure beneath Lake Ontario: crustal-scale Grenville subdivisions. Canadian Journal of Earth Sciences, 31, 255–270.

Frarey, M.J., 1985. Proterozoic geology of the Lake Panache–Collins Inlet area, Ontario. Geological Survey of Canada, Paper 83–22, 61 pp.

Gariépy, C., Verner, D. & Doig, R., 1990. Dating Archean metamorphic minerals southwest of the Grenville Front, western Quebec, using Pb isotopes. Geology, 18, 1078–1081.

Gill, J.E., 1948. Mountain building in Canada. 18th International Geological Congress, pt. XIII, 97–104.

Gordon, M.B. & Hempton, M.R., 1986. Collision-induced rifting: the Grenville orogeny and the Keweenawan rift of North America. Tectonophysics, 127, 1–25.

Gower, C.F., 1985. Correlations between the Grenville Province and Sveconorwegian orogenic belt—implications for Proterozoic evolution of the southern margins of the Canadian and Baltic shields. In: Tobi, A.C. & Touret, J.L.R. (editors), The deep Proterozoic crust in the North Atlantic provinces. NATO ASI Series, ser. C, 158, 247–257.

Gower, C.F., 1990. Mid-Proterozoic evolution of the eastern Grenville Province, Canada. Geologiska Föriningens i Stockholm Förhandlingar, 112, 127–139.

Gower, C.F. & Tucker, R.D., 1994. Distribution of pre-1400 Ma crust in the Grenville province: implications for rifting in Laurentia-Baltica during geon 14. Geology, 22, 827–830.

Gower, C.F., Rivers, T. & Ryan, A.B. (editors), 1990. Mid-Proterozoic Laurentia-Baltica. Geological Association of Canada, Special Paper 38, 581 pp.

Gower, C.F., Heaman, L.M., Loveridge, W.D., Schärer, U. & Tucker, R.D., 1991. Grenvillian magmatism in the eastern Grenville Province, Canada. Precambrian Research, 51, 315–336.

Gower, C.F., Schärer, U. & Heaman, L.M., 1992. The Labradorian orogeny in the Grenville Province, eastern Labrador, Canada. Canadian Journal of Earth Sciences, 29, 1944–1957.

Gower, C.F., van Nostrand, T. & Evans-Lamswood, D., 1994. Geology of the Pinware River region, southeast Labrador. In: Current Research (1994). Newfoundland Department of Mines and Energy, Report 94-1, 347–369.

Grant, S.M., 1989. Tectonic implications from sapphirine-bearing lithologies, south-west Grenville Province, Canada. Journal of Metamorphic Geology, 7, 583–598.

Green, A.G., Milkereit, B., Davidson, A., Spencer, C., Hutchinson, D.R., Cannon, W.F., Lee, M.W., Agena, W.F., Behrendt, J.C. & Hinze, W.J., 1988. Crustal structure of the Grenville Front and adjacent terranes. Geology, 16, 788–792.

Griffin, W.L., 1987. 'On the eclogites of Norway'—65 years later. Mineralogical Magazine, 51, 333–343.

Haggart, M.J., Jamieson, R.A., Reynolds, P.H., Krogh, T.E., Beaumont, C. & Culshaw, N.G., 1993. Last gasp of the Grenville orogeny: thermochronology of the Grenville Front tectonic zone near Killarney, Ontario. Journal of Geology, 101, 575–589.

Hanmer, S., 1988. Ductile thrusting at mid-crustal level, southwestern Grenville Province. Canadian Journal of Earth Sciences, 25, 1049–1059.

Hanmer, S. & Ciesielski, A., 1984. A structural reconnaissance of the northwest boundary of the Central Metasedimentary Belt, Grenville Province, Ontario and Quebec. *In* Current Research, Part B. Geological Survey of Canada, Paper 84-1B, 121–131.

Hanmer, S. & McEachern, S., 1992. Kinematical and rheological evolution of a crustal-scale ductile thrust zone, Central Metasedimentary Belt, Grenville orogen, Ontario. Canadian Journal of Earth Sciences, 29, 1779–1790.

Harnois, L. & Moore, J.M., 1991. Geochemistry of two metavolcanic arc suites from the Central Metasedimentary Belt of the Grenville Province, southeastern Ontario. Canadian Journal of Earth Sciences, 28, 1429–1443.

Hauser, E.C., 1993. Grenville foreland thrust belt hidden beneath the eastern U.S. midcontinent. Geology, 21, 61–64.

Haynes, S.J., 1986. Metallogenesis of U–Th, Grenville Supergroup, Peterborough County, Ontario. In: Moore, J.M., Davidson, A. & Baer, A.J. (editors), The Grenville Province. Geological Association of Canada, Special Paper 31, 271–280.

Heaman, L.M. & LeCheminant, A.N., 1993. Paragenesis and U–Pb systematics of baddeleyite (ZrO_2). Chemical Geology, 110, 95–126.

Hervet, M., van Breemen, O. & Higgins, M.D., 1994. U–Pb igneous crystallization ages of intrusive rocks near the southeastern margin of the Lac-St-Jean anorthosite complex, Grenville Province, Quebec. In: Radiogenic age and isotopic studies: report 8. Geological Survey of Canada, Current Research 1994-F, 115–124.

Heyn, T. 1990. Tectonites of the northwest Adirondack Mountains, New York: structural and metamorphic evolution. Ph.D. thesis, Cornell University, Ithaca, New York, 203 pp.

Higgins, M.D. & Doig, R., 1981. The Sept Iles anorthosite complex: field relationships, geochronology, and petrology. Canadian Journal of Earth Sciences, 18, 561–573.

Higgins, M.D. & van Breemen, O., 1992. The age of the Lac-Saint-Jean anorthosite complex and associated mafic rocks, Grenville Province, Canada. Canadian Journal of Earth Sciences, 29, 1412–1423.

Hoffman, P.F., 1988. United plates of America, the birth of a craton: Early Proterozoic assembly and growth of Laurentia. Annual Review of Earth and Planetary Sciences, 16, 543–603.

Hoffman, P.F., 1989a. Precambrian geology and tectonic history of North America. In: Bally, A.W. & Palmer, A.R. (editors), The geology of North America—an overview. Geological Society of America, The geology of North America, A, ch. 16, 447–511.

Hoffman, P.F., 1989b. Speculations on Laurentia's first gigayear (2.0 to 1.0 Ga). Geology, 17, 135–138.

Hoffman, P.F., 1991. Did the break-out of Laurentia turn Gondwana inside-out? Science, 252, 1409–1412.

Hoffman, P.F., 1992. Does the Central Metasedimentary Belt of the Grenville orogen encompass a klippe rooted 550 km to the southeast? Eos, 73, 340.

Hoffman, P.F. & Grotzinger, J.P., 1993. Orographic precipitation, erosional unloading, and tectonic style. Geology, 21, 195–198.

Holm, P.E., Smith, T.E., Huang, C.H., Gerasimoff, M., Grant, B. & McLaughlin, L., 1986. Geochemistry of metavolcanic rocks and dykes from the Central Metasedimentary Belt, Grenville Province, southeastern Ontario. In: Moore, J.M., Davidson, A. & Baer, A.J.

(editors), The Grenville Province. Geological Association of Canada, Special Paper 31, 25–269.

Indares, A., 1993. Eclogitized gabbros from the eastern Grenville Province: textures, metamorphic context, and implications. Canadian Journal of Earth Sciences, 30, 159-173.

Indares, A. & Martignole, J., 1989. The Grenville Front south of Val-d'Or. Tectonophysics, 157, 221–239.

Indares, A. & Martignole, J., 1990a. Metamorphic constraints on the tectonic evolution of the allochthonous monocyclic belt of the Grenville Province, western Quebec. Canadian Journal of Earth Sciences, 27, 371–386.

Indares, A. & Martignole, J., 1990b. Metamorphic constraints on the evolution of the gneisses from the parautochthonous and allochthonous polycyclic belts, Grenville Province, western Quebec. Canadian Journal of Earth Sciences, 27, 357–370.

Jamieson, R.A., Culshaw, N.G., Wodicka, N., Corrigan, D. & Ketchum, J.W.F., 1992. Timing and tectonic setting of Grenvillian metamorphism—constraints from a transect along Georgian Bay, Ontario. Journal of Metamorphic Geology, 10, 321–332.

Kamo, S., Gower, C.F. & Krogh, T.E., 1989. A birthdate for the Iapetus Ocean? A precise U–Pb zircon and baddeleyite age for the Long Range dykes, S.E. Labrador. Geology, 17, 602–605.

Kerr, A., Krogh, T.E., Corfu, F., Schärer, U., Gandhi, S.S. & Kwok, Y.Y., 1992. Episodic Early Proterozoic granitoid plutonism in the Makkovik Province, Labrador: U–Pb geochronological data and geological implications. Canadian Journal of Earth Sciences, 29, 1166–1179.

Ketchum, J.W.F., Jamieson, R.A., Heaman, L.M., Culshaw, N.G. & Krogh, T.E., 1994. 1.45 Ga granulites in the southwestern Grenville Province: geologic setting, P–T conditions, and U–Pb geochronology. Geology, 22, 215–218.

Krogh, T.E., 1989. U–Pb systematics of zircon and titanite in metasediments and gneisses near the Grenville Front, Ontario. Geological Association of Canada, Program with Abstracts, 14, A52.

Kumerapeli, S.P., St. Seymour, K., Fowler, A. & Pinston, H., 1990. The problem of the magma source of a giant, radiating dyke swarm. In: Parker, A.J., Rickwood, P.C. & Tucker, D.H. (editors), Mafic dykes and emplacement mechanisms. Balkema, Rotterdam, 163–171.

Logan, W.E., 1863. Report on the geology of Canada. Geological Survey of Canada, Report of Progress from its Commencement to 1863, 963 pp.

Loveridge, W.D., 1986. U–Pb ages on zircon from rocks of the Lac de Morhiban map area, Quebec. In: Current research, Part A. Geological Survey of Canada, Paper 86-1A, 523–530.

Lumbers, S.B., Heaman, L.M., Vertolli, V.M. & Wu, T.-W., 1990. Nature and timing of middle Proterozoic magmatism in the Central Metasedimentary Belt, Grenville Province, Ontario. In: Gower, C.F., Rivers, T. & Ryan, A.B. (editors), Mid-Proterozoic Laurentia-Baltica. Geological Association of Canada, Special Paper 38, 243–276.

Lumbers, S.B., Wu, T.-W., Heaman, L.M., Vertolli, V.M. & MacRae, N.D., 1991. Petrology and age of the A-type Mulock granite batholith, northern Grenville Province, Ontario. Precambrian Research, 53, 199–231.

Machado, N., David, J., Carignan, J., Zhang, Q. & Gariépy, C., 1991. Géochronologie U-Pb du territoires québecois, 2ième rapport intérimaire: résultats 1990–1991. Ministère de l'Énergie et des Ressources du Québec, Rapport Interne.

Marcantonio, F., McNutt, R.H., Dickin, A.P. & Heaman, L.M., 1990. Isotopic evidence for the crustal evolution of the Frontenac Arch in the Grenville Province of Ontario, Canada. Chemical Geology, 83, 297–314.

Martignole, J. & Pouget, P., 1993. Contrasting zoning profiles in high-grade garnets: evidence for the allochthonous nature of a Grenville Province terrane. Earth and Planetary Science Letters, 120, 177–185.

Martignole, J. & Pouget, P., in press. A two-stage emplacement for the Cabonga allochthon: evolution from orthogonal to oblique collision in the central part of the Grenville Province. Canadian Journal of Earth Sciences.

Martignole, J. & Schrijver, K., 1970. Tectonic setting and evolution of the Morin anorthosite, Grenville Province, Quebec. Bulletin of the Geological Society of Finland, 42, 165–209.

Martignole, J., Indares, A. & Kish, L., 1987. Le supergroupe de Wakeham dans la partie nord-est de la province de Grenville. Ministère de l'Énergie et des Ressources du Québec, Rapport DV 87-25, 91–94.

Martignole, J., Machado, N. & Nantel, S., 1993. Timing of intrusion and deformation of the Rivière-Pentecôte anorthosite (Grenville Province). Journal of Geology, 101, 652–658.

Martignole, J., Machado, N. & Indares, A., 1994. The Wakeham terrane: a Mesoproterozoic terrestrial rift in the eastern part of the Grenville Province. Precambrian Research, 68, 291–306.

McEachern, S.J. & van Breemen, O., 1993. Age of deformation within the Central Metasedimentary Belt boundary thrust zone, southwest Grenville Orogen: constraints on the collision of the Mid-Proterozoic Elzevir terrane. Canadian Journal of Earth Sciences, 30, 1155–1165.

McLelland, J.M., 1986. Pre-Grenvillian history of the Adirondacks as an anorogenic, bimodal caldera complex of mid-Proterozoic age. Geology, 14, 229–233.

McLelland, J.M., 1989. Crustal growth associated with anorogenic, mid-Proterozoic anorthosite massifs in northeastern North America. Tectonophysics, 161, 331–341.

McLelland, J.M. & Chiarenzelli, J.R., 1990. Geochronological studies in the Adirondack Mountains and the implications of a Middle Proterozoic tonalitic suite. In: Gower, C.F., Rivers, T. & Ryan, A.B. (editors), Mid-Proterozoic Laurentia-Baltica. Geological Association of Canada, Special Paper 38, 175–194.

McLelland, J., Chiarenzelli, J., Whitney, P. & Isachsen, Y., 1988. U-Pb zircon geochronology of the Adirondack Mountains and implications for their geologic evolution. Geology, 16, 920–924.

McMenamin, M.A.S. & McMenamin, D.L.S., 1990. The emergence of animals. The Cambrian breakthrough. Columbia University Press, New York, 217 pp.

Mezger, K., Essene, E.J., van der Pluijm, B.A. & Halliday, A.N., 1993. U-Pb geochronology of the Grenville orogen of Ontario and New York: constraints on ancient crustal tectonics. Contributions to Mineralogy and Petrology, 114, 13–26.

Mezger, K., Rawnsley, C.M., Bohlen, S.R. & Hanson, G.N., 1991. U-Pb garnet, sphene, monazite, and rutile ages: implications for the duration of high-grade metamorphism and cooling histories, Adirondack Mts., New York. Journal of Geology, 99, 415–428.

Miller, R.R. & Lenz, D.R., 1993. Kinematical and rheological evolution of a crustal-scale ductile thrust zone, Central Metasedimentary Belt, Grenville orogen, Ontario: discussion. Canadian Journal of Earth Sciences, 30, 647–649.

Moore, J.M. & Thompson, P.H., 1980. The Flinton Group:

a late Precambrian metasedimentary succession in the Grenville Province of eastern Ontario. Canadian Journal of Earth Sciences, 17, 1685–1707.

Moore, J.M., Davidson, A. & Baer, A.J. (editors), 1986. The Grenville Province. Geological Association of Canada, Special Paper 31, 358 pp.

Moores, E.M., 1991. Southwest U.S.–East Antarctica (SWEAT) connection: a hypothesis. Geology, 19, 425–428.

Murthy, G., Gower, C., Tubrett, M. & Pätzold, R., 1992. Paleomagnetism of Eocambrian Long Range dykes and Double Mer Formation from Labrador, Canada. Canadian Journal of Earth Sciences, 29, 1224–1234.

Nadeau, L. & Hanmer, S., 1992. Deep-crustal, break-back stacking and slow cooling of the continental footwall beneath a thrusted marginal basin, Grenville orogen, Canada. Tectonophysics, 210, 215–233.

Nadeau, L. & van Breemen, O., 1994. Do the 1.45–1.39 Ga Montauban Group and the La Bostonnais complex constitute a Grenvillian accreted terrane? Geological Association of Canada, Program with Abstracts, 19, A81.

Nelson, B.K. & DePaolo, D.J., 1985. Rapid production of continental crust 1.7 to 1.9 b.y. ago: Nd isotopic evidence from the basement of the North American mid-continent. Geological Society of America, Bulletin, 96, 746–754.

Nyman, M.W., Karlstrom, K.E., Kirby, E. & Grabaud, C.M., 1994. Mesoproterozoic contractional orogeny in western North America: evidence from ca. 1.4 Ga plutons. Geology, 22, 901–904.

Owen, J.V. & Erdmer, P., 1990. Middle Proterozoic geology of the Long Range Inlier, Newfoundland: regional significance and tectonic implications. In: Gower, C.F., Rivers, T. & Ryan, A.B. (editors), Mid-Proterozoic Laurentia-Baltica. Geological Association of Canada, Special Paper 38, 215–231.

Owens, B.E., Dymek, R.F., Tucker, R.D., Brannon, J.C. & Podosek, F.A., 1994. Age and radiogenic isotopic composition of a late- to post-tectonic anorthosite in the Grenville Province: the Labrieville massif, Quebec. Lithos, 31, 189–206.

Patchett, J.P. & Arndt, N.T., 1986. Nd isotopes and tectonics of 1.9–1.7 Ga crustal genesis. Earth and Planetary Science Letters, 78, 329–338.

Philippe, S., Wardle, R.J. & Schärer, U., 1993. Labradorian and Grenvillian crustal evolution of the Goose Bay region, Labrador: new U–Pb geochronological constraints. Canadian Journal of Earth Sciences, 30, 2315–2327.

Rankin, D.W. et al., 1993. Proterozoic rocks east and southeast of the Grenville front. In: Reed, J.C., Jr., Bickford, M.E., Houston, R.S., Link, P.K., Rankin, D.W., Sims, P.K. & Van Schmus, W.R. (editors), Precambrian: Conterminous U.S. Geological Society of America, The geology of North America, C-2, ch. 5, 335–461.

Ratcliffe, N.M., Aleinikoff, J.N., Burton, W.C. & Karabinos, P., 1991. Trondhjemitic, 1.35-1.31 Ga gneisses of the Mount Holly complex of Vermont: evidence for an Elzevirian event in the Grenville basement of the United States Appalachians. Canadian Journal of Earth Sciences, 28, 77–93.

Rivers, T., 1983. Progressive metamorphism of pelitic and quartzofeldspathic rocks in the Grenville Province of Labrador—tectonic implications of bathozone 6 assemblages. Canadian Journal of Earth Sciences, 20, 1791–1804.

Rivers, T. & Chown, E.H., 1986. The Grenville orogen in eastern Quebec and western Labrador – definition, identification and tectonometamorphic relationships of autochthonous, parautochthonous and allochthonous terranes. In: Moore, J.M., Davidson, A. & Baer, A.J. (editors), The Grenville Province. Geological Association of Canada, Special Paper 31, 31–50.

Rivers, T., Martignole, J., Gower, C.F. & Davidson, A., 1989. New tectonic divisions of the Grenville Province, southeast Canadian Shield. Tectonics, 8, 63–84.

Rivers, T., van Gool, J.A.M. & Connelly, J.N., 1993. Contrasting tectonic styles in the northern Grenville Province: implications for the dynamics of orogenic fronts. Geology, 21, 1127–1130.

Rondot, J., 1986. Géosutures dans le Grenville. In: Moore, J.M., Davidson, A. & Baer, A.J. (editors), The Grenville Province. Geological Association of Canada, Special Paper 31, 313–325.

Ruiz, J., Patchett, P.J. & Ortega-Gutierrez, F., 1988. Proterozoic and Phanerozoic basement terranes of Mexico from Nd isotopic studies. Geological Society of America, Bulletin, 100, 274–281.

Sager-Kinsman, E.A. & Parrish, R.R., 1993. Geochronology of detrital zircons from the Elzevir and Frontenac terranes, Central Metasedimentary Belt, Grenville Province, Ontario. Canadian Journal of Earth Sciences, 30, 465–473.

Schau, M., Davidson, A. & Carmichael, D.M., 1986. Granulites and granulites. Geological Association of Canada, Field Trip 6 Guidebook, 36 pp.

Schwerdtner, W.M. & van Berkel, J.T., 1991. The origin of fold abutments in the map pattern of the westernmost Grenville Province, central Ontario. Precambrian Research, 49, 39–59.

Sims, P.K. & Peterman, Z.E., 1986. Early Proterozoic Central Plains orogen: a major buried structure in the north-central United States. Geology, 14, 488–491.

Sleep, N.H., 1990. Monteregian hotspot track: a long-lived mantle plume. Journal of Geophysical Research, 95, ser. B, 21329–21344.

Stewart, A. & Clarke, G., 1993. Extension of the Woodroffe Thrust, Musgrave Block, into Western Australia. AGSO Research Newsletter, 18, 5–6.

Stockwell, C.H., 1964. Fourth report on structural provinces, orogenies, and time-classification of rocks of the Canadian Precambrian Shield. In: Age determinations and geological studies; part II, geological studies. Geological Survey of Canada, Paper 64-17 (Part II), 1–21.

Storey, B.C., Pankhurst, R.J. & Johnson, A.C., 1994. The Grenville Province within Antarctica: a test of the SWEAT hypothesis. Journal of the Geological Society, London, 151, 1–4.

Sun, S. & Sheraton, J., 1992. Zircon U/Pb chronology, tectono-thermal and crust-forming ages in the Tomkinson Ranges, Musgrave Block, Central Australia. AGSO Research Newsletter, 17, 9–11.

Sun, S.-S., Gray, C.M., Sheraton, J.W., Glikson, A.Y. & Stewart, A.J., in press. Zircon U–Pb chronology and neodymium isotope study of tectonothermal and crust-forming events in the Tomkinson Ranges, western Musgrave Block, central Australia. AGSO Journal of Australian Geology & Geophysics.

Tucillo, M.E., Mezger, K., Essene, E.J. & van der Pluijm, B.A., 1992. Thermobarometry, geochronology and the interpretation of P–Tt data in the Britt domain, Ontario Grenville orogen, Canada. Journal of Petrology, 33, 1225–1259.

Tucker, R.D. & Gower, C.F., 1994. A U–Pb geochronological framework for the Pinware terrane, Grenville Province, southeast Labrador. Journal of Geology, 102, 67–78.

van Breemen, O. & Davidson, A., 1988a. Northeast

extension of Proterozoic terranes of mid-continental North America. Geological Society of America, Bulletin, 100, 630–638.

van Breemen, O. & Davidson, A., 1988b. U–Pb zircon ages of granites and syenites in the Central Metasedimentary Belt, Grenville Province, Ontario. In: Radiogenic age and isotopic studies: report 2. Geological Survey of Canada, Paper 88-2, 45–50.

van Breemen, O. & Davidson, A., 1990. U-Pb zircon and baddeleyite ages from the Central Gneiss Belt, Ontario. In: Radiogenic age and isotopic studies: report 3. Geological Survey of Canada, Paper 89-2, 85–92.

van Breemen, O. & Higgins, M.D., 1993. U–Pb zircon age of the southwest lobe of the Havre-Saint-Pierre anorthosite complex, Grenville Province, Canada. Canadian Journal of Earth Sciences, 30, 1453–1457.

van Breemen, O., Davidson, A., Loveridge, W.D. & Sullivan, R.W., 1986. U–Pb zircon geochronology of Grenville tectonites, granulites and igneous precursors, Parry Sound, Ontario. In: Moore, J.M., Davidson, A. & Baer, A.J. (editors), The Grenville Province. Geological Association of Canada, Special Paper 31, 191–207.

van der Pluijm, B.A. & Carlson, K.A., 1989. Extension in the Central Metasedimentary Belt of the Ontario Grenville: timing and tectonic significance. Geology, 17, 161–164.

van der Pluijm, B.A., Mezger, K., Cosca, M.A. & Essene, E.J., 1994. Determining the significance of high-grade shear zones by using temperature–time paths, with examples from the Grenville orogen. Geology, 22, 743–746.

Van Schmus, W.R. et al., 1993. Transcontinental Proterozoic provinces. In: Reed, J.C., Jr., Bickford, M.E., Houston, R.S., Link, P.K., Rankin, D.W., Sims, P.K. & Van Schmus, W.R. (editors), Precambrian: Conterminous U.S. Geological Society of America, The geology of North America, C-2, ch. 4, 171–334.

Wardle, R.J., Rivers, T., Gower, C.F., Nunn, G.A.G. & Thomas, A., 1986. The northeastern Grenville Province: new insights. In: Moore, J.M., Davidson, A. & Baer, A.J. (editors), The Grenville Province. Geological Association of Canada, Special Paper 31, 13–29.

Wardle, R.J., Ryan, B., Philippe, S. & Schärer, U., 1990. Proterozoic crustal development, Goose Bay region, Grenville Province, Labrador, Canada. In: Gower, C.F., Rivers, T. & Ryan, A.B. (editors), Mid-Proterozoic Laurentia-Baltica. Geological Association of Canada, Special Paper 38, 197–214.

White, D.J., Easton, R.M., Culshaw, N.G., Milkereit, B., Forsyth, D.A., Carr, S., Green, A.G. & Davidson, A., 1994. Seismic images of the Grenville orogen in Ontario. Canadian Journal of Earth Sciences, 31, 293–307.

Windley, B.F., 1986. Comparative tectonics of the western Grenville and the western Himalaya. In: Moore, J.M., Davidson, A. & Baer, A.J. (editors), The Grenville Province. Geological Association of Canada, Special Paper 31, 341–348.

Windley, B.F., 1989. Anorogenic magmatism and the Grenvillian orogeny. Canadian Journal of Earth Sciences, 26, 479–489.

Windley, B.F., 1993. Proterozoic anorogenic magmatism and its orogenic connections. Journal of the Geological Society of London, 150, 39–50.

Wodicka, N., Parrish, R.R., Jamieson, R.A. & Culshaw, N.G., 1994. Was the Parry Sound allochthon rooted in the Central Metasedimentary Belt? Geological Association of Canada, Program with Abstracts, 19, A120.

Wynne-Edwards, H.R., 1972. The Grenville Province. In: Price, R.A. & Douglas, R.J.W. (editors), Variations in tectonic styles in Canada. Geological Association of Canada, Special Paper 11, 263–334.

AGSO Journal of Australian Geology & Geophysics, 16 (1/2), 25–39

Grenville-age belts and associated older terranes in Australia and Antarctica

G.L. Clarke[1], S.-S. Sun[2] & R.W. White[3]

During 1.3–1.0 Ga, multiple magmatic/tectonic events, causally linked to extensive mantle melting, markedly affected the Musgrave Block, the Albany–Fraser belt and parts of the east Antarctic shield. It is possible that southern parts of the central Australian Arunta Block were also affected by this event. Equivalent terranes can be juxtaposed in conventional Gondwana reconstructions of southwestern Australia and Antarctica. Effects of a ~1060 Ma Gondwana-wide magmatism include areally extensive dyke swarms and volcanics of the central Australian Bentley Supergroup. It is unclear to what extent the effects of a ~550 Ma convergent event that resulted in significant crustal overthickening and high-P recrystallisation in Musgrave Block rocks can be extrapolated to neighbouring terranes. Nonetheless, this event may be indicative of plate margin processes of latest Neoproterozoic age that controlled the assembly of central Australia.

Introduction

The geology of central Australia is dominated by high-grade rocks of the early Proterozoic Arunta Block and mid-Proterozoic Musgrave Block, which are separated by unconformably overlying sedimentary rocks of the late Proterozoic Amadeus Basin (Fig. 1A). Complex tectonic histories are inferred for both high-grade terranes, involving multiple phases of magmatism, deformation, metamorphism and sedimentation (e.g. Stewart et al. 1984; Clarke et al. 1995—this issue; Collins & Shaw in press). Refined methods of isotopic rock dating mean that these tectonic histories are now sufficiently well constrained to allow comparison with those of adjacent Proterozoic belts in Gondwana to test for the regional correlation of events. The aim of this paper is to review the tectonic histories of the metamorphic complexes in Australia and parts of Antarctica that were grossly affected by orogeny in the period 1300–1000 Ma, and place the ~1200 Ma and 1080 Ma deformation and magmatism that grossly affected the Musgrave Block into a regional context. Orogeny in the period 1300 to 950 Ma can be correlated with the extensive Grenville belts of the North America shield (e.g. Davidson 1995—this issue), and controversial Gondwana reconstructions have been inferred on the basis of spatial correlations between Grenville-aged belts in Australia, Antarctica, and the North American shield (e.g. Moores 1991). Grenville-aged belts in both North America and Australia superimpose intense deformation and high-grade metamorphism on composite older structural and metamorphic provinces (e.g. Krogh 1994), so it is appropriate to review the evolution of terranes adjacent to the Grenville belts to test for equivalent protoliths.

Grenville-aged complexes in Australia comprise the Musgrave Block, the Rudall Complex of the Paterson Orogen in north Western Australia (Clarke 1991) and the Albany–Fraser Orogen in south Western Australia (Nelson et al. in press). Parts of the east Antarctic shield that were adjacent to Western Australia in the Proterozoic also evidence Grenville-aged metamorphism and magmatism (Tingey 1991; Fig. 1A). The tectonic histories of the various terranes will be reviewed briefly, and then regional correlations tested by the construction of a time–space diagram.

Paterson Orogen

The Paterson Orogen (Williams 1990) is a belt of metamorphic, sedimentary, and igneous rocks of Archaean to late Proterozoic age that trend northwesterly through northern Western Australia (Fig. 1A). In northwestern Australia, high-grade parts of the orogen are restricted to amphibolite facies metamorphic rocks of the Rudall Complex (Fig. 1B), which were metamorphosed and deformed at ~1330 Ma (Chin & deLaeter 1981) before being re-exposed and unconformably overlain by late Proterozoic sedimentary rocks of the Yeneena Group and Karara Formation. The Paterson Orogen has been extrapolated southeastwards to incorporate the Musgrave Block (Williams 1990), since an elongate gravity anomaly, called the Ankatell Regional Gravity Ridge (Fraser 1976), extends southeastwards from the Rudall Complex to the Musgrave Block.

The Rudall Complex consists of two tectonically interlayered metamorphic sequences (Chin et al. 1980; Clarke 1991; Hickman & Clarke 1993): (1) older banded orthogneiss and metasediments of the Yandagooge Formation; and (2) younger quartzite and schist of the Tjingkulatjatjarra Formation. The Yandagooge Formation occurs as inclusions in, and is intimately interlayered with, a composite orthogneiss that is the dominant rock type of the Rudall Complex. The Tjingkulatjatjarra Formation is not disrupted by orthogneiss, and is interpreted as being younger than both the composite orthogneiss and Yandagooge Formation, possibly forming a cover sequence to these rocks. Sm–Nd model ages (McCulloch 1987) and preliminary U–Pb dating of zircons (D.Nelson, GSWA, unpublished data) from samples of the orthogneiss suggest that a significant component may be Archaean in age. The Yandagooge Formation and orthogneiss record a tectonic event, D_1, that predates the Tjingkulatjatjarra Formation, but all rock units were intensely deformed and metamorphosed during the Watrara Orogeny, which comprises events D_{2-3}. On the basis of whole-rock Rb–Sr analysis of orthogneiss that was pervasively recrystallised during D_2 (Chin & DeLaeter 1981), the Watrara Orogeny occurred at 1333±44 Ma. Macroscopic recumbent folds produced during D_2 reflect crustal shortening along a northeast-trending axis (Clarke 1991) that produced kyanite+staurolite+biotite and garnet+staurolite+biotite S_2 assemblages in metapelites, consistent with the Rudall Complex having been buried to depths of ~20 km during the Watrara Orogeny (G.L. Clarke, unpublished data). The Rb–Sr dating of pegmatite that cuts S_3 in the Rudall Complex constrains orogeny to have been over by 1132±21 Ma (Chin & deLaeter 1981). A ~1060 Ma biotite monzogranite crops out among sand dunes to the southeast of the Rudall Complex (Chin & deLaeter 1981).

The Rudall Complex, the Pilbara Craton, and 1050–1100 Ma sedimentary rocks of the Bangemall Basin are unconformably overlain by a sequence of low-grade metasedimentary rocks called the Yeneena Group (Williams 1990; Fig. 1B). The Yeneena Group includes a basal conglomerate where it overlies the Rudall Complex, and passes upwards with apparent conformity into sheet sandstone, graphitic shale, dolomite, and siltstone. The position of the Yeneena Group in regional Proterozoic stratigraphy is controversial, since outcrop is discontinuous. However, it is thought to be between 750 and 1000 Ma in age (Williams 1990): 940 Ma epigenetic galena

1 Department of Geology & Geophysics, University of Sydney, NSW 2006, Australia
2 Australian Geological Survey Organisation, GPO Box 378 Canberra, ACT 2601, Australia
3 School of Earth Sciences, Macquarie University, Sydney, NSW 2109, Australia

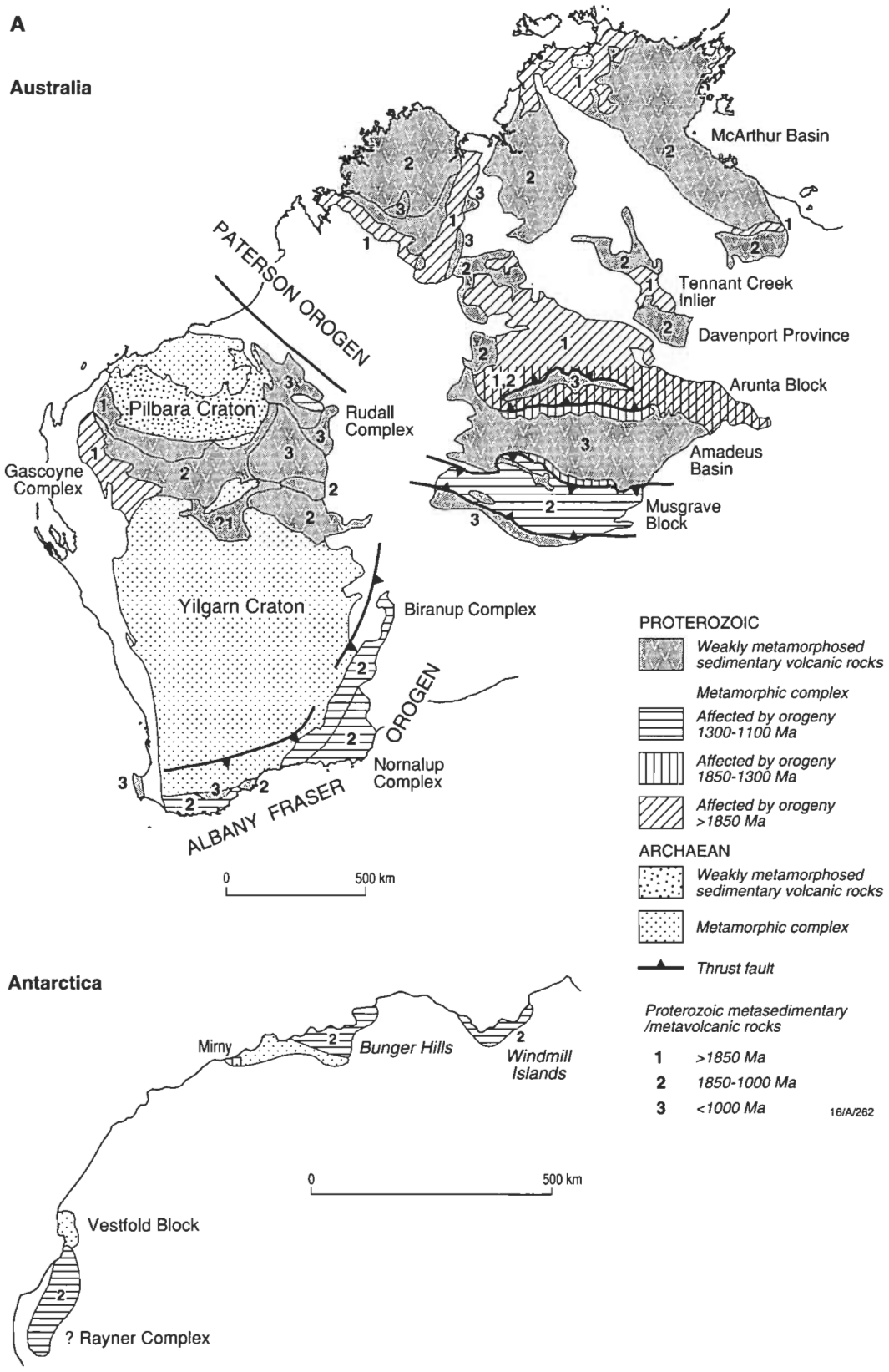

Figure 1. (A) Geological map showing Precambrian rocks of north and western Australia (after Palfreyman et al. 1976; Myers & Hocking 1988) and parts of Antarctica that were adjacent in the Gondwana reconstruction (after Veevers & Eittreim 1988). The subdivision of the Proterozoic era is based on that proposed by Dunn et al. (1966) and refined by Plumb (1985), Page (1988), and other workers discussed in the text. (B) Detail of the geological setting of the Rudall Complex and adjacent Proterozoic basins. (C) Detail of the geological setting of the Musgrave and Arunta Blocks, showing the location of areas and geological features discussed in the text.

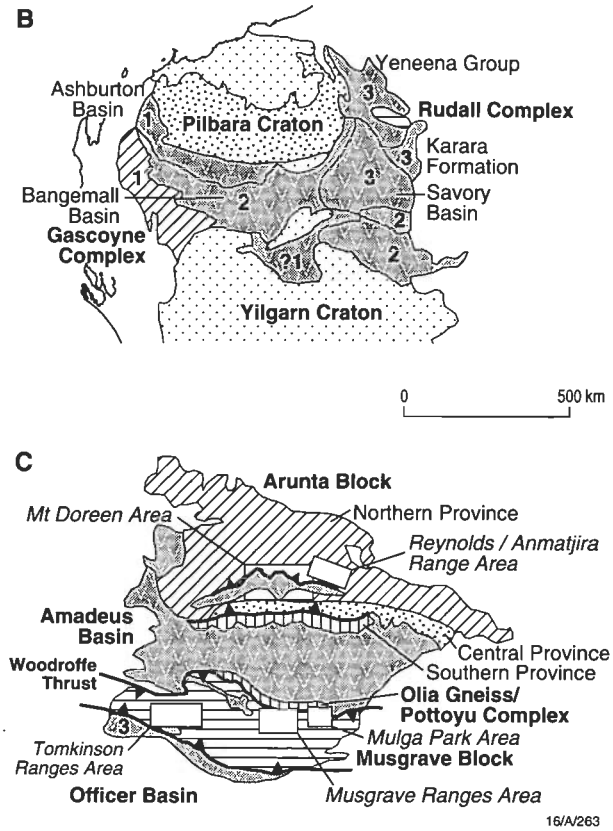

mineralisation (I.R. Fletcher, unpublished data) and 820±40 Ma syngenetic Cu mineralisation (McKnight 1992) occur in older parts of the Yeneena Group. It was affected by folding and thrusting prior to the intrusion of 690±48 Ma granite bodies, which cut deformed Yeneena Group rocks in the Telfer area (McNaughton & Goellnicht 1990). The Yeneena Group is unconformably overlain by two successions of late Proterozoic sedimentary rocks (Fig. 1B), which are in fault contact with each other: the Karara Formation to the southeast, and the Savory Basin to the southwest of the Rudall Complex. The Savory Basin contains glacigene sediments that are correlated with parts of the Amadeus Basin (Fig. 1a; Williams 1990).

The Arunta Block

Following a geochronological framework based mostly on Rb–Sr dating (Black et al. 1983), Shaw et al. (1984) divided the areally extensive (200 000 km^2) Arunta Block into three tectonic provinces (southern, central, and northern; Fig. 1C) and three lithostratigraphic units (Divisions 1, 2, and 3). The central and northern provinces would appear to be broadly equivalent (Collins & Shaw in press): both contain equivalent rocks from two metasedimentary sequences that are separated by an unconformity (Stewart 1981) and both were intruded by areally extensive granites ranging in age from ~1880 Ma to ~1580 Ma (Sun et al. in press). Rocks in the two provinces were patchily affected by at least three major phases of areally restricted metamorphism, with effects of the youngest event having been significantly more pronounced and widespread in the central province (Clarke et al. 1990; Black & Shaw 1992). On the basis of recent zircon dating, Black & Shaw (1992) have discounted previous chronostratigraphic correlations between these rocks and the southern province, and inferred that rocks of the southern province, which are separated from the rest of the Arunta Block by the north-dipping Redbank–Mount Zeil thrust zone (Glikson 1987), may represent a distinct terrane. Despite covering such a large area, no outcropping Archaean basement has been located for the Arunta Block, although dismembered Archaean basement is inferred on the basis of inherited Archaean zircons (Black & Shaw 1992) and very low initial ε Nd values (Sivell et al. 1992; Zhao & McCulloch 1993; Sun et al. 1995) in some of the Proterozoic granites and mafic rocks. All three provinces of the Arunta Block are extensively dissected by shear zones of several ages, and interpretations of the tectonic relationships between units are continually being revised as on-going U–Pb dating of zircons provides more precise geochronological control.

Metamorphic grade varies considerably throughout the northern province: there are large areas of poorly exposed greenschist to amphibolite facies metasediments (Shaw et al. 1984) and localised areas of well-exposed high-grade rocks, which record a complex history for at least parts of the terrane. Metasediments are dominantly Division 2 turbidites of the Lander Rock beds, which have been correlated with the 1870 Ma Warramunga Group in the Tennant Creek Inlier (Fig. 1A; Blake et al. 1986; Blake & Page 1988) and may be equivalent to low-grade greywackes and metavolcanics of the Granites–Tanami Province to the northwest of the Arunta Block (Fig. 1A). The Lander Rock beds are unconformably overlain by Division 3 quartzose platform sedimentary rocks of the 1820 to 1780 Ma (Collins & Shaw in press) Reynolds Range Group (Stewart 1981), which has been correlated with the Hatches Creek Group in the Tennant Creek Inlier (Blake et al. 1986). The Lander Rock beds are inferred as having been deformed and locally metamorphosed to granulite facies before the intrusion of the 1880±5 Ma Ngadarunga Granite in the Mount Doreen area (Fig. 1C; Young et al. 1995). This interpretation conflicts with the generally accepted 1870 Ma age of the Lander Rock beds, and it is possible that the Ngadarunga Granite represents local basement to the sedimentary sequence (see Collins & Shaw in press). However, if the Lander Rock beds are older than 1880 Ma, then any deformation and metamorphism that predate the Ngadarunga Granite could be equivalent to the loosely defined Barramundi Orogeny (Etheridge et al. 1987), which grossly affected Proterozoic terranes to the north and northwest of the Arunta Block (Fig. 1A; Page & Williams 1988; Young et al. 1995). The precise timing and regional extent of the Barramundi Orogeny are undergoing redefinition with the collection of new data from northwestern Australia (Shaw 1994). Regionally extensive 1820 Ma granitoids cut granulite facies Lander Rock beds in the Reynolds/Anmatjira Range area (Fig. 1C; Vernon et al. 1990; Collins & Williams 1995). The Lander Rock Beds were then re-exposed before deposition of the Reynolds Range Group (Stewart 1981; Hand et al. 1992) and, in the Mount Doreen area, probable equivalents, comprising the 1772±5 Ma Nicker beds and 179910 Ma Patamungala beds (Fig. 1C; Young et al. 1995). A phase of tectonism, granite intrusion, and localised granulite facies metamorphism at ~1770 Ma (e.g. Clarke et al. 1990; Collins & Shaw in press) produced east-trending folds and sub-concordant high-strain zones in Lander Rock beds, Reynolds Range Group, Patmungala beds, and earlier orthogneiss. This event can be correlated with the Late Strangways event that had widespread effects in the central province (Black & Shaw 1992). In the Mt Doreen area, an episode of late faulting juxtaposed low and high-grade metasediments (Young et al. 1995). This faulting may correlate with shear zone development in the Reynolds/Anmatjira Range area at ~1660 Ma (Dirks & Hand 1991) or with the Chewings orogeny, evident in the southern province at ~1600 Ma (Collins & Williams 1995). Post-tectonic mafic to felsic magmatism occurred in the Mount Doreen area at 1635±9 Ma and a regionally extensive megacrystic granite and pegmatite suite intruded Reynolds Range Group rocks at ~1580 Ma (Collins & Williams 1995; Young et al. 1995).

The central province comprises multiply deformed mafic

and felsic orthogneiss intercalated with subordinate aluminous, siliceous, and calcareous metasedimentary rocks (Division 1; Shaw et al. 1984), which were deformed and metamorphosed by the ~1770 Late Strangways event (Black & Shaw 1992) at conditions of up to about 800°C and 8 kbar (Warren 1983; Norman & Clarke 1990). Based on the presence of comparatively high-pressure assemblages in the extensive granulite facies rocks of the central province, some metasediments were inferred to be older than the Division 2 rocks of the northern province and thought to represent a deeper, possibly older crustal segment (Shaw et al. 1984). For example, extensive exposures of garnet–two pyroxene granulite in the southwestern portion of the province have been interpreted as an exhumed fragment of a mafic lower crust (Glikson 1986). However, there were few isotopic data to directly constrain the interpretation that these rocks are older than Division 2 sequences, and recent Pb-isotope studies suggest the contrary: extensive metasedimentary gneisses of the central province are inferred as having been deposited in the period 1810–1790 Ma (Warren 1994), possibly contemporaneously with deposition of the Reynolds Range Group in the northern province. In addition, petrological, chemical and Nd isotope data support the concept of back-arc opening and intrusion of large igneous complexes into metasediments of the central province shortly before the Late Strangways event (Foden et al. 1988; Sivell 1988). However, other sections of the central province show a complex tectonic history that includes them having been metamorphosed at low-P, high-T conditions before the ~1770 Ma Late Strangways event (Norman & Clarke 1990; Goscombe 1992a 1992b; Zhao & Cooper 1992; LaFrance et al. 1995). Whole-rock Rb–Sr dates of approximately 1850–1820 Ma, obtained from rocks in the Strangways Range (Iyer et al. 1976; Black et al. 1983), could represent the age of an 'Early Strangways event' (LaFrance et al. 1995) and make the event equivalent to pre-1820 Ma metamorphism observed in the northern province. Alternatively, the 'Early Strangways event' may be only 20 Ma older than the ~1770 Ma Late Stangways event (Black & Shaw 1992; Colins & Shaw 1995), but such an interpretation does not account for the ~1850 Ma ages. The ~1770 Ma Late Strangways event involved significant crustal thickening (Norman & Clarke 1990; Goscombe 1992a, 1992b), which developed regional-scale sheath folds in metasediments of the central province (Goscombe 1991), most probably related to continental convergence. Kilometre-wide retrograde shear zones separate blocks of the central province (Warren 1983) and the correlation of local deformation events and magmatic phases between blocks can be problematical (e.g. Mortimer et al. 1987; Cooper et al. 1988), possibly owing to patchy overprinting during the Late Strangways event. As a generalisation, the history of the central province can be interpreted as broadly similar to that of the northern province, but with effects of the ~1770 Ma Late Strangways event significantly more intense and having overprinted effects of the pre-1820 Ma metamorphism throughout most of the central province (Norman & Clarke 1990). In comparison, in the Arunta Block to the north and west of the Reynolds Range (Fig. 1C), the effects of Strangways event appear to have been mild or absent (Clarke et al. 1990) and effects of the pre-1820 Ma event are readily recognised (e.g. Vernon et al. 1990).

The southern tectonic province is composed of banded quartzofeldspathic and granitic gneiss unconformably overlain by silicic and aluminous rocks (Shaw et al. 1984). There are limited isotopic data to constrain geological events that affected the province, but two orthogneisses are inferred to have crystallised at 1663±13 Ma (Black & Shaw 1992) and 1678±14 Ma (Collins et al. 1995) before deformation and metamorphism (Teyssier et al. 1988) related to the 1610–1600 Ma Chewings orogeny (Majoribanks & Black 1974; Collins & Shaw in press). The limited zircon data constrain the silicic and aluminous rocks of the southern province to be significantly younger than the Division 3 Reynolds Range Quartzite of the northern province (cf. Shaw et al. 1984). If representative, the data suggest that the southern province is a different terrane to the central and northern provinces of the Arunta Block (Black & Shaw 1992), although felsic intrusions of similar age are observed in the Mt Doreen area of the northern province. Crustal-scale thrusting, evident in the north-dipping Redbank thrust zone, most probably joined the southern province to the rest of the Arunta Block at about 1500–1400 Ma (Shaw & Black 1991). The ~1140 Ma Ormiston event (Shaw et al. 1984), now referred to as the Teapot thermal event (Collins & Shaw in press), resulted in open folding, localised anatectic granite, such as the 'enriched-type' Teapot Complex (Sun et al. 1995), 1137^{+9} Ma pegmatites (Black & Shaw 1992), and the intrusion of t-7 alkaline Mordor Complex (Langworthy & Black 1978; Nelson et al. 1989) in the southern province. Whereas the effects of this event seem to be restricted to the southern province of the Arunta Block, felsic magmatism of this age is common in the Musgrave Block (see below).

The southern province of the Arunta Block was intruded by the 1076±33 Ma Stuart Dyke swarm (Zhao & McCulloch 1993; cf. Black et al. 1980). The basal units of the Amadeus Basin, the Heavitree Quartzite and equivalent Dean and Townsend Quartzites, unconformably overlie both the Arunta Block and the Musgrave Block. Parts of the basin stratigraphy constrain tectonic events in the Musgrave Block, and these are discussed further below. The 400 to 300 Ma Alice Springs Orogeny (Dunlap et al. 1991; Shaw & Black 1991) caused basement uplift, folding, faulting and thrusting of the northern margin of the Amadeus Basin, mostly in a thick-skinned fashion (Shaw et al. 1992). Crustal shortening seems to have been accommodated by the progressive denudation of an upthrust wedge centred near the current northern margin of the Amadeus Basin (Shaw et al. 1992). However, intense ductile faulting occurred in, for example, the case of the Arltunga Nappe Complex (Teyssier 1985), where basement and cover were tectonically interleaved into a nappe 10 km thick. In addition, shear zones of this age are observed throughout the early Proterozoic metamorphic basement of the Arunta Block (e.g. Collins & Teyssier 1988). The event is not discussed further here.

The Musgrave Block

Parts of the mid-Proterozoic Musgrave Block (Fig. 1A) are interpreted as having volcanic and/or sedimentary precursors (Gray 1971, 1977; Daniels 1974; Moore & Goode 1978) of at least two ages. Whole-rock Rb–Sr isochron ages of 1564±12 and 1327±7 Ma are inferred to date distinct protolith ages of rocks north and south of the D_6 Hinckley fault (Gray 1971, 1978; see below). This interpretation is consistent with U–Pb zircon dating of samples from the same area (Sun & Sheraton 1992), and U–Pb dates of zircons obtained by the analysis of granulites from the Amata area in South Australia (Maboko et al. 1991). Inherited zircons of ~1650 Ma have also been found in some granitoids (Sun et al. in press). Although it is probable that different terranes will be defined with further work in the Musgrave Block, currently there is no such clear definition. In the western Musgrave Block, isoclinal, gently inclined to recumbent D_2 folding accompanied the intrusion of pre-S_1 mafic and felsic orthogneisses and post-S_1, pre-S_2 felsic orthogneisses under peak conditions of 5±1 kbar and >750°C at c.1200 Ma (Gray 1978; Sun & Sheraton 1992; Clarke et al. 1995—this issue). Post-S_2 mafic to ultramafic magmatism resulted in the large layered intrusions of the Giles Complex, whilst the terrane was at 6±1 kbar.

Collerson et al. (1972) divided rocks exposed in the central Musgrave Ranges (Fig. 1C) into three terranes separated by east-trending faults, and inferred that these terranes experienced

distinct structural and metamorphic histories. The shallowly south-dipping Woodroffe Thrust (Fig. 1C) separates overlying granulites of the Musgrave Block from an underlying gneiss terrane comprising amphibolite facies rocks of the Olia Gneiss and the Pottoyu Igneous Complex (Forman 1965, 1972). The Olia Gneiss is dominated by orthogneiss that crystallised as early as 1683±56 Ma (Maboko et al. 1992) and was metamorphosed to amphibolite facies as early as 1607±14 Ma, but probably also experienced deformation at 1429±38 Ma (Maboko et al. 1992). Collerson et al. (1972) sub-divided Musgrave Block rocks above the Woodroffe Thrust into central and southern terranes, but Maboko (1988) argued that the only difference between these was that the southern terrane experienced more extensive retrogression.

Granites and gneisses in the Mulga park area of the eastern Musgrave Block (Fig. 1C) have been divided into the Fregon and Mulga Park terranes (Camacho et al. 1991; Edgoose et al. 1993; Camacho & Fanning in press). The Fregon terrane comprises all granulite and transitional granulite facies gneisses that lie above the Woodroffe Thrust and would be broadly equivalent to the central and southern terranes of Collerson et al. (1972; Camacho & Fanning in press). Rocks of the Fregon terrane are as old as ~1550 Ma (Gray 1978; Camacho et al. 1991; Edgoose et al. 1993; Camacho & Fanning in press) and were multiply deformed and metamorphosed to granulite facies at 1200 Ma (Gray 1978). Amphibolite facies rocks below the Woodroffe Thrust are collectively known as the Mulga Park terrane, which includes exposures of what has also been mapped as the Olia Gneiss (Forman 1972) and would be equivalent to the Gneiss terrane of Collerson et al. (1972). However, Camacho & Fanning (in press) infer that the Mulga Park and Fregon terranes are equivalent, with the distinction simply reflecting different metamorphic grades for the ~1200 Ma metamorphic event. Thus, there is complexity in the unit currently defined as the Olia Gneiss (Forman 1965) and further work is needed to delimit the ~1680 Ma gneiss terrane defined in the northern Musgrave Ranges (Collerson et al. 1972; Maboko et al. 1992).

Two complexes of granites, the Ayers Ranges Adamellite and the Kulgera Adamellite intruded the Fregon terrane soon after peak metamorphism, at 1150±12 Ma and 1159±17 Ma respectively (U–Pb on zircons, Edgoose et al. 1993). The Kulgera Adamellite is of the 'enriched' type (Gray, personal communication, 1994). Movement along the Woodroffe Thrust is constrained to between 560 and 520 Ma on the basis of K–Ar and Rb–Sr dating of syn-kinematic muscovite and biotite (Camacho & Fanning 1994).

Whereas significant burial of parts of the currently exposed Musgrave Block most probably occurred owing to over-accretion of Giles Complex sills at ~1080 Ma, parts of the Musgrave Block west of the Tomkinson Ranges were re-exposed before the eruption of the near-contemporaneous Tollu Group volcanics (Daniels 1974; Sun et al. in press). The Tollu Group volcanics are part of the Bentley Supergroup (Daniels 1974), which is inferred to be approximately 7 km thick and includes basalt, rhyolite, rhyodacite, and lesser dolomite and conglomerate. Comagmatic microgranitoid dykes and veins intruded Giles Complex sills in the Tomkinson Ranges, whilst that part of the Musgrave Block remained at considerable depth (Sun et al. in press). This magmatic event is also represented by the Kulgera dyke swarm in the eastern Musgrave Block (Rb–Sr age of 1054±14 Ma, Camacho et al. 1991; Sm–Nd age of 1090±32 Ma, Zhao & McCulloch 1993), the 1076±33 Ma Stuart Dyke swarm in the southern Arunta Block, and possibly by Type A mafic dykes in the Tomkinson Ranges (Clarke et al. 1995—this issue). A third deformation event, D_3, resulted in a system of steep, southeast-trending mylonite zones, which define S_3 and contain a well-developed down-dip L_3 stretching lineation. Type A mafic dykes show marginal to complete recrystallisation to granulite facies mylonitic S_3 assemblages at conditions of about 11 kbar and 700°C (Clarke et al. 1995—this issue). Near-isothermal decompression returned such parts of the Musgrave Block 4–5 kbar late in D_3 (Clarke & Powell 1991b; Clarke et al. 1995—this issue). Parts of the Tollu Group volcanics in the western Tomkinson Ranges were also intensely mylonitised by this D3 event, but these parts of the Musgrave Block probably remained close to the Earth's surface during D_3.

Coarse-grained, ~800 Ma, Type B mafic dykes (Sun & Sheraton 1992; Sun et al. in press) and ~1000 Ma aphanitic Type C mafic dykes cut S_3. The Type B dykes are correlated with the 790±40 Ma Amata dyke swarm in the central Musgrave Block and the southeasterly trending 802±35 Ma Gairdner dyke swarm of the Gawler Craton and Stuart Shelf (Sm–Nd ages, Zhao et al. 1994). In the Tomkinson Ranges, all dykes are cut by a system of mylonite and retrograde shear zones, D_{4-7}. East-trending D_6 ultramylonite ± pseudotachylite zones are the most prominent of the shear zones that represent the effects of the Late Proterozoic to Cambrian Petermann Orogeny (Forman 1965). Examples include the Hinckley and Champs de Mar faults in the Tomkinson Ranges, and the Woodroffe Thrust and related Petermann Nappe in the central Musgrave Block.

The Dean and Townsend Quartzites represent basal units of the southwestern Amadeus Basin (Daniels 1974). They unconformably overlie the Musgrave Block and tectonically overlie the Bentley Supergroup, and are correlated with the Heavitree Quartzite of the northern and eastern Amadeus Basin (Forman 1965; Daniels 1974). Mafic volcanics in the Bitter Springs Formation—which overlies the Heavitee Quartzite in the northern Amadeus Basin—are correlated with the ~800 Ma dykes (Zhao et al. 1994), constraining basin formation as being somewhat older than ~800 Ma. The basin contains several unconformities and Neoproterozoic glacigene sequences (Sturtian, Marinoan) that can be correlated over large areas of Australia (Fig. 1A; Shaw et al. 1991) and may be used to constrain tectonism in adjacent basement rocks. Initial deposition resulted in areally extensive sheets of the basal Heavitree Quartzite and equivalents, followed by the development of a large asymmetric east–west sub-basin in the south, separated by a narrow arch from another shallower sub-basin to the north (Korsh & Kennard 1991, and references therein; Shaw et al. 1991). A profound change in basin morphology occurred near the end of the Proterozoic era, when the main axis of deposition shifted northwards, owing to plate convergence. This tectonism is evident as the Petermann Ranges Orogeny, which thrust the Musgrave Block and juvenile southern Amadeus Basin northwards in nappe complexes (Forman 1965; Forman & Shaw 1973). Crustal overthickening must have occurred in basement rocks, since syntectonic molasse deposits occur in the southern Amadeus Basin: the Mt Currie Conglomerate in the central part of the Amadeus Basin (Korsch & Lindsay 1989; Shaw et al. 1991; Sweet & Crick 1992) and the Sir Frederick Conglomerate in the western Amadeus Basin (Grey 1990). These are thick, poorly sorted conglomerate lenses, which may have clasts up to one metre across (Sweet & Crick 1992), and unconformably overlie equivalents of the 670 Ma Marinoan glacigene sediments in the Amadeus Basin (Grey 1990). Whereas conglomerates are restricted to the southern part of the basin, they interfinger with sandstone lateral equivalents further north (Sweet & Crick 1992). However, effects of the Petermann Orogeny cannot be recognised in the northern Amadeus Basin, where sedimentary rocks that span the period before and after the orogeny were deposited with apparent conformity (Korsch & Lindsay 1989; Shaw et al. 1991).

These restricted molasse deposits developed in shortening basins, causally linked to crustal overthickening which mostly

occurred within basement rocks (Forman 1965; Korsch & Lindsay 1989), although staurolite+kyanite-bearing metapelitic assemblages occur in metamorphosed late Proterozoic sediments along the southern margin of the central Amadeus Basin (Forman 1965). North–south convergence is recorded in large fault zones that cut the Musgrave Block, which are spatially associated with the development of garnet–clinopyroxene–rutile–plagioclase–hornblende–quartz–kyanite assemblages in post-S_3 dykes (Clarke et al. 1995—this issue). These assemblages reflect metamorphic conditions of 14±1 kbar and 700–750°C (Clarke et al. 1995—this issue; see also Ellis & Maboko 1992). To date the metamorphic assemblages, mineral separates of garnet, hornblende, plagioclase, and clinopyroxene were prepared from two samples (9485a and 9485b) of recrystallised dyke from near the western extension of the Woodroffe Thrust (Stewart 1993). The dyke has bulk-rock chemistry and a Nd-isotope initial ratio consistent with it being part of the Type C suite (Sun & Sheraton 1992; Sun et al. in press). The mineral separates and whole-rock samples were then analysed for Sm–Nd values, but isochrons were not obtained, owing to problems of isotopic equilibrium having not been attained between coexisting minerals during metamorphism. Analytical procedure is described in Sun et al. (in press) and results presented in Table 1 and Fig. 2. The data were reduced following the method of Ludwig (1990). Diopside has a closure temperature for Sm diffusion (>850°C; Becker 1993) that is higher than temperature estimates obtained for the D_6 event (Clarke et al. 1995—this issue). Accordingly, an age of 768±110 Ma (Fig. 2), from a two-point line connecting Sm–Nd isotopic ratios from whole rock and clinopyroxene mineral separates, is inferred to be close to the emplacement age, and is consistent with the age inferred for the Type B dykes. Moreover, the clinopyroxene grains in this sample are texturally disequilibrated: they are mostly large igneous porphyroclasts enveloped by S_6 hornblende, although neoblastic grains are observed on grain margins. Neoblastic and porphyroclastic clinopyroxene grains could not be distinguished using microprobe analyses. Garnet in both samples has intergrown fine-grained kyanite and grains are not strongly zoned, but show a restricted range of compositions inferred to reflect variations in the chemistry of the local equilibration volumes that controlled garnet growth. Plagioclase shows a large range in composition (andesine to bytownite) in the recrystallised dykes, which reflects the partial recrystallisation of calcic igneous grains to more sodic metamorphic grains. Complete recrystallisation of the phenocrysts was probably inhibited by kinetic problems related to the paired $NaSiCa_{-1}Al_{-1}$ exchange involved in the recrystallisation. Hornblende composition was uniform throughout the analysed samples.

On the $^{147}Sm/^{144}Nd$ versus $^{143}Nd/^{144}Nd$ plot (Fig. 3), the analysed minerals and whole-rock sample do not fall on a single isochron; they clearly show isotopic disequilibrium. Whereas the data thus require interpretation in terms of

Table 1. Duplicated $^{143}Nd/^{144}Nd$ versus $^{147}Sm/^{144}Nd$ data for mineral separates and a whole-rock sample of rock 9485a, a recrystallised ~800 Ma mafic dyke. Method of analysis is described by Sun et al. (1994). The data are plotted in Figure 2.

Mineral	*Sm (ppm)*	*Nd (ppm)*	$^{147}Sm/^{144}Nd$	$^{143}Nd/^{144}Nd$
plag (1)	1.74	7.57	0.1393	0.512672±7
plag (2)	1.25	5.11	0.1485	0.512701±6
wr (1)	1.64	4.91	0.2020	0.512913±7
wr (2)	1.73	5.08	0.2057	0.512937±6
grt (1)	0.95	2.77	0.2069	0.512908±6
grt (2)	0.96	2.85	0.2036	0.512896±6
cpx (1)	0.94	2.32	0.2447	0.513121±6
cpx (2)	0.83	2.11	0.2387	0.513102±6
hbl (1)	1.30	2.57	0.3055	0.513339±7
hbl (2)	1.08	2.16	0.3025	0.513320±6

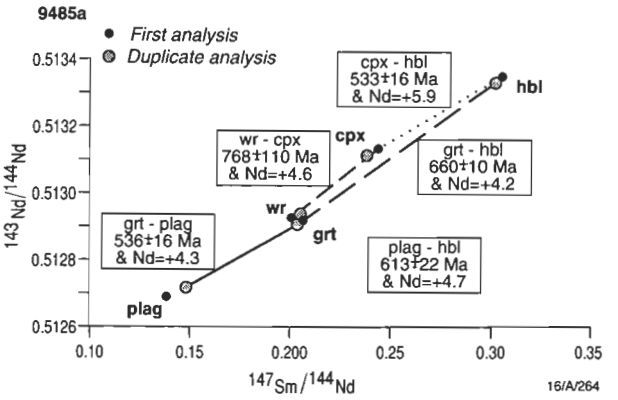

Figure 2. Plot of $^{143}Nd/^{144}Nd$ versus $^{147}Sm/^{144}Nd$ data for mineral separates and a whole rock sample of a recrystallised ~800 Ma mafic dyke prepared following the analytical procedure described in Sun et al. (1994). No isochron was obtained, owing to problems of incomplete isotopic equilibration (discussed in the text). The two-point dates were obtained following the procedure of Ludwig (1990), and their significance is also discussed.

precursor minerals and some speculation (e.g. Thoni & Jagoutz 1992; Jagoutz 1994), such difficulties would appear to be common in 'lower temperature' eclogites where rare-earth elements seem to be less mobile than major elements during recrystallisation (e.g. Gebauer 1990). Sm–Nd data for garnet and plagioclase mineral separates in sample 9485a give a two-point line that defines an age of 536±16 Ma (after Ludwig 1990; Fig. 3) and the hornblende–clinopyroxene pair gives an age of 533±16 Ma. These 'ages' are consistent with the ~530–550 Ma age inferred for the Woodroffe Thrust 200 km further east (Maboko et al. 1992; Camacho & Fanning in press) and are younger than the 670 Ma maximum age of the Petermann Orogeny, which is constrained by the age of Marinoan glacigene sediments that underlie the causally related molasse deposits (Grey 1990). A possible explanation for agreement of these ages can be given in terms of isotopic inheritance of precursor minerals; i.e. garnet inherited the Nd isotopic composition of its precursor mineral plagioclase, whereas hornblende inherited the Nd isotopic composition of its precursor clinopyroxene. The non-radiogenic Nd isotopic composition and low Sm/Nd observed in garnet, in contrast to its normal characteristics (e.g. Jagoutz 1994), are consistent with its derivation from plagioclase. Following this line of reasoning, the ages for the garnet–hornblende pair (660±10 Ma) and plagioclase–hornblende pair (613±22 Ma) have no geological meaning.

Albany–Fraser Orogen

The Albany–Fraser Orogen (Myers & Hocking 1988) extends along the southern and southeastern margin of the Yilgarn Craton (Fig. 1A), and is partially formed from rocks of Yilgarn Craton tectonically reworked during Grenvillean events. It is exposed in two discontinuous segments. The western segment extends from the Darling Fault eastwards to Bremer Bay, where it continues offshore (Whittaker 1989). The eastern segment is exposed between Hopetoun and the Fraser Range, and is composed of two main parts: the Biranup Complex to the northwest, which includes basic rocks of the Fraser Complex, and the Nornalup Complex to the southeast (Fig. 1A; Myers 1994). The boundary between the Biranup Complex and the Nornalup Complex is defined on the basis of discontinuous outcrop, the interpretation of regional aeromagmetic survey data (Myers 1994), and limited U–Pb zircon dating of orthogneiss (Nelson et al. 1994).

On the basis of U–Pb zircon microprobe analyses, Black et al. (1992) found that the northern part of the western segment was derived mostly from Archaean rocks tectonically

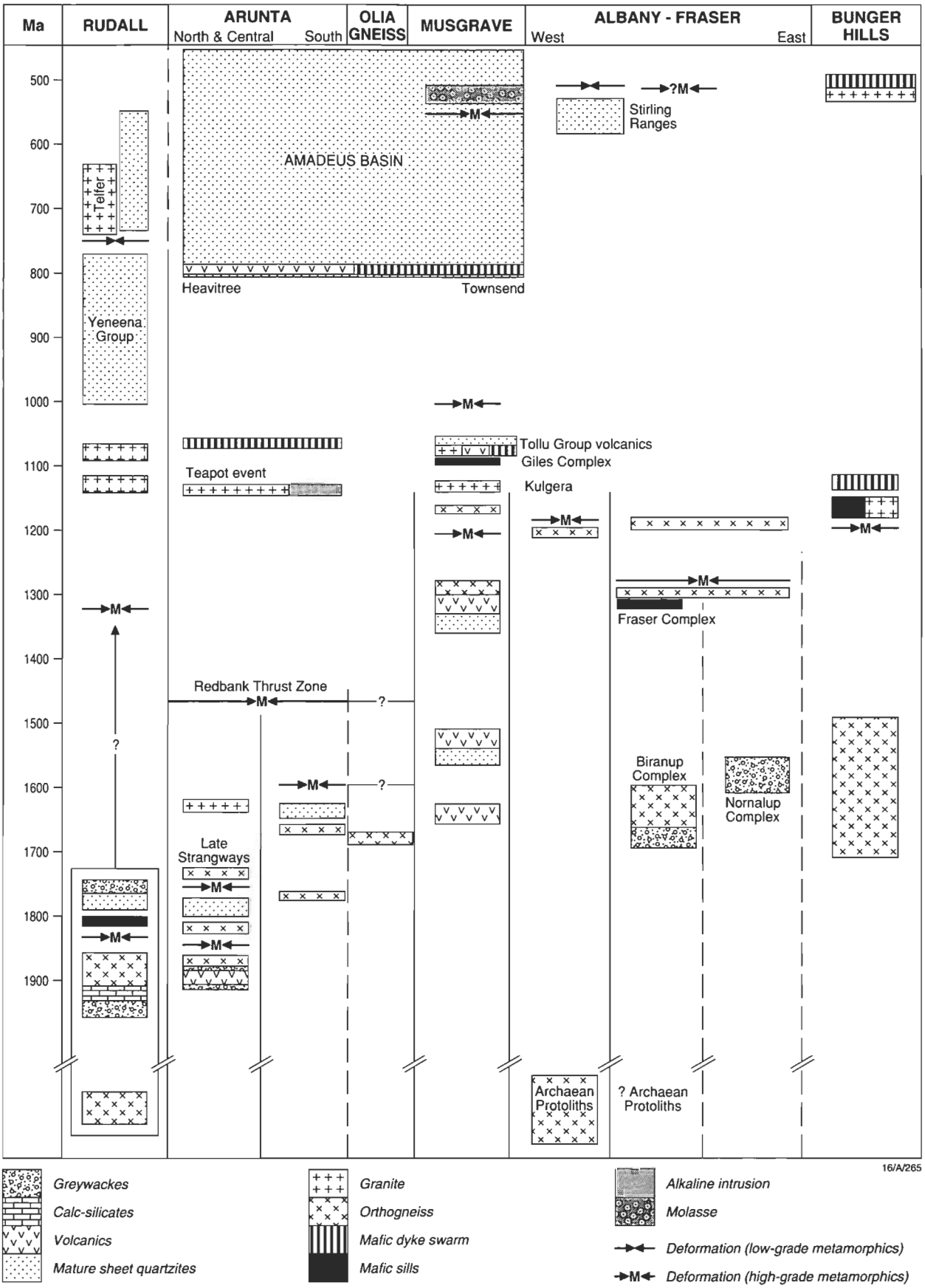

Figure 3. Time–space diagram summarising the geological evolution of the terranes discussed in the text. The thick vertical lines represent terrane distinctions; the lines end where terrane boundaries are transgressed by a magmatic, tectonic or sedimentary event that joins two or more terranes. As described in the text, note the strong correlation of the ~1200 Ma magmatic and metamorphic event through the Musgrave Block, Albany Fraser Orogen, Bunger Hills and (not shown) Windmill Islands. It is possible that 'enriched' style granitoids that intrude both the Arunta and Musgrave Blocks at ~1150 Ma represent a late stage of this event.

reworked during an 1190 Ma (Pidgeon 1990) granulite facies metamorphic and magmatic event. The southern part of the western segment includes protoliths of several ages. Early Proterozoic protolith rocks have been inferred on the basis of ~2100 Ma Sm–Nd model ages, and 1290 Ma enderbitic intrusions are reported from the central part of the segment, on the basis of U–Pb dating of zircons (Black et al. 1992). There is some concern (Nelson et al. in press) that the 2200–2100 Ma Sm–Nd age may reflect mixing of Archaean and younger source rocks, given that the ages have not been confirmed by zircon dating. Black et al. (1992) have inferred that early and mid-Proterozoic rocks were juxtaposed with reworked sections of the Yilgarn Craton during the 1190 Ma metamorphic and deformation event (Beeson et al. 1988). Uplift and cooling of the terrane occurred during the following 100 Ma, on the basis of Rb–Sr mineral ages that are distinctly younger than the zircon ages (Turek & Stephenson 1966; Stephenson et al. 1977; Black et al. 1992).

The eastern part of the Albany–Fraser Orogen contains heterogeneous banded orthogneiss and lesser paragneiss of the Biranup Complex (Myers 1994), which were intruded by regionally extensive gabbros of the Fraser Complex (Doepel 1973; Wilson 1969a, 1969b; Myers 1988). U–Pb analysis of zircons in orthogneiss from the Biranup Complex indicates that they were formed from granitoid intrusion between 1700 and 1600 Ma (Nelson et al. in press). A mineral Sm–Nd date of 1291±21 Ma, interpreted as a crystallisation age, was obtained by Fletcher et al. (1991) on a sample of gabbro from the Fraser Complex. The Biranup and Fraser Complexes were affected by a short-lived granite intrusion and granulite facies metamorphic event at ~1300 Ma (Arriens & Lambert 1969; Bunting et al. 1976; Nelson et al. in press). Owing to the intensity of deformation associated with the metamorphism, the temporal relationship of paragneiss and orthogneiss in the Biranup Complex is unclear. Since the petrology of gneisses in the Fraser and Biranup Complexes is not readily available, details are summarised here (after Ahmat 1983, 1985; G.L. Clarke, unpublished data). The pervasive foliation in metapelitic gneisses is commonly defined by biotite, quartz, K-feldspar, plagioclase, rutile, and idioblastic sillimanite grains that envelop large (up to 3mm diameter) anhedral garnet grains. Foliated cordierite and hercynitic spinel occur in some samples. Average pressure calculations (Powell & Holland, 1988; Holland & Powell 1990) made on a metapelitic gneiss constrain the 1300 Ma event to have involved metamorphic conditions of 6.1±0.4 kbar and 700°C (G.L. Clarke, unpublished data). Occurring with the metapelitic gneisses are orthopyroxene-bearing, biotite-bearing and amphibole-bearing felsic gneisses, quartzite and thinly layered banded iron formation (BIF). Gneisses with the bulk composition of adamellite are made up of well-foliated quartz, plagioclase, mesoperthite, garnet, biotite, hornblende and ilmenite. Garnet is generally coarse-grained and sieve-like, but some occurs as fine-grained symplectites with biotite, quartz and opaque grains that partially replace hornblende. The symplectites are attributed to a second metamorphic event (discussed further below). The cores of many gabbroic bodies preserve ophitic textures, but commonly show limited recrystallisation related to sub-solidus cooling, with igneous olivine replaced by metamorphic orthopyroxene plus hercynitic spinel, and igneous clinopyroxene replaced by metamorphic clinopyroxene plus spinel. The margins of the bodies were more intensely deformed and pervasively recrystallised to hornblende-bearing pyroxene granofels during the ~1300 Ma metamorphic event.

Southeast of the Biranup Complex, extensive orthogneiss, granite and minor metasedimentary gneiss outcrops, which are lithologically similar to the Biranup Complex, have been distinguished as the Nornalup Complex by Myers (1994). On the basis of U–Pb analyses of zircons (Nelson et al. 1994), metasediments as old as ~1570 Ma were intruded by granite, and deformed and metamorphosed at ~1300 Ma before an extensive phase of granite intrusion at ~1150 to 1100 Ma. The Nornalup Complex is inferred to have been accreted to the southeastern margin of the Yilgarn Craton and intruded by granite during the ~1300 Ma orogeny that grossly recrystallised the Biranup and Fraser Complexes.

Close to the (obscured) contact of the Yilgarn Craton, garnet+clinopyroxene±hornblende-bearing amphibolite facies gneisses predominate, in comparison to the pyroxene granofels further to the southeast. The amphibolite facies assemblages partially to pervasively retrogress the earlier granulite facies assemblages (Ahmat 1983, 1985; G.L. Clarke, unpublished data). There are no isotopic data to directly constrain the age of this recrystallisation. Nonetheless, there are two distinct metamorphic events with the overprinting effects of the amphibolite facies recrystallisation becoming progressively more intense (to the northwest) as the Archaean–Proterozoic boundary is approached. The partially retrogressed pyroxene granofels shows reaction textures similar to those in the garnet-bearing gneisses of adamellite composition, described above. In other samples, symplectic intergrowths of garnet, biotite, and quartz replace plagioclase and orthopyroxene grains. The symplectites are random (Ahmat 1985), and thus post-date the pervasive ~1300 Ma granulite facies foliation (Nelson et al. in press). Minor green to brownish green hornblende may occur as thin coronas to orthopyroxene, clinopyroxene or ilmenite grains, but not as separate grains. Biotite is also intergrown with ilmenite. Quartz is present in small amounts and the bulk of the rock is commonly made up of elongate, foliated plagioclase. Metagabbros that were pervasively recrystallised during the M_2 event comprise clinopyroxene (20%), garnet (20%), plagioclase (50%), quartz (5%), and ilmenite (2%), with or without green to brownish green hornblende; ragged, retrogressed grains of orthopyroxene occur in some. Garnet is weakly amoebic and commonly has inclusions of quartz and clinopyroxene. Apatite, K-feldspar and carbonate are common in small amounts. Gneisses with a tonalitic protolith comprise well-foliated plagioclase (40%), quartz (29%), garnet (20%), clinopyroxene (10%), opaques and minor hornblende. Average pressure calculations made on these rocks constrain M_2 conditions to have been 9.3±1.0 kbar and >550°C (Clarke, unpublished data). The effects of this M_2 event in granulite facies gneisses further southeast can be recognised in kyanite-bearing amphibolite facies shear zones (Ahmat 1985) that cut the granulites.

On the basis of regional Rb–Sr and K–Ar dates of ~1270–1220 Ma (Wilson et al. 1960), Fletcher et al. (1991) and Nelson et al. (in press) infer that the ~1300 Ma regional metamorphism in the eastern segment of the Albany–Fraser Orogen was terminated by rapid uplift. Cooling and uplift are inferred to have been induced by the westward thrusting of the orogen onto the Yilgarn Craton (Myers 1988). However, the *retrograde* high-P M_2 assemblages prevalent in the northeast of the orogen segment imply significant post-granulite facies burial of the Biranup and Fraser Complexes. If this burial occurred soon after 1300 Ma, it would be difficult to reconcile with the inferred rapid cooling of the orogen. The field setting of the late high-P rocks is similar to the 550 Ma high-P assemblages in the Musgrave Block, and it is tempting to correlate them, given that tectonism at about this time is evident in the northwards thrusting of post-590 Ma Ediacaran fossil-bearing rocks (Jenkins 1994) of the Stirling Range Formation (Cruse et al. 1993; Cruse & Harris 1994). These rocks unconformably overlie the western segment of the Albany–Fraser Orogen.

East Antarctic Shield

Discontinuous coastal exposures of the Antarctic shield east of 40°E are dominated by a belt of ~1000–1200 Ma magmatism and metamorphism, which is called the Rayner Complex (Sheraton et al. 1980; Tingey 1991) in Enderby and MacRobertson Lands. This belt envelopes Archaean cratons of the Napier Complex, the Vestfold Block, and the southern Prince Charles Mountains, and is diverse, both in terms of protolith (Black et al. 1987; cf. Clarke 1988) and metamorphic characteristics (see Harley & Hensen 1990, and references therein). It may extend to parts of Antarctica that were adjacent to Western Australia in Precambrian times (Fig. 1A), as ~1200 Ma magmatism and granulite facies metamorphism are evident in rocks of the Bunger Hills (Sheraton et al. 1990, 1993; Black et al. 1992). On the basis of U–Pb dating of zircon, igneous precursors to granodioritic orthogneiss were emplaced between 1700 and 1500 Ma, and late Archaean (2640 Ma) tonalitic orthogneiss occurs in the nearby Obruchev Hills (Black et al. 1992; Sheraton et al. 1993). Granulite facies metamorphism and polyphase deformation (Stüwe & Powell 1989, Stüwe & Wilson 1990) at 1190±15 Ma (Sheraton et al. 1993) were followed by emplacement of 1170–1150 Ma plutonic rocks, ranging from gabbro, through quartz monzogabbro and quartz monzodiorite, to granite. The intrusion of abundant dolerite dykes of four chemically distinct suites at about 1140 Ma (Sheraton et al. 1990) was associated with shear zone formation. Later deformation involved extensive pseudotachylite formation in ultramylonite zones (Stüwe & Wilson 1990), and alkaline mafic dykes were emplaced 500 Ma ago.

Metamorphic rocks between Mirny and the Bunger Hills (Fig. 1A) include tonalitic orthogneiss emplaced about 3000 Ma ago and metamorphosed at about 2890 Ma (Black et al. 1992); there is no clear evidence that the ~1200 Ma event affected these rocks (Sheraton et al. 1993). Extensive syenitic to granite plutonism, with post-orogenic or anorogenic (A-type) chemical characteristics, took place at about 516 Ma (Sheraton et al. 1992). To the east of the Bunger Hills are the Windmill Islands, which include amphibolite to granulite facies metabasites, felsic orthogneiss and metapelitic gneiss that were intruded by charnockite and a variety of tholeiitic to alkaline dykes. There seem to have been at least two main phases of metamorphism and magmatism. Some felsic igneous rocks were emplaced during metamorphism as early as ~1500 Ma (Williams et al. 1983), but tectonism and magmatism also occurred at 1172±68 Ma, as the Ardery Charnockite was emplaced at that time (Rb–Sr isochron, Tingey 1991). Granite plutonism also occurred at 1070±36 Ma (Rb–Sr isochron), and biotite Rb–Sr and K–Ar ages of 1160–1060 Ma (Tingey 1991) probably record cooling of the terrane. Thus, there are marked similarities between rocks from this area and those from the Bunger Hills (Sheraton et al. 1993).

Regional correlations

On the basis of current isotopic data (Gray 1978; Sun et al. in press), the ~1650–1300 Ma protoliths of the Musgrave Block were grossly affected by three periods of tectonism: (1) a 1200–1180 Ma event, including metamorphism, granitic intrusion and, possibly, mantle melting; (2) a phase of extensive mantle melting and, most probably, deformation at ~1080 Ma, which gave rise to the Giles Complex and volcanics of the 7 km thick Bentley Supergroup (Daniels 1974), and the Stuart and Kulgera dyke swarms (Zhao & McCulloch 1993); and (3) a ~550 Ma convergent event, which resulted in crustal overthickening in basement rocks (Clarke et al. 1995—this issue) and the thrusting of the Musgrave Block northwards onto a juvenile Amadeus Basin during the Petermann Orogeny (Forman 1965).

These events and those that affected all the other Grenville belts described above have been summarised on a space–time diagram (Fig. 3) to test for regional correlations and equivalent terranes. The ~1200 Ma magmatic and deformation event has strong correlations, which are discussed further below. Whereas the ~1080–1060 Ma magmatism was a Gondwana-wide dyke event (Fig. 3), the tectonism inferred to have shortly followed it in the Musgrave Block appears to be of only local significance. Interpretations linking this magmatism and dyke emplacement to incipient crustal extension that consequently lead to the large Neoproterozoic intracratonic basins throughout the Australian sector of Gondwana (Korsch & Lindsay 1989) are now largely discredited on the basis of the inferred ~800 Ma age for mafic magmatism in the Bitter Springs Formation and the dating of older units of the Adelaide 'Geosyncline' at 80210 Ma (Fanning et al. 1986). Features of these basins are reviewed elsewhere (Preiss & Forbes 1981; Lindsay & Korsch 1991; Korsch & Kennard 1991; Shaw et al. 1991). Effects of high-P recrystallisation in parts of the Musgrave Complex during the ~550 Ma Petermann Orogeny have only recently been recognised (Clarke et al. 1995—this issue), though such effects were predicted on the basis of the large Petermann Nappe Complex and related molasse in the southern Amadeus Basin (Forman 1965; Forman & Shaw 1973). However, significant crustal overthickening at about this time is difficult to place in current regional models, since a widely held view is that central Australia was already within an intracratonic setting at this time (e.g. Shaw et al. 1991). Accordingly, the following discussion concentrates on regional correlations of the ~1080 Ma and ~550 Ma movements. An aspect of regional geology often ignored in regional correlations involves the ephemeral nature of terrane boundaries: the current margins to any metamorphic terrane may have no relevance to the crustal processes that caused its burial and metamorphism. For example, the latitudinal trend of the Musgrave Block has no direct implication for the form of the ~1080 Ma orogeny, since the trend was caused during the ~550 Ma Petermann Orogeny. In rocks that have undergone high-grade metamorphism and polyphase deformation, it should be self-evident that the processes leading to linear geological boundaries occurred very late in the terranes' histories.

A 1200 Ma Gondwana-wide orogen

Magmatic and metamorphic events grossly affected the Musgrave Block, the western Albany–Fraser Orogen, the Bunger Hills and Windmill Islands in the period 1300–1080 Ma (Fig. 3). These events are characterised by extensive mantle-derived magmatism, most extensively developed in the case of the Giles Complex, and contemporaneous low to mid-P granulite facies metamorphism. Although some components have protoliths of distinct lithology and age, this correlation and the juxtaposition of the Albany–Fraser, Bunger Hills, and Windmill Island components in the Gondwana reconstruction (Fig. 1A) suggest that they were also most probably continuous at the time of the ~1200 Ma event. Protolith ages for the Biranup and Nornalup Complexes, the Bunger Hills, and the Windmill Islands would appear to correlate, but are imprecise. Nontheless, all these areas experienced high-grade metamorphism, magmatism and deformation during the ~1200 Ma event. It seems probable that the 1200 Ma orogen extended further west than the Bunger Hills, through Antarctic parts of Gondwana to Rayner Complex rocks (Moores 1991), but there are sufficient complexities in the case of the Albany–Fraser Orogen to caution sweeping correlations. The ~1300 Ma magmatic and tectonic event that grossly affected the eastern segment of the Albany–Fraser Orogen was not as regionally extensive as the ~1200 Ma event, which is evident as felsic plutonism in the eastern segment of the orogen. Whereas it is convincing that the Musgrave Block experienced contemporary orogeny and magmatism, extensive intervening cover

rocks make it difficult to assess the relative positions of these rocks and the Albany–Fraser Orogen at 1200 Ma. Regional AGSO aeromagnetic and gravity data indicate that the Biranup and Nornalup Complexes are not continuous with the Musgrave Block, although the Biranup Complex does have similar magnetisation (high to moderate intensity) and gravity values (high) to those of the Musgrave Block.

The stratigraphic and early tectonic history of the north and central provinces of the Arunta Block shows many similarities with Proterozoic terranes in northern Australia (Page 1988), and it is possible the 1880 Ma orogeny evident in the Mt Doreen area can be correlated with the apparently widespread, but ill-defined, Barramundi Orogeny in Northern Australia (Page 1988; Young et al. 1995). However, the mid-Proterozoic histories of these provinces are quite dissimilar to those of the Grenville-aged belts to the south and southwest (Figs 1a, 3). The three provinces were assembled into the Arunta Block by ~1500–1400 Ma, when the Redbank Thrust Zone developed (Shaw & Black 1991). Whereas the ~1660 Ma orthogneisses that form most of the southern province seem to have no equivalents in the central and northern provinces of the Arunta Block (Black & Shaw 1992; Young et al. 1995), their history appears to be identical to parts of the Olia Gneiss north of the Musgrave Ranges (Maboko et al. 1992): orthogneisses in both areas crystallised at ~1660 Ma, and were metamorphosed once at ~1600 Ma and again at ~1450 Ma. Thus, on the basis of these limited isotopic data, it is possible they are related to or originate from the same terrane. If so, this terrane could then underlie the Amadeus Basin and would have docked with the Arunta Block at ~1450 Ma. Some Musgrave granitoids contain ~1650 Ma inherited zircons (Sun et al. in press), which may indicate a relationship to the Olia Gneiss–southern province terrane. In addition, extensive dyke emplacement characterises all three areas, giving them similarities lacking from the central and northern provinces of the Arunta Block. However, more data are needed for both the southern Arunta province and the composite Olia Gneiss (Maboko et al. 1992; cf. Camacho & Fanning in press) to confirm the correlation. Accepting the correlation between the Olia Gneiss and at least parts of the southern province of the Arunta Block, the original geological features related to the docking of the Musgrave Block can be understood despite the sedimentary cover of the Amadeus Basin (Fig. 1A). On the basis of the temporal and magnetic pole equivalence of the Stuart and Kulgera dyke swarms (Camacho et al. 1991; Zhao & McCulloch 1993), the Arunta and Musgrave Blocks were certainly in their current disposition by the time the 1080 Ma Tollu Group volcanics erupted. Dyke swarms of equivalent age cut rocks in the Bunger Hills. However, the ~1150 Ma intraplate Kulgera Adamellite on the northern margin of the Musgrave Block is contemporary with the enriched intraplate magmatism of the Teapot thermal event near the southern margin of the Arunta Block (Fig. 3). The short 35 Ma interval between the Kulgera granite and the block-wide 1200–1180 Ma magmatism and orogenic events mean the two could be causally related. If so, it is possible that the Teapot thermal event (Black & Shaw 1992) is an expression of the ~1200 Ma event in the southern Arunta Block.

The early stratigraphic and tectonic history of the Rudall Complex is currently poorly constrained, but it has similarities in style with the 1870–1770 Ma history of the Arunta Block (Fig. 3). The 1330 Ma Watrara Orogeny could be equivalent to the 1300 Ma orogeny in the eastern Albany–Fraser Orogen. However, better age data are required to constrain the history of this complex, which must have had its current disposition with respect to the Pilbara Craton by the time the Yeneena Group was deposited at ~1000 Ma (Williams 1990).

A late Proterozoic suture through central Australia?

The northwest-trending Paterson Orogeny has been correlated with the late Proterozoic Petermann Orogeny in central Australia (Myers & Hocking 1988). However, the two appear to be significantly different in age (Fig. 3)—pre-690±48 Ma in the case of the Paterson Orogeny and ~550 Ma for the Petermann Orogeny—but more data are required to confirm the age of the post-670 Ma high-P metamorphism in the Musgrave Block. On the basis of current data, it is more likely that the Paterson Orogeny is equivalent in age to pre-670 Ma unconformities recorded in the Amadeus Basin stratigraphy (see Lindsay & Korsch 1991; Shaw et al. 1991).

P–T estimates of D_6 assemblages, made on the basis of high-P mineral assemblages defining D_6 shear zones, which include the Woodroffe Thrust, are consistent with parts or all of the Musgrave Block and Olia Gneiss having been overthrust by a 30 km thick continental slab, some time after the development of S_3 and before the development of the Woodroffe Thrust (Clarke et al. 1995—this issue). Such tectonism suggests that crustal thickening as a consequence of convergence at ~550 Ma was the principal tectonic event in shaping the regional structure of south-central Australia (Shaw et al. 1991; Moores 1991). It is unclear where any boundary between two previously separate continental plates would lie with respect to the Musgrave Block. Further work may indicate that the Musgrave Block comprises several unrelated terranes, since Gray (1978) inferred distinct protoliths north and south of the Hinckley Fault and the Musgrave Block is tectonically interleaved with the Olia Gneiss and cover rocks in the Petermann Nappe (Forman 1965). Positioning a plate boundary anywhere near the Musgrave Block at ~550 Ma is controversial, given that the Musgrave Block may represent an emergent area surrounded by areally extensive, possibly interconnected, intracratonic superbasins that covered much of central, northern and northwestern Australia (e.g. Walter et al. 1994). Whereas convincing correlations exist between these superbasins, models for their spatial relationships require further testing and palaeomagnetic information.

From a regional perspective, the Paterson Orogeny seems to be the wrong age to be equivalent to the ~550 Ma event and no molasse has been reported from the Yeneena Group (cf. Myers 1990). Also, on the basis of available isotopic data, no high-grade rocks of equivalent age have been reported from the Albany–Fraser Orogen. However, the garnet+clinopyroxene M_2 assemblages along the northwestern margin of the Fraser Range are remarkably similar in field setting to the ~550 Ma assemblages of the Musgrave Block, and we speculate that the two could be contemporary. Tectonism of similar age affected the Albany–Fraser Orogen, since Ediacaran fossil-bearing strata were thrust northwards after 590 Ma. If these three tectonic events can be correlated, we speculate that the Petermann Orogeny could reflect the convergence of part of the east Antarctic Shield with the Musgrave Block and Yilgarn Craton. The segment of east Antarctic shield would comprise rocks currently beneath the Officer Basin, the eastern segment of the Albany–Fraser Complex, and the Windmill Islands. Certainly, further work is required to date the M_2 assemblages in the Fraser Range and obtain apparent magnetic pole data on dykes from the Bunger Hills and the Albany–Fraser Orogen to clarify these theories.

Acknowledgements

D. Nelson, D. Young, A. Camacho, and W.J. Collins generously provided unpublished isotopic data. R. Shaw, G. Warren, J. Sheraton, and A. Camacho made useful comments on parts of earlier versions of the manuscipt. We thank Shuguang Li for helping with the interpretation of the Sm–Nd isotopic

systematics of sample 9485a and A. Whittaker for a helpful review. GLC acknowledges support from the Division of Regional Geology and Minerals, Western Musgrave Project (211.14), of the Australian Geological Survey Organisation, and Australian Research Council Grant No. A39230559. RWW acknowledges support from an Australian post-graduate award. This is a contribution to IGCP project 304 'Lower Crustal Processes'.

References

Ahmat, A.L., 1983. Petrological Report 1250, Fraser Range, Norseman & Zanthus 1:250,000 sheets. Geological Survey of Western Australia, Perth (unpublished).

Ahmat, A.L. 1985. Petrological Report 1380, High-grade gneisses and basic granulites from Fraser Range. Geological Survey of Western Australia, Perth (unpublished).

Arriens, P.A. & Lambert, I.B., 1969. On the age and strontium isotopic geochemistry of granulite facies rocks from the Fraser Range, Western Australia, and Musgrave Ranges, central Australia. In: Granulites facies, Geological Society of Australia Special Publication 2, 377–388.

Becker, H., 1993. Garnet peridotite and eclogite Sm–Nd mineral ages from the Lepontine dome (Swiss Alps): new evidence for Eocene high-pressure metamorphism in the central Alps. Geology, 21, 599–602.

Beeson, J., Delor, C.P. & Harris, L.B., 1988. A structural and metamorphic traverse across the Albany Mobile Belt, Western Australia. Precambrian Research, 40/41, 117–136.

Black L.P. & Shaw, R.D., 1992. U–Pb zircon chronology of prograde Proterozoic events in the central and southern provinces of the Arunta Block, central Australia. Australian Journal of Earth Sciences, 39, 153–171.

Black L.P., Harley, S.L., Sun, S.S. & McCulloch, M.T., 1987. The Rayner Complex of East Antarctica: complex isotopic systematics within a Proterozoic mobile belt. Journal of Metamorphic Geology, 5, 1–26.

Black, L.P., Harris, L.B. & Delor, C.P., 1992. Reworking of Archaean and Early Proterozoic components during a progressive, Middle Proterozoic tectonothermal event in the Albany Mobile Melt, Western Australia. Precambrian Research, 59, 95–123.

Black, L.P., Shaw, R.D. & Offe, L.A., 1980. The age of the Stewart Dyke swarm and its bearing on the onset of late Precambrian sedimentations in central Australia. BMR Journal of Australian Geology & Geophysics, 8, 129–138.

Black, L.P., Shaw, R.D. & Stewart, A.J., 1983. Rb–Sr geochronology of Proterozoic events in the Arunta Inlier, central Australia. BMR Journal of Australian Geology & Geophysics, 8, 129–138.

Black L.P., Sheraton, J.W., Tingey, R.J. & McCulloch, M.T., 1992. New U–Pb ages from the Denman Glacier area, east Antarctica, and their significance for Gonwana reconstruction. Antarctic Science, 4, 447–460.

Blake, D.H. & Page, R.W. 1988. The Proterozoic Davenport Province, central Australia: regional geology and geochronology. Precambrian Research, 40/41, 341–362.

Blake, D.H., Stewart, A.J. & Sweet, I.P., 1986. The Proterozoic Hatches Creek Group, an ensialic sandstone–bimodal volcanic association in association in central Australia. Transactions of the Geological Society of South Africa, 89, 243–251.

Bunting, J.A., de Laeter, J.R. & Libby, W.G., 1976. Tectonic subdivisions and geochronology of the northeastern part of the Albany–Fraser Province, Western Australia. Geological Survey of Western Australia, Annual Report 1975, 117–126.

Camacho, A. & Fanning, C.M., in press. Some isotopic constraints on the evolution of the granulite and upper amphibolite facies terranes in the eastern Musgrave Block, central Australia. Precambrian Research.

Camacho, A., Simons, B. & Schmidt, P.W., 1991. Geological and palaeomagnetic significance of the Kulgera Dyke Swarm, Musgrave Block, NT, Australia. Geophysical Journal International, 107, 37–45.

Chin R.J. & deLaeter J.R. 1981. The relationship of new Rb–Sr isotopic dates from the Rudall Metamorphic Complex to the geology of the Paterson Province. Geological Survey of Western Australia Annual Report, 1980, 80–87.

Chin R.J., Williams I.R., Williams S.J. & Crowe R.W.A. 1980. Rudall 1:250,000 Geological Map sheet and Explanatory Notes. Geological Survey of Western Australia, Perth.

Clarke, G.L., 1988. Structural constraints on the Proterozoic reworking of Archaean crust in the Rayner Complex, MacRobertson and Kemp Land coast, East Antarctica. Precambrian Research, 40/41, 137–156.

Clarke, G.L., 1991. Proterozoic tectonic reworking in the Rudall Complex, Western Australia. Australian Journal of Earth Sciences, 38, 31–44.

Clarke, G.L. & Powell, R., 1991a. Proterozoic granulite facies metamorphism in the southeastern Reynolds Range, central Australia: geological context, P–T path and overprinting relationships. Journal of Metamorphic Geology, 9, 267–281.

Clarke, G.L. & Powell, R., 1991b. Decompressional corona and symplectite textures in granulites of the Musgrave Complex, central Australia. Journal of Metamorphic Geology, 9, 441–450.

Clarke, G.L., Collins, W.J. & Vernon, R.H., 1990. Successive early Proterozoic metamorphic events in the Anmatjira Range, central Australia. Journal of Metamorphic Geology, 8, 65–88.

Clarke, G.L., Buick, I.S., Glikson, A.Y., & Stewart, A.J., 1995. Timing of Giles Complex intrusion and multiple high-P events in the western Musgrave Block, central Australia. AGSO Journal of Australian Geology & Geophysics, this issue.

Collerson, K.D., Olliver, R.L. & Rutland, R.W.R., 1972. An example of structural and metamorphic relationships in the Musgrave Orogenic Belt, central Australia. Journal of the Geological Society of Australia, 18, 379–393.

Collins, W.J. & Shaw, R.D., in press. Geochronological constraints on orogenic events in the Arunta Inlier. Precambrian Research.

Collins, W. J. & Tessyier, 1989. Crustal scale ductile fault systems in the Arunta Inlier, central Australia. Tectonophysics,158, 49–66.

Collins, W.J. & Williams, I.S., in press. Short-lived Proterozoic tectonic cycles in the northern Arunta Inlier, central Australia. Precambrian Research.

Collins, W.J., Vernon, R.H. & Clarke, G.L., 1991. Discrete Proterozoic structural terranes associated with high-T, low-P metamorphism, Anmatjira Range, Arunta Inlier, central Australia: tectonic implications. Journal of Structural Geology, 13, 1157–1171.

Collins, W.J., Williams, I.S. & Shaw, S.E., in press. Age of the Ormiston Pound Granite: implications for Mesoproterozoic evolution of the Arunta Inlier, central Australia. Precambrian Research.

Cooper, J.A., Mortimer, G.E. & James, P.R.,1988. Rate of Arunta Inlier evolution at the eastern margin of the Entia Dome, Central Australia. Precambrian Research,40/41, 217–232.

Cruse, T. & Harris, L.B., 1994. Ediacaran fossils from the Stirling Range Formation, Western Australia. Precam-

brian Research, 67, 1–10.
Cruse, T., Harris, L.B. & Rasmenn, B., 1993. The discovery of Ediacaran trace and body fossils in the Stirling Range Formation, Western Australia: Implications for sedimentation and deformation during the 'Pan-African' orogenic cycle. Australian Journal of Earth Sciences, 40, 293–296.
Daniels J.L. 1974. The geology of the Blackstone Region Western Australia. Bulletin of the Geological Survey of Western Australia, 123, 257 pp.
Davidson, A., 1995. A review of the Grenville orogen in its North American type area. AGSO Journal of Australian Geology & Geophysics, this issue.
Doepel, J.J.G., 1973. Norseman, Western Australia, 1:250,000 geological mapsheet and explanatory notes. Geological Survey of Western Australia, Perth.
Dunlap, J., Teyssier, C., McDougall, I. & Baldwin, S., 1991. Ages of deformation from K/Ar and $^{40}Ar/^{39}Ar$ dating of white micas. Geology, 19, 1213–1216.
Dunn P.R., Plumb K.A. & Roberts H.G., 1966. A proposal for time-stratigraphic subdivision of the Australian Precambrian. Journal of the Geological Society of Australia, 13, 593–608.
Edgoose, C.J., Camacho, A., Wakelin-King, G.A. & Simons, B.A., 1993. Kulgera 1:250,000 geological map sheet and explanatory notes. Northern Territory Geological Survey, Darwin, Australia.
Ellis, D.J. & Maboko, M.A.H., 1992. Precambrian tectonics and the physicochemical evolution of the continental crust. I. The gabbro eclogite transition revisited. Precambrian Research, 55, 491–506.
Etheridge, M.A., Rutland, R.W.R. & Wyborn, L.A., 1987. Orogenesis and tectonic processes in the early Proterozoic of northeastern Australia. In: Kroner, A. (editor), Precambrian lithospheric evolution. American Geophysical Union Geodynamic Series, 17, 131–147.
Fanning, C.M., Ludwig, K.R., Forbes, B.G. & Preiss, W.W., 1986. Single and multiple grain U–Pb zircon analyses for the early Adelaidean Rook Tuff, Willouran ranges, South Australia. 8th Australian Geological Convention, Adelaide, Geological Society of Australia, 15, 71–72 (abstract).
Fletcher, I.R., Myers, J.S. & Ahmat, A.L., 1991. Isotopic evidence on the age and origin of the Fraser Complex, Western Australia: a sample of mid-Proterozoic lower crust. Chemical Geology, 87, 197–216.
Foden, J., Buick, I. & Mortimer, G., 1988. The petrology and geochemistry of granitic gneisses from the east Arunta Inlier, central Australia: implications for Proterozoic crustal development. Precambrian Research, 40/41, 233–259.
Forman D.J. 1965. Ayers Rock, Northern Territory, 1:250,000 Geological Map Sheet. Bureau of Mineral Resources, Geology & Geophysics, Canberra.
Forman, D.J., 1972. Petermann Ranges 1:250,000 Geological Map Sheet. Bureau of Mineral Resources, Geology & Geophysics, Canberra.
Forman D.J. & Shaw R.D., 1973. Deformation of the crust and mantle in central Australia. Bureau of Mineral Resources, Australia, Bulletin 144.
Fraser, A.R., 1976. Gravity provinces and their nomenclature. BMR Journal of Australian Geology & Geophysics, 1, 350–352.
Gebauer, D., 1990. Isotopic systems—geochronology of eclogites. In: Carswell, D.A. (editor), Eclogite facies rocks. Blackie, London, p. 141–159.
Glikson, A.Y., 1986. An upthrusted early Proterozoic basic granulite–anorthosite suite and anatectic gneisses, southwest Arunta block, central Australia: evidence on the nature of the lower crust. Transactions of the Geological Society of South Africa, 89, 263–283.
Glikson, A.Y., 1987. Regional structure and evolution of the Redbank–Mount Zeil thrust zone: a major lineament in the Arunta inlier, central Australia. BMR Journal of Australian Geology & Geophysics, 10, 89–107.
Goscombe, B., 1991. Intense non-coaxial shear and the development of mega-scale sheath folds in the Arunta Block, central Australia. Journal of Structural Geology, 13, 299–318.
Goscombe, B., 1992a. High-grade reworking of central Australian granulites. Part 1. Structural evolution. Tectonophysics, 204, 361–399.
Goscombe, B., 1992b. High-grade reworking of central Australian granulites: metamorphic evolution of the Arunta Complex. Journal of Petrology, 33, 917–962.
Gray, C.M., 1971. Strontium isotopic studies on granulites. Ph.D. thesis, Australian National University, Canberra (unpublished).
Gray, C.M., 1977. The geochemistry of central Australian granulites in relation to the chemical and isotopic effects of granulite facies metamorphism. Contributions to Mineralogy and Petrology, 65, 79–89.
Gray C.M. 1978. Geochronology of granulite facies gneiss in the Western Musgrave Block, central Australia. Journal of the Geological Society of Australia, 25, 403–414.
Grey, K., 1990. Amadeus Basin. In: Trendall, A. (editor). Geology and mineral resources of Western Australia. Geological Survey of Western Australia, Memoir 3, p. 335–348.
Hand, M., Dirks, P., Powell, R. & Buick, I., 1992. How well established is isobaric cooling in Proterozoic orogenic belts? An example from the Arunta Inlier, central Australia. Geology, 20, 649–652.
Harley, S.L. & Hensen, B.J., 1990. Archaean and Proterozoic high-grade terranes of east Antarctica (40–80° E): a case study of diversity in granulite facies metamorphism. In: Ashworth, J.R. & Brown, M. (editors). High temperature metamorphism and crustal anatexis. Mineralogical Society Special Publication, 320–370.
Hickman, A.H. & Clarke, G.L., 1993. Broadhurst 1:100,000 Special Mapsheet and Explanatory Notes. Geological Survey of Western Australia, Perth.
Holland, T.J.B. & Powell, R., 1990. An enlarged and updated internally consistent dataset with uncertainties and correlations: the system K_2O–Na_2O–CaO–MgO–MnO–FeO–Fe_2O_3–Al_2O_3–TiO_2–SiO_2–C–H_2O–O_2. Journal of Metamorphic Geology, 8, 89–124.
Iyer,S. S., Woodford, P. J. & Wilson, A. F., 1976. Rb–Sr isotopic studies of a polymetamorphic granulite terrain, Strangways Range, central Australia. Lithos, 9, 211–224.
Jagoutz, E., 1994. Isotopic systematics of metamorphic rocks. In: Lanphere, M.A.,Dalrymple, G.B. & Turrin, B.D. (editors), Abstracts of the Eighth International Conference on Geochonology, Cosmochronology, and Isotope Geology. United States Geological Survey, Circular 1107, 156.
Jenkins, R.J.F., 1984. Ediacaran events: boundary relationships and correlation of key sections, especially in 'Amorica'. Geological Magazine, 121, 635–643.
Korsch, R.J. & Kennard, J.M. (editors), 1991. Geological and geophysical studies in the Amadeus Basin, central Australia. Bureau of Mineral Resources, Australia, Bulletin 236, 594 pp.
Korsch, R.J. & Lindsay, J.F., 1989. Relationship between deformation and basin evolution in the intracratonic Amadeus Basin, central Australia. Tectonophysics, 158, 5–22.
Krogh, T.E., 1994. Precise U–Pb ages for Grenvillean and pre-Grenvillean thrusting of Proterozoic and Archaean

metamorphic assemblages in the Grenville Front tectonic zone, Canada. Tectonics, 13, 963–982.

LaFrance, B., Clarke, G.L., Collins, W.J. & Williams, I.S., in press. The emplacement of the Wuluma granite: melt generation during gravitational collapse of a thickened crust, Arunta Block, central Australia. Precambrian Research.

Langworthy, A.P. & Black, L.P., 1978. The Mordor Complex: a highly differentiated potassic intrusion with kimberlitic affinities in central Australia. Contributions to Mineralogy & Petrology, 67, 51–62.

Lindsay, J.F. & Korsch, R.J., 1991. The evolution of the Amadeus Basin, central Australia. Bureau of Mineral Resources, Australia, Bulletin 236.

Ludwig, K.R., 1990. ISOPLOT—a plotting and regression program for radiogenic-isotope data for IBM-PC compatible computers, version 2.11. US Geological Survey, Open File Report 88–557, Revision of August 7, 1990, 33 pp.

Maboko, M.A.H., 1988. Metamorphic and geochronological evolution in the Musgrave Ranges, central Australia. Unpublished Ph.D. thesis, Australian National University.

Maboko M.A.H., Williams I.S. & CompstonW. 1991. Zircon U–Pb chronometry of the pressure and temperature history of granulites in the Musgrave Ranges, central Australia. Journal of Geology, 99, 675–697.

Maboko M.A.H., Williams I.S. & CompstonW., 1992. Geochronological evidence for ~530–550 Ma juxtaposition of two Proterozoic metamorphic terranes in the Musgrave Ranges, central Australia. Australian Journal of Earth Sciences, 39, 457–471.

Majoribanks, R.W. & Black, L.P., 1974. Geology & geochronology of the Arunta Complex, north of Ormiston George, central Australia. Journal of the Geological Society of Australia, 21, 291–299.

McCulloch, M.T., 1987. Sm–Nd isotopic constraints on the evolution of Precambrian crust in the Australian continent. In: Proterozoic lithospheric evolution. American Geophysical Union Geodynamic Series, 17, 115–130.

McKnight, R., 1992. Constraints on the origin of Broadhurst stratabound Cu mineralization with emphasis on stratigraphic setting and timing of mineralization. B.Sc (Hons) thesis, University of Western Australia, Nedlands, W.A., 81pp (unpublished).

McNaughton N.J. & Goellnicht N.M. 1990. The age and radiothermal properties of the Mount Crofton Granite, Telfer area, Western Australia. Australian Journal of Earth Sciences,37, 103–106.

Moore A.C. & Goode A.D.T. 1978. Petrography and origin of granulite facies rocks in the western Musgrave Block, central Australia. Journal of the Geological Society of Australia, 25, 341–358.

Moores, E.M., 1991. Southwest U.S.–east Antarctic (SWEAT) connection: a hypothesis. Geology, 19, 425–428.

Mork, M.B. & Mearns, E.W., 1986. Sm–Nd isotopic systematics of a gabbro–eclogite transition. Lithos, 19, 255–267.

Mortimer, G.E., Cooper, J.A. & James, P.R., 1987. U–Pb and Rb–Sr geochronology and geological evolution of the Harts Range ruby mine area of the Arunta inlier, central Australia. Lithos,20, 445–467.

Myers, J.S., 1988. The Fraser Complex—a major layered intrusion in Western Australia. Geological Survey of Western Australia, Annual Report 1987, 57–66.

Myers, J.S., 1990. Precambian tectonic evolution of part of Gondwana, southwestern Australia. Geology, 18, 537–540.

Myers, J.S., 1994. Esperence 1:1,000,000 geological map sheet and explanatory notes. Geological Survey of Western Australia, Perth.

Myers J.S. & Hocking R.M. 1988. Geological map of Western Australia, and explanatory notes. Geological Survey of Western Australia, Perth.

Nelson, D.R., Black, L.P. & McCulloch, M.T., 1989. Nd–Pb isotopic characteristics of the Mordor Complex, Northern Territory: mid-Proterozoic potassic magmatism from an enriched mantle. Australian Journal of Earth Sciences, 36, 541–551.

Nelson, D.R., Nutman, A.P. & Myers, J.S., in press. Chronology of geological events in the eastern part of Albany–Fraser Orogen, Western Australia. Precambrian Research.

Norman, A.R. & Clarke, G.L., 1990. A barometric response to late compression in the Strangways Metamorphic Complex, Arunta Block, central Australia. Journal of Structural Geology, 12, 667–684.

Page R.W. 1988. Geochronology of early to middle Proterozoic fold belts in northern Australia: a review. Precambrian Research, 40/41, 1–19.

Page R.W. & Williams, I.S., 1988. Age of the Barramundi Orogeny in northern Australia by means of ion-probe and conventional U–Pb zircon studies. Precambrian Research, 40/41, 21–36.

Palfreyman W.D., Stewart A.J., Bultitude J.M. & Chan R.A. 1976. Geology of Australia map sheet. Bureau Mineral Resources, Geology & Geophysics, Canberra.

Pidgeon, R.T., 1990. Timing of plutonism in the Proterozoic Albany Mobile Belt, southwestern Australia. Precambrian Research, 47, 157–167.

Plumb, K.A., 1985. Sub-division and correlation of late Precambrian serquences in Australia. Precambrian Research, 29, 303–329.

Powell, R. & Holland, T.J.B., 1988. An internally consistent dataset with uncertainties and correlations: 3. Applications to geobarometry, worked examples and a computer program. Journal of Metamorphic Geology, 6, 173–204.

Preiss, W.V. & Forbes, B.G., 1981. Stratigraphy, correlation and sedimentary history of Adelaide (late Proterozoic) basins in Australia. Precambrian Research, 15, 255–304.

Shaw, R.D., 1994. Structure and tectonic development of the Mt Doreen 1:250K sheet area. Australian Geological Survey Organisation, Record 1994/54.

Shaw, R.D. & Black, L.P., 1991. History and tectonic implications of the Redbank Thrust Zone, central Australia, based on structural, metamorphic and Rb–Sr isotopic evidence. Australian Journal of Earth Sciences, 38, 307–332.

Shaw, R.D., Stewart, A.J. & Black, L.P., 1984. The Arunta Inlier: a complex ensialic mobile belt in central Australia. Part 2: Tectonic history. Australian Journal of Earth Sciences, 31, 457–486.

Shaw, R.D., Etheridge, M.A. & Lambeck, K., 1991. Development of the Late Proterozoic to Mid-Palaeozoic, intracratonic Amadeus Basin in central Australia: a key to understanding tectonic forces in plate interiors. Tectonics, 10, 688–721.

Shaw R.D., Zeitler, P.K., McDougall, I. & Tingate, P.R., 1992. The Palaeozoic history of an unusual intracratonic thrust belt in central Australia based on ^{40}Ar–^{39}Ar, K–Ar and fission track dating. Journal of the Geological Society, London, 149, 937–954.

Sheraton, J.W. & Sun, S-S., 1995. Geochemistry and origin of felsic igneous rocks of the western Musgrave Block. AGSO Journal of Australian Geology & Geophysics, this issue.

Sheraton, J.W., Offe, L.A., Tingey, R.J. & Ellis, D.J. 1980. Enderby Land, Antarctica—an unusual Precambrian

high grade terrain. Journal of the Geological Society of Australia, 27, 1–18.

Sheraton, J., Black, L.P., McCulloch, M.T. & Oliver, R.L., 1990. Age and origin of a compositionally varied mafic dyke swarm in the Bunger Hills, east Antarctica. Chemical Geology, 85, 215–246.

Sheraton, J., Black, L.P. & Tindle, A.G., 1992. Petrogenesis of plutonic rocks in a Proterozoic granulite facies terrane—the Bunger Hills, east Antarctica. Chemical Geology, 97, 163–198.

Sheraton, J.W., Tingey, R.J., Black, L.P. & Oliver, R.L., 1993. Geology of the Bunger Hills area, Antarctica: implications for Gondwana reconstructions. Antarctic Science, 5, 85–102.

Sivell, W.J., 1988. Geochemistry of metatholiites from the Harts Range, central Australia: implications for mantle source heterogeneity in a Proterozoic mobile belt. Precambrian Research, 40/41, 261–275.

Sivell, W.J. & McCulloch, M.T., 1991. Neodymium isotope evidence for ultra-depleted mantle in the early Proterozoic. Nature, 354, 384–387.

Sivell, W.J., Mortimer, G.E. & McCulloch, M.T., 1992. Sm–Nd isotopic study of mantle crust interaction in the Harts Range meta-igneous complex: implications for the origin of anorthosites. Geological Society of Australia, Abstracts, 32, p. 21.

Stephenson, N.C.N., Russell, T.G., Stubbs, D. & Kalocsai, G.I.Z., 1977. Potassium–argon ages of hornblendes from Precambrian gneisses from the south coast of Western Australia. Journal of the Royal Society of Western Australia, 59, 105–109.

Stewart A.J., 1981. Reynolds Range Region, Northern Territory 1:100,000 special sheet. Bureau Mineral Resources, Geology & Geophysics, Canberra.

Stewart, A.J., 1993. Western extension of the Woodroffe Thrust Musgrave Block, central Australia. AGSO Research Newsletter, 18, 5–6.

Stewart A.J., Shaw R.D. & Black L.P. 1984. The Arunta Inlier: a complex ensialic mobile belt in central Australia. Part 1: stratigraphy, correlations and origin. Australian Journal of Earth Sciences, 31, 445–455.

Stüwe, K. & Powell, R., 1989.Metamorphic evolution of the Bunger Hills, east Antarctica: evidence for substantial post-metamorphic peak compression with minimal cooling in a Proterozoic orogenic event. Journal of Metamorphic Geology,7, 449–464.

Stüwe, K.& Wilson, C.J.L., 1990. Interaction between deformation and charnockite emplacement in the Bunger Hills, east Antarctica. Journal of Structural Geology, 12, 767–783.

Sun, S-S. & Sheraton, J., 1992. Zircon U/Pb chronology, tectonothermal and crust-forming events in the Tomkinson Ranges, Musgrave Block, central Australia. AGSO Research Newsletter, 17, 9–10.

Sun, S-S., Warren, R.G. & Shaw, R.D., 1995. Nd isotope study of granites from the Arunta Inlier, central Australia: constraints on geological models and limitation ofthe method. Precambrian Research, 71.

Sun, S-S., Gray, C.M.,Sheraton, J.W., Glikson, A.Y. & Stewart, in press. Zircon U–Pb chronology and neodymium isotope study of tectonothermal and crust-forming events in the Tomkinson Ranges, western Musgrave Block, central Australia. AGSO Journal of Australian Geology & Geophysics.

Sweet, I.P. & Crick, I.H., 1992. Uluru & Kata Tjuta; A geological history. Australian Geological Survey Organisation, Canberra, 27 pp.

Teyssier, C., 1985. A crustal scale system in an intracratonic environment. Journal of Structural Geology, 7, 689–700

Teyssier, C., Amri, C. & Hobbs, B.E.,1988. Southern Arunta Block: the internal zones of a Proterozoic overthrust in central Australia. Precambrian Research, 40/41, 157–173.

Thoni, M. & Jagoutz, E., 1992. Some aspects of dating eclogites in orogenic belts: Sm–Nd, Rb–Sr, and Pb–Pb isotopic results from the Austroalpine Saualpe and Koralpe type-locality (Carinthia/Styria, southeastern Austria). Geochemica et Cosmochimica Acta, 56, 347–368.

Tingey, R.J., 1991. The regional geology of Archaean and Proterozoic rocks in Antarctica. In: Tingey, R.J. (editor). The geology of Antarctica. Clarendon Press, Oxford. 1–73.

Turek, A. & Stephenson, N.C.N., 1966. The radiometric age of the Albany Granite and the Stirling Range Beds, south-west Australia. Journal of the Geological Society of Australia, 13, 449–456.

Veevers, J.J. & Eittreim, S.L., 1988. Reconstruction of Antarctica and Australia at break-up (955 Ma) and before rifting (160 Ma). Australian Journal of Earth Sciences, 35, 355–362.

Vernon, R.H., Clarke, G.L. & Collins, W.J., 1990. Local, mid-crustal granulite facies metamorphism and melting: an example in the Mt Stafford area, central Australia. In: Ashworth, J.R. & Brown, M. (editors). High temperature metamorphism and crustal anatexis. Mineralogical Society Special Publication, 272–319.

Walter, M.R., Veevers, J.J., Calver, C.R. & Grey, K., in press. Neoproterozoic stratigraphy of the Centralian Superbasin, Australia. Precambrian Research.

Warren, R.G., 1983. Metamorphism and tectonic evolution of granulites, Arunta Block, central Australia. Nature, 305, 300–303.

Warren, R.G., 1994. Implications of Pb-isotope data for tectonstratigraphic correlations in the Proterozoic of central Australia. AGSO Research Newsletter, 20,11–13.

Whittaker, A., 1989. A geophysical model of the Precambrian of the Albany 1:1M sheet, Western Australia, and its relevance to economic geology. Exploration Geophysics, 20, 195–199.

Williams, I.R., 1990. Rudall Complex & Yeneena Basin. In: Geology and mineral resources of Western Australia. Geological Survey of Western Australia, Memoir 3, 276–282.

Williams, I.S., Compston, W., Collerson, K.D., Arriens, P.A. & Lovering, J.F., 1983. A reassessment of the age of the Windmill Metamorphics, Casey area. In: Oliver, R.L., James, P.R.& Jago, J.B. (editors), Antarctic earth science. Australian Academy of Sciences, Canberra. 73–76.

Wilson, A.F., 1969a. The pyroxene granulites and associated gabbros of the Fraser Range, Western Australia, and their economic significance. Proceedings of the Australasian Institute of Mining and Metallurgy, 231, 47–57.

Wilson, A.F., 1969b. Some structural, geochemical and economic aspects of the metamorphosed East Fraser Gabbro and associated pyroxene granulites of the Fraser Range, Western Australia. Indian Mineralogist, 10, 1–21.

Wilson, A.F., Compston, W., Jeffrey, P.M. & Riley, G.H., 1960. Radioactive ages from the Precambrian rocks of Australia. Journal of the Geological Society of Australia, 6, 179–195.

Windrum, D. P. & McCulloch, M. T., 1984. Nd and Sr isotopic systematics of central Australian granulites: chronology of crustal development and constraints on the evolution of lower continental crust. Contributions to Mineralogy and Petrology,94, 289–303.

Zhao, J. & Cooper, J., 1992. Precambrian Research, 56, 227–253.

Zhao, J. & McCulloch, M.T., 1993. Sm–Nd mineral isochron

ages of Late Proterozoic dyke swarms in Australia: evidence for two distinctive events of mafic magmatism and crustal extension. Chemical Geology, 109, 341–354.

Zhao, J., McCulloch, M.T. & Korsch, R.J., 1994. Characterisation of a plume related ~800 Ma magmatic event and its implications for basin formation in central-southern Australia. Earth and Planetary Science Letters, 121, 349–367.

AGSO Journal of Australian Geology & Geophysics, 16 (1/2), 41–67

Geological framework and crustal evolution of the Giles mafic–ultramafic complex and environs, western Musgrave Block, central Australia

A.Y. Glikson[1], C.G. Ballhaus[2], G.L. Clarke[3], J.W. Sheraton[1], A.J. Stewart[1] & S.-S. Sun[1]

Layered mafic–ultramafic intrusions of the Giles Complex, western Musgrave Block are confined to a southern granulite facies block thrust northward over an amphibolite facies block and southward over sediments of the Officer Basin. The Tomkinson Ranges to Jameson Range region, at the westernmost end of the southern granulite facies terrane, consists of 17 medium to large-scale faulted segments or intact layered mafic–ultramafic sills and lopoliths emplaced into felsic to intermediate or mafic granulite facies orthogneiss. Protoliths of these gneisses, giving ages of ~1.55 and 1.3 Ga, were metamorphosed at ~1.2 Ga. Emplacement of the mafic–ultramafic bodies into multiply deformed felsic granulites (D_1 and D_2—pure shear; T>750°C, P=5±1 kb), previously believed to have occurred at about 1200–1188 Ma, is now thought more likely to be of 1.08–1.06 Ga—coeval with the Tollu Group volcanics. The western Musgrave Block displays crustal zonation of near-contemporaneous units, from deep crustal ultramafic-dominated intrusions in the north (south of the Woodroffe Thrust), to gabbro–pyroxenite intrusions in the Tomkinson Ranges, to troctolite intrusions in the southwest, to upper crustal volcanics of the Tollu Group—i.e. a southward rise in crustal level. The layered intrusions include: (1) large olivine–clinopyroxene–plagioclase troctolite to troctolite–anorthosite bodies, with Fe-rich olivine and plagioclase as liquidus phases, crystallised from highly evolved silica-undersaturated liquids and representing high-pressure orthopyroxene fractionation prior to intrusion. These bodies are commonly magnetite-rich, representing high oxygen fugacities, and include little or no ultramafic component, e.g. Jameson, Blackstone, Cavenagh, and Bell Rock intrusions; (2) large orthopyroxene–clinopyroxene–plagioclase gabbronorite to norite intrusions, including a significant (up to about 30%) ultramafic component, e.g. Michael Hills, Mount Davies, Kalka; (3) small to medium-sized layered pyroxenite–peridotite–gabbro intrusions, e.g. Murray Range, Claude Hills, The Wart, Gosse Pile, Ewarara, and (4) stratiform anorthosites forming lenses and recrystallised tongues interlayered with felsic granulites, mainly around Teizi bore. Ultramafic increments crystallised from little-fractionated primitive basaltic magmas saturated with olivinespinel form late magmatic pulses injected into above-solidus resident gabbroic bodies. Intrusion was followed by isobaric cooling (Wingellina Hills: P=6±1 kb; Blackstone: ~4 kb). Near-coeval relations between the Giles Complex and the Tollu Group volcanics imply rapid uplift and erosion of deep crustal zones followed by volcanic activity. Feeders for the volcanics are represented by type-A dykes correlated with the ~1.05–1.07 Ga Kulgera swarm of the eastern Musgrave Block, and by extensive granite veining and related granulite facies recrystallisation of large sectors of the Giles Complex (D_3—simple shear; early stage T=650–700°C, P=11 kb; late stage P=4.5±1.1 kb). Northward thrusting of the granulite facies block over amphibolite facies gneisses along the western extension of the Woodroffe Thrust ~550 Ma was associated with elevated pressures along the fault zone (P=14.0±1.1 kb; T=750°C), contemporaneous with the Petermann Ranges deformation.

Introduction

The Giles Complex is defined as a suite of massive gabbroic to gabbro/pyroxenite and gabbro/pyroxenite/peridotite intrusions emplaced in the southern granulite facies block of the middle to upper Proterozoic Musgrave Block (Fig. 1). The suite is locally deformed, extensively faulted and partly recrystallised under granulite facies conditions. The southern granulite facies block occupies an east–west belt approximately 500 x 50 km and mafic/ultramafic intrusions concentrate in an area of about 3000 km^2 in the Tomkinson Ranges–Blackstone Ranges–Jameson Ranges region in the westernmost part of the Musgrave Block (Figs 2, 3). These intrusions represent one of the most extensive mafic plutonic suites recognised in deep levels of the continental crust worldwide (Nesbitt et al. 1970; Goode 1970; Moore 1971; Daniels 1974; Thomson 1977 1980; Thomson et al. 1962; Webb 1985; Glikson et al. 1990). Investigations of the field relations between the Giles Complex and country rocks in the western Musgrave Block (Glikson 1989, 1990; Glikson et al. 1990; Pharaoh 1990; Stewart & Glikson 1991; Clarke et al. 1992;), petrology/geochemistry of the mafic/ultramafic rocks (Ballhaus & Glikson 1989; Ballhaus & Berry 1991; Ballhaus 1992; Ballhaus et al. 1992; Ballhaus & Glikson, 1995—this issue), felsic igneous rocks (Stewart, 1995—this issue; Sheraton & Sun, 1995—this issue), isotopic ages (Sun & Sheraton 1992: Sun et al. in press), tectonic fabrics and thermobarometric indices (Clarke et al. 1992, 1993; Clarke et al. 1995—this issue), boundary thrust faults (Stewart 1993; Stewart 1995—this issue) and remotely sensed multispectral imagery (Glikson 1994; Glikson & Creasey 1995—this issue) were conducted during 1987–1994, within the framework of the National Geological Mapping Accord. This paper highlights some of the major results of this project with reference to the crustal evolution of the upper Proterozoic crust in the western part of the Musgrave Block.

Some of the principal suggestions made by previous studies of the Tomkinson Ranges, mainly in South Australia, include: (1) an interpretation of the Giles Complex in terms of tectonic slices of an originally contiguous lopolith (Nesbitt et al. 1970); (2) a view of the latitudinal Hinckley fault as a lineament separating a high-pressure older terrane to the north from a lower pressure younger terrane to the south (Nesbitt et al. 1970; Gray 1978); (3) metamorphism of the northern terrane under pressures of about 100–120 Mpa (Goode & Moore 1975), (4) increased differentiation with higher stratigraphic levels in some of the mafic–ultramafic intrusions, and (5) coeval age relations between the Giles Complex and the Tollu Group of the Bentley Supergroup (Nesbitt et al. 1970; Daniels 1974).

Major questions pertaining to the origin of the Giles Complex include: (1) the crustal environment in which the mafic/ultramafic intrusions were emplaced, including the pressure and temperature of the host country rocks; (2) original spatial relationships between the separate mafic/ultramafic bodies; (3) age of emplacement of the Giles Complex in relation to the metamorphic and tectonic history of the Musgrave Block; (4) the effects of emplacement on the felsic granulites and possible genetic relations between the Giles Complex and intrusive granitoids; (5) the relations between the Giles Complex and associated basic dyke swarms, including identification of feeders of the layered intrusions; (6) deformation history of the Giles Complex and associated rocks; (7) significance of the Tollu Group volcanics, and (8) the origin of the basic igneous activity and its possible lateral extent across central Australian infracrustal Precambrian terranes. This paper addresses these questions with specific reference to the Tomkinson Ranges, with implications for the Musgrave Block as a whole.

Structural and temporal framework

The Giles Complex is confined to the granulite facies, felsic

1 Division of Regional Geology & Minerals, Australian Geological Survey Organisation, GPO Box 378, Canberra, ACT 2601
2 University of Freiburg and Max Planck Institute for Chemistry, Mainz, Germany
3 Department of Geology and Geophysics, University of Sydney

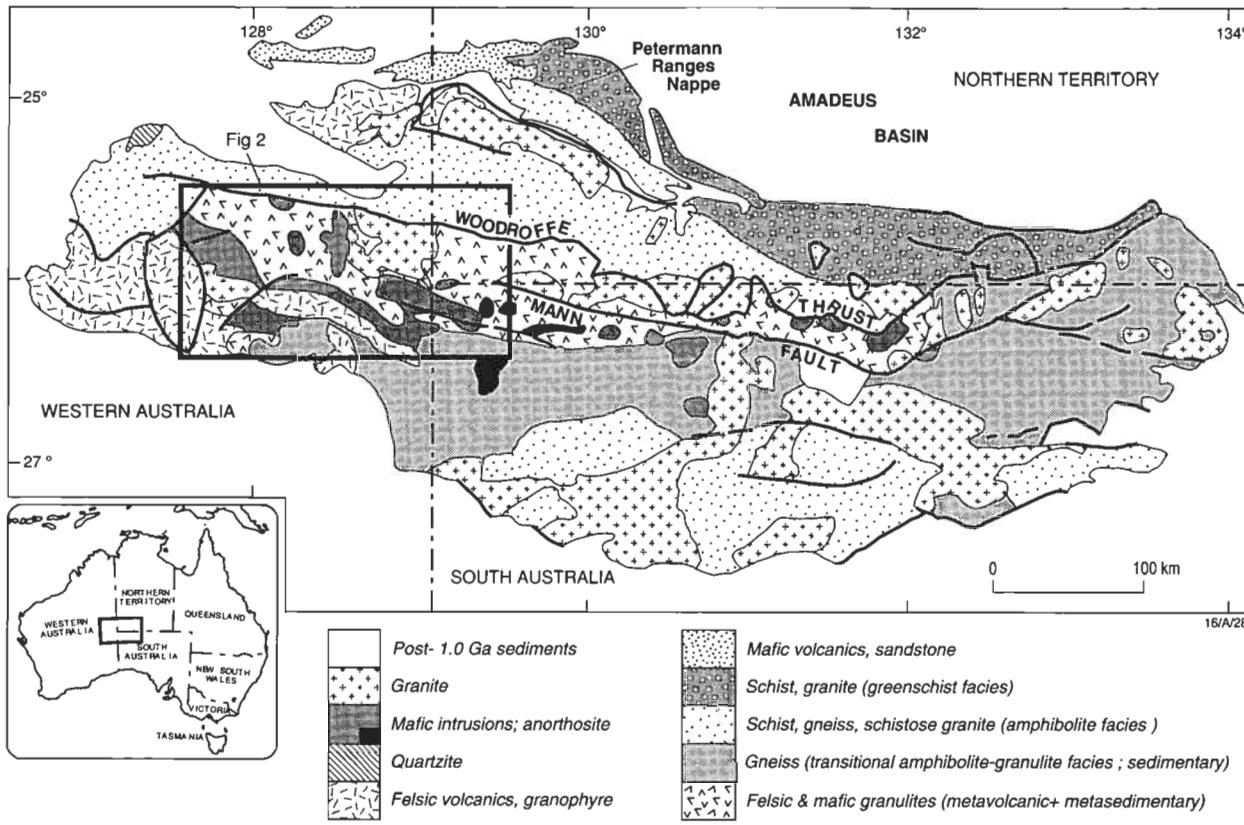

Figure 1. Geological sketch map of the Musgrave Block.

to intermediate, east–west terrane bound to the north by the Woodroffe Thrust (Collerson et al. 1968; Nesbitt et al. 1970; Gray & Compston 1978; Gray & Goode 1981). The Woodroffe Thrust to the north of the Mann Range is defined by well-pronounced magnetic and gravity lineaments (Fig. 4). Mapping in the Bates 1:100 000 sheet area, north of the Tomkinson Ranges has identified a northwest-trending mylonitic shear zone which may represent a splay of the Woodroffe Thrust in this area (Stewart 1993, 1995—this issue). This zone is up to 3 km wide and places upper amphibolite facies garnet–hornblende granite and rapakivi granite in the south over mid-amphibolite facies granitic gneiss in the north. The southern block is cut by doleritic dykes containing metamorphic garnet–clinopyroxene assemblages which indicate pressures of 131±21 Mpa for T=725C°—suggesting the sole of the thrust in this area represents the deepest structural level identified in the western Musgrave Block. As indicated below, progressively shallower crustal levels southward of the Woodroffe Thrust are consistent with the transition from ultramafic-dominated intrusions formed under intermediate pressure (Wingellina Hills—Ballhaus & Berry 1991—and probably Murray Range, Claude Hills, Ewarara, Kalka and Gosse Pile) to gabbro and silica-undersaturated troctolite-dominated intrusions (Bell Rock, Blackstone, Cavenagh, Jameson) formed under lower pressures. Further palaeo-pressure/temperature studies of the felsic granulites and granitoids required for assessment of palaeo-PT variations are underway (White & Clarke, studies in progress)..

The relationships between rock units and between structural elements as unravelled in the present study are portrayed in Figures 5 and 6. Comparisons between the total magnetic intensity (TMI) and Bouguer anomaly (BA) maps with the solid geology map of the Tomkinson Ranges and environs indicates the following features:

1. TMI 'highs' may coincide with layered intrusions of the Giles Complex, notably the Bell Rock intrusion, or may coincide with felsic granulite terranes, for example Mount Aloysius, Kunatjara and much of the Ewarara–Teizi ridge.
2. TMI 'lows' may coincide with layered intrusions of the Giles Complex, i.e. the Hinckley intrusion and the Mount Davies, Gosse Pile and Ewarara and Kalka intrusions.
3. Some intrusions include zones corresponding to TMI highs and TMI lows, i.e. the Michael Hills and Kalka intrusions. This suggests that remagnetisation of the high-grade terrane during metamorphism and faulting controls the TMI patterns to a greater extent than original lithological characteristics (Mutton et al. 1983).
4. Boundaries between TMI 'highs' and 'lows' commonly coincide with major fault lineaments, principal examples being (1) the fault-bounded western and eastern boundaries of the Bell Rock intrusion; (2) the northeastern boundary of the Bell Rock intrusion, which *may* signify a western extension of the Hinckley fault, and (3) part of the Numbunja fault between the Mount Davies and Gosse Pile intrusions. However, anomaly boundaries are more commonly displaced from, although they may parallel, major faults, i.e. the Champ de Mars fault, much of the Hinckley fault, the Wingellina fault and part of the Numbunja fault.
5. A close coincidence is observed between Bouguer anomaly 'highs' and the central parts of layered intrusions of the Giles Complex, including the Bell Rock, Michael Hills, Hinckley and Mount Davies intrusions. Conversely, Bouguer anomaly 'lows' coincide with felsic granulite/granite terranes, i.e. Mount West, Champ de Mars, Wandu Hill. The Mount Aloysius felsic granulite massif and the Ewarara–Teizi felsic granulite ridges are marked by steep northward sloping gradients. Steep gradients also mark the fault boundary between the Bell Rock intrusion and the felsic plutonic basement and overlying Tollu Group volcanics to the southwest.

The temporal–tectonic relationships of the Giles Complex are summarised in Table 1. Regional foliation in granulite facies felsic gneisses trend broadly east–west in the North Hinckley–Ewarara–Teizi Ranges, with marked strike deflections in

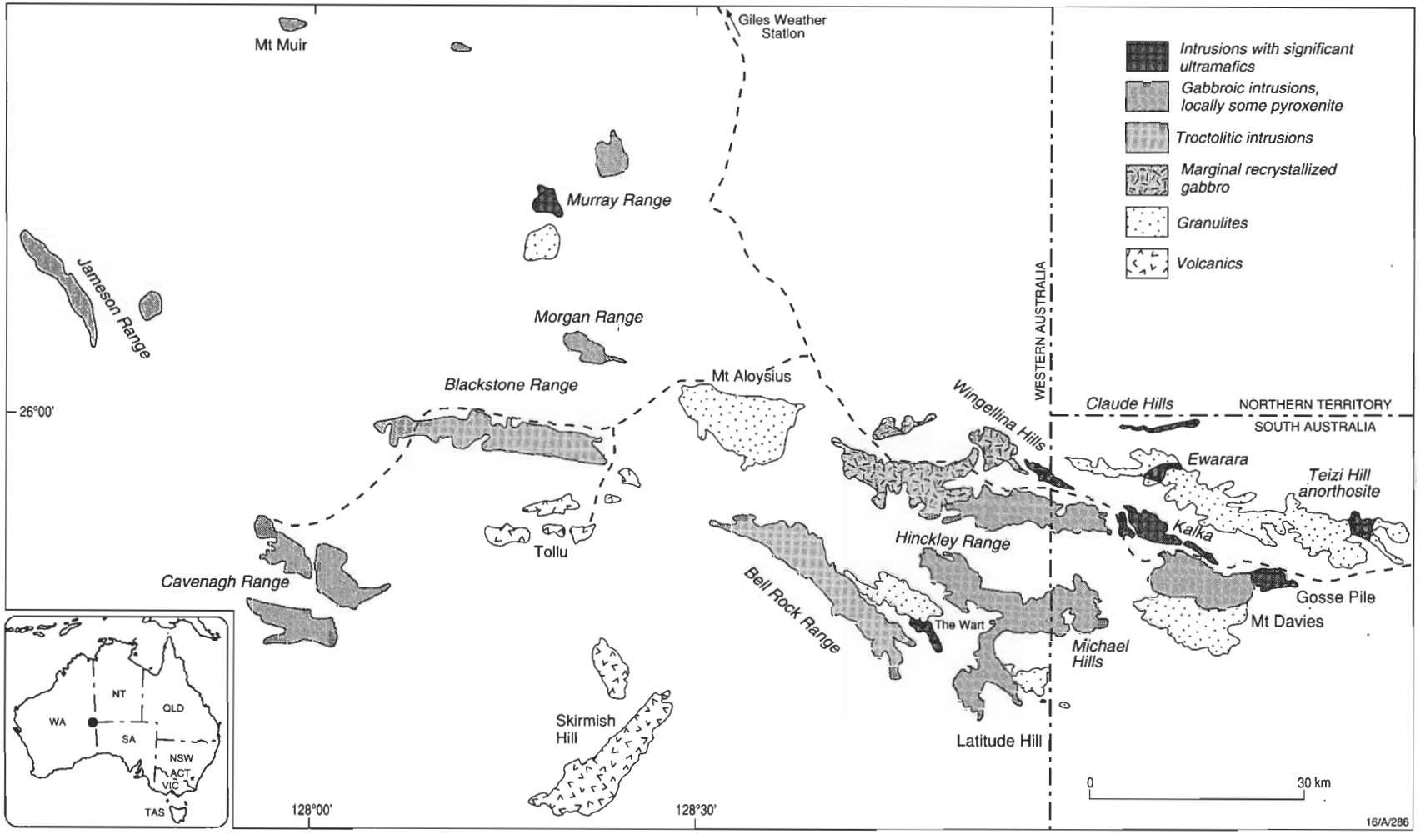

Figure 2. Geological sketch map of the Tomkinson Ranges–Blackstone–Jameson region.

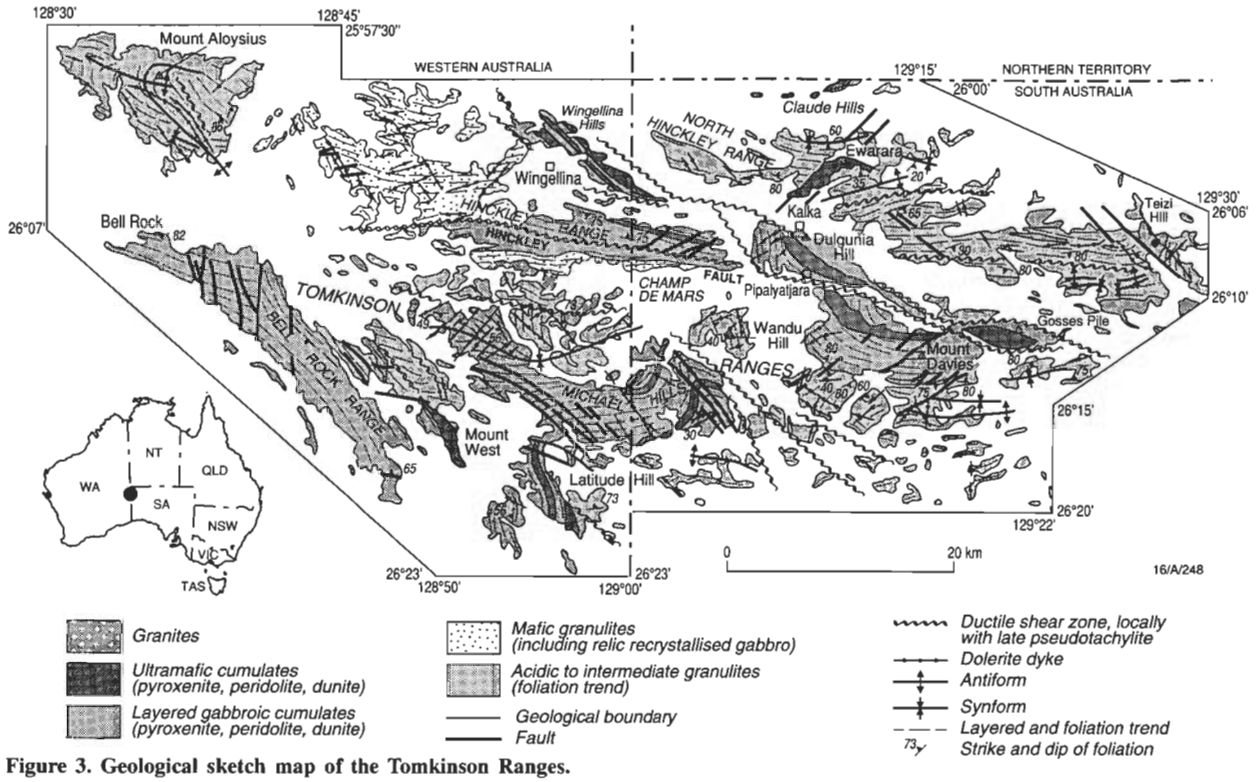

Figure 3. Geological sketch map of the Tomkinson Ranges.

the Mount West, Wandu Hill and south of Mount Davies. In general, the sill-like to lopolithic intrusions of the Giles Complex are emplaced with their longer axes parallel or subparallel to the regional foliation S_3. Notable exceptions are the Ewarara, Mount Davies and Murray Range intrusions (Figs 2, 3). In general, the degree of deformation of layered intrusions decreases from east to west and from north to south—the eastern bodies are mostly steeply dipping, cut by mylonitic shears and by pervasive pseudotachylite/brittle vein–breccia systems (i.e. Kalka, Mount Davies, Hinckley, Wingellina Hills). By contrast, the western intrusions are little deformed to flat lying (i.e. Bell Rock–Blackstone, Jameson, Cavenagh). The density of dykes is also variable—dykes are less common in the Blackstone and Jameson intrusions, but a penetrative dyke system forms about one-quarter of the outcrop in parts of the Cavenagh gabbro.

Internal folding of the layered intrusions is locally observed, but is generally difficult to discern in the massive gabbros. The Michael Hills intrusion outlines a northward-concave flexure, local dome and basin structures in near-flat lying zones in the western part of the intrusion, and marked strike deviations in the south, producing the Latitude Hills sliver (Fig. 3). The layered intrusions are cut and separated from each other by major mylonitic shears, which form an anastomosing fault pattern associated in part with felsic granulite/granite core zones, which occupy intermediate positions between the layered intrusions. Examples are (1) Champ de Mars fault–north Mount Davies fault, which truncates the tops of the north-younging Michael Hills intrusion and the base of the Mount Davies intrusion; (2) Wingellina–Kalka fault,

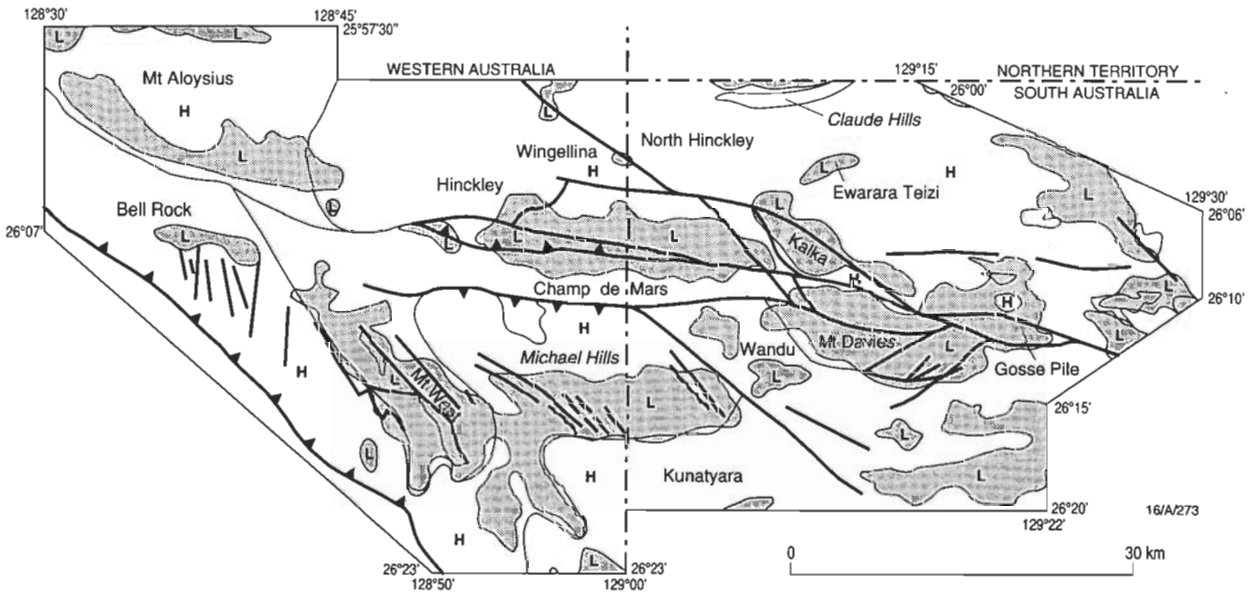

Figure 4. Total Magnetic Intensity overlay to a raster grey-scale map of the Tomkinson Ranges, showing the main outcrops of the Giles Complex.

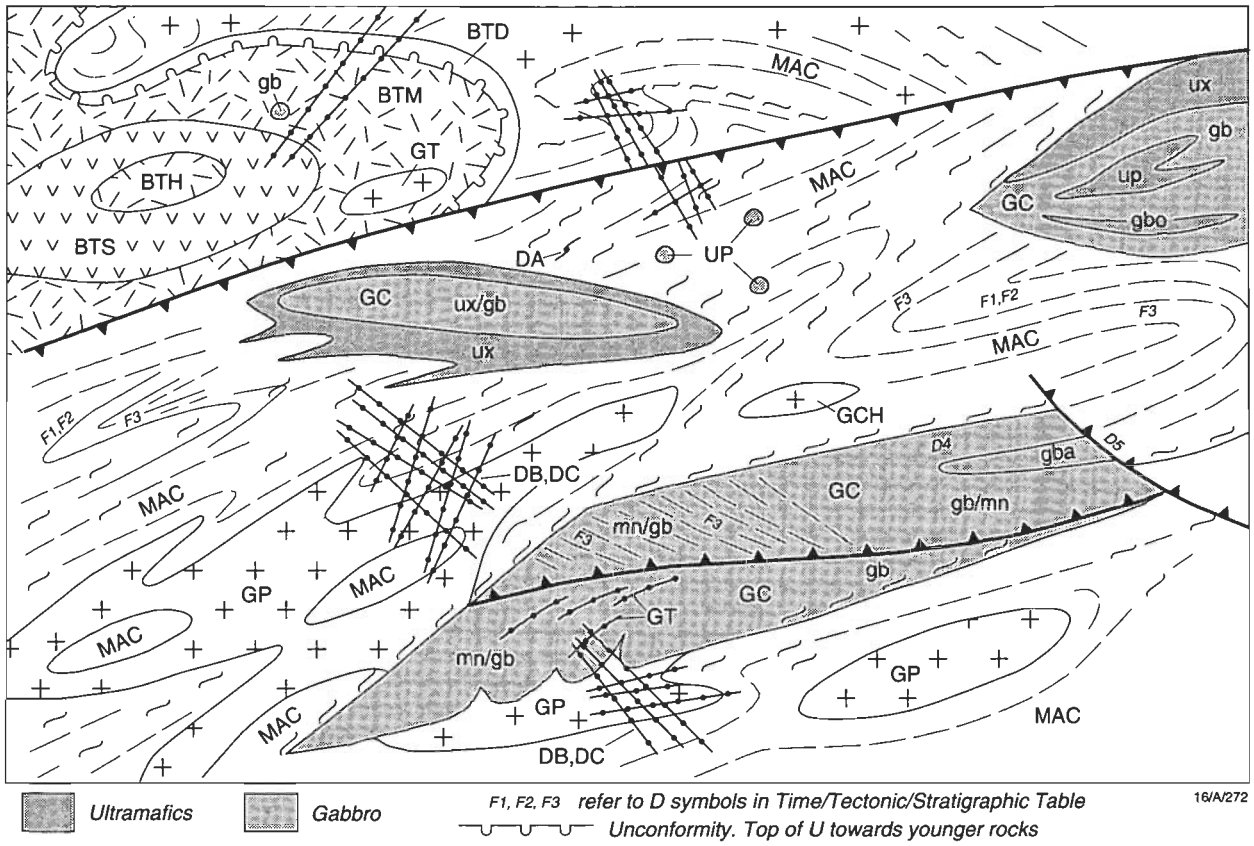

Figure 5. Schematic diagram of relationships between rock units in the Tomkinson Ranges.

which truncates the tops of the Wingellina Hills and Kalka intrusions; (3) the Mount Davies–Numbunja Creek fault, which truncates the base of the Mount Davies intrusion and the top of the Gosse Pile intrusion; (4) the Bell Rock–Blackstone magnetic lineament, which truncates the tops of the Bell Rock and Blackstone gabbroic bodies—considered to be parts of one and the same intrusion (Daniels 1974). Fault zones developed along the base of mafic/ultramafic intrusions include the Hinckley fault (as defined here—restricted to the southern edge of the Hinckley gabbro) and the multiple Mount West shear zones which underlie the Bell Rock gabbro (Fig. 3).

It is likely that some of the above fault zones constituted ductile loci, allowing the rise of granitic magmas. Principal examples of such granite-rich core zones are (1) the Champ de Mars complex, which consists of migmatised and porphyritic granite-intruded felsic granulites; (2) a granite vein-rich zone of recrystallised gabbro south and west of the Wingellina fault; (3) the southern fault-bound annealed portion of the Gosse Pile intrusion (Moore 1971); (4) the heavily sheared felsic granulites/banded orthogneiss and paragneiss of the Mount West complex, located below the Bell Rock intrusion and intruded by the The Wart (southeast of Mount West) layered gabbro/pyroxenite body.

The oldest components identified in the Tomkinson Ranges are granulite facies orthogneisses, including interlayered supracrustal paragneisses, including orthoquartzite units, minor garnet–sillimanite gneiss and minor calc silicates. Evidence of two early deformation events (D_1 and D_2) accompanying granulite facies metamorphism is preserved (Table 1). Igneous components include pre-S_1 mafic granulites and post-S_1/pre-S_2 lenses of orthogneiss and orthopyroxene-bearing charnockitic granite. A penetrative S_1 gneissosity is deformed by isoclinal F2 folds. Except for F1 hinges, S_1 has been rotated into parallelism with S_2. Where unaffected by subsequent deformation, D_2 is characterised by meso- to macroscopic, tight to isoclinal F2 folds with east to east-southeast-trending axes and reclined axial planes, resulting in a shallow east-dipping S_2 foliation. Whereas an S_1–S_2 intersection lineation is common, mesoscopic F_2 folds are not associated with mineral stretching lineation, implying deformation involving mainly pure shear. S_{1-2} fabrics typically comprise granoblastic interlocking mineral assemblages, in contrast to later mylonitic foliations enveloping residual S_{1-2} minerals.

Crosscutting contacts of the Hinckley Gabbro with the felsic granulites indicate its emplacement has postdated S_2, although gabbro–granulite contacts have mostly been disrupted by later deformation. Well-exposed intrusive contacts are observed along the northern margin of the Kalka intrusion and the southern margin of the Mount Davies intrusion (Nesbitt et al. 1970). Regionally extensive K-feldspar megacrystic granite and microgranite dykes and stocks intrude gabbro or gabbro-derived mafic granulite of the Giles Complex, and commonly contain xenoliths of mafic granulites. As is shown by Sun et al. (in press), at least some of the finer grained granites are related to the ~1.06 Ga Tollu Group volcanic event. Megacrystic granite stocks grade into microgranite. Charnockitic and rapakivi granites, in places grading into megacrystic granite and containing inclusions of gabbro and recrystallised derivatives, intrude the southern margin of the Hinckley Gabbro.

The above units are intruded by at least three generations of basic dykes: (1) type-A dykes, dated by U–Pb zircon as 1060 Ma and by Sm–Nd (plg–cpx) as ~1100 Ma (Sun et al. in press), consist mostly of northwest-trending and some northeast and north-trending dykes deformed by D_3. They display marginal to complete recrystallisation of primary igneous textures into granulite facies S_3 assemblages; their trend results from D_3 folding and is mostly aligned with the southeast-trending S_3 foliation. (2) Type-B, northwest-trending dykes dated as ~800 Ma (Sun et al. in press), consist of post-S_3 granoblastic dolerite with coarse-grained plagioclase phenocrysts. They crosscut S_3 foliations and, thus, postdate

D_3. (3) Type-C, post-metamorphic dykes, are fine-grained to aphanitic, occasionally pyrite-bearing, mostly northwest and northeast-trending, and dated at ~1000 Ma (Sun & Sheraton 1992; Sun et al. in press; Clarke et al. 1995—this issue).

D_3 structures comprise upright to reclined, tight to isoclinal, mesoscopic F3 folds with amplitude and wavelength from a few metres to tens of metres, with steeply dipping soouth-east-trending S_3 axial plane mylonitic foliations. In the felsic granulites, D_3 resulted in widespread rotation to sub-parallelism of earlier S_{1-2} granoblastic assemblages to S_3–L_3 mylonitic fabrics. These fabrics consist of steeply plunging southwest-trending L_3 stretching lineations within the southeast-striking steeply south-dipping S_3 foliation, suggesting southwest-directed compression and recrystallisation under dominantly simple (rotational) shear. In general, D_3 is difficult to detect in massive gabbro. However, in felsic vein-injected mafic granulites, derived by recrystallisation of gabbro, S_3–L_3 fabrics are dominant and include penetrative rodding of felsic stringers related to simple shear rotation. Since at least some of the felsic veins are related to the ~1.08 Ga Tollu Group (Sun et al. in press), it follows that D_3 postdated the latter volcanic event.

The Hinckley Gabbro and Kalka layered intrusion are bound to the south by east–west mylonitic to ultramylontic shear zones, referred to as the Hinckley Fault (Goode 1978), and its offshoots. This D_4 deformation (Clarke 1992; Clarke et al. 1995—this issue) resulted in zones of intense recrystallisation, 10–100 m wide, with throws of up to about 100 m, estimated from basic dykes displacement. Southeast-directed transport is indicated by S_4–L_4 geometry. D_4 shears are offset by north-trending D_5 ultramylonite zones dipping steeply east, with D_5–L_5 relations indicating southwest-directed transport and apparent dextral reverse throw of a few hundred metres. Broad east-trending D_6 ultramylonite zones form prominent faults, the primary example being the Champ de Mars fault (Fig. 6). The zone of pervasive D_6 recrystallisation is up to 500 m wide where felsic rocks are affected, or up to 150 m wide through gabbro; in the latter, the mylonite is imprinted by extensive pseudotachylite (Glikson & Mernagh 1990). The fault dips steeply south and has a steeply plunging L_6 mineral stretching lineation, suggesting its correlation with the Woodroffe Thrust zone and related faults. The latter involved northward transport of the Musgrave Block over the late Proterozoic to Palaeozoic Amadeus Basin during the Cambrian Petermann Orogeny (Collerson et al. 1972; Forman & Shaw 1973; Glikson et al. 1990). Poorly exposed east-trending mica-rich D_7 retrograde shear zones dip north and preserve a reverse sense of movement.

Isotopic age determinations for the Tomkinson Ranges (Table 1) define protolith ages of banded granulites at about 1.55 to 1.30 Ga (felsic granulite from Mount Aloysius: U–Pb ion-probe age of 1530 Ma, Sun & Sheraton 1992; Rb–Sr isochron age of 1564±12 Ma and 1358 Ma, Gray 1978; felsic granulite E of Michael Hills, 1305±8 Ma U–Pb ion-probe age; inherited zircon cores in Minno Granite, 1296±10 Ma, Sun & Sheraton 1992). A close contemporaneity pertains between peak metamorphism of the older banded granulite (represented by metamorphic zircon overgrowth of 1223±7 Ma in felsic granulites and Rb–Sr isochron ages of about 1200 Ma) and the intrusion of porphyritic and rapakivi granites (Minno

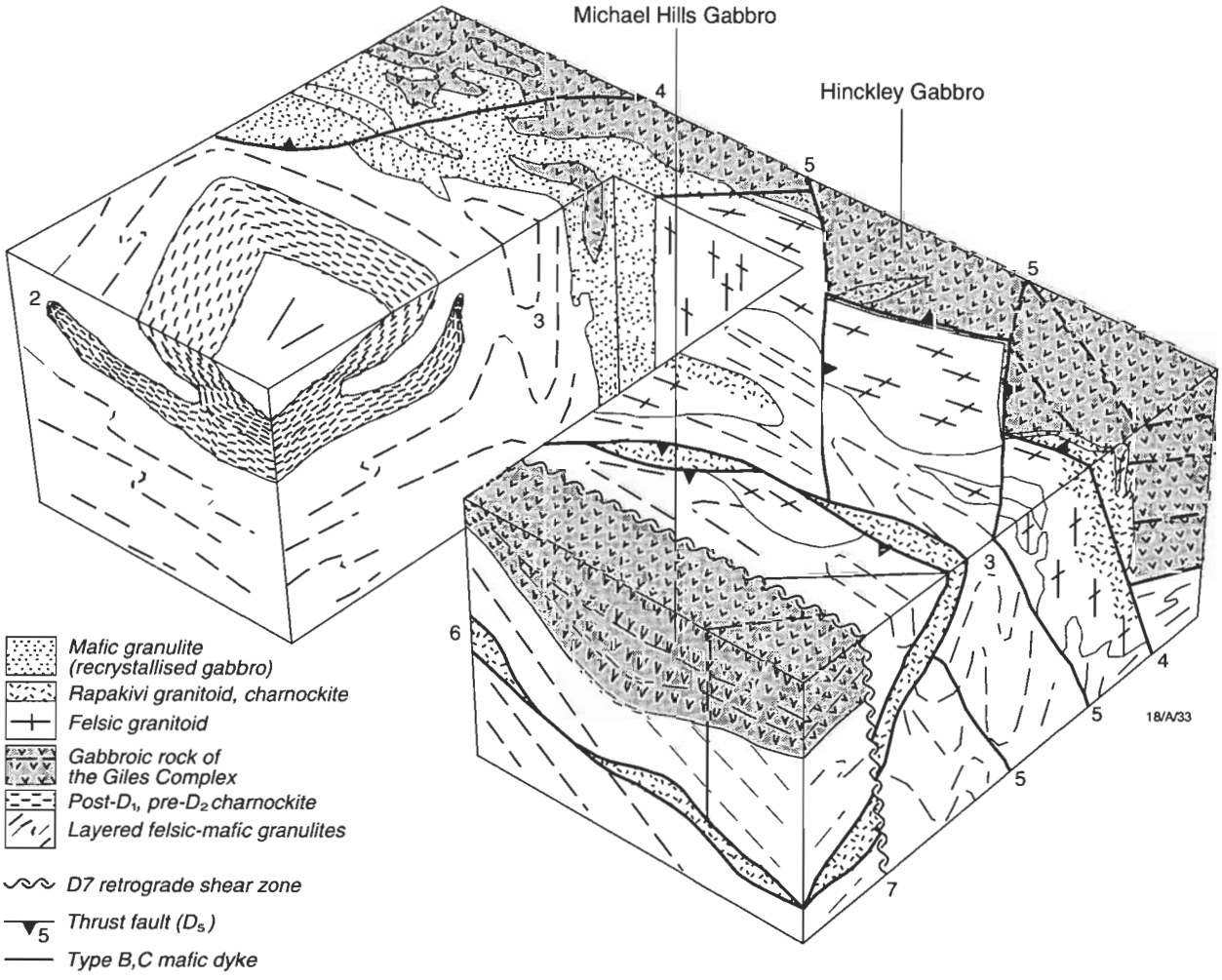

Figure 6. Structural block diagram of the Champ de Mars felsic complex (after Clarke 1992).

Granite, U–Pb ion probe zircon age of 1198±6 Ma, Sun & Sheraton 1992; Rb–Sr isochron age of 1204±17 Ma, Gray 1978).

Pre-Giles Complex felsic granulites

Banded to massive quartzofeldspathic granulites of mostly felsic composition form country rocks to the Giles Complex, including the principal outcrops of Mount Aloysius (Stewart 1995—this issue), North Hinckley range, Ewarara–Teizi Ranges, Wandu Hill, Mount West and isolated inselbergs scattered around the Tomkinson Ranges (Figs 2, 3). The banded granulites, including both meta-igneous and metasedimentary components, are cut concordantly to discordantly by the Giles Complex, as shown by their older structural fabrics and isotopic ages (Glikson & Stewart 1990; Sun & Sheraton 1992; Sun et al. in press; Clarke et al. 1995—this issue). The massive pods and lenses of granitic gneiss, migmatite and charnockite within the banded granulites include (1) units which possibly predate the Giles Complex (Clarke et al. 1992); (2) units contemporaneous with and genetically related to the emplacement of the Giles Complex; and (3) post-Giles Complex units, which, in part, represent plutonic counterparts of felsic volcanics of the Tollu Group. Opx–qz–feld gneisses (commonly <4% strongly pleochroic orthopyroxene) contain K-feldspar, plagio-

Table 1. Isotopic ages, tectonic elements and palaeo-pressure/temperature parameters for units and tectonic events in the Tomkinson Ranges.

Age (Ma)	Event	Metamorphic conditions	STRUCTURAL FABRICS		
			Folds	Dominant foliation	Lineation, dominant movement
1550[1]	Protolith of felsic granulites (North of Hinckley fault)				
1300[1]	Protolith of felsic granulites (South of Hinckley fault)				
	D_1		Rarely preserved	Layer parallel S_1, reoriented during D_2	None observed
1200[1]	Intrusion of charnockite				
	D_2	P=5±1 kbar,T>750°C F_2 folds, oriented parallel to L_2	Reclined isoclinal 335/15NE	Pervasive S_2 gneissosity L_2 15 --> 105	Pervasive intersection
1188 ±4[5]	Intrusion of fine grained granite and K-feldspar megacrystic granitoids				
1100[5]	Intrusion of mafic dykes Type A				
1080[5]	Intrusion of Giles Complex	P=6±1 kbar; uplift,erosion; extrusion of Tollu Group volcanics			
1060[5]	D_3 early late	P=11 kbar,T=650-700°C P=4.5±1 kbar	Open to isoclinal Upright F_3 folds	135/80NE	Down-dip mineral and stretching 80 -->025
1000[5]	Intrusion of mafic dykes Type C (including olivine+plagioclase dykes)				
800 Ma[3]	Intrusion of mafic dykes Type B				
	D_4 ultramylonite (SE transport)	Amphibolite facies		095/65N	42 -->325 Reverse
	D_5 mylonite/ultramylonite (SW transport)	Greenschist facies	160/80E	50 -->025 common fracture cleavage	Reverse
550 Ma[4,5]	D_6 **Petermann Orogeny** ultramylonite with psuedotachylite north - directed thrusting e.g. Champs de Mar Fault, Woodroffe Thrust	P=14.0±1.1 kbar, T=750°C	Large shear zones, extensive pseudotachylite	100/80S 085/60N	80 -->175 Reverse 60 -->350 Normal
	D_7 retrograde shear zones	Contains muscovite and biotite	Broad "crush" zones		80 -->030

16/A/249

[1] Rb-Sr whole rock isochrons,Gray (1971, 1977); [2] U-Pb on zircons, Maboko (1988); [3] U-Pb on zircons, Sun & Sheraton (1992); [4] Ar^{39}-Ar^{40}, Maboko (1988); [5] Sun et al., in press

clase (calcic plagioclase or andesine), accessory zircon, apatite and iron oxides, and may contain clinopyroxene-bearing mafic bands. K-feldspar is markedly perthitic, plagioclase is antiperthitic and many gneisses are dominated by mesoperthite. Recrystallisation and mylonitic textures, dominated by D_3, are common and these rocks contain secondary red-brown biotite and less brownish-green hornblende replacing pyroxene. The widespread mesoperthite indicates high T and very low P_{H2O} conditions, reflecting crystallisation under peak alkali-feldspar solvus conditions, corresponding to high An contents and high feldspar solidus under dry conditions (Morse 1968). This agrees with the essentially anhydrous mineral assemblages of the undeformed gneisses, whereas the development of mica and amphibole occurred during later deformation under more hydrous conditions.

Most gneisses are of granitic (s.s) composition. The more fractionated siliceous gneisses may have negative Sr anomalies, reflecting residual plagioclase. The age of these source rocks may be reflected by 1550 Ma zircons from orthopyroxene-gneiss from Mount Aloysius and 1300 Ma from other areas, whereas metamorphism is dated at 1200 Ma (Sun & Sheraton 1992). Another example is furnished by a Y-undepleted gneiss from north of Mount Davies, with U–Pb zircon ion-probe ages of 1305±8 and 1223±7 Ma, representing precursor and metamorphic ages, respectively. Some orthopyroxene-bearing gneisses have high Ce/Y and are depleted in Y and HREE (heavy rare earth elements), possibly representing partial melting of feldspar-poor hornblende±garnet-bearing mafic source (Sheraton & Black 1988). These gneisses are typically high in Sr and have positive Sr anomalies, indicating that plagioclase was not a major residual phase (Sheraton & Sun 1995—this issue). Granodioritic gneisses are less common and tonalitic gneisses are rare. As distinct from other granulite facies terranes, where metamorphic depletion in large-ion lithophile elements (LILE: K, Rb, Th, U) is widespread (Tarney et al. 1972), K/Rb ratios of the Musgrave gneisses are not high (mostly 200–300), implying little loss of Rb. By contrast, a tonalitic gneiss sample has a K/Rb ratio of 609. These differences reflect the role of K-feldspar in concentrating Rb relative to K. As pointed out by Gray (1977), the Th/U ratios (<80) of Musgrave gneisses are markedly higher than crustal averages (~3.8: Taylor & McLennan 1985), representing metamorphic depletion of uranium.

Most orthopyroxene-bearing gneisses are metaluminous or slightly peraluminous—the alumina saturation index (ASI—molecular $Al_2O_3/(CaO+Na_2O+K_2O+3.33P_2O_5)$) being mostly <1.1, representing I-type granites derived from igneous precursors (Chappell & White 1974). Massive felsic to intermediate granulite units may be of volcanic or sedimentary origin. Gnt–qz–feld gneisses (gnt <6%) are similar to orthopyroxene gneisses and Gnt–opx assemblages are present, but no garnet is seen to coexist with clinopyroxene or hornblende. By analogy with the orthopyroxene gneisses, many garnet-bearing gneisses have near-eutectic granitic (s.s.) compositions, are slightly peraluminous (ASI: 1.0–1.1), and are, thus, probably orthogneisses. Most analyses have high Y and low Ce/Y and Sr—consistent with intracrustal melting of precursor felsic materials and derived sediments (Tarney et al. 1987). K/Rb ratios are similar to those of orthopyroxene gneisses whereas Th/U ratios (~20) are lower.

Whereas the bulk of the orthopyroxene-bearing gneisses are likely derivatives of volcanic or granitic protoliths, sedimentary components are represented by some of the garnet-bearing varieties, quartz-rich varieties and quartzite units, rare garnet–sillimanite gneiss (i.e. in Mount Aloysius) and calc-silicates. Impure quartzites commonly contain orthopyroxene and K-feldspar. Calc-silicates are represented by gneisses containing clinopyroxene, calcic plagioclase (labradorite–bytownite), sphene or allanite and, in some rocks, orthopyroxene or garnet. These rocks typically have high Al_2O_3, CaO and Sr and low SiO_2, FeO, MgO and K_2O.

Mafic granulites of volcanic or hypabyssal derivation form thin units and are volumetrically minor. They consist chiefly of orthopyroxene, clinopyroxene and plagioclase, accompanied by minor biotite and/or hornblende, and are Ol-normative or slightly Q-normative tholeiites. Incompatible elements, particularly LILE, show a wide range of abundances, reflecting original mantle source variations, magmatic contamination, and superimposed metamorphic effects.

Igneous stratigraphy of the Giles Complex

The Giles Complex in the Tomkinson Ranges and adjoining ranges to the west consists of 17 medium to large units, including (from east to west): Teizi anorthosite suite, Claude Hills, Ewarara, Kalka, Gosse Pile, Mount Davies, Wingellina Hills, Hinckley, Michael Hills, The Wart, Bell Rock, Blackstone, Cavenagh, Morgan, Murray Hills (two bodies) and Jameson. Some of these bodies are believed to have been originally contiguous, for example Blackstone–Bell Rock (Daniels 1974), The Wart–Bell Rock, Kalka–Gosse Pile (Moore 1971), and possibly Michael Hills–Mount Davies. The Kalka, Ewarara, Gosse Pile, Mount Davies and Teizi intrusions in South Australia have been the subject of detailed investigations by staff and students of the University of Adelaide (Nesbitt & Kleeman 1964; Nesbitt & Talbot 1966; Nesbitt et al. 1970; Goode & Krieg 1967; Goode & Moore 1975; Goode 1976, 1977, 1978; Moore & Goode 1978; Gray & Oversby 1972; Gray & Goode 1989). Only the principal features of these bodies are summarised below; the layered intrusions in Western Australia are described in more detail (Ballhaus & Glikson 1995—this issue).

Layered intrusions in the eastern part of the Tomkinson Ranges display a general progression from ultramafic-dominated bodies in the north and the east, i.e. Claude Hills, Ewarara (Goode & Krieg 1967) and Gosse Pile (Moore 1971) to interlayered ultramafic/mafic intrusions, i.e. Kalka (Goode 1970; 1976; 1977) and Mount Davies (Nesbitt & Kleeman 1964). For a review of these intrusions refer to Nesbitt et al. 1970).

The ***Ewarara pyroxenite*** (>500 m thick, 6 km along strike) is a small, most completely preserved, layered intrusion, consisting of a lower zone of olivine bronzitite (or harzburgite) and an upper zone of pyroxenite and melagabbro. The body is keel-shaped, as shown by structural attitudes and a gravity profile, and is discordantly intruded into, and in places intertongued with, banded felsic granulites, which include augen gneiss. Well-defined chilled to hybrid contacts against the felsic granulites are characterised by sharp elevation in the pyroxene/plagioclase ratio, abundant biotite and occasional felsic xenoliths. A steepening of igneous layering along the southeastern lobe is interpreted as a possible feeder zone.

The ***Kalka intrusion*** (>5000 m thick, 11 km along strike) consists of (1) a basal pyroxenite zone, consisting of orthopyroxenite and websterite; (2) a thick norite consisting of opx–cpx–plg norite, minor pyroxenite, clinopyroxene–plagioclase gabbro, anorthosite, olivine-bearing norite, and olivine–websterite. Phase layering and grain-size cm-scale pyroxene–plagioclase layering, which is gradational or sharply bounded, occur locally; (3) a lens of harzburgite occurs within the norite zone, occupying a conspicuous topographic depression; (4) an olivine gabbro zone (<600 m, up to 6.5 km along strike) within the norite zone, including also minor orthopyroxene-bearing cumulates, clinopyroxene–pyroxenite, and olivine-bearing pyroxenite. Centimetre-scale graded layering and isomodal sharp-bounded layering are present, especially in an upper 5 m thick horizon traced over a strike length of about 3 km (Johnson member, Goode 1976); (5) an anorthosite zone, forming low hills at the western end of the intrusion. This

unit includes locally finely banded leucogabbro and anorthositic gabbro, with olivine and magnetite as minor phases and local magnetite–ilmenite-rich bands.

The ***Gosse Pile intrusion*** (>2000 m thick; strike length >7 km) consists of a near-vertically dipping sequence of pyroxenite-dominated cumulates, separated by a major fault from the Mount Davies intrusion. Thin noritic intrusives at the base of the body are interdigitated with felsic granulites. These are overlain by a discrete, deeply weathered and valley-forming, body of serpentinised peridotite, consisting of poikilitic pyroxene and finer grained olivine and plagioclase. A finer grained marginal facies with xenoliths of olivine pyroxenite is present. The overlying layered sequence consists of orthopyroxenite, olivine orthopyroxenite, websterite and norite, and includes a stratigraphically distinct band of gabbro. The southern part of the intrusion consists of sheared recrystallised derivates of these rock types. Moore (1971) suggested three southward-younging magmatic cycles whose feldspar-dominated tops have been mostly removed—correlating Gosse Pile with the lower ultramafic section of the Kalka intrusion to the northwest.

The ***Mount Davies intrusion*** (Nesbitt & Kleeman 1964)—the largest layered mafic/ultramafic body of the Giles Complex (>7000 m thick, 15 km along strike) consists of (1) a lower gabbro zone with pyroxenite intercalations; (2) a central valley-forming serpentinised peridotite unit; (3) a zone of pyroxenite and olivine gabbro intercalations within gabbro; (4) a thick upper gabbroic zone, which discordantly intrudes felsic granulites, featuring a several hundred metre wide hybrid transition zone. The body is cut by numerous faults, including the near-strike Greenwood fault. As the Mount Davies intrusion constitutes sacred Aboriginal ground, it remains little known relative to other parts of the Giles Complex.

Wingellina Hills norite/pyroxenite intrusion

A detailed petrological study has been conducted of the Wingellina Hills intrusion, which is typical of the northern layered mafic–ultramafic intrusions of the Giles Complex (Ballhaus & Glikson 1989). It consists of a 1600 m thick succession of olivine gabbro and gabbronorite which alternate with lenticular stratabound intercalations of pyroxenite and peridotite. The ultramafic units are underlain by hybrid footwall zones, representing basal mixing of ultramafic increments with the resident gabbro. The mg′ numbers of olivine range from 89 to 77, below which olivine is replaced by cumulus orthopyroxene. Clinopyroxene mg′ numbers (91–77) are higher than for coexisting orthopyroxene and olivine. The mg′ numbers correlate with An content of plagioclase. Highly calcic antiperthites ($An_{65}Ab_{15}Or_{20}$), signifying crystallisation under high-T anhydrous conditions, occur as interstitial constituents of pyroxenites. Variations in mg′ of gabbros with stratigraphic level indicate weak Fe enrichment upward, whereas the ultramafic units display sharp compositional reversals. The origin of this composite body is interpreted in terms of continuous fractionation of of a resident ol–cpx–plg-saturated magma, periodically replenished by increments of olivine-saturated ultramafic melts, which crystallised peridotite, wehrlite, clinopyroxenite and olivine gabbro. Orthopyroxene-rich cumulates form by mixing of ultramafic increments with resident siliceous gabbro. The temperature difference between the host gabbro and the ultramafic pulses resulted in rapid quench crystallisation of the latter.

Murray Range pyroxenite/peridotite/gabbro intrusion

The Murray Range intrusion hosts the highest proportion of peridotites and the most primitive cumulates recognised in the Giles Complex. The magmatic sequence is well layered from megascale to centimetre scale and consists predominantly of pyroxenite, peridotite, harzburgite, and dunite, with subordinate gabbroic to gabbronoritic cumulates (Ballhaus & Glikson 1995—this issue). As such, it is closely comparable with the sequences of the Wingellina Hills, Kalka, and Ewarara intrusions to the east (Ballhaus & Glikson 1990). Outcrop at Murray Range is almost continuous for 2600 m and magmatic layering dips steeply between 80 and 90°.

The Murray Range sequence is characteristic of a magma chamber that experienced repeated episodes of primitive magma addition into a stagnant body of more fractionated multiply saturated resident melt. The first 500 m of the sequence, i.e. those units interpreted to be the bottom series, is composed of massive, poorly layered uniform pyroxenites. Following this unit is an exceptionally well-layered sequence of gabbroic to gabbronoritic units, alternating with wehrlite and peridotite layers (~600 to at least 1500 m). These rocks are interpreted as cumulates that separated from small pulses of primitive magma fed into a magma body of plagioclase-saturated, more evolved, resident melt of the same parentage. The stratigraphically higher units consist of ultramafic rocks, mostly coarse-grained orthopyroxenite, harzburgite, and subordinate dunite orthocumulates. Plagioclase in the upper part of the sequence is exclusively intercumulus and rarely exceeds five per cent.

Superimposed on the megascale layering are several shear zones concordant with the magmatic layering. Sheared cumulates are altered and variably deformed to mylonite. In places shearing was followed by intense hydration and in places intrusion of granitic and aplitic veins. Formerly magmatic contacts of the layered series of the Murray Range intrusion with granulites are obliterated by faulting and no chilled margins have been observed.

The Wart gabbro/pyroxenite intrusion

The Wart layered intrusion, south of Mount West and east of Bell Rock (Fig. 3) is a small sliver of interlayered mafic/ultramafic rocks intruded into felsic granulites. The magmatic sequence is at least 1900 m thick. Dip angles vary between 50 and 90°. The western part of the intrusion consists of homogeneous gabbro, possibly originally contiguous with the Bell Rock gabbro, from which it is separated by the Poonawarra valley (Fig. 3). If so, The Wart intrusion constitutes the basal ultramafic zone of the Bell Rock intrusion. Intrusive contacts are commonly marked by back-intruded felsic apophysae. The sequence consists of an exceptionally well-layered suite of clinopyroxenite cumulates, with numerous highly primitive wehrlite and, locally, peridotite intercalations and some olivine melagabbro, all overlying a sequence of gabbroic cumulates. Compared with pyroxenites of other mafic sequences of the Giles Complex, these pyroxenites are very poor in plagioclase. The most fractionated units exposed are olivine-bearing melagabbros with less than 40 vol. per cent calcic plagioclase.

The sequence also hosts a few stratiform microgabbro units and a number of crosscutting basaltic dykes. Most significant in elucidating the evolution of the Giles Complex is one set of basaltic dykes, where orthopyroxene is the only phenocryst phase in addition to some plagioclase microphenocrysts in the groundmass. This dyke offers evidence that possible feeders of the Giles Complex may have experienced pre-emplacement high-pressure fractionation. Most other dykes in this area carry phenocryst assemblages that disqualify them as reasonable parent melts to the layered sequence.

Michael Hills/Latitude Hill gabbro/pyroxenite intrusion

The Michael Hills gabbro/pyroxenite is the largest layered intrusion in the Tomkinson Ranges, forming a northward-concave flexure which deforms a shallowly northward-dipping and younging to near flat-lying sequence of gabbro, containing locally abundant thin (1–20 m thick) pyroxenites. The Latitude Hill tectonic sliver forms a north–south striking sequence, up to 8000 m thick, containing a pyroxenite-rich section at its base (Ballhaus & Glikson 1995—this issue). The sequence

Figure 7. Banded felsic to intermediate granulites.

has been sampled along three separate, but consecutive, traverses with minimal stratigraphic overlap or lateral displacement. Dips of the magmatic layers vary between 80 and 90°. The most common rock types are gabbros and microgabbros with unusually immature cumulate textures, along with cumulate-textured gabbros, orthopyroxenites, and, rarely, olivine-bearing ultramafic cumulates. It is debatable whether the cumulates exposed at Latitude Hill represent one continuous and genetically coherent sequence, or are a tectonically dismembered composite with up to three genetically and temporally different units. Rock types of the central part of the sequence (from about 2900 m to at least 4250 m) are highly deformed and far more fractionated than cumulates of lower and upper sections. The underlying and overlying cumulates are undeformed, except along some localized shear zones, significantly more mafic, and texturally quite different from the central deformed sliver.

Hinckley Range gabbro intrusion

The Hinckley Range gabbro is delimited and cut by major east–west shear zones and is, in places, intruded by granites. The magmatic sequence is approximately 5800 m thick and dips 70 to 80° northward. Cryptic layering patterns, and graded and crosscutting laminations suggest northward younging, i.e. the same as the Michael Hills intrusion, but the reverse of the juxtaposed Wingellina Hills intrusion. The Hinckley Range gabbro is one of the more deformed intrusions of the Giles Complex. Its western units are affected by a metamorphic overprint, producing mafic granulites (formerly magmatic gabbros) interleaved with intrusive granitic veins, owing to their deformation by D_3. In this part of the Hinckley Range, cumulate textures and magmatic layering are poorly preserved. The eastern extension of the intrusion has, however, largely escaped deformation and metamorphic overprint. The most common rock types in the eastern part of the Hinckley Range include troctolites, olivine gabbros, gabbronorites, and anorthosites, as well as their deformed equivalents (Ballhaus & Glikson 1995—this issue). These rocks are intruded by thin (~5 m) layers and pods of finer grained microgabbros. Since crystallisation sequences in the latter are identical to the cumulus mineralogy of the coarser grained host gabbro, they are interpreted as the more rapidly cooled equivalents of similar magma. However, as in other intrusions, the coarser grained country rocks back-intrude the microgabbro sills, suggesting their emplacement at late magmatic stages.

The layered sequence is also cut by several generations of basaltic dykes, including an olivine–spinel-phyric dyke generation primitive enough to be mantle-derived. This composition probably qualifies as parental melt to the ultramafic olivine-rich units at Wingellina Hills, Murray Range, and the Kalka intrusions. It may also represent the primary melt composition from which all derivative parental liquids to the Giles Complex have been derived.

Along the western margin, the layered sequence is infiltrated and crosscut by felsite veins to very coarse-grained granitic material, where quartz and K-feldspar may occur in graphic intergrowth. In addition, there are several major mylonite zones near-parallel to the magmatic layering. The most prominent is the extension of the Hinckley thrust fault (Goode 1978), a series of layer-parallel splay faults and pseudotachylite veins within the Hinckley Range sequence. Nowhere in the Giles Complex are pseudotachylite veins more abundant and of greater thickness than in the Hinckley Range, where superimposed vein networks may be over 50 m thick (Glikson & Mernagh 1990).

Bell Rock–Blackstone gabbro/troctolite intrusion

The Bell Rock gabbro and Blackstone gabbro, separated by an unexposed zone marked by a magnetic lineament representing a fault south of Mount Aloysius (Fig. 2), are considered as segments of the same body (Daniels 1974) and are, therefore, discussed together.

The ***Bell Rock gabbro*** consists of a fractionated well-layered 3800 m thick sequence of troctolites, gabbroic troctolites, anorthosites, some dunitic cumulates, and several thin massive oxide horizons. The stratigraphic column, as deduced from thin-section microscopy and field observations, is illustrated in (Ballhaus & Glikson 1995—this issue). The sequence dips at approximately 70° toward the southwest. The lower quarter comprises gabbroic troctolites and some olivine gabbro, gabbronorite, and microgabbro units. The remainder is dominated by oxide-bearing troctolites, anorthosites, and thin dunite horizons. Further up the sequence, magnetite changes from intercumulus to cumulus, culminating in several decimetre-thick massive magnetite layers. This uppermost iron-rich unit forms a consistent marker along the Bell Rock gabbro and is conspicuous on aerial photographs, owing to its more-oxidised red color. Apart from the magnetite units and a few dunite layers, monomineralic units are rare in the Bell Rock sequence, and there are few departures from cotectic crystallisation relationships. Magmatic layering, therefore, is mainly developed on a small centimetre-to-metre scale. Megascale cyclicity, such as in the Murray Range or Wingellina Hills intrusions, is absent.

The ***Blackstone gabbro*** is strikingly similar to the Bell Rock gabbro in mineralogy, magmatic stratigraphy, styles of magmatic layering, and degree of fractionation. Both bodies comprise several fine-grained stratiform microgabbro units and crosscutting dykes, whose phenocryst mineralogy resembles the cumulus mineralogy and crystallisation sequence in the layered cumulates. The Blackstone Range gabbro consists of a thick (>3600 m) south-younging and south-dipping (~70°) sequence of highly fractionated troctolites, olivine gabbros, anorthosites, a few dunite layers, and some tens of centimetre-thick monomineralic magnetite layers (Ballhaus & Glikson 1995—this issue). Along the north, the intrusion is recrystallised into phlogopite-bearing mafic granulites, whereas contacts with the felsic igneous and metamorphic country rocks are unexposed. Along its southern contact, the intrusion is faulted against the Tollu Group volcanics. The fault shows as a marked lineament on the total magnetic intensity map, but is otherwise unexposed. With the exception of one dunite layer and several thin magnetite layers, there is little evidence for megascale phase layering. Instead, the cumulates are well layered on a smaller scale, with olivine/plagioclase layers, a few centimetres thick, being common.

Jameson Range gabbro/troctolite

This intrusion consists of roughly 2500 m of well-layered olivine–plagioclase cumulates (Ballhaus & Glikson 1995—this issue). The Jameson Range sequence includes some of the most fractionated cumulates of the Giles Complex. It comprises

variably well-layered and partly deformed troctolites, gabbroic troctolites, and anorthosite adcumulates. Extreme chemical differentiation in the upper part of the sequence led to the formation of several massive titaniferous and vanadiferous magnetite layers. Exposure is comparatively poor and about two thirds of the magmatic sequence is covered by alluvium. The bottom and top contacts of the intrusion are not exposed and the nature of the contacts with the country rocks is unknown.

Cavenagh gabbro. This body consists of nearly flat-lying sheets of gabbro and gabbronorite cut penetratively by dense swarms of subvertical dolerite dykes on a variety of scales. In places, dykes are spaced every 10–100 m or so. The body forms a dissected plateau and a group of low table-top hills, which occupy an area of about 10 x 10 km. As the bulk of the body occurs within Aboriginal sacred ground, only the northernmost part was examined and the intrusion remains a subject for future work.

Morgan Range gabbro. This 5 km long, northwest-trending body consists mainly of intensely recrystallised gabbro and mafic granulite, intruded by pegmatite and granite veins, and cut by both northwest and northeast-trending dykes. The extensive recrystallisation resulted in obliteration of most primary magmatic structures and textures.

Teizi anorthosites

The felsic granulite sequence of the Ewarara–Teizi Ranges between north of Gosse Pile and the Teizi bore area is extensively intruded by lenses of little-deformed, coarse-grained, magmatically textured to gneissose anorthosites and by numerous sills of recrystallised, fine-grained, granoblastic meta-anorthosite. Discrimination between fine-grained granoblastic anorthosites and feldspathic felsic granulites in outcrop hinges on the occurrence of quartz in the latter. The anorthosites have a clay-rich weathering crust, owing to the lower stability of calcic plagioclase, allowing its depiction by clay indicators of Landsat-5 TM (Glikson & Creasy 1995—this issue). The Teizi anorthosites (Gray 1967) consist of anorthosites (100% plg), orthopyroxene–plagioclase gneiss, and rare orthopyroxene rocks. The sequence is about 1500 m thick, and is classified in terms of nine mappable lithological units, which define an antiformal structure. Boundaries between the anorthosite and country rock felsic granulites are difficult to define. The core of the antiform contains even-grained gabbroic anorthosite, consisting of interlocking antiperthitic plagioclase (~85%) and interstitial orthopyroxene (~15%). Deformation has produced complex interlayering, with gradational contacts between pyroxene–plagioclase gneiss, foliated gabbroic anorthosite, and pure anorthosite. The major component of the Teizi anorthosites is coarse-grained blue-grey anorthosite, with pyroxene occasionally exceeding 10 per cent. Antiperthitic plagioclase occurs as serrated interlocking grains, forming a metamorphic texture. Pyroxene may form foliated aggregates and augen-shaped clots. The unit includes a sheared recrystallised fine-grained equivalent of the anorthosite, containing relic coarse-grained anorthosite. This variety dominates the narrow, heavily sheared and recrystallised, fine-grained anorthositic sills mapped north and west of Teizi bore. Alteration is associated with development of carbonate. Advanced to cataclastic deformation of anorthosites is marked by a general decrease in twinning and bending of relic twinning, undulose extinction, shearing, areas of granulation, and grain alignment with long axes parallel. Layered anorthositic units within massive anorthositic units form useful structural markers. Layering, on a scale of a few to about 30 cm, is defined by varying pyroxene/plagioclase proportions. Mineral assemblages may include garnet and hornblende. The plagioclase in the layered units is not antiperthitic and the texture is granoblastic. Pegmatitic units consist of very coarse-grained orthopyroxene. The Teizi anorthosites include a transitional contact unit of mafic granulite, consisting of opx–cpx–plg–gnt assemblages.

Petrology of the Giles Complex

The layered intrusions of the Giles Complex can be classified in terms of several types: (1) large (10–40 km along strike) gabbroic bodies with a small or no ultramafic component, e.g. Jameson, Blackstone, Cavenagh, Bell Rock, Hinckley, Michael Hills, and Mount Davies; (2) small to medium-sized (<10 km along strike) layered intrusions with a significant ultramafic component, e.g. Murray Range, The Wart, Ewarara, Kalka, Gosse Pile, and (4) small to medium-scale bodies of anorthosite, i.e. Teizi anorthosites (Figs. 2, 3). Four types of bodies are distinguished (listed in terms of increasing ultramafic component): (1) anorthosites (Teizi); (2) troctolite-dominated, commonly magnetite-rich, intrusions, containing little or no ultramafic component (Jameson, Blackstone, Bell Rock); (3) cpx–opx–plg-dominated gabbroic intrusions, consisting of norite, gabbronorite and clinopyroxene-rich gabbro and commonly containing units of pyroxenite, anorthosite and, less commonly, peridotite (Hinckley, Michael Hills, Mount Davies, Kalka, Wingellina Hills); and (4) intrusions dominated by pyroxenite and peridotite (Murray Hills, Ewarara, Gosse Pile, Claude Hills). Ultramafic units crystallised from unfractionated, mantle-derived, primitive basaltic magmas that were only saturated with olivine ± spinel at the time of emplacement. The gabbroic magmas were derived from slightly to moderately fractionated liquids, multiply saturated with olivine or orthopyroxene, clinopyroxene, and plagioclase upon emplacement. The most fractionated troctolitic intrusions crystallised from highly evolved, extremely silica-undersaturated, parent liquids with Fe-rich olivine and plagioclase as liquidus phases.

Chemically, it is difficult to relate the above magma types to a single liquid line of descent from a unique parent magma. In other words, the ultramafic units intercalated in the gabbro-dominated sills do not represent local crystal fractionation of the resident gabbroic magmas within the magma chamber, although some fractionation in situ is evident from upward iron enrichment, for example in the Bell Rock intrusion (Ballhaus & Glikson 1995—this issue). Furthermore, the sills differ from each other with regard to the degree of fractionation of their parent gabbroic magmas, as represented by the point at which olivine was replaced on the liquidus by orthopyroxene. Thus, in ultramafic sequences, the olivine–melt peritectic occurs at Fo_{77}, in primitive gabbro at $Fo_{68–57}$, while in the undersaturated troctolites, olivine persists to $Fo_{50–40}$. The variations in the composition of the least-fractionated basic magmas in each intrusion suggest that the parent magmas were fractionated, owing to high-pressure orthopyroxene precipitation, before their intrusion as sills.

The Wingellina Hills body (Ballhaus & Glikson 1989) is an example of the third type of intrusion. It consists of a poorly fractionated sequence of dunite, wehrlite, pyroxenite, gabbro, and gabbronorite. Chemical fractionation is limited: the Mg number (Mg/Mg+Fe) of olivine and orthopyroxene ranges from 0.89 at the base to 0.74 at the top of the intrusion. Orthopyroxene replaces olivine on the liquidus at Mg number about 0.77–0.78. Microprobe data have demonstrated a multiple intrusive history for the Wingellina Hills body, with batches of olivine–spinel saturated parent magma periodically emplaced into cooler and more evolved orthopyroxene–clinopyroxene–plagioclase-saturated resident magma. Intrusive events are recognised by coarse-grained ultramafic orthocumulate horizons resting on partly resorbed fine-grained footwalls of fractionated gabbronoritic adcumulates. These contacts are marked by sharp reversals in the composition of olivine, plagioclase, and clinopyroxene.

Examples of microscopic textures of the more common rock types of which the Giles Complex consists are given in Figure 8. Some of the results of the petrological study of the

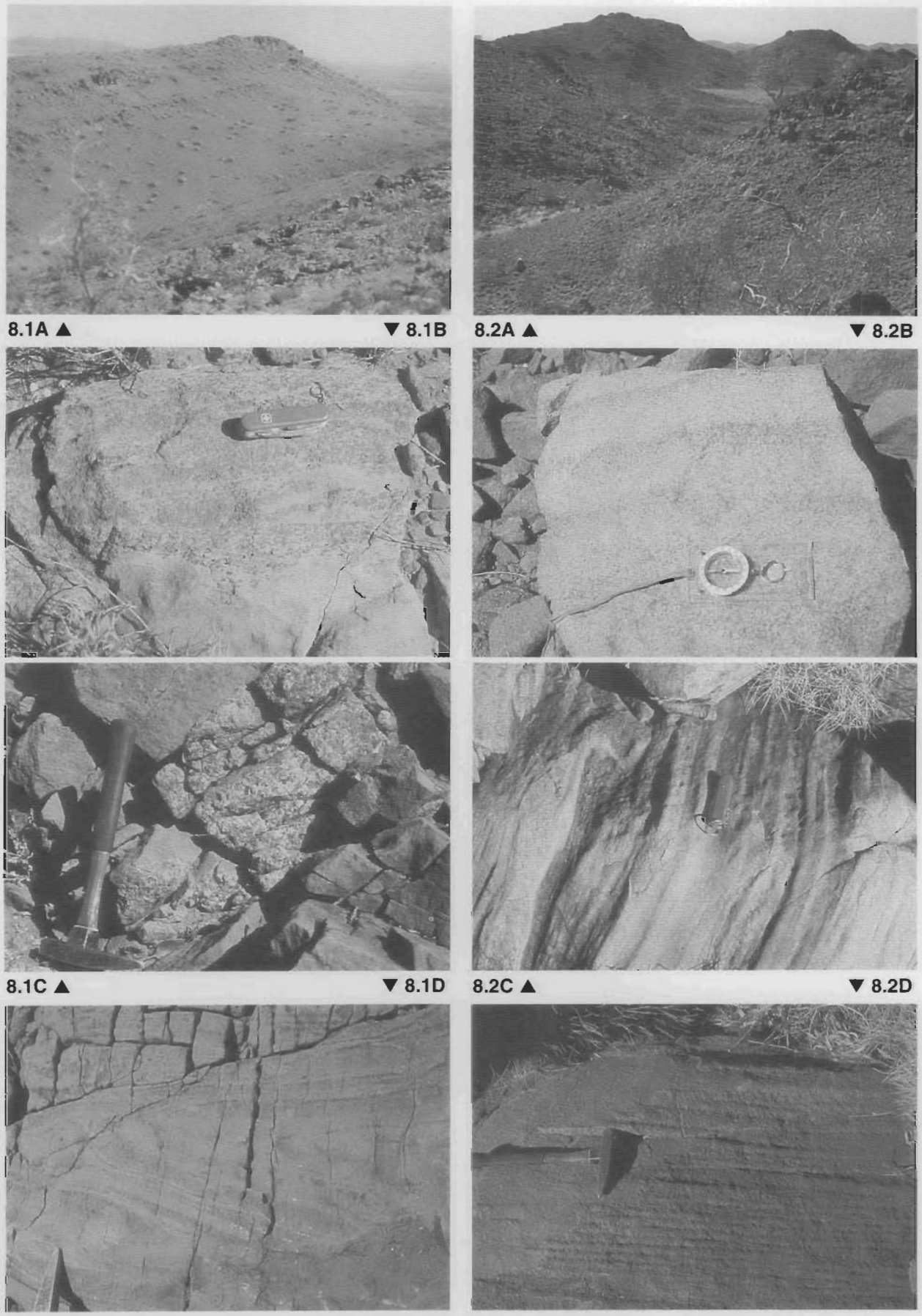

Figure 8. Intrusions of the Giles Complex. 8.1—Wingellina Hills intrusion: A, ravine section of gabbro (smooth slope) and pyroxenite (dark banks); B, mixed zone of gabbronorite and pyroxenite; C, folded flow segregated gabbronorite; D, pegmatoid pyroxenite unit, including chromitite pods. 8.2—Bell Rock intrusion: A, outcrops of gabbro truncated by a dyke, northern Bell Rock range; B, cross-layered gabbro; C, rhythmically laminated gabbro; D, rhythmically laminated gabbro;

8.2E ▲ ▼ 8.2F

8.3A ▲ ▼ 8.3B

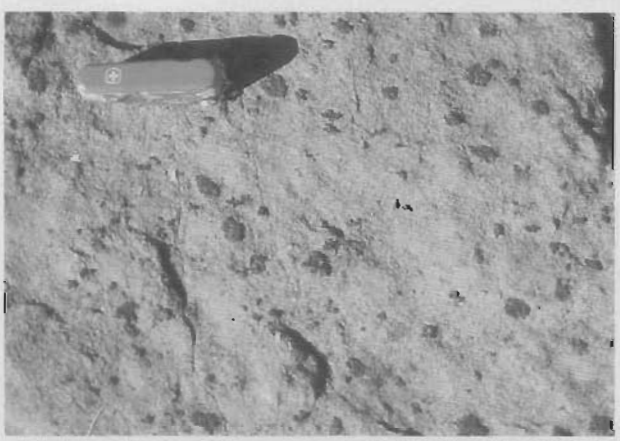

8.2G ▲ ▼ 8.2H

8.4A ▲ ▼ 8.4B

Figure 8 continued. **E, mixed coarse grained and medium grained gabbro; F, cumuloblasts of pyroxene in gabbro; G, microgranite-veined contact with the Mt West orthogneiss; H, microgranite-veined contact with the Mt West orthogneiss. 8.3—Murray Range intrusion: A, layered gabbro, recrystallised gabbro, pyroxenite and peridotite, looking northeast; B, layered peridotite. 8.4—Jameson Range intrusion: A, layered troctolites; B, olivine and clinopyroxene rock unit in banded troctolite;**

8.4C ▲ ▼ 8.4D

8.5C ▲ ▼ 8.5D

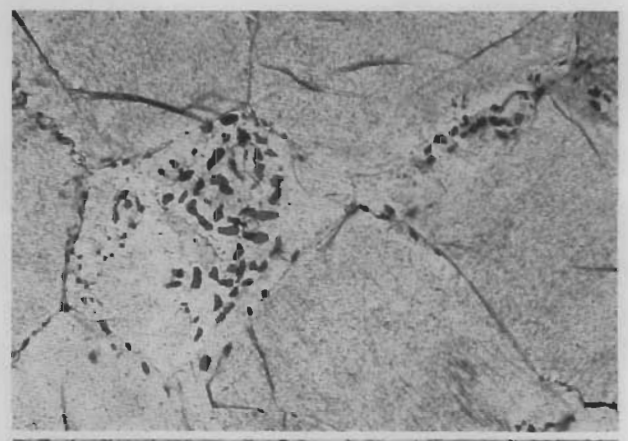

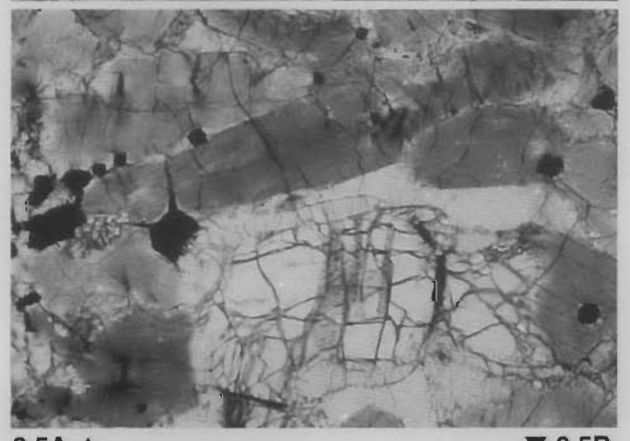

8.5A ▲ ▼ 8.5B

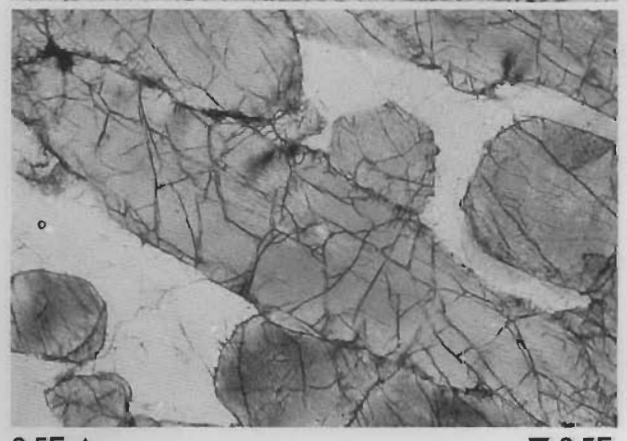

8.5E ▲ ▼ 8.5F

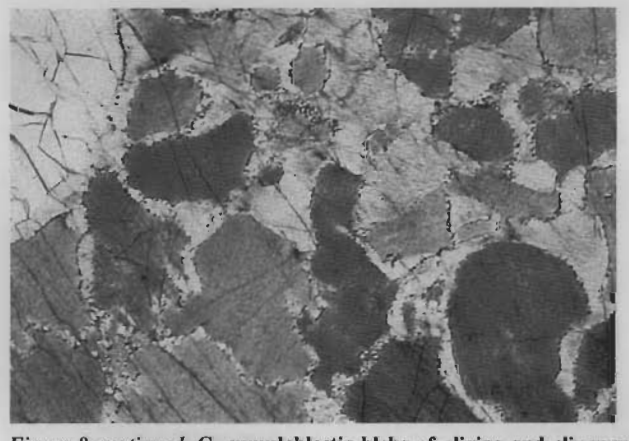

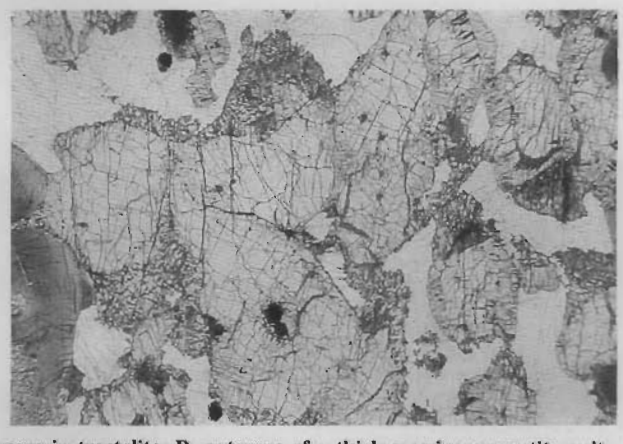

Figure 8 continued. C, cumuloblastic blebs of olivine and clinopyroxene in troctolite; D, outcrops of a thick massive magnetite unit. 8.5—Photomicrographs of ultramafic cumulates: A, harzburgite, Murray Range intrusion, showing cracked olivine, blades of orthopyroxene clouded by exsolved spinel and opaque chromite grain; B, wehrlite, Murray Range intrusion, showing cracked olivine and adcumulus clinopyroxene with late exsolved lamella of orthopyroxene; C, feldspathic orthopyroxenite cumulate, Murray Range

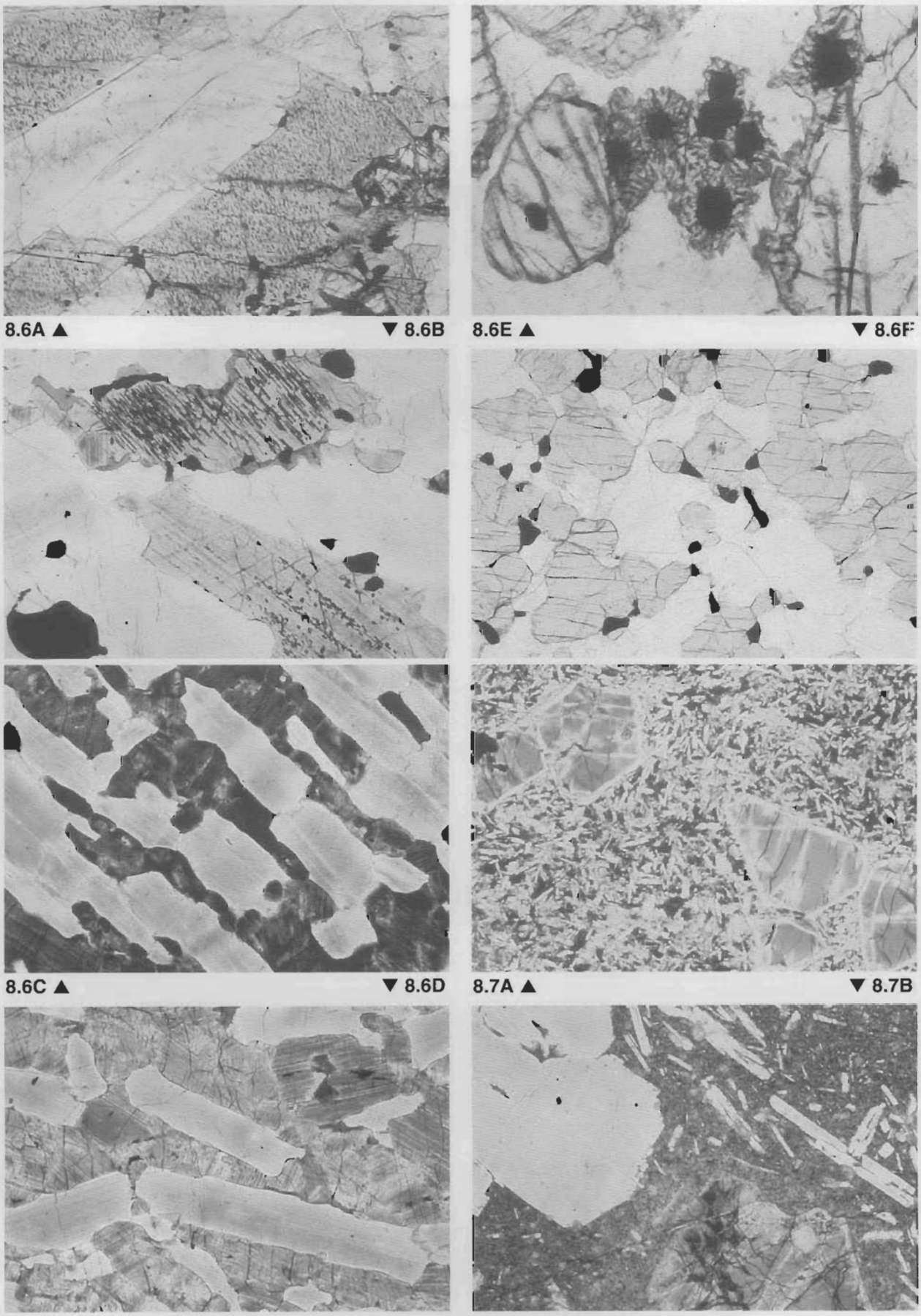

Figure 8 continued. **intrusion, showing euhedral clouded orthopyroxene, intercumulus plagioclase, poikilitic clinopyroxene and accessory oxides; D, orthopyroxenite adcumulate, Murray Range intrusion, showing interlocked orthopyroxene intergrowth and granular spinel; E, orthopyroxenite orthocumulate, Latitude Hill (part of the Michael Hills intrusion), showing orthopyroxene and intercumulus plagioclase; F, olivine-rich wehrlite, Wingellina Hills, showing olivine grains rimmed by spinel–cpx–opx symplectite in contact with intercumulus plagioclase. Cumulus clouded clinopyroxene grain shows on the right. 8.6—Photomicrographs of gabbroic and troclolitic rocks: A, troctolite, Bell Rock intrusion, showing small grains of olivine, medium-grained clouded clinopyroxene pokilitically enclosing plagioclase;**

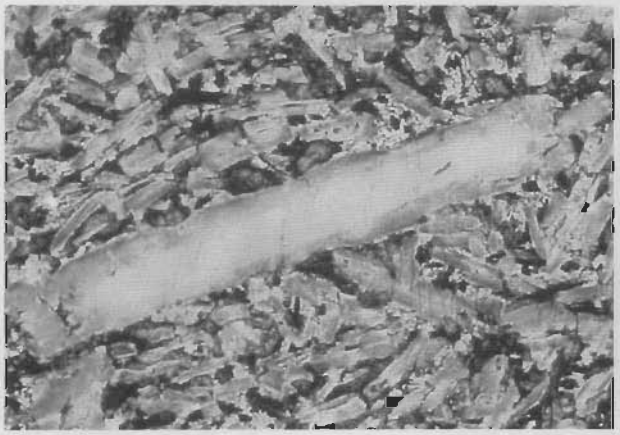

8.7C ▲

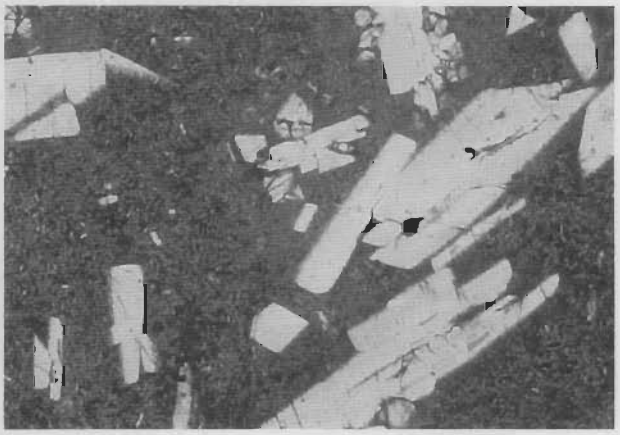

8.7D ▲

Figure 8 continued. **8.6B, gabbronorite, Bell Rock intrusion, showing orthopyroxene with spinel exsolutions interlocked with cumulus plagioclase; accessory oxides; C, anorthositic adcumulate, Latitude Hill, showing cumulus plagioclase and intercumulus clouded clinopyroxene; D, dolerite-textured gabbronorite, Latitude Hill, showing cumulus plagioclase and cumulus clinopyroxene (with exsolved lamella) rimmed by orothopyroxene; E, troctolite, Wingellina Hills, showing cumulus olivine, plagioclase and oxide grains—note the symplectite (spinel–cpx–opx) corona around olivine and oxides; F, microgabbro, Hinckley Range intrusion, showing interlocked clinopyroxene, orthopyroxene, plagioclase and exsolved oxides. 8.7—Photomicrographs of hypabyssal sills and dykes emplaced within the Giles Complex: A, olivine-phyric dyke intruded into the Hinckley Range intrusion, showing orthopyroxene-rimmed porphyritic olivine in groundmass dominated by plagioclase, oxides and alteration products; B, plagioclase and olivine-phyric dyke intruded into anorthosites of the Bell Rock intrusion; C, plagioclase and olivine-phyric sill intruded into the Bell Rock intrusion; D, plagioclase lath in clinopyroxene–magnetite-rich groundmass of a dyke intruded into the Bell Rock intrusion.**

Giles Complex (Ballhaus & Glikson 1989; Ballhaus 1992; Ballhaus & Glikson 1995—this issue) are summarised below.

The layered mafic/ultramafic bodies experienced a history of multiple intrusion, as documented in the Wingellina Hills, where fractionated gabbronorite resident magma was periodically replenished by batches of more primitive, olivine-saturated melt. Similar relationships exist in other bodies with a significant ultramafic component, i.e. the Murray Range, The Wart, and Latitude Hill layered intrusions. The intrusions crystallised from several distinct magmas of different composition and degree of fractionation, but all related to a single parent magma fractionated before emplacement. The Mg number at which olivine is replaced by orthopyroxene on the liquidus is positively related to the silica activity of the melt, in turn reflecting the fractionation and assimilation history of the parent magma. The Wingellina Hills, Murray Range and The Wart intrusions were derived from an unfractionated hypersthene-normative MORB-type (mid-oceanic-ridge basalt) magma, with orthopyroxene replacing olivine at an Mg number of about 0.78–0.76; a composition possibly close to the parent magma. The Bell Rock, Jameson, and Blackstone gabbros were derived from fractionated olivine (± nepheline)-normative melts, with the most primitive olivine of Mg number around 0.67, persisting down to 0.55–0.5. The Latitude Hill and Hinckley intrusions fall between these extremes, with values of 0.82–0.65.

Some intrusions show an exponential increase in the degree of fractionation of their cumulus phases within about 200 m of their present hanging-wall contacts (Ballhaus & Glikson 1995—this issue), suggesting that the present upper contacts approximate the original upper intrusive boundaries, and that each intrusion followed its liquid line of descent, intermittently interrupted by replenishment.

The penetrative dyke swarm within the Giles Complex includes compositions that may be correlated with those of the parental precursor and derivative magmas of the layered intrusions, with phenocryst compositions and crystallisation sequences matching those in the spatially associated intrusions.

The intrusions display at least two generations of gabbro: (a) massive medium to coarse-grained gabbro, and (b) relic concordant units of microgabbro up to a few metres thick. The microgabbro is minor to very minor in volume as compared to the medium-grained gabbro. It appears that the main intrusions were followed by small and more rapidly cooled gabbroic pulses, forming sills under above-solidus conditions of the resident gabbro chambers.

The above suggests that the present structural pattern of the layered intrusions closely reflects the shapes of the original magmatic bodies, which were only related through magma parentage, i.e. they are not slices of an originally contiguous Bushveld-like lopolith. The exponential increases in degree of fractionation at the upper contacts of most intrusions indicate that each intrusion represents a discrete magma chamber that followed its individual fractionation path. However, it is difficult to relate all intrusions to a single liquid line of descent of one continually fractionating parent magma, where the primitive olivine-rich intrusions constitute basal units and the more-evolved intrusions, the fractionated end-members.

Phase-equilibrium considerations demand that, once olivine is replaced on the liquidus by orthopyroxene, the magma cannot revert to olivine-normative conditions and simultaneously continue its normal fractionation path with respect to the Mg number of olivine and orthopyroxene and to the Ca/Ca+Na ratio of plagioclase. The olivine/plagioclase relations are best explained in terms of high-pressure orthopyroxene (±clinopyroxene) fractionation of a common parent, i.e. the source magma of gabbroic intrusions (Blackstone, Bell Rock, and Jameson) suffered extensive orthopyroxene fractionation at greater depth before emplacement. The Giles Complex is thus defined as a series of discrete coeval intrusions, sills and associated feeder dykes related through a common magma parentage.

Granitoids associated with the Giles Complex

Units of granitic gneiss to massive charnockite occur within the banded granulites as lenses and pods, with a range of age relationships to the mafic/ultramafic intrusions of the Giles Complex. Examples of the various granite types are given in Figure 9. Clarke et al. (1992) identified lenses of post-D_1, pre-D_2 charnockite in the western end of the Hinckley Range, and such relationships are supported by U–Pb ion-probe data for an isolated outcrop of pre-D_2 granitic gneiss between the Mount Davies and Kalka layered intrusions (Minno granite gneiss)(Fig. 3). Extensive porphyritic granites, of the Champ de Mars area, locally dated as 1188±4 Ma, are now considered

to predate the Giles Complex (Sun et al. in press). Back-intrusion-like relations of granitoid veins into gabbro along gabbro–felsic granulite boundaries suggest contemporaneity of at least some granitic veins with the emplacement of the Giles Complex (Glikson & Stewart 1991). The age of at least some of these veins approximates the ~1.08 Ga Tollu Group volcanics.

The felsic intrusive rocks range from veins and dykes to small plutons which intrude both felsic granulites and recrystallised layered mafic/ultramafic intrusions—particularly where the latter are recrystallised into mafic granulites. Most are of granitic (s.s.) composition, with subordinate quartz monzodiorite and quartz syenite; granodiorite and tonalite appear to be rare or absent. Three varieties of granite are identified in the Champ de Mars complex, including (1) orthopyroxene granite (charnockite); (2) rapakivi granite, and (3) porphyritic (megacrystic) to even-grained granite. The orthopyroxene-bearing granites represent dry magmas, whereas biotite and/or hornblende-bearing granites may represent younger more hydrous melting. In the following, each of the granite groups is discussed separately:

Orthopyroxene-bearing granite, quartz monzonite and quartz monzodiorite have been documented in several areas (Minno, Chanockite Flats, Champ de Mars, Blackstone–Murray Range area). Pre-Giles Complex intrusions may be represented by a pre-D_2 biotite granite gneiss—constituting a likely deformed derivative from associated orthopyroxene granite—at Minno. This rock yields a U–Pb zircon age of 1198±6 Ma (Sun & Sheraton 1992), within the error of a Rb–Sr age of 1205±23 m.y. (Gray 1978). No contacts were observed between the Minno granite and the nearby shear-bounded Mount Davies and Kalka layered intrusions.

The Champs de Mars granites include conformable pods and stocks of foliated, locally porphyritic, cpx–opx–hbl–biotite granite within felsic granulites, dominated by perthite and antiperthitic oligoclase–andesite. Orthopyroxene (<3%), red-brown biotite and green-brown hornblende form minor phases; Fe–Ti oxides, apatite and zircon are accessory minerals. Similar granites are associated with, and probably related to, rapakivi/porphyritic granites. Mesoperthite may be present in orthopyroxene granites, e.g. Blackstone–Murray Range area. The mafic mineral content rises in contact zones associated with the Giles Complex: a zone of quartz monzodiorite associated with the southern contact of the Mount Davies layered intrusion has a higher mafic minerals content (opx 5–7%; cpx <3%; antiperthitic andesine; quartz– K-feldspar granophyre (Sheraton & Sun, 1995—this issue).

The porphyritic pre-Giles Complex granitoids in the Champ de Mars valley, and hosts of granitic dykes and veins which cut gabbro and derived basic granulite in the western Hinckley Range, were originally considered to represent manifestations of the same event (Glikson et al. 1990). Rapakivi granites consist of corroded megacrysts of perthitic K-feldspar, commonly microcline, rimmed by relatively fine-grained plagioclase associated with hornblende, pyroxene, or quartz. The distribution of rapakivi megacrysts is irregular, and unmantled K-feldspar and plagioclase (oligoclase–andesine) megacrysts are common. Rapakivi granite grading into quartz monzonite contains brown-green hornblende (<10%), red-brown biotite (<5%), clinopyroxene (<3%) and minor orthopyroxene, and accessory apatite, zircon, Fe–Ti oxides and ?chevkinite. Pervasive crystallisation, syn-D_3 and later events, resulted in the development of augen gneiss in places. The more-deformed gneisses may contain minor pale-golden garnet. Pyroxene appears to be confined to less-deformed granitoids. Fine-grained biotite–hornblende–quartz aggregates may signify replacement of pyroxene.

Fine to even-grained and porphyritic granitoid varieties are petrographically similar to the rapakivi granites, apart for the absence of mantled K-feldspar. Perthitic K-feldspar phenocrysts are commonly partly resorbed. Minor phases include hornblende (both dark-green primary and pale-green secondary)(<4%), dark to red-brown biotite (<4%), orthopyroxene (<2%) and rare relic clinopyroxene. Recrystallisation is widespread and may be accompanied by minor secondary garnet. Accessories include Fe–Ti oxide, apatite, zircon, allanite and, less commonly, sphene. Granitic dykes and veins which intrude the Hinckley Gabbro contain biotite (<2%), hornblende (<3%), rare clinopyroxene and accessory Fe–Ti oxides, apatite, zircon, sphene, rare allanite and ?chevkinite.

The Tollu Group (Bentley Supergroup) volcanics

The Bell Rock Gabbro and Blackstone Gabbro are bound to the southwest and south by structural discontinuities, manifested as magnetic lineaments, which are probably normal faults, where volcanics of the 1080 Ma Tollu Group (U–Pb ion-probe zircon age; Sun et al. in press) are downfaulted against the Giles Complex (Fig. 2). No exposures of this fault zone have been observed, although, at one locality, felsic volcanics crop out within a few hundred metres of the gabbro. The southern block consists of a gently dipping to flat-lying volcanic sequence, which overlies granitic basement inliers through a major unconformity capped by a basal conglomerate. Examples of outcrops of the Tollu Group volcanics are given in Fig. 10. The basement consists of biotite granite (s.s.) (biotite <3%), quartz, perthitic microcline, sericitised oligoclase, minor Fe–Ti oxides, apatite, zircon, sphene, allanite, ?chevkinite, fluorite). These rocks are similar to, although they tend to be more siliceous than, the porphyritic/rapakivi biotite–hornblende granites of the Champ de Mars area. Some of these granites are characterised by low HFSE and high Ce/Y, and are interpreted in terms of partial melting of plagioclase-poor mafic source materials (Sheraton & Sun, 1995—this issue). Granites of probable coeval relationship with the Tollu Group, i.e. fluorite and garnet-bearing hornblende granite, are emplaced into, and are of similar chemistry to, the Smoke Hill Volcanics.

Volcanics of the Tollu Group include mafic and felsic lavas overlying a basal quartz pebble-bearing conglomerate with arkose and gritstone intercalations. The Mummawarrawarra Basalt includes a variety of fine-grained amygdaloidal basalts with textures from hypocrystalline to subophitic. Relict clinopyroxenes are present, but mafic phases are generally replaced by chlorite, epidote and /or amphibole, and plagioclase is commonly sericitised or saussuritised. Most samples are markedly Q-normative tholeiites, ranging from basalt, through basaltic andesite, to andesite, according to the classification of Le Maitre (1989). Several basaltic and basaltic andesite dykes intruding the basement underlying the Tollu Group are chemically similar to the Mummawarrawarra Basalt.

The felsic Smoke Hill Volcanics include subordinate mafic and intermediate rocks, and are, in places, intruded by stocks of gabbro and granite. Rhyolites (defined on the alkali–SiO_2 diagram after Le Bas 1986) grade into dacite and trachydacite. The dacites contain sericitised plagioclase phenocrysts and amphibole-altered clinopyroxene in fine-grained magnetite-rich quartz–feldspar matrix and are, in places, epidote-rich (Giles 1981). Rhyolites are K-feldspar–plagioclase(albite–oligoclase)–quartz-phyric and contain fine-grained dark-green hornblende (<5%), dark-brown biotite, stilpnomelane, Fe–Ti oxides, sphene, apatite, zircon and secondary chlorite, epidote and garnet. Many rhyolites show relict, tectonically modified, volcanic lamination, and some display relict eutaxitic structures, devitrification textures, and units of crystal to lithic tuff. The quartz–feldspar groundmass is invariably recrystallised and phenocrysts are broken or recrystallised (Giles 1981). These rocks show typical A-type features (Sheraton & Sun, 1995—this issue). Slightly porphyritic trachyte veins cut the Mummawar-

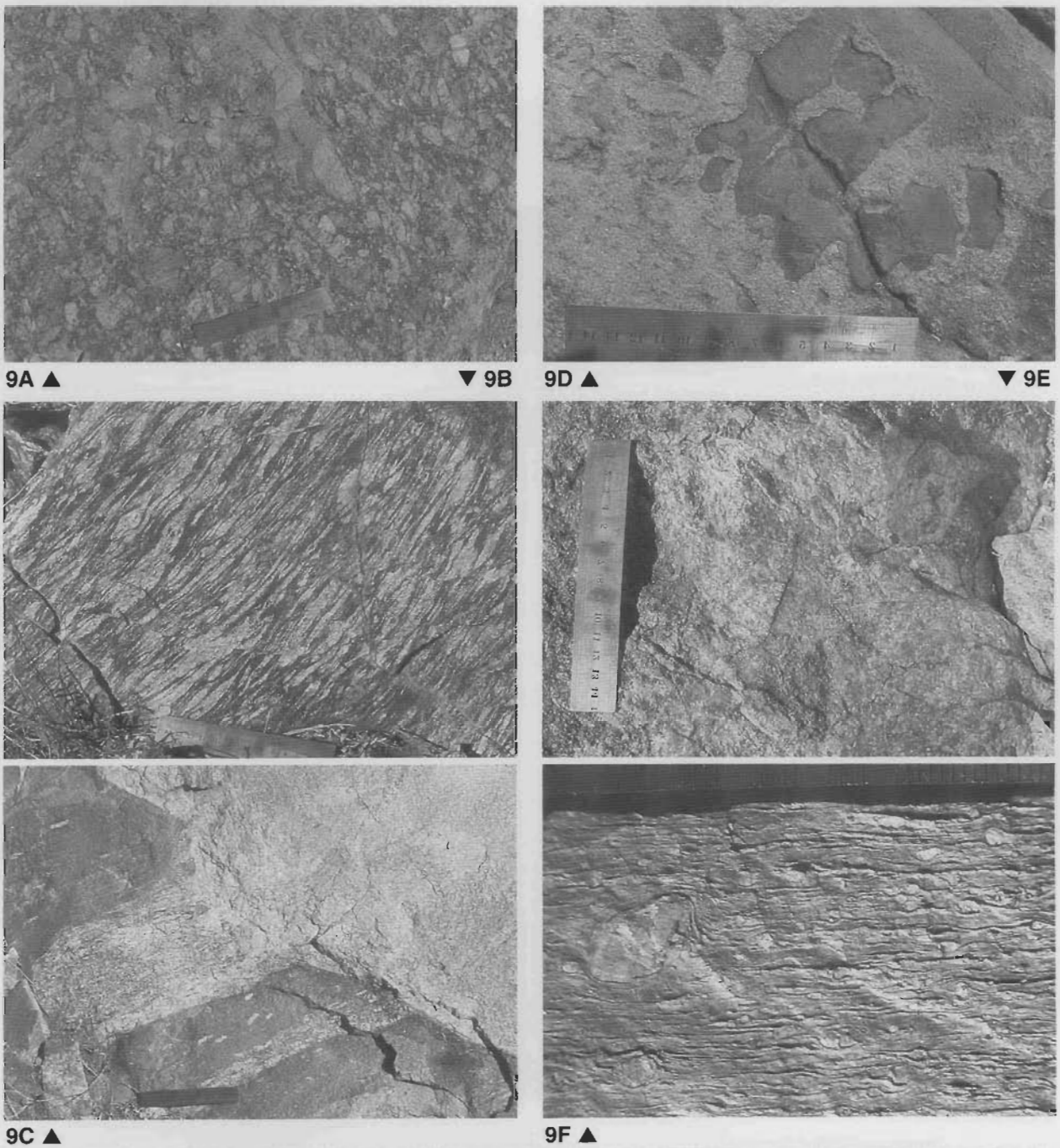

Figure 9. Granitoid outcrops. A, porphyroblastic rapakivi granite including a relic band of felsic granulite or microgranite, Champ de Mars valley; B, intermediate segregated granulite or orthogneiss; basement of the Tollu Group south of Blackstone Range; C, banded porphyritic granite and microgranite intruded by leucogranite (upper left), basement of the Tollu Group south of Blackstone Range; D, mafic xenoliths within porphyritic granitoids, south Tomkinson Ranges; E, relics of quartzite within recrystallised felsic granulite/granitoid, south Tomkinson Ranges. F, mylonitised granite, south Tomkinson Ranges.

rawarra Basalt at McDougall Bluff; they comprise rare altered alkali feldspar phenocrysts in trachytic groundmass, with minor quartz, Fe–Ti oxides, and fluorite.

Giles (1981) tested alternative models for derivation of the bimodal Tollu Group volcanics by geochemical least-square mixing calculations—observing that crystal fractionation of basic magmas of Mummawarrawarra Basalt composition (involving residual hornblende, plagioclase, clinopyroxene, magnetite, apatite) is unable to give rise to the rhyolites of the Smoke Hill Volcanics. A derivation of at least some of the felsic volcanics by crystal fractionation of the basic magma cannot be ruled out from present geochemical considerations, especially in connection with the trachyte veins mentioned above. However, this interpretation raises difficulties regarding the low Ce/Y ratios, high Nb/Zr ratios and the need for K-feldspar fractionation, inherent in the model. The alternative model involves partial melting of felsic granulites of the type presently exposed in the Tomkinson Ranges (see above), but gives rise to inconsistencies between the degrees of partial melting indicated by the bulk composition of the dacites and that required by the high field strength elements (HFSE) enrichment. Assuming instead the anatexis of an unexposed intermediate/felsic source, leaving residual plagioclase, but little residual mafic phases, allows the production of Sr-depleted, low Ce/Y magmas, similar to the dacites/rhyolites. Such a model is consistent with considerations based on Nd

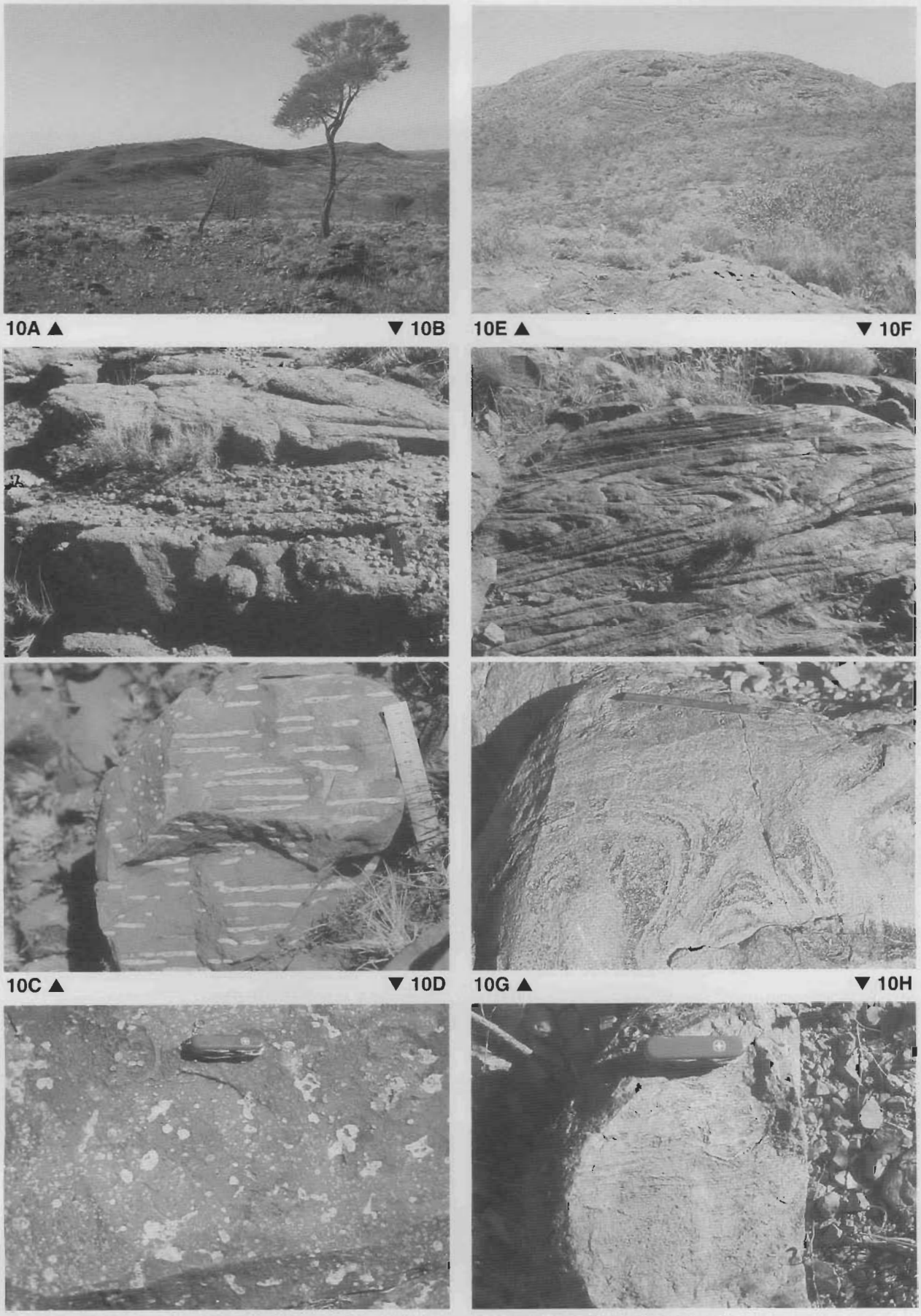

Figure 10. Volcanic rocks of the Tollu Group. A, low-dipping sequence of basalt and andesite at MacDougall Bluff; B, basal quartz pebble conglomerate at the base of the Bentley Supergroup, MacDougall Bluff; C, pipe-structured quartz amygdales in andesite, MacDougall Bluff; D, large quartz-filled vugs in andesite, MacDougall Bluff; E, outcrop of felsic volcanics at Mt Maria; F, folds in felsic volcanics, Tollu Hill; G, folds in felsic volcanics, Tollu Hill; H, flow banding in felsic pyroclastics, Tollu Hill.

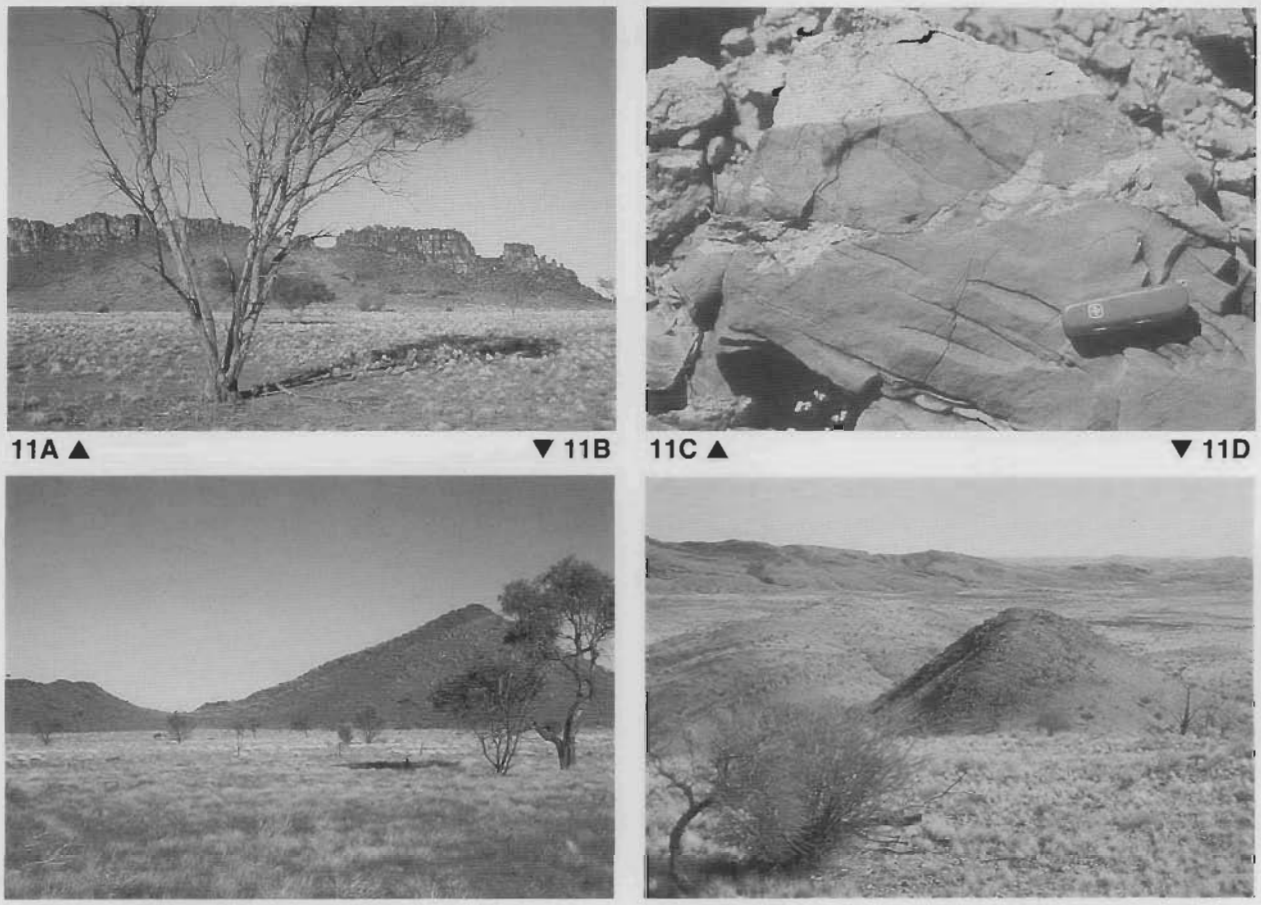

Figure 11. Mafic dykes. A, ridge-forming gabbro dyke in the Charnockite Flats area, west of the Hinckley Range; B, low-dipping dolerite dyke forming a ridge top to felsic granulites at Mount Aloysius; C, mafic dyke cutting through anorthosite near Teizi bore; D, ultramafic plug intruded into felsic granulites south of Ewarara Range.

isotopic data (DePaolo et al. 1992). Such intermediate/felsic source materials would be of normal undepleted high field strength elements (HFSE) composition, for example tonalitic to granodioritic source rocks which have not undergone previous melt depletion, bearing in mind that a derivation of A-type granites by anatexis of HFSE-depleted granulite facies sources (Collins et al. 1982) is not matched by the non-refractory composition of high-grade terranes (Sheraton & Black 1988). Further, the HFSE levels of partial melts may be enhanced by high fluorine (Collins et al. 1982), considering the high fluorine of some of the Tollu Group rhyolites and coeval granitoids.

The underlying factor for the A-type anatexis may have been the rise of mantle-derived magmas into the crust, probably represented by the Mummawarrawarra Basalt, contemporaneous or near-contemporaneous with emplacement of the Giles Complex. The difference in depleted-mantle (DM) Nd model maximum mantle-derivation ages of source material of the Smoke Hill Volcanics (1460–1570 Ma) and source materials of basement felsic granulites (1610–1900 Ma)(Sun & Sheraton 1992) suggests that the volcanics could not have been derived by anatexis of the latter, but represent the introduction of juvenile crustal components.

Basic dyke swarms

Dolerite dykes in the central and eastern part of the Musgrave Block give two distinct Sm–Nd isochron ages: (1) 1054±14 Ma in the Amata region, central Musgrave Block (Camacho et al. 1990, 1991), probably contemporaneous with the 1090±94 Ma Kulgera dyke swarm of similar age to the Stuart dyke swarm in the Arunta Block (1076±33 Ma and 1049±94 Ma), and (2) 790±40 Ma and 797±49 Ma for dykes at Amata, similar in age to the Gairdner dyke swarm of the Gawler Craton (802±35 and 867±47, Zhao & McCulloch 1993). Nesbitt et al. (1970) recognised four post-Giles Complex sets of dolerite dykes (A–D) in the eastern Tomkinson Ranges, subject to a geochemical study by A.J. Crawford (pers. comm. 1992). In the present study, three suites of post-Giles Complex basic dykes: type-A, type-B and type-C, are recognised on structural grounds in the Mount Aloysius and Champ de Mars areas (Clarke 1992). At least three types of dykes are also identified on petrographic and chemical criteria. Examples of dyke outcrops are given in Figure 11.

Type-A dykes—post-D_2, pre-D_3, intergranular-textured dolerites, typically containing phenocrysts of plagioclase embedded in intergranular groundmass, regarded as recrystallised igneous textures. The dykes mostly consist of clinopyroxene (~20%), orthopyroxene (~20%), plagioclase (andesine–labradorite: 55–60%), Fe–Ti oxides (1–5%), and apparently primary red-brown biotite (%). The chemistry is Ol-normative or slightly Q-normative tholeiitic (mg′ = 57–64). The age of this dyke set is estimated as ~1100 Ma, from Sm–Nd plagioclase–clinopyroxene studies (Sun et al. in press).

Type-B dykes—these mainly northwest-trending quartz dolerite dykes postdate or intrude D_3 and pre-D_4. The dykes are up to 30 m thick, but commonly 3–5 m, displaying typical subophitic textures and, commonly, cut by thin mylonitic zones. Principal constituents are plagioclase (labradorite: 55–60%), clinopyroxene (35–40%, locally uralitised), Fe–Ti oxides (2–4%) and quartz (<2%). Minor biotite and hornblende are present. Chemically, these are slightly Q-normative tholeiites (mg′ = 53–60), but distinct from type-A dolerites. The

age of these dykes is defined as ~800 Ma from Sm– Nd and U–Pb zircon studies (Sun et al. in press).

Type-C dykes—olivine dolerites: These northeast-trending and, rarely, northwest trending, strongly olivine-normative dykes are mostly thinner (1–2 m) than type-B dykes. Textures range from subophitic to porphyritic, with olivine and plagioclase phenocrysts. Coarser grained dykes contain plagioclase (50–60%), clinopyroxene (20–35%), olivine (5–12%, partly serpentinised), Fe–Ti oxides (4–6%) and biotite (<4%). The rocks are little fractionated (mg′ = 62–69; Cr = 373–606 ppm; Ni = 202–329 ppm), although higher fractionation (mg′ = 50) in type-C dykes is recorded from the Murray Range area. Type-C dykes display similarities to type-A dykes, but are much more SiO_2-undersaturated and heterogeneous. The age of these dykes is defined as ~1000 Ma on the basis of Sm–Nd mineral isochrons (Sun et al. in press).

The gabbroic cumulates of the Giles Complex are extensively intruded by conformable layers and pods of microgabbro, which are back-intruded by the coarser grained host gabbro. These relationships are interpreted in terms of late-stage intrusion of increments of basaltic magma into resident magma chambers at above-solidus conditions. No direct links have been seen between these dykes and cumulates of the Giles Complex, and the observed dykes cut through the Giles Complex. From a petrological viewpoint, some olivine–plagioclase and olivine–clinopyroxene-phyric dykes are consistent with feeders of fractionated troctolitic and gabbroic intrusions. Thus, assemblages crystallised under high pressure conditions have been identified in dykes cutting the Hinckley Range and The Wart intrusion, some containing intratelluric orthopyroxene as the only phenocryst generation (Ballhaus 1992). Some of the fine-grained dykes have a primitive olivine and aluminous spinel normative basaltic composition, qualifying as parental liquids for ultramafic pulses. The post-Giles Complex dykes reflect uplift of the terrane and recrystallisation under lower grade and, in places, brittle regimes. Type-A dykes may predate the Giles Complex as well as the earliest mylonitic deformation of D_3. The post-metamorphic type-B dykes may be correlated with feeders of mafic volcanics, such as are observed in the Bitter Springs carbonates of the Amadeus Basin.

Models of crustal evolution

Sm–Nd isotopic data from the felsic granulites indicate protolith T_{TM} model ages in the range 1770–1890 Ma (McCulloch 1987) and 1460–1910 Ma (Sun & Sheraton 1992) for Musgrave Block samples, as compared to 2120–2190 Ma for the Arunta Block (McCulloch 1987). Relatively young protolith ages pertain to volcanics of the 1080 Ma (U–Pb zircon ion-probe) Tollu Group (D_{TM} 1460–1570). Banded granulites, constituting the oldest recognised units in the Musgrave Block, were studied in detail at Mount Aloysius, where Rb–Sr isochron ages of 1564±12 Ma and 1327±7 Ma were defined as protolith ages (Gray 1978), and are confirmed by U–Pb zircon ages (Sun et al. in press) is summarised in Table 1 and Figure 13. At least seven phases of deformation are recognised by Clarke et al. (1992): (1) pre-Giles Complex pure shear (D_{1-2}); (2) post-Giles Complex simple shear (D_3); (3) younger mylonitic and retrograde shear zones (D_{4-7}). Intrusion of the Giles Complex is now considered to be indicated by Sm–Nd clinopyroxene–plagioclase–whole-rock ages of 1047±14 and 1079±16 for little recrystallised segments of the Wingellina mafic–ultramafic intrusion and U–Pb zircon ages of granophyre veins within the Bell Rock intrusion (Sun et al., in press).

The likely contemporaneity of the Giles Complex and the Tollu Group volcanics vindicates the suggestions by Nesbitt et al. (1970) and Daniels (1974), with the following implications: (1) The Giles Complex and the Tollu Group represent a 1.08–1.06 Ga coeval plutonic–volcanic suite; (2) since the Tollu Group volcanics unconformably overlie basement gneisses similar to those into which the Giles Complex was intruded, a coeval relationship between the plutonic and volcanic mafic rocks implies relatively rapid uplift and erosion following the deep-seated emplacement of the mafic–ultramafic sills and preceding the Tollu Group; (3) emplacement of the Giles Complex was associated with extensive back-intrusion of partial melts of felsic wall rock, affecting recrystallisation of the gabbro to mafic granulites, e.g. in the western Hinckley Range and northeastern Michael Hills areas; (4) the mylonitic D_3 deformation followed closely on the emplacement of the Giles Complex and Tollu Group volcanics; (5) the granophyre-bearing veins in the Bell Rock gabbro can be regarded as an intrinsic late phase of this intrusion.

The Giles Complex has long been cited as an example of basaltic magmas emplaced in lower to middle crustal levels, on the basis of pressures calculated from subsolidus reactions between (1) olivine and plagioclase reacting to produce orthopyroxene, clinopyroxene, spinel, and Ca-poor plagioclase; (2) orthopyroxene and plagioclase reacting to produce garnet; and (3) spinel and orthopyroxene reacting to produce garnet (Goode & Moore 1975). Clinopyroxene and orthopyroxene are enriched in Ca–Al and Mg–Al Tschermak components. Ballhaus & Berry (1991) conducted thermobarometric studies of the Wingellina Hills intrusion, where orthopyroxene–clinopyroxene–spinel symplectites along olivine–plagioclase boundaries yield a medium-pressure isobaric cooling path of 1150–750°C at 65–62 Mpa, respectively. Some ultramafic cumulates contain highly potassic calcic antiperthites ($An_{75}Ab_5Or_{20}$) which allow palaeothermometric estimates of about 1200°C based on the An–Or solvus of Ai & Green (1989).

High-pressure features have previously been recorded only from layered intrusions north of the Hinckley fault, including the Wingellina Hills, Kalka, Ewarara, Gosse Pile, Teizi, and possibly Claude Hills, intrusions. In other intrusions, olivine and plagioclase are in stable coexistence, except for rare amphibole–spinel coronas at olivine–plagioclase contacts in altered units in The Wart body. Consequently, it has been postulated that intrusions south of the Hinckley fault and also the westernmost intrusions (Blackstone, Cavenagh, Jameson) have been emplaced at shallower crustal levels (Nesbitt et al. 1970; Goode & Moore 1975). This view is consistent with the general shallowing in crustal level southward postulated from increased magmatic fractionation of layered intrusions in this direction. However, the Hinckley fault is considered to involve only limited vertical displacement. The lack of high-pressure reaction textures in some intrusions may be a consequence of phase compositions unfavourable for the development of spinel coronas and thus is not necessarily indicative of emplacement at shallower crustal levels.

Recent PT studies of granulite facies gneisses and dykes from the Tomkinson Ranges and the Woodroffe Thrust to the north indicate at least two stages of high-pressure metamorphism (Clarke et al. 1992)(Fig. 12):

1. Garnet–orthopyroxene-bearing granulites from Mount Aloysius (Stewart 1995—this issue) preserve coarse-grained mineral assemblages formed under relatively low pressures of ca. 400 Mpa (T = 750°C). A Rb–Sr isochron age of 1200 Ma was reported by Gray, (1978) and this event is correlated with D_1 and D_2 deformation events by Clarke et al. (1992). Core to rim zonation of garnet reflects subsequent cooling.
2. Porphyritic hornblende–biotite granitoids in the Tomkinson Ranges represent a 1188±4 Ma intrusive event (Sun & Sheraton 1992). These rocks were recrystallised to garnet–hornblende gneiss during development of a mylonitic D_3 foliation. The assemblages yield values of ca. 1100 Mpa (T = 650°C), indicating greater than two-fold increase in pressure between D_{1-2} and D_3.

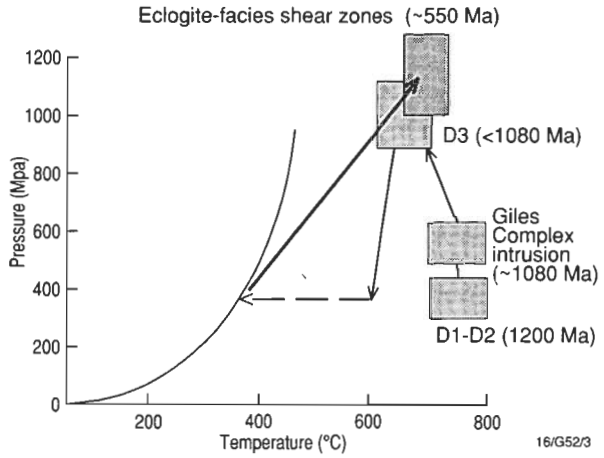

Figure 12. Pressure–temperature–time history of the Tomkinson Ranges (after Clarke et al. 1993).

3. Coarse-grained garnet and orthopyroxene in Mount Aloysius felsic granulites are surrounded by syn-D_3 to post-D_3 garnet– orthopyroxene–plagioclase symplectites, indicating decompression to ca. 450 Mpa. This late-D_3 decompression is correlated with formation of spinel–cordierite coronas surrounding garnet in pelitic gneisses at Cohn Hill about 70 km west of the Tomkinson Ranges (Clarke & Powell 1991).
4. Garnet–clinopyroxene assemblages occur within ultramylonite shears south of the south-dipping Woodroffe Thrust and oriented at high angles to this structure. They may predate the Woodroffe Thrust, which contains hydrous upper greenschist to upper amphibolite facies (biotite–sericite± amphibole) assemblages. The overlying thrust sheet also contains mafic dykes overprinted by garnet–clinopyroxene–hornblende–plagioclase–rutile–quartz assemblages and displaying garnet–clinopyroxene coronas around orthopyroxene. Thermobarometric determinations, based on recrystallised mafic dykes, give pressure estimates up to 1300 Mpa (T = 725°C).

The PT history of the western Musgrave Block as suggested by the above and by earlier studies is portrayed in Figure 12. The diagram reflects (1) an increase in pressure from the ca. 1200 Ma D_{1-2} metamorphism to the post-1080 Ma D_3 deformation; (2) late to post-D_3 decompression, and (3) a sharp late or post-D_3 increase in pressure. The significant crustal thickening represented by the late-D_3 pressure–temperature values, which correspond to lithostatic pressures at depths of about 30 km, may be closely related to emplacement of the thick (>5 km) dense mafic–ultramafic sills of the Giles Complex. Two alternative interpretations of the post-dykes eclogite facies conditions can be made: (1) the granulites and mylonites south of the Woodroffe Thrust represent basal structural levels of the overlying south-dipping thrust sheet, and originated at deep crustal levels of 30–40 km, or (2) the eclogite facies assemblages were developed in conjunction with late Proterozoic to Cambrian movements along the thrust.

Eclogite facies rocks have been reported earlier from the Amata area, central Musgrave Block. The results of the present investigation are in agreement with the observations of Goode & Moore (1975) and require further work regarding possible PT changes through the granulite facies terrane. Such suggested changes include a decrease in pressure south of the Hinckley fault (Nesbitt et al. 1970) and possible shallower crustal level for the Blackstone, Cavenagh and Jameson gabbroic intrusions to the west (Daniels 1974; Ballhaus 1992). Further studies are required to elucidate the PT–time evolution associated with the Giles Complex and the Woodroffe Thrust.

The Giles Complex is extensively recrystallised in the granulite facies in the western part of the Hinckley Range and parts of the Michael Hills and other intrusions. These zones have been interpreted as a marginal contaminated facies of the gabbro (Daniels 1974). However, evidence for intrusion of veins and stocks of granitoid into fractured consolidated gabbro and the common occurrence of angular mafic xenoliths within the granites suggest an interpretation in terms of back-intrusion of felsic magma, contemporaneous with emplacement of the gabbro.

From the present study, the late Proterozoic Giles Complex constitutes a suite of discrete primary sills preserved in their near-original form, rather than tectonic slices of an originally contiguous Bushveld-type lopolith. These intrusions, emplaced within the orthogneiss/paragneiss assemblage of the southern granulite facies terrane of the Musgrave Block, show a general increase in the degree of magmatic fractionation from north to south and east to west. This is manifested by the abundance of peridotite and pyroxenite-rich intrusions in the north (Murray Range, Wingellina Hills, Claude Hills, Ewarara, Kalka, Gosse Pile), to interlayered gabbro/pyroxenite in the south and southeast (Michael Hills, Mount Davies), to gabbro and troctolite in the southwest (Jameson, Blackstone–Bell Rock, Cavenagh). This trend is consistent with an interpretation of the terrane in terms of progressively shallower crustal levels southward—a consequence of northward-directed lifting along the Woodroffe Thrust marked by an east–west mylonite zone associated with upthrust garnet–pyroxene assemblages. The deeper level sills were emplaced at depths of about 20 km, defining an isobaric cooling path from a PT regime of 65 Mpa/1150° to 62 Mpa/750° (Ballhaus & Berry 1990). Compositionally contrasted magma types in these sills were derived from a parent magma fractionated at depth by polybaric precipitation of orthopyroxene (±clinopyroxene) before intrusion. Fractionation of these phases resulted in the generation of Fe-rich SiO_2-poor troctolitic magmas, generally emplaced at higher crustal levels under ~4 kb, as shown by the equilibrium of silicification reactions (olivine + SiO_2 = orthopyroxene; Ca-Tschermak + SiO_2 = anorthite; jadeite + SiO_2 = albite). A history of multiple intrusion is suggested within the sills, including (1) voluminous gabbronorite, gabbro and troctolite; (2) late pulses of primitive ultramafic olivine and spinel-dominated magmas; and (3) numerous small pulses of microgabbro emplaced within the still hot and plastic host intrusions.

The origin of the Giles Complex and its extensive equivalents in the Tollu Group is thought to be related to the formation of a transient thermal anomaly in the upper mantle. The emplacement of at least some of the intrusions has occurred at depths of ca. 20 km, i.e. Wingellina Hills (Ballhaus & Berry 1991), whereas the western intrusions—Blackstone and Jameson, formed at shallower levels of about 10–12 km. In broad terms, therefore, the Giles Complex represents multiple intrusion at different crustal levels, and including basaltic underplating of the sialic crust.

Thermal and magmatic modelling of deep-seated basaltic intrusions (Campbell & Turner 1987; Huppert & Sparks 1988) underpins the extremely efficient convective heat transfer and attendant intracrustal melting in and above roof zones of magmatic cupolas. At infracrustal levels about 20 km and deeper, melting of roof rocks, already at near-solidus temperatures under the attendant geotherm, will result in extensive intracrustal melting and high rates of cooling. This contrasts with the slower melting and thereby heat loss in the roof zones of shallower crustal cupolas emplaced within colder rocks, where heat transfer through the country rocks would take place mainly by conduction. The degree of melting of roof materials depends on their composition. Melting of country rocks of near-granite (s.s.) eutectic composition would produce largely phenocryst-free rhyolites, whereas anatexis of more refractory materials would result in restite-rich granitoid plutons

whose composition may reflect that of the source (Wyborn & Chappell 1986). Partial melting of refractory materials would be accompanied by extensive recrystallisation in the interior of the roof melt layer as it forms, producing phenocryst-rich silicic magmas (Huppert & Sparks 1989). Repeated remelting of such anatectic country rocks by new increments of basaltic magma of alkaline felsic materials, producing A-type granites.

The above model predicts loci of anatectic granites to occur above the roofs of the layered intrusions. The occurrence of major faults truncating the tops of the Kalka intrusion (Hinckley fault), Wingellina Hills (Wingellina fault), Michael Hills intrusion (Champ de Mars fault), and south and west of the Blackstone–Bell Rock intrusion (magnetic lineament), as well as lack of outcrop elsewhere, complicates identification of primary roof zones in these areas. The lack of a clear melt zone along the southern top of the Mount Davies intrusion, which shows a wide gradational transition of granoblastic mafic to felsic granulites, is surprising in view of the great thickness of this body (>6 km). The widespread occurrence of granite/migmatite zones and pods within older felsic granulites located away from or below exposed layered intrusions—i.e. Mount Aloysius, North Hinckley–Ewarara–Teizi range, isolated outcrops south of Michael Hills and Mount Davies, and south of Blackstone Range—suggests regional partial anatexis of an as yet undefined age. The generally low ratio of granite to granulite in these terranes

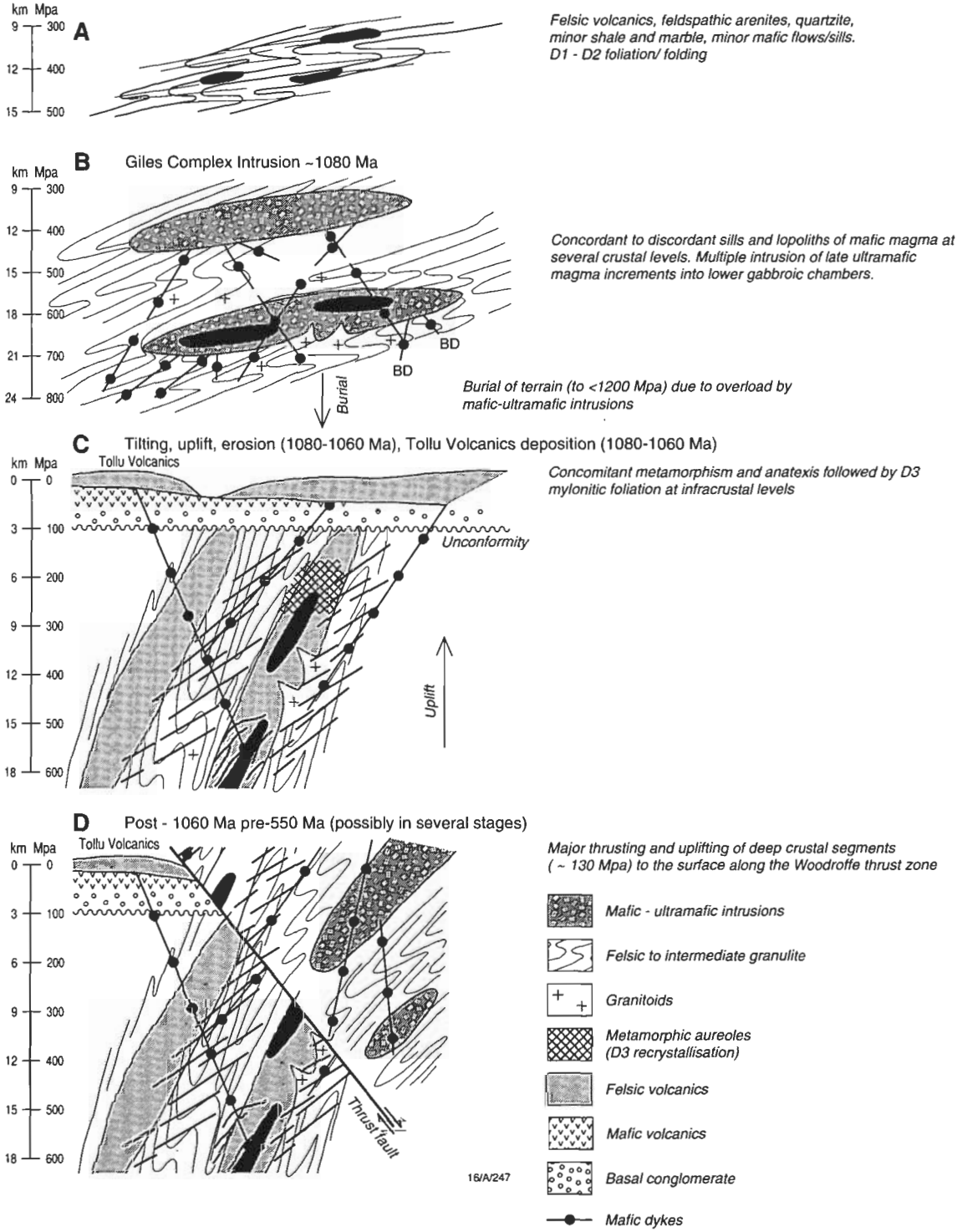

Figure 13. Crustal evolution model for the Giles Complex in the Tomkinson Ranges and adjoining areas, western Musgrave Block, as controlled by pressure–temperature–time history described in this report.

and the lack of major continuous zones of migmatite place limits on the extent of melting. Considering the volume of the Giles Complex, the relatively low degree of anatexis is interpreted in terms of the dry composition and high solidi temperatures of the granulites (mostly <1% H_2O).

The conditions under which sialic crust is subject to anatexis and palingenesis are portrayed in Figure 14. According to the model of Lambert (1983), elevation of the geothermal gradient by emplacement of a 4000 m thick mafic sill at a depth of 10 km would result in elevation of the geothermal gradient and intersection of the wet granite, tonalite and gabbro solidi at 11–13 km depth. Melting of plagioclase would occur about 16 km and hornblende, at about 19 km depth. The dry gabbro solidus would be intersected at about 20 km depth. Similarly drastic melting consequences would ensue from emplacement of thick mafic/ultramafic bodies at greater depth, as indicated for the Giles Complex by the abundance of contemporaneous granite veins. However, the paucity of granophyre and migmatite at the top of intrusions suggests extremely dry compositions and, thereby, high solidi of the felsic granulite country rocks during intrusion of the Giles Complex.

Basaltic underplating may be widespread in infracrustal regions throughout wider tracts of the central and northern Australian crust, as suggested by a transitional seismic layer above the MOHO. The general increase in degree of fractionation of the layered intrusions with higher crustal levels, namely from ultramafic-rich intrusions at deep crustal levels along the Woodroffe Thrust in the north to gabbro-dominated intrusions and troctolite–anorthosite intrusions in the south and west (Fig. 3), reflects a relationship between magma density and crustal level. Bouguer anomaly data suggest that the Amadeus Basin is underlain by mainly amphibolite facies rocks of the type that dominate the north of the Musgrave Block and the south of the Arunta Block (Glikson 1986, 1987). The extent of granulite facies infracrustal zones beneath the Amadeus Basin and the Officer Basin, however, remains unknown, leaving the original spatial distribution of the mafic–ultramafic igneous activity undefined. Thus, it remains possible that effects of the 1.3 Ga and 1.08 Ga mantle melting events were not necessarily limited to narrow linear zones such as the Albany–Fraser and Musgrave belts. The location of primary borders of these belts remains subject for palaeomagnetic studies. In the Albany–Fraser belt (Clarke et al. 1995—this issue), as in the North American Grenville belt (Davidson 1995—this issue), the borders are, in places, thrust over older Archaean terranes, although whether these represent near-original boundaries or are the result of accretion of allochtonous terranes remains unclear. The absence of older

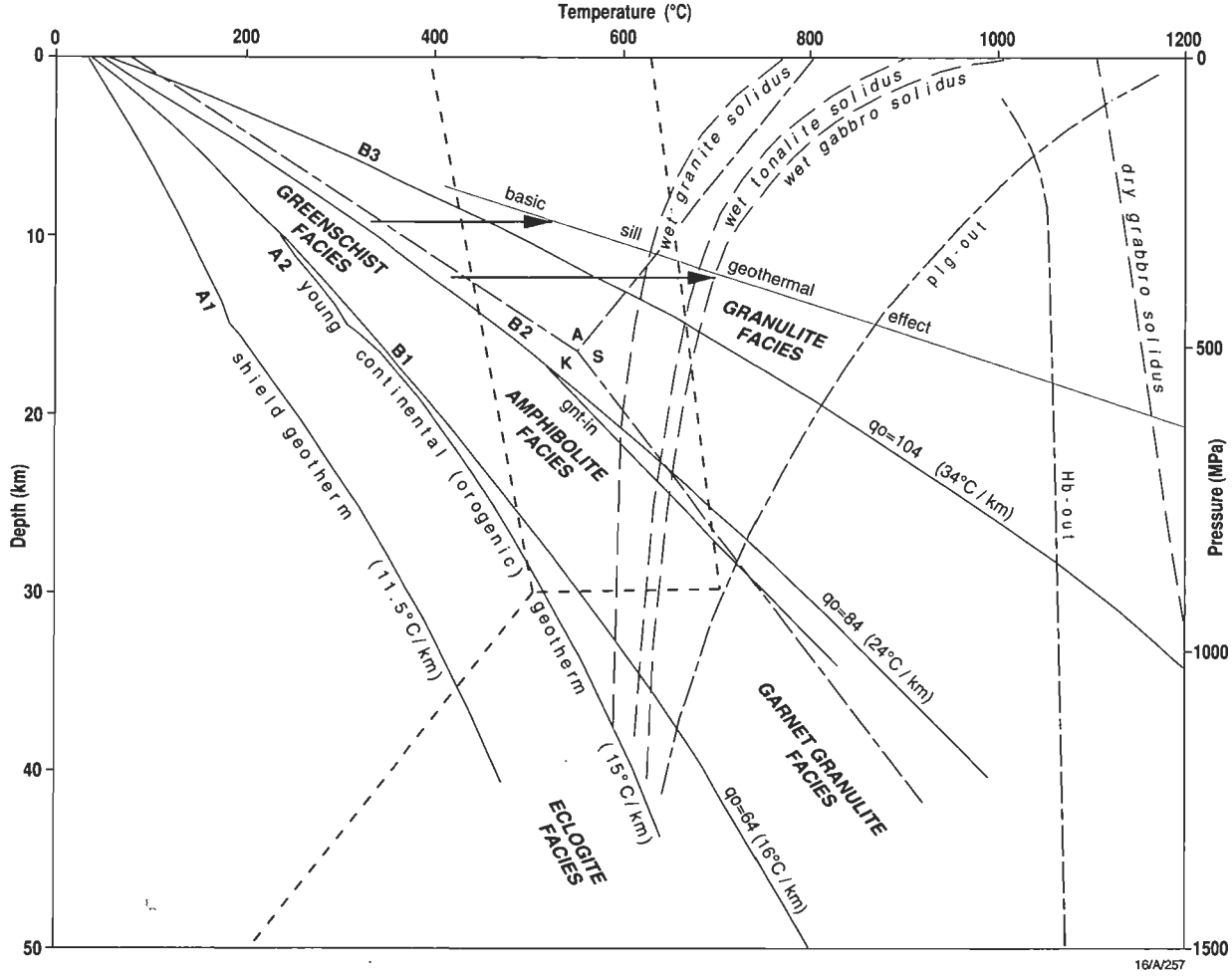

Figure 14. Phase relations diagram of the pressure–temperature parameters of the wet granite solidus, wet tonalite solidus, wet gabbro solidus, dry gabbro solidus, plagioclase and hornblende in relation to shield geotherm (A1) and young continental geotherm (A2) (Ringwood 1975); model Proterozoic geotherms computed by Lambert (1983) for a crustal section of 22 km pyroxene granulite, 10 km amphibolite and gneiss and 8 km metasediments and felsic gneiss. Heating of the crustal section by emplacement of a 4 km thick mafic sill at a depth of 10 km under a geotherm of 24C°/km during a period of 4 m.y. is denoted by black arrows. Metamorphic phase boundaries are after Lambert & Wyllie (1972) and Kerrick (1972); the field of andalusite–sillimanite–kyanite triple point after Holdaway (1971) and Winkler (1978); the field of granulite facies (GF) and transitional hornblende granulite facies (TGF) after Newton & Hansen (1983), and the fields of greenschist, amphibolite, granulite, garnet granulite and eclogite facies after Winkler (1978).

terranes juxtaposed with the Musgrave Block renders this question even more difficult to resolve, pending further seismic reflection surveys, further isotopic age studies, and a redefinition of apparent polar wander paths.

Acknowledgements

We are grateful to the Ngganyatjarra Aboriginal Council and to members of the Wingellina, Blackstone, Jameson, Kalka and Pipalyatjarra communities in Western Australia and South Australia for assisting the field work through the provision of guides and logistic support. In particular we are indebted to Rob Shelton, community advisor at Wingellina, whose generous assistance and friendship made all the difference in otherwise difficult circumstances, and to Nugget, the Aboriginal tribal elder. We thank other Aboriginal elders and field guides and the community advisors—Ruth Raintree, Murray Wells, David Brooks and Diana James—for logistic help in connection with field work in the Tomkinson Ranges, Blackstone Range and Jameson Range region.

References

Ballhaus, C.G., 1992. Petrology of the Giles Complex, Musgrave Block, central Australia: the Jameson, Blackstone, Bell Rock, Murray, The Wart, Latitude Hill and Hinckley intrusions. Australian Geological Survey Organisation Record 1992/73.

Ballhaus, C.G. & Berry, R.F., 1991. Crystallisation pressure and cooling history of the Giles layered igneous complex, central Australia. Journal of Petrology, 32, 1–28.

Ballhaus, C.G. & Glikson, A.Y., 1989. Magma mixing and intraplutonic quenching in the Giles Complex, central Australia. Journal of Petrology, 30, 1443–1469.

Ballhaus, C.G., Berry, R.F. & Green, D.H., 1991. High pressure experimental calibration of the olivine-orthopyroxene-spinel oxygen geobarometer: implications for the oxidation state of the upper mantle. Contributions to Mineralogy and Petrology, 107, 27–40.

Ballhaus, C.G., Glikson, A.Y. & Keays, R.R., 1992. Magmatic and metamorphic evolution and economic potential of the mafic/ultramafic Giles Complex, western Musgrave Block, W.A.. BMR Research Newsletter, 16, 6–9.

Ballhaus, C.G. & Glikson, A.Y., 1995. Petrology of layered mafic–ultramafic intrusions of the Giles Complex, western Musgrave Block, Western Australia, AGSO Journal of Australian Geology & Geophysics, this issue.

Camacho, A., Simons, B., Schmidt, P.W. & Gray, C.M., 1990. Middle to late Proterozoic mafic dykes of central Australia. 2nd International Dyke Conference, Adelaide, Excursion Guide.

Camacho, A., Simons, B. & Schmidt, P.W., 1991. Geological and palaeomagnetic significance of the Kulgera dyke swarm, Musgrave Block, N.T., Australia. Geophysics Journal International., 107, 37–45.

Campbell, I.H., 1987. Distribution of orthocumulate textures in the Jimberlana intrusion. Journal of Geology, 95, 35–54.

Campbell, I.H. & Turner, J.S., 1987. A laboratory investigation of assimilation at the top of a basaltic magma chamber. Journal of Geology, 95, 155–173.

Chappell, B.W., & White, A.J.R., 1974. Two contrasted granite types. Pacific Geology, 8, 173-175.

Clarke, G.L., 1992. Field relations and tectonic history of the Hinckley Gabbro, felsic to mafic granulites and ganitoids, western Hinckley Range and Champ de Mars areas, Tomkinson Ranges, Musgrave Block, Western Australia. Bureau of Mineral Resources, Australia, Record 1992/33.

Clarke, G.L. & Powell, R., 1991. Decompressional coronas and symplectites in granulites of the Musgrave Block, central Australia. Journal of Metamorphic Geology, 9, 441–450.

Clarke, G.L., Buick, I.S. & Glikson, A.Y., 1992. Contact relationships and structure of the Hinckley Gabbro and host rocks, Giles Complex, western Musgrave Block, W.A. BMR Research Newsletter, 17, 6–8.

Clarke, G.L, Stewart, A.J. & Glikson, A.Y., 1993. High pressure eclogite facies metamorphism associated with the Woodroffe Thrust. AGSO Research Newsletter, 18, 6–7.

Clarke, G.L., Sun, S.-S. & White, R.W., 1995. Grenville age belts and adjacent older terranes in Australia and Antarctica. AGSO Journal of Australian Geology & Geophysics, this issue.

Clarke, G.L., Buick, I.S., Glikson, A.Y. & Stewart, A.J., 1995. Structural and pressure-temperature evolution of host rocks of the Giles Complex, western Musgrave Block, central Australia: evidence for multiple high-pressure events, AGSO Journal of Australian Geology & Geophysics, this issue.

Collerson, K.D., Oliver, R.L. & Rutland, R.W.R., 1972. An example of structural and metamorphic relationships in the Musgrave Orogenic Belt, central Australia. Journal of the Geological Society of Australia, 18, 379–393.

Collins, W.J., Beans, S.D., White, A.J.R. & Chappell, B.W., 1982. Nature and origin of A-Type granites with particular reference to southeastern Australia. Contributions to Mineralogy and Petrology, 80, 189–200.

Daniels, J.L., 1974. The geology of the Blackstone region, Western Australia. Geological Survey of Western Australia, Bulletin 123, 257 pp.

Davidson, A., 1995. A review of the Grenville orogen in its North American type area. AGSO Journal of Australian Geology & Geophysics, this issue.

Forman, D.J. & Shaw, R.D., 1973. Deformation of crust and mantle in central Australia. Bureau of Mineral Resources, Australia, Bulletin 144.

Giles, C.W., 1981. A comparative study of Archaean and Proterozoic felsic volcanic associatisons in southern Australia. Ph.D. Thesis (unpublished), University of Adelaide.

Glikson, A.Y. 1986. Regional structure and evolution of the Redbank-Mt Zeil thrust zone: a major lineament in the Arunta Inlier, central Australia. BMR Journal of Australian Geology & Geophysics, 10, 89–107.

Glikson, A.Y., 1987. An upthrusted early Proterozoic basic granulite–anorthosite suite and anatectic gneisses, southwestern Arunta Block, central Australia: evidence on the nature of the lower crust. Transactions of the Geological Society of South Africa, 89, 263–283.

Glikson, A.Y., 1989. Significance of ultrabasic components of the Giles Complex, central Australia. BMR Research Newsletter, 10, 4–6.

Glikson, A.Y., 1994. Landsat-5 Thematic Mapper image correlations: application to NGMA mapping of the western Musgrave Block, central Australia. Australian Geological Survey Organisation Record 1994/17.

Glikson, A.Y. & Creasey, J.W., 1995. Landsat-5-TM correlations of mafic-ultramafic intrusions and granulite facies gneisses, western Musgrave Block, central Australia, AGSO Journal of Australian Geology & Geophysics, this issue.

Glikson, A.Y. & Mernagh, T.P., 1990. Significance of pseudotachylite vein systems, Giles basic/ultrabasic complex, Tomkinson Ranges, western Musgrave Block, central Australia. BMR Journal of Australian Geology & Geophysics, 11, 509–519.

Glikson, A.Y., Ballhaus, C.G., Golbey, B.R. & Shaw, R.D., 1990. Major thrust faults and crustal zonation of the

middle to upper Proterozoic crust in central Australia. NATO Advanced Study Institute on exposed cross sections through the continental crust. Kluwer Academic Publishers, Netherlands, 285–304.

Glikson, A.Y., Ballhaus, C.G. & Pharaoh, T., 1990. The Giles Complex, central Australia: new insights into tectonics and metamorphism. BMR Research Newsletter, 12, 18–20

Goode, A.D.T., 1970. The petrology and structure of the Kalka and Ewarara layered basic intrusions, Giles Complex, central Australia. Ph.D. Thesis, University of Adelaide.

Goode, A.D.T., 1975. A transgressive picrite suite from the western Musgrave Block, central Australia. Journal of the Geological Society of Australia, 22, 187–194.

Goode, A.D.T., 1976. Small-scale primary cumulus igneous layering in the Kalka layered intrusion, Giles Complex, central Australia. Journal of Petrology, 17, 379–397.

Goode, A.D.T., 1977. Intercumulus igneous layering in the Kalka layered intrusion, central Australia. Geological Magazine, 114, 215–218.

Goode, A.D.T., 1978. High Temperature, High Strain Rate Deformation in the Lower Crustal Kalka Intrusion, Central Australia. Contributions to Mineralogy and Petrology, 66, 137–148.

Goode, A.D.T. & Krieg, G.W., 1967. The geology of the Ewarara intrusion, Giles Complex, central Australia. Journal of the Geological Society of Australia, 14, 185–194.

Goode, A.D.T. & Moore, A.C., 1975. High pressure crystallization of the Ewarara, Kalka and Gosse Pile Intrusions, Giles Complex, central Australia. Contributions to Mineralogy and Petrology, 51, 77–97.

Gray, C.M., 1967. The geology, petrology and geochemistry of the Teizi anorthosite. B.Sc. Honours Thesis, University of Adelaide (unpubl.)

Gray, C.M., 1977. The geochemistry of central Australian granulites in relation to the chemical and isotopic effects of granulite facies metamorphism. Contributions to Mineralogy and Petrology, 65, 79–89.

Gray, C.M. 1978. Geochronology of granulite-facies gneisses in the western Musgrave block, central Australia. Journal of the Geological Society of Australia, 25, 403–414.

Gray, C.M. & Compston, W., 1978. A Rb-Sr chronology of the metamorphism and prehistory of central Australian granulites. Geochimica et Cosmochimica Acta., 42, 1735–1748.

Gray, C.M. & Goode, A.D.T., 1981. Strontium isotopic resolution of magma dynamics in a layered intrusion. Nature, 294, 155–158.

Gray, C.M. & Goode, A.D.T., 1989. The Kalka layered intrusion, central Australia. A strontium isotopic history of contamination and magma dynamics. Contributions to Mineralogy and Petrology, 103, 35–43.

Gray, C.M. & Oversby, V.M., 1972. The behaviour of lead isotopes during granulite facies metamorphism. Geochimica et Cosmochimica Acta, 36, 939–952.

Holdaway, M.J., 1971. Stability of andalusite and the aluminium silicate phase diagram. American Journal of Science, 27, 97–131.

Huppert, H.E. & Sparks, S.J., 1988. The generation of granitic magmas by intrusion of basalt into continental crust. Journal of Petrology, 29, 599–624.

Kerrick, D.M., 1972. Experimental determination of muscovite–quartz stability with pH2O = P total. American Journal of Science, 272, 946–958.

Lambert, R.St.J., 1983. Metamorphism and thermal gradients in the Proterozoic continental crust. Geological Society of America, Memoir 161, 155–166.

Lambert, I.B. & Wyllie, P.J., 1972. Melting of gabbro (quartz-eclogite) with excess water to 35 kilobar, with geological implications. Journal of Geology, 80, 693–708.

Le Maitre, R.W., 1989. A classification of igneous rocks and glossary of terms. Blackwell Scientific Publications, Oxford.

Maboko, M.A.H., Williams, I.S. & Compston, W., 1991. Zircon U–Pb chronometry of the pressure and temperature history of granulites in the Musgrave Ranges, central Australia. Journal of Geology, 99, 675–697.

McCulloch, M.T., 1987. Sm–Nd isotopic constraints on the evolution of the Precambrian crust in the Australian continent. American Geophysical Union, Geodynamic Series, 17, 115–130.

Moore, A.C., 1971. Some aspects of the geology of the Gosse Pile ultramafic intrusion, central Australia. Journal of the Geological Society of Australia, 18, 69–80.

Moore, A.C. & Goode, A.D.T., 1978. Petrography and origin of granulite-facies rocks in the western Musgrave Block, central Australia. Journal of the Geological Society of Australia, 25, 341–358.

Morse, S.A., 1968. Feldspars. Yearbook of the Carnegie Institute, Washington, 67, 120–126.

Mutton, A.J., Shaw, R.D. & Wilkes, P, 1983. Analysis of geological, geophysical and physical property data from the southwest Arunta Block, N.T. Bureau of Mineral Resources, Australia, Record 1983/1.

Nesbitt, R.W. & Kleeman, A.W., 1964. Layered intrusions of the Giles Complex, Central Australia. Nature, 203, 391–393.

Nesbitt, R.W & Talbot, J.L., 1966 The layered basic and ultrabasic intrusives of the Giles Complex, central Australia. Contributions to Mineralogy and Petrology, 13, 1–11.

Nesbitt, R.W., Goode, A.D.T., Moore, A.C. & Hopwood, T.P., 1970. The Giles Complex, central Australia: a stratified sequence of mafic and ultramafic intrusions. Geological Society of South Africa Special Publication, 1, 547–564.

Newton, R.C. & Hansen, E.C., 1983. The origin of Proterozoic and late Archaean charnockites: evidence from field relations and experimental petrology. Geological Society of America, Memoir 161, 167–178.

Pharaoh, T.C., 1990. Aspects of structural geology of the Giles layered mafic/ultrmafic complex, Tomkinson Range, Musgrave Block, central Australia. Bureau Mineral Resources, Australia, Record 1990/6

Ringwood, A.E., 1975. Composition and petrology of the Earth's mantle. McGraw Hill, New York, 618 pp.

Sheraton, J.W. & Black, L.P., 1988. Chemical evolution of granitic rocks in the east Antarctic shield with particular reference to post-orogenic granites. Lithos, 21, 37–52.

Sheraton, J.W. & Sun, S.-S., 1995. Geochemistry and origin of felsic igneous rocks of the western Musgrave Block. AGSO Journal of Australian Geology & Geophysics, this issue.

Stewart, A.J., 1993. Western extension of the Woodroffe Thrust, Musgrave Block, central Australia. AGSO Research Newsletter, 18, 5–6.

Stewart, A.J., 1995a. Extension of the Woodroffe Thrust, Musgrave Block, central Australia. AGSO Journal of Australian Geology & Geophysics, this issue.

Stewart, A.J., 1995b. Resolution of conflicting structures and deformation history of the Mount Aloysius granulite massif, western Musgrave Block, central Australia. AGSO Journal of Australian Geology & Geophysics, this issue.

Stewart, A.J. & Glikson, A.Y., 1991. The felsic metamor-

phic/igneous core complexes hosting the Giles Complex. BMR Research Newsletter, 14, 6–7.

Sun, S.-S. & Sheraton, J.W., 1992. Zircon U/Pb chronology, tectono-thermal and crust-forming events in the Tomkinson Ranges, Musgrave Block, central Australia. AGSO Research Newsletter, 17, 9–10.

Sun, S.S., Gray, C.M., Sheraton, J.W., Glikson, A.Y. & Stewart, A.J., in press. Zircon U–Pb chronology and neodymium isotopic study of tectono-thermal and crust-forming events in the Tomkinson Ranges, western Musgrave Block, central Australia. AGSO Journal of Australian Geology & Geophysics.

Tarney, J., Skinner, A.C. & Sheraton, J.W., 1972. A geochemical comparison of major Archaean gneiss units from northern Scotland and east Greenland. 24th International Geological Congress., section 1, 162–174.

Tarney, J., Wyborn, L.A.J., Sheraton, J.W. & Wyborn, D., 1987. Trace element differences between Archaean, Proterozoic and Phanerozoic crustal components: implications for crustal growth processes. In: L.B. Ashwell (editor), Workshop on the growth of continental crust. Lunar Planetary Institute Technical Report, 88.02, 139–140.

Taylor, S.R. & McLennan, S.M., 1985. The continental crust: its composition and evolution. Blackwell Scientific Publications, Oxford, 312 pp.

Thomson, B.P., 1977. The Musgrave Block, S.A., N.T., W.A. In: C.L. Knight (editor), Economic geology of Australia and Papua New Guinea. Australasian Institute of Mining and Metallurgy Monograph 5, 451–460.

Thomson, B.P., 1980. Geological map of South Australia, 1:1 M scale. South Australia Department of Mines and Energy.

Thomson, B.P., Miriams, R.C. & Johnson, J., 1962. Mann, South Australia, 1:250,000 Geological Sheet, Explanatory Notes, Geological Survey of South Australia.

Webb, A.W., 1985. Geochronology of the Musgrave Block. Mineral Resourses Review, South Australia Department of Mines and Energy, 23–37.

Winkler, H.G.F., 1978. Petrogenesis of metamorphic rocks. Springer Verlag, New York, 334 pp.

Wyborn, D. & Chappell, B.W., 1986. The petrogenetic significance of chemically related plutonic and volcanic rock units. Geological Magazine, 123, 619–628.

Zhao, J.X. & McCulloch, M.T., 1993. Sm–Nd mineral isochron ages of late Proterozoic dyke swarms in Australia; evidence for two distinctive events of mafic magmatism and crustal extension. Chemical Geology, 109, 341–354.

AGSO Journal of Australian Geology & Geophysics, 16 (1/2), 69–89

The petrology of layered mafic–ultramafic intrusions of the Giles Complex, western Musgrave Block, Western Australia

Chris Ballhaus[1] & Andrew Y. Glikson[2]

The Musgrave Block hosts about twenty major layered intrusions and several generations of compositionally diverse sills and dykes collectively referred to as the Giles Igneous Complex. All were emplaced in middle Proterozoic intermediate to felsic granulites and amphibolites. On the basis of crystallisation sequences within the cumulates, we distinguish between (1) ultramafic olivine–clinopyroxene rich cumulate sequences, (2) mafic clinopyroxene–plagioclase-rich sequences, and (3) evolved troctolitic olivine–plagioclase ± magnetite-rich sequences. The layered igneous rocks are intruded by several generations of dykes, whose phenocryst assemblages resemble the crystallisation sequences in the cumulates. On this basis, at least three discrete parental melt compositions are identified, namely (1) a near-primitive olivine±clinopyroxene saturated melt, (2) a slightly fractionated olivine–(orthopyroxene)–clinopyroxene–plagioclase saturated melt, and (3) a strongly fractionated fayalitic olivine–plagioclase ± magnetite saturated melt. These magmas represent derivatives of a parental liquid that experienced various degrees of polybaric orthopyroxene–clinopyroxene ± olivine fractionation prior to emplacement, at depths significantly greater than the emplacement levels of the Giles intrusions and the dykes.

Introduction

The upper Proterozoic Giles Complex is one of the most extensive suites of layered mafic/ultramafic intrusions in the world. It comprises about twenty major intrusions, numerous smaller bodies of layered cumulates, and several swarms of dykes, all intruded into middle Proterozoic mafic to felsic granulite to upper amphibolite facies gneisses (Nesbitt et al. 1970). Age determinations (Sun & Sheraton 1992) suggest that the melts were emplaced about 1.18–1.2 Ga, whereas more recent data may suggest a younger age of ~1.08 Ga, coeval with volcanics of the Bentley Supergroup (Sun et al. in press). From east to west, the major intrusions include the Teizi Hill anorthosite; Gosse Pile pyroxenite intrusion; Mt Davies, Kalka, and Ewarara pyroxenite-rich intrusions and Claude Hills ultramafics; Michael Hills and Hinckley Range gabbros; Wingellina Hills ultramafic intrusion; Latitude Hill gabbro–pyroxenite (a segment of the Michael Hills intrusion); The Wart pyroxenite; Bell Rock and Blackstone Range troctolites; Murray Range ultramafic intrusion; Morgan and Cavenagh Range gabbros; and, finally, Jameson Range troctolite. In addition, there are several mafic intrusives in the eastern Musgrave Ranges in South Australia near Mt Woodroffe, which have a similar setting to the Giles intrusions in Western Australia.

The Giles Complex is an important target for petrological studies, for several reasons. It is one of the largest accumulations of layered mafic igneous rocks in Australia, and, therefore, of potential interest for exploration for platinum-group element (PGE) mineralisation. The Giles Complex represents a major thermal event in the crustal evolution of the Musgrave block, and its relationships with the granulite-metamorphic event or events need to be clarified. It is an example of the type of magmatic intrusive activity that can be expected at lower to middle crustal levels (Goode & Moore 1975; Ballhaus & Berry 1990), and is, therefore, relevant to the compositional evolution of the lower crust. To address these issues, the compositional relationships between the different intrusions need to be understood, i.e. are they tectonised segments of a formerly larger complex? (e.g. Sprigg & Wilson 1959) or individual intrusions derived from chemically distinct magmas (Nesbitt et al. 1970; Ballhaus & Glikson 1989; Gray & Goode 1989, Ballhaus 1993)

This paper documents the magmatic sequences of seven major intrusions of the Giles Complex in WA, i.e. the Murray Range, Hinckley Range, Latitude Hill, The Wart, Bell Rock, Blackstone Range, and Jameson Range intrusions. It presents geological maps and petrographic sections compiled from sampling traverses, thin-section petrography (Ballhaus 1993), systematic airphoto evaluation (Pharaoh 1990), and Landsat-5 TM satellite imagery (Glikson 1994). The nature and extent of chemical fractionation in each intrusion are illustrated by cryptic variation diagrams based on microprobe analysis of about 300 cumulate samples (Ballhaus 1993). The results suggest that the intrusions cannot be related by continuous in-situ fractionation of a single parental melt in a single magma chamber, and resulted from batches of chemically diverse parent melts derived from high-pressure fractionation of one common parental liquid.

Regional distribution of the Giles Complex

Figure 1 illustrates the generalised geology of the larger Giles intrusions. The intrusions are subdivided according to the principal cumulus phases. Ultramafic intrusions have an essential component of primitive (i.e. Mg-rich) olivine-rich orthocumulates in which plagioclase is a late poikilitic or intercumulus phase (for a cumulus terminology cf. Irvine 1982). The mafic gabbroic intrusions are composed of olivine–(orthopyroxene)–clinopyroxene–plagioclase adcumulates as well as subordinate pyroxenites. Intrusions termed troctolitic are dominated by fractionated (i.e. Fe-rich) olivine–plagioclase±magnetite adcumulates, locally containing magnetite seams. Most of the ultramafic intrusions (Murray Range, Wingellina Hills, Claude Hills, Ewarara, and Kalka) are concentrated along the northern periphery of the Giles Complex; most mafic gabbroic intrusions (Hinckley, Michael Hills Mt Davies, and Latitude Hill) occupy central parts of the complex; and the troctolitic intrusions (Jameson Range, Blackstone Range, and Bell Rock Range) define its southern margin. In so far as the Tollu volcanics of the Bentley Supergroup (1.08 Ga) are coeval with the Giles Complex (Sun et al. in press), they represent the highest level in a crustal section which becomes progressively shallower south of the Woodroffe Thrust (Glikson et al. 1995—this issue).

Murray Range intrusion

Figure 2 illustrates the generalised geology of the Murray Range intrusion. The stratigraphic succession is continuous for about 2600 m, with layering dipping steeply between 80 and 90°. The sequence is illustrated schematically in Figure 3 along a traverse from the southwestern to the northeastern contact (cf. Fig. 2). The magmatic sequence starts with about 500 m of poorly layered, uniform olivine-free feldspathic pyroxenite to melagabbro adcumulates with minor intercalations of peridotite orthocumulates. Following this unit to the 1800 m

[1] Max-Planck-Institut für Chemie, Abt. Kosmochemie, Postfach 3060, 55122 Mainz, Germany

[2] Division of Regional Geology & Minerals, Australian Geological Survey Organisation, GPO Box 378, Canberra, ACT 2601

elevation is a well-layered gabbroic to gabbronoritic suite with olivine-bearing pyroxenite, wehrlite, and peridotite/dunite intercalations. The sequence then changes to predominantly ultramafic lithologies, where coarse-grained pyroxenites alternate with harzburgite, peridotite, and dunite orthocumulate layers. Superimposed on the magmatic layering are several layer-parallel mylonite zones, along which the cumulates are highly strained and locally hydrated to light-green amphibolite (tremolitic amphibole in a matrix of sodic plagioclase). The contacts of the magmatic series of the Murray Range sequence with the granulite country rocks are covered by alluvium, and their relationships are unclear.

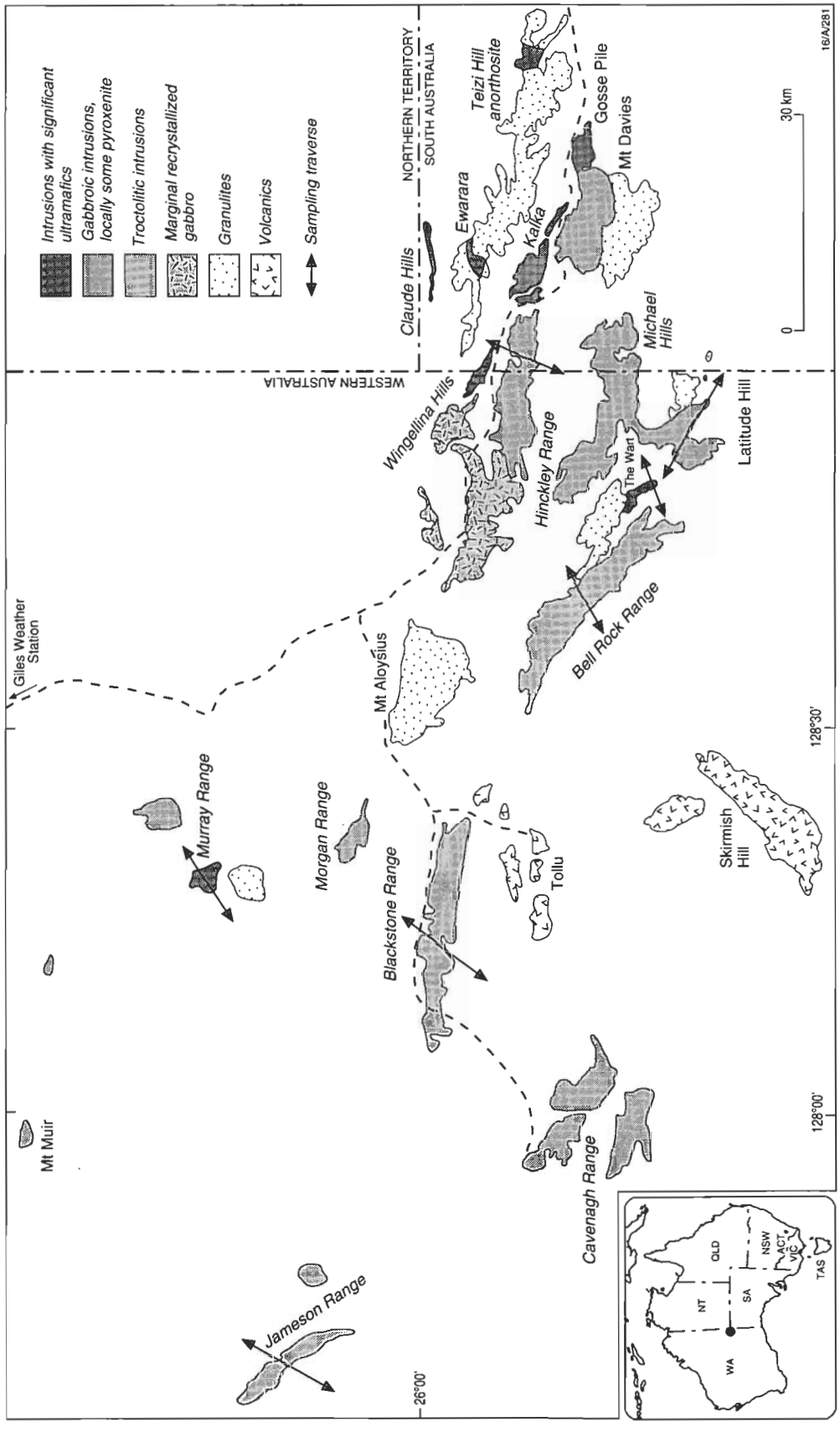

Figure 1. Major intrusions of the Giles Complex and granulite outcrops in the western Musgrave block, central Australia.

The range in mineral compositions is summarised in Figure 4 and plotted against Mg/(Mg+Fe) or Mg-number of orthopyroxene. Olivine ranges from Fo_{88} to Fo_{77}, with maximum forsterite in the well-layered ultramafic sequence around the 2000 m elevation. Orthopyroxene replaces olivine as the liquidus phase at about Fo_{77}. Clinopyroxene is, at a given olivine composition, significantly more magnesian than coexisting orthopyroxene. This applies especially to small neoblasts that have equilibrated to low temperature. Cr/(Cr+Al) in clinopyroxene is the ratio most sensitive to chemical fractionation. Up to 0.25 in the most magnesian olivine-rich cumulates, it drops to about 0.05 in the most fractionated gabbronorites. In cumulus spinel and coexisting clinopyroxene Cr/(Cr+Al) varies coherently. Ca/(Ca+Na) in plagioclase ranges from about 0.8 to 0.2 and shows little sympathetic variation with olivine composition. Plagioclase is, for a given Mg-number of coexisting olivine or orthopyroxene, comparatively sodic (cf. Ballhaus & Glikson 1989).

The Murray Range sequence is a clear example of a multiply replenished magma chamber (cf. Irvine 1980). The cryptic layering pattern in Figure reveals two gradual chemical reversals toward more primitive (i.e. more Mg and Ca-rich)

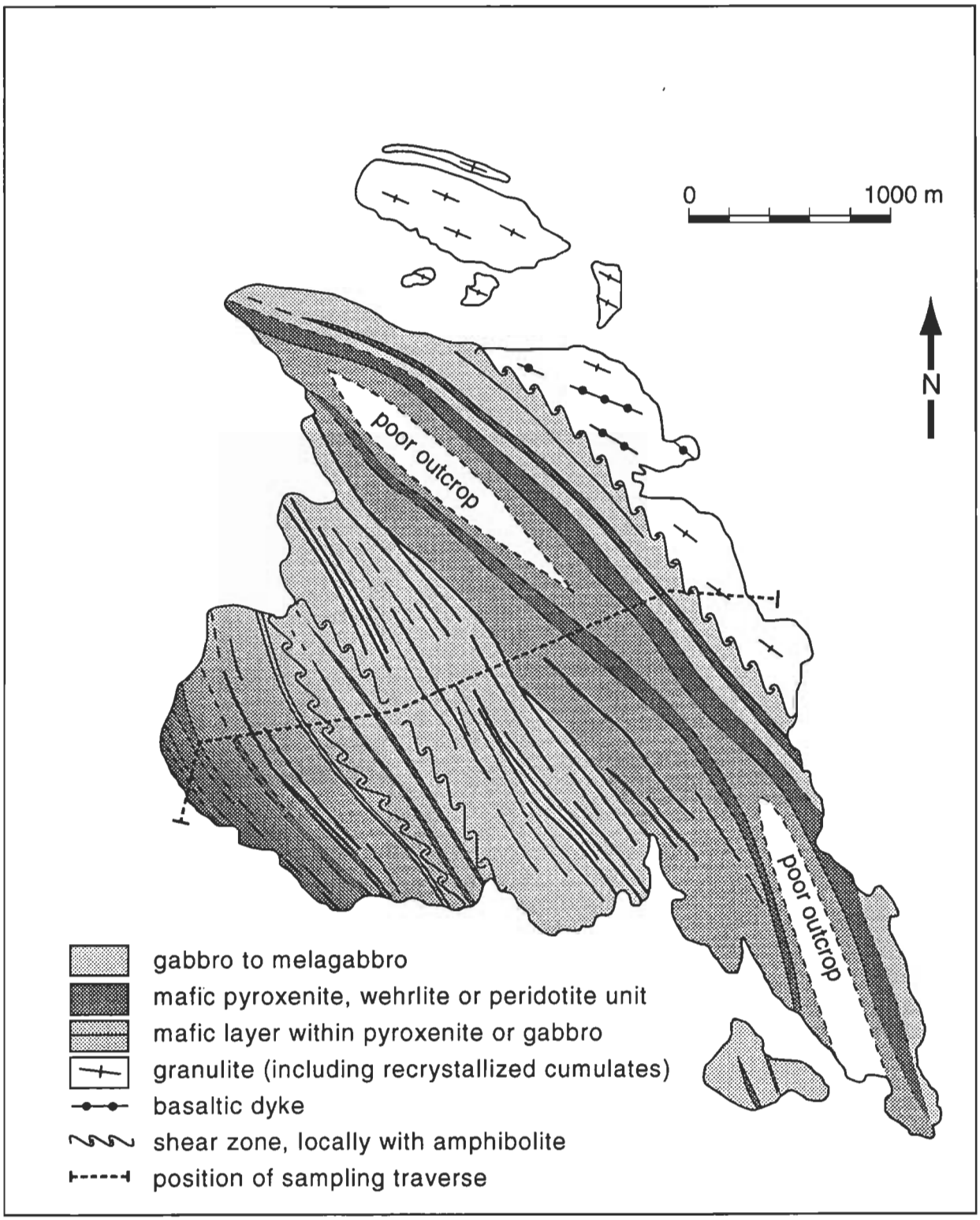

Figure 2. Schematic geology of the Murray Range ultramafic intrusion.

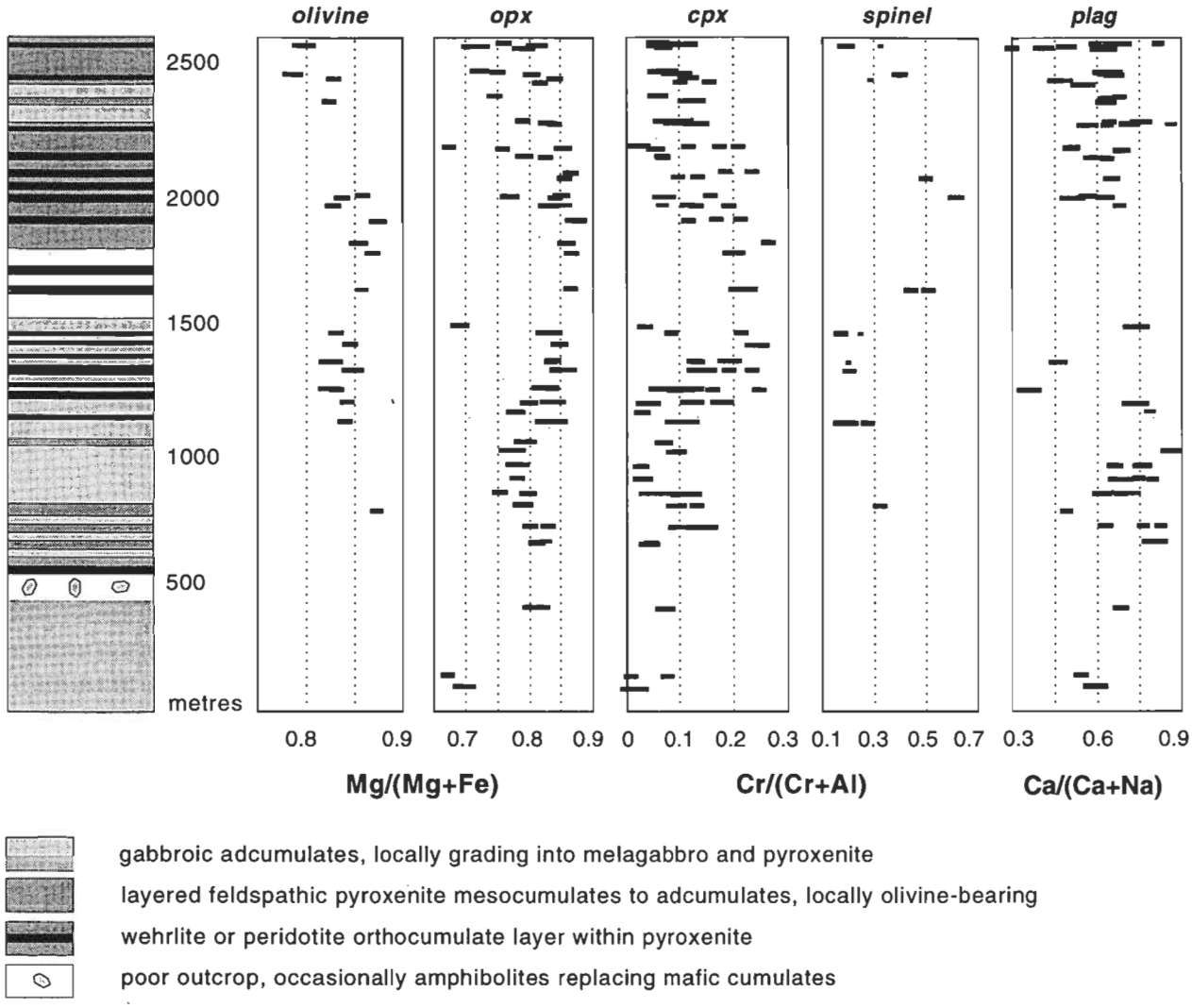

Figure 3. Magmatic stratigraphy and cryptic layering of the Murray Range ultramafic intrusion (for position of the sampling traverse see Fig. 2).

mineral compositions, each followed by extended periods of normal fractionation. The lack of overall chemical differentiation makes it difficult to decide which way the sequence may be younging. We believe that the southern contact marks the bottom of the intrusion, for three reasons: (1) the chemical reversals are broadly situated where the sequence changes from predominantly gabbroic to predominantly ultramafic lithologies; (2) the bases of ultramafic cycles are typically orthocumulates, suggesting that they formed in a high thermal gradient (Campbell 1987; Ballhaus & Glikson 1989); and (3) several ultramafic intercalations are preceded by hybrid zones in which patches and schlieren of ultramafic cumulate material occur intermingled with more fractionated gabbroic material (cf. Ballhaus & Glikson 1989). Such hybrid zones may form when the first batches of a major pulse collect on the magma chamber floor and freeze before they can homogenise with the cooler resident melt. As such, they must define the footwall contact of an ultramafic unit. Accordingly, the stratigraphic sequence of the Murray Range intrusion youngs toward the northeast.

We infer from crystallisation sequences and mineral compositions in the most mafic units that the parental melt to the Murray Range intrusion was saturated with olivine and an aluminous spinel, and was near-primitive with respect to MgO content. The crystallisation sequence was (1) olivine±aluminous spinel, (2) olivine(orthopyroxene)–clinopyroxene, and (3) (olivine)–orthopyroxene–clinopyroxene–plagioclase. The megascale layering is a direct consequence of the undersaturated nature of the replenished melt. Any pulse of olivine-only saturated liquid into multiply saturated resident melt must have resulted in the loss of at least one liquidus phase, commonly two, and a corresponding change in cumulate mineralogy.

The Wart intrusion

The Wart intrusion is an ultramafic intrusion situated east of the southwestern tip of the Bell Rock intrusion (Fig. 5). The magmatic sequence along the traverse (Fig. 6) dips steeply between about 80 and 90°. The intrusion is composed of an exceptionally well-layered suite of clinopyroxenite to melagabbro mesocumulates to adcumulates. Many (several tens) layers of lenticular wehrlite to peridotite orthocumulate are intercalated, as well as numerous microgabbro sills with textural transitions from rapidly chilled rocks to genuine cumulate layers (cf. Ballhaus 1993). The cumulates and sills, in turn, are cut by at least three compositionally different generations of basaltic dykes; one with subhedral clinopyroxene and elongate plagioclase laths as phenocrysts, a second with olivine and plagioclase, and a third with partially resorbed orthopyroxene phenocrysts. Total thickness of the cumulate pile exceeds 1800 m. Most contacts are covered by alluvium, although the northeastern margin features cumulates with intrusive relationships into felsic granulites. Original chilled margins have not been seen.

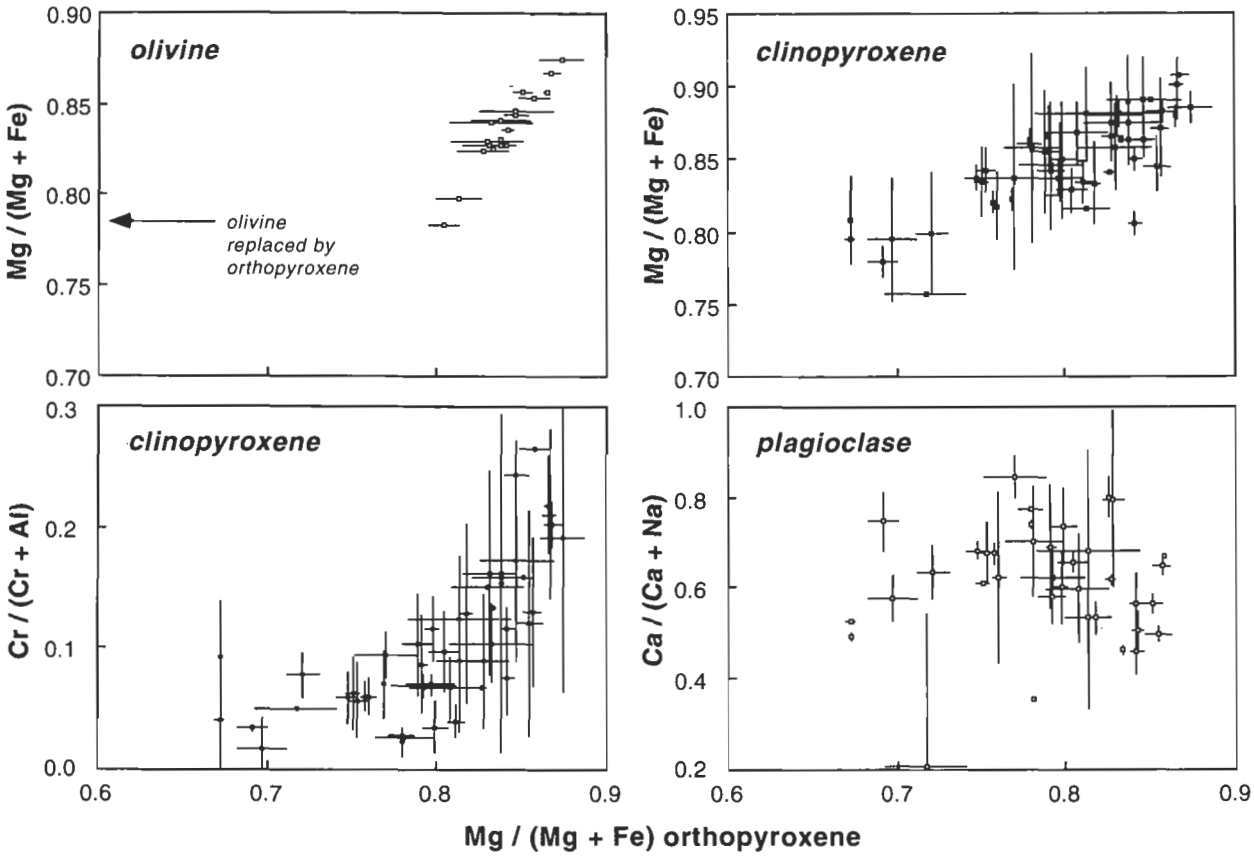

Figure 4. Average phase compositions in the Murray Range cumulates (error bars are two standard deviations).

In terms of phase composition (Fig. 7), The Wart sequence is nearly as primitive as the Murray Range or Wingellina Hills (Ballhaus & Glikson 1989) sequences. Olivine falls within a compositional range of Fo_{87-78}, below which it becomes replaced by orthopyroxene. In comparison with the Murray Range sequence, orthopyroxene is much rarer and clinopyroxene is more fractionated, with Cr/(Cr+Al) ratios not exceeding 0.16. A cumulus spinel phase is not observed, probably because the magma was depleted in Cr by extensive clinopyroxene crystallisation. Plagioclase is, for a given olivine composition, far more calcic than in the Murray Range intrusion.

The modal layering in The Wart sequence arises from the intrusion of numerous small to medium-sized batches of primitive parent magma, into a continuously differentiating body of somewhat more fractionated resident melt. From stratigraphic relationships, it is suggested that this layered sequence youngs to the southwest and could, therefore, form the base of the Bell Rock intrusion. Most ultramafic units commence with a sharp modal change to olivine-rich orthocumulates, followed by an upward gradation to wehrlite and then pyroxenite. This cyclic pattern is likely to result when olivine-rich liquid ponds on the magma chamber floor and gradually mixes with the overlying cooler resident melt. The lower northeastern half of the sequence, up to the 1050 m stratigraphic level, signifies a period of multiple magma addition, while the upper half indicates chemically more stagnant conditions with fewer magmatic replenishment events.

The parent melt characteristics are similar to those of the Murray Range intrusion. The melt was near-primitive with respect to its Mg-number. The common lack of orthopyroxene and spinel indicates that silica activity and Cr contents may have been slightly lower than in the Murray Range magma, possibly because the magma experienced some pyroxene fractionation prior to emplacement into the crustal magma chamber.

Latitude Hill intrusion

The Latitude Hill intrusion (Fig. 8), a folded segment of the Michael Hills gabbro, is one of the thickest cumulate sequences in the Giles Complex. Classified as mafic gabbroic in character, it consists of two steeply dipping (80–90°), uniform, olivine-bearing gabbro units with numerous layers and lenses of olivine-bearing pyroxenite and rare peridotite, altogether about 8000 m thick (Fig. 9). The two magmatic units are separated by a zone of altered, highly strained, recrystallised gabbro, infiltrated by pseudotachylite veins. The magmatic suites of the Latitude Hill intrusion feature several unusually fine-grained 'doleritic-textured' units, which Ballhaus (1993) interpreted as intraplutonic chill zones. The Latitude Hill gabbro is one of the few cumulate packages of the Giles Complex with demonstrably intrusive contacts with felsic granulites.

Mineral compositions are displayed in Figure 10. The Latitude Hill sequence is significantly more fractionated than the primitive Murray or The Wart sequences. Olivine is relatively rare and ranges in composition from Fo_{83} to Fo_{67}. Mg-numbers of orthopyroxene are slightly offset relative to olivine to more magnesian values and range from 0.85 in the most primitive ultramafic units to about 0.58 in the central deformed granulitic zone. Orthopyroxene replaces olivine at Fo_{68}. Cr/(Cr+Al) in clinopyroxene varies sympathetically with Mg-numbers of orthopyroxene and rarely exceeds 0.1. Ca/(Ca+Na) in plagioclase ranges from about 0.5 to 0.85 and varies coherently with Mg-numbers of olivine and orthopyroxene.

The stratigraphic orientation of the sequence, as inferred in Figure 9, is arbitrary, as there is no textural indication of where bottom and top contacts are situated, nor does the shape of the cryptic fractionation patterns (Fig. 9) provide a clue. The two magmatic piles on either side of the central deformed zone feature a major chemical reversal followed by a similarly

extensive period of normal fractionation. Abrupt changes in modal mineralogy and megascale layering are rarer and less obvious than in the more primitive Murray Range and The Wart cumulate sequences.

The parent melt to the Latitude Hill sequences was close to multiple saturation with olivine, pyroxenes, and plagioclase. As a result, megascale layering is poorly developed because new magma pulses did not lead to major changes in the crystallisation sequence. Suggested crystallisation sequences are: (1) olivine+orthopyroxene, (2) orthopyroxene+clinopyroxene, and (3) orthopyroxene+clinopyroxene+plagioclase. Cr/(Cr+Al) in clinopyroxene and the Mg-numbers at which olivine became replaced by orthopyroxene are lower than in the ultramafic sequences. This indicates that the Latitude Hill liquids were more fractionated and lower in silica activity than the melts of the ultramafic intrusions, possibly owing to pyroxene fractionation before emplacement.

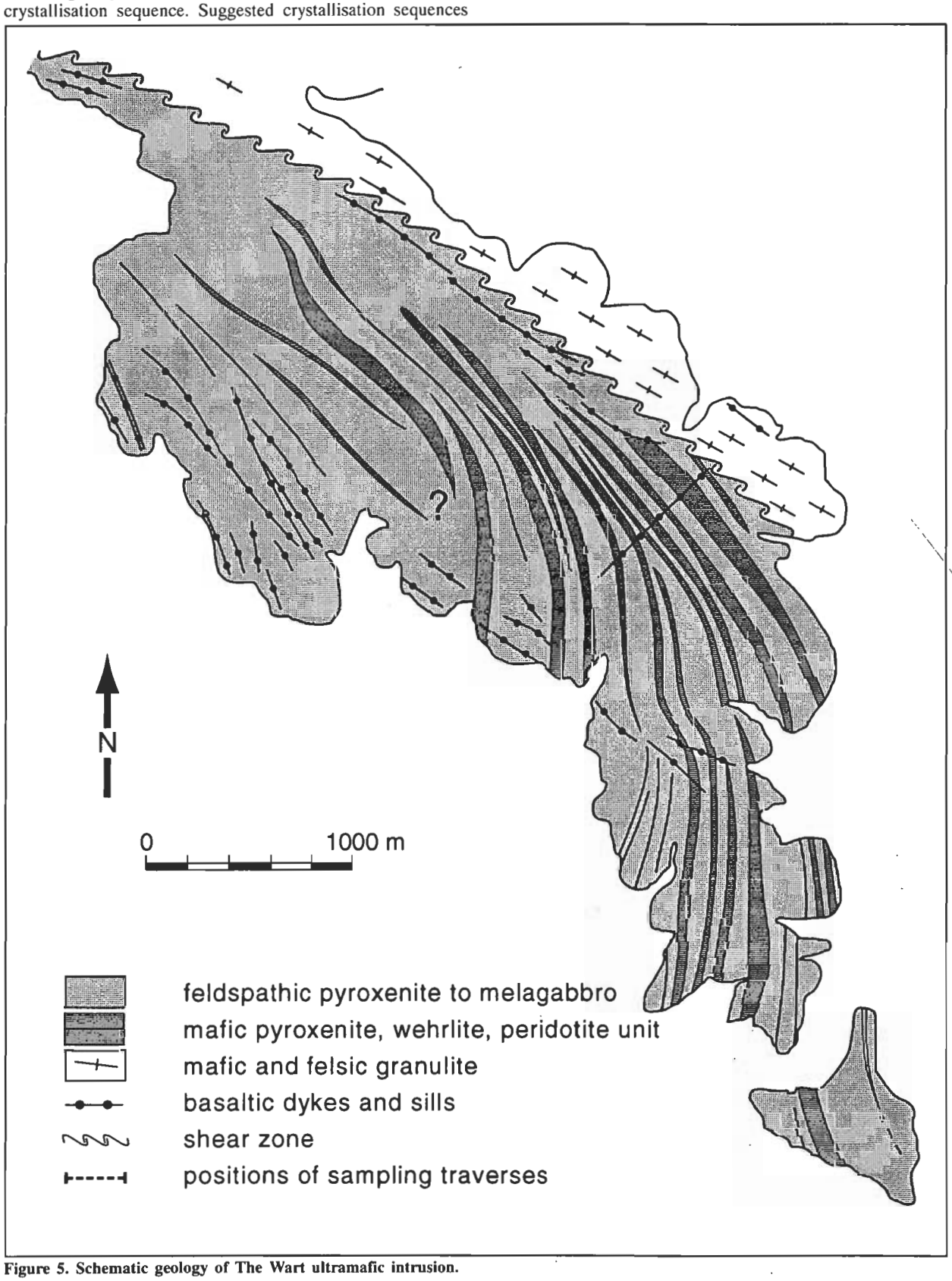

Figure 5. Schematic geology of The Wart ultramafic intrusion.

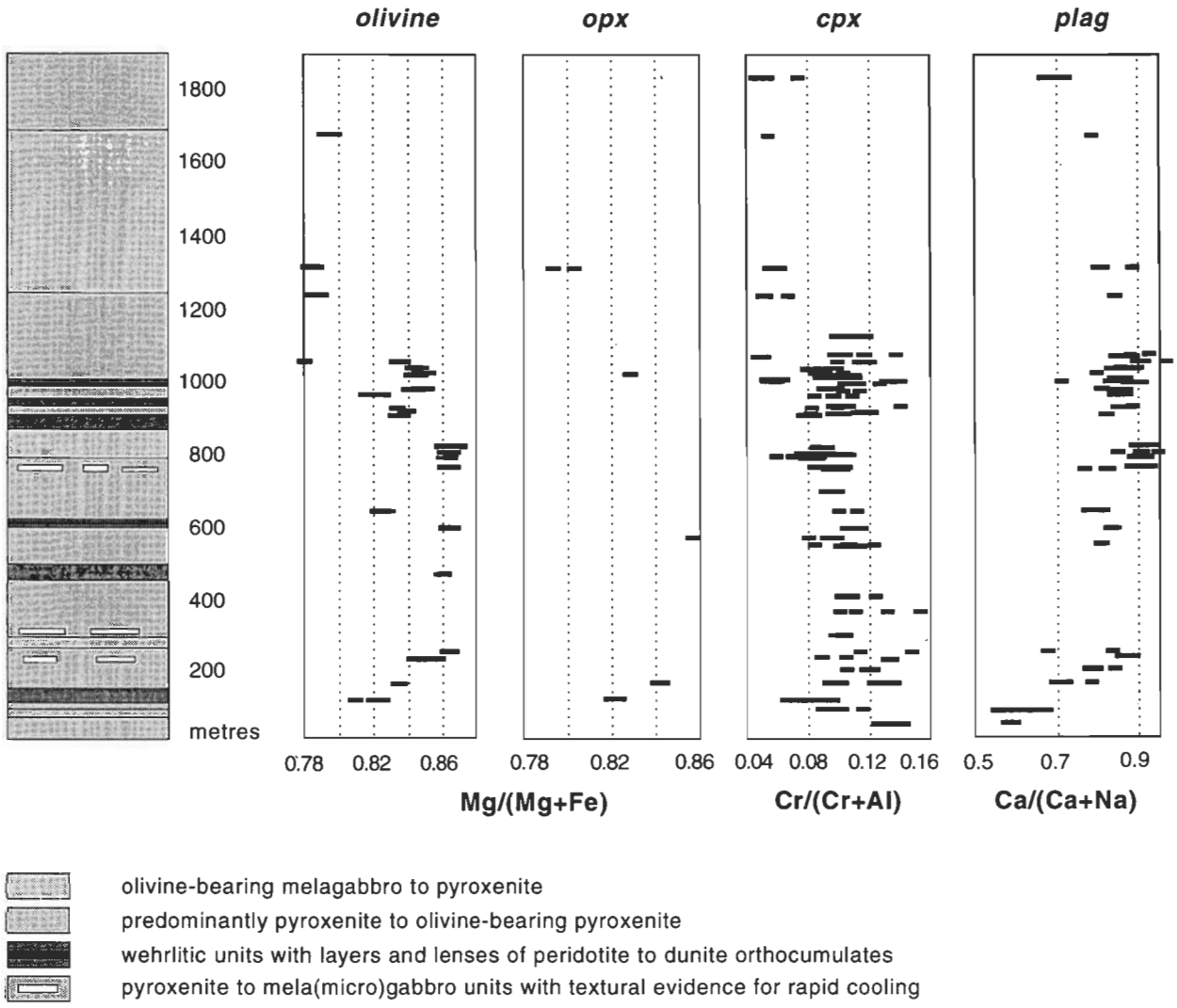

Figure 6. Magmatic stratigraphy and cryptic layering pattern of The Wart intrusion (for position of the sampling traverse see Fig. 5).

Hinckley Range intrusion

The Hinckley Range intrusion (Fig. 11) is one of the largest and most deformed intrusions of the Giles Complex. The magmatic sequence is approximately 5800 m thick and dips steeply north at 70 to 80°. Its western and northwestern units are affected by a metamorphic overprint, identified by Glikson & Stewart (1990) and Clarke (1992) as recrystallised gabbros intruded by felsic veins (cf. Fig. 1). Cumulate textures and magmatic layering are poorly preserved. The eastern (magmatic) extension of the intrusion is well layered and has largely escaped the metamorphic overprint evident in the west.

The Hinckley Range intrusion is mainly gabbroic, with the most common cumulates being gabbroic troctolite, troctolitic gabbro, gabbronorite, anorthosite, and locally minor pyroxenite (Fig. 12). The sequence is interlayered with multiple intraplutonic chill zones, i.e. multiple repetitions of fine-grained 'marginal' layered microgabbros and doleritic-textured (Ballhaus 1993) gabbroic sills. Phenocryst populations in these finer grained units resemble the phase assemblages in the surrounding layered cumulates. Parts of the sequence are cut by layer-parallel mylonite zones rich in pseudotachylite veins. The most prominent is the Hinckley thrust fault (Goode 1978), where pseudotachylite networks superimposed onto each other and gabbroic fragments are several metres thick (Glikson & Mernagh 1990).

Mineral compositional trends are summarised in Figure 13 and plotted against Mg-numbers of orthopyroxene. The Hinckley Range sequence is comparatively fractionated. Olivine ranges from Fo_{75} to Fo_{59}, below which it is replaced by orthopyroxene. Cr/(Cr+Al) in clinopyroxene is low, reflecting significant fractionation of the melt prior to emplacement. Plagioclase composition is highly variable in single samples and single grains, especially in more recrystallised cumulates. With protracted fractionation, there is a poorly defined trend toward more sodic average plagioclase compositions.

Cryptic layering patterns (Fig. 12) are consistent with normal fractionation from the south to the north, interrupted by a poorly defined reversal above the 2000 m level. With protracted fractionation upward in the sequence there is a steady increase in modal orthopyroxene and clinopyroxene at the expense of olivine. The morphology of the cryptic layering profiles and graded and cross-layering features suggest that the Hinckley Range gabbro youngs towards its northern contact, i.e. an opposite orientation to the Wingellina Hills intrusion (Ballhaus & Glikson 1989).

The parent magma of the Hinckley Range suite must have been fairly fractionated. At the time of emplacement, the magma was multiply saturated with olivine and plagioclase, and just undersaturated with clinopyroxene. The increase in orthopyroxene and clinopyroxene upwards indicates that the fractionating phase assemblages were, mostly, lower in bulk silica content than the parent melt.

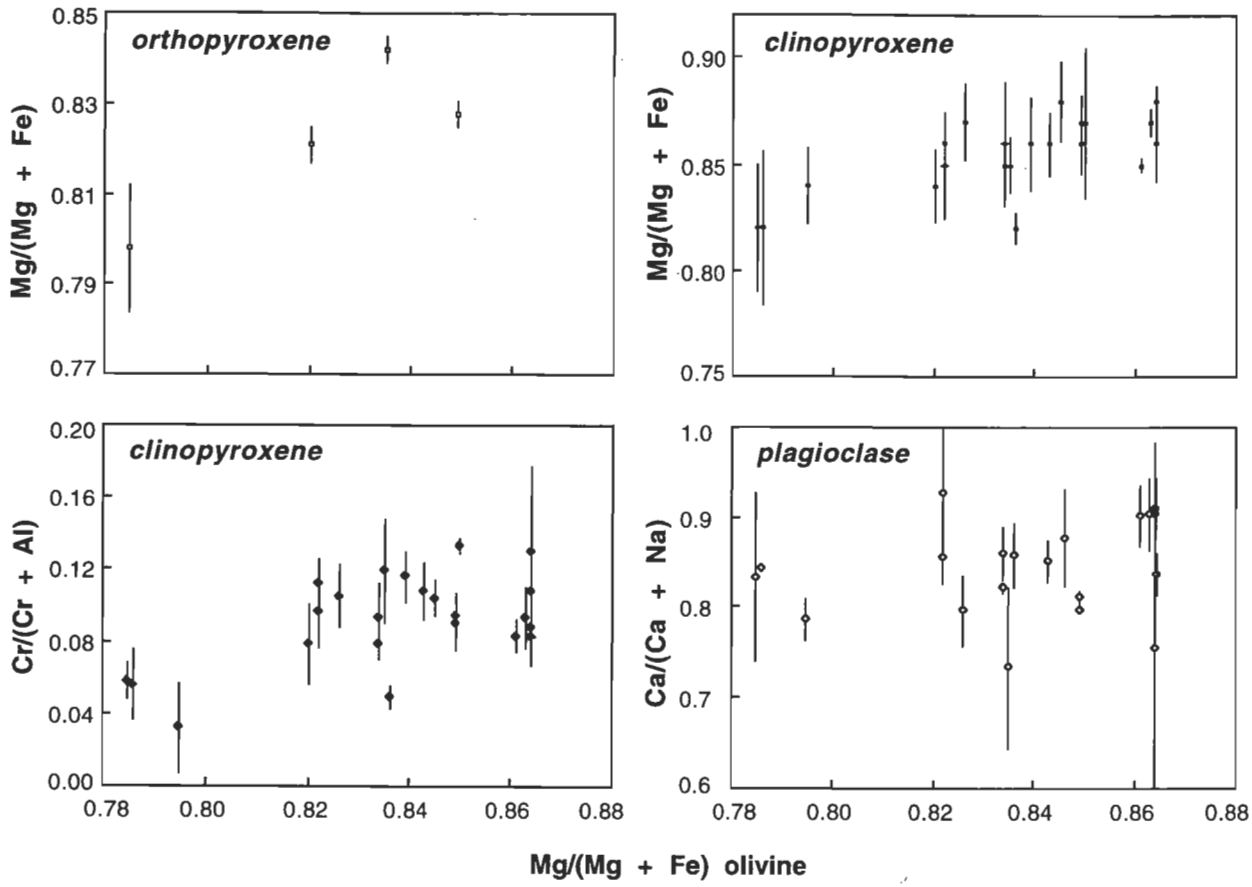

Figure 7. Average phase compositions in The Wart cumulates (error bars are two standard deviations).

Bell Rock Range intrusion

The Bell Rock Range intrusion (Fig. 14) hosts one of the most fractionated magmatic sequences of the Giles Complex and belongs to the troctolitic suite (Fig. 1). Total exposed thickness is around 3800 m. The sequence dips steeply at 70° southwest. Most contacts with country rocks are hidden by alluvium. The units are composed of massive, laterally continuous magnetite-bearing troctolites, gabbroic troctolites, and anorthosites, each being several hundreds of metres thick (Fig. 15). A few thin dunite layers and magnetite seams, several centimetres thick, are intercalated with the gabbroic sequence. Part of the sequence displays numerous stratiform repetitions of microgabbro sills, which may be chilled equivalents of the coarser grained cumulates. Modal layering only occurs on a centimetre to metre scale (cf. Boudreau 1987). The megascale cyclicity, so typical of the more mafic intrusions of the Giles Complex, is poorly developed.

Mineral compositional ranges are shown in Figure 16. Olivine ranges from Fo_{68} to about Fo_{56}. No textural evidence is observed to indicate that olivine becomes replaced by orthopyroxene (i.e. no peritectic reaction relationship with the melt); for example, modal orthopyroxene does not increase with falling Mg number upward in the sequence, in contrast to the gabbroic and ultramafic intrusions. Relative to olivine, orthopyroxene is displaced to higher Mg-numbers and varies from 0.72 to 0.62. Clinopyroxene compositions show no systematic chemical trend, probably because clinopyroxene is a late intercumulus phase. Mg-numbers of clinopyroxene are poor indicators of magmatic differentiation because clinopyroxene becomes more magnesian as it exsolves orthopyroxene during subsolidus equilibration. Ca/(Ca+Na) of plagioclase is highly variable between 0.85 and 0.55 and shows little systematic variation with coexisting olivine compositions.

The stratigraphic orientation of the Bell Rock Range sequence (Fig. 15) remains ambiguous; clearly, the morphology of the cryptic layering pattern could be interpreted either way. However, unless it is overturned, the general dip of the cumulate units suggests that the sequence youngs to the southwest. Grading and cross-layering structures also suggest southwestward younging, and there is also a tendency for modal magnetite to increase in the same direction. The parent magma must have been highly fractionated and saturated with olivine and plagioclase (and possibly also clinopyroxene and magnetite) at the time of emplacement. As a direct consequence, there is no departure from olivine–plagioclase co-precipitation even at stratigraphic levels where chemical reversals signify influxes of fresh melt. Silica activity does not seem to increase with protracted fractionation; i.e. there is no increase in modal orthopyroxene upward in the sequence, probably because the fractionating phase assemblages were at all times richer in silica than the equilibrium melt.

Blackstone Range intrusion

The Blackstone Range intrusion is a major troctolitic magmatic sequence (Fig. 17). Similar to the Bell Rock Range intrusion, it consists of fractionated troctolites, olivine gabbros, and anorthosites, with occasional monomineralic dunite and massive magnetite layers (Fig. 18). Megascale phase layering is poorly developed. The stratigraphic sequence is continuous for about 3900 m and magmatic layers dip south at 70 to 75°. Along the northern periphery, cumulates are recrystallised to fine-grained massive phlogopite-bearing mafic granulite, possibly incorporating former chilled margins. Along the southern contact the sequence is faulted against the Bentley Supergroup (cf. Daniels 1974). Contacts with felsic granulite country rocks are not exposed.

Mineral compositional variations are plotted against orthopyroxene composition in Figure 19. Olivine ranges from

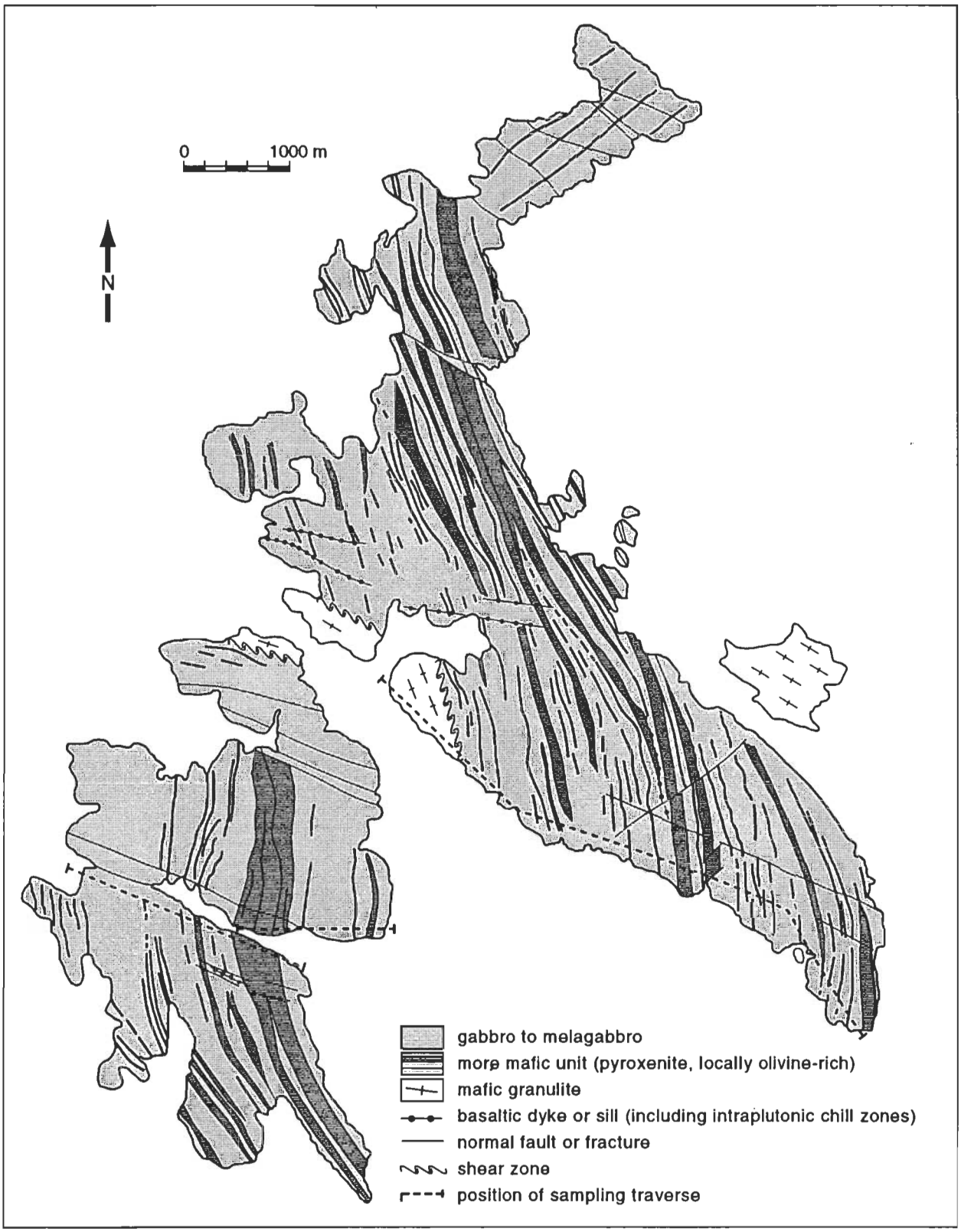

Figure 8. Schematic geology of the Latitude Hill gabbroic intrusion.

Fo_{67} to Fo_{40}, the latter being the most fractionated olivine reported from the Giles Complex. Mg numbers of coexisting orthopyroxenes vary from about 0.7 to 0.55 and are slightly compressed relative to those of olivine. Cr contents in clinopyroxene are close to detection limit and show no sensible stratigraphic trend. Ca/(Ca+Na) of plagioclase is highly variable and ranges from above 0.8 to about 0.5.

The cryptic layering pattern strikingly resembles that of the Bell Rock Range intrusion (Fig. 18). It is suggested that the minimum Mg number at the 2400 m level coincides with a similar minimum at the 3600 m level in the Bell Rock Range sequence. Likewise, the dunite layers at the 400–450 m level of the Blackstone Range sequence may correlate with a similar sequence at the 1500 m level at Bell Rock. There is again no clear indication which way chemical fractionation was directed and where the bottom and top contacts may have

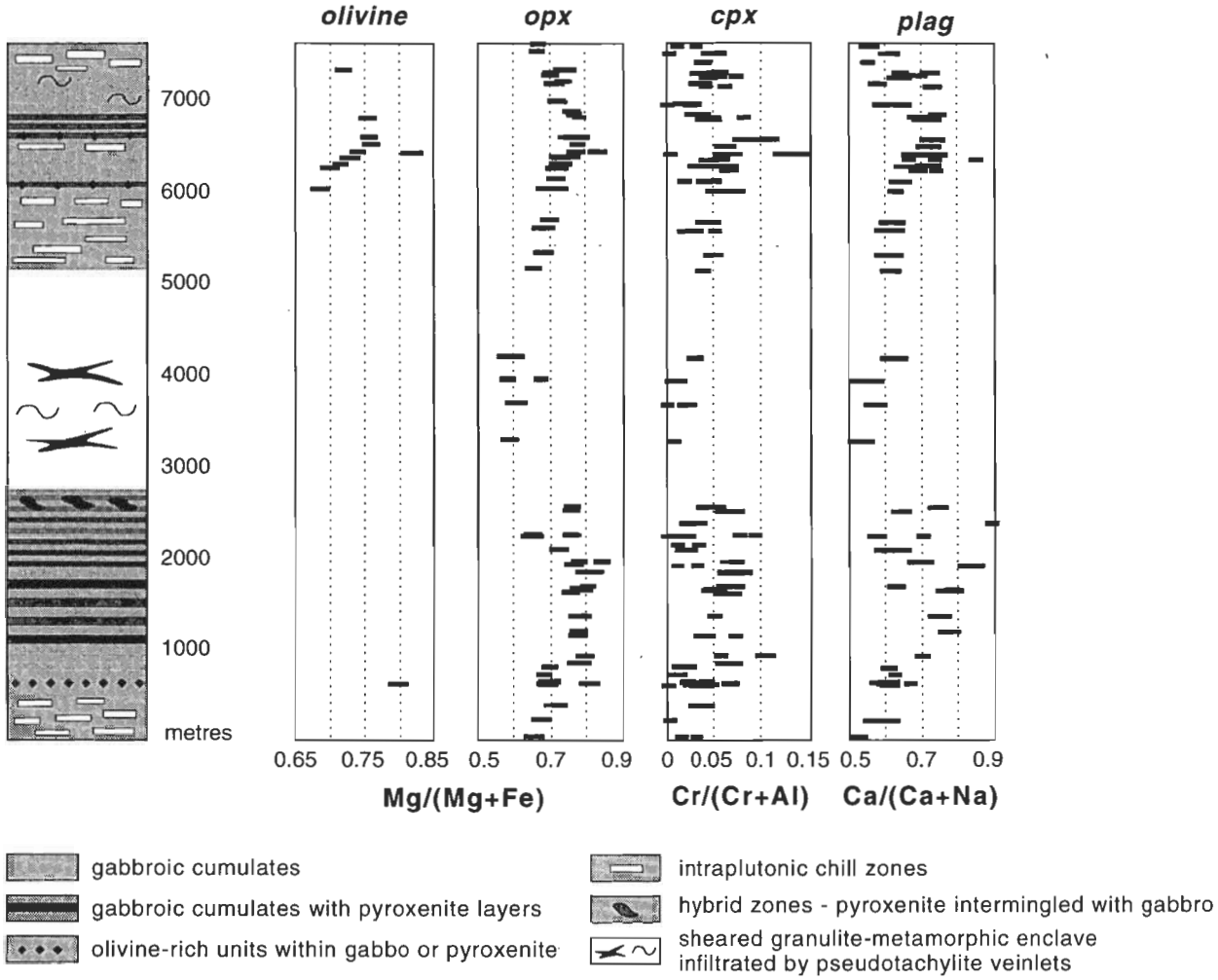

Figure 9. Magmatic stratigraphy and cryptic layering pattern of the Latitude Hill intrusion (for position of the sampling traverse see Fig. 8).

been situated. However, unless the sequence is overturned, it youngs toward the south. We concur with Daniels (1974) that the Bell Rock Range and Blackstone Range sequences originally formed one coherent intrusion.

Jameson Range intrusion

The Jameson Range intrusion is composed of approximately 2500 m of layered Fe-rich troctolite, gabbroic troctolite, and anorthosite adcumulates with various proportions of disseminated magnetite (Fig. 20). About two-thirds of the magmatic sequence is covered by alluvium. Closely interlayered centimetre-scale units are common. The Jameson sequence hosts several massive vanadiferous titano-magnetite seams (Daniels 1974). Bottom and top contacts of the intrusion are not exposed and the nature of the contacts remains unknown. The intrusion hosts some of the most fractionated cumulates in the Giles Complex (Fig. 21). Olivine ranges from about Fo_{65} to Fo_{51}, and Mg numbers of coexisting orthopyroxenes from 0.72 to 0.62. There is again no indication of a peritectic relationship between olivine and orthopyroxene, nor does modal orthopyroxene increase with increasing degree of fractionation. Clinopyroxene is significantly more magnesian than orthopyroxene and Cr is at detection limit. Ca/(Ca+Na) in plagioclase varies randomly from 0.75 to 0.49, sometimes with a 20 per cent variation within single grains. This can be attributed to incomplete plagioclase equilibriation during subsolidus recrystallisation.

Sampling density across strike is insufficient to identify any clear cryptic variation pattern (Fig. 20), nor can abrupt changes in cumulus mineralogy or any megascale layering be identified except where the massive magnetite seams occur, i.e. between the 1200 and 1700 m levels. Mineralogic phase layering occurs through gradual variation in (olivine+pyroxene)/plagioclase modal ratios and variation in disseminated magnetite. There is no obvious stratigraphic variation in modal olivine/orthopyroxene ratio or any correlation of that ratio with chemical fractionation, implying that the magma was too Fe-rich for olivine to react with its equilibrium melt, nor is there clear geochemical evidence to indicate younging direction. The shallow southerly dip of the magmatic layers makes it likely that the sequence youngs to the southwest.

Discussion

The Giles Complex consists of three major types of cumulates—ultramafic, gabbroic, and troctolitic. In the following sections we identify, in broad terms, the parent melt compositions that gave rise to these types of cumulates and discuss how they may be related.

Parental magmas to the Giles intrusions

Although chilled margins occur locally (Kalka, Mount Davies), their contaminated state requires reconstruction of parent melt compositions from crystallisation sequences and phase compositions of the most primitive cumulates in each intrusion. Implicit in this is that the crystallisation sequences in the cumulates resemble the liquidus relations of the parent melts. On this basis we identify three major types of parental magmas;

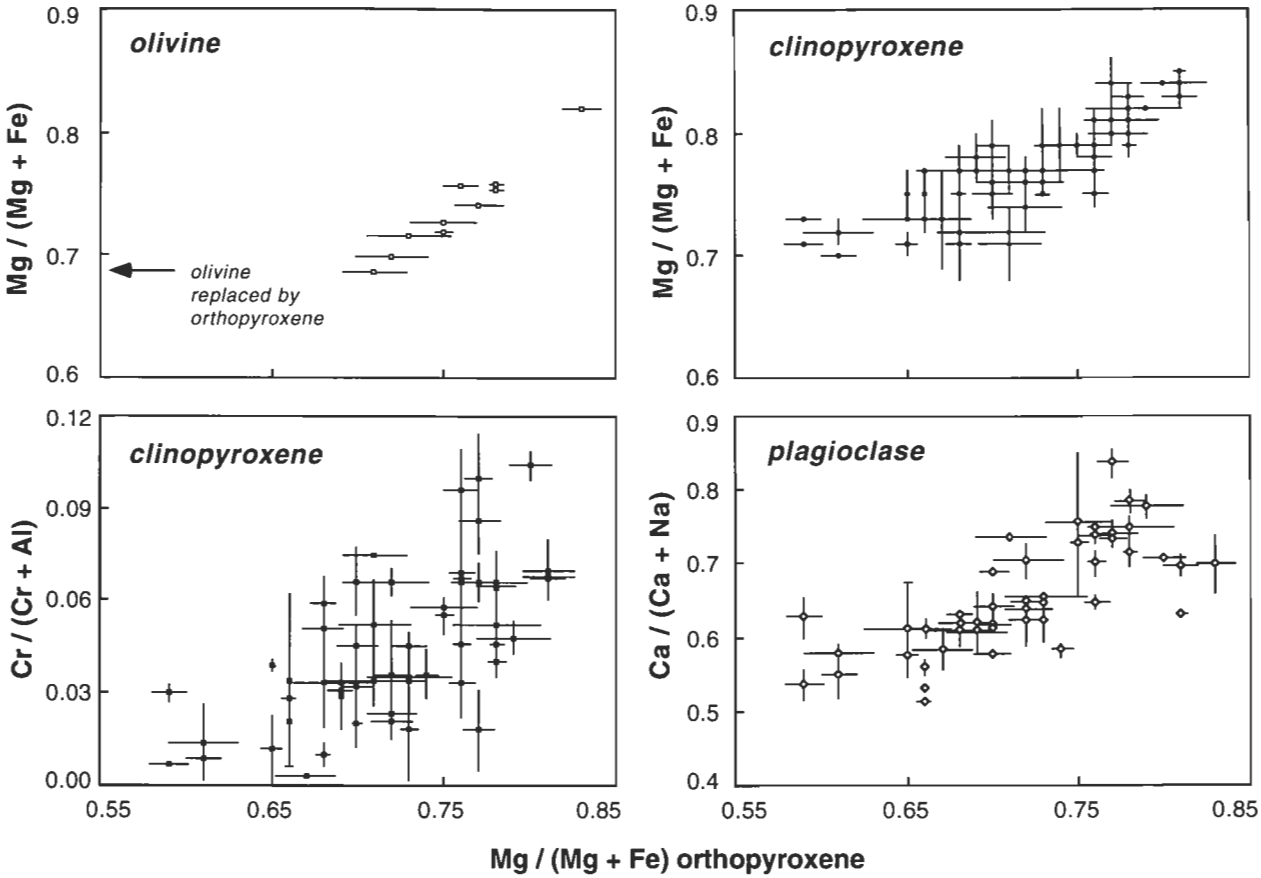

Figure 10. Average phase compositions in the Latitude Hill cumulates (error bars are two standard deviations).

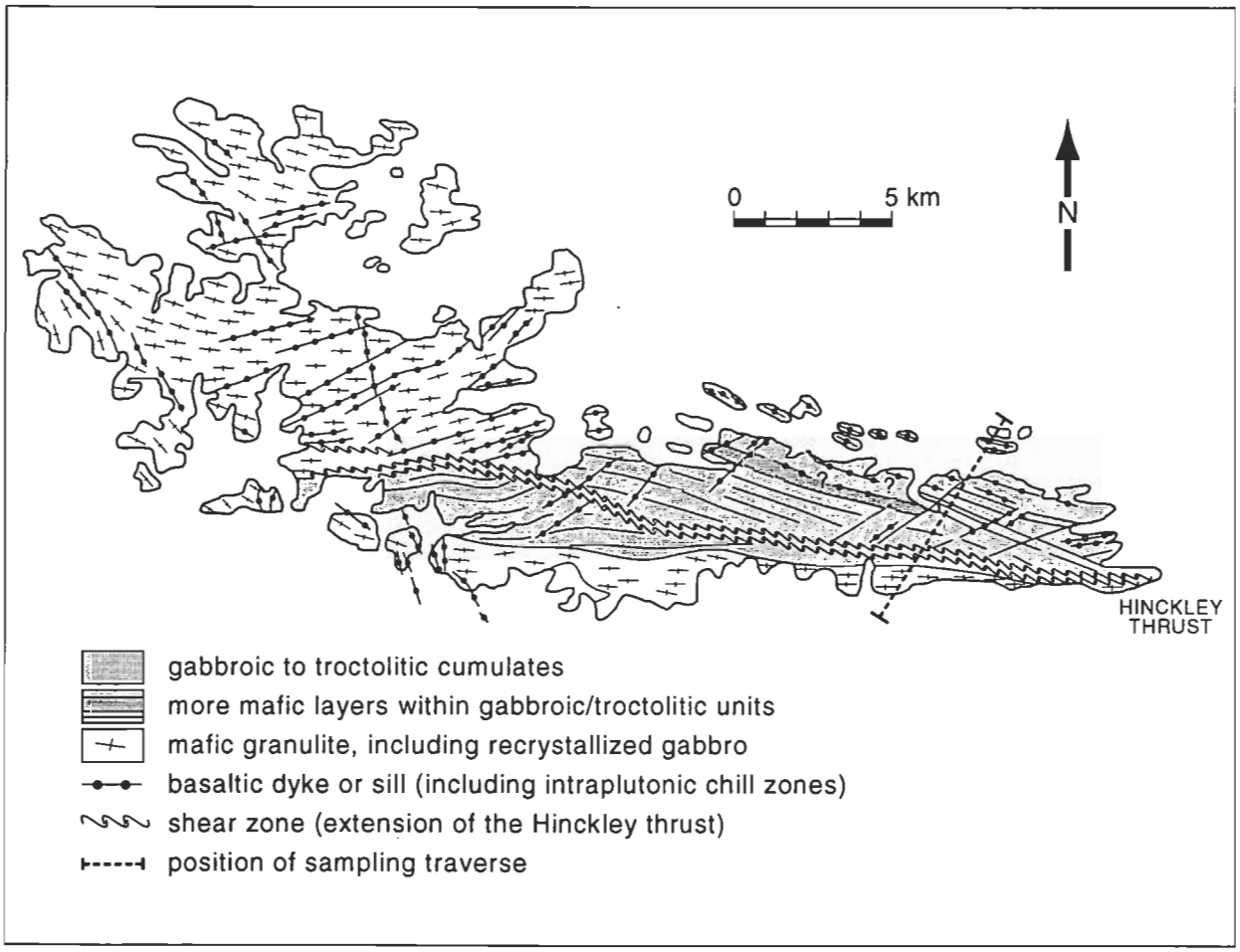

Figure 11. Schematic geology of the Hinckley Range mafic gabbroic intrusion.

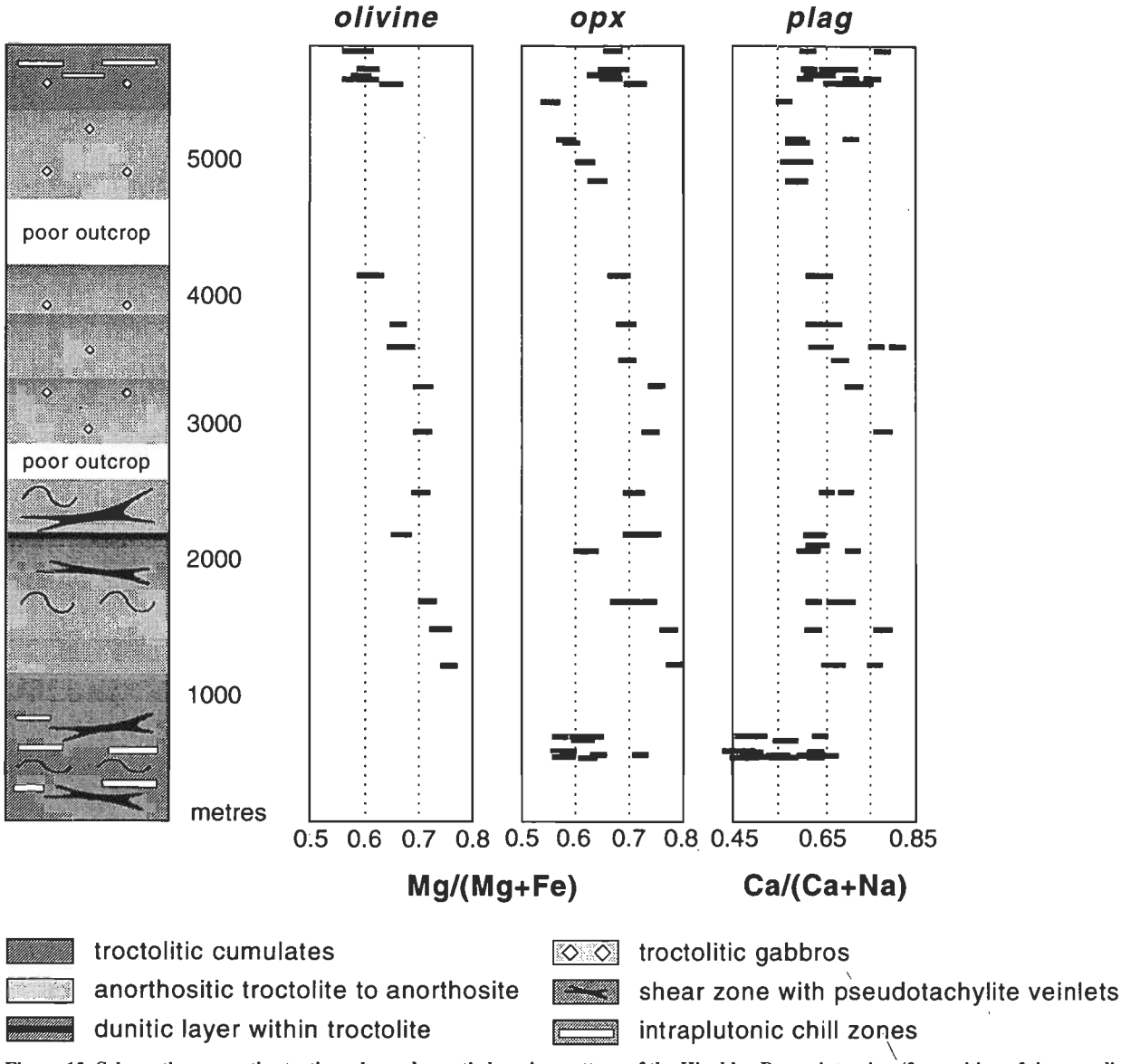

Figure 12. Schematic magmatic stratigraphy and cryptic layering pattern of the Hinckley Range intrusion (for position of the sampling traverse see Fig. 11).

(1) a primitive olivine-normative olivine–spinel saturated liquid, (2) a moderately fractionated quartz-normative pyroxene–plagioclase saturated gabbroic melt, and (3) a highly evolved nepheline-normative olivine–plagioclasemagnetite saturated troctolitic melt.

Primitive parental melt. Examples of cumulate sequences derived from a primitive melt are the Murray Range, The Wart, and Wingellina Hills intrusions (Ballhaus & Glikson 1989), and possibly the Kalka and Ewarara intrusions (Goode & Moore 1975, Goode & Krieg 1967), for which systematic phase compositions are not available. The following criteria allow characterisation of the parent melt:

- Olivine became replaced from the liquidus at Fo_{77} (Figs 4, 7); this, in combination with the observation that dunite cumulates are volumetrically minor rock types in all ultramafic intrusions of the Giles Complex, suggests that the normative olivine content of the melt could not have been very high.
- The most primitive cumulates (Murray Range and Wingellina Hills intrusions) are dunitic orthocumulates where the most magnesian olivine is Fo_{88-89}. Assuming that total Fe as FeO in the melt was around 10 wt per cent (reasonable for continental tholeiitic melts), this gives an MgO content in the melt of around 12 wt per cent (Roeder & Emslie 1970).
- Typical Ni content in the most primitive olivines is around 2500 ppm; available partition coefficients constrain Ni in the equilibrium melt to around 200 ppm (Henderson 1982; Hirschmann & Ghiorso 1994).
- Maximum Cr content of the texturally earliest cumulus clinopyroxene ranges from 1800 to 2200 ppm, suggesting a Cr content of the equilibrium melt of around 150–200 ppm (e.g. Philpotts 1990).
- Every reversal in the cryptic layering patterns of the ultramafic intrusions is matched in the cumulate sequence by loss of at least one cumulus phase, commonly two (clinopyroxene and plagioclase). This suggests that, at the pressure of emplacement, the primitive magma was only saturated with olivine (+ spinel).

The above points summarise the chemical characteristics of a low-pressure basaltic melt in near-equilibrium with mantle parageneses (cf. Green & Ringwood 1967a; Jaques & Green 1980). We conclude that the parent melt to the ultramafic intrusions of the Giles Complex was broadly tholeiitic and just olivine normative. It experienced negligible phase fractionation or contamination prior to emplacement in the crustal magma reservoirs.

Gabbroic parental melt. The cumulate series of the gabbroic intrusions (Hinckley and Latitude Hill) formed from multi-

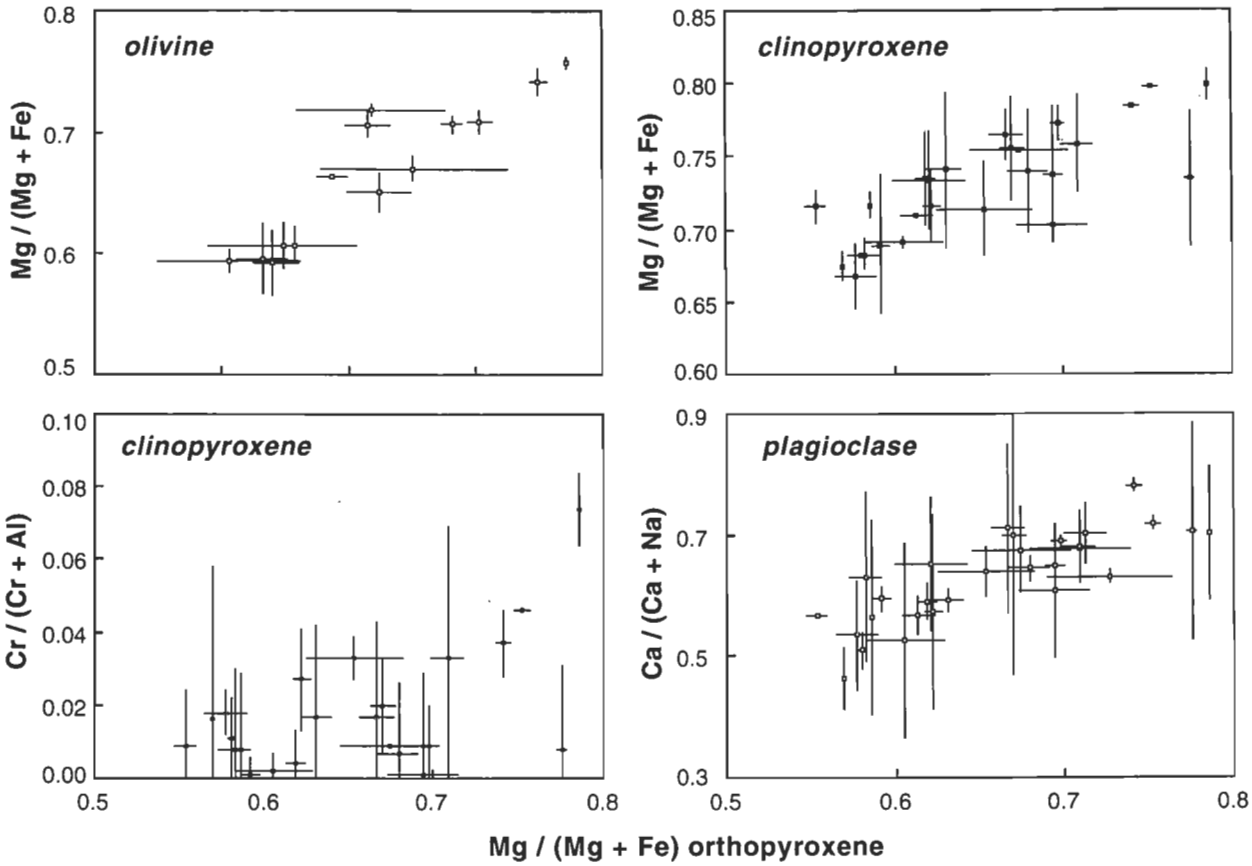

Figure 13. Average phase compositions in the Hinckely Range cumulates (error bars are two standard deviations).

ply-saturated parental melts significantly more evolved than the parent liquids to the ultramafic intrusions. The melts must have been saturated with olivine–(orthopyroxene), clinopyroxene, and plagioclase at the time of emplacement. As a direct result there is little change in cumulus mineralogy, even where reversals in mineral composition signify a major influx of new magma into the magma chamber. A new melt pulse can only change cumulate mineralogy (and initiate megascale layering) if it is compositionally far removed from a cotectic. In cases where a melt is close to multiple phase saturation, a modal change will only result if the mass ratio of added (more primitive) to resident (more fractionated) melt is high.

Overall, the gabbroic parent magma must have experienced appreciable pyroxene±olivine fractionation prior to emplacement. The most primitive olivine compositions encountered are Fo_{83} at Latitude Hill and Fo_{75} in the Hinckley Range sequence, and these became replaced by orthopyroxene when olivine had evolved to Fo_{67} and Fo_{56}, respectively. Cr in the gabbroic parental melt was also severely depleted. Cr/(Cr+Al) in clinopyroxenes of the Latitude Hill sequence is below 0.15, while in the Hinckley Range sequence it is near detection limit.

Troctolitic parental melt. The parent melt to the troctolitic intrusions (Bell Rock, Jameson, and Blackstone Ranges) was saturated with Fe-rich olivine and sodic plagioclase, and close to magnetite saturation. Silica activity in the melt was low and the bulk silica content of the fractionating phases (olivine, plagioclase, magnetite) must have been higher than that of the equilibrium melt. Consequently, there was no silica enrichment in the melt and no increase in modal orthopyroxene with protracted fractionation upward in the sequence, as confirmed by the scarcity of orthopyroxene in the most Fe-rich cumulates as well as the most primitive samples. The melt that gave rise to the troctolitic suites must have been enriched in ferrous iron, resulting in a stable cotectic relation between Fe-rich olivine and orthopyroxene and between these phases and the melt (cf. Bowen & Schairer 1935). In addition, the magma was low in normative clinopyroxene in comparison with the gabbroic and the mafic parental melts, and despite clinopyroxene increasing in modal abundance with falling Mg number (increasing degree of fractionation) in the gabbroic intrusions (Hinckley Range or Latitude Hill).

The low silica activity, high Fe contents, and low normative clinopyroxene are chemical fingerprints of a melt that experienced severe fractionation prior to emplacement. The enrichment of the melt in terms of FeO resulted in the equilibrium olivine being no longer in peritectic reaction relationship with its melt (cf. Bowen & Schairer 1935). To derive strongly undersaturated troctolite melts, the fractionating assemblages must have had a bulk silica content at least as high as that of their equilibrium melt. As suggested below, this can ensue from pre-emplacement high-pressure pyroxene fractionation.

Chemical relationships among the parent melts

At first sight, it seems straightforward to derive all parent melt compositions and cumulates from one primitive mantle liquid, by simply fractionating the phase assemblages that occur as cumulate layers in intrusions of the Giles Complex. Implicit in this model is that the ultramafic cumulate suites form the basal sequence, the gabbroic intrusions the main section, and the troctolitic intrusions the highly evolved roof section of a single magma chamber (Sprigg & Wilson 1959), and that the complex later became dismembered by post-granulite metamorphic thrusting (cf. Harley 1990).

The above model, however, is consistent with the behaviour of olivine. Olivine persists as a fractionating phase through a range of cumulates, from Fo_{89} in the Murray Range intrusion down to Fo_{40} in the Blackstone Range intrusion (cf. Fig. 22). The expected trend in a single basaltic magma chamber would be that olivine temporarily disappears from the liquidus when

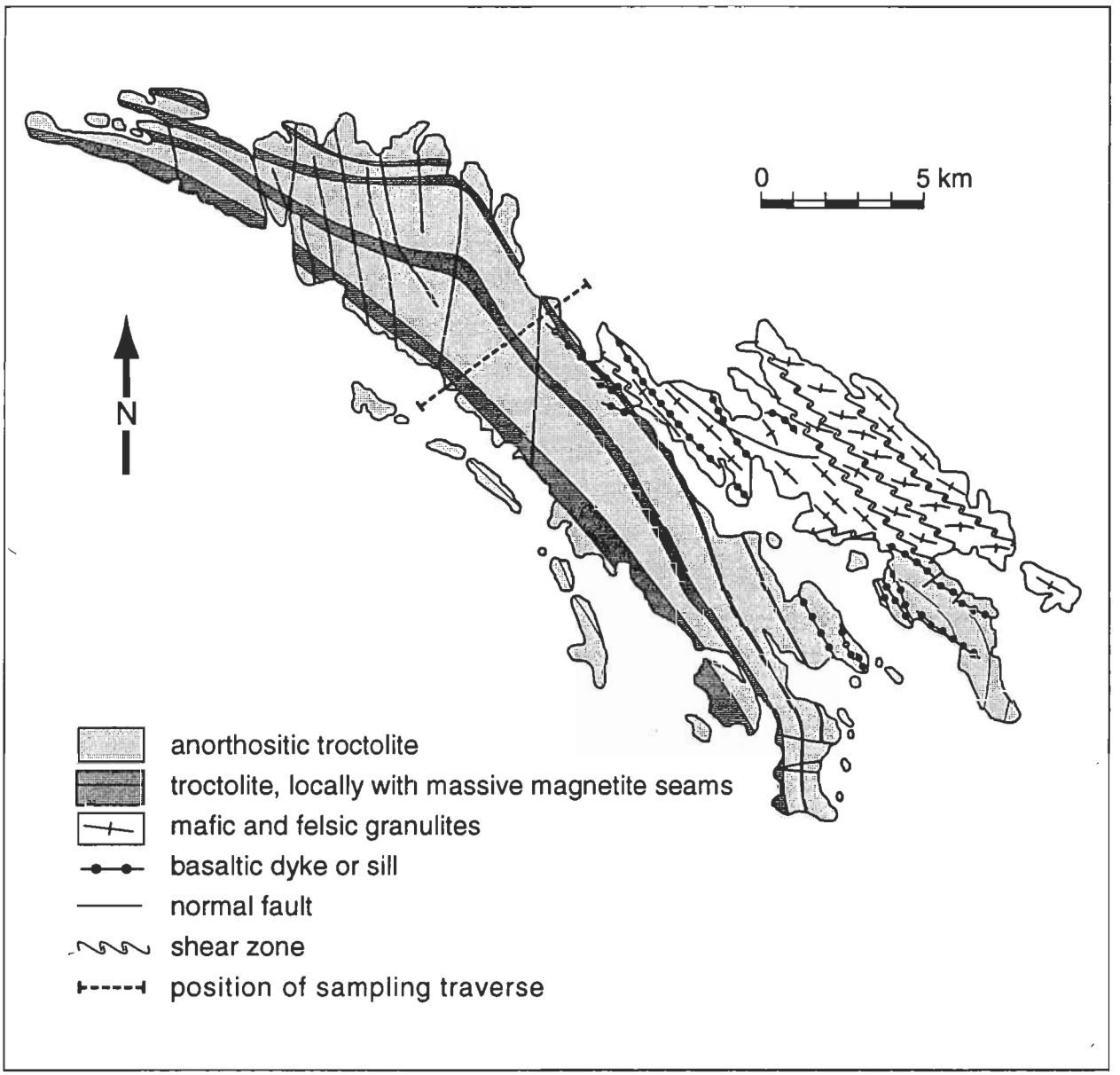

Figure 14. Schematic geology of the Bell Rock Range troctolitic intrusion.

the silica activity of the melt exceeds that of the olivine–orthopyroxene peritectic of the melt, to reappear as a fayalite-rich olivine when FeO is high enough that olivine and orthopyroxene are in cotectic relationships. A classic example where this happens is the Bushveld sequence (Willemse 1969). Most Giles Complex intrusions indeed show replacement of olivine by orthopyroxene: at Fo_{78} in the Murray Range and Wingellina Hills sequences; at Fo_{68} in the Latitude Hill intrusion; and at Fo_{59} in the Hinckley Range gabbro. However, it is unlikely that olivine could reappear on the liquidus in successive cumulate piles while Mg numbers continued to fall (cf. Fig. 22).

High-pressure pyroxene fractionation?

The trend in Figure 22 suggests derivation from a single magma composition, if the fractionating assemblages had bulk MgO, CaO, and silica contents higher than their equilibrium melts. An elegant way to achieve this is by high-pressure fractionation (Ballhaus & Glikson 1992). At low confining pressure, up to about 0.8 GPa, a tholeiitic melt initially in equilibrium with mantle assemblages will fractionate olivine followed by clinopyroxene and plagioclase (cf. Green & Ringwood 1967a). A typical intrusive cycle within a replenished magma chamber will thus commence with the deposition of primitive dunite and peridotite orthocumulates followed by more fractionated olivine-bearing pyroxenites, pyroxenites, and then gabbros (cf. Ballhaus & Glikson 1989). Chemical evolution will be along an olivine control line, whereby Mg numbers of the cumulus phases fall and the activity of silica in the equilibrium melt rises. The fractionating mineral assemblages have at all times lower bulk silica content than the magma from which they separated. When silica exceeds that of the olivine–orthopyroxene peritectic, olivine will be replaced by orthopyroxene and further fractionation will not include olivine until high FeO terminates the peritectic relationship between olivine and melt.

This scenario changes if crystallisation takes place at higher confining pressure. The olivine–orthopyroxene peritectic shifts toward the olivine stability field until it becomes a cotectic phase boundary. The clinopyroxene and spinel stability fields expand at the expense of the olivine and plagioclase fields until troctolitic assemblages (olivine plus plagioclase) become unstable (Green & Ringwood 1967a,b; Presnall et al. 1978). A direct consequence is that the silica content of melts along the olivine–orthopyroxene cotectic will be lower than the silica content of the equilibrium orthopyroxene (e.g. Kushiro 1969;

Presnall et al. 1978, 1979). Crystal fractionation under such conditions will consist of pyroxene+olivine and will deplete the melt in MgO and CaO relative to FeO and Na_2O without enrichment in silica, because the fractionating phases have bulk silica contents as high, or higher than, their equilibrium melts.

It is suggested that the fractionation trends observed in the Giles Complex can be explained by high-pressure fractionation followed by low-pressure fractionation. The range in parent melt compositions could have been produced by high-pressure pyroxene±olivine fractionation when olivine and orthopyroxene were in cotectic relationships, preventing a buildup in silica in the melt (Fig. 22). The individual fractionation trends inside the intrusions must have originated at lower pressure, when olivine was in a reaction relationship with the melt. It is envisaged that fractions of the evolving high-pressure melt were periodically squeezed off into shallower pressure magma reservoirs in the crust at various degrees of chemical fractionation. As a result, melts that were fractionating pyroxeneolivine at high pressure experienced a relative compositional shift into the olivine-only stability field when decompression occurred. Further fractionation at low pressure was then dominated by olivine, allowing silica activity to increase as fractionation continued. Depending on the stage in the high-pressure fractionation history at which a derivative melt fraction became squeezed off its high-pressure reservoir, the liquid crystallised to gabbroic or troctolitic cumulates.

Evidence in support of high-pressure crystallisation. Ample evidence exists to support high-pressure fractionation for parts of the Giles Complex (cf. Goode & Moore 1975):

- In all troctolitic intrusions, clinopyroxene remains a minor phase and appears late (if at all) in the crystallisation sequence. This is only understandable if the parental melts were severely depleted in normative clinopyroxene through a prolonged history of high-pressure fractionation, prior to emplacement in their crustal reservoirs.
- The Murray Range sequence includes cumulates where olivine and orthopyroxene coexist as cumulus phases at an olivine composition as primitive as Fo_{88} (Ballhaus 1993). This may suggest that both minerals crystallised along a cotectic phase boundary very early in the fractionation history. The minimum pressure to achieve this must have been at least 0.7 to 0.8 GPa judging from the work of Green & Ringwood (1967a), assuming that the parental liquid was a tholeiitic low-pressure mantle melt and just olivine-normative.

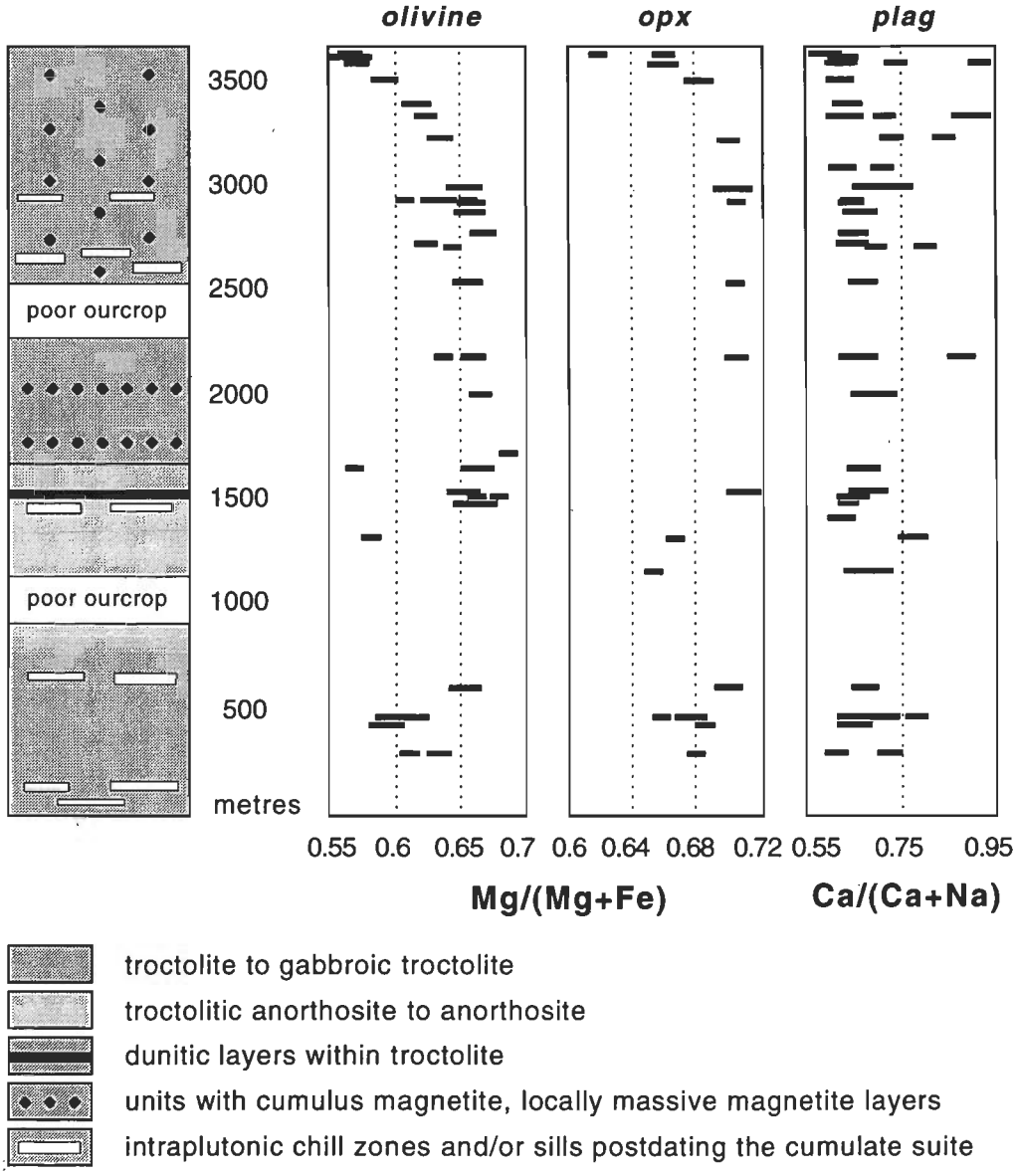

Figure 15. Schematic magmatic stratigraphy and cryptic layering pattern of the Bell Rock Range intrusion (for position of the sampling traverse see Fig. 14).

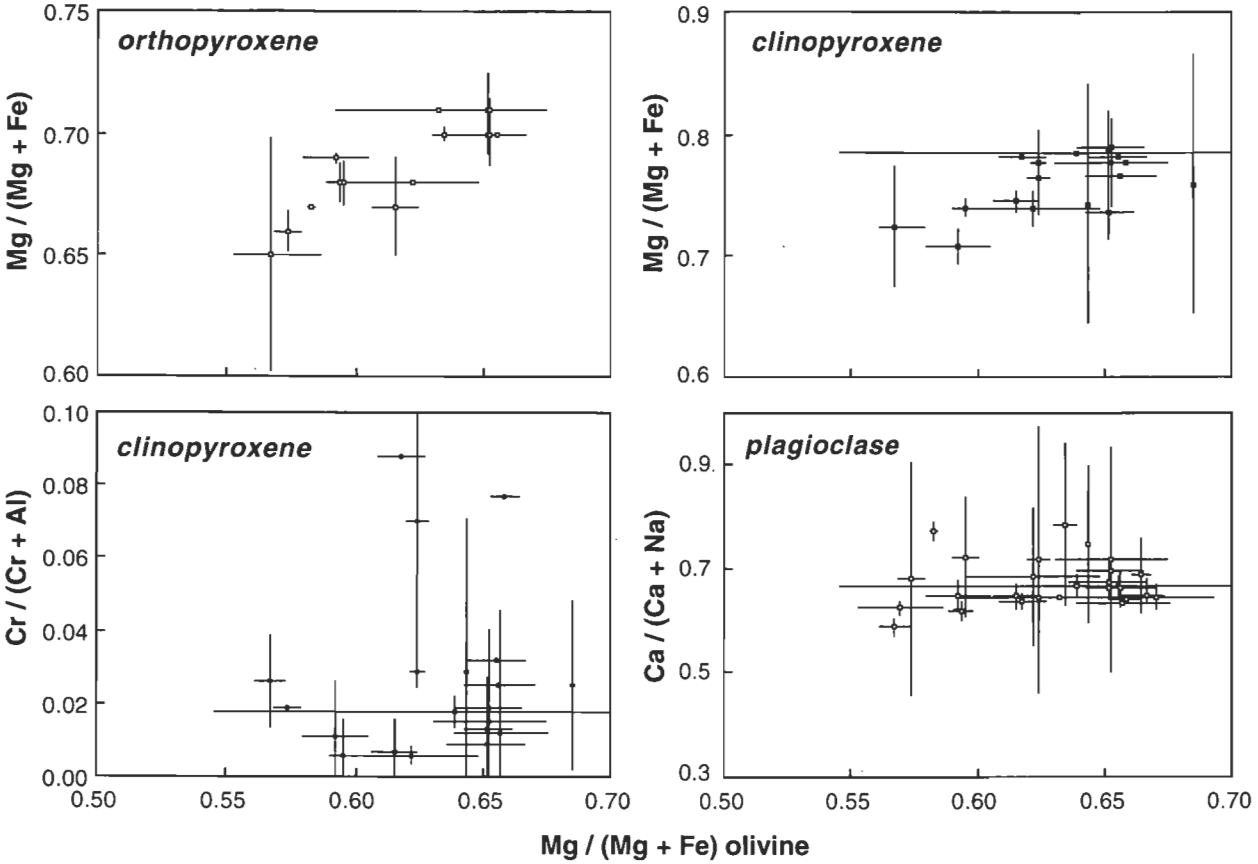

Figure 16. Average phase compositions in the Bell Rock Range cumulates (error bars are two standard deviations).

- Plagioclase in the Murray Range sequence is more sodic at any given olivine composition than in other, similarly mafic sequences of the Giles Complex. This may in part be attributed to the fact that, in the Murray Range intrusion, plagioclase appears later in the crystallisation sequence than olivine and clinopyroxene, i.e. crystallised from a magma that was depleted in CaO and enriched in silica by olivine–clinopyroxene fractionation. Both factors will tend to stabilise more sodic plagioclases. On the other hand, elevated pressure will also stabilise diopside and aluminous spinel relative to anorthite (Green & Ringwood 1967b; Green & Hibberson 1970; Presnall et al. 1979), and thus delay nucleation of plagioclase.
- Pyroxenes are high in alumina and other non-quadrilateral components, notably in the ultramafic cumulates of the Murray Range sequence (cf. Ballhaus & Glikson 1989). The primary reason for this must be a high crystallisation temperature; indirectly, however, high temperature may indicate high confining pressure, since pressure displaces the liquidus of a dry basaltic melt to higher temperature.
- One set of dykes includes partially resorbed orthopyroxene as the only phenocryst generation, in a matrix containing olivine microphenocrysts (Ballhaus 1993). These dykes may represent quenched fractions of a high-pressure basaltic melt, tapped from greater depths, that managed to preserve samples of the high-pressure fractionating phase as intratelluric phenocrysts.

Towards an emplacement model for the Giles Complex

Magmatism of the Giles Complex and associated metamorphism may have resulted from a thermal anomaly situated in the upper mantle below the Musgrave Block (see also Sun & Sheraton 1992). Emplacement of melts into the crustal reservoirs must have coincided with an extensional period during the granulite–metamorphic event, possibly as a result of lithospheric thinning above a thermal anomaly in the upper mantle. Some fractions of the primitive mantle-derived magma were emplaced directly into crustal reservoirs where pressures were low enough to allow extensive olivine fractionation, followed by clinopyroxene and plagioclase fractionation. The cumulate sequences from these batches of primitive magma are denoted as 'primitive' in Figure 1, i.e. the Murray Range, Wingellina Hills, Kalka, Ewarara, Gosse Pile, and Claude Hill intrusions.

Other fractions of the primitive mantle magma must have ponded at greater depths, possibly in reservoirs within the lower crust or even in the shallow lithosphere. Owing to higher confining pressure, the stable liquidus phases included orthopyroxene and clinopyroxene in addition to olivine. These melts experienced silica depletion with progressive fractionation.

Development of particular tectonic conditions may have resulted in the squeezing of fractions of the evolving high-pressure melt into shallower crustal (secondary) reservoirs. Decompression caused an expansion of the olivine and plagioclase stability fields relative to those of pyroxene and spinel, and a relative shift in melt composition away from multiple saturation into the olivine stability field. Following emplacement at shallow pressure, these melts now fractionated predominantly olivine and plagioclase. Depending on the stage at which these melts became squeezed off their high pressure reservoirs, they gave rise to either gabbroic or troctolitic cumulate sequences.

Conclusions

The mafic–ultramafic intrusions of the Giles Complex formed from separate batches of variably fractionated parent melts (cf. Nesbitt et al. 1970; Daniels 1974). The parent melt compositions can be related chemically to a primitive man-

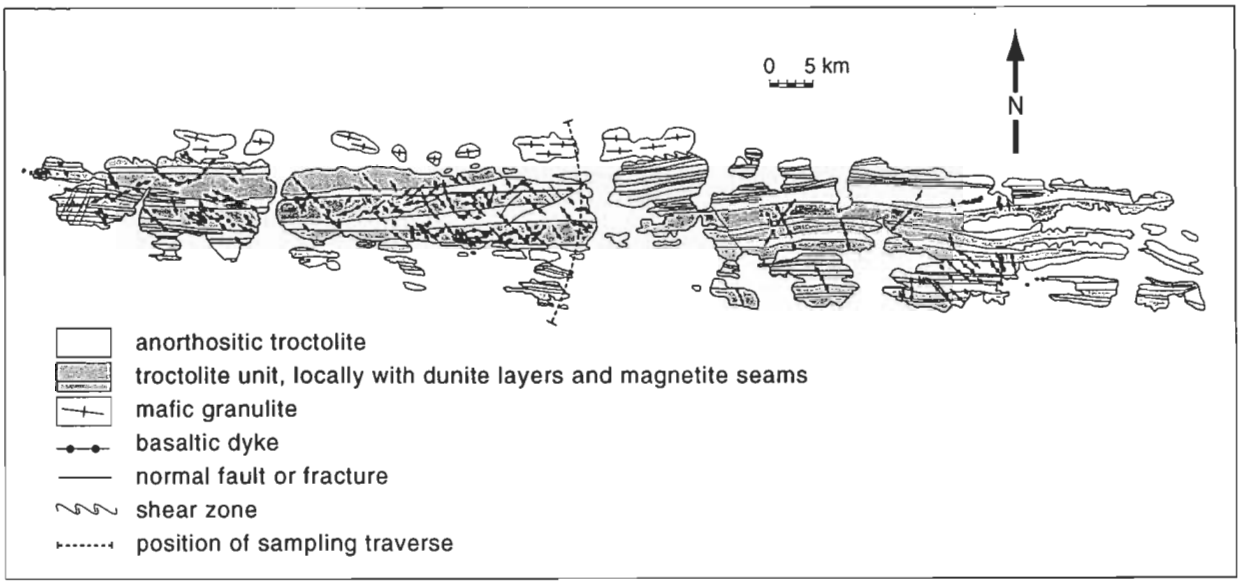

Figure 17. Schematic geology of the Blackstone Range troctolitic intrusion.

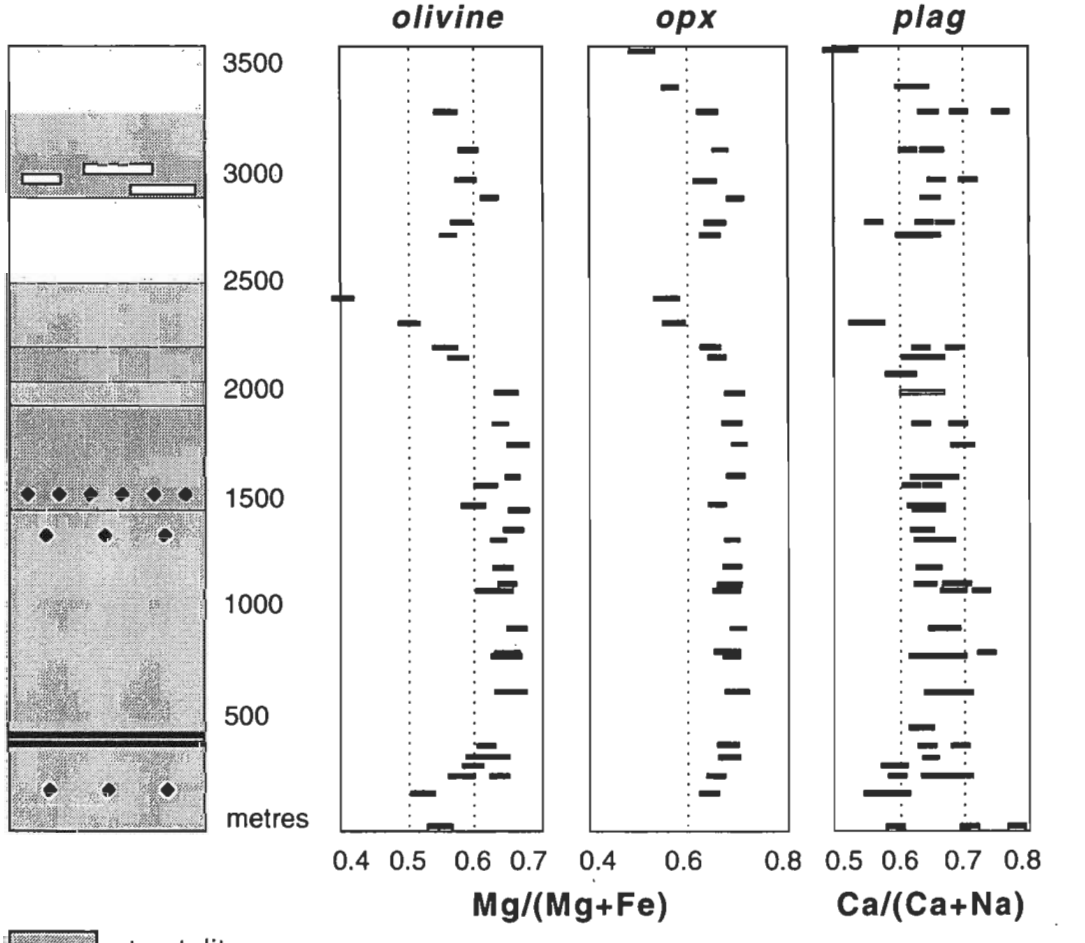

Figure 18. Schematic magmatic stratigraphy and cryptic layering pattern of the Blackstone Range intrusion (for position of the sampling traverse see Fig. 17).

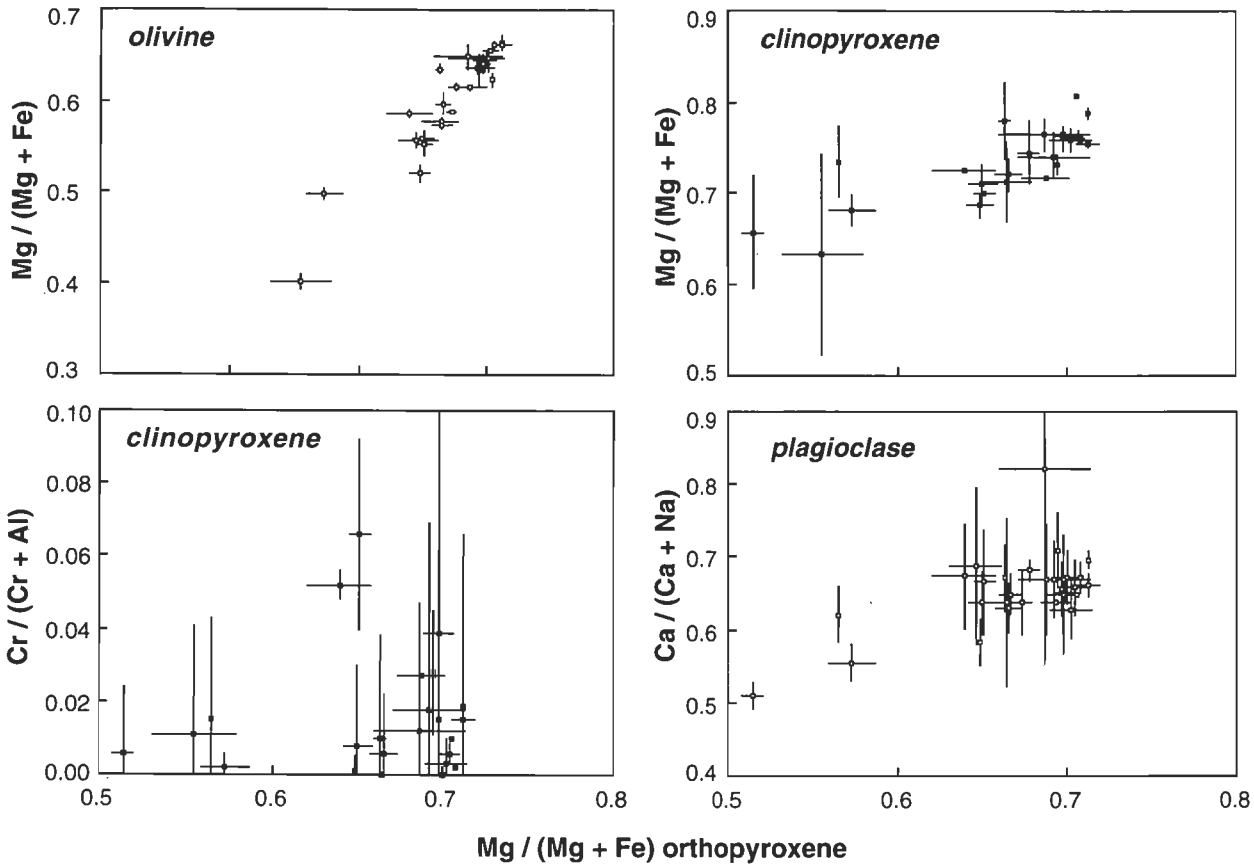

Figure 19. Average phase compositions in the Blackstone Range cumulates (error bars are two standard deviations).

tle-derived parental liquid by polybaric pyroxene±olivine fractionation.

The present-day dimensions of the intrusions approximately reflect the sizes of individual middle to upper crustal magma chambers. Their geographic distribution may reflect vertical stacking of individual magma chambers within the Proterozoic crustal section exposed in the Tomkinson Ranges.

Identification of extensive high-pressure fractionation precursors of the Giles Complex implies that the lower crust of the Musgrave Block may host other pyroxene-dominated high-pressure intrusions, unexposed at present-day erosion levels. These high-pressure cumulates, if they exist, would be characterised by high modal pyroxene/olivine ratios and high-temperature/high-pressure crystallisation features, such as high Cr and Al contents in pyroxenes and very aluminous spinels. Plagioclase (if present) will be a minor phase and comparatively sodic. The only intrusions exposed at present-day erosion levels that fit these characteristics are the Murray Range intrusion and, possibly, the Ewarara and Gosse Pile intrusions, described by Goode (1967), Moore (1971a,b), and Goode & Moore (1975).

The geographic distribution of the Giles intrusions may have been controlled by magma densities, i.e. buoyancy differences between the magmas and the surrounding crust. Judging from high modal plagioclase in the cumulates, the parental liquids to the gabbroic and troctolitic sequences must have been less dense and more buoyant than the primitive parental liquid. As such, they intruded shallower crustal levels than the denser mantle-derived basaltic liquids, which ponded in deeper levels of the crust. Intrusions with similar parentage tend to occur in discrete belts, parallel to the regional compositional layering in the felsic granulites of the Musgrave Block (Fig. 1), as follows: (1) ultramafic intrusions along the northeastern margin of the Tomkinson Ranges; (2) the most fractionated troctolitic intrusions along the southern and western margins; and (3) gabbroic intrusions in positions intermediate between (1) and (2). It is suggested that this pattern was controlled by magma density, where each magma type intruded the crust at its level of neutral buoyancy. Implicit in this model is that the crustal section exposed in the Tomkinson Ranges progressively shallows from the Woodroffe Thrust in the northeast toward the southwest.

Prospects for the Giles Complex having potential for magmatic chromite–sulphide–PGE mineralisation are considered to be limited, as these intrusions have important differences from economically important complexes such as the Bushveld, Great Dyke or Stillwater intrusions (cf. Naldrett et al. 1986). Cumulate textures illustrated by Ballhaus (1993) suggest that the Giles Complex intrusions cooled faster than the above layered intrusions, leaving less chance for efficient accumulation of incompatible elements, such as the PGE (see Morse 1986 for cumulate growth mechanisms). Chromitite layers, often spatially associated with stratiform sulphide–PGE mineralisation, are also lacking, probably because the melt became depleted in Cr at an early stage, owing to high-pressure clinopyroxene fractionation (cf. Goode & Moore 1975). Should sulphide–PGE mineralisation be identified in the future, it may be restricted to single cumulate sequences, in view of the discrete nature of individual intrusive bodies and the difficulty in correlating cumulate sequences between intrusions.

Acknowledgments

This project was funded jointly by ASGO Division of Regional Geology & Minerals, through the Musgrave project of the National Geological Mapping Accord and by the German Research Council (DFG) through its post-doctoral program. Prof. D.H. Green kept a continuing interest in the progress of the Giles project and supported C.B. during 1991 through his ARC program grant. Our thanks go to Dean Hoatson for

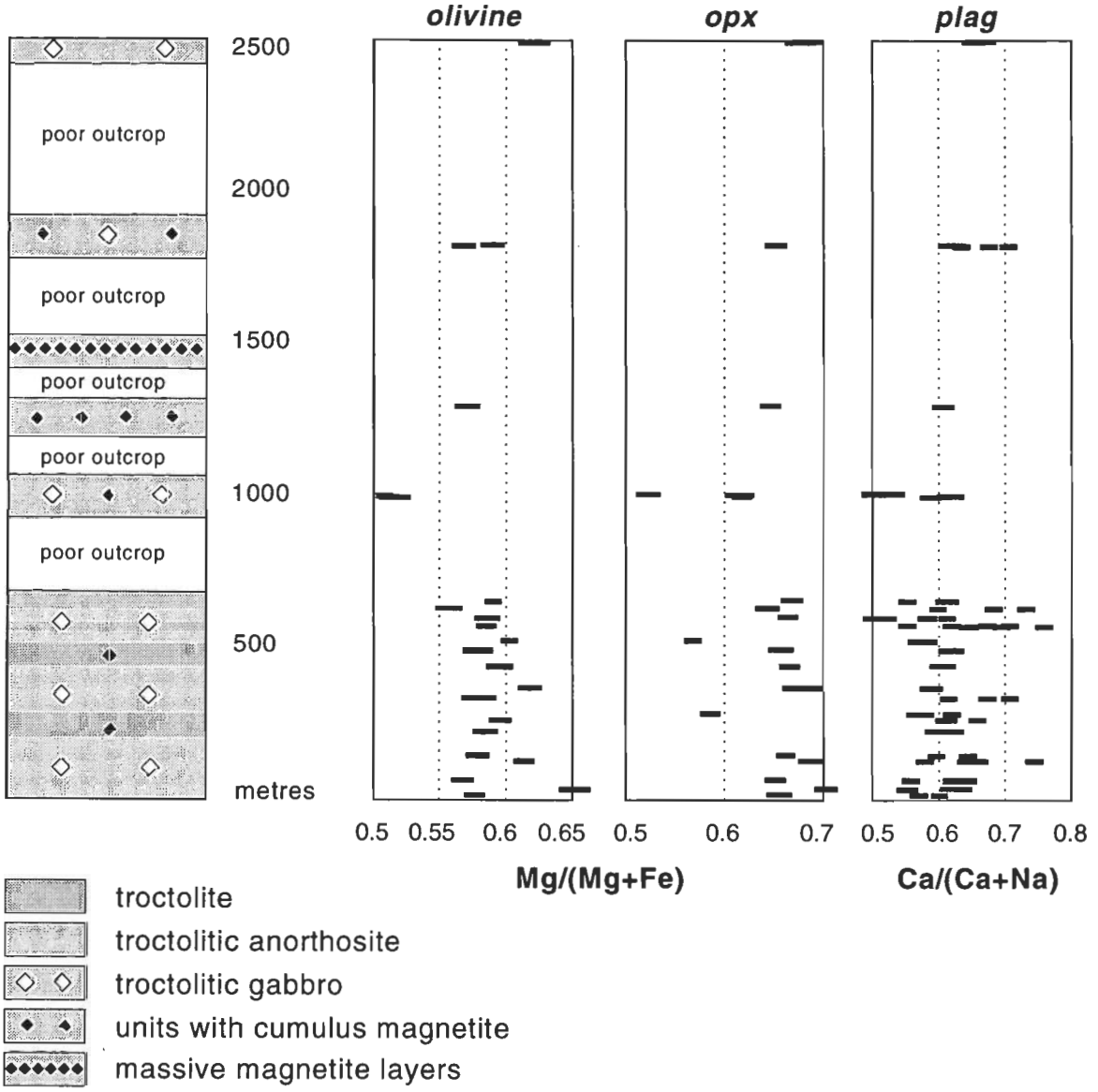

Figure 20. Schematic magmatic stratigraphy and cryptic layering pattern of the Jameson Range intrusion.

commenting extensively on the manuscript. Wieslav Jablonsky (Central Science Lab, University of Tasmania) maintained the microprobe in running order.

References

Ballhaus, C., 1993. Petrology of the layered mafic/ultramafic Giles Complex, Western Musgrave Block, Western Australia: Igneous stratigraphy, mineralogy and petrogenesis of the Jameson Range, Murray Range, Blackstone Range, Hinckley Range, Bell Rock Range, south Mt. West and Latitude Hill intrusions. Bureau of Mineral Resources, Australia, Record 1992/73.

Ballhaus, C.G. & Glikson, A.Y., 1989. Magma mixing and intraplutonic quenching in the Wingellina Hills Intrusion, Giles Complex, central Australia. Journal of Petrology, 30, 1443–1469.

Ballhaus, C.G. & Berry, R.F., 1991. Crystallization pressure and cooling history of the Giles layered igneous complex, central Australia. Journal of Petrology, 32, 1–28.

Ballhaus, C.G. & Glikson, A.Y., 1992. Magmatic and metamorphic evolution and economic potential of the mafic/ultramafic Giles Complex, western Musgrave Block, W.A. BMR Research Newsletter 16, 6–9.

Boudreau, A.E., 1987. Pattern formation during crystallization and the formation of fine-scale layering. In: Parsons, I. (editor), Origins of igneous layering. D. Reidel Publishing Company, Dordrecht, 453–471.

Bowen, N.L. & Schairer, J.F., 1935. The system MgO–FeO–SiO_2. American Journal of Science, 29, 151–217.

Campbell, I.H., 1987. Distribution of orthocumulate textures in the Jimberlana intrusion. Journal of Geology, 95, 35–54.

Clarke, G.L., 1992. Field relationships and tectonic history of the Hinckley gabbro felsic to mafic granulites and granitoids, West Hinckley Range and Champ de Mars areas, Tomkinson Ranges, Musgrave Block, W.A. Bureau of Mineral Resources, Australia, Record 1992/33.

Daniels, J.P., 1974. The geology of the Blackstone region, Western Australia. Geological Survey of Western Australia, Bulletin 123, 257 pp.

Glikson, A.Y., 1994. Landsat-5 thematic mapper image correlations: Applications to NGMA mapping of the western Musgrave Block, central Australia. Australian Geological Survey Organisation, Record 1994/17.

Glikson, A.Y. & Mernagh, T.P., 1990. Significance of

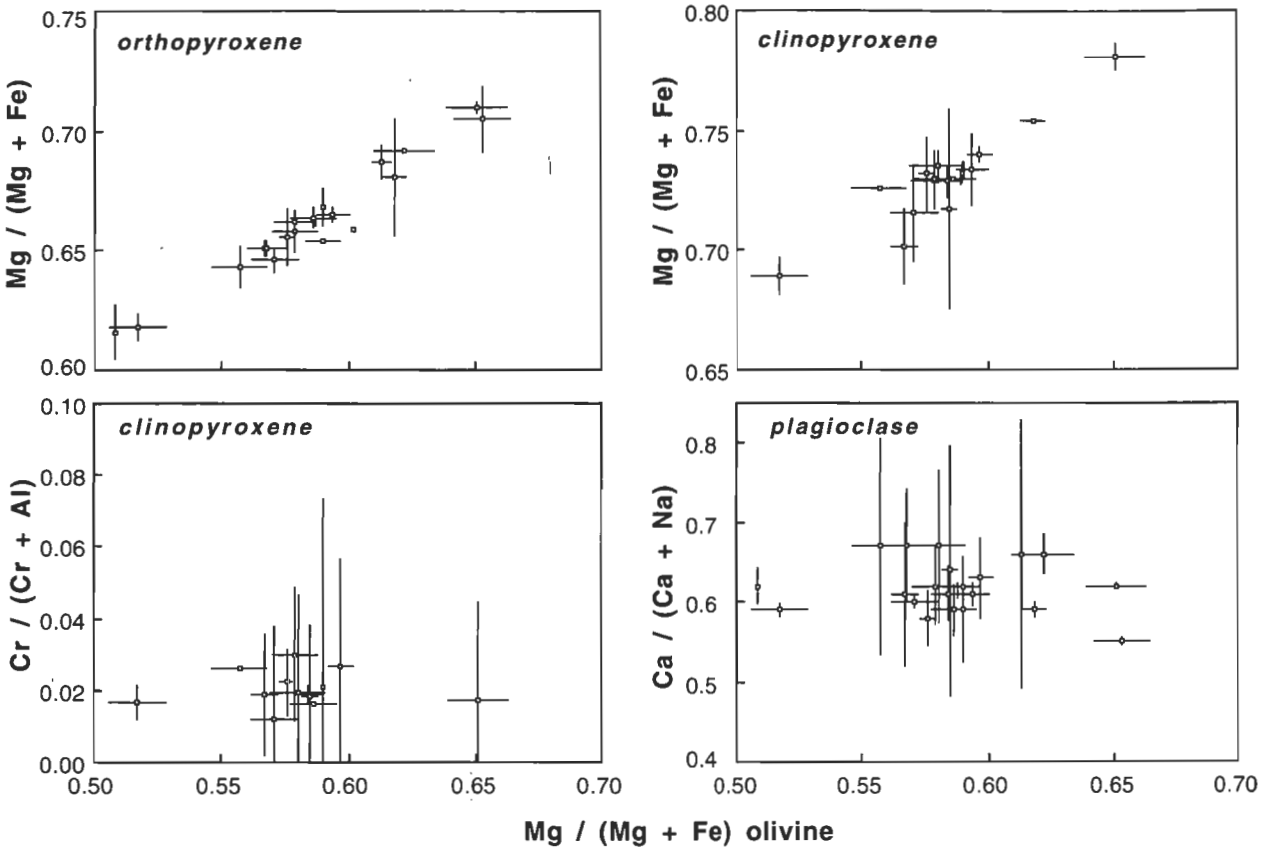

Figure 21. Average phase compositions in the Jameson Range cumulates (error bars are two standard deviations).

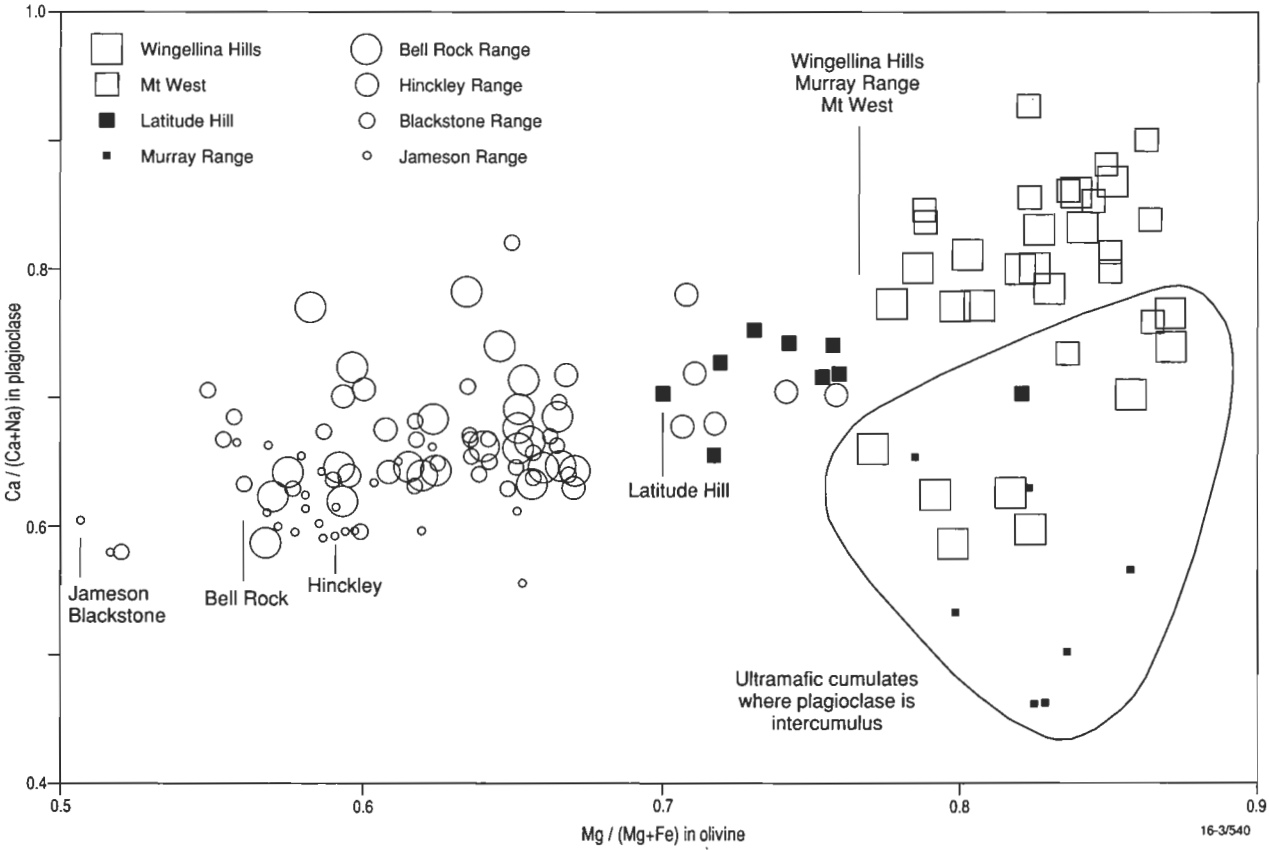

Figure 22. Olivine and plagioclase (average compositions) in cumulates of the Giles Complex. Arrows mark the most Fe-rich olivine composition of each cumulate suite. In the ultramafic and mafic gabbroic sequences, the most Fe-rich olivine marks the point in fractionation history where olivine became replaced by orthopyroxene. For implications see text.

pseudotachylite vein systems, Giles basic/ultrabasic complex, Tomkinson Ranges, western Musgrave Block, central Australia. BMR Journal of Australian Geology & Geophysics, 11, 509–519.

Goode, A.D.T., 1978. High temperature, high strain rate deformation in the lower crustal Kalka intrusion, central Australia. Contributions to Mineralogy and Petrology, 66, 137–148.

Goode, A.D.T. & Krieg, G.W., 1967. The geology of Eawara intrusion, Giles Complex, central Australia. Journal of the Geological Society of Australia, 14, 185–194.

Goode, A.D.T. & Moore, A.C., 1975. High-pressure crystallization of the Ewarara, Kalka and Gosse Pile intrusions, Giles Complex, central Australia. Contributions to Mineralogy and Petrology, 51, 77–97.

Gray, C.M. & Goode, A.D.T, 1989. The Kalka layered intrusion, central Australia. A strontium isotopic history of contamination and magma dynamics. Contributions to Mineralogy and Petrology, 103, 35–43.

Green, D.H. & Hibberson, W., 1970. The instability of plagioclase in peridotite at high pressure. Lithos, 3, 209–221.

Green, D.H. & Ringwood, A.E., 1967a. The genesis of basaltic magmas. Contributions to Mineralogy and Petrology, 15, 103–190.

Green, D.H. & Ringwood, A.E., 1967b. An experimental investigation of the gabbro to eclogite transformation and its petrological application. Geochimica et Cosmochimica Acta, 31, 767–833.

Harley, S.M., 1990. The origins of granulites: a metamorphic perspective. Geological Magazine, 126, 215–247.

Henderson, P., 1982. Inorganic geochemistry. Pergamon Press, Oxford, 353 pp.

Hirschmann, M.M. & Ghiorso, M.S., 1994. Activities of nickel, cobalt, and manganese silicates in magmatic liquids and applications to olivine/liquid and to silicate/metal partitioning. Geochimica et Cosmochimica Acta, 58, 4109–4126.

Irvine, T.N., 1980. Magmatic infiltration metasomatism, double-diffusive fractional crystallization, and adcumulus growth in the Muskox Intrusion and other layered intrusions. In: Hargraves, R.B. (editor), Physics of magmatic processes. Princeton University Press, Princeton, 325–385.

Irvine, T.N., 1982. Terminology for layered intrusions. Journal of Petrology, 23, 127–162.

Jaques, A.L. & Green, D.H., 1980. Anhydrous melting of peridotite at 0–15 kbar pressure and the genesis of tholeiitic basalts. Contributions to Mineralogy and Petrology, 73, 287–310.

Kushiro, I., 1969. The system forsterite-diopside-silica with and without water at high pressures. American Journal of Science, 267-A, 269–294.

Moore, A.C., 1971a. Some aspects of the geology of the Gosse Pile ultramafic intrusion, central Australia. Journal of the Geological Society of Australia, 18, 69–80.

Moore, A.C., 1971b. The mineralogy of the Gosse Pile ultramafic intrusion, central Australia. II. Pyroxenes. Contributions to Mineralogy and Petrology, 18, 243–258.

Morse, S.A., 1986. Convection in aid of adcumulus growth. Journal of Petrology, 27, 1183–1214.

Naldrett, A.J., Cameron, G., Von Gruenewaldt, G. & Sharpe, M.R., 1986. The formation of stratiform PGE deposits in layered intrusions. In: Parsons, I. (editor), Origins of igneous layering. D. Reidel Publishing Company, Dordrecht, 313–397.

Nesbitt, R.W., Goode, A.D.T., Moore, A.C., & Hopwood, T.P., 1970. The Giles Complex, central Australia: a stratified sequence of mafic and ultramafic intrusions. Geological Society of South Africa, Special Publication, 1, 547–564.

Pharaoh, T.C., 1990. Aspects of structural geology of the Giles layered basic/ultrabasic complex and associated felsic granulites, Tomkinson Range, Musgrave Block, central Australia. Bureau of Mineral Resources, Australia, Record 1990/5.

Philpotts, A.R., 1990. Principles of igneous and metamorphic petrology. Prentice Hall, New Jersey, 498 pp.

Presnall, D.C., Dixon, S.A., Dixon, J.R., O'Donnell, T.H., Brenner, N.L., Schrock, R.L. & Dykus, D.W., 1978. Liquidus phase relations on the join diopside–forsterite–anorthite from 1 atm to 20 kbar: their bearing on the generation and crystallization of basaltic magma. Contributions to Mineralogy and Petrology, 66, 203–220.

Presnall, D.C., Dixon, J.R., O'Donnell, T.H. & Dixon, S.A., 1979. Generation of mid-ocean ridge tholeiites. Journal of Petrology, 20, 3–36.

Roeder, P.L. & Emslie, R.F., 1970. Olivine liquid equilibrium. Contributions to Mineralogy and Petrology, 29, 275–289.

Sprigg, R.C. & Wilson, R.B., 1959. The Musgrave mountain belt in South Australia. Geologische Rundschau, 47, 531–542.

Sun, S.-S. & Sheraton, J.W., 1992. Zircon U/Pb chronology, tectono-thermal and crust-forming events in the Tomkinson Ranges of the Musgrave Block, central Australia. ASGO Research Newsletter, 17, 9-11.

Willemse, J., 1969. The geology of the Bushveld Igneous Complex, the largest repository of magmatic ore deposits in the world. In: Wilson, H.D.B. (editor), Magmatic ore deposits: a symposium. Economic Geology Monograph, 4, 187–208.

AGSO Journal of Australian Geology & Geophysics, 16 (1&2), 91–105

Resolution of conflicting structures and deformation history of the Mount Aloysius granulite massif, western Musgrave Block, central Australia

A.J. Stewart[1]

The Mount Aloysius massif comprises complexly folded high-pressure Mesoproterozoic granulites, typical of those making up much of the western Musgrave Block. The granulites host the well-studied mafic–ultramafic layered intrusions of the Giles Complex, but up to now have not been mapped in detail. Previous lithological mapping and airphoto interpretation produced conflicting synformal and antiformal interpretations of the structure of the massif. New mapping reported here resolves this conflict, and shows that the massif preserves four episodes of folding. The first formed small, initially recumbent (now reclined), F_1 folds, which are earlier than any previously known in the massif. Two major episodes formed a large west-inclined isoclinal, gently doubly plunging, F_2 antiform, which was subsequently folded early in D_3 to a steeply doubly plunging antiform and then bent late in D_3 to an arcuate shape. With each episode, the intensity of deformation decreased, from isoclinal F_1 folds with a strong axial-plane granoblastic-textured foliation to open F_4• folds with spaced axial-plane cleavage and local greenschist retrogression, reflecting decreasing ductility as the rocks cooled. Formation of the F_2 antiform was helped by the presence of a stiff buttress of relatively massive granulite in the east of the massif, against which well-layered granulite to the west was squashed and flattened. Subsequently, the same near-massive granulite provided a stiff *auge*-like core, around which the well-layered granulite was wrapped during D_3.

Introduction

The Musgrave Block (Fig. 1a) consists chiefly of metavolcanics and metasediments intruded by layered mafic intrusions (Giles Complex; Nesbitt et al. 1970), granites, and mafic dykes. Metamorphic facies ranges from greenschist to granulite. The parent volcanics and sediments accumulated between about 1550 and 1330 Ma, and were metamorphosed at about 1200 Ma (Gray 1978). The Bureau of Mineral Resources (now the Australian Geological Survey Organisation) began a detailed investigation of the Giles Complex in the west of the block in 1987, and in 1990, as part of the National Geoscience Mapping Accord (NGMA), the study was broadened to include detailed mapping of the granulites hosting the Giles Complex, as these had previously been mapped only at reconnaissance level (Thomson et al. 1962; Daniels et al. 1970a, b; Forman et al. 1972), except for a detailed map of the central part of the Mount Aloysius massif by Gray (1971). The aims of the present study were to analyse the structure of the massif and, particularly, to resolve the previously determined conflicting antiformal and synformal interpretations; to determine the presence or absence of a recently recognised episode of folding older than all those known hitherto in the western Musgrave Block; and to determine the sequence of deformational events. These results help to refine the tectonic history for the western part of the Musgrave Block as an integral part of NGMA mapping. In brief, the massif preserves four generations of folding, the major ones forming a west-inclined isoclinal F_2 antiform, subsequently folded early in D_3 to a steeply doubly plunging antiform and then bent late in D_3 to an arcuate shape. The folds were formed during the regional deformation and granulite-facies metamorphism at 1200 Ma that affected the western (Gray 1978) and central (Maboko et al. 1989) Musgrave Block, and are found throughout the Tomkinson Ranges region (Fig. 1b; Nesbitt et al. 1970; Pharaoh 1990; Clarke 1992; Clarke et al. 1992–3).

The Mount Aloysius massif is part of the Tomkinson Ranges of Western Australia (Fig. 1b), and is a roughly triangular range of granulite hills rising to 982 m ASL at Mount Aloysius itself, 400 m above the surrounding plain. The triangular plan of the massif reflects a major west-plunging F_3 antiformal axis through its centre.

Detailed mapping of the whole massif by the author in 1990–91 used 1:20 000 scale colour aerial photographs. A detailed account of the Mount Aloysius area appears in Glikson et al. (in preparation).

[1] Division of Regional Geology & Minerals, Australian Geological Survey Organisation, GPO Box 378, Canberra, ACT 2601

Previous investigations

The Mount Aloysius massif was initially mapped as part of 1:250 000 systematic mapping of Western Australia, and appears on the Cooper (Daniels et al. 1970a) and Scott (Daniels et al. 1970b) 1:250 000 geological maps published by the Geological Survey of Western Australia. The massif was examined only in the south and northwest, and was depicted as a single unit of well-banded granulite cut by dolerite dykes. Flaser structures, complex repeated folding, and migmatisation were recognised, and the granulites were regarded as largely of sedimentary origin (Daniels 1971, 1972). In the comprehensive bulletin describing the entire Blackstone area (Cooper, Scott, Bentley, and Talbot 1:250 000 sheet areas; Daniels 1974), it was recognised that the granulites probably represented a variety of igneous and sedimentary rocks, and mylonitisation was recognised as a late deformational process.

Gray (1971; Gray & Compston 1978) recognised four granulite units in the centre of the massif, and delineated the map closure that is the major F2 antiform of this report (Fig. 2). His boundaries delineating the map closure have been transferred to the Tomkinson Ranges 1:100 000 geological map (Glikson et al. in preparation), and used in Figure 2. He interpreted the closure as a west-plunging F_1 synform, recorded the existence of mesoscopic F_1 similar folds, and recognised mesoscopic and macroscopic F_2 folds (F_3 in this study) overprinting the F_1 folds; the double closure of the major F_1 synform was linked to this F_2 folding about an east-trending axis. Gray also determined Rb–Sr whole-rock isochron dates on felsic granulite rock types, and pooled these to obtain an age of 1578 ± 20 Ma (Gray 1978, Gray & Compston 1978). He interpreted this as the protolith age, because the individual isochrons described large bodies of rock or entire lithological units, possessed a large spread in Rb/Sr ratio, and most of them were precise. Furthermore, initial ratios of felsic granulite layers were quite distinct from those of interlayered mafic granulite units. The time of granulite metamorphism was determined at 1222 ± 39 Ma (Gray 1978, Gray & Compston 1978). The compositions of the granulites were 'consistent with both igneous and sedimentary materials' (Gray 1977).

Pharaoh (1990) worked in the area immediately east of the Mount Aloysius massif, but photointerpreted a steeply plunging macroscopic antiformal fold axis (D_{2F}) trending northwest through the massif. Pharaoh's antiformal interpretation conflicts with Gray's synform. The southern part of Pharaoh's antiform approximates the major F_2 antiform of this study, but he did not recognise the folding of the antiform around the west-plunging F_3 axis. He also interpreted the existence of steeply dipping northwest-striking coplanar de-

formation zones which attenuated the limbs of the D_{2F} antiform, but these were not confirmed by the present study.

Clarke (1992, Clarke et al. 1992–3) mapped in detail two areas of the same granulite sequence 30 km east of Mount Aloysius, and recognised seven episodes of deformation, including rare, previously unrecognised mesoscopic folds folded by, and therefore older than, the F_1 generation of Nesbitt et al. (1970) and Gray (1971), and four episodes of shear zone formation, i.e. ductile faulting D_{4-7}. The F_1 folds of Nesbitt et al. (1970), Gray (1971), and Pharaoh (1990)

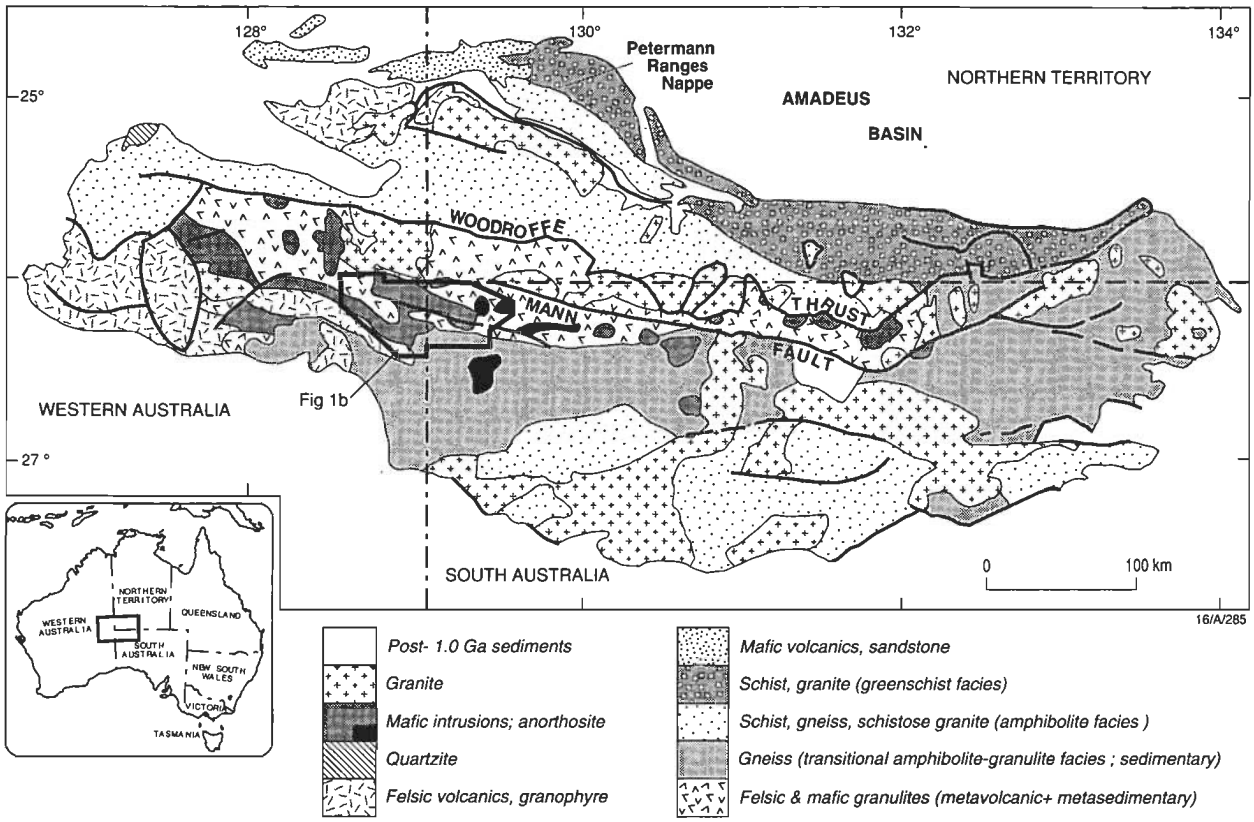

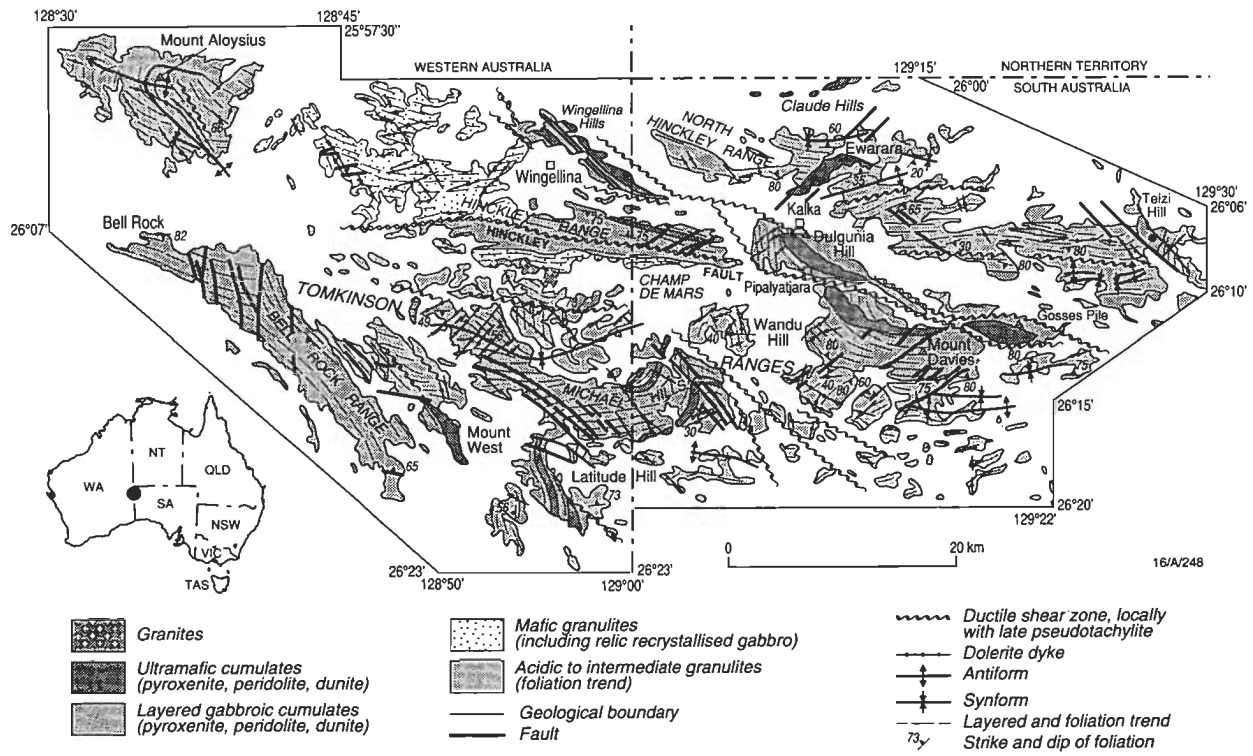

Figure 1. (a, upper) Geological map of Musgrave Block, compiled from: Daniels (1974, pl. 2), Stewart, A.J. (1992, pl. 3); Mann, Woodroffe, Alberga, Abminga, Birksgate, Everard, and Lindsay 1:250 000 geological maps, Geological Survey of South Australia. (b, lower) Geological sketch map of Tomkinson Ranges (after Pharaoh 1990), showing location of study area.

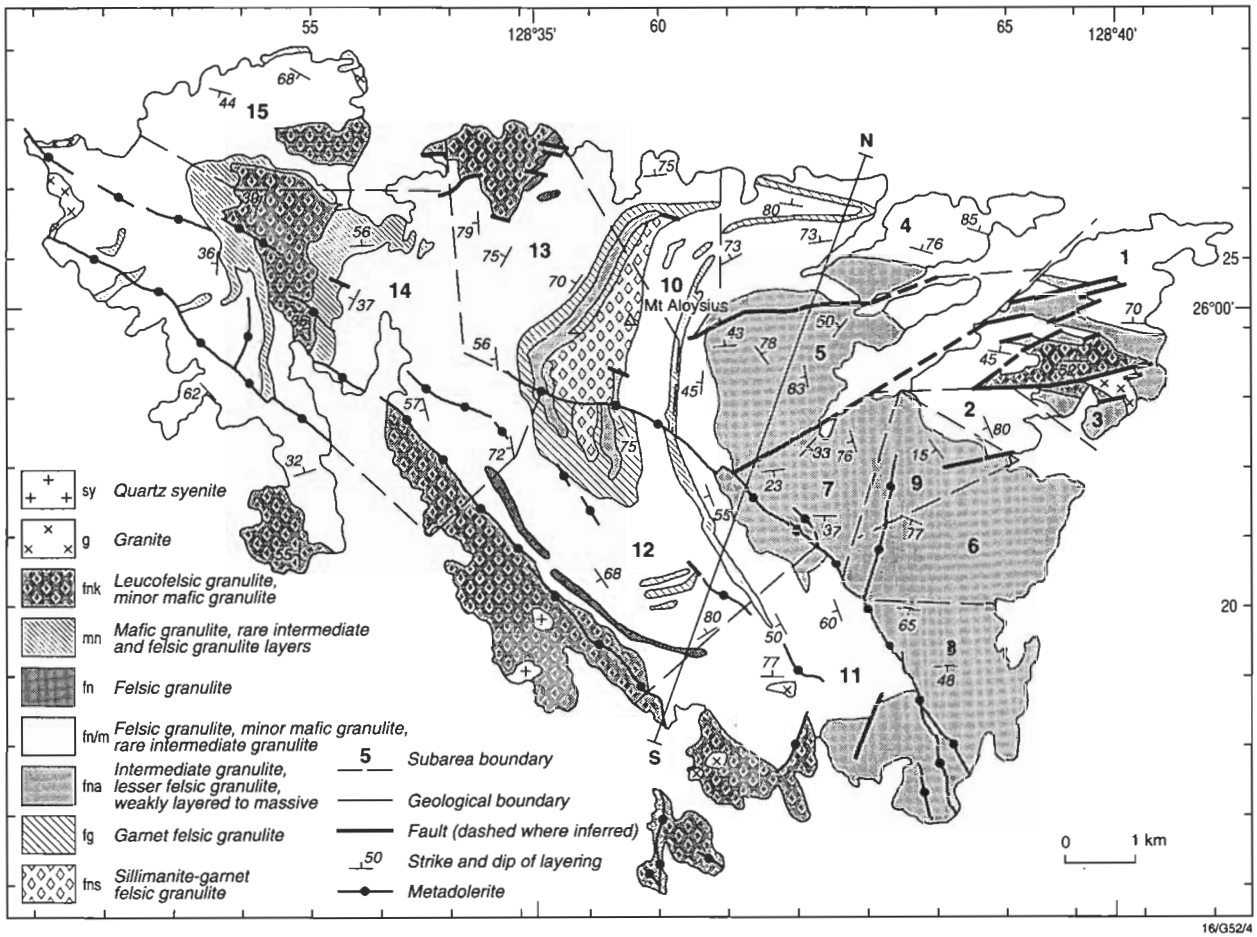

Figure 2. Generalised geological map of Mount Aloysius massif; mapping by A.J. Stewart except boundaries of units forming fold closure around Mount Aloysius by Gray (1971). N–S is position of cross-section in Figure 12. Boundaries of structural subareas also shown. Numbered ticks at margin of this and other similar diagrams are 1 km intervals of Australian Map Grid, Zone 52.

correspond to F_2 of Clarke and this study, and F_2 of Nesbitt et al., Gray, and Pharaoh to F_3 of Clarke and this study.

Sun & Sheraton (1992) determined a SHRIMP U–Pb zircon date of about 1530 Ma on a banded felsic granulite from the Mount Aloysius massif, confirming the 1578 Ma Rb–Sr protolith age of Gray (1978). They also confirmed Gray's time of granulite metamorphism at about 1200 Ma.

The Mount Aloysius massif is part of the Fregon Subdomain of Major & Conor (1993), which is the portion of the Musgrave Block south of the Woodroffe Thrust (Fig. 1a).

Terminology

Terms used are as defined in the Glossary of Geology (Bates & Jackson 1980). Fold terminology follows Fleuty (1964).

Lithology

The Mount Aloysius massif is a sequence of felsic, intermediate, and mafic granulites, interlayered on scales ranging from centimetres to hundreds of metres and intruded by small bodies of granite, syenite, pegmatite, and by three generations of mafic dykes. Details of lithology and petrography are set out in Glikson et al. (in preparation). Layering, called S_{1a}, is compositional and is imparted by changes in mineral proportions and grain size. Thin layers commonly narrow, widen, bifurcate, or lens out along strike distances of less than a few metres, and in places crosscut each other at low angles. Some mafic layers have even more mafic selvedges. These observations indicate that the layering is of metamorphic differentiation origin superimposed on original volcanic or sedimentary layering. On the other hand, compositional variations on the hundreds of metres scale, e.g. the units of garnet felsic granulite and sillimanite–garnet felsic granulite in the centre of the massif and the mafic granulite in the northwest (Fig. 2) are probably original sedimentary and volcanic rock bodies, respectively, as concluded by Gray (1971). The metamorphic layering is broadly parallel to these macroscopic layers, and may be palimpsest bedding in rocks of sedimentary composition. Gray (1971) and Moore & Goode (1978) considered that the layering in the granulites approximates the original lithological variations.

Deformation and structure

The events recognised in the Mount Aloysius massif are set out in Table 1, together with the relevant events recognised by Clarke (1992, Clarke et al. 1992–3). The Mount Aloysius rocks were affected by an additional episode of mesoscopic folding between D_3 and D_4 of Clarke et al. (1992–3), denoted as D_{4*} in Table 1. D_{4-7} have not been recognised in the Mount Aloysius massif.

The map area was divided into fifteen structural subareas (Fig. 2). Equal-area stereograms of poles to S_{1a} layering, lineations, mesoscopic fold axes, and poles to axial-plane foliations are shown in Figure 3. Each subarea's pi-axis to the great circle of poles to S_{1a} layering represents an 'average' fold axis in that subarea (Fig. 4).

D_1

D_1 formed the S_{1a} layering in the granulites, which is shown on the map as airphoto trends (Fig. 5). S_{1a} normally has a massive granuloblastic texture. In places in the west, however (grid reference 538229-540240), there is a tectonic foliation

Table 1. Sequence of structural events in the Mount Aloysius massif.

Event	*Age (Ma)*	*This report*	*Clarke et al. (1992–3)*
Mylonitisation		**Post-D_{4*} mylonite**	
Mafic intrusion	820[2]	Type B dykes soon after D_3; NW strike, moderately metamorphosed	Type B dykes
D_{4*}		F_{4*} upright gentle to open folds, NNE trend and S_{4*} axial plane foliation; local greenschist facies retrogression	
Mafic intrusion	1000[2]	Type C dykes: aphanitic to porphyritic, unmetamorphosed, NE to NNE strike	Type C dykes
D_3		F_3 upright gentle to tight folds, NW to WNW plunge; S_3 axial-plane foliation strikes SE to E, cataclastic to mylonitic, granulite facies; partial melt; syn-D_3 mylonites	D_3
Mafic intrusion	1060[2]	Type A dykes; strongly metamorphosed, subparallel to and folded with S_{1a}	Type A dykes
Felsic intrusion	1180[2]	Syenite plugs	
D_2	1200[1] 1200[3]	F_2 upright to W-inclined close to isoclinal NNW-trending folds (where not refolded) with S_2 granoblastic axial-plane foliation, granulite facies; syn-D_2 mylonites	D_2
Felsic intrusion	ca. 1200[2]	Granite bosses	Charnockite
D_1		S_{1a}layering, granoblastic, with foliation parallel to layering in south; F_{1b} reclined (originally recumbent) close to isoclinal folds, no axial-plane foliation; granulite facies	D_1
Felsic and mafic volcanism, sedimentation	1578[1]	Protolith of felsic, mafic, calcareous granulites, quartzite	Protolith of paragneisses

[1] *Rb-Sr whole rock, Gray (1971, 1978);* [2] *U–Pb on zircons, Sun et al. (in press);* [3] *U–Pb on zircons, Sun & Sheraton (1992).*

parallel to the layering, shown principally by flattening of quartz grains, boudins of mafic granulite or coarsely crystalline quartz, or ellipsoidal garnet aggregates. Weakly or non-layered granulites also show this grain-flattening foliation parallel to layering nearby.

F_{1b} folds (Figs 6, 7a–d) affect S_{1a} layering (the b subscript indicating that they began forming after the initiation of S_{1a}). The folds are observed only in widely separated parts of the massif, and are characterised by an absence of axial-plane foliation. In the northeast (Fig. 6a, b) and south (Fig. 6c), the folds are close to isoclinal (Fig. 7a–c), reclined, and are preserved in the hinge regions of large-scale F_2 folds, the axial planes of the F_{1b} folds being at right angles to the S_2 axial-plane foliation. In places, F_{1b} folds are transected by S_2 (Figs 6b, 7b, c). In the west, around grid reference 567225, several exposures of tight southwest-plunging upright folds (Figs 6e, f, 7d) are assigned to F_{1b} because they trend southwest at right angles to a nearby large-scale F_2 fold, and have no axial-plane foliation of their own; some are transected by S_2 (Fig. 6f). F_{1b} folds are too few to warrant a stereogram.

D_2

D_2 formed large-scale upright north to north-northwest-trending F_2 folds in the centre and southeast in unit fna and, to the west, an overturned (west-inclined) antiform–synform pair in units fg, fns, and fn/m (Fig. 5). The antiform and synform are now steeply plunging, but this is a D_3 effect, and the D_2 plunges would have been gentle. Both folds are tight to isoclinal, and have southwest-dipping axial planes in the south of the massif, which are bent around large-scale F_3 axes to a northwest and eventual north dip in the north of the massif (Fig. 5). Similarly, the antiform and synform plunge west (Fig. 3m) to southwest (Fig. 3n) in the south, and northwest in the north (Fig. 3f).

In unit fna, F_2 folds are outlined by weak S_{1a} layering trends, are tight to isoclinal, and plunge 40–50° north-northwest in the north (Fig. 3g), whereas in the south they are open and plunge 4–70° south (Figs 3h, i, k, 4, 5). A northeast-striking D_3 fault separates the two areas, and an east-striking D_3 fault forms the northern margin of the northern area.

The closed map pattern of units fns, fg, and fna (Figs 2, 5) outlines the major northerly-trending F_2 antiform that passes through Mount Aloysius itself. At two localities (grid references 593220 and 596225) on the eastern limb, axial-plane foliation S_2 dips at a lesser angle than S_{1a} layering, and at grid references 577234 and 581247 on the western limb, parasitic F_2 folds verge southeast and northeast, respectively; these observations (Fig. 8) confirm the antiformal nature of the fold.

Mesoscopic F_2 folds are close to isoclinal, asymmetric (Figs 7e, f, 9c) and parasitic on the limbs of large-scale F_2 folds. They typically have thickened hinges and weak to strong S_2 axial-plane foliation which cuts S_{1a} layering at a low angle on both limbs of the folds (Fig. 10a, b, c, d). Rarely, S_2 parallels the longer limb and cuts the shorter limb obliquely (Fig. 10c). S_2 is generally imparted to the rock by flattening of quartz grains and growth of a granoblastic texture. Elongation of grains or mineral clots or ellipsoidal garnet aggregates defines L_2 lineation, but is rare. In the hinge of the antiform at grid reference 592237, L_2 lineation parallels the axis of gently north-plunging F_2 folds in S_2, and has obliterated layering in unit fns. Leucofelsic granulite around grid reference 567225 has a strong lineation imparted by rod-shaped quartz grains parallel to the southwest fold plunge. However, the F_2 plunge in this area is also southwest, and so the lineation could be L_1 or L_2. Mafic rocks are only weakly foliated, and metadolerites preserve relict blastophitic texture. Rarely (e.g., at grid reference 580248) S_2 is cataclastic to mylonitic, with kinked orthopyroxene, flattened plagioclase, and lenticular strained quartz.

Stereograms of S_2 are shown for subareas 1 (Fig. 3b) and 12 (Fig. 3o) only, these being where S_2 is best developed; S_2 elsewhere is too sparse to warrant stereograms. Stereograms including F_2 are shown in Figures 3a, f, g, h, i, m, n, and L_2 is plotted in Figures 3a, f, g, i, j, m, n.

In places, F_2 folds are transected by S_3 foliation, which cuts undeviated through both F_2 limbs (Fig. 10e, f, g,). L_2 also is folded by F_3 (Fig. 11d).

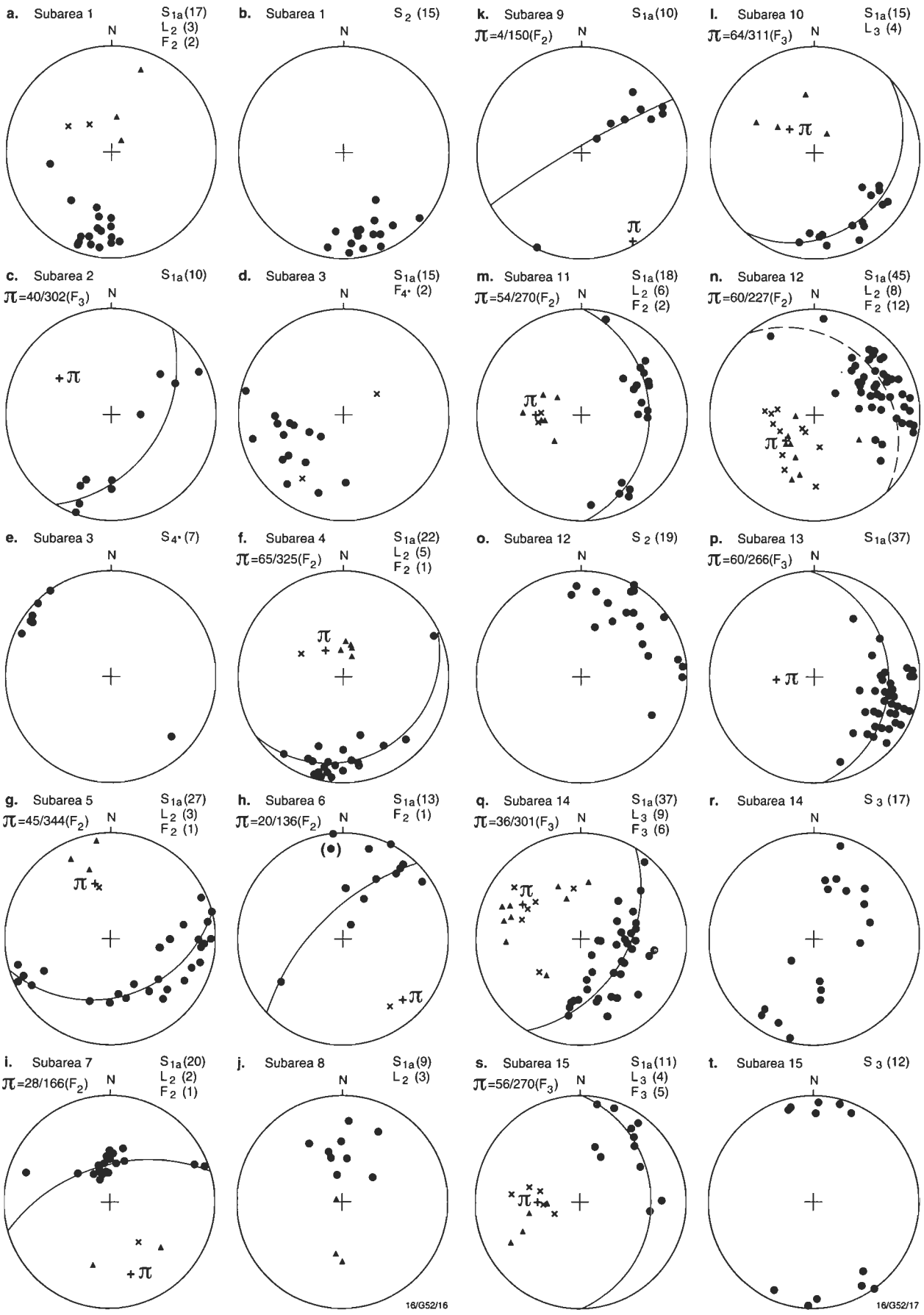

Figure 3. Stereograms of poles to S_{1a} layering (solid circles), L_2, L_3 lineations (triangles), F_2, F_3, F_{4*} mesoscopic fold axes (diagonal crosses), and poles to S_2, S_3, S_{4*} axial-plane foliations (solid circles) in 15 subareas of Mount Aloysius massif. Upright crosses are pi-axes of great-circle girdles of S_{1a} poles.

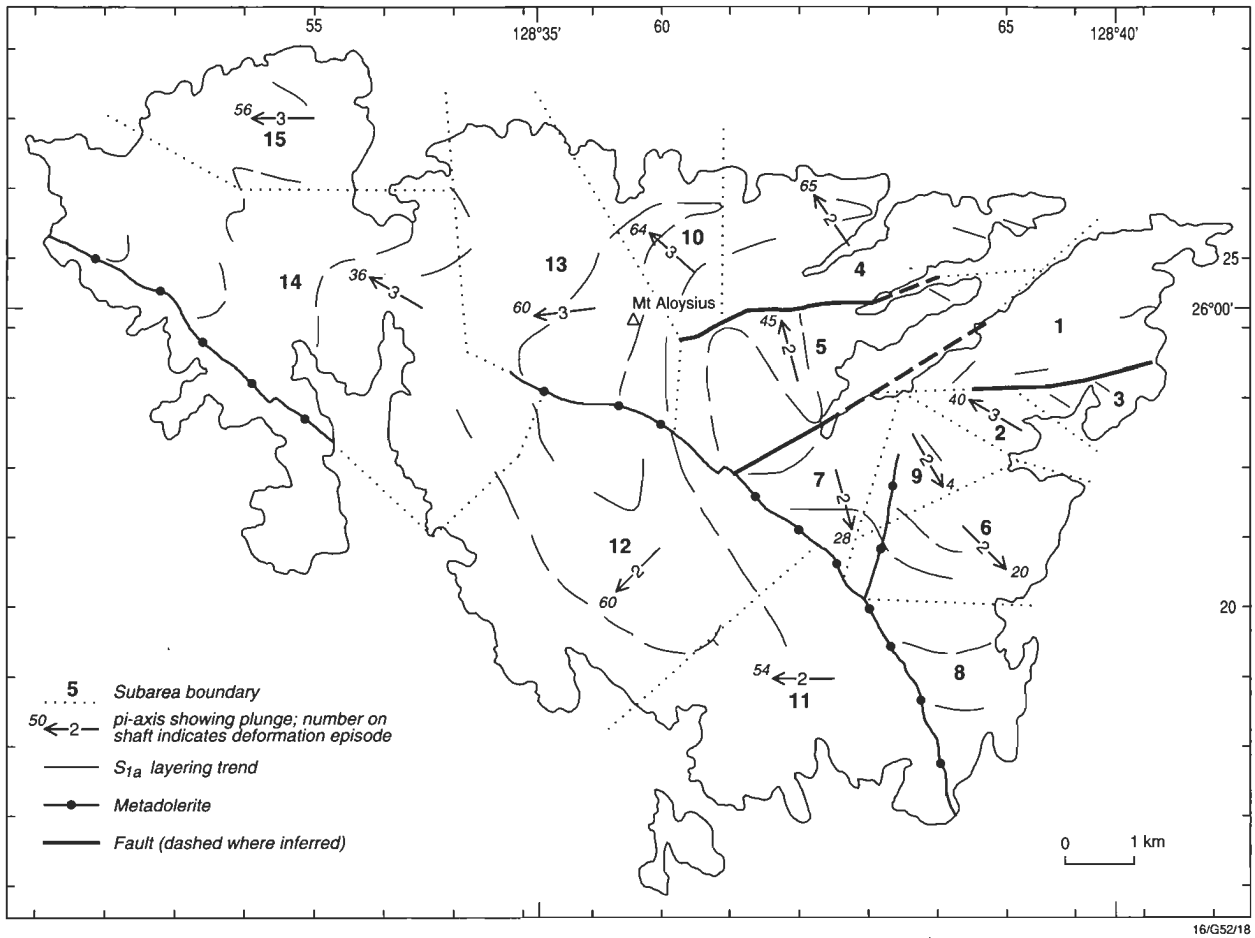

Figure 4. Map of Mount Aloysius massif, showing structural subareas and average pi-axes.

D_3

D_3 formed the major west to west-northwest-trending upright F_3 folds in the centre and northwest (Figs 3c, p, q, s, 4, 5). The folds are open in the northwest, close in the centre and east, and are outlined by layering trends in unit fn/m (Fig. 5) and by the map pattern of units fg and mn in the northwest (Fig. 2). Plunges range from 28° northwest in the east to 60° northwest in the west and 68° northwest in the central north (Fig. 5). Interference by D_3 with the major isoclinal F_2 antiform folded it into its present shape, with plunges of 63-65° northwest in the north of the massif, and 60° west-southwest in the south (Figs 4, 5).

Numerous easterly striking faults in the east are interpreted as contractional, and the result of the space problem in the hinge of the largest F_3 antiform. The two faults bounding the group of three tight to isoclinal F_2 folds in the north of the unit of weakly layered to massive intermediate and felsic granulites (fna; Fig. 5) are similarly interpreted as contractional, and bound a block that moved down from the hinge region of the antiform to the more roomy lower region of the fold (Fig. 12).

Mesoscopic F_3 folds are found mostly in the northwest. The folds are upright, and range from gentle in the east (Fig. 11a, b, c) to tight in the northwest (Figs 9d; 11d, e). Plunges are steep, reflecting the pre-existing steep attitude of layering resulting from D_2 folding. Tight folds in the northwest are asymmetric and parasitic on the large-scale F_3 limbs. Many folds have a steep axial-plane S_3 foliation which crosscuts S_{1a} layering and in places transects F_{1b} and F_2 folds. In the east and southeast, S_3 is a spaced cleavage with a weak cataclastic texture. In the northwest, S_3 is a strong grain-flattening penetrative foliation with occasional grain elongation forming a lineation. S_3 texture is cataclastic to mylonitic, and characterised by twisted, kinked, bent, and broken plagioclase with recrystallised grain boundaries, flat lenses of recrystallised mosaic quartz, strained K-feldspar augen, cracked or marginally recrystallised garnet, orthopyroxene with sutured boundaries, and fine-grained aggregates of recrystallised clinopyroxene. In places, relict S_2 granoblastic texture is preserved. Type B metadolerite dykes and granite pegmatites have a weak S_3 foliation. At grid reference 529255, S_3 is a spaced crenulation cleavage with parallel partial melt stringers along the cleavage, and crenulates the S_{1a} layering (Fig. 11f). In unit fna in the east, disrupted blocks of granulite with gentle to isoclinal F_2 folds are enclosed in massive leucosome (Fig. 9a, b), which is also interpreted as D_3 melt. At one locality (grid reference 609250), S_3 is a finely spaced cleavage with small offsets of the layering. Stereograms of S_3 are shown in Figure 3r, t.

In the northeast, bending of the F_2 inclined antiform into parallelism with the northern limb of the major F_3 antiform means that S_2 and S_3 (if both are present) are also parallel. The existence of tight to isoclinal F_2 folds with axial-plane foliation implies that the foliation is S_2, and the east-striking foliation in this area is identical with S_2 in texture, being generally granulo- to granoblastic rather than cataclastic to mylonitic, which is typical of S_3.

L_3 lineation is found only in the north and northwest, and arises from grain elongation parallel to F_3 fold axes. Stereograms are shown in Figure 3l, q, s.

Interference of F_2 and F_3 folds is well displayed on the large scale by the map-pattern of units fn/m, fg, and fns (Fig. 2), the isoclinal F_2 antiform and synform being folded to their present Type 2 (Ramsay 1967) irregular arcuate shapes (Fig. 13a). The axes of the antiformal map closure plunge 63–65° northwest in the north and 60° southwest in the south

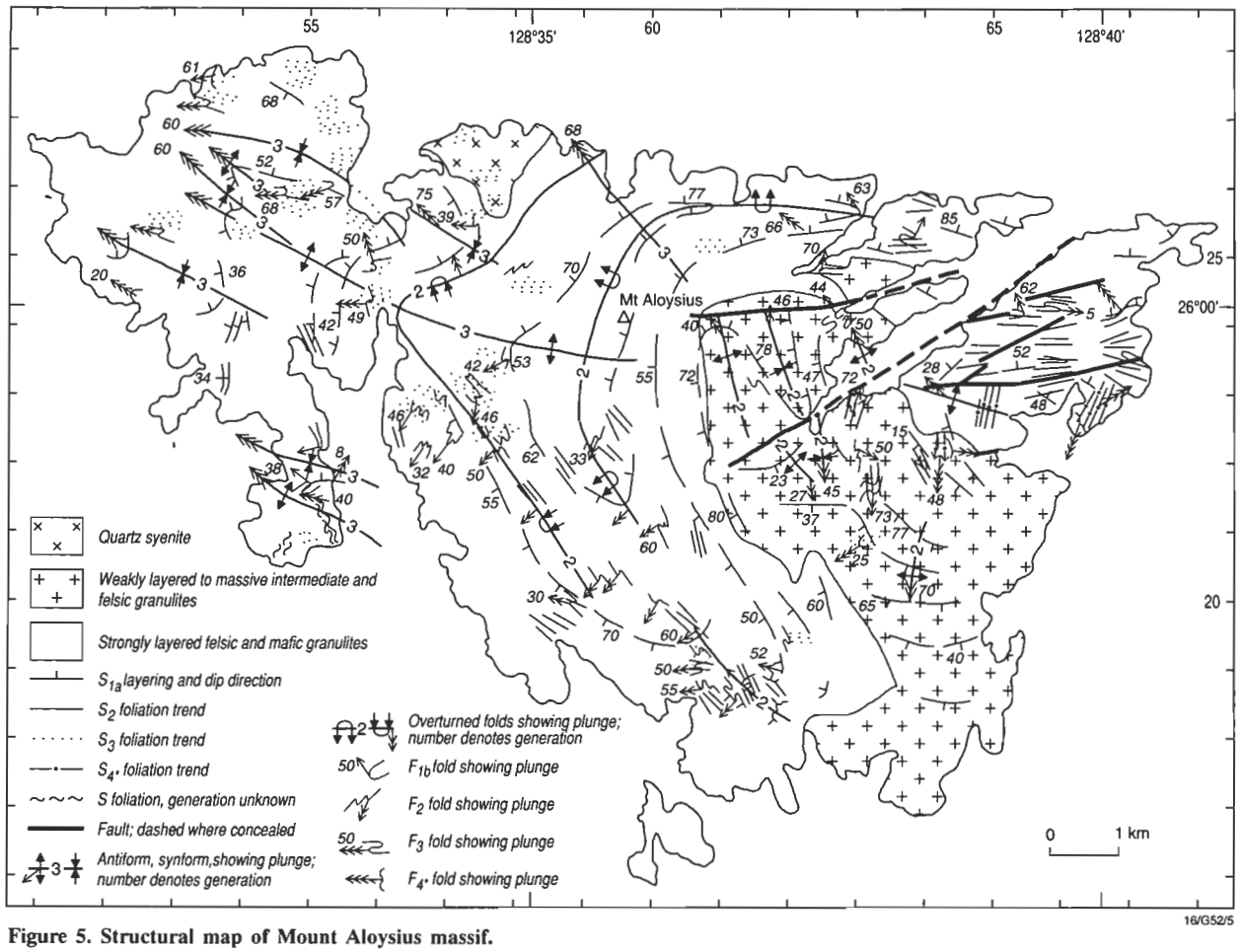

Figure 5. Structural map of Mount Aloysius massif.

(Figs 4, 5). If the F_3 folds are unfolded, the closure reverts to a northerly trending west-inclined doubly plunging F_2 antiform with an axis bending through about 90° in the axial plane (Fig. 13b). The 90° bend probably formed early in D_3, the strain increasing an originally gentle plunge at each F_2 hinge to its presently steep attitude, forming a Type 1 (Ramsay 1967) elongate isoclinal antiform. An alternative process, large-scale D_2 shear of the antiform to form an F_2 sheath fold, the crest of which the F2 antiform resembles (Fig. 13b), is less likely because of the lack of intense L_2 stretching lineation, and because the axes at each hinge are far from parallel, as a sheath fold shape requires.

F_{1b}–F_2 and F_2–F_3 interference patterns are well displayed on the mesoscopic scale in the south, forming Type 1 domes, saddles, and basins, and Type 2 crescents in thinly interlayered felsic and mafic granulites (Figs 9e, 14).

D_{4*}

D_{4*} effects are mesoscopic only, and of restricted though widely scattered extent. F_{4*} folds (Fig. 15) are upright, gentle to open, and have a north-northeast-striking axial-plane cleavage, ranging from spaced cleavage seams 10 cm apart to a mild flattening of quartz and K-feldspar grains (Fig. 9f) with growth of new small grains at their margins. Texture is granuloblastic to granoblastic. Scattered epidote, abundant disseminated calcite, and chlorite rims around opaque grains have formed in the northeast (grid reference 665226). Stereograms of F_{4*} folds and cleavage are shown for subarea 3 only (Fig. 3d, e).

Mafic dykes

Mafic dykes were intruded at three different times during the deformation sequence. Type A, strongly metamorphosed orthopyroxene-rich dolerite dykes, were intruded after D_2 and before D_3. The dykes strike northwest on the southwest limb of the major F_3 antiform that trends west-northwest through the Mount Aloysius massif, and northeast to east-northeast on the northern limb (Fig. 16). Type C, unmetamorphosed olivine-rich dolerite dykes, were intruded after D_3 folding, and strike northeasterly across the axial plane of the major F_3 antiform. Type B, moderately metamorphosed clinopyroxene-rich dolerite dykes, were intruded long after D_3 folding. They are large dykes parallel or subparallel to the axial plane of the major west-trending F_3 antiform, with a few offshoots striking north (Fig. 16).

Mylonite

A total of 17 mesoscopic mylonite zones were observed in the Mount Aloysius massif (Fig. 17). The zones are a few metres wide and all consist of strongly foliated and lineated granulite facies fine-grained gneiss (less commonly augen gneiss) with extreme elongation of quartz to ribbons. The mylonites are assigned to the various deformation events based on their effects (or lack of) on mafic dykes, or where there is no such relationship, on their orientation and distribution with respect to major fold axes and foliations. Mylonitization took place at syn-D_2, syn-D_3, and post-D_{4*} times. Mesoscopic kinematic information was observed in only seven of the mylonites, despite careful search, and in all cases indicated contractional movement, ranging from reverse dip slip through oblique slip to strike slip in a few places. Where kinematic information is lacking, the mylonites are presumed to have a reverse movement sense, and are so depicted in Figure 17.

Three syn-D_2 mylonites were observed; they have no effect

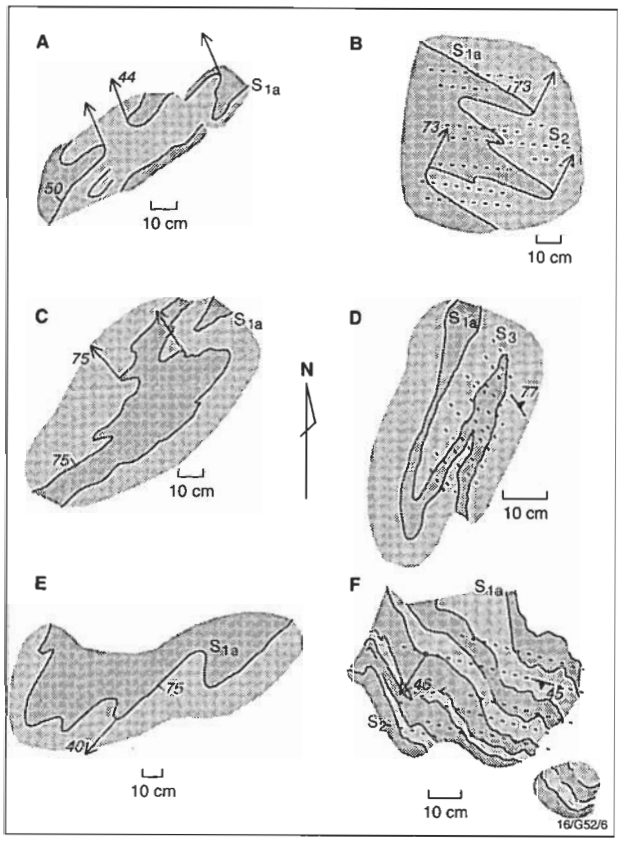

Figure 6. Sketches of mesoscopic F_{1b} folds in Mount Aloysius massif. (a) Tight to isoclinal reclined folds in weakly layered felsic granulite of unit fna, grid reference 626239. (b) Tight reclined folds transected by S_2 foliation in weakly layered leucofelsic granulite of unit fn/m, grid reference 636251. (c) Tight reclined folds in felsic granulite with mafic interlayers, unit fn/m, grid reference 615187. (d) Tight fold in quartz layer in felsic granulite of unit fn/m transected by S_3 foliation, grid reference 531284; same locality as Figure 7c. (e) Close to tight upright folds in thinly interlayered mafic and felsic granulites of unit fn/m, grid reference 571223. (f) Open upright folds transected by S_3 foliation in thinly interlayered mafic and felsic granulites of unit fn/m, grid reference 565227; same locality as Fig. 7d.

on and are therefore older than adjoining Type A metadolerite. They have an easterly strike, moderately steep dips (>60°), and shallow to steep lineation, indicating strike slip to dip slip. Data are too few to allow any kinematic conclusions.

Ten syn-D_3 mylonites were noted; they affect Type A metadolerites as well as the granulites, but the effects in the mafic rocks, such as microjointing, spaced cleavage, or marginal mylonitic foliation, are weaker than in the adjoining mylonitised granulites. The mylonites strike easterly, dips are moderate to steep (33–78°), and lineations plunge from 5° to steeply down-dip. All but one of the mylonites on the northern limb of the major F_3 antiform dip north and, similarly, those on the southern limb dip south (Fig. 17). In both limbs the mylonites dip more gently than the granulite layering. The mylonites are interpreted as conjugate shears that helped to accommodate the space problem in the core of the F_3 antiform, allowing the core rocks to move out and down from the hinge region (Fig. 12).

Four post-D_{4*} mylonites were observed. Two cut granulite and have bordering veinlets of ultramylonite. Two coincide with and brecciate or cleave Type C dolerites. The mylonites strike north through northeast to east, and dip from 45° to vertical. Data are too few to allow any kinematic conclusions to be drawn. The post-D_{4*} mylonites do not appear to correlate with the D_4 mylonites of Clarke (1992, Clarke et al. 1992–3) in the Champ de Mars area, as the D_4 mylonites there are an order of magnitude larger in thickness and throw, and differ significantly in orientation and metamorphic facies (amphibolite; Clarke 1992) from the post-D_{4*} mylonites at Mount Aloysius.

Discussion and conclusions

- The granulites in the Mount Aloysius massif preserve evidence of four episodes of folding, the intensity gradually lessening from isoclinal to close (F_{1b}, F_2) through tight to gentle (F_3), to open to gentle (F_{4*}); axial-plane cleavage shows a similar progression from strong with granoblastic texture (S_2) through strong with cataclastic/mylonitic texture with local partial melt streaks and patches (S_3) to mild grain-flattening or spaced cleavage with local greenschist retrogression (S_{4*}). These effects point to decreasing ductility of the rock as temperature waned from a maximum >750°C (and a pressure of about 700 MPa) during D_1 to about 700°C and 400–500 MPa during late D_3 (Clarke et al. 1992–3).
- The conflicting interpretations of the major fold through Mount Aloysius are resolved—it is an interference fold which began as a west-inclined isoclinal gently doubly plunging F_2 antiform which was steepened early in D_3 to a steeply doubly plunging F_2 antiform, and was subsequently refolded to an arcuate shape late in D_3.
- The major F_2 antiform through Mount Aloysius was just one fold in a train of northerly trending folds, and became strongly flattened to an isoclinal profile. The presence of the relatively massive unit of granulite (fna) immediately next to the isoclinal antiform suggests that the near-massive granulite may have acted as a stiff buttress against which the well-layered granulite to the west was squashed and flattened.
- The same mass of relatively massive granulite again acted as a buttress during D_3, and provided a stiff *auge*-like core around which the well-layered granulite was wrapped like an envelope.
- The Mount Aloysius area strongly resembles the Champ de Mars and west Hinckley areas, 30 km to the east (Clarke 1992). The presence of small F_{1b} folds, now reclined, but originally recumbent, noted by Clarke (1992) in the Champ de Mars area, is confirmed. These predate the F_1 folds of Nesbitt et al. (1970), Gray (1971), and Pharaoh (1990), which, accordingly, become F_2 in this study. Mount Aloysius also has an additional generation of F_{4*} folds, and F_2 axial planes dip moderately to steeply, which contrasts with the gentle dip observed by Clarke (1992).

Acknowledgements

I thank C.M. Gray for permission to use the geological map in his Ph.D. thesis, and R.S. Blewett, K.A. Plumb, A.L. Jaques, I.S. Buick, M.J. Rickard, C.M. Gray, and an anonymous referee for critical reviews of the paper. The text-figures were drawn by John Convine of the AGSO Cartographic Services Unit.

References

Bates, R.L. & Jackson, J.A., 1980. Glossary of geology (Second edition). American Geological Institute, Falls Church, Virginia, 751 pp.

Clarke, G.L., 1992. Field relationships and tectonic history of the Hinckley Gabbro, felsic to mafic granulites and granitoids, west Hinckley Range and Champ de Mars areas, Tomkinson Ranges, Musgrave Block, WA. Bureau of Mineral Resources, Australia, Record 1992/33 (Minerals and Land Use Program, Mineral Provinces 13), 48 pp.

Clarke, G.L., Buick, I.S., Glikson, A.Y. & Stewart, A.J.,

1992–3. Contact relationships and structure of the Hinckley Gabbro and environs, Giles Complex, Western Musgrave Block, W.A. AGSO Research Newsletter 17, 6–8 and 18, 15.

Daniels, J.L., 1971. Cooper, W.A. 1:250 000 Geological Series Explanatory Notes SG52-10, 22 pp. Bureau of Mineral Resources, Geology and geophysics, Canberra.

Daniels, J.L., 1972. Scott, W.A. 1:250 000 Geological Series, Explanatory Notes SG52-6, 21 pp. Australian Government Publishing Service, Canberra.

Daniels, J.L., 1974. The geology of the Blackstone Region, Western Australia. Geological Survey of Western Australia, Bulletin 123, 257 pp., 3 pl.

Daniels, J.L., Horwitz, R.C., Kriewaldt, M.J.B., Doepel, J.J.G. & Fairbridge, R.A., 1970a. Cooper, W.A. 1:250 000 Geological Map (First edition), SG52-10. Geological Survey of Western Australia, Perth.

Daniels, J.L., Horwitz, R.C. & Kriewaldt, M.J.B., 1970b.

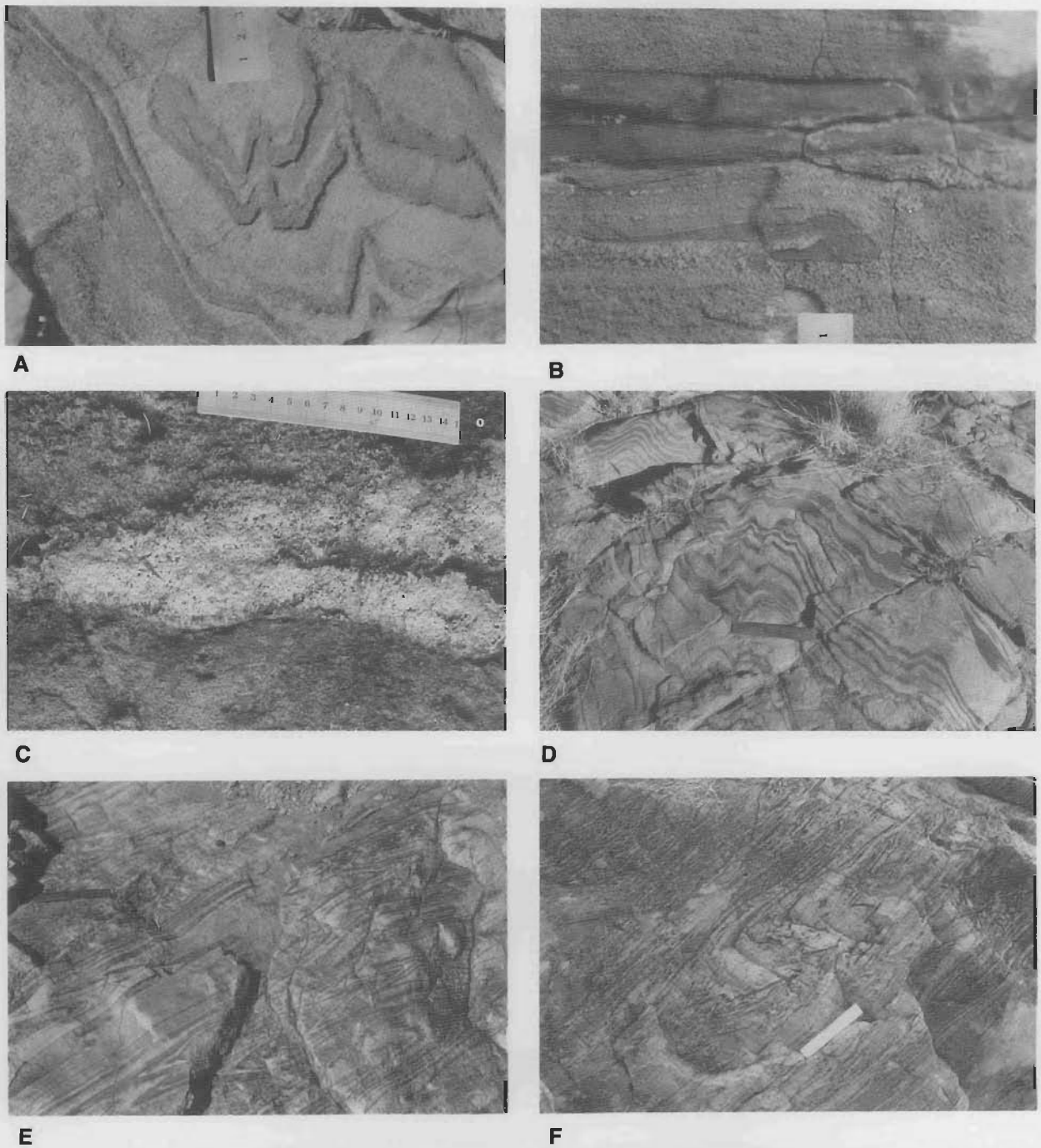

Figure 7. Field photographs of mesoscopic folds, Mount Aloysius massif. (a) Isoclinal F_{1b} fold in interlayered felsic and mafic granulites of unit fn/m, folded into Type 2 crescent and partly disrupted by tight upright F_2 folds. Scale in cm and mm. Grid reference 608188. (b) Isoclinal F_{1b} fold in mafic and felsic granulites of unit fn/m transected by S_3 foliation well-shown in coarse-grained leucolayers. Scale in cm and mm. Grid reference 549277. (c) Tight to isoclinal F_{1b} fold in quartz layer in felsic granulite of unit fn/m, obliquely transected by S_3 foliation. Scale 15 cm. Grid reference 531284. Same locality as Figure 6d. (d) Open upright F_{1b} folds in thinly interlayered felsic and mafic granulites of unit fn/m. Scale 15 cm. Grid reference 565227. Same locality as Figure 6f. (e) Tight F_2 folds in thinly interlayered felsic and mafic granulites of unit fn/m. Scale 15 cm. Grid reference 577222. (f) Tight F_2 folds in thin-layered (S_{1a}) calc-silicate granulite (modal percentages: labradorite 64, diopside 20, quartz 10, titanite 5, opaque grains 1) of unit fn/m. Scale 15 cm. Grid reference 577234.

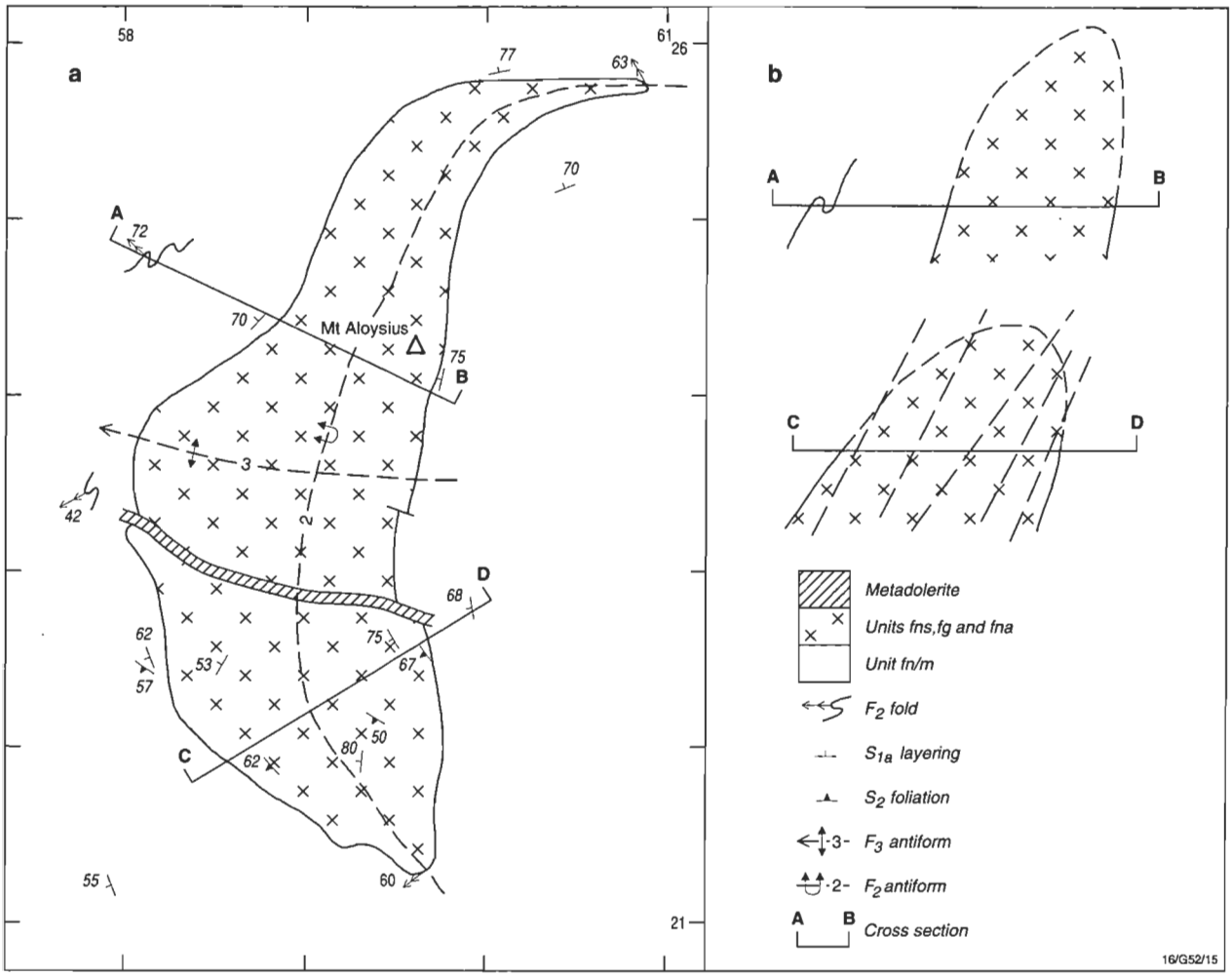

Figure 8. (a) Geological map and (b) cross-sections of central part of Mount Aloysius massif, showing S_2 foliation dipping less steeply than S_{1a} layering on eastern limb of F_2 fold, and parasitic folds with easterly component of vergence on western limb, indicating antiformal shape of the F_2 fold.

Scott, W.A. 1:250 000 Geological Map (First edition), SG52-6. Geological Survey of Western Australia, Perth.

Fleuty, M.J., 1964. The description of folds. Proceedings of the Geologists' Association 75, 46–492.

Forman, D.J., Shaw, R.D., Hancock, P.M., Stewart, A.J. & Ivanac, J.F., 1972. Petermann Ranges, N.T. 1:250 000 Geological Map (First edition), SG 52-7. Bureau of Mineral Resources, Geology and Geophysics, Canberra

Glikson, A.Y., Ballhaus, C.G., Clarke, G.L., Stewart, A.J., Sheraton, J.W., Sun, S.-S., & Feeken, E.H.J., in preparation. Geology of the Giles Complex Special 1:100 000 Map, western Musgrave Block. Australian Geological Survey Organisation, Canberra.

Gray, C.M., 1971. Strontium isotopic studies on granulites. Ph.D. thesis, Australian National University, Canberra (unpublished).

Gray, C.M., 1977. The geochemistry of central Australian granulites in relation to the chemical and isotopic effects of granulite facies metamorphism. Contributions to Mineralogy and Petrology 65, 79–89.

Gray, C.M., 1978. Geochronology of granulite-facies gneisses in the western Musgrave Block, central Australia. Journal of the Geological Society of Australia 25, 403–414.

Gray, C.M. & Compston, W., 1978. A rubidium-strontium chronology of granulite-facies rocks in the western Musgrave Block, central Australia. Geochimica et Cosmochimica Acta, 42, 1735–1747.

Maboko, M.A.H., McDougall, I. & Zeitler, P.K., 1989. Metamorphic P-T path of granulites in the Musgrave Ranges, central Australia. In: Daly, J.S., Cliff, R.A. & Yardley, B.W.D. (editors), Evolution of metamorphic belts. Geological Society Special Publication 43, 303–307.

Major, R.B. & Conor, C.H.H., 1993. Musgrave Block. In: Drexel, J.F., Preiss, W.V. & Parker, A.J. (editors), The geology of South Australia. 1: The Precambrian. Geological Survey of South Australia, Bulletin 54, 156–167.

Moore, A.C. & Goode, A.D.T., 1978. Petrography and origin of granulite-facies rocks in the western Musgrave Block, central Australia. Journal of the Geological Society of Australia 25, 341–358.

Nesbitt, R.W., Goode, A.D.T., Moore, A.C. & Hopwood, T.P., 1970. The Giles Complex, central Australia: a stratified sequence of mafic and ultramafic intrusions. Geological Society of South Africa, Special Publication 1, 547–564.

Pharaoh, T.C., 1990. Aspects of structural geology of the Giles layered basic/ultrabasic complex and associated felsic granulites, Tomkinson Range, Musgrave Block, central Australia. Bureau of Mineral Resources, Australia, Record 1990/5, 28 pp., 2 pl.

Ramsay, J.G., 1967. Folding and fracturing of rocks. McGraw-Hill, New York, 568 pp.

Stewart, A.J., 1992. Structural map of the Amadeus Basin, 1:1 000 000. In: Lindsay, J.F. (editor), Geological atlas of the Amadeus Basin. Australian Geological Survey Organisation, Canberra.

Sun, S.-S., Gray, C.M., Sheraton, J.W., Glikson, A.Y. & Stewart, A.J., in press. Zircon U–Pb chronology and neodymium isotopic study of tectono-thermal and crust-forming events in the Tomkinson Ranges, western Musgrave Block, central Australia. AGSO Journal of Australian Geology & Geophysics.

Sun, S.-S. & Sheraton, J.W., 1992. Zircon U/Pb chronology, tectono-thermal and crust-forming events in the Tomkinson Ranges, Musgrave Block, central Australia. AGSO Research Newsletter 17, 9–11.

Thomson, B.P., Mirams, R.C. & Johnson, J., 1962. Mann, S.A., 1:250 000 Geological Map (First edition), SG 52-11. Geological Survey of South Australia, Adelaide.

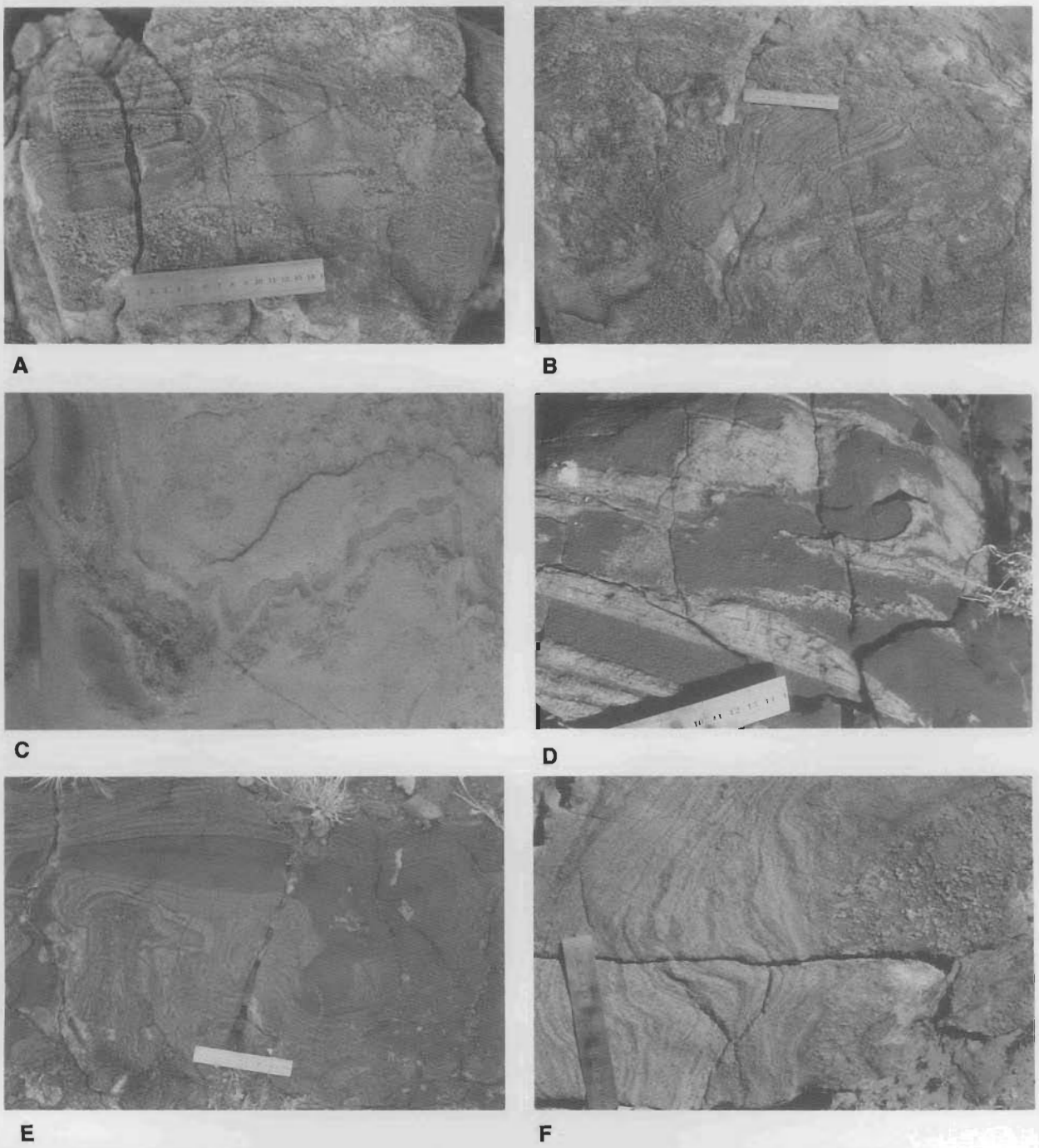

Figure 9. Field photographs of mesoscopic folds, Mount Aloysius massif. (a, b) Blocks of thin-layered garnet felsic granulite: (a) with isoclinal F_2 fold enclosed in massive, very coarse-grained, garnet felsic leucosome of unit fna. Scale 15 cm. Grid reference 641219. (c) Open to close F_2 folds in interlayered felsic and boudinaged mafic granulites of unit fn/m. Scale 15 cm. Grid reference 608188. (d) Open to tight F_3 folds in felsic granulite melt patches in mafic granulite of unit mn. Scale in cm and mm. Grid reference 558251. (e) Interference folds in interlayered felsic and mafic granulites of unit fn/m. Scale 15 cm. Grid reference 613187. Explanatory sketch shown in Figure 14. (f) Gentle to open F_{4^*} fold in weakly layered felsic granulite of unit fna, with axial-plane foliation visible in coarse-grained granulite (right). Scale in cm and mm. Grid reference 666227.

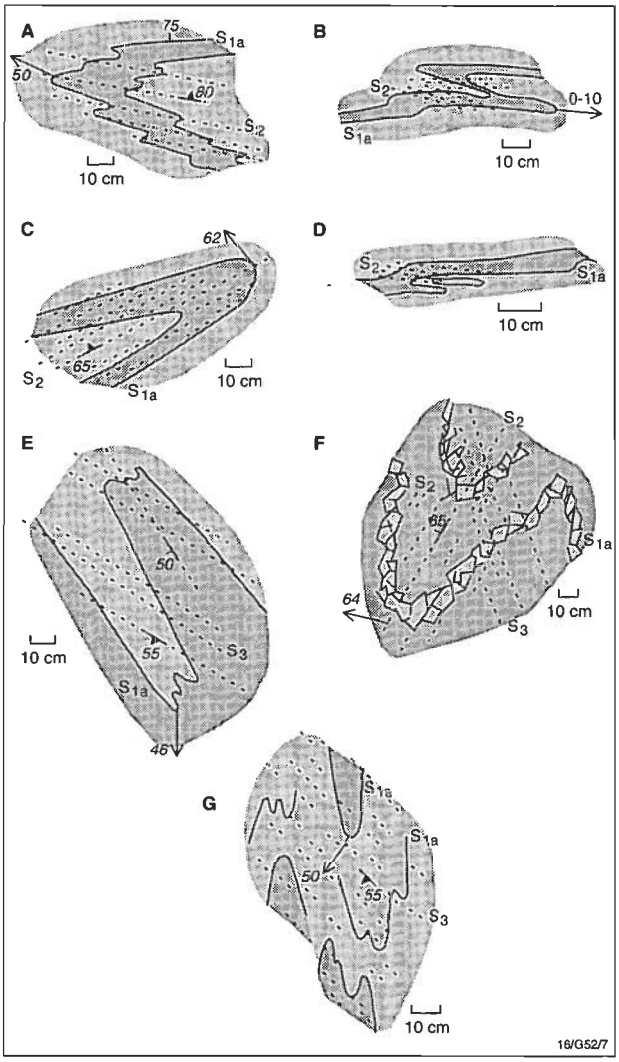

Figure 10. Sketches of mesoscopic F_2 folds in Mount Aloysius massif. (a, b) Tight upright folds with axial-plane foliation in thin-layered felsic granulite of unit fna. Grid reference 658242. (c) Tight reclined fold with S_2 foliation parallel to one limb and oblique to other limb in leucofelsic granulite of unit fn/m. Grid reference 653240. (d) Isoclinal folds in laminated to thin-layered felsic granulite of unit fna. Grid reference 656241. (e) Tight folds transected by S_3 foliation in thin-layered felsic granulite of unit fn/m. Grid reference 574229. (f) Close reclined fold with S_2 axial-plane foliation transected by S_3 foliation in garnet felsic granulite with very coarse-grained quartz laminae S_{1a}, unit fn/m. Grid reference 607192. (g) Tight inclined folds transected by S_3foliation in thinly layered felsic granulite with mafic to intermediate layers. Grid reference 576222.

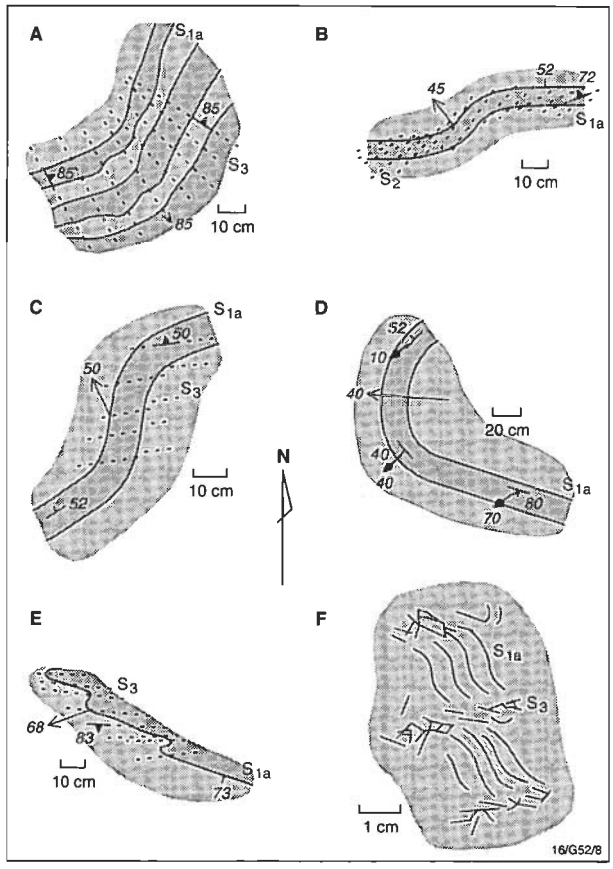

Figure 11. Sketches of mesoscopic F_3 folds in Mount Aloysius massif. (a) Gentle upright fold with axial-plane foliation in medium-grained compositionally layered felsic granulite of unit fna. Grid reference 643221. (b) Gentle upright fold which bends S_{1a} layering and S_2 foliation in leucofelsic granulite of unit fn/m. Grid reference 669241. (c) Gentle reclined fold with axial-plane foliation in thin to medium-layered felsic granulite of unit fn/m. Grid reference 560249. (d) Close upright fold, which folds L_2 lineation in medium-layered felsic granulite of unit fn/m. Grid reference 551217. (e) Tight upright folds with axial-plane foliation in weakly compositionally layered leucofelsic granulite of unit fnk. Grid reference 548259. (f) Spaced crenulation cleavage S_3 with partial melt quartz–feldspar stringers parallel to S_3 and crenulating earlier S_1 layering in garnet felsic granulite of unit fn/m. Grid reference 529256.

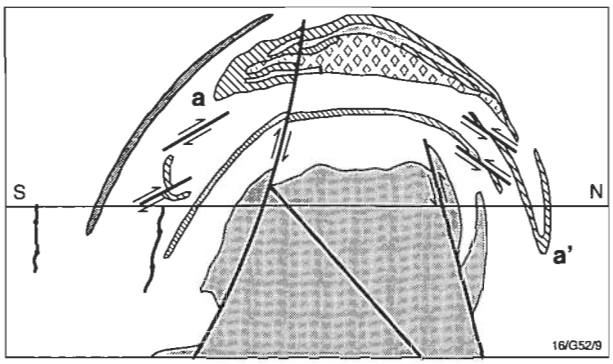

Mafic granulite, rare intermediate and felsic granulite layers

Felsic granulite

Felsic granulite, minor mafic granulite, rare intermediate granulite

Intermediate granulite, lesser felsic granulite, weakly layered to massive

Garnet felsic granulite

Sillimanite-garnet felsic granulite

Metadolerite

Figure 12. North-south vertical cross-section through Mount Aloysius massif, showing major F_2 and F_3 antiforms, block displaced down from hinge region of F_3 antiform, and schematic syn-D_3 mylonite zones on limbs of F_3. At a and a', F_2 antiform has synformal orientation because of rotation on limbs of F_3 antiform. Same lithological patterns as Figure 2. Vertical and horizontal scales equal.

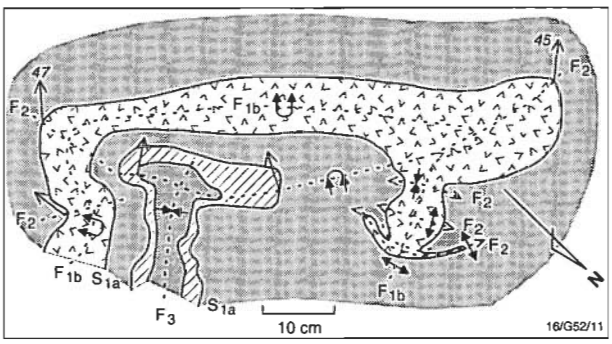

Figure 14. Explanatory sketch of interference folds shown in Figure 9e. F_{1b} is an isoclinal antiform bent into Type 2 crescents (Ramsay 1967) by F_2 reclined folds (in left and right of figure) and squashed into Type 1 domes and saddles by F_2 (right) and into a Type 1 basin by F_3 (slightly left of centre). Grid reference 613187.

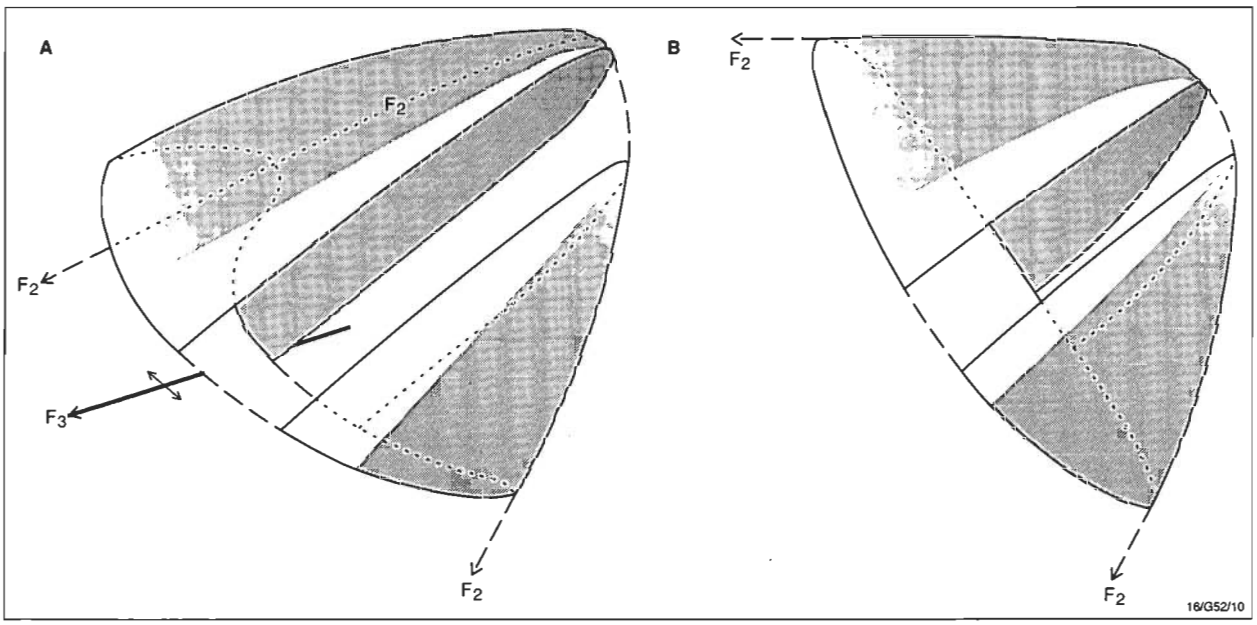

Figure 13. (a) Sketch of F_2–F_3 interference antiform folded into Type 2 arc late in D_3. (b) Sketch of Type 1 steeply doubly plunging isoclinal F_2–F_3 interference antiform formed early in D_3.

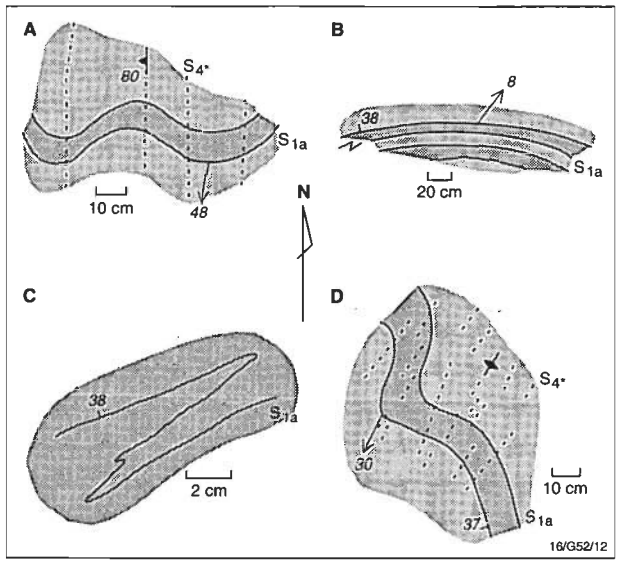

Figure 15. Sketches of mesoscopic F_{4*} folds in Mount Aloysius massif. (a) Open upright fold with spaced axial-plane cleavage in thin-layered weathered granulite (magnetite–goethite–quartz) of unit fna. Grid reference 642219. (b) Gentle inclined fold with F_{1b} reclined fold preserved in left limb in thinly interlayered felsic granulites (massive medium-grained leucolayers and coarse-grained hackly leucolayers) of unit fn/m. Grid reference 551216. (c) Enlargement of F_{1b} fold at left of (b). (d) Open upright fold with axial-plane cleavage in magnetite felsic granulite of unit fna. Grid reference 663224.

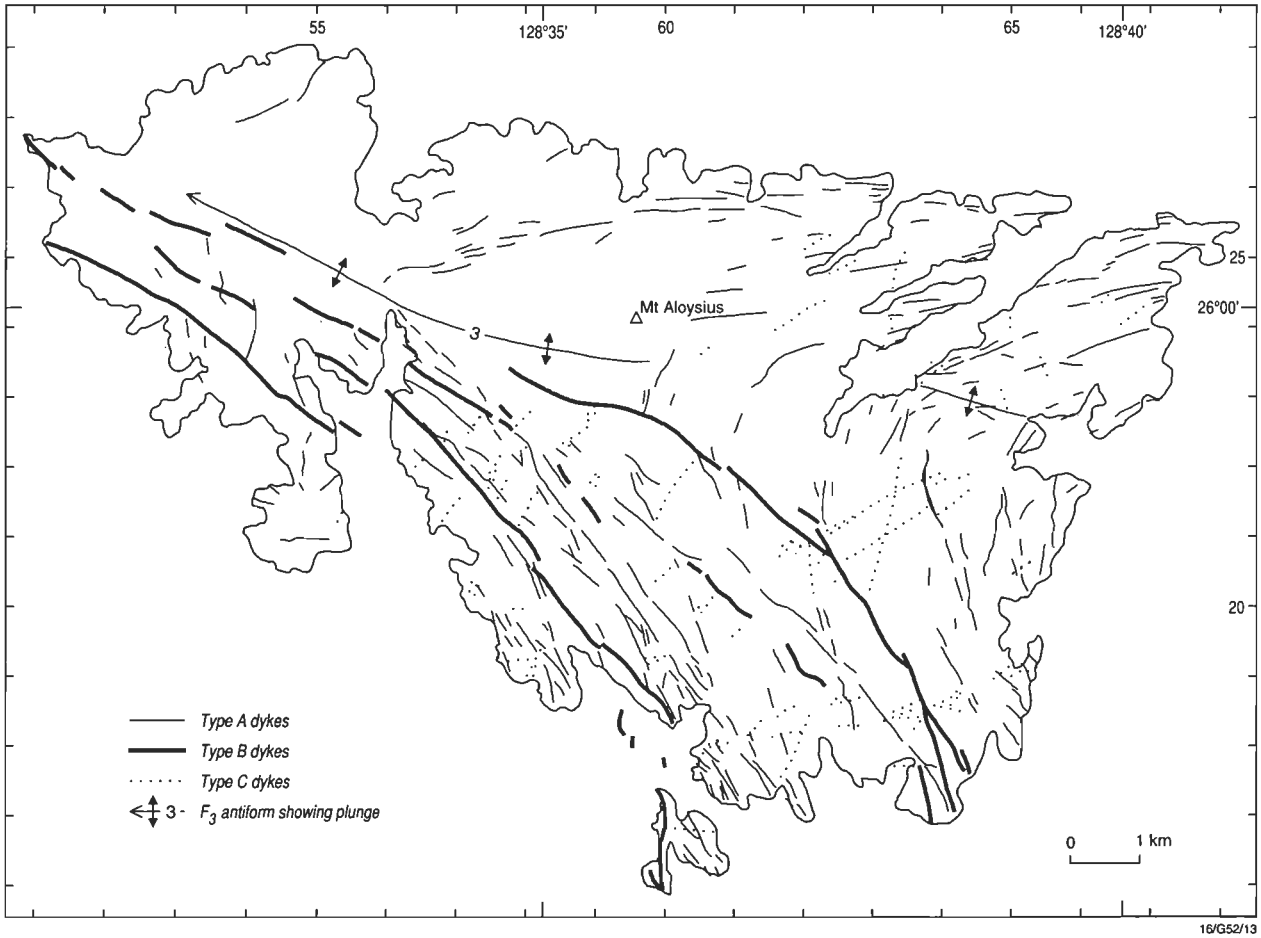

Figure 16. Map of Mount Aloysius massif, showing Type A, B, and C mafic dykes. Type A dykes are folded around F_3 antiform, Type B are subparallel to axial plane of F_3 antiform, and Type C crosscut F_3 antiform.

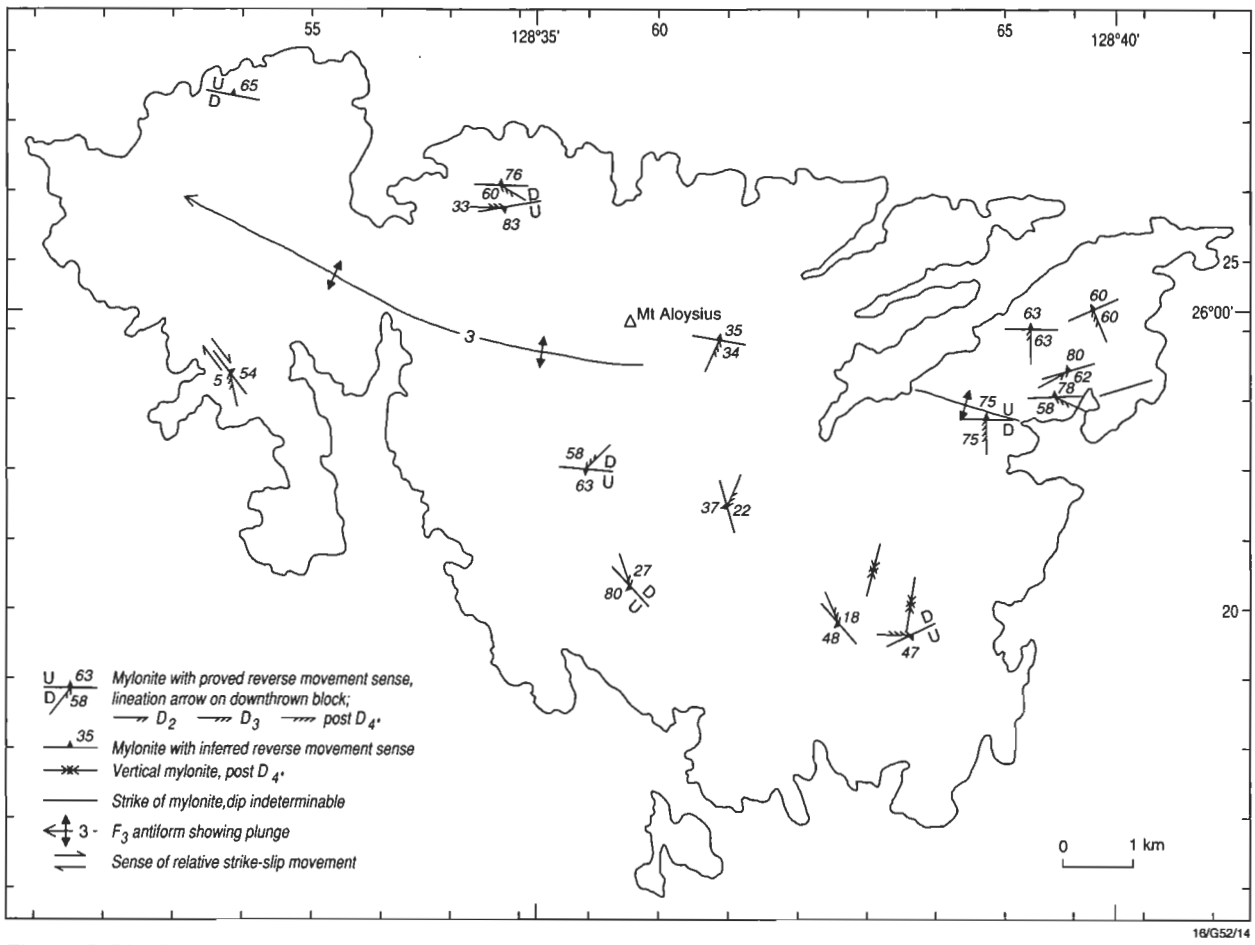

Figure 17. Distribution and attitudes of mesoscopic mylonites in Mount Aloysius massif.

AGSO Journal of Australian Geology & Geophysics, 16 (1/2), 107–125

Geochemistry and origin of felsic igneous rocks of the western Musgrave Block

John W. Sheraton[1] & Shen-Su Sun[1]

Granulite facies country rocks of the Giles Complex in the western Musgrave Block are predominantly of felsic igneous (intrusive or extrusive) origin and were metamorphosed at about 1200 Ma. The protoliths of some Y-depleted orthogneisses may represent primary felsic crust derived by partial melting of a hornblende±garnet-bearing, but feldspar-poor, mafic source, whereas others (including syn-metamorphic orthopyroxene granites) have geochemical features (notably depletion in Sr, but not Y) more consistent with intracrustal melting. 1188±4 Ma and ~1060 Ma hornblende–biotite granitoids (including rapakivi varieties) south of the Hinckley Range mostly have compositions (high HFSE, LREE, and Th/U, and low Sr) consistent with relatively high-temperature partial melting of near-anhydrous granulite facies crustal rocks, at least partly caused by emplacement of mafic magmas (including the Giles Complex). Granitic basement rocks to the Bentley Supergroup in the western Musgrave Block differ from granitoids of the Hinckley Range area in including a significant proportion of Y-depleted, Sr-undepleted rocks which may represent new felsic crust. The 1078±5 Ma felsic Smoke Hill Volcanics of the Bentley Supergroup have compositions (high HFSE, LREE, and Ga/Al, and low *mg*) typical of A-type and intraplate granitoids. Like the Hinckley Range hornblende–biotite granitoids, they may have been derived by partial melting of granulite facies lower crustal rocks during emplacement of mantle-derived magma (e.g., the associated Mummawarrawarra Basalt), or, alternatively, by fractionation of basaltic magma. However, the relatively high Nb of the felsic volcanics implies a source compositionally different from either the exposed felsic crustal rocks or mafic volcanics. The somewhat younger Nd T_{DM} model ages (1460–1570 Ma) of the Smoke Hill Volcanics compared to granulite facies metamorphics west of the Hinckley Range (1610–1900 Ma) are consistent with derivation of the former either from a relatively young crustal underplate or directly from mantle-derived magma.

Introduction

The western part of the Mesoproterozoic Musgrave Block in central Australia consists of high-grade (amphibolite to granulite facies) metamorphic rocks of both igneous and sedimentary origin (Fig. 1) (Stewart & Glikson 1991; Glikson et al. in press, 1995—this issue). Felsic orthogneiss is the most abundant, whereas rocks of clearly sedimentary origin, such as metapelite, metaquartzite, and calc-silicate, are much less common; mafic granulite, although widespread, is volumetrically minor. The metamorphic rocks are intruded by major layered mafic–ultramafic bodies of the Giles Complex, as well as a variety of granitic rocks and mafic dykes (Figs 1, 2). Igneous protoliths of felsic orthogneiss in the Tomkinson Ranges area were emplaced between 1300 and 1550 Ma, and high-grade metamorphism occurred at about 1200 Ma (Gray 1978; Maboko et al. 1991; Sun & Sheraton 1992; Sun et al. in press), accompanied by two deformation events (D_1 and D_2). Clarke et al. (1995—this issue) estimated peak metamorphic conditions of at least 750°C at 5±1 kb during D_2.

The post-D_2, pre-D_3 Giles Complex forms the largest exposures of deep-seated layered mafic-ultramafic intrusions in Australia (Nesbitt et al. 1970; Glikson et al. 1990; Ballhaus & Berry 1991), and was apparently emplaced significantly later than the high-grade metamorphism, probably at about 1080 Ma (Sun et al. in press). Emplacement of several suites of mafic dykes, formation of open to isoclinal upright folds (D_3), and at least four episodes of mylonite/retrograde shear zone formation (D_{4-7}) followed emplacement of the Giles Complex (Clarke 1992; Clarke et al. 1995—this issue). Mafic to felsic volcanic rocks of the Tollu Group (Bentley Supergroup), which unconformably overlie granitic basement rocks west of the Tomkinson Ranges, apparently in cauldron subsidence areas (Daniels 1974), have been dated at 1078±5 Ma, i.e. roughly coeval with the Giles Complex (Sun et al. in press).

In this paper, the geochemistry and origin of the various felsic igneous rocks in the western Musgrave Block are examined. These comprise pre-Giles Complex felsic orthogneisses and orthopyroxene-bearing granitoids, a variety of pre to syn-Giles Complex hornblende–biotite granitoids, and felsic volcanics of the Bentley Supergroup.

[1] Division of Regional Geology & Minerals, Australian Geological Survey Organisation, GPO Box 378, Canberra, ACT 2601

Field relations and petrography

Felsic orthogneiss

Orthopyroxene-bearing felsic gneiss is widespread in the western Musgrave Block. It commonly contains up to 4 per cent of strongly pleochroic orthopyroxene, as well as quartz, K-feldspar, plagioclase (typically calcic oligoclase or andesine), and accessory zircon, apatite, and opaque minerals. Clinopyroxene occurs in some layers, particularly the more mafic ones. Most such gneiss has a granitic (s.s.) composition; granodiorite is less common, and tonalite, quartz monzodiorite, and diorite are rare. K-feldspar is commonly strongly perthitic, plagioclase is antiperthitic, and in some rocks mesoperthite is the only feldspar. However, many gneisses are partly or wholly recrystallised and some have mylonitic textures. Reddish-brown biotite and, less commonly, brownish-green hornblende are present in many of these deformed rocks, and appear to be mostly retrograde, replacing pyroxene.

Garnet-bearing gneiss is also common and, apart from the presence of garnet (up to about 6%), rather than orthopyroxene, is petrographically similar to the orthopyroxene gneiss. A few gneisses contain both garnet and orthopyroxene, but the former does not appear to coexist with either clinopyroxene or hornblende, except in secondary assemblages formed during later deformations. Some garnet leucogneiss is thought to be of igneous origin (see below), although in some places (e.g. Mount Aloysius) more garnet-rich paragneiss is interlayered with other metasedimentary rocks (garnet+sillimanite-bearing metapelite, metaquartzite, and calc-silicate).

The widespread occurrence of mesoperthite indicates crystallisation of the original feldspar at high temperature and very low water pressure. Calcic alkali feldspar cannot form at high water pressure, because the temperature of the alkali feldspar solvus crest rises steeply with increasing An content, and would intersect the feldspar solidus, which is lowered with increasing P_{H2O} (Morse 1968). Low P_{H2O} is consistent with the essentially anhydrous assemblages present in most undeformed felsic gneisses.

Felsic igneous rocks

A variety of felsic intrusive rocks, ranging from veins and dykes to small plutons, crops out in the Tomkinson Ranges. Most are of granitic (s.s.) composition, with subordinate quartz monzodiorite, quartz monzonite, and quartz syenite; granodiorite and tonalite appear to be absent. Apparent back intrusion relationships and a spatial association with Giles Complex

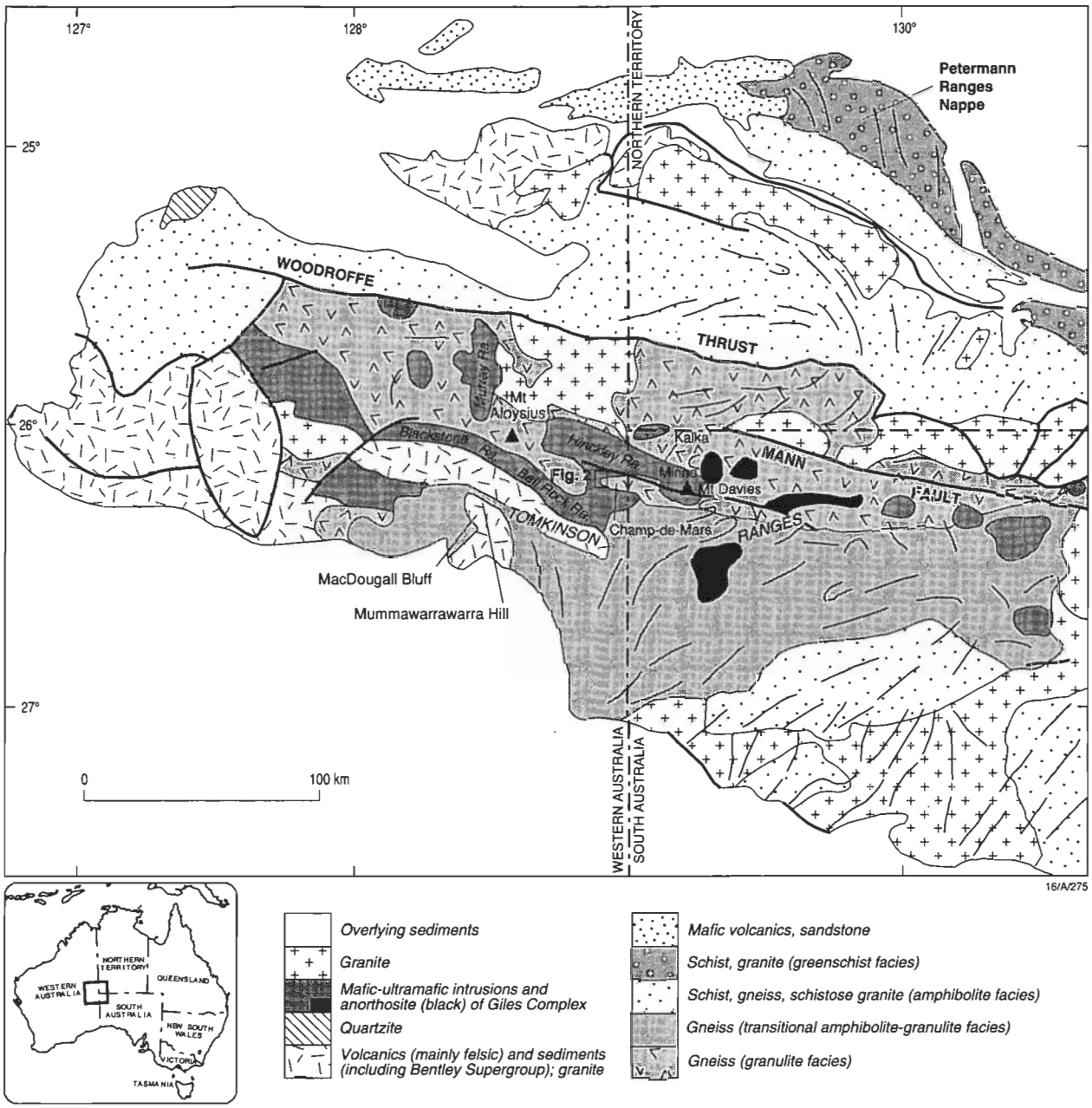

Figure 1. Generalised geological map of the western Musgrave Block (after Stewart 1995—this issue), showing main localities mentioned in text.

intrusions (Stewart & Glikson 1991; Clarke 1992; Clarke et al. 1995—this issue) suggest that emplacement of some of these granitoids was closely associated with that of the Giles Complex (i.e. they are post-D_2). In the western Champ de Mars area (Fig. 2), south of the Hinckley Range, three main varieties—orthopyroxene granite ('charnockite'), rapakivi granite, and porphyritic ('megacrystic') to even-grained granite—were recognised by Clarke et al. (1995—this issue), who suggested that the more melanocratic varieties of orthopyroxene and rapakivi granite may have been derived by contamination of porphyritic granite with mafic material. However, foliated orthopyroxene granitoids were shown to be of pre-Giles Complex age (post-D_1 and pre-D_2), and some rapakivi granites are also pre-Giles (Sun et al. in press).

Farther west, south of the Blackstone and Bell Rock Ranges, mostly biotite-bearing granitic rocks form the basement to the mafic to felsic volcanics (and subordinate sedimentary rocks) of the Tollu Group of the Bentley Supergroup. Within the latter, the Smoke Hill Volcanics consist predominantly of rhyolitic extrusives.

Orthopyroxene granitoids. Orthopyroxene-bearing granite, quartz monzonite, and quartz monzodiorite (charnockites of Clarke et al. 1995—this issue) crop out near the Mount Davies and Kalka layered intrusions, in the western Hinckley Range, and in areas flanking the Murray and Blackstone Ranges. Biotite granite gneiss at Minno (about 10 km northwest of Mount Davies), emplaced before D_2 and possibly the deformed equivalent of nearby orthopyroxene granite, has given a zircon U–Pb ion microprobe age of 1198±6 Ma (Sun & Sheraton 1992; Sun et al. in press), within error of the Rb–Sr age (1204±17 Ma: Gray 1978). This defines an older limit to the time of emplacement of the Giles Complex (Gray 1978), although the granite is separated from the Kalka intrusion by the Hinckley Fault.

In the Charnockite Flats and Champ de Mars areas (west and south of the Hinckley Range, respectively), small, locally discordant pods and larger stocks of foliated, locally porphyritic granite contain up to 3 per cent of orthopyroxene, with smaller amounts of reddish-brown biotite and, less commonly, greenish-brown hornblende and clinopyroxene. Perthite is generally

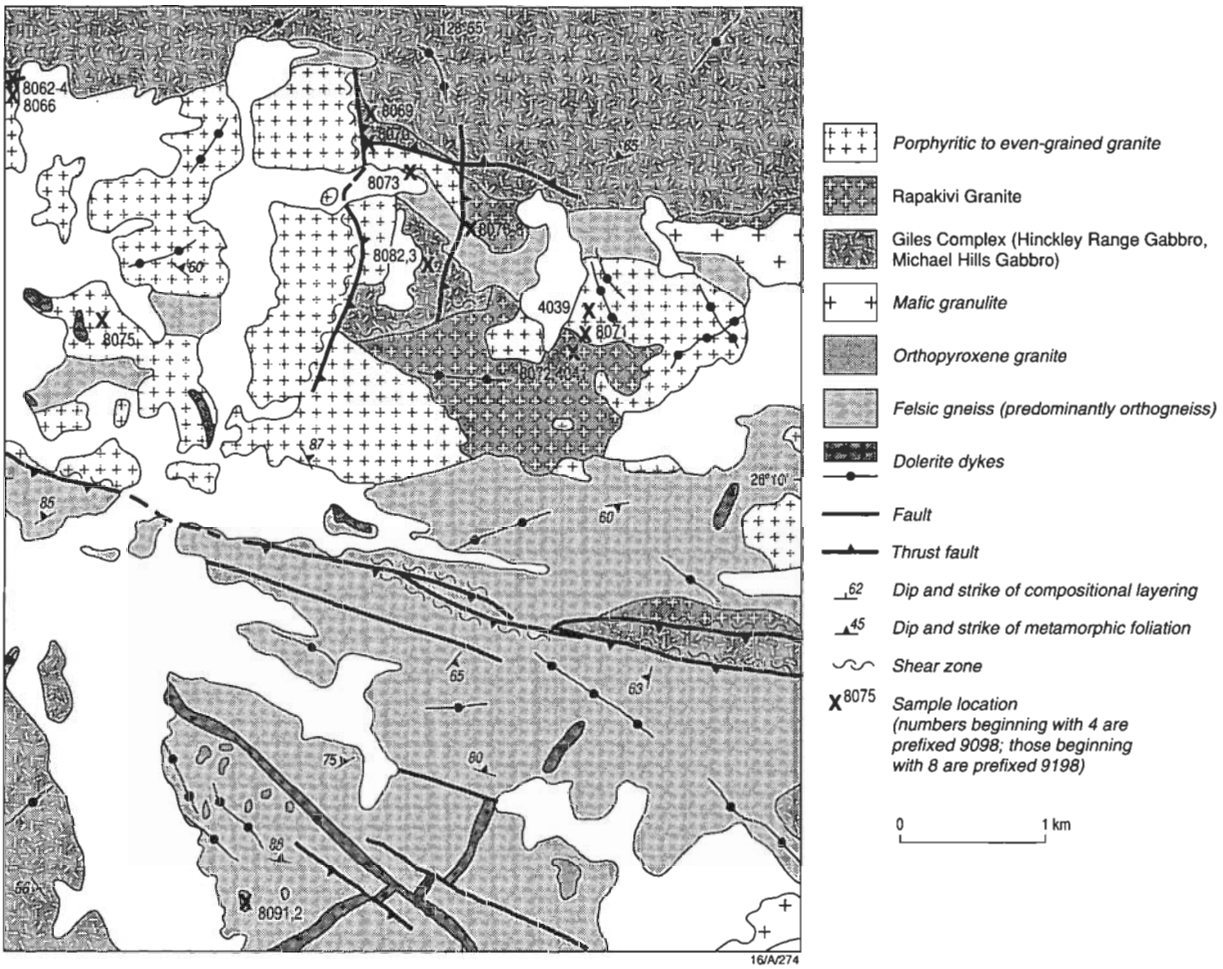

Figure 2. Geological map of the western Champ-de-Mars area, south of the Hinckley Range (after Glikson et al. 1995—this issue), showing sample localities for intrusive rocks. Sample numbers starting with 4 are prefixed '9093'; those starting with 8 are prefixed '9198'.

more abundant than (commonly antiperthitic) oligoclase–andesine. Accessory minerals comprise Fe–Ti oxides, apatite, and zircon. These pre-D_2 granitoids are petrographically distinct from post-D_2 orthopyroxene granitoids, with more biotite and hornblende, which are spatially associated with, and apparently genetically related to, the rapakivi/porphyritic granitoids (see below). Quartz monzodiorite intruding metamorphics southwest of Mount Davies contains more (5–7%) orthopyroxene and clinopyroxene (up to 3%), and feldspar is predominantly antiperthitic andesine; granophyric intergrowths of quartz and K-feldspar are conspicuous. Orthopyroxene granite in the Murray Range area contains mesoperthite.

Hornblende–biotite granitoids of the Hinckley Range area. These include the porphyritic and rapakivi granites in the Champ de Mars area, some with charnockitic affinities (Clarke et al. 1995—this issue), as well as granite dykes cutting Hinckley Range gabbronorite in the western Hinckley Range. Rapakivi granite forms stocks and dykes, commonly associated with, and gradational into, porphyritic and even-grained granite. This suggests that many of these petrographically rather diverse rocks are genetically closely related. However, not all are of the same age. A porphyritic granite has been dated at 1188±4 Ma, and a rapakivi granite, which clearly intrudes the Giles Complex, at about 1060 Ma, both by the U–Pb zircon ion microprobe technique (Sun et al. in press).

Rapakivi granite contains corroded megacrysts of perthitic K-feldspar (commonly microcline) rimmed by relatively fine-grained plagioclase, associated with or including hornblende, pyroxene, or quartz. However, the distribution of mantled K-feldspars is markedly irregular, and other K-feldspar, as well as oligoclase–andesine, phenocrysts are unmantled. Rapakivi granite, which grades into quartz monzonite, typically contains brownish-green hornblende (up to 10%) and reddish-brown biotite (up to 5%), with clinopyroxene (up to 3%) and minor orthopyroxene in some rocks. Accessories comprise apatite, zircon, Fe–Ti oxides, and ?chevkinite. Most granites were extensively recrystallised during D_3 and later events, more extreme deformation resulting in the formation of augen gneiss. Small amounts of pale golden garnet are widespread in the more deformed rocks, whereas pyroxene appears to be confined to less-deformed granitoids. Much, although by no means all, the biotite and hornblende forms fine-grained aggregates with quartz, presumably replacing pyroxene.

Porphyritic to even-grained granite is petrographically quite similar to the rapakivi granite, apart from the absence of mantled K-feldspars, and perthitic K-feldspar phenocrysts are commonly partly resorbed. Up to 4 per cent of dark brownish-green primary or paler green secondary hornblende is present in some granites, whereas dark brown to reddish-brown biotite (up to 4%) is ubiquitous; orthopyroxene (up to 2%) and relict clinopyroxene occur in a few rocks. Many granites are much recrystallised and small amounts of secondary garnet are common. Accessory minerals comprise Fe–Ti oxides, apatite, zircon, allanite, and, less commonly, sphene.

Locally porphyritic granite dykes which intrude the Hinckley Range gabbronorite in the western Hinckley Range contain biotite (up to 2%), hornblende (up to 3%), and rare clinopyroxene, as well as accessory Fe–Ti oxides, apatite, zircon, sphene, and rare allanite and ?chevkinite. They may be related to the younger hornblende–biotite granitoids, having given a

U–Pb zircon age (~105211 Ma) similar to that of the Tollu Group felsic volcanics (Sun et al. in press).

Quartz syenite of Mount Aloysius. Several small (~100 m across) stocks of quartz syenite crop out on the western side of Mount Aloysius. The rocks are bluish-grey and unfoliated, and contain clinopyroxene with exsolved blebs and lamellae of orthopyroxene (possibly after pigeonite: ~5%), fayalite (~1%), and minor orthopyroxene, greenish-brown hornblende, and biotite. Orthopyroxene also occurs as granular rims (with clinopyroxene) around primary clinopyroxene. Abundant accessory minerals include Fe–Ti oxides, apatite, zircon, ?chevkinite, and fluorite; K-feldspar is strongly perthitic. Although there is little evidence of deformation and recrystallisation, the quartz syenite appears to be of similar age (~1190 Ma) to the older hornblende–biotite granitoids (Sun et al., in press).

Granitic rocks of the basement to the Bentley Supergroup. The basement to the predominantly volcanic Bentley Supergroup in the westernmost Musgrave Block consists mainly of biotite granite. Typical rocks contain dark brown biotite (up to 3%), quartz, slightly perthitic microcline, sericitised oligoclase, and minor Fe–Ti oxides, apatite, zircon, sphene, and, less commonly, allanite, ?chevkinite, and fluorite. Some granites contain K-feldspar phenocrysts and many are foliated. Secondary epidote, chlorite, and muscovite are common. A distinctive hornblende granite (AGSO sample 91988006) which crops out about 6 km south of Bell Rock is closely associated with, and may actually intrude (although the contact is not exposed) the Smoke Hill Volcanics. It contains conspicuous fluorite and is quite strongly foliated, with minor secondary garnet.

Tollu Group felsic volcanics. The Tollu Group consists mainly of mafic to felsic volcanic rocks with basal sandstone and conglomerate, unconformably overlying metamorphic and granitic basement rocks (Daniels 1974; Giles 1981).

The 1078±5 Ma Smoke Hill Volcanics are largely felsic, but include subordinate mafic and intermediate rocks. Rhyolites (according to the total alkali–SiO_2 classification of Le Maitre 1989), grading into dacite and trachydacite, predominate. Dacitic rocks contain phenocrysts of partly sericitised sodic plagioclase and clinopyroxene (largely altered to amphibole) in a fine-grained quartzo-feldspathic matrix with abundant magnetite (Giles 1981). One dacite contains about 12 per cent of epidote. Rhyolites are K-feldsparplagioclase(albite–oligoclase)quartz-phyric and contain dark green hornblende (fine-grained aggregates or prismatic crystals: up to 5%), with smaller amounts of dark brown biotite, stilpnomelane (in one sample), opaque minerals, sphene, apatite, zircon, and secondary chlorite, epidote, and garnet. The quartzo-feldspathic groundmass is invariably recrystallised, phenocrysts are commonly broken or partly recrystallised, and many rocks have a strong lamination (probably largely primary, but tectonically modified in some rocks). However, relict eutaxitic structures, devitrification textures, and the presence of intercalated crystal and lithic tuffs attest to a pyroclastic origin for at least some of the volcanics (Giles 1981).

A slightly porphyritic trachyte vein cutting Mummawarrawarra Basalt at McDougall Bluff comprises rare altered alkali feldspar phenocrysts in a trachytic groundmass with minor quartz, opaque minerals, and fluorite.

Geochemistry

Forty-six samples of felsic gneiss and 86 intermediate to felsic igneous rocks (including Smoke Hill felsic volcanics) were analysed for major and trace elements. FeO was determined volumetrically; Li, Be, and Ag by atomic absorption spectrophotometry; and the remaining elements by X-ray fluorescence spectrometry (XRF), using the methods of Norrish & Hutton (1969) and Norrish & Chappell (1977). Further details of methods and accuracy are given by Cruikshank & Pyke (1993). For reasons of space, only representative analyses are given in Tables 1–3, but a complete list is available from the first author.

Felsic orthogneiss

Chemical data (Tables 1–3, Fig. 3), mainly for rocks from the western Hinckley Range area, are consistent with a felsic igneous origin for most orthopyroxene-bearing gneisses, which are metaluminous or only slightly peraluminous. ASI (alumina-saturation index: molecular $Al_2O_3/(CaO - 3.33P_2O_5 + Na_2O + K_2O)$ values are less than 1.1 (Fig. 3), so they are equivalent to I-type (derived by partial melting of igneous precursors) granitoids on the classification of Chappell & White (1974). However, it is unclear whether they represent metamorphosed intrusive or extrusive rocks. More massive orthogneisses may well be intrusive, whereas many of those interlayered with metasedimentary rocks could be of volcanic origin.

Many orthopyroxene-bearing gneisses (mostly granodioritic to granitic) belong to the Y- (and heavy rare-earth elements: HREE) depleted suite of Sheraton & Black (1983) (Fig. 5),

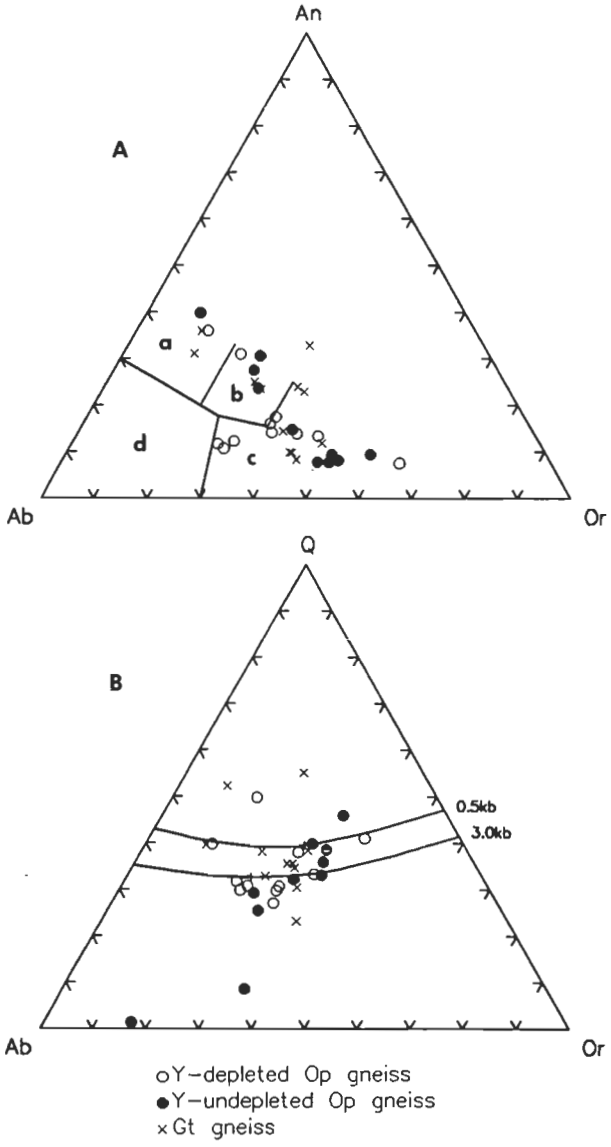

Figure 3. A—Normative Ab–Or–An diagram for felsic gneisses, showing the a, tonalite; b, granodiorite; c, granite; and d, trondhjemite fields of Barker (1979). B—Normative Q–Ab–Or diagram, showing quartz–feldspar field boundaries and positions of quaternary isobaric minima at 0.5 and 3.0 kb P_{H2O} (after Tuttle & Bowen 1958).

which is thought to represent new (i.e. primary) continental crust derived by partial melting of a hornblende±garnet-bearing, but feldspar-poor, mafic source (such as subducted hydrated oceanic crust or a mafic underplate). Y-depleted gneisses tend to have high Sr and Ce/Y (Fig. 6), and spidergrams show little or no Sr depletion (Fig. 7), because plagioclase was not a major residual (nor presumably a fractionating) phase; some show marked positive Sr anomalies. Zircons from one such gneiss from Mount Aloysius indicate a protolith age of about 1550 Ma and metamorphic age of about 1200 Ma (U–Pb ion-microprobe data: Sun et al. in press).

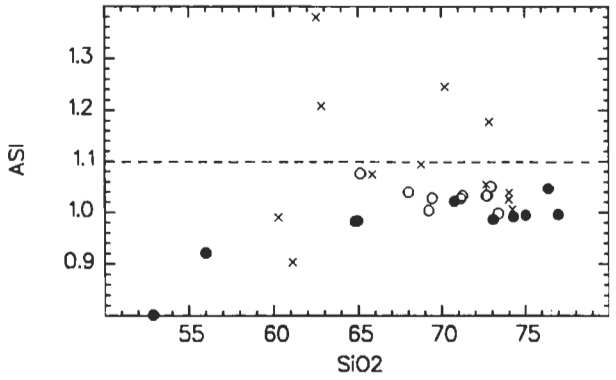

Figure 4. Plot of alumina saturation index (ASI = molecular $Al_2O_3/(Na_2O+K_2O+CaO-3.33P_2O_5)$) against SiO_2 for felsic gneisses. The dashed line separates the fields of I-type (igneous-derived; lower field) and S-type (sedimentary-derived) granitiods of Chappell & White (1974). Some garnet-bearing gneisses are markedly peraluminous. Symbols as in Figure 3.

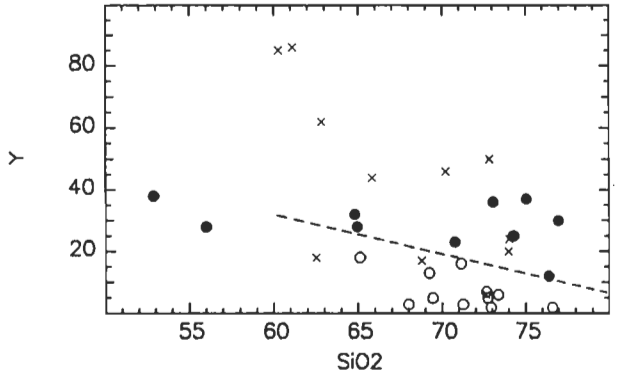

Figure 5. Plot of Y against SiO_2 for felsic gneisses. Dashed line indicates the approximate boundary between fields of Y-depleted (lower field) and Y-undepleted felsic orthogneisses of the Archaean Napier Complex, Enderby Land, Antarctica (after Sheraton & Black 1983). Symbols as in Figure 3.

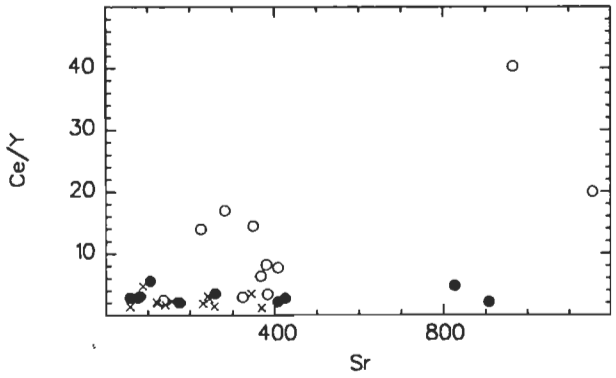

Figure 6. Plot of Ce/Y against Sr for felsic gneisses. Y-depleted orthogneisses commonly have high Sr and Ce/Y, consistent with derivation by partial melting of a hornblendegarnet-bearing mafic source. Symbols as in Figure 3.

In contrast, many (predominantly granitic) gneisses are not depleted in Y (nor presumably HREE) (Fig. 5), and these probably mainly represent partial melts of predominantly felsic crustal rocks. They tend to have low Sr and Ce/Y (Fig. 6), and spidergrams, particularly for the more fractionated siliceous granites, have significant negative Sr anomalies (Fig. 7), consistent with residual plagioclase and/or plagioclase fractionation. However, two high-Sr gneisses, which have quartz monzodioritic and dioritic compositions without significant Sr anomalies, were probably derived by melting and subsequent fractionation of a mantle source. A Y-undepleted granitic gneiss from west of Mount Davies has given zircon U–Pb ion-microprobe ages of 1305±8 and 1223±7 Ma, attributed, respectively, to those of the igneous protolith and high-grade metamorphism (Sun et al. in press).

Many garnet-bearing gneisses also have near-minimum melt (i.e. granitic, s.s.) compositions (Fig. 3), suggesting that, like the orthopyroxene gneisses, they are orthogneisses. This is supported by their only slightly peraluminous compositions (ASI 1.0–1.1: Fig. 4). However, other garnet gneisses are more strongly peraluminous and some are relatively quartz-rich,

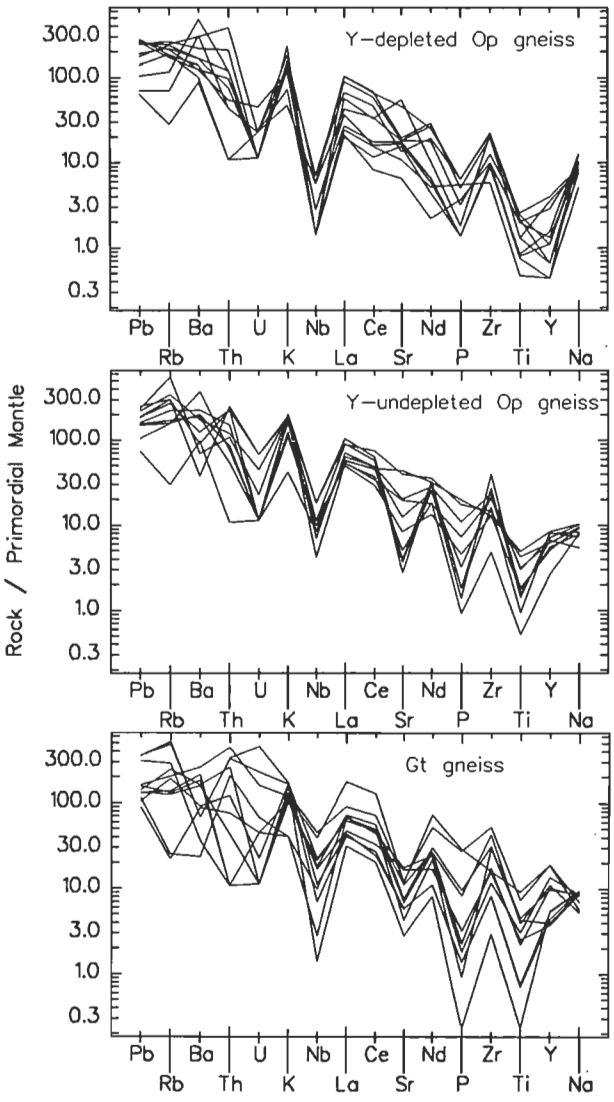

Figure 7. Primordial mantle-normalised incompatible element abundance diagrams (spidergrams) for felsic gneisses. Normalising values (Pb, 0.20; Rb, 0.63; Ba, 6.91; Th, 0.092; U, 0.022; K, 230; Nb, 0.71; La, 0.70; Ce, 1.81; Sr, 20.9; Nd, 1.35; P, 95; Zr, 11.1; Ti, 1270; Y, 4.52; Na, 2890 ppm) after Sun & McDonough (1989). Most Y-depleted orthogneisses do not have significant Sr anomalies, whereas Y-undepleted orthogneisses have marked negative Sr anomalies, consistent with partial melting of felsic crustal rocks.

more consistent with a sedimentary origin. Most analysed garnet gneisses have relatively high Y, but low Sr and Ce/Y (Figs 5, 6), typical of both felsic igneous rocks formed by intracrustal melting and clastic sedimentary rocks derived therefrom (Tarney et al. 1987); spidergrams show marked negative Sr anomalies (Fig. 7).

Unlike many other granulite terranes, which appear to have undergone depletion in large-ion lithophile elements (LILE: K, Rb, Th, U, etc.) during metamorphism (Tarney et al. 1972), K/Rb ratios are not particularly high (mostly 200–300), implying little loss of Rb relative to K. However, this may reflect the rarity of K-feldspar-free rocks (e.g. tonalitic gneisses) which, because they do not contain a phase capable of retaining much Rb, are the most susceptible to such depletion (Tarney & Windley 1977). The only analysed tonalitic orthogneiss has a K/Rb ratio of 609. On the other hand, as pointed out by Gray (1977), Th/U ratios are much higher (up to about 80) than the estimated crustal average (~3.8: Taylor & McLennan 1985), consistent with metamorphic depletion of U, possibly during dehydration.

Orthopyroxene granitoids

All the analysed orthopyroxene granites (Table 3, Fig. 8) are I-type. They are metaluminous or only slightly peraluminous (ASI < 1.1) and define a trend of increasing ASI with SiO_2 (Fig. 9). Most rocks do not show depletion in Y (and, by implication, HREE) (Figs 10,11), and spidergrams are markedly irregular, with negative Nb, Sr, P, and Ti anomalies (Fig. 12). These features are consistent with melting of plagioclase-rich, predominantly felsic crustal rocks (Tarney et al. 1987; Sheraton & Black 1988). In contrast, quartz monzodiorites intruding metamorphic rocks in the Mount Davies area do not have Sr anomalies (Fig. 12), and probably represent new felsic crust derived either directly from the mantle (Stern & Hanson 1991), by fractionation of mantle-derived magma or by hydrous melting of a plagioclase-poor mafic source (e.g. amphibolite) (Sheraton & Black 1983). Most orthopyroxene granites have lower Rb, Th, U, Zr, Nb, La, Ce, Y, and Ga/Al and higher K/Rb than the hornblende–biotite granitoids of the Champ de Mars area (Fig. 10), and are, therefore, unrelated. Indeed, as already pointed out, most or all are significantly older (pre-D_2).

Hornblende–biotite granitoids of the Hinckley Range area

There are no clear chemical differences between the various hornblende–biotite granitoids in the Champ de Mars area, even though rocks of significantly different ages are present. Rapakivi and porphyritic to even-grained granites have, with few exceptions, similar ranges of SiO_2 and trace element abundances, although both types are compositionally rather varied. However, as a group, they tend, for a given SiO_2 content, to be more enriched in many incompatible elements (Rb, Th, U, Zr, Nb, La, Ce, and Y) than the pre-D_2 orthopyroxene granites (Fig. 10), which could be explained by either derivation from a different source or lower degrees of melting of a similar source. Like these orthopyroxene granites, they are metaluminous or slightly peraluminous (I-type) (Fig. 9) and show a K-rich trend on an Ab–Or–An diagram (Fig. 8). High HFSE (high field strength elements: Zr, Nb, Y), LREE, and Ga/Al compared to most granites suggest A-type ('anorogenic') affinities (Collins et al. 1982; Whalen et al. 1987), in common with other rapakivi granites (Rogers & Greenberg 1990). However, *mg* (atomic 100Mg/(Mg + Fe^2)) values (17–48) are not as low as for typical A-types, suggesting that they are not truly anorogenic. Like most rapakivi granites, they are Sr-depleted and Y-undepleted (Fig. 11) and have irregular spidergrams (large negative Nb, Sr, P, and Ti anomalies: Fig. 13), typical of melts derived from felsic crust.

Most of these features are explicable in terms of relatively high-temperature partial melting of virtually anhydrous granulite facies crustal rocks, probably, in some cases, caused by emplacement of Giles Complex mafic–ultramafic intrusions. For example, Zr is relatively soluble in high-temperature melts (Watson & Harrison 1983). Although high Th/U (mostly 10–25) is consistent with melting of a granulite facies source, absolute abundances of Th and U are much higher than in typical granulite facies gneisses, ranging up to 158 and 28 ppm, respectively. This feature suggests derivation from a different source (or at least the presence of a distinct ?mantle-derived source component) to that of the orthopyroxene granitoids, because degrees of melting are unlikely to have been significantly lower for these comparatively melanocratic granitoids. Nd isotopic data are consistent with melting of felsic crustal rocks presently exposed in the area, which have similar depleted mantle (DM) model ages (1610–1900 Ma) to those of the

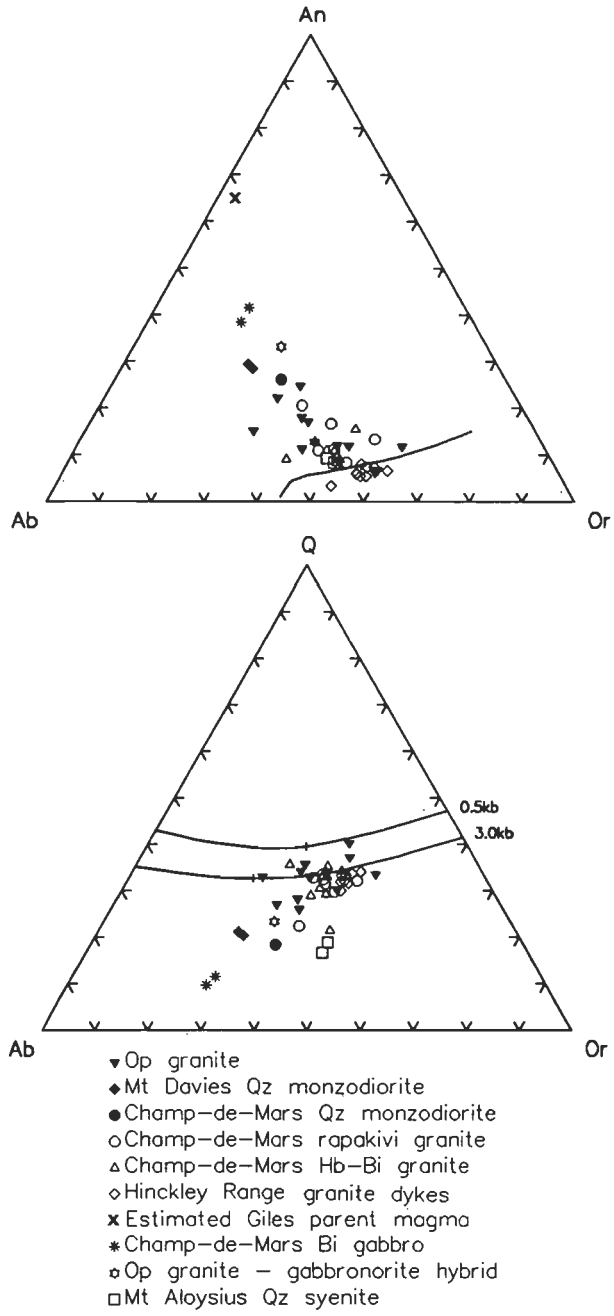

Figure 8. Normative Ab-Or–An and Q–Ab–Or diagrams for granitoids from the Tomkinson Ranges. The former shows the plagioclase–alkali feldspar field boundary at 1 kbar P_{H2O}, projected onto the Ab–Or–An face of the tetrahedron (after James & Hamilton 1969).

granitic rocks (1680–1860 Ma: Sun et al. in press). The relatively potassic compositions of many Champ de Mars granites (Fig. 8) are consistent with the experimental data of Ebadi & Johannes (1991) and Beard et al. (1994), which show that low P_{H2O} melting of felsic crustal rocks produces liquids with high Or/Ab; incorporation of calcic plagioclase (i.e. the An component) into the melt would enhance this effect (James & Hamilton 1969).

Clarke et al. (1995—this issue) suggest that some of the less siliceous rapakivi granitoids may have formed by contamination of more felsic magma (which produced the porphyritic granite) by gabbroic material. Nd isotopic data lend some support to this proposal, because rapakivi granites have slightly younger Nd T_{DM} model ages and higher $_{Nd}$ (1675–1787, and –1.4 to –3.1, respectively) than porphyritic granites (1877 & 1912, and –3.6 & –3.7) (Sun et al. in press). However, apart from the few SiO_2-poor quartz monzonites and quartz monzodiorites, the rapakivi and porphyritic hornblende-biotite granitoids show a wide, but broadly similar range of SiO_2 content (~65–75%). The two least siliceous (i.e., intermediate) rocks (sample 91988073, an orthopyroxene–biotite–clinopyroxene quartz monzodiorite and sample 91988072, a rapakivi biotite–hornblende quartz monzonite) have abundances of many elements consistent with formation by mixing of mafic and felsic end-members, but contents of other elements do not support such a model. In particular, TiO_2, P_2O_5, Zr, Nb, Y, La, and Ce are too high and Al_2O_3, MgO, Cr, and Ni too low for simple mixing. This contrasts with a sample (91988063) of porphyritic gabbronorite containing irregular veins and patches of orthopyroxene granite (i.e., a quartz monzodioritic bulk composition), which has the chemistry (and $\varepsilon_{Nd} = -1.5$) expected of such a hybrid. For example, Cr and Ni are much higher and TiO_2, P_2O_5, Zr, Nb, Y, La, and Ce are lower in this mixed rock than in the other intermediate rocks. A more complex origin for the various intermediate to felsic intrusives is thus indicated.

Spidergrams (Fig. 13) of these two intermediate intrusive rocks (as well as the least siliceous rapakivi granite, sample

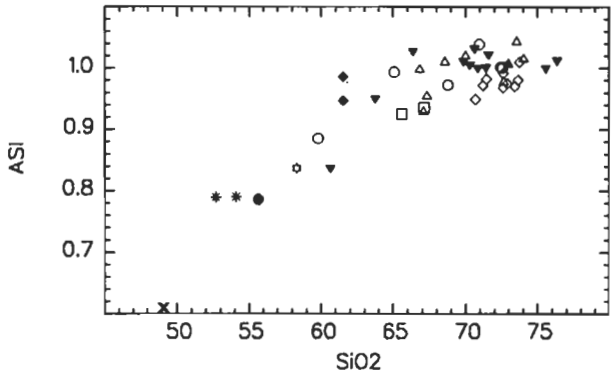

Figure 9. Plot of alumina saturation index against SiO_2 for granitoids from the Tomkinson Ranges. Symbols as in Figure 8.

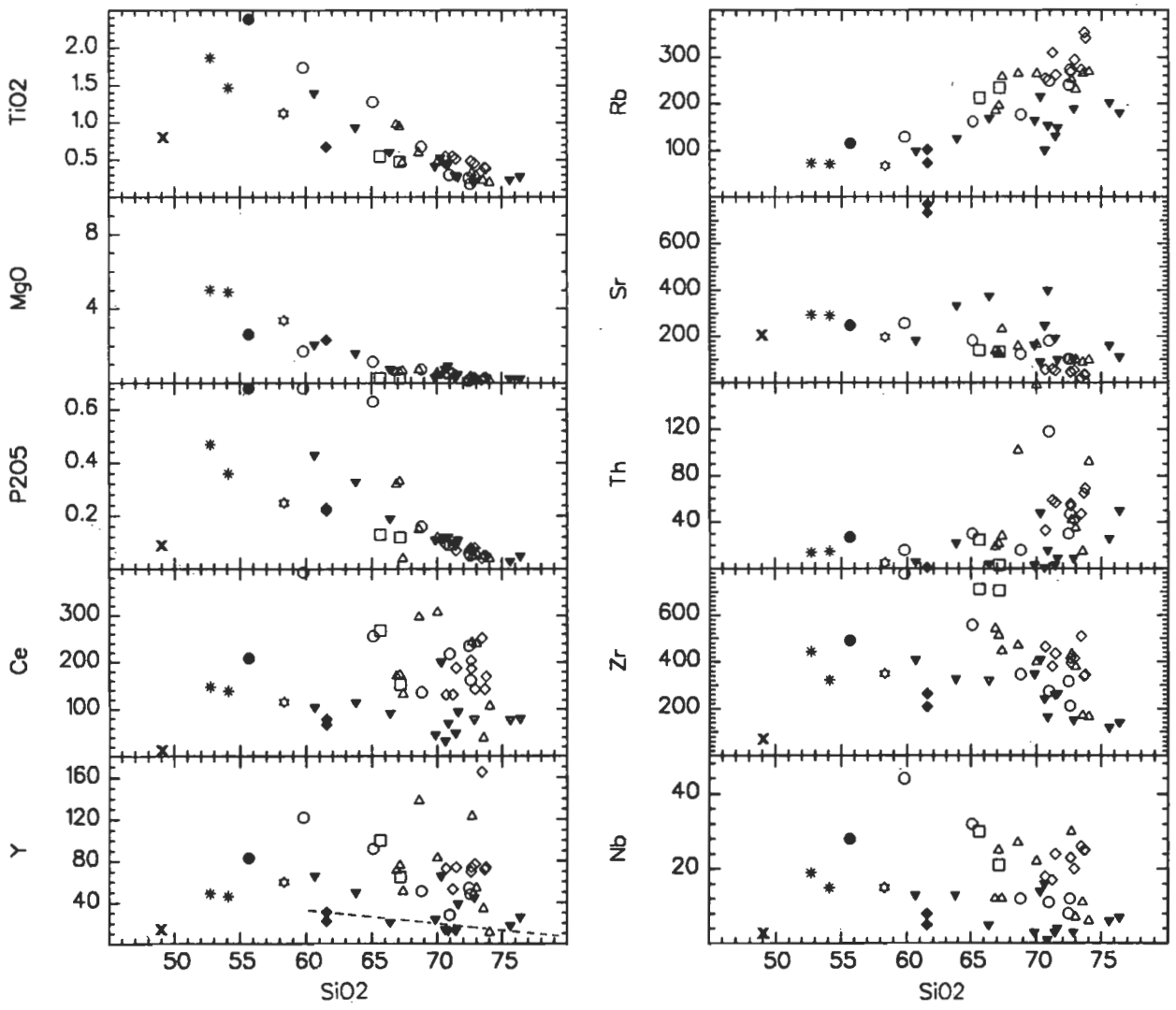

Figure 10. SiO_2 variation diagrams for granitoids from the Tomkinson Ranges. Symbols as in Figure 8 and boundary between Y-depleted and Y-undepleted orthogneisses from Sheraton & Black (1983).

Table 1. Chemical analyses of representative felsic gneisses from western Musgrave Block.

Sample no.	90984005	91988087	91989009	90984007	90984057	91988015	90984019	91988033
Locality	Mount Aloysius (central)	Western Champ-de-Mars	Murray Range	Western Champ-de-Mars	Western Champ-de-Mars	Mount Aloysius (east)	Mount Aloysius (central)	Mount Aloysius (south)
Lithology	Op-Kf-Qz-Pl gneiss	Bi-Op-Pl-Qz-Kf gneiss	Bi-Op-Mp gneiss	Bi-Hb-Op-Qz-Kf-Pl gneiss	Bi-Hb-Op-Qz-Mp gneiss	Op-Cp-Qz-Kf-Pl gneiss	Op-Gt-Pl-Qz-Kf gneiss	Bi-Gt-Qz-Mp gneiss
Group	Y-dep.	Y-dep.	Y-dep.	Y-undep.	Y-undep.	Y-undep.	Y-undep.	Y-undep.
SiO_2	65.14	73.37	69.45	64.97	74.28	56.01	68.79	74.00
TiO_2	0.55	0.42	0.52	0.67	0.37	0.90	0.53	0.15
Al_2O_3	15.86	13.30	15.05	16.36	13.10	17.07	15.71	13.90
Fe_2O_3	1.51	0.85	1.35	2.22	0.78	2.92	0.88	0.66
FeO	4.57	0.76	1.10	2.19	0.47	4.63	2.42	0.46
MnO	0.10	0.03	0.08	0.11	0.03	0.13	0.04	0.03
MgO	2.45	0.62	0.78	1.43	0.47	4.35	1.03	0.16
CaO	4.29	1.86	2.13	4.16	1.41	5.61	3.18	1.34
Na_2O	3.45	3.29	3.98	3.73	3.04	3.58	3.42	3.70
K_2O	1.32	4.36	4.21	3.06	5.44	3.09	2.88	4.71
P_2O_5	.07	0.08	0.14	0.16	0.10	0.38	0.07	0.03
LOI	.51	0.34	0.29	0.45	0.40	0.52	0.44	0.31
Rest	.20	0.15	0.26	0.31	0.20	0.52	0.27	0.16
Total	100.02	99.43	99.34	99.82	100.09	99.71	99.66	99.61
	C.I.P.W. norms							
Q	24.45	32.85	24.77	20.54	32.41	4.58	28.40	31.38
C	1.12	-	0.41	-	-	-	1.35	0.35
Or	7.80	25.76	24.88	18.08	32.15	18.26	17.02	27.83
Ab	29.19	27.84	33.68	31.56	25.72	30.29	28.94	31.31
An	20.83	8.65	9.65	18.86	6.03	21.38	15.32	6.45
Di	-	0.05	-	0.59	0.24	3.20	-	-
Hy	12.52	1.58	2.14	4.56	1.06	14.12	5.47	0.51
Mt	2.19	1.23	1.96	3.22	0.54	4.23	1.28	0.96
Il	1.04	0.80	0.99	1.27	0.70	1.71	1.01	0.28
Ap	0.17	0.19	0.33	0.38	0.24	0.90	0.17	0.07
mg	48.9	59.3	55.8	53.8	64.1	62.6	43.1	38.3
	Trace elements in parts per million							
Ba	614	694	1135	1391	862	2565	1258	474
Li	15	11	33	11	6	8	11	12
Rb	18	116	137	100	171	99	82	326
Sr	383	138	282	407	176	827	345	121
Pb	13	28	38	30	37	21	31	72
Th	<2	<2	7	8	21	7	<2	31
U	0.5	<0.5	<0.5	<0.5	<0.5	<0.5	1.0	10
Zr	140	112	241	228	145	160	175	92
Hf	2	4	7	6	5	8	4	5
Nb	4	<2	5	7	8	8	12	8
Y	18	6	5	28	25	28	17	20
La	30	15	47	38	35	62	33	31
Ce	62	15	85	62	53	135	60	44
Nd	24	3	26	24	18	48	23	15
Pr	4	<2	10	8	6	15	<2	<2
Sc	20	6	7	15	7	18	11	3
V	107	22	16	60	11	130	61	7
Cr	31	7	3	14	4	62	73	1
Ni	10	6	3	6	3	28	17	2
Cu	5	2	<1	4	<1	20	7	<1
Zn	66	29	51	67	20	85	63	35
Sn	<2	3	8	4	3	2	<2	5
Ga	16	13	16	18	14	20	21	21
S	<100	100	20	100	70	100	<100	10
Be	1	<1	2	3	1	4	1	2

mg, atomic $100Mg/(Mg+Fe^{2+})$; LOI, loss on ignition.
Bi, biotite; Cp, clinopyroxene; Fl, fluorite; Gt, garnet; Kf, K-feldspar; Mp, mesoperthite; Op, orthopyroxene; Pl, plagioclase; Qz, quartz.

Table 2. Chemical analyses of representative gabbroic and granitic rocks from the Tomkinson Ranges. Abbreviations as in Table 1.

Sample no.	91980267A	91985001A	91988092	91988100		91988082	91988063	91988073
Locality	SW of Mount Davies	North of Ewarara Range	Western Champ-de-Mars	Western Champ-de-Mars	Estimated Giles Complex parent	Western Champ-de-Mars	Western Champ-de-Mars	Western Champ-de-Mars
Lithology	Bi-Cp-Op grano-diorite	Cp-Op granite gneiss	Foliated Op granite	Porphyrit. Op granite	magma*	Cp-Op-Bi-Hb gabbro	Granite/ granulite hybrid	Op-Bi-Cp quartz monzodior.
SiO_2	61.54	69.85	75.60	72.85	49.0	52.70	58.33	55.66
TiO_2	0.68	0.42	0.24	0.20	0.8	1.87	1.13	2.38
Al_2O_3	17.20	14.40	12.40	13.75	14.0	15.32	15.44	13.96
Fe_2O_3	2.20	1.48	0.45	1.00	-	2.39	3.43	2.98
FeO	3.00	1.25	0.54	1.14	11.0	8.62	4.91	7.71
MnO	0.07	0.05	0.02	0.05	0.17	0.16	0.12	0.14
MgO	2.35	0.32	0.26	0.30	12.0	5.02	3.39	2.63
CaO	5.04	1.79	0.83	1.59	11.0	7.72	6.14	6.10
Na_2O	3.93	2.95	2.56	3.53	1.6	2.79	2.85	2.96
K_2O	2.85	5.90	6.23	4.74	0.3	1.75	2.95	3.16
P_2O_5	0.23	0.11	0.03	0.07	0.09	0.47	0.25	0.68
LOI	0.44	0.41	0.32	0.35	-	1.15	0.68	0.88
Rest	0.48	0.29	0.18	0.17	-	0.38	0.32	0.46
Total	100.01	99.22	99.66	99.74	-	100.34	99.94	99.70
O=F,S,Cl	0.04	0.00	0.00	0.00	-	0.03	0.01	0.05
Total	99.96	99.22	99.66	99.74	-	100.30	99.93	99.65
	C.I.P.W. norms							
Q	13.46	25.90	34.67	30.05	-	4.44	12.67	9.86
C	-	0.17	0.01	0.09	-	-	-	-
Or	16.84	34.86	36.81	28.01	1.8	10.34	17.43	18.67
Ab	33.25	24.96	21.66	29.87	13.5	23.61	24.12	25.05
An	20.87	8.16	3.92	7.43	30.1	24.11	20.62	15.47
Di	2.12	-	-	-	19.3	9.16	6.65	8.62
Hy	7.52	1.27	0.91	1.78	20.0	19.04	9.74	10.27
Ol	-	-	-	-	11.0	-	-	-
Mt	3.19	2.15	0.65	1.45	2.7	3.47	4.97	4.32
Il	1.29	0.80	0.46	.38	1.5	3.55	2.15	4.52
Ap	0.54	0.26	0.07	0.17	0.2	1.11	0.59	1.61
mg	58.3	31.3	46.2	31.9	69.6	50.9	55.2	37.8
	Trace elements in parts per million							
Ba	1725	1525	723	655	100	637	928	1042
Li	7	2	6	6	-	19	6	1
Rb	73	165	203	190	-	73	67	115
Sr	733	164	161	104	200	293	198	248
Pb	24	28	43	54	-	20	24	32
Th	<2	3	26	9	-	14	5	27
U	<0.5	<0.5	1.0	3.0	-	2.5	<0.5	1.5
Zr	264	349	121	152	70	444	350	491
Hf	6	11	2	3	-	10	9	11
Nb	8	3	6	3	3	19	15	28
Y	31	24	18	45	18	49	60	83
La	43	27	44	50	7	81	64	96
Ce	79	46	78	79	17	148	116	209
Nd	32	19	27	33	10	67	52	97
Pr	5	5	6	8	-	11	12	28
Sc	13	5	3	3	-	30	24	25
V	66	18	8	11	-	197	158	197
Cr	26	3	4	4	-	55	93	11
Ni	22	10	3	1	-	51	59	14
Cu	21	7	<1	<1	-	27	78	16
Zn	76	51	17	49	-	139	90	147
Sn	4	4	3	<2	-	<2	3	2
Ga	21	19	12	19	-	19	20	23
S	900	30	10	10	-	690	200	920
Be	3	1	<1	2	-	2	3	<1

* From Sun & Sheraton (1992); norm calculated assuming $Fe^{2+} = 0.85Fe^{total}$.

Table 2 (cont.)

Sample no.	91988064	91988072	91988076	90980506	90984039	91988070	91988060	91988044
Locality	Western Champ-de-Mars	Western Champ-de-Mars	Western Champ-de-Mars	Champ-de-Mars	Western Champ-de-Mars	Western Champ-de-Mars	West Hinckley Range	Mount Aloysius (west)
Lithology	Rapakivi Cp-Bi granite	Rapakivi Bi-Hb Qz monzonite	Rapakivi Cp-Bi-Hb granite	Foliated porphyrit. Bi granite	Porphyrit. Bi granite	Cp-Bi-Hb granite	Foliated Bi granite dyke	Ol-Hb-Cp quartz syenite
SiO_2	68.79	59.80	72.57	73.56	70.01	66.86	73.76	65.63
TiO_2	0.68	1.74	0.18	0.23	0.47	0.98	0.39	0.55
Al_2O_3	13.69	14.07	14.21	13.57	14.13	13.21	13.01	15.52
Fe_2O_3	2.77	2.23	0.76	0.55	1.38	3.42	1.44	1.17
FeO	1.40	6.29	0.55	0.85	1.63	2.93	0.63	3.31
MnO	0.06	0.12	0.02	0.02	0.05	0.10	0.02	0.09
MgO	0.74	1.73	0.15	0.28	0.57	0.60	0.30	0.27
CaO	2.17	4.49	1.25	1.23	1.64	2.36	.79	2.28
Na_2O	2.39	3.03	3.22	3.73	3.25	2.44	2.83	3.77
K_2O	6.08	4.04	6.24	4.39	5.37	5.27	6.38	6.22
P_2O_5	0.16	0.68	0.05	0.05	0.12	0.32	0.05	0.13
LOI	0.42	0.96	0.44	0.50	0.46	0.45	0.36	0.34
Rest	0.29	0.49	0.23	0.17	0.35	0.37	0.22	0.45
Total	99.64	99.67	99.87	99.13	99.43	99.31	100.18	99.73
O=F,S,Cl	0.00	0.00	0.00	0.00	0.00	0.00	0.00	0.01
Total	99.64	99.67	99.87	99.13	99.43	99.30	100.18	99.72
	C.I.P.W. norms							
Q	26.55	14.29	27.14	31.80	26.00	26.96	30.88	13.72
C	-	-	0.01	0.57	0.28	-	0.13	-
Or	35.93	23.87	36.87	25.94	31.73	31.14	37.70	36.76
Ab	20.22	25.64	27.25	31.56	27.50	20.65	23.95	31.90
An	8.67	12.86	5.87	5.78	7.35	9.53	3.59	7.06
Di	0.82	4.18	-	-	-	0.07	-	2.97
Hy	1.46	9.26	0.50	1.46	2.59	2.58	0.75	3.49
Ol	-	-	-	-	-	-	-	-
Mt	2.73	3.23	1.10	0.80	2.00	4.96	.96	1.70
Il	1.29	3.30	0.34	0.44	0.89	1.86	0.74	1.04
Ap	0.38	1.61	0.12	0.12	0.28	0.76	0.12	0.31
mg	48.5	32.9	32.7	37.0	38.4	26.7	45.9	12.7
	Trace elements in parts per million							
Ba	1187	1431	791	556	1123	1429	409	1622
Li	6	14	12	39	10	5	10	9
Rb	177	129	273	265	264	186	340	213
Sr	124	257	102	89	166	137	35	141
Pb	39	41	49	48	63	45	44	48
Th	16	16	47	15	158	19	69	25
U	1.0	2.5	2.0	1.0	9.5	1.0	10.5	<0.5
Hf	9	18	4	4	11	13	11	16
Zr	347	777	212	171	401	542	345	712
Nb	12	44	12	11	22	12	25	30
Y	51	122	48	34	83	71	74	100
La	74	172	78	20	106	87	94	136
Ce	136	393	162	39	307	171	170	268
Nd	58	168	67	18	95	81	61	119
Pr	12	37	18	4	22	19	16	27
Sc	8	22	4	2	6	12	5	6
V	36	112	5	8	23	22	12	2
Cr	9	8	<1	3	4	3	4	3
Ni	8	7	2	3	2	5	8	2
Cu	12	13	<1	<1	4	17	5	2
Zn	55	152	31	31	72	120	38	88
Sn	3	2	3	2	3	4	8	4
Ga	17	21	20	20	18	19	16	25
S	70	60	40	20	<100	70	20	180
Be	3	5	4	3	4	4	4	3

Table 3. Chemical analyses of representative granitic and volcanic rocks from the Bentley Supergroup and basement in the westernmost Musgrave Block. Abbreviations as in Table 1.

Sample no.	91988011	91989395	90984015	91988007	91988101	91988006	91988002	91989416
Locality	McDougall Bluff	McDougall Bluff	West of Mummawarr. Hill	McDougall Bluff	West of Bell Rock Range	West of Bell Rock Range	West of Bell Rock Range	Mount Jane
Lithology	Bi granite	Foliated Bi granite	Bi granite	Slightly porphyrit. Bi granite	Porphyrit. Fl-Bi granite	Porphyrit. Fl-Hb granite	Slightly porphyrit. rhyolite	Porphyrit. rhyolite
Group	Y-dep.	Y-dep.	Y-undep.	Y-undep.				
SiO2	74.37	72.97	74.54	68.00	73.22	72.38	68.61	71.85
TiO2	0.18	0.24	0.19	0.62	0.27	0.34	0.58	0.42
Al2O3	13.39	13.45	12.61	14.46	12.57	12.54	12.60	12.35
Fe2O3	0.93	0.81	0.63	1.94	0.84	2.26	3.08	1.82
FeO	0.15	0.49	1.10	1.16	1.13	1.15	2.45	1.63
MnO	0.04	0.04	0.04	0.05	0.02	0.05	0.06	0.06
MgO	0.17	0.32	0.10	0.89	0.22	0.11	0.18	0.15
CaO	0.99	0.79	0.93	2.34	1.13	1.01	1.66	0.94
Na2O	3.74	3.21	2.93	3.54	2.54	4.01	3.81	3.27
K2O	4.77	6.06	5.53	4.57	6.28	5.14	4.89	5.62
P2O5	0.05	0.06	0.03	0.22	0.05	0.01	0.07	0.08
LOI	0.45	0.37	0.79	0.75	0.95	0.42	0.63	0.51
Rest	0.16	0.19	0.22	0.41	0.37	0.36	0.55	0.37
Total	99.39	99.00	99.64	98.95	99.59	99.78	99.17	99.07
O=F,S,Cl	0.00	0.00	0.00	0.02	0.00	0.00	0.01	0.00
Total	99.39	99.00	99.64	98.94	99.59	99.78	99.16	99.07
	C.I.P.W. norms							
Q	32.13	29.11	33.70	24.22	31.56	27.93	24.67	29.27
C	0.39	0.32	0.19	-	-	-	-	-
Or	28.19	35.81	32.68	27.01	37.11	30.37	28.90	33.21
Ab	31.65	27.16	24.79	29.95	21.49	33.93	32.24	27.67
An	4.58	3.53	4.42	10.07	4.35	1.04	2.84	2.42
Di	-	-	-	0.08	0.78	0.59	3.05	1.46
Wo	-	-	-	-	-	1.32	0.57	-
Hy	0.42	0.80	1.51	2.18	1.12	-	-	0.53
Mt	0.09	1.01	0.91	2.10	1.22	2.88	4.47	2.64
Il	0.34	0.46	0.36	1.18	0.51	0.65	1.10	0.80
Ap	0.12	0.14	0.07	0.52	0.12	0.02	0.17	0.19
mg	66.9	53.7	13.9	57.8	25.8	14.6	11.6	14.1
	Trace elements in parts per million							
Ba	416	681	298	1358	562	680	1404	1388
Li	11	11	46	24	15	1	3	8
Rb	237	241	481	269	406	216	179	225
Sr	208	243	45	397	93	50	86	78
Pb	60	54	69	51	82	9	21	44
Th	36	30	131	63	225	49	41	40
U	4.0	2.5	14	8.0	37	7.0	5.5	4.5
Zr	116	138	217	327	330	826	1329	560
Hf	4	4	5	8	10	19	34	15
Nb	9	6	18	24	19	90	103	28
Y	10	6	75	58	58	197	205	110
La	47	43	108	150	339	153	150	114
Ce	65	76	187	216	578	316	328	210
Nd	21	17	55	69	177	144	161	90
Pr	4	7	18	18	52	37	39	22
Sc	2	1	3	6	4	1	3	5
V	7	7	<2	33	8	3	11	4
Cr	3	3	4	13	<1	2	2	3
Ni	2	3	1	6	2	<1	2	2
Cu	<1	<1	1	5	<1	3	30	6
Zn	28	32	37	78	40	67	160	96
Sn	3	6	15	8	14	23	16	6
Ga	19	15	21	21	17	37	38	19
S	20	20	<100	310	50	<100	200	50
Be	5	4	9	5	7	4	7	5

Table 3 (cont.)

Sample no.	91989403	91988014
Locality	McDougall Bluff	McDougall Bluff
Lithology	Porphyrit. trachyte	Slightly amygdal. basalt
Group		
SiO2	64.66	50.84
TiO2	0.07	1.33
Al2O3	15.71	13.46
Fe2O3	1.17	3.22
FeO	0.27	8.13
MnO	0.01	0.15
MgO	0.20	6.65
CaO	2.93	8.75
Na2O	5.64	2.26
K2O	5.62	1.34
P2O5	0.02	0.18
LOI	2.65	3.33
Rest	0.44	0.26
Total	99.39	99.90
O=F,S,Cl	0.01	0.00
Total	99.38	99.90
C.I.P.W. norms		
Q	6.73	3.95
C	-	-
Or	33.21	7.92
Ab	47.72	19.12
An	0.95	22.62
Di	1.07	15.98
Wo	5.04	-
Hy	-	19.08
Mt	0.70	4.67
Il	0.13	2.53
Ap	0.05	0.43
mg	56.9	59.3
Trace elements in parts per million		
Ba	75	369
Li	3	14
Rb	390	49
Sr	20	185
Pb	13	9
Th	82	6
U	6.5	0.5
Zr	1300	156
Hf	45	<2
Nb	420	5
Y	225	29
La	99	19
Ce	252	39
Nd	116	22
Pr	31	4
Sc	2	35
V	8	261
Cr	3	296
Ni	3	163
Cu	5	115
Zn	6	108
Sn	41	<2
Ga	51	19
S	250	80
Be	23	3

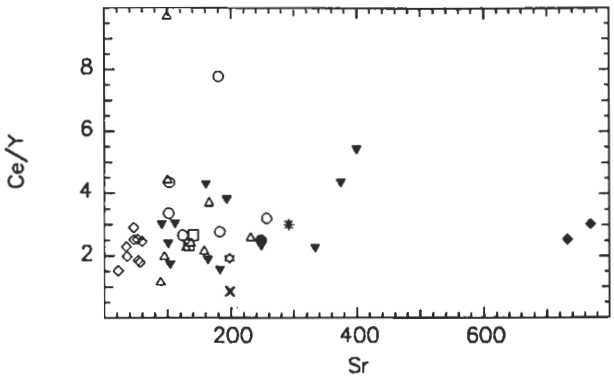

Figure 11. Plot of Ce/Y against Sr for granitoids from the Tomkinson Ranges. Symbols as in Figure 8.

90984041) are quite similar to, although more enriched than, those of two unusually biotite±hornblende-rich gabbronorites (which have similar ε_{Nd} (–2.1) to the rapakivi suite) from a small body about 0.5 km south of the main Hinckley Range gabbronorite intrusion near Champ de Mars (Fig. 2). These biotite–hornblende gabbronorites are considerably older than the Giles Complex (11765 Ma: Sun et al. in press). They are much more enriched than the estimated Giles Complex parent magma (Sun & Sheraton 1992), as well as typical non-cumulate samples of Giles gabbronorites, which have much flatter patterns. This might indicate that the intermediate intrusives (quartz monzonites and quartz monzodiorites) were formed by either progressive contamination (with felsic crustal material) or fractionation of such an enriched gabbroic magma (cf. Sheraton et al. 1992). Trace-element contents and ratios are perhaps more consistent with the latter process, because incompatible element/Zr ratios (e.g., K/Zr, Ba/Zr, Nb/Zr, P/Zr, and Ce/Zr) are essentially constant for the whole range of compositions, whereas at least some of these ratios (e.g., P/Zr) would be expected to decrease upon contamination with felsic crust or a granitic melt. Of the two intermediate rocks, the quartz monzodiorite has a similar S content (920 ppm) to the postulated gabbronorite parent (~700 ppm), whereas the rapakivi quartz monzonite has much lower S (60 ppm), more typical of Giles Complex rocks. Unfortunately, without more geochronological data, it is difficult to make more definitive correlations between these various rock types.

Although the range of granitic (s.s.) rocks could, in theory, have been derived by mixing of an intermediate magma with a felsic end-member, this seems unlikely because intermediate compositions are much less common than felsic ones. Moreover, there appears to be a compositional gap between the intermediate and granitic rocks, and the latter have distinctive, much more irregular spidergrams with larger Nb anomalies (Fig. 13). Hence, we consider it more likely that most hornblende–biotite granites were derived from different parent magmas to that of the intermediate rocks (quartz monzodiorites and quartz monzonites). Some degree of contamination of felsic magma with mafic material may well have occurred, but much of the chemical variation of the granitic rocks is probably due to other processes, such as crystal fractionation, different extents of melting, cumulate unmixing (Cullers et al. 1993), or combinations of these. The marked decreases of both *mg* and K/Rb with increasing SiO_2 suggest at least some degree of fractional crystallisation.

Biotite–hornblende granite dykes in the western Hinckley Range are quite strongly fractionated (high K_2O, Rb, Th, U, Sn, and Rb/Sr, and low CaO, Na_2O, Ba, Sr, and K/Rb), with highly irregular spidergrams (Fig. 13). Although compositionally similar to the more evolved variants of the Champ de Mars rapakivi and porphyritic granites, they have higher Nb, Sn, and $_{Nd}$ (–1.6 & –2.4, i.e., 1 to 2 units higher than the latter at 1060 Ma), implying the presence of a younger source component.

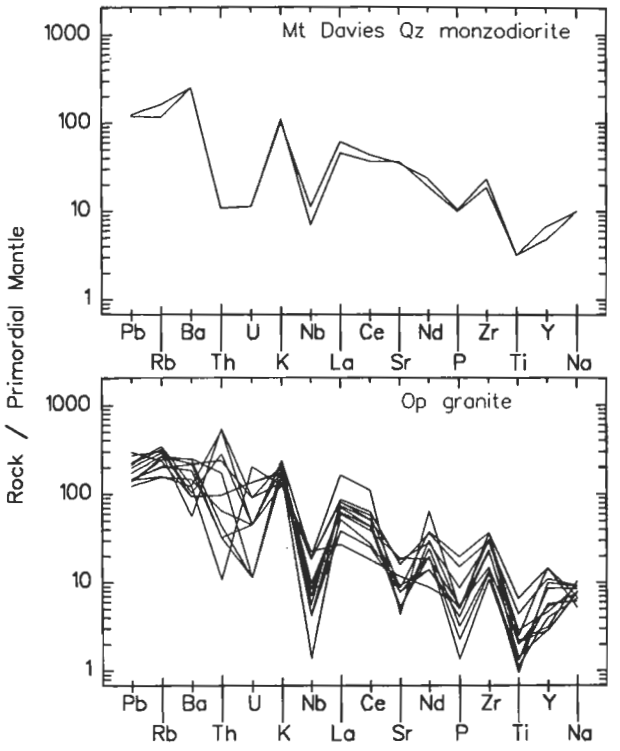

Fig.12. Spidergrams for orthopyroxene granitoids from the Tomkinson Ranges.

Quartz syenites of Mount Aloysius

The quartz syenites are highly fractionated (Fig. 14) rocks with high K_2O, Ba, Zr, Nb, Y, La, Ce, and Ga and low MgO, Sr, Cr, Ni, Sc, and V. High HFSE and Ga/Al, and low *mg* (12–13) are all characteristic of A-type granitoids, and are consistent with high-temperature melting of lower crustal granulites (Sheraton & Black 1988), although an origin by fractionation of mafic magma, possibly combined with crustal assimilation, has also been suggested for such syenitic rocks (see various papers in Fitton & Upton 1987; Zhao et al. in press). Unfortunately, the strong fractionation of the Mount Aloysius quartz syenites complicates attempts to estimate the composition of their parent magma, but the presence of 1300 Ma inherited zircons and ε_{Nd} of –2.0 (similar to those of country rock orthogneisses at 1200 Ma: Sun et al. in press) indicates a major crustal component in these rocks. Whatever their origin, the higher Zr (Fig. 10) and much lower *mg* compared to the rapakivi/porphyritic granitoids of the Champ de Mars area imply that they are unrelated.

Granitic rocks of the basement to the Bentley Supergroup

In many respects, most of these biotite granites are compositionally similar to the Champ de Mars granitoids, but tend to be more siliceous (all analysed samples are granite, s.s; Figs 15,17). They are also I-type (Fig. 16) and have the irregular spidergrams typical of intracrustal melts (Fig. 19). However, many rocks, in particular those from McDougall Bluff, differ in having higher Sr, Be, and Sn. Several of these are characterised by relatively low Zr, Nb, Y, La, and Ce and high Ce/Y (Figs 17,18); spidergrams show marked Y depletion and only very small negative Sr anomalies (Fig. 19). Hence, although quite siliceous (73.0–74.5% SiO_2), they cannot be related to any other Bentley Supergroup basement granites by crystal fractionation processes and were probably derived from a distinct, more plagioclase-poor (possibly hornblende±garnet-bearing mafic) source. They are thus equivalent to the Y-depleted suite of Sheraton & Black (1983) and, in contrast to most granitic rocks in the western Musgrave Block, they may represent new felsic crust.

Two fluorite-bearing biotite granites from southeast of Mummawarrawarra Hill have particularly high K_2O and Rb and low Na_2O, Sr, *mg*, and K/Rb, and were probably derived from a further distinct parent magma. One contains accessory allanite and has very high Th, U, La, and Ce. The fluorite–hornblende granite (sample 91988006) apparently represents yet another magma type. It has quite a different composition to all other analysed samples: low MgO, P_2O_5, Sr, Ni, Cr, Sc, V, Li, *mg* (15), and Ce/Y and high HFSE (Zr, Nb, Y), LREE, Sn, Ga, Ga/Al, and ε_{Nd} (+0.8 at 1080 Ma: Sun et al. in press); the spidergram is particularly irregular (fractionated)

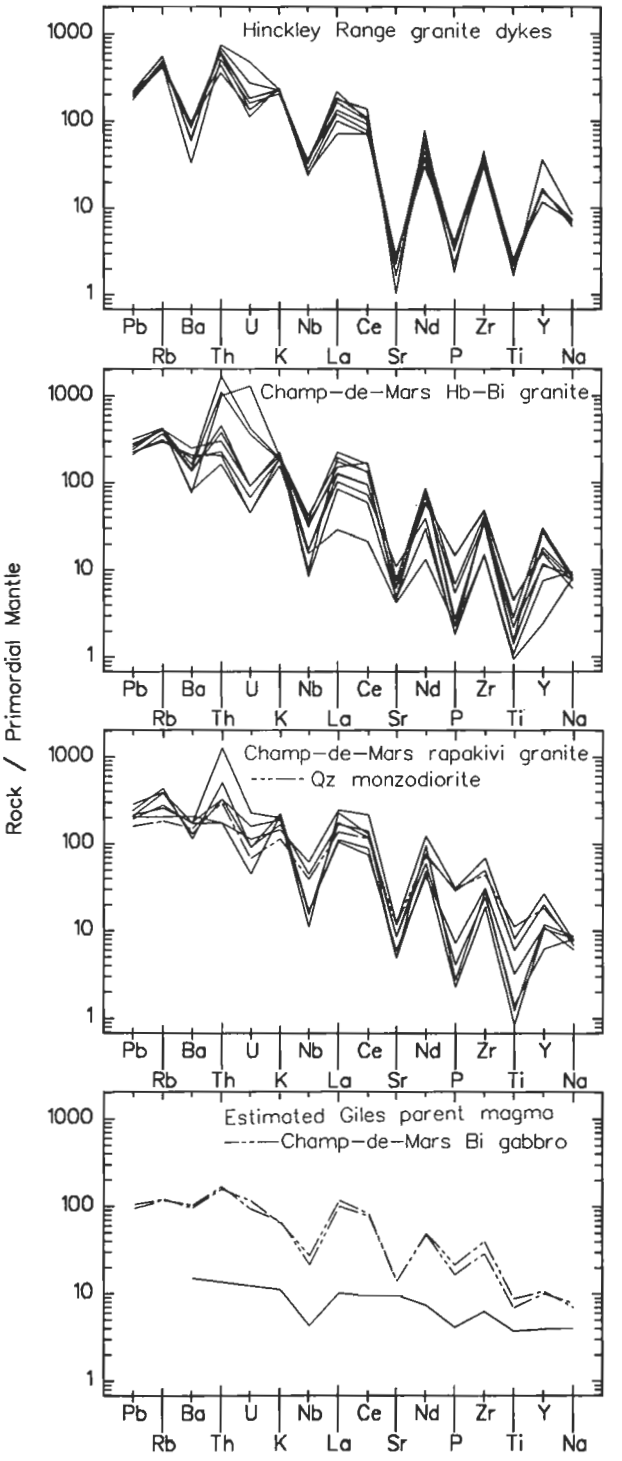

Fig.13. Spidergrams for gabbroic rocks and granitoids from the Hinckley Range area.

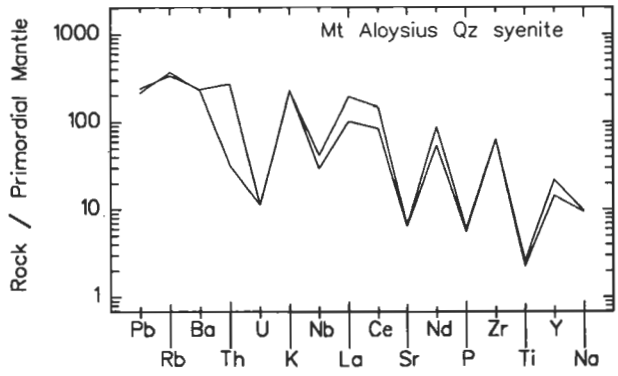

Figure 14. Spidergrams for quartz syenites from Mount Aloysius.

(Fig. 19). Such features are characteristic of A-type granitoids and can be explained by high-temperature melting of dry (but possibly F-rich) granulite facies felsic crustal rocks (Collins et al. 1982; Sheraton & Black 1988). Alternatively, derivation by fractionation of a mafic parent magma is possible; both models are considered in the discussion of the compositionally and isotopically almost identical rhyolites of the Smoke Hill Volcanics, which are clearly the extrusive equivalents of the granite (see next section).

Tollu Group felsic volcanics

The Smoke Hill Volcanics have typical A-type characteristics: low MgO, P_2O_5, Sr, V, Cr, Ni, *mg* (mostly 6–14), and Ce/Y and high Zr, Nb, Y, La, Ce, Ga, and Ga/Al (Figs 17,18). Spidergrams are highly irregular, with large negative Sr, P, and Ti anomalies (Fig. 20). Virtually all analysed rocks are metaluminous (diopside-normative) (Fig. 16). The trachydacites are compositionally similar, but poorer in SiO_2. The epidote-rich dacite has anomalously high CaO and low K_2O, Rb, and Ba, presumably as a result of alteration. The rhyolites show quite wide variations in Na_2O and K_2O contents, probably also the result of late or post-magmatic redistribution of alkalies (Fig. 15).

The Mummawarrawarra trachyte has an extremely fractionated composition with, for its SiO_2 content (64.7%), much higher Al_2O_3, Na_2O, Nb, Y, Ga, Sn, and Be, and lower TiO_2, FeO, MgO, P_2O_5, Ba, Sr, Sc, and V than the other felsic volcanics (Figs 15, 17, 20); it cannot, therefore, be genetically related.

Giles (1981) carried out least-squares mixing calculations to investigate the possible generation of the felsic volcanics by either fractionation of mafic magma or partial melting of granulite facies crustal rocks. He concluded that a fractionation model (involving amphibole, plagioclase, clinopyroxene, magnetite, and apatite) could not explain the trace element compositions of the felsic rocks and that the mafic and felsic volcanics are, therefore, unrelated. He further concluded that a source similar to the felsic granulites presently exposed in the Musgrave Block is unlikely because excessive degrees of partial melting would be required to produce a suitable dacitic parent magma and hence the required degrees of enrichment in HFSE could not be attained. Therefore, a mafic–intermediate (possibly residual) source was considered probable.

However, the presently exposed country rocks are not necessarily representative of the presumed lower crustal source, and an intermediate–felsic source would be much less refractory than mafic granulite, which would require an excessive heat input to melt significantly. Experimental data (Beard et al. 1994) show that water-undersaturated melting of a dioritic source produces siliceous (>72% SiO_2) liquids, even for degrees of melting as high as 50 per cent. DePaolo et al. (1992) have shown from Nd isotopic data that crustally derived granitic magmas are typically melted from intermediate to felsic, rather than mafic, source rocks. An intermediate–felsic

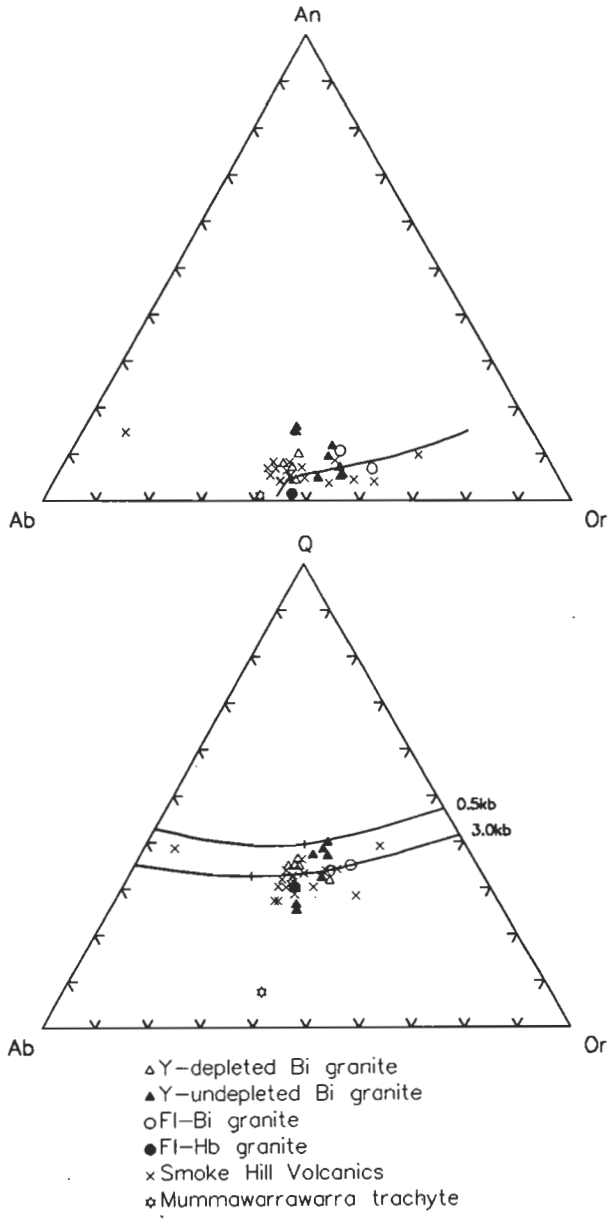

Figure 15. Normative Ab–Or–An and Q–Ab–Or diagrams for granitoids and felsic volcanics from the westernmost Musgrave Block.

source could more easily explain certain trace element data, i.e. strong Sr depletion on the spidergrams, implying a high proportion of residual plagioclase, combined with unfractionated REE patterns (low Ce/Y), implying little or no residual (or fractionating) amphibole or garnet and only relatively minor clinopyroxene. Moreover, there seems to be no compelling reason to assume a refractory residual source for A-type granitoids, as suggested by Collins et al. (1982), as even the highest-grade metamorphic terranes do not have particularly refractory compositions (Sheraton & Black 1988) and both experimental (Skjerlie & Johnston 1993) and geochemical (Anderson & Morrison 1992) data are more consistent with melting of predominantly felsic igneous (granitic, *s.l.*) rocks. The HFSE contents of A-type granitoids would be enhanced by high F in the parent melt, which increases the solubility of minor phases such as zircon and Fe–Ti oxides (Collins et al. 1982; Keppler 1993). This is certainly the case for some Tollu Group volcanics and associated intrusive rocks containing significant amounts of fluorite. However, a significant argument against an intracrustal melting model is provided by the relatively small Nb anomalies of the Smoke Hill Volcanics, which contrast with the much larger anomalies of other

granitoids and metamorphic rocks in the area (and indeed most felsic crustal rocks).

The ultimate cause of A-type magmatism was presumably emplacement of mantle-derived magma into the crust. The observed association with mafic volcanics, such as the Mummawarrawarra Basalt, is thus significant. In view of the fact that Nd isotopic data (Sun et al. in press) are consistent with generation of the Smoke Hill Volcanics (ε_{Nd} +0.3 to +0.7, compared to –1.8 for the Mummawarrawarra Basalt) by an AFC (assimilation–fractional crystallisation) process (DePaolo 1981) from a basaltic parent magma, and the difficulties with a crustal melting model, this possible alternative origin was re-examined. There are, however, also problems with this model. Least-squares mixing calculations for major elements (Wright & Doherty 1970) are broadly consistent with about 90 per cent fractionation of clinopyroxene (~20%), orthopyroxene (35%), plagioclase (45%), and minor Ti-magnetite from typical Mummawarrawarra Basalt to give the least siliceous rhyolite. Significant amphibole fractionation would produce a marked increase in Ce/Y and is, therefore, unlikely. Rayleigh fractionation calculations for many trace elements are compatible with this model, but show that fractionation of K-feldspar would also be necessary to produce the lesser degrees of enrichment shown by K_2O, Ba, and Rb compared to other minor elements; however, the major element modelling program cannot be reconciled with K-feldspar fractionation, and crustal assimilation would be unlikely to produce the observed abundances. It is also difficult to produce the observed degrees of Nb and Y enrichment and Sr depletion. In particular, the felsic rocks have significantly smaller Nb anomalies (Nb/La 0.30–0.65) than the basalts (Nb/La 0.25–0.35). Moreover, there appear to be no suitable intermediate compositions and extensive (~90%) fractionation of large quantities of mafic magma would be required to produce the felsic differentiates. The volumetrically minor trachytes within the Mummawarrawarra Basalt are perhaps the most likely products of extensive fractionation of such a basaltic parent magma, but certain element ratios (e.g., extremely high Nb/Zr (0.32) and Nb/La (4.2) and positive Nb anomalies) appear to preclude a direct relationship with the Mummawarrawarra Basalt itself. It is worth pointing out that extreme fractionation of mantle-derived mafic magma through AFC processes was proposed for the economically significant highly Nb-rich (up to 3200 ppm) trachytic volcanics of the Halls Creek Mobile Zone, Western Australia (Taylor et al. 1995).

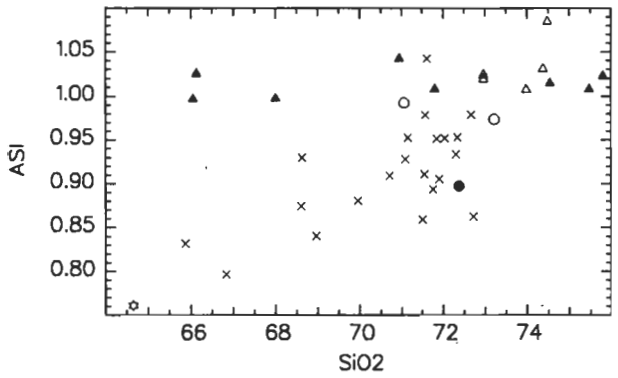

Figure 16. Plot of alumina saturation index against SiO_2 for granitoids and felsic volcanics from the westernmost Musgrave Block. Symbols as in Figure 15.

In summary, like the hornblende–biotite granitoids of the Hinchley Range area, many of the chemical features of the Smoke Hill Volcanics appear to be generally consistent with partial melting of intermediate to felsic granulite facies lower crustal rocks (possibly with an additional mantle-derived component: Kerr & Fryer 1993), possibly caused by heating due to emplacement of mantle-derived magma. The somewhat younger Nd T_{DM} model ages and high ε_{Nd} of the Smoke Hill

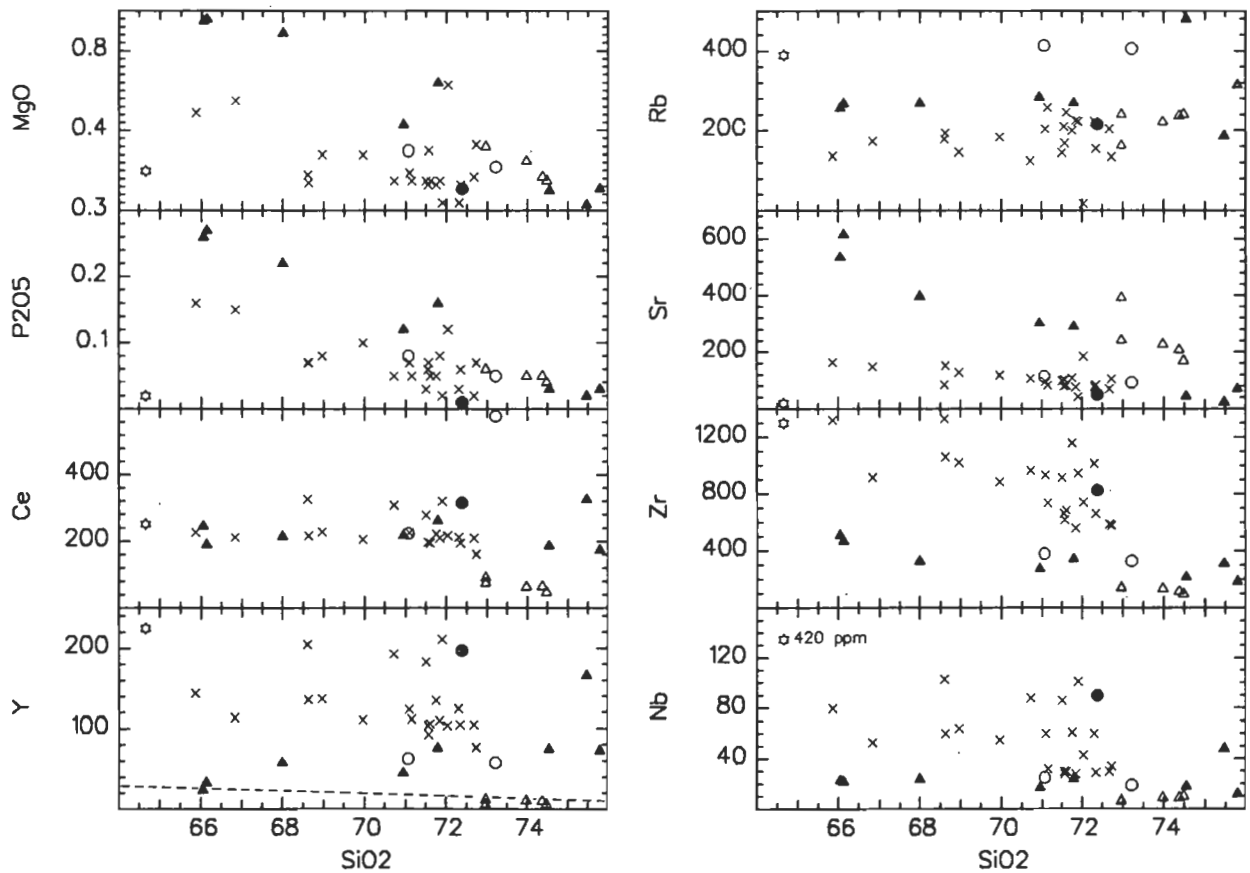

Figure 17. SiO_2 variation diagrams for granitoids and felsic volcanics from the westernmost Musgrave Block. Symbols as in Figure 15.

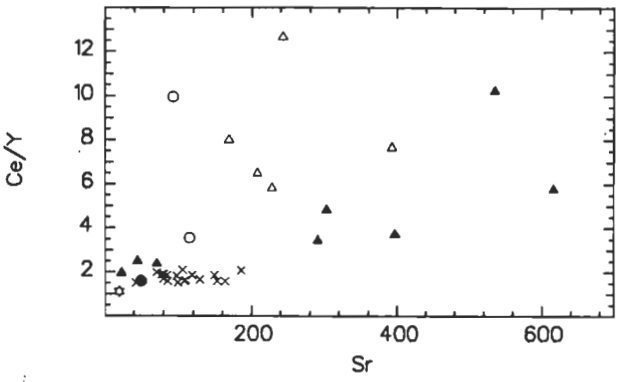

Figure 18. Plot of Ce/Y against Sr for granitoids and felsic volcanics from the westernmost Musgrave Block. Symbols as in Figure 15.

Volcanics (1540–1570 Ma: Sun et al. in press), compared to granulite facies metamorphics in the western Hinckley Range area (1610–1900 Ma) may be a result of derivation from a relatively young crustal underplate. Indeed, as discussed above, some Y-depleted granitic rocks in the basement to the Bentley Supergroup may represent new felsic crust. On the other hand, generation of the felsic volcanics by direct fractionation of a basaltic magma is also feasible. Although model calculations are not entirely consistent with such an origin, the discrepancies may be due to inappropriate choices of K_d values or parent magma or fractionating mineral compositions. DePaolo et al. (1992) concluded from Nd isotopic data that high-silica rhyolitic ignimbrites of the western United States were commonly formed primarily by fractionation of basaltic magma, and a similar origin for A-types was proposed by Javoy & Weis (1987) and Turner et al. (1992). However, because neither the exposed felsic country rocks nor the associated basaltic rocks are entirely suitable chemically as a source for the Smoke Hill Volcanics, their origin is presently uncertain. Eby (1990) emphasised that A-type granitoids can be produced by a variety of processes, including fractionation of basaltic magma, intracrustal melting, or interaction of mantle-derived magma with continental crust.

Discussion and conclusions

1200 Ma granulite facies country rocks of the Giles Complex in the western Musgrave Block are predominantly of felsic igneous origin (intrusive or extrusive), and obvious metasedimentary rocks are much less common. The protoliths of some Y-depleted orthopyroxene-bearing felsic orthogneisses may represent primary felsic crust derived by partial melting of a hornblende±garnet-bearing, but feldspar-poor, mafic source (possibly subducted hydrated oceanic crust). Other orthopyroxene and/or garnet-bearing orthogneisses have geochemical features (notably depletion in Sr, but not Y) more consistent with intracrustal melting. Chemical effects of high-grade metamorphism were apparently minor, being confined to loss of U relative to Th.

Post-D_1, pre-D_2 orthopyroxene granites represent intracrustal melts formed during granulite facies metamorphism, although minor quartz monzodiorites are likely to have been derived either directly from the mantle, or by hydrous melting of a mafic crustal source.

1188±4 Ma and ~1060 Ma hornblende–biotite granitoids in the Champ de Mars area, south of the Hinckley Range, include rapakivi, porphyritic, and even-grained varieties. Some show close spatial and probably temporal associations with Giles Complex intrusions, suggesting a relationship, but only in so far as emplacement of mantle-derived magmas provided a source of heat for intracrustal melting. Most of the geochemical features of these granitoids (high HFSE, LREE, and Th/U,

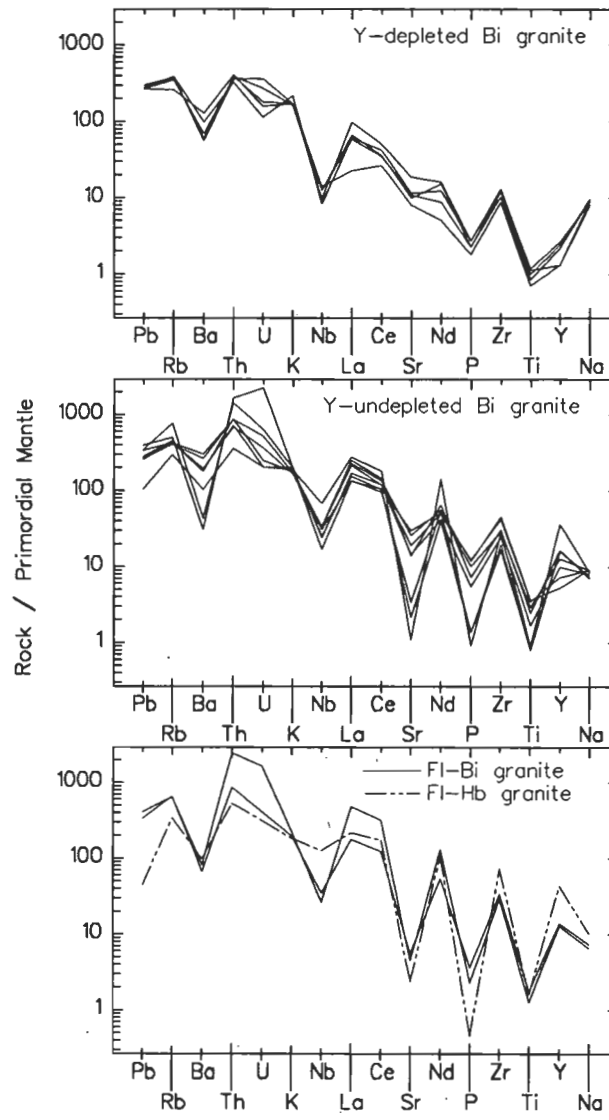

Figure 19. Spidergrams for granitoids from the basement to the Bentley Supergroup, westernmost Musgrave Block.

and low Sr) can be explained by relatively high-temperature partial melting of near-anhydrous granulite facies felsic crustal rocks. However, some intermediate rocks (quartz monzodiorite and quartz monzonite) may have been formed by fractionation of gabbroic magma or, less likely, by progressive contamination with felsic crustal material. The wide compositional range of the hornblende–biotite granitoids cannot be due entirely to mixing of mafic (or intermediate) and felsic magmas, although some degree of mixing may well have occurred. Much of the variation is probably due to crystal fractionation, different extents of melting, and/or cumulate unmixing, although distinct parent magmas of different ages were also involved. Quartz syenite of Mount Aloysius represents a distinct magma type with A-type chemical features (high LILE, HFSE, LREE, and Ga, and low *mg* and Sr), derived from a distinct crustal, or possibly mantle, source.

Granitic basement rocks to the Bentley Supergroup differ from those of the Champ de Mars area in including a significant proportion of Y-depleted, Sr-undepleted rocks which may represent new felsic crust. The 1078±5 Ma felsic Smoke Hill Volcanics of the Bentley Supergroup have typical A-type compositions (high HFSE, LREE, and Ga, and low *mg*). Like the Champ de Mars hornblende–biotite granitoids, these features may be due to partial melting of granulite facies lower crustal rocks during emplacement of mantle-derived magma (the

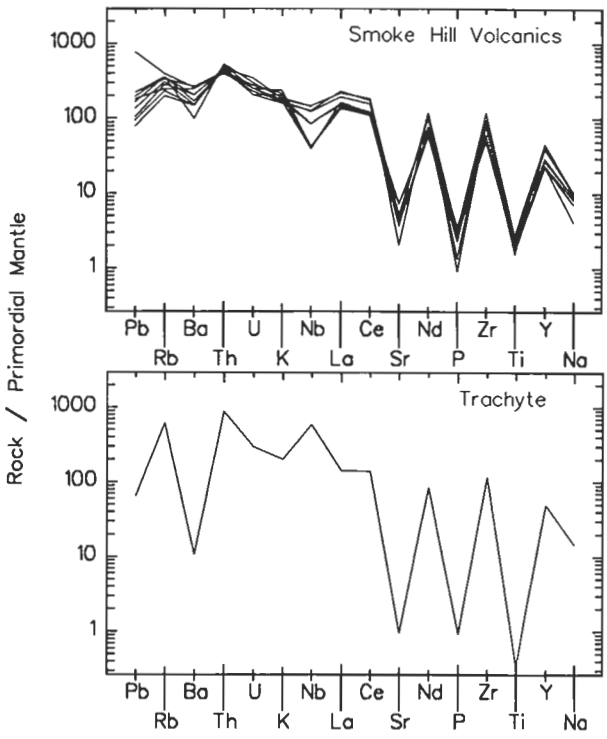

Figure 20. Spidergrams for Smoke Hill Volcanics and trachyte from the Bentley Supergroup, westernmost Musgrave Block.

Mummawarrawarra Basalt and, possibly, the Giles Complex, Sun et al. in press). Alternatively, generation of the felsic volcanics by AFC fractionation of basaltic magma is possible, although petrogenetic modelling is not consistent with a parent magma similar to the Mummawarrawarra Basalt. In particular, the relatively small negative Nb anomalies of the felsic volcanics (and the positive Nb anomaly of the Mummawarrawarra trachyte) are difficult to explain by either model, and imply a source different from either the exposed felsic crustal rocks or the mafic volcanics. This lack of major Nb depletion is perhaps more consistent with a mafic, rather than a felsic crustal, source, because continental crustal rocks typically have large negative Nb anomalies. The somewhat younger Nd T_{DM} model ages (1460–1570 Ma) of the Smoke Hill Volcanics compared to granulite facies metamorphics in the western Hinckley Range area (1610–1900 Ma) may reflect derivation of the former either from a relatively young crustal underplate or directly from mantle-derived magma. If the first alternative is correct, then this regional difference in model ages may suggest that the two areas form parts of two different tectonic plates, although more isotopic data are obviously needed to confirm this.

It is noteworthy that both major episodes of felsic magmatism (at about 1190–1180 and 1080–1060 Ma) in the western Musgrave Block appear to have been associated with mafic (to ultramafic) magmatism. However, in the case of the Champ de Mars granitoids, the relationship appears to have been indirect, in that the mafic magmas were the cause of intracrustal melting, rather than being parental to the felsic magmas. Both felsic suites have many compositional features of A-type granitoids, but only the younger appears to be truly anorogenic in its tectonic setting. Granitoids with 'A-type' geochemical characteristics are thus not necessarily confined to anorogenic settings, but may form in any environment in which emplacement of mantle-derived magma provides enough heat to cause high-temperature intracrustal melting (with or without significant mixing of the mantle and crustal components). Nevertheless, only the Smoke Hill Volcanics and the Mummawarrawarra trachyte have the high Nb (and thus only small negative, or positive, Nb anomalies) typical of intraplate granitoids (Pearce et al. 1984). These rocks may thus contain a Nb-rich OIB (ocean island basalt) type mantle component (Sun & McDonough 1989). Most other granitoids in the area have the high LILE/HFSE ratios and, consequently, the large negative Nb anomalies characteristic of subduction-related magmatism, including typical continental crust derived directly or indirectly from enriched lithospheric mantle (Brown et al. 1984).

In view of the very large scale of mafic–ultramafic magmatism represented by the Giles Complex, it is rather surprising that intracrustal melting was not more extensive. This is particularly so, as it appears that many of the granitoids in the Champ de Mars area, at least, are considerably older. It is possible that much of the granitic magma was emplaced at higher crustal levels, now removed by erosion. The relatively poorly exposed basement to the Bentley Supergroup consists largely of biotite granite and may represent such a higher crustal level, although neither the age nor the tectonic relationships of these rocks with those of the Tomkinson Ranges have been established. The dry nature of the granulite facies country rocks would, of course, limit the extent of melting, although the hornblende–biotite granitoids clearly represent 'wetter' magmas than the older orthopyroxene granitoids. If the country rocks could not be the source of the water in these magmas, it was presumably derived either directly from mafic magma (including the Giles Complex) or as a hydrous fluid associated with emplacement of the latter. Either way, it was, presumably, mantle-derived.

Tectonic events of similar age to those in the Musgrave Block (i.e. about 1200 and 1300 Ma) have also been reported from the Albany–Fraser Block to the southwest (Pidgeon 1990; Black et al. 1992), suggesting that both areas formed parts of the same mobile belt (Sun et al. in press). The same belt may well have extended into the Bunger Hills area of Antarctica, where high-grade metamorphism also occurred about 1190 Ma ago (Sheraton et al. 1993); Moores (1991) proposed that these terranes represent parts of a global Grenvillean belt which extended to the Appalachians of North America. More detailed geochemical and isotopic studies may help to shed light on the geological evolution of this major feature, the formation of which was one of the most important events in Proterozoic Earth history.

Acknowledgements

We thank John Pyke, Bill Pappas and Elizabeth Webber for chemical analyses, Lance Black, David Champion and Andrew Glikson for invaluable comments on the manuscript, and AGSO's Cartographic Services Unit for drafting two of the figures.

References

Anderson, J.L. & Morrison, J., 1992. The role of anorogenic granites in the Proterozoic crustal development of North America. In: Condie, K.C. (editor). Proterozoic crustal evolution. Elsevier, Amsterdam, 263–299.

Ballhaus, C. & Berry, R.F., 1991. Crystallization pressure and cooling history of the Giles layered igneous complex, central Australia. Journal of Petrology, 28, 1–28.

Barker, F.; 1979. Trondhjemite: definition, environment and hypotheses of origin. In: Barker, F. (editor). Trondhjemites, dacites, and related rocks. Elsevier, Amsterdam, 1–12.

Beard, J.S., Lofgren, G.E., Sinha, A.K. & Tollo, R.P., 1994. Partial melting of apatite-bearing charnockite, granulite, and diorite: melt compositions, restite mineralogy, and petrologic implications. Journal of Geophysical Research, 99, 21591–21603.

Black, L.P., Harris, L.B. & Delor, C.P., 1992. Reworking

of Archaean and Early Proterozoic components during a progressive, Middle Proterozoic tectonothermal event in the Albany Mobile Belt, Western Australia. Precambrian Research, 59, 95–123.

Brown, G.C., Thorpe, R.S. & Webb, P.C., 1984. The geochemical characteristics of granitoids in contrasting arcs and comments on magma sources. Journal of the Geological Society of London, 141, 413–426.

Chappell, B.W. & White, A.J.R., 1974. Two contrasting granite types. Pacific Geology, 8, 173–174.

Clarke, G.L., 1992. Field relationships and tectonic history of the Hinckley Gabbro, felsic to mafic granulites and granitoids, west Hinckley Range and Champ-de-Mars areas, Tomkinson Ranges, Musgrave Block, WA. Bureau of Mineral Resources, Australia, Record 1992/33.

Clarke, G.L., Buick, I.S., Glikson, A.Y. & Stewart, A.J., 1995. Structural and pressure–temperature evolution of host rocks of the Giles Complex, western Musgrave Block, central Australia: evidence for multiple high-pressure events. AGSO Journal of Australian Geology & Geophysics, this issue.

Collins, W.J., Beams, S.D., White, A.J.R. & Chappell, B.W., 1982. Nature and origin of A-type granites with particular reference to southeastern Australia. Contributions to Mineralogy and Petrology, 80, 189–200.

Cruikshank, B.I. & Pyke, J.G., 1993. Analytical methods used in Mineral and Land Use Program's geochemical laboratory. Australian Geological Survey Organisation, Record 1993/26.

Cullers, R.L., Stone, J., Anderson, L., Sassarini, N. & Bickford, M.E., 1993. Petrogenesis of Mesoproterozoic Oak Creek and West McCoy Gulch plutons, Colorado: an example of cumulate unmixing of a mid-crustal, two-mica granite of anorogenic affinity. Precambrian Research, 62, 139–169.

Daniels, J.L., 1974. The geology of the Blackstone region, Western Australia. Geological Survey of Western Australia, Bulletin 123.

DePaolo, D.J., 1981. Trace element and isotopic effects of combined wallrock assimilation and fractional crystallisation. Earth and Planetary Science Letters, 53, 189–202.

DePaolo, D.J., Perry, F.V. & Baldridge, W.S., 1992. Crustal versus mantle sources of granitic magmas: a two-parameter model based on Nd isotopic studies. Transactions of the Royal Society of Edinburgh: Earth Sciences, 83, 439–446.

Ebadi, A. & Johannes, W., 1991. Beginning of melting and composition of first melts in the system Qz-Ab-Or-H_2O-CO_2. Contributions to Mineralogy and Petrology, 106, 286–295.

Eby, G.N., 1990. The A-type granitoids: a review of their occurrence and chemical characteristics and speculations on their petrogenesis. Lithos, 26, 115–134.

Fitton, J.G. & Upton, B.G.J., 1987. Alkaline igneous rocks. Geological Society of London, Special Publication 30.

Giles, C.W. 1981. A comparative study of Archaean and Proterozoic felsic volcanic associations in southern Australia. Unpublished PhD Thesis, University of Adelaide.

Glikson, A.Y., Ballhaus, C. & Pharaoh, T, 1990. The Giles Complex, central Australia. New insights into tectonics and metamorphism. BMR Research Newsletter, 12, 18–20.

Glikson, A.Y., Ballhaus, C., Clarke, G.L., Sheraton, J.W., Stewart, A.J. & Sun, S-S., in press a. Geology of the Giles Complex, Tomkinson Ranges and environs, western Musgrave Block, central Australia. Australian Geological Survey Organisation, Record.

Glikson, A.Y., Stewart, A.J., Ballhaus, C., Clarke, G.L., Sheraton, J.W. & Sun, S-S., 1995. Geological and geophysical framework of the Tomkinson Ranges, western Musgrave Block, central Australia. AGSO Journal of Australian Geology & Geophysics, this issue.

Gray, C.M., 1977. The geochemistry of central Australian granulites in relation to the chemical and isotopic effects of granulite facies metamorphism. Contributions to Mineralogy and Petrology, 65, 79–89.

Gray, C.M., 1978. Geochronology of granulite-facies gneisses in the western Musgrave Block, central Australia. Journal of the Geological Society of Australia, 25, 403–414.

James, R.S. & Hamilton, D.L., 1969. Phase relations in the system $NaAlSi_3O_8$–$KAlSi_3O_8$– $CaAl_2Si_2O_8$–SiO_2 at 1 kilobar water vapour pressure. Contributions to Mineralogy and Petrology, 21, 111–141.

Keppler, H., 1993. Influence of fluorine on the enrichment of high field strength trace elements in granitic rocks. Contributions to Mineralogy and Petrology, 114, 479–488.

Kerr, A. & Fryer, B.J., 1993. Nd isotope evidence for crust-mantle interaction in the generation of A-type granitoid suites in Labrador, Canada. Chemical Geology, 104, 39–60.

Le Maitre, R.W., 1989. A classification of igneous rocks and glossary of terms. Blackwell, Oxford.

Maboko, M.A.H., Williams, I.S. & Compston, W., 1991. Zircon U-Pb chronometry of the pressure and temperature history of granulites in the Musgrave Ranges, central Australia. Journal of Geology, 99, 675–697.

Moores, E.M., 1991. Southwest U.S.-East Antarctica (SWEAT) connection: a hypothesis. Geology, 19, 425–428.

Morse, S.A., 1968. Feldspars. Yearbook of the Carnegie Institute, Washington, 67, 120–126.

Nesbitt, R.W., Goode, A.D.T., Moore, A.C. & Hopwood, T.P., 1970. The Giles Complex, central Australia: a stratified sequence of mafic and ultramafic intrusions. Geological Society of South Africa, Special Publication 1, 547–564.

Norrish, K. & Chappell, B.W., 1977. X-ray fluorescence spectrometry. In: Zussman, J. (editor). Physical methods in determinative mineralogy. Academic Press, London, 201–272.

Norrish, K & Hutton, J.T., 1969. An accurate X-ray spectrographic method for the analysis of a wide range of geological samples. Geochimica et Cosmochimica Acta, 33, 431–453.

Pearce, J.A., Harris, N.B.W. and Tindle, A.G., 1984. Trace element discrimination diagrams for the tectonic interpretation of granitic rocks. Journal of Petrology, 25, 956–983.

Pidgeon, R.T., 1990. Timing of plutonism in the Proterozoic Albany Mobile Belt, southwestern Australia. Precambrian Research, 47, 157–167.

Rogers, J.J.W. & Greenberg, J.K., 1990. Late-orogenic, post-orogenic, and anorogenic granites: distinction by major-element and trace-element chemistry and possible origins. Journal of Geology, 98, 291–309.

Sheraton, J.W. & Black, L.P., 1983. Geochemistry of Precambrian gneisses: relevance for the evolution of the East Antarctic Shield. Lithos, 16, 273–296.

Sheraton, J.W. & Black, L.P., 1988. Chemical evolution of granitic rocks in the East Antarctic Shield, with particular reference to post-orogenic granites. Lithos, 21, 37–52.

Sheraton, J.W., Black, L.P. & Tindle, A.G., 1992. Petrogenesis of plutonic rocks in a Proterozoic granulite-facies terrane—the Bunger Hills, East Antarctica. Chemical Geology, 97, 163–198.

Sheraton, J.W., Tingey, R.J., Black, L.P. & Oliver, R.L., 1993. Geology of the Bunger Hills area, Antarctica: implications for Gondwana correlations. Antarctic Science, 5, 85–102.

Skjerlie, K.P. & Johnston, A.D., 1993. Fluid-absent melting behavior of an F-rich tonalitic gneiss at mid-crustal pressures: implications for the generation of anorogenic granites. Journal of Petrology, 34, 785–815.

Stern, R.A. & Hanson, G.N., 1991. Archean high-Mg granodiorite: a derivative of light rare earth element-enriched monzodiorite of mantle origin. Journal of Petrology, 32, 201–238.

Stewart, A.J., 1995. Resolution of conflicting structures and deformation history of the Mount Aloysius granulite massif, western Musgrave Block, central Australia. AGSO Journal of Australian Geology & Geophysics, this issue.

Stewart, A.J. & Glikson, A.Y., 1991. The felsic metamorphic/igneous core complexes hosting the Giles Complex. BMR Research Newsletter, 14, 6–16.

Sun, S-S. & Sheraton, J.W., 1992. Zircon U/Pb chronology, tectono-thermal and crust-forming events in the Tomkinson Ranges, Musgrave Block, central Australia. AGSO Research Newsletter, 17, 9–11.

Sun. S-S. & McDonough, W.F., 1989. Chemical and isotopic systematics of oceanic basalts: Implications for mantle composition and processes. In: Saunders, A.D. & Norry, M.J. (editors). Magmatism in ocean basins. Geological Society of London, Special Publication 42, 313–345.

Sun, S.-S., Gray, C.M., Sheraton, J.W., Glikson, A.Y. & Stewart, A.J., 1995. Zircon U–Pb chronology and neodymium isotope study of tectonothermal and crust-forming events in the Tomkinson Ranges, western Musgrave Block, central Australia. AGSO Journal of Australian Geology & Geophysics, this issue.

Tarney, J. Skinner, A.C. & Sheraton, J.W., 1972. A geochemical comparison of Archaean gneiss units from northwest Scotland and East Greenland. 24th International Geological Congress, Section 1, 162–174.

Tarney, J. & Windley, B.F., 1977. Chemistry, thermal gradients and evolution of the lower continental crust. Journal of the Geological Society of London, 134, 153–172.

Tarney, J., Wyborn, L.E.A., Sheraton, J.W. & Wyborn, D., 1987. Trace element differences between Archaean, Proterozoic and Phanerozoic crustal components—implications for crustal growth processes. In: Ashwal, L.D. (editor). Workshop on the growth of continental crust. Lunar and Planetary Institute, Technical Report 88.02, 139–140.

Taylor, S.R. & McLennan, S.M., 1985. The continental crust: its composition and evolution. Blackwell, Oxford.

Taylor, W.R., Esslemont, G. & Sun, S.-S., 1995. Geology of the volcanic-hosted Brockman rare-metals deposit, Halls Creek Mobile Zone, northwest Australia. II. Geochemistry and petrogenesis of the Brockman volcanics. Mineralogy and Petrology, 52, 231–255.

Tuttle, O.F. & Bowen, N.L., 1958. Origin of granite in the light of experimental studies in the system $NaAlSi_3O_8$ - $KAlSi_3O_8$ - SiO_2 - H_2O. Geological Society of America, Memoir 74.

Watson, E.B. & Harrison, T.M., 1983. Zircon saturation revisited: temperature and composition effects in a variety of crustal magma types. Earth and Planetary Science Letters, 64, 295–304.

Whalen, J.B., Currie, K.L. & Chappell, B.W., 1987. A-type granites: geochemical characteristics, discrimination and petrogenesis. Contributions to Mineralogy and Petrology, 95, 407–419.

Wright, T.L. & Doherty, P.C., 1970. A linear programming and least squares computer method for solving petrologic mixing programs. Geological Society of America, Bulletin 81, 1995–2008.

Zhao, J-X., Shiraishi, K., Ellis, D.J. & Sheraton, J.W., in press. Geochemical and isotopic studies of syenites from the Yamato Mountains, East Antarctica: implications for the origin of syenitic magmas. Geochimica et Cosmochimica Acta.

AGSO Journal of Australian Geology & Geophysics, 16 (1/2), 127–146

Structural and pressure–temperature evolution of host rocks of the Giles Complex, western Musgrave Block, central Australia: evidence for multiple high-pressure events

G.L. Clarke[1], I.S. Buick[2], A.Y. Glikson[3] & A.J. Stewart[3]

The history of Mid-Proterozoic metasedimentary gneisses, felsic and mafic orthogneisses of the Tomkinson Ranges, western Musgrave Block, involved multiple low- to high-P metamorphic events and polyphase deformation. Isoclinal, gently inclined to recumbent $D_{1/2}$ folding accompanied the intrusion of pre-S_1 mafic and felsic orthogneisses and post-S_1, pre-S_2 felsic orthogneisses under peak conditions of P=5±1 kbar and T≥750°C at ~1200 Ma. K-feldspar megacrystic granitoid stocks formed at ~1188 Ma. Post-S_2 mafic to ultramafic magmatism resulted in the large layered intrusions of the Giles Complex at ~1080 Ma, whilst the terrane was at conditions of P=6±1 kb. At ~1080–1060 Ma, microgranitoid dykes and veins intruded Giles Complex sills in the Tomkinson Ranges, while comagmatic volcanics of the Tollu Group unconformably overlie other parts of the Musgrave Block further west. Type A mafic dykes, which may represent feeder veins to the Tollu Group, intruded rocks of the Tomkinson Ranges before a third deformation event, D_3, resulted in a system of steep, southeast-trending mylonites with a granulite facies S_3 foliation and a well-developed down-dip L_3 stretching lineation. Type A mafic dykes and their host felsic granite gneiss show marginal to complete recrystallisation to granulite facies mylonitic S_3 assemblages at conditions of P≈11 kb and T≈700°C. Near-isothermal decompression returned such parts of the Musgrave Block to conditions of P≈4–5 kb late in D_3. Parts of the Musgrave Block that are unconformably overlain by the Tollu Group probably remained closer to the earth's surface during D_3. Coarse-grained, ~800 Ma Type B mafic dykes and aphanitic, ~1000 Ma Type C mafic dykes cut S_3, and are cut by a system of mylonite and retrograde shear zones, D_{4-7}. East-trending ~550 Ma D_6 ultramylonite pseudotachylite zones represent the effects of the Late Proterozoic to Cambrian Petermann Orogeny, which resulted in significant dislocation of parts of the Musgrave Block and the partial to complete recrystallisation of post-S_3 dykes near the Woodroffe thrust zone at sub-eclogite facies conditions of P=14±1 kb and T=700–750°C. These late high-pressure assemblages suggest that the structural grain in rocks of south-central Australia resulted, to a major extent, from Late Proterozoic to Cambrian compression.

Introduction

Granulite facies supracrustal gneisses and orthogneisses of the mid-Proterozoic Musgrave Block (Hossfeld 1954) define an east-trending gravity high, with a strike extent of over 700 km, that straddles the South Australian–Northern Territory border and extends into Western Australia (Fig. 1). The granulites were intruded by large layered basic to ultrabasic bodies of the Proterozoic Giles Complex (Sprigg & Wilson 1959), representing significant mantle-derived contributions to a previously deformed and metamorphosed continental crust (Nesbitt & Kleeman 1964; Nesbitt & Talbot 1966; Goode & Krieg 1967; Nesbitt et al. 1970; Daniels 1974; Goode 1978; Moore & Goode 1978; Ballhaus & Glikson, 1989; Glikson et al. 1990; Ballhaus & Berry 1991). We describe below the results of field and petrological studies of rocks from the western Musgrave Block; a detailed sequence of intrusive and deformation events is integrated with quantitative pressure and temperature estimates and isotopic age constraints (Sun & Sheraton 1992; Sun et al. 1995—this issue). The data suggest a dynamic history for the western Musgrave Block involving (1) ~1200 Ma granulite facies metamorphism; (2) ~1080 Ma mafic–ultramafic plutonic activity and near-contemporaneous mafic–felsic volcanic activity; and (3) ~550 Ma high-temperature sub-eclogite facies metamorphism, owing to the convergence of parts of the Musgrave Block with a juvenile late Proterozoic foreland basin.

Regional geology

This paper is primarily concerned with granulite facies gneisses forming the Tomkinson Ranges and outcrops to the north of these ranges, in the western part of the Musgrave Block (Fig. 1). The oldest exposed rocks are mid-Proterozoic granulite facies metasedimentary gneisses and felsic and mafic orthogneisses. Parts of these are interpreted as having volcanic and/or sedimentary precursors (Gray 1971 1977; Daniels 1974; Moore & Goode 1978) of at least two ages, ~1550 and ~1300 Ma, on the basis of Rb-Sr whole rock isochron ages and U-Pb zircon dating using the Australian National University's SHRIMP (Sensitive High Resolution Ion Micro Probe) (Gray 1971, 1978; Sun & Sheraton 1992; Sun et al. in press). Distinct protolith ages were obtained from rocks north and south of the Hinckley fault (Fig. 1), and are further supported by SHRIMP dates of granulites from the Amata area in South Australia (Maboko et al. 1991).

Metamorphism at granulite facies conditions produced orthopyroxene garnet-bearing felsic gneisses and rare garnet + sillimanite-bearing metapelitic rocks (Gray 1978; Moore & Goode 1978). High-grade metamorphism was synchronous with deformation and granitic magmatism, with pre-S_1 felsic and mafic orthogneisses and post-S_1, pre-S_2 felsic orthogneisses (Clarke 1992). D_2 resulted in mesoscopic to macroscopic isoclinal reclined F2 folds with an axial-planar foliation, S_2, i.e. the pervasive gneissosity in the felsic-mafic granulites. D_2 involved mostly pure shear, with only a small component of rotational strain and resulted in a shallowly dipping reclined or recumbent terrane (Clarke 1992). Rb–Sr isochron dating of syn-metamorphic intrusions constrains peak metamorphism to 1204±17 Ma (Gray 1971, 1978).

Features of the layered mafic and ultramafic bodies of the Giles Complex are consistent with post-S_2 pre-S_3 intrusion (Clarke 1992), a high crystallisation pressure, unusually high liquidus temperatures because of the high confining pressure, and rapid near-isobaric cooling (Nesbitt et al. 1970; Goode & Moore 1975, Ballhaus & Glikson 1990; Daniels 1974). Early petrographic work on mineral corona textures from the Ewarara, Kalka and Gosse Pile ultramafic to mafic bodies inferred that intrusion occurred whilst the terrane was at pressures of 10–12 kb (Goode & Moore 1975), whereas more recent work on the Wingellina Hills layered intrusion suggests a significantly lower pressure of 6±1 kb (Ballhaus & Berry 1991). Possible explanations for these differing estimates are discussed below. The nature of magmatic layering and olivine–plagioclase relations in several of the intrusions suggest that the multiple mafic/ultramafic bodies constituted discrete original magma chambers or sills rather than tectonic slices derived from an originally continuous lopolith (Ballhaus 1992;

[1] Department of Geology & Geophysics, University of Sydney, NSW 2006, Australia
[2] Department of Geology, La Trobe University, Bundoora, Victoria 3083, Australia
[3] Australian Geological Survey Organisation, GPO Box 378, Canberra, ACT 2601, Australia

Ballhaus & Glikson 1995—this issue). Magma increments emplaced into the sills were derived from a parent magma which underwent pre-emplacement orthopyroxene clinopyroxene fractionation (Ballhaus 1992).

Regionally extensive granitoids were intruded during at least two stages: (1) during and following the 1.2 Ga metamorphism (Daniels 1974; Maboko et al. 1991), and (2) as granitic vein systems contemporary with the emplacement of the Giles Complex and the extrusion of volcanics of the Tollu Group at ~1060 Ma (Sun et al. in press). Type A mafic dykes cut 1188 Ma granitoid stocks (Clarke 1992), but their field relationships with the 1080 Ma granitic veins are not known. Another major phase of folding, F_3, resulted in the near-vertical southeast-trending granulite facies S_3 mylonitic foliation ob-

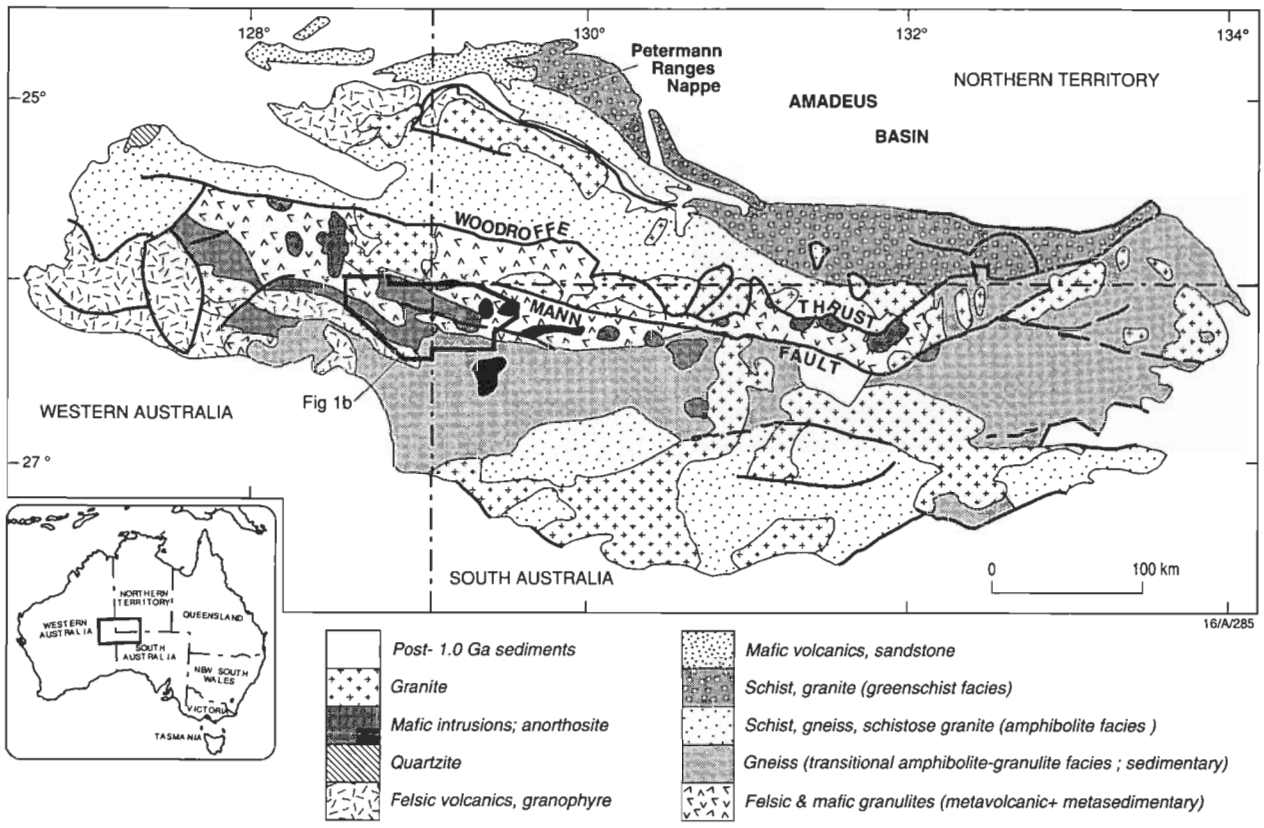

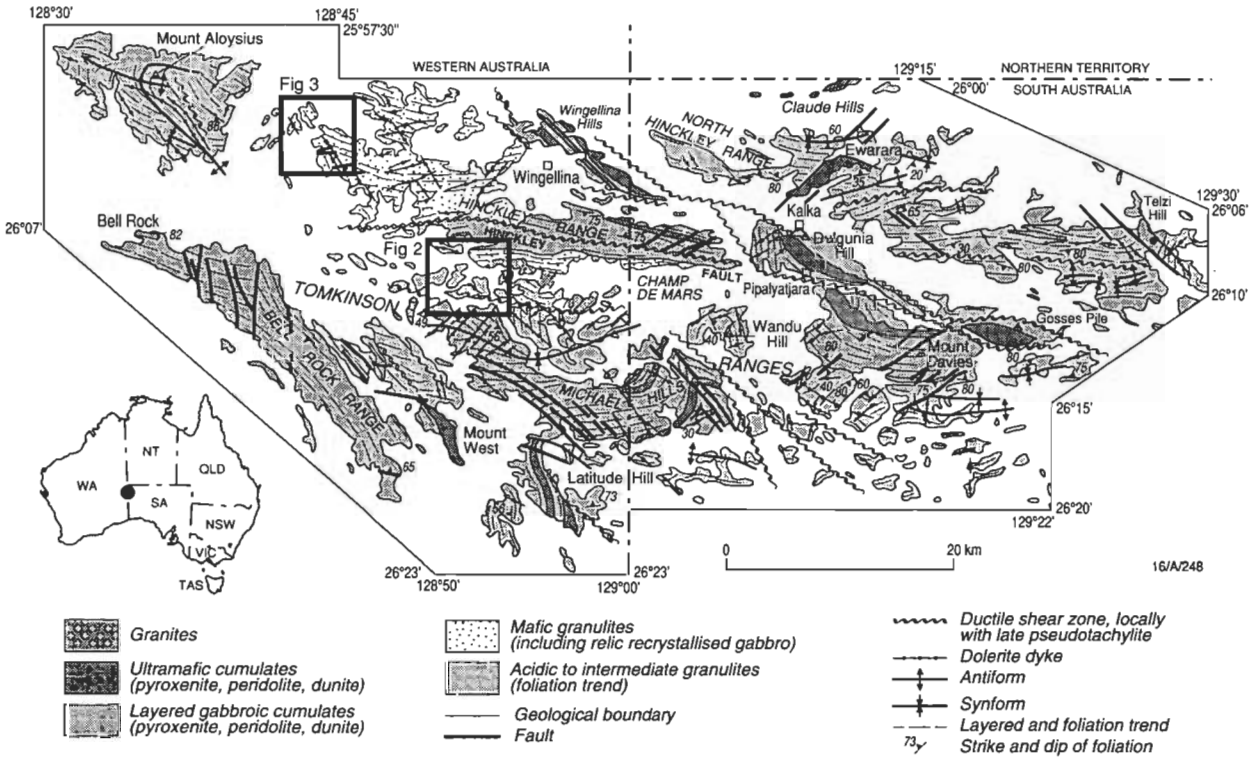

Figure 1. (a, upper) Structure of the Musgrave Block, showing location of the Bates 1:100 000 sheet area; (b, lower) Geological sketch map of the Tomkinson Ranges, showing the location of the two areas mapped in detail.

served throughout much of the western Musgrave Block. Intrusions of the Giles Complex were deformed by D_3, which resulted in marginal recrystallisation of gabbro to mafic granulite (Glikson 1990). Effects of D_3 are evident in the granulites as open concentric folds superimposed on S_1 and S_2 (Nesbitt et al. 1970; Gray 1971; Clarke 1992). On the basis of mineral assemblages in metapelitic rocks from Cohn Hill on the western part of the Cooper 1:250 000 sheet area, Clarke & Powell (1991) inferred a syn-S_3 decompressional P–T path for that part of the Musgrave Block, which is consistent with the P–T path derived from mineral assemblages in mafic dykes near Amata in the eastern part of the Musgrave Block (Maboko et al. 1991).

Coarse-grained, northwest-trending, ~800 Ma Type B dykes (Sun & Sheraton 1992) and smaller, northeast-trending, fine-grained to aphanitic ~1000 Ma Type C dykes cut S_3 (Clarke 1992). All dykes are cut by a system of steep mylonites and ultramylonites that have been divided into discrete deformation events, D_{4-7} (Clarke 1993). However, it is probable that the series D_{4-7} represents a single evolving orogen. D_4 ultramylonites with either normal or reverse movement are observed; these zones form the boundaries of the Hinckley gabbro, and are cut by steep north-trending D_5 ultramylonites that preserve southwest-directed deformation. D_4 and D_5 ultramylonite zones involved maximum displacements of several hundred metres, and significant uplift and/or dissection of the terrane, and are defined by mineral assemblages that imply greenschist to amphibolite facies conditions. East-trending D_6 ultramylonite pseudotachylite zones are the most prominent of all shear zones (Clarke 1992) and are best developed on the Bates 1:100 000 sheet area, where they represent the western extension of the Woodroffe Thrust (Forman 1965; Stewart 1993; Fig. 1). They were generated during the Late Proterozoic to Cambrian Petermann Orogeny, which resulted in north-verging folds, thrusts and metamorphism in cover rocks (Forman 1965), and the easterly trend of the Musgrave Block. Garnet+clinopyroxene-bearing assemblages occur in ultramylonites a few kilometres south of the south-dipping Woodroffe Thrust in the Bates 1:100 000 sheet area, oriented at acute to obtuse angles to this structure (Stewart 1993; Fig. 1A). Sm–Nd data for mineral separates from these assemblages, which straddle the boundary between the granulite and eclogite facies at high pressures (here termed sub-eclogites), suggest that a late Proterozoic to Cambrian crustal suture shaped the late evolution of rocks forming south central Australia (cf. Moores 1991).

Field relationships and petrology

The Hinckley gabbro forms the spine of the west-trending Hinckley Range, and has been extensively recrystallised in its western part to form mafic granulites (Glikson 1990). It is flanked on its westernmost extremity by layered felsic–mafic granulites (Daniels 1974) and to its south by felsic granulites and granitoids (Fig. 1). Two areas were selected for detailed study: (1) the Champ de Mars area (Fig. 2), which presents a microcosm of the Musgrave Block, with gabbroic intrusions of the Giles Complex, felsic and mafic granulites, microgranites, K-feldspar megacrystic granite and rapakivi granite; and (2) the western Hinckley Range and Charnockite Flats area (Fig. 3), which contains good exposures of what Daniels (1974) interpreted as a contaminated, marginal phase to the Hinckley gabbro. As justified below, the 'contaminated' gabbro represents recrystallised gabbro and, to avoid confusion with the older layered felsic–mafic granulites, is referred to as *mafic granulites (recrystallised gabbro)*. The aim of the mapping was to investigate the field relationships between the gabbros, mafic granulites, layered felsic–mafic granulites, and granitic stocks. A similar geological history is inferred for rocks located to the north of the Tomkinson Ranges (Fig. 1), on the basis of geological mapping completed for preparation of the Bates 1:100 000 sheet area (Stewart in press). However, rocks in this area also contain evidence of a late, high temperature sub-eclogite facies metamorphic event, whose effects are less clear in the Tomkinson Ranges, as discussed below.

We discuss below the field relationships and petrology of units that were distinguished in the mapping. The field relationships and structures of the Champ de Mars and west Hinckley areas are illustrated in Figures 2–5, and the temporal relations of structural and pressure–temperature features are summarised in Table 1.

Layered felsic and mafic granulites

The oldest rocks in the Tomkinson Ranges are well-layered felsic and mafic granulites that preserve evidence of one or two early deformation events, D_1 and D_2 . Daniels (1974) divided these rocks into two types: (1) (areally restricted) well-banded granulites characterised by lithological variations on a metre–centimetre scale (Fig. 4A) after primary sedimentary layering; and (2) (areally extensive) poorly banded felsic granulites, which include charnockitic gneisses, inferred to be orthogneisses. Principal locations for the well-banded variety in Western Australia include Mt Aloysius (Stewart 1995—this issue) (Fig. 1), Mt West in the southern part of the Tomkinson Ranges, and the area between Winburn Rocks and Lightning Rocks (western part of the Cooper 1:250 000 sheet); these rocks were interpreted to unconformably overly the poorly banded variety (Daniels 1974, p. 34). A migmatitic variant of the poorly banded felsic granulites was mapped in the Champ de Mars area by Daniels (1974), but minor amounts of quartzite occur. Mafic granulites are interlayered with the felsic granulites on a centimetre scale. Daniels (1974) inferred that these mafic rocks were genetically related to the Giles Complex; however, the mafic granulites record identical deformation histories to the felsic granulites and evidence of tectonic events that predated the large gabbroic intrusions. Felsic granulites predominate, but minor quartzite, calc-silicate and amphibolite are also present, indicating a metasedimentary precursor to part of the layered granulite sequence, as inferred by Daniels (1974), Gray (1977, 1978), Stewart (1995—this issue), and Sheraton & Sun (1995—this issue) for the well-banded granulites of Mt Aloysius (Fig. 1).

Metasedimentary gneisses and orthogneisses that were minimally affected by D_3 can be distinguished on textural grounds from those that were intensely recrystallised during D_3: the composite S_1 and S_2 foliation is granoblastic with interlocking coarse-grained minerals, whereas S_3 is a fine-grained mylonitic foliation,. typically with quartz ribbons enveloping relic S_2 mineral grains (Fig. 4B, C). This distinction becomes critical in the interpretation of parageneses, and is corroborated by differences in mineral chemistry between S_2 and S_3 grains in individual samples . The rare metasedimentary gneisses are most useful in constraining the metamorphic history, since they commonly contain garnet. Granulite facies metapelites with a pristine S_1 assemblage have coarse-grained poikiloblastic garnet (5 mm diameter) intergrown with, and wrapped round by, a granoblastic S_2 foliation comprising sillimanite, quartz, K-feldspar, plagioclase and ilmenite. Garnet may have inclusions of sillimanite that are oriented at an angle to the enveloping S_2 foliation, consistent with the interpretation of there having been an earlier S_1 foliation. The metapelites are commonly interlayered with intermediate garnet+orthopyroxene-bearing gneisses, which may be metapsammites or metamorphosed felsic volcanics (Gray 1978). Coarse-grained (<5 mm in diameter) granoblastic garnet, orthopyroxene, plagioclase, quartz and ilmenite, with or without K-feldspar or perthite define a pervasive foliation that is most probably a composite of S_1 and S_2. The calc-silicate gneisses preserve only a weak foliation and contain granoblastic garnet, clinopyroxene, plagioclase, ilmenite and sphene. The mafic and felsic

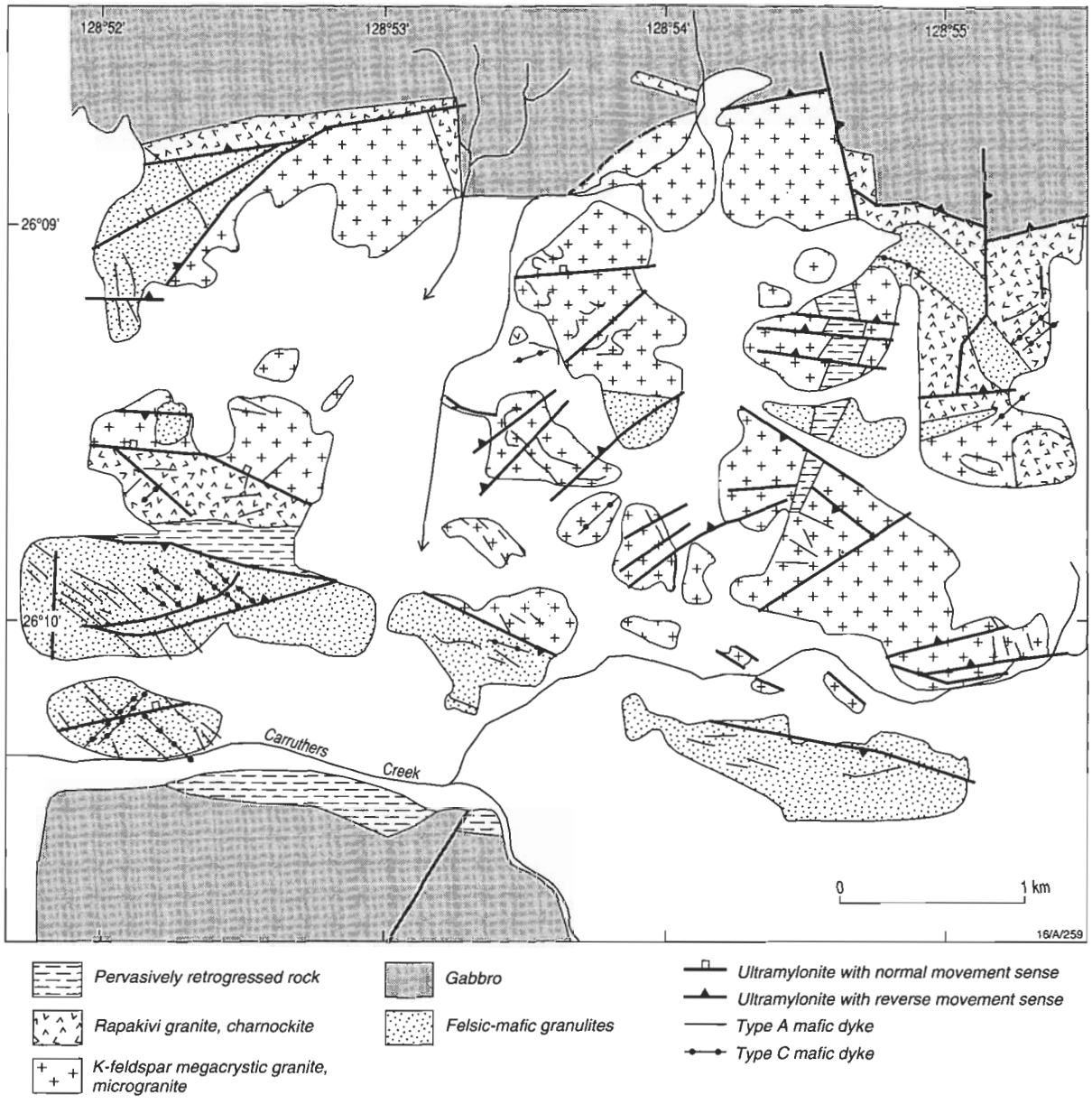

Figure. 2. Geology of the Champ de Mars area.

granulites comprise hypersthene, clinopyroxene, plagioclase, quartz and opaque minerals, with or without orthoclase, biotite and amphibole. Mafic minerals can vary from modal abundances of less than 5 per cent to more than 40 per cent, with the range forming a continuum between felsic and mafic granulite end-members. Whereas orthopyroxene is usually present in greater abundance than clinopyroxene in the felsic granulites, the mafic granulites lack K-feldspar and clinopyroxene is usually present in greater abundance than orthopyroxene. Large, zoned and simply twinned plagioclase grains, and large pyroxene grains that contain abundant fine-grained inclusions aligned along cleavages are common in the mafic granulite layers, suggesting that many of these were derived from recrystallised gabbroic rock.

In the Charnockite Flats area, a body of charnockitic gneiss and charnockitic dykes cuts S_1 in adjacent layered granulites, but contains S_2 (Clarke 1992), confirming an intrusive origin for at least some of the orthogneisses (cf. Gray 1978). The absence of the intense S_1 gneissosity in the charnockite gneiss gives the rocks a massive outcrop habit. Apophyses and dykes of the charnockite pervasively intrude adjacent layered granulites, with the numerous narrow veins giving the composite rocks a migmatitic appearance. Small xenoliths in these veins preserve an S_1 foliation, which is truncated at the margins of the xenolith.

Garnet+orthopyroxene-bearing gneisses from Mt Aloysius (Fig. 1) that were partially recrystallised during D_3 are of two types. In the first type, S_2 orthopyroxene and ilmenite are enveloped and partially replaced by S_3 amphibole and haematite. Garnet, plagioclase, K-feldspar, biotite and quartz were extensively recrystallised during development of the mylonitic S_3 foliation (Fig. 4C), and large garnet grains are strongly zoned. The second type involves patchy recrystallisation of the granoblastic S_2 grains, with the effects of D_3 being mostly restricted to narrow (<2 mm in width) S_3 shear zones that are mostly defined by recrystallised feldspar and quartz. Random, fine-grained symplectites of orthopyroxene, plagioclase and biotite, with or without garnet, partially replace large S_2 garnet grains, and symplectites of garnet and quartz partially to completely enclose S_2 orthopyroxene grains. Garnet occurs in two forms in the symplectites that enclose the large S_2 garnet grains: (1) grains interspersed with and of similar size to the symplectic orthopyroxene and plagiclase grains; and (2) as very narrow grains enclosing, and being at least an order of magnitude smaller than, the symplectic orthopyroxene. Whereas the first type are probably relicts of S_2 garnet

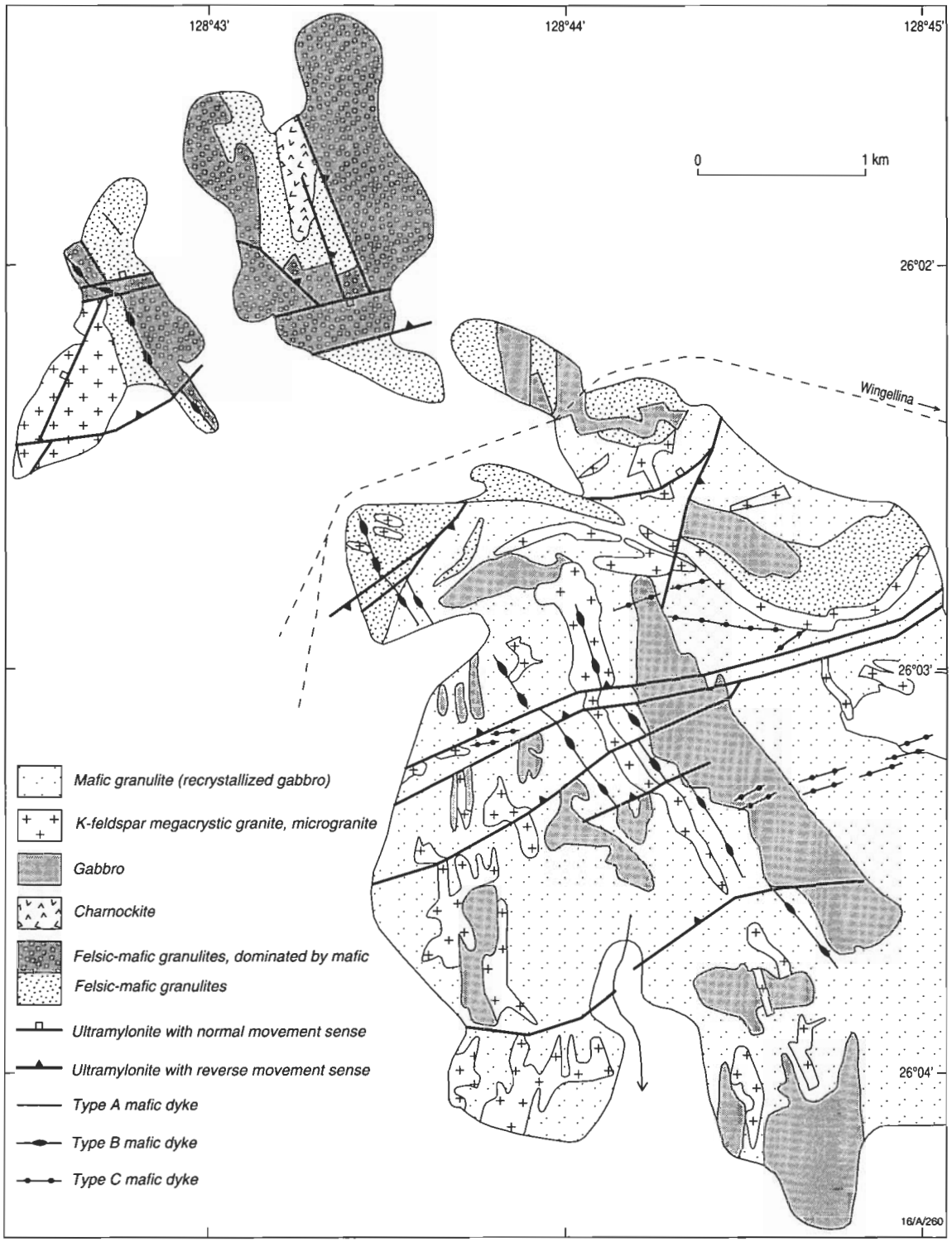

Figure 3. Geology of the west Hinckley Range.

incompletely consumed by the S_3 orthopyroxene and plagioclase (see below), the significantly finer grained garnet may represent the effects of recrystallisation during D6 (R.W. White & G.L. Clarke, unpublished data). The symplectites are drawn into the S_3 foliation and are cut by the narrow shear zones. Syn-S_3 to late-S_3 corona textures are also observed in metapelitic gneisses from near Cohn Hill, approximately 100 km west of the Tomkinson Ranges, which contain large grains of garnet (<5 mm diameter) and sillimanite (<2 mm diameter) enveloped by a mylonitic S_3 foliation, comprising fine-grained (typically <0.5 mm diameter) quartz, K-feldspar, biotite, cordierite, ilmenite and hercynitic spinel. Well-developed coronas separate garnet and sillimanite from each other, and from the matrix S_2 minerals. Most of the minerals defining the coronas are elongate in S_3, but some also appear to transect S_3. These coronas have been described in detail by Clarke & Powell (1991), and similar textures are observed in metapelitic rocks of the Tomkinson Ranges and adjacent areas (Moore 1969).

~1188 Ma and ~1080 Ma felsic granitoids

K-feldspar megacrystic granite and microgranite dykes and stocks dominate outcrops in the Champ de Mars area, where a U-Pb zircon age of 1188 Ma is recorded (Sun et al. in press). These bodies pervasively intrude, and contain xenoliths

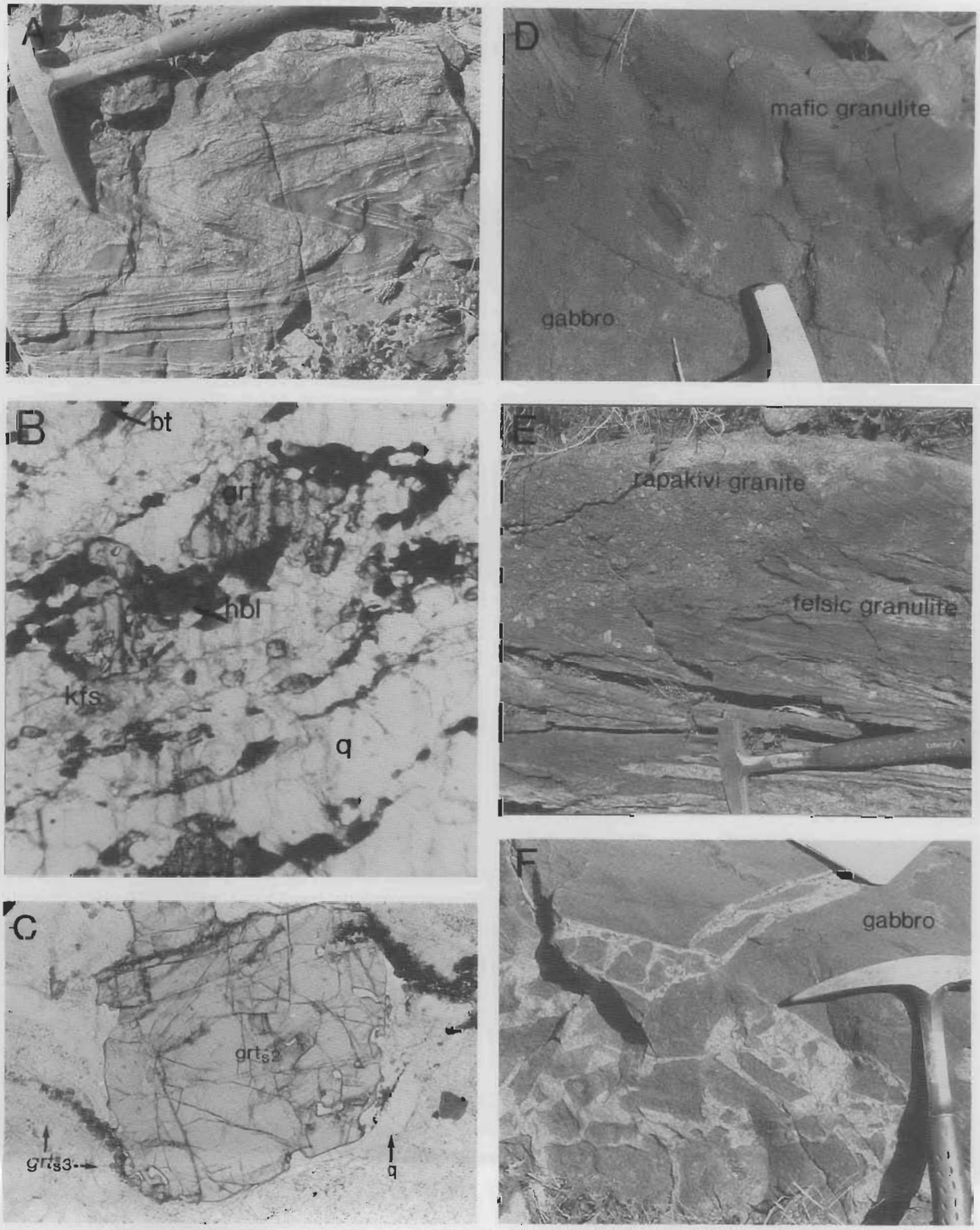

Figure 4. (A) Layered felsic–mafic granulite, showing F_2 folds refolding F_1 in a mixed felsic and mafic granulite. The felsic layers are discontinuous and the complex fabric is interpreted as having been developed by felsic veins sourced from a post-S_1 pre-S_2 charnockite that injected mafic granulite. Charnockite Flats, west Hinckley area. (B) Mylonitic S_3 foliation in an intermediate gneiss, defined by garnet (grt), hornblende (hbl), biotite (bt), quartz (q) and alkali feldspar (kfs). Plane-polarised light, sample 9198-9455. Width of field of view ~ 4 mm. (C) Mylonitic S_3 foliation in an intermediate gneiss, defined by quartz (q), biotite (bt), fine grained garnet (grt_{S3}). The S_3 foliation wraps a porphyroclast of S_2 garnet (grt_{S2}). S_2 and S_3 garnet have distinctly different compositions, as discussed in the text. Plane-polarised light, sample 9198-9567B (Bates sheet). Width of the field of view ~ 4 mm. (D) Gabbro intruding layered mafic granulite. Although the local geology is extensively disrupted by felsic intrusions and shear zones, this appears to be a rare example of an intrusive contact between the Hinckley gabbro and surrounding layered granulites. West Hinckley area. (E) Xenoliths of felsic granulite in rapakivi granite with megacrysts of K-feldspar. Champ de Mars area. (F) Felsic dyke containing xenoliths of gabbro and recrystallised gabbro. West Hinckley area.

of, the felsic granulites (Fig. 4E). Stocks and dykes of K-feldspar megacrystic and microgranite are mutually cross-cutting. Xenoliths of one occur in the other, and gradations between the two end-members are observed. Outcrops of these lithologies could not be differentiated on the scale mapped and on the basis of the field relationships they appear contemporary. In the west Hinckley Range, granitoid veins and dykes dated as ~1080 Ma (Sun et al. in press) intrude and contain xenoliths and mafic granulite derived from the Hinckley gabbro (Fig. 4F). It is difficult to separate the ~1.88 Ga from the ~1.08 Ga granitoids on the basis of field relations, since they are both post-S_2 and pre-S_3. All the felsic granitoids were pervasively recrystallised during D_3, and they typically contain K-feldspar and subordinate plagioclase megacrysts enveloped by a mylonitic S_3 foliation defined by K-feldspar, plagioclase, quartz, amphibole and haematite with or without garnet, biotite or ilmenite. Microgranitoids commonly comprise S_3 quartz, antiperthite, perthite, orthopyroxene, and ilmenite with minor biotite and/or garnet.

Rapakivi granites and charnockites

Dykes of post-S_2 charnockite and rapakivi granite that contain abundant angular to partially resorbed xenoliths of mafic rock occur along the southern margin of, and intrude, the Hinckley gabbro in the Champ de Mars area (Fig. 2). Larger stocks of ~1188 Ma rapakivi granite predate the Hinckley gabbro. Some of these rocks contain relic orthopyroxene that is now mostly pseudomorphed by biotite, suggesting a high solidus temperature. Typically, the charnockites contain large igneous clinopyroxene, orthopyroxene and perthite grains in a fine-grained groundmass of quartz, microcline, plagioclase, amphibole, biotite and ilmenite. Orthoclase megacrysts have plagioclase rims, and hornblende partially pseudomorphs magmatic pyroxene grains and encloses ilmenite. Coarse-grained symplec-

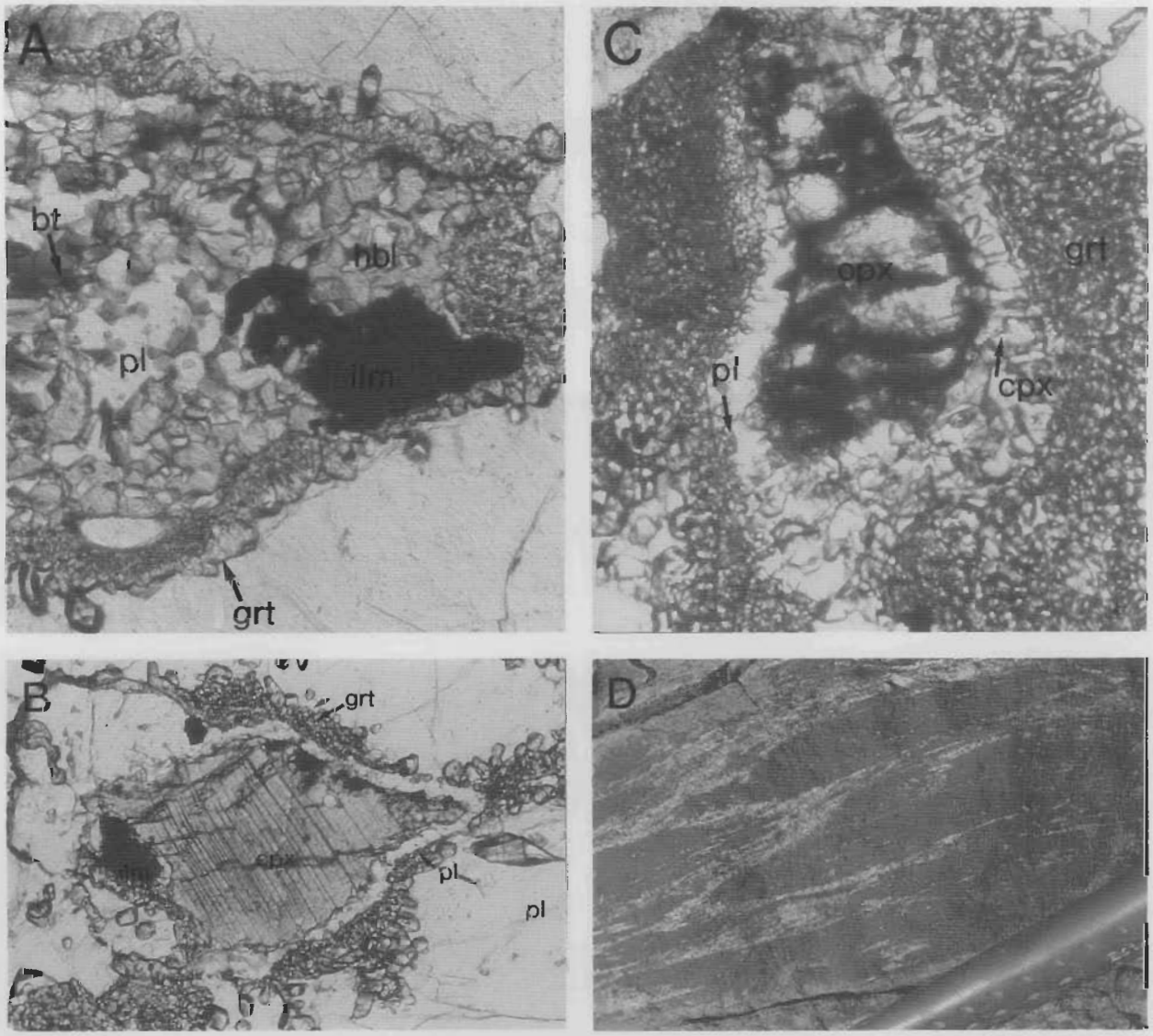

Figure 5. (A) A corona of garnet (grt) enclosing a symplectite of hornblende (hbl), biotite (bt), plagioclase (pl) and ilmenite (ilm), which is inferred to replace magmatic clinopyroxene (cpx). Plane-polarised light, sample 9198-9445b (charnockite). Width of field of view ≈ 2 mm. (B) Corona of plagioclase (pl) and garnet (grt) surrounding magmatic clinopyroxene (cpx) and ilmenite (ilm) Note the garnet corona continues away from clinopyroxene, along old plagioclase grain boundaries. Plane-polarised light, sample 9198-9445b (charnockite). Width of field of view ≈ 2 mm. (C) Relict magmatic orthopyroxene (opx) surrounded by a structured corona comprising a) an inner zone of symplectitic clinopyroxene (cpx) and plagioclas (pl), with or without biotite, and b) an outer corona of garnet (grt) against groundmass plagioclase (pl). Plane-polarised light, sample 9198-9458 (charnockite). Width of field of view ≈ 2 mm. (D) Close-up of the S_3 foliation in the mafic granulite (recrystallised gabbro), illustrating the discontinuous nature of the felsic layers in the unit. The impersistence of the felsic stringers contrasts with the thin laterally persistent felsic layers in the older layered felsic-mafic granulites (see Fig. 4A).

Table 1. Summary of the geological evolution of the western Musgrave Block.

Age (Ma)	Event	Metamorphic conditions	STRUCTURAL FABRICS		
			Folds	Dominant foliation	Lineation, dominant movement
1550[1]	Protolith of felsic granulites (North of Hinckley fault)				
1300[1]	Protolith of felsic granulites (South of Hinckley fault)				
	D_1		Rarely preserved	Layer parallel S_1, reoriented during D_2	None observed
1200[1]	Intrusion of charnockite				
	D_2	P=5±1 kbar,T>750°C F_2 folds, oriented parallel to L_2	Reclined isoclinal 335/15NE	Pervasive S_2 gneissosity L_2 15 --> 105	Pervasive intersection
1188 ±4[5]	Intrusion of fine grained granite and K-feldspar megacrystic granitoids				
1100[5]	Intrusion of mafic dykes Type A				
1080[5]	Intrusion of Giles Complex	P=6±1 kbar; uplift,erosion; extrusion of Tollu Group volcanics			
1060[5]	D_3 early late	P=11 kbar,T=650-700°C P=4.5±1 kbar	Open to isoclinal Upright F_3 folds	135/80NE	Down-dip mineral and stretching 80 -->025
1000[5]	Intrusion of mafic dykes Type C (including olivine+plagioclase dykes)				
800 Ma[3]	Intrusion of mafic dykes Type B				
	D_4 ultramylonite (SE transport)	Amphibolite facies		095/65N	42 -->325 Reverse
	D_5 mylonite/ultramylonite (SW transport)	Greenschist facies	160/80E	50 -->025 common fracture cleavage	Reverse
550 Ma[4,5]	D_6 **Petermann Orogeny** ultramylonite with psuedotachylite north - directed thrusting e.g. Champs de Mar Fault, Woodroffe Thrust	P=14.0±1.1 kbar, T=750°C	Large shear zones, extensive pseudotachylite	100/80S 085/60N	80 -->175 Reverse 60 -->350 Normal
	D_7 retrograde shear zones	Contains muscovite and biotite	Broad "crush" zones		80 -->030

16/A/249

[1] Rb-Sr whole rock isochrons,Gray (1971, 1977); [2] U-Pb on zircons, Maboko (1988);
[3] U-Pb on zircons, Sun & Sheraton (1992); [4] Ar^{39}-Ar^{40}, Maboko (1988); [5] Sun et al., in press

tites of amphibole, plagioclase, orthopyroxene, clinopyroxene and magnetite (3 cm diameter) are most probably related to the hydration of large magmatic pyroxenes. Narrow garnet coronas enclose magmatic clinopyroxene, orthopyroxene and/or magnetite in these symplectites (Fig. 5A, B, C), and garnet and biotite symplectites separate amphibole from K-feldspar. The mineral assemblages in these coronas and symplectites may be correlated with similar assemblages that define S_3 in ~1188 Ma felsic granitoids. Alternatively, they may correlate with much later garnet-bearing assemblages that occur in the post-S_3 mafic dykes.

Gabbroic rocks of the southern Hinckley Range are intruded by abundant feldspathic stringers and may contain isolated feldspar megacrysts. These rocks involve plagioclase and K-feldspar megacrysts (2–3 cm in diameter) surrounded by fine-grained plagioclase, quartz, orthopyroxene, clinopyroxene, biotite and opaque minerals. Stringers of charnockite are also observed cutting S_2 in the felsic granulites (Fig. 5D), but the stringers are deformed by S_3.

Rapakivi granite in some of the pre-Giles Complex stocks along the southern margin of the Hinckley Gabbro is gradational into the more common ~1188 Ma K-feldspar megacrystic granite on a scale of ten to one hundred metres. Zones rich in rapakivi-textured feldspars occur in a host with limited rapakivi-textured feldspar, or amongst zones of simple K-feldspar megacrystic granitoid. Zones of microgranite may accompany such gradations.

The Hinckley and Michael Hills gabbros

Concordant to discordant gabbroic bodies forming the Hinckley and Michael Hills gabbros intrude the layered felsic–mafic granulites (Fig. 4D), but in most places the contacts of the gabbro bodies have been extensively modified by later deformation. Along the northern margin of the Michael Hills gabbro in the Champ de Mars area, primary igneous banding on a macroscopic scale is truncated by a large retrograde shear zone (Fig. 2), with marginal recrystallisation of the gabbro forming amphibolite along this zone. Retrogression has occurred within 200 m of the shear zone, but elsewhere the gabbro shows only minor recrystallisation. The southern margin of the Hinckley gabbro is cut by a D4 ultramylonite, with recrystallisation restricted to within a few metres at the shear zone. The gabbroic to leucogabbroic rocks commonly retain an ophitic texture defined by coarse-grained (2 mm diameter), zoned and simply twinned, interdigitating plagioclase grains, with subordinate fine-grained (0.1 mm diameter) pyroxene.

Field work accompanied by interpretation of aerial photographs and Landsat Thematic Mapper images (Glikson & Creasey 1995—this issue) indicates consistent stratigraphic markers through some of the Giles Complex intrusions, allowing reasonable thickness estimates. For example, the Bell Rock Range intrusion is at least 9 km across and has a mean northeasterly dip of 60–70°, giving a true thickness of over 4 km along a strike of more than 25 km. Well-developed igneous banding is observed on all scales in much of the Michael Hills Gabbro. In places, this layering dips shallowly and has resulted in benches approximately 16 m high. Although disrupted by faulting, the Michael Hills body is at least 6 km across and crops out over 260 km2 that straddle the Western Australia–South Australia border (Daniels 1974). The magmatic layering has a mean dip of 70° (Daniels 1974), yielding a thickness estimated in excess of 5 km. However, it is difficult to estimate the thickness of the Hinckley gabbro, owing to its homogeneous composition and occurrence of shear zones, although it also could be over 5 km thick (Ballhaus 1992).

Mafic granulite (recrystallised gabbro)

In the west Hinckley Range, abundant dykes and small stocks of ~1080 Ma (Sun et al. in press) K-feldspar megacrystic granitoid and microgranite cut mafic granulite and residual pods of gabbro on all scales (Glikson 1990; Clarke 1992). This resulting heterogeneous unit is mapped as mafic granulite (recrystallised gabbro), and contains granite veined-mafic granulite that envelopes bodies of gabbro, amphibolite, and foliated granitoid. It has a banded, streaky expression on colour aerial photographs, owing to the intense development of the S_3 foliation. Compositional variations occur on a scale of 1–100 m. Large dykes of granitoid (>5 m diameter) commonly include angular xenoliths of foliated amphibolite derived from recrystallised gabbro (Fig. 4F). Numerous smaller granitoid dykes range from outcrop scale and veins to hand-specimen scale; most granitoid was intensely recrystallised during the development of S_3. The mafic granulite (recrystallised gabbro) is significantly finer grained than the layered felsic–mafic granulites, and, in thin section, does not generally have a well-developed gneissic layering.

Pods of gabbro may retain coarse-grained igneous textures that are cut by undeformed K-feldspar-rich veins and stringers and that are surrounded by a narrow zone of alteration/recrystallization. The granite veins contain quartz and microcline (with myrmekite), and have distinct angular margins without selvedges. Poikiloblastic plates of orthopyroxene and clinopyroxene, together with interdigitating plagioclase laths preserve the igneous fabric of the undeformed gabbro. However, aggregates of amphibole, ilmenite (minor haematite exsolution) and secondary orthopyroxene replace some clinopyroxene grains, and non-aligned grains of biotite and amphibole partially replace some pyroxene grains. The pseudomorphous textures and effects of recrystallisation increase in intensity towards the margins of the granite veins. The effects are observed at several scales: the size and density of the feldspathic stringers increase toward the margin of the gabbro bodies, with a concomitant increase in the intensity of the S_3 fabric (Fig. 5D) until the only mafic rock that can be recognised is mafic granulite (recrystallised gabbro). Similarly, granitoid veins and sheets may show gradational contacts with the mafic granulite, with a discontinuous S_3 gneissic layering developed in the mafic granulite by alternations of mafic and felsic rock. The mafic granulite commonly consists of a fine-grained (~0.5 mm diameter) recrystallised assemblage of hypersthene, clinopyroxene, plagioclase, biotite, haematite and quartz, which define a mylonitic S_3 foliation and envelop coarse-grained (2 mm diameter) igneous porphyroclasts of orthopyroxene, clinopyroxene and plagioclase. The pyroxene porphyroclasts have rutile and opaque minerals aligned in cleavage traces, and are distinct from the S_3 pyroxenes.

Mafic dykes

On the basis of field relationships, mafic dyke swarms of at least three distinct generations (Types A, B and C) have been recognised. Type A dykes cut all the above rock rock types, but their relation with the 1080 Ma felsic dykes is not known. Type A dykes are usually northwest-trending in the Champ de Mars area (Fig. 2), but north-trending and northeast-trending Type A dykes occur. The dominant trend of these dykes is due to post-intrusion deformation: Type A dykes were folded during the D_3 deformation, and, in most places, were aligned with the southeast-trending S_3 foliation. Thus, the present orientation of the Type A dyke swarm has little to do with regional stresses that may have been present during intrusion. Type A dykes dip steeply and typically have a granular texture, involving orthopyroxene, clinopyroxene, plagioclase, ilmenite and haematite with or without amphibole or biotite. The cores of the dykes commonly preserve a coarse-grained sub-ophitic texture defined by randomly oriented, zoned and simply twinned plagioclase laths with interstitial aggregates of orthopyoxene and clinopyroxene, which are commonly rimmed by biotite. Although there is no penetrative foliation in the cores of such dykes, a recrystallised mylonitic S_3 foliation, which contains clinopyroxene, orthopyroxene, plagioclase, biotite, quartz and haematite, occurs along their margins. Dykes that intrude the felsic granitoids commonly show recrystallisation to amphibolite; they contain S_3 amphibole, plagioclase and ilmenite with or without quartz. Where the dykes cut gabbro, they appear to have been protected from recrystallization associated with D_3 and primary igneous features are well preserved. We infer this to be due to the D_3 conditions in the gabbroic bodies having involved lower water activities than those for the surrounding felsic gneisses. The dykes cut igneous layering in the Michael Hills gabbro and rapakivi granite that intrudes the Hinckley gabbro. Consequently, whereas feeder dykes of the Giles Complex undoubtedly exist (Ballhaus 1992), the dykes observed in the present study post-date this basic plutonic phase. Sun et al. (in press) have determined the age of Type A dykes as 1100 Ma.

In the Champ de Mars area, S_3 is cut by large (3–5 m diameter), coarse-grained northwest-trending Type B dykes and smaller, fine-grained to aphanitic Type C dykes. Type B dykes are generally wide and coarse-grained, and preserve a clear ophitic texture, defined by interlocking plagioclase laths up to 1 cm long. Type C dykes trend dominantly northwest and northeast, and commonly contain olivine and plagioclase phenocrysts. A dyke in the southern part of the Champs de Mar area, with field relationships and geochemistry consistent with it being Type B, has been dated at ~ 800 Ma, whereas the age of Type C dykes is given as ~1000 Ma (Sun et al. in press). All dykes are displaced by D_{4-7} shear zones (Figs. 2 &

3).

Post-S_3 mafic dykes that occur near near D_6 ultramylonites on the Bates 1:100 000 sheet (Fig. 1), including olivine+plagioclase-bearing dykes correlated on geochemical grounds with Type C dykes in the Tomkinson Ranges (Sun & Sheraton 1992), are partially to completely recrystallised to garnet+clinopyroxene-bearing assemblages. Intensely recrystallised dykes contain amphibole, garnet, plagioclase, scapolite, clinopyroxene, clinozoisite, rutile and quartz, with or without kyanite, that define a pervasive S_6 foliation (Figs 6A, B, C, D). Large clinopyroxenes in these rocks include igneous porphyroclasts enveloped by amphibole, but small neoblastic clinopyroxene grains indicate partial recrystallisation of clinopyroxene (Fig. 6B). Kyanite, when present, is fine-grained and intergrown with garnet and rutile. Post-S_3 dykes that were less affected by shearing preserve sub-ophitic textures defined by intermeshing plagioclase, clinopyroxene and ilmenite grains, with or without olivine and/or orthopyroxene. Orthopyroxene, clinopyroxene and ilmenite are partially to completely replaced by symplectites of secondary clinopyroxene, plagioclase, amphibole and rutile, with or without biotite (Figs 6b, c). The symplectites or phenocrysts are surrounded by structured mineral coronas, involving an inner rim of quartz with or without plagioclase, a rarely developed intermediate rim of rutile, and an outer rim of garnet, which embays plagioclase with or without clinozoisite. Ilmenite phenocrysts are commonly enclosed by a structured mineral corona, involving an inner discontinuous rim of clinopyroxene and plagioclase, and then an outer rim of garnet or garnet+quartz symplectite. In dykes with primary olivine, plagioclase and orthopyroxene, olivine and plagioclase are separated by coronas involving metamorphic orthopyroxene adjacent to olivine, and garnet adjacent to plagioclase (Fig. 6E). Similarly, igneous orthopyroxene and plagioclase are separated by structured mineral coronas involving metamorphic clinopyroxene adjacent to orthopyroxene, and amphibole adjacent to plagioclase. Garnet has also formed along plagioclase–plagioclase grain boundaries.

Mineral chemistry

Analyses of samples appropriate to constraining the P–T history of the western Musgrave Block were made on the University of Sydney ETEC autoprobe and the University of Melbourne Cameca SX-50 Camebax microprobe, both operating with an accelerating voltage of 15 kV, a beam width of 1-10 m. Data were reduced using ZAF (Sydney) and PAP (Melbourne) matrix corrections. The major features of mineral chemistry for samples that are used for geothermobarometry are presented below. Representative microprobe analyses are listed in Table 2.

S_2 garnets in garnet+orthopyoxene-bearing gneisses from Mt Aloysius are grossular-poor and mostly spessartine-poor almandines, with a variable proportion of pyrope. X_{Fe} (=Fe/(Fe+Mg)) in the core of large garnet grains is 0.76 and 0.81, respectively, in samples 9117 and 9082. Whereas garnet in samples 9117 and 9082 has less than 2 wt% MnO, garnet in sample 9407a contains up to 10 wt% MnO. Garnet in rocks that show minimal effects of D_3 have a minor rimward increase in almandine, whereas garnet in rocks recrystallised during the development of S_3 are commonly strongly zoned in grossular content. For example, sample 9082 contains S_2 garnet and orthoproxene, with S_2 orthopyroxene enveloped and partially replaced by S_3 amphibole. Garnet in this rock shows appreciable rimward increase in grossular content (X_{gross} = Ca/(Fe+Mn+Mg+Ca) = 0.12 to 0.25) at the expense of almandine and pyrope contents (Fig. 7). S_2 garnet (X_{gross} = 0.07 to 0.09) and orthopyroxene in sample 9567B occur as porphyroclasts (Fig. 4C) that are wrapped in a foliation defined by clusters of fine-grained S_3 garnet. (X_{gross} = 0.20 to 0.23; Fig. 7). Garnet in the S_3 orthopyroxene+ plagioclase symplectites enclosing S_2 garnet in sample 9117 have similar grossular and almandine contents to the S_2 grains, consistent with it being relict S_2 garnet. S_3 garnet in the garnet+amphibole gneisses (recrystallised 1188 Ma granitoids) are essentially almandine and grossular mixtures. X_{Fe} and X_{gross} of garnet in sample 9455 are 0.87 and 0.25, respectively, and in sample 28-141-11 are 0.95 and 0.31. S_6 garnet in ultramylonites and recrystallised mafic dykes is a mixture of almandine, grossular and pyrope. X_{Fe} and X_{gross} of garnet in recrystallised dyke 9453 are 0.63 and 0.26, respectively, in recrystallised dyke 9480 are 0.60–0.65 and 0.22–0.29, and in ultramylonite 9435a are 0.80 and 0.28. S_6 garnet in recrystallised dyke 9485b varies from X_{Fe}= 0. 59, X_{gross}= 0.27 to X_{Fe}=0. 69, X_{gross}= 0.30, with pyrope and grossular contents varying antithetically. S_6 garnet in coronas developed around pyroxene and ilmenite in the partially recrystallised dykes is also an almandine, pyrope and grossular mixture and shows a restricted range in composition within individual samples. In sample 9497, garnet developed as a corona to ilmenite tends to be slightly richer in almandine and poorer in grossular (X_{Fe}= 0. 74, X_{gross}= 0.20) than garnet formed as a corona to clinopyroxene or along plagioclase–plagioclase grain boundaries (X_{Fe}= 0. 70, X_{gross}= 0.27 to 0.30). These variations in S_6 garnet composition within individual samples are interpreted as reflecting variations in chemistry of the local equilibration volumes that controlled garnet growth.

S_2 orthopyroxene in the garnet+orthopyroxene-bearing gneisses straddles the enstatite–ferrosillite boundary, with X_{Fe} between 0.51 and 0.55 in sample 9407a, 0.46 and 0.49 in sample 9117, and 0.49 and 0.51 in sample 9082. S_2 orthopyroxene is characterised by low (0.89–1.02 wt %; sample 9407a) to moderate (1.53–2.54 wt %; sample 9117) Al-contents. In the case of sample 9117, Al-contents increase from orthopyroxene cores to rims. S_6 clinopyroxene has Ca contents close to the top of the augite field, X_{Fe} ranging from 0.21 to 0.45 and up to 14% jadeite content. As for garnet, there is some variation in clinopyroxene composition within samples, depending on the textural context, but no systematic variation could be established in the mineral chemistry of porphyroclastic versus neoblastic clinopyroxene grains.

Whereas S_2 biotite has X_{Fe} ranging from 0.3 to 0.45, S_3 biotite has X_{Fe} ranging from 0.45 to 0.7. S_3 amphibole is pargasite, with X_{Fe} ranging from 0.6 to 0.8, and variable, but significant contents of both K and Na (Table 2). S_6 amphibole shows a range in composition that straddles the edenite–pargasite–hornblende–tschermakite join, but has a restricted range in X_{Fe} from 0.31 to 0.35. They are Na-poor and, in rocks that contain S_6 scapolite, have trivial Na content.

S_2 plagioclase in the garnet+orthopyroxene-bearing gneisses is labradorite in samples 9082 (An_{55-58}) and 9117 (An_{55-69}), and bytownite in sample 9407a (An_{84-90}). Symplectic S_3 plagioclase in sample 9117 is richer in Ca than large S_2 plagioclase grains (An_{69} cf. An_{55}). S_3 plagioclase in the garnet+amphibole gneisses (recrystallised ~1188 Ma granitoids) is oligoclase in samples 28-141-11 (An_{25}) and 9455 (An_{19-29}). Plagioclase shows a large range in composition in the recrystallised dykes, which is interpreted as representing the partial recrystallisation of igneous plagioclase grains. In the recrystallised mafic dykes 9485a and 9485b, plagioclase ranges from andesine to bytownite (An_{34-83}). In sample 9497, it ranges from oligoclase to andesine (An_{17-39}), with Na-rich plagioclase in coronas around clinopyroxene phenocrysts.

D_6 Scapolite in mafic dyke 9453 is close to mizzonite in composition (Eq_{An} = 62 to 70; where Eq_{An} = 100(Al-3)/3 for (Al + Si) = 12; Evans et al. 1969), is fully carbonated, and co-exists with D_6 plagioclase of An_{42} to An_{47}. Mafic dyke 9485a also contains coexisting D_6 intermediate scapolite ($Eq_{An65-67}$) and plagioclase (An_{30-40}).

D_6 clinozoisite from recrystallised mafic dykes is an epidote–clinozoisite solid solution, with approximately 35 to

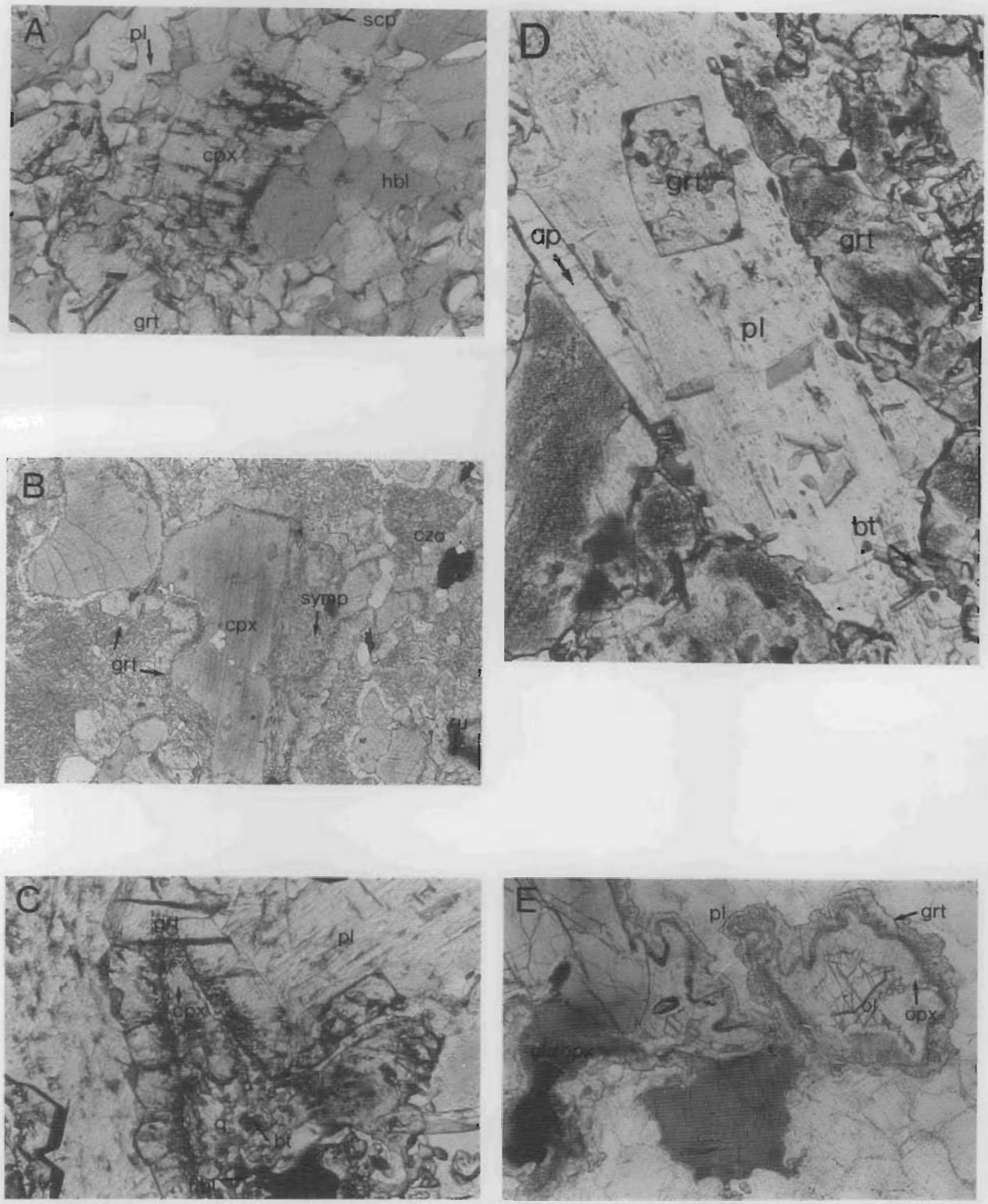

Figure 6. (A) D_6 sub-eclogite facies assemblage in metadolerite sample 9198-9453, comprising intergrown garnet (grt), scapolite (scp), hornblende (hbl) and plagioclase (pl), which enclose relict igneous clinopyroxene (cpx). Plane-polarised light, width of field of view ~ 2 mm. (B) D_6 sub-eclogite facies assemblage in metadolerite dyke sample 9198-9569d. The original magmatic clinopyroxene has been partially replaced by garnet (grt) and symplectites of neoblastic clinopyroxene (cpx) + hornblende (hbl) + plagioclase (pl), whereas magmatic calcic plagioclase has been replaced by acicular needles of clinozoisite (czo) in a matrix of sodic plagioclase. Note also the presence of rutile (ru) in the groundmass. Plane-polarised light, width of the field of view ~ 1.8 mm. (C) Structured D_6 corona, comprising an inner symplectite of neoblastic clinopyroxene (cpx), quartz (q), hornblende (hbl), plagioclase (pl) and biotite (bt; inferred as being after magmatic clinopyroxene), and an outer corona of garnet (grt). Plane-polarised light, sample 9198-9442 (metadolerite dyke). Width of field of view ~ 2 mm. (D) Magmatic plagioclase (pl) with interstital clinopyroxene being replaced along its margin by high-relief garnet (grt). Plagioclase contains inclusions of biotite, and is bordered on one side by prismatic apatite (ap). Plane-polarised light, sample 9198-9442 (metadolerite dyke). Width of field of view ~ 2 mm. (e) Structured D_6 corona, comprising an inner zone of orthopyroxene (opx) mantling igneous olivine (ol), and an outer zone of garnet (grt) mantling igneous plagioclase (pl). Garnet also mantles igneous orthopyroxene (old opx). Plane-polarised light, sample 9198-9550c (type C mafic dyke).

Table 2. Representative electron microprobe analyses of minerals from S_2, S_3 and S_6 assemblages.

mineral	*grt*	*grt*	*opx*	*bi*	*grt*	*grt*	*opx*	*bi*	*hbl*	*grt*	*hbl*	*bi*	*grt*	*grt*	*bi*	*cpx*	*hbl*	*grt*	*grt*	*ky*	*plag*
sample	*9117*	*9117.00*	*9117*	*9117*	*9082*	*9082*	*9082*	*9082*	*9082*	*9455*	*9455*	*9455*	*9445b*	*9445b*	*9445b*	*9445b*	*9485b*	*9485b*	*9485b*	*9485b*	*9485b*
paragenesis	*S2*	*S3*	*S2*	*S2*	*S2*	*S3*	*S2*	*S3*	*S3*	*S3*	*S3*	*S3*	*S6*	*S6*	*S6*	*S6*	*S6*	*S6*	*S6*	*S6*	*S6*
	rim	*symp*	*core*	*in g*									*with plag*	*co symp*	*in symp*	*in symp*					
SiO_2	38.27	35.45	50.79	37.64	38.61	42.52	50.50	36.78	40.97	38.21	40.34	36.66	38.22	37.90	37.34	51.48	44.283	38.567	36.069	36.669	57.911
TiO_2	0.06	3.36	0.04	6.55	0.12	0.05		5.50		0.10	1.83	4.92	0.01	0.05	5.75	0.14	0.723	0.031	0.026	0	0.023
Al_2O_3	21.60	21.09	1.53	14.13	21.44	20.67	1.62	14.27	14.15	20.78	12.13	13.28	21.45	20.86	12.99	2.03	13.357	22.184	22.163	63.193	26.256
Cr_2O_3	0.07																0	0.008	0.004	0.035	0
FeO	28.92	28.88	28.74	12.90	31.34	24.43	30.00	17.65	16.33	28.25	20.90	20.95	28.74	29.75	17.67	13.52	10.898	23.24	21.234	0.955	0.276
MnO	1.19	0.98	0.28	0.20	1.70	1.51	0.42	0.09	0.22	1.84	0.20	0.05	1.27	1.51	0.05	0.23	0.075	0.65	0.567	0.084	0.04
MgO	5.15	5.08	18.64	14.27	3.86	3.15	16.69	12.23	9.08	2.22	7.54	10.39	2.88	3.40	12.27	10.52	13.821	9.348	7.567	0.016	0
CaO	5.45	6.76	0.30	0.30	4.66	8.50	0.53		11.56	9.47	11.10		8.26	6.59	0.00	21.12	12.06	5.891	9.262	0.072	7.846
Na_2O			0.01	0.17				0.11	1.40		1.94	0.14			0.01	1.19	1.586	0.01	0.023	0.03	7.014
K_2O				8.34				9.82	2.27		1.99	9.53			9.61		0.57	0	0.024	0.016	0.153
TOTAL	**100.71**	**101.60**	**100.33**	**94.50**	**101.73**	**100.83**	**99.76**	**96.45**	**95.98**	**100.87**	**97.97**	**95.92**	**100.83**	**100.06**	**95.69**	**100.23**	**97.373**	**99.935**	**99.939**	**101.07**	**99.519**
O	12	12	6	22	12	12	6	22	23	12	23	22	12	12	22	6	23	12	12	5	8
Si	2.99	2.78	1.95	5.59	3.01	3.24	1.95	5.52	6.26	3.02	6.24	5.62	3.01	3.01	5.65	1.96	6.4514	2.9541	2.9890	0.9850	2.6048
Ti	0.00	0.19	0.00	0.73	0.01	0.00		0.62		0.01	0.21	0.57	0.00	0.00	0.65	0.00	0.0792	0.0018	0.0015	0.0000	0.0008
Al	1.99	1.95	0.07	2.47	1.97	1.86	0.07	2.52	2.58	1.93	2.21	2.40	1.99	1.95	2.31	0.09	2.2941	2.0033	1.9990	2.0012	1.3923
Cr	0.00																0.0000	0.0005	0.0002	0.0007	0.0000
Fe	1.89	1.89	0.92	1.60	2.05	1.56	0.97	2.22	2.11	1.87	2.70	2.69	1.89	1.98	2.23	0.43	1.3278	1.4891	1.3586	0.0215	0.0104
Mn	0.08	0.07	0.01	0.02	0.11	0.10	0.01	0.01	0.03	0.12	0.03	0.01	0.08	0.10	0.01	0.01	0.0093	0.0422	0.0367	0.0019	0.0015
Mg	0.60	0.59	1.06	3.16	0.45	0.36	0.96	2.73	2.09	0.26	1.74	2.37	0.34	0.40	2.76	0.60	3.0008	1.0671	0.8628	0.0006	0.0000
Ca	0.46	0.57	0.01	0.05	0.40	0.69	0.02		1.91	0.80	1.84		0.70	0.56	0.00	0.86	1.8826	0.4835	0.7593	0.0021	0.3781
Na			0.00	0.05				0.03	0.42		0.58	0.04			0.00	0.09	0.4480	0.0015	0.0034	0.0016	0.6117
K				1.58				1.88	0.45		0.39	1.86			1.85		0.1059	0.0000	0.0023	0.0005	0.0088
TOTAL	**8.01**	**8.04**	**4.02**	**15.25**	**8.00**	**7.81**	**3.98**	**15.53**	**15.85**	**8.01**	**15.94**	**15.56**	**8.01**	**8.00**	**15.46**	**4.04**	**15.5993**	**8.0430**	**8.0128**	**3.0151**	**5.0085**
XFe	0.76	0.76	0.46	0.34	0.82	0.81	0.50	0.45	0.50	0.88	0.61	0.53	0.85	0.83	0.45	0.42	0.31	0.58	0.61		
Xgross	0.15	0.18			0.13	0.25				0.26			0.23	0.18				0.16	0.25		

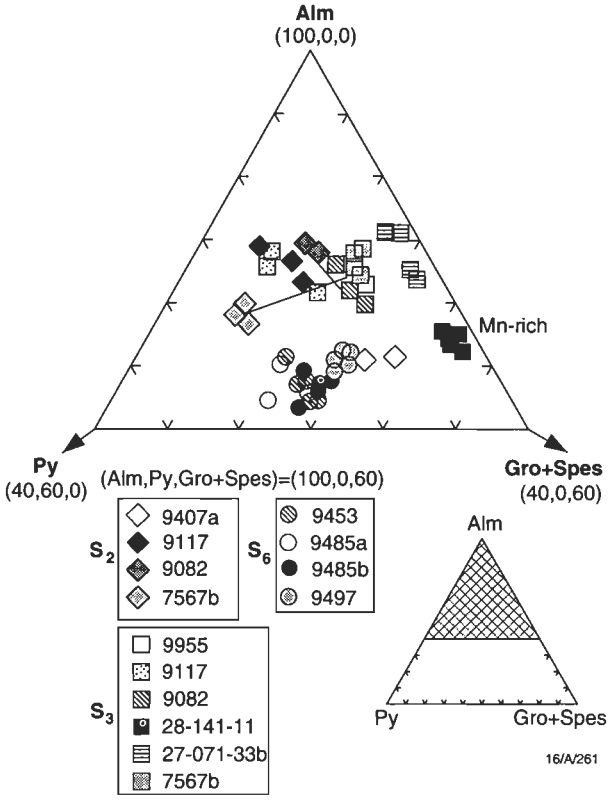

Figure 7. Compositional trends in representative garnets from the study area within the ternary Alm–Py–(Gr+Spes).

40 mol.% of epidote end-member.

The ilmenite end-member in ilmenite ranges from 0.87 to 1. Haematite is mostly pure. Kyanite may contain up 1% Fe_2O_3, but the proportion of Mn_2O_3 is negligible.

Pressure and temperature conditions

The mineral assemblages described above have potential for the estimation of pressure and temperature conditions, using a variety of directly calibrated geothermometers and geobarometers and the average pressure approach of Powell & Holland (1988) with the expanded, internally consistent dataset of Holland & Powell (1990). The essence of the latter approach is the combination of the pressures, calculated for each reaction in an independent set at an estimated temperature, involving *all* the mineral end-members shared between an (equilibrium) mineral assemblage and the dataset. In this way, the calculations maximise the information available from a mineral assemblage. The application of the average pressure approach to the Musgrave Block rocks is complicated by problems involving garnet and plagioclase composition–activity relations. However, owing to the complex history and range in P–T conditions experienced by Musgrave Block, the diverse mineral assemblages give an indication of the suitability of composition–activity models to various conditions. The results of the application of various geothermometers and barometers are summarised in Table 3.

Peak temperatures associated with the development of S_2 were at least 750°C on the basis of core analyses and garnet–orthopyroxene geothermometry (Harley 1984) for samples 9117, 9407a and 9082 (Table 3). The 873°C estimate for sample 9407a is unreliable, given the high MnO conent of both garnet and orthopyroxene. However, garnet–clinopyroxene geothermometry (after Ellis & Green 1979) for sample 28-142-25c, a calc-silicate gneiss, also returns a high estimate of 909°C. Pressure for the development of S_2 can be estimated by a variety of methods; a temperature of 750°C is assumed. Garnet–plagioclase–clinopyroxene–quartz exchange equilibria return an estimate of 5.1 kb for sample 28-142-25c, following the method of Eckert et al. (1991) with the plagioclase activity model corrected after Newton & Perkins (1982). This estimate is confirmed using garnet–orthopyroxene–plagioclase–quartz exchange equilibria and sample 9117, following the methods of Perkins & Chipera (1985), Eckert et al. (1991), and Bohlen et al. (1983), which all give results near 5.0 kb (Table 3). This estimate is consistent with results obtained by the average pressure approach of Powell & Holland (1988) and assuming ideal mixing on sites, which gives a pressure estimate of 5.0±1.0 kb for sample 9117, using the assemblage garnet, orthopyroxene, plagioclase, quartz and biotite. An inconsistent estimate of 8.61.7 kb is obtained from the average pressure approach of Powell & Holland (1988) with garnet A–X relations corrected after Berman (1990). This inconsistency suggests that for almandine-rich, grossular-poor garnets like those defining S_2, the average pressure method is best completed assuming ideal mixing on sites. Calculations made using samples 9407a and 9082 return estimates for S_2 conditions close to 5 kb (Table 3), which is considerably lower than inferred by earlier workers (Nesbitt et al. 1970; Goode & Moore 1975). The slightly disparate results obtained for sample 9082 probably reflect effects of incomplete recrystallisation during the development of S_3, which involves S_2 orthopyroxene replaced by S_3 hornblende and strongly zoned garnet. Garnet core compositions were used for estimates of S_2 conditions, and rim compositions for estimates of S_3.

Goode & Moore (1975) estimated high confining pressures in the range 10–12 kb for crystallisation of the Ewarara, Kalka, and Gosse Pile layered mafic/ultramafic intrusions of the Giles Complex on the basis of sub-solidus reactions between: (1) olivine and plagioclase reacting to produce orthopyroxene, clinopyroxene, spinel, and Ca-poor plagioclase; (2) orthopyroxene and plagioclase reacting to produce garnet; and (3) spinel and orthopyroxene reacting to produce garnet. More recent studies of the Wingellina Hills gabbronorite–pyroxenite body (Ballhaus & Berry 1991) indicate cooling of this intrusion from T=1150°C to 750°C at pressures of 6±1 kb, based on the reaction of olivine and plagioclase to produce symplectites involving orthopyroxene–clinopyroxene–spinel, olivine–spinel and spinel–clinopyroxene. As discussed further below, different intrusion depths could be expected because the intrusions are diverse in composition (and hence density; Ballhaus 1992), and the currently exposed structural level of the Musgrave Block was being pushed to greater crustal depths at about the same time as sill emplacement. Moreover, some of the garnet coronas may be completely unrelated to isobaric cooling of the Giles Complex.

Temperatures associated with the development of S_3 can be estimated using garnet–amphibole geothermometry in the recrystallised ~1188 Ma granitoids, since both garnet and amphibole formed during metamorphism. Approximately 700°C has been estimated for samples 9455 and 28-141-11, using the method of Graham & Powell (1984). Garnet in the S_3 orthopyroxene–plagioclase symplectites of sample 9117 could be used to give an estimate of 700°C (after Harley 1984), but this garnet is probably relict from the S_2 assemblage. Assuming a temperature of 700°C, the method of Kohn & Spear (1990) gives a pressure estimate for S_3 of 9 kb for sample 9082, compared with approximately 13 kb suggested by average pressure calculations (Powell & Holland 1988) using the assemblage garnet–hornblende–plagioclase–quartz–biotite. Although these estimates indicate a significant increase in pressure, they are possibly unreliable, owing to incomplete chemical re-equilibration during the development of S_3. However, the significant increase in pressure conditions is confirmed by sample 9455, a recrystallised felsic granitoid from the Bates 1:100 000 sheet area. The S_3 minerals, garnet,

Table 3: Summary of the results from the application of geothermometers and geobarometers.

Rock	*Location*	*Foliation*	*Assemblage*	*Assumed*		*T °C*	*P kbar*	*Method*
28-142-25c	Charnockite Flats	S_2	$Gr_{80}Alm_{20}$-$Woll_{50}Hed_{78}$-An_{97}-qtz	P=4		909		1
			$Gr_{80}Alm_{20}$-Hed_{78}-An_{97}-qtz	T=750			5.1	2
9117	Mt Aloysius	S_2	$Alm_{67}Py_{20}Gr_{10}$-Fs_{49}	P=4	cores	780		3
		S_2	$Alm_{67}Py_{20}Gr_{10}$-Fs_{49}-An_{78}-qtz	T=750	cores		P_{Fe}= 6.1	4
							4.9	5
							5.2	6
							5.5	7
			$Alm_{67}Py_{20}Gr_{10}$-Fs_{49}-An_{78}-Ann_{30}				5.0±1.0	8
							8.6±1.7	9
9407a	SE Bell Rock 100K	S_2	$Alm_{57}Py_{18}Gr_{15}$-Fs_{55}	P=4	cores	873		
			$Alm_{54}Py_{11}Gr_{16}$-Fs_{56}		rims	641		
			$Alm_{57}Py_{18}Gr_{15}$-Fs_{55}	T=750			P_{Fe}=5.5	4
			(Mn-rich garnet)				6.7	5
							4.0	6
							5.6	7
							3.8±1.1	8
							4.8±1.0	9
9082	Mt Aloysius	S_2	$Alm_{69}Py_{16}Gr_{12}$-Fs_{49}-An_{55}-qtz	T=750	cores		P_{Mg}=6.8 P_{Fe}=6.3	4
							2.9	5
							5.5	6
							6.2	7
							6.0±1.3	8
							6.4±1.2	9
		S_3	$Alm_{56}Py_{18}Gr_{25}$-Parg-An_{55}-qtz	T=700	rims		P_{Mg}=8.8 P_{Fe}=8.3	10
			$Alm_{56}Py_{18}Gr_{25}$-Parg-An_{55}-qtz-Ann_{45}				13.0±2.4	8
							13.5±1.7	9
9455	Bates 100K	S_3	$Alm_{62}Py_{10}Gr_{25}$-Parg			699		11
			$Alm_{62}Py_{10}Gr_{25}$-Parg-An_{29}-qtz	T=700			P_{Mg}=11.9 P_{Fe}=12.1	10
							13.6±3.0	8
							13.8±2.4	9
28-141-11	Champs de Mar	S_3	$Alm_{57}Py_3Gr_{32}$-Parg			670-754		11
			$Alm_{57}Py_3Gr_{32}$-Parg-An_{25}-qtz	T=700°C			P_{Mg}=11.1 P_{Fe}=11.2	10
			$Alm_{57}Py_3Gr_{32}$-Parg-An_{25}-qtz-Ksp90-Ann_{70}	T=700°C			9.8±2.5	8
9480	Bates 100K	S_6	$Alm_{46}Py_{24}Gr_{28}$-$Woll_{47}Hed_{18}$	P=12		764		1
			$Alm_{46}Py_{24}Gr_{28}$-Parg			762		11
			$Alm_{46}Py_{24}Gr_{28}$-Parg-An_{30}-qtz	T=700			P_{Mg}=12.7 P_{Fe}=12.4	10
			$Alm_{46}Py_{24}Gr_{28}$-Parg-An_{30}-qtz-$Cz_{64}Ep_{36}$				14.1±1.9	8
							14.4±1.7	9
9435a	Bates 100K	S_6	$Alm_{57}Py_{14}Gr_{29}$-$Woll_{42}Aug_{45}$	P=12		875		1
9453	Bates 100K	S_6	$Alm_{45}Py_{26}Gr_{29}$-Parg			811		11
			$Alm_{45}Py_{26}Gr_{29}$-$Woll_{46}Hed_{22}$	P=14		821		1
			$Alm_{45}Py_{26}Gr_{29}$-$Woll_{46}Hed_{22}$-An_{43}-qtz	T=750			9.7	2
			$Alm_{45}Py_{26}Gr_{29}$-$Woll_{46}Hed_{22}$-An_{43}-qtz-Parg			12.2±2.2	8	
							12.9±1.9	9
9485a	Bates 100K	S_6	$Alm_{47}Py_{32}Gr_{22}$-Parg			731		11
			$Alm_{47}Py_{32}Gr_{22}$-Parg-An38-qtz	T=750			P_{Mg}=11.7 P_{Fe}=11.8	10
			$Alm_{47}Py_{32}Gr_{22}$-Parg-An_{38}-qtz-Ky				14.0±1.1	8
							14.3±1.2	9
9485b	Bates 100K	S_6	$Alm_{45}Py_{29}Gr_{26}$-Parg			738		11
			$Alm_{45}Py_{29}Gr_{26}$-Parg-An_{35}-qtz	T=750			P_{Mg}=11.0 P_{Fe}=10.8	10
			$Alm_{45}Py_{29}Gr_{26}$-Parg-An_{35}-qtz-Ky				13.7±1.6	8
							14.3±1.6	9
9497	Bates 100K	S_6	$Alm_{49}Py_{23}Gr_{28}$-$Woll_{42}Aug_{39}$	P=14	(corona to S_3 hmte)	708		1
			$Alm_{49}Py_{23}Gr_{28}$-$Woll_{42}Aug_{39}$-An_{17}-qtz	T=750	(corona to cpx_{ig})		12.5	2
			$Alm_{49}Py_{23}Gr_{28}$-Parg-An_{17}-qtz	T=750	(corona to cpx_{ig})		P_{Mg}=14.0 P_{Fe}=13.5	10

Rock	*Location*	*Foliation*	*Assemblage*	*Assumed*		*T °C*	*P kbar*	*Method*
27-071-33b	Champs de Mar	S_6	$Alm_{30}Py_3Gr_{30}$-Parg	P=14	sympl	591		
			$Alm_{63}Py_4Gr_{23}$-$Woll_{43}Aug_{69}$		sympl	501		
			$Alm_{63}Py_4Gr_{23}$-$Woll_{43}Aug_{69}$-An_{26}-qtz	T=750	sympl		P_{Mg}=6.3 P_{Fe}=8.4	10
28-142-15a	Champs de Mar	S_6	$Alm_{66}Py_4Gr_{30}$-Parg		sympl	568		
			$Alm_{66}Py_4Gr_{30}$-Parg-An_{33}-qtz	T=750	sympl		P_{Mg}=6.8 P_{Fe}=8.7	10
				T=650			P_{Mg}=6.7 P_{Fe}=8.0	10

Methods: 1- Ellis &Green (1979); 2 - Eckert et al. (1991), corrected plag model after Newton & Perkins (1982); 3 - Harley (1984); 4 - Perkins & Chipero (1985) after Ganguly & Saxena (1984); 5 - Eckert et al. (1991), corrected plag model after Newton & Perkins (1982); 6 - Bohlen et al. (1983) with garnet A-X after Ganguly & Saxena (1984); 7 - Bohlen et al. (1983) with garnet A-X after Newton & Perkins (1982); 8 - Powell & Holland (1988), assuming ideal mixing on sites; Powell & Holland (1988) with garnet A-X after Berman (1990); 10 - Kohn & Spear (1990); 11 - Graham & Powell (1984).

Alm=Fe/(Fe+Mn+Mg+Ca); Py=Mg/(Fe+Mn+Mg+Ca); Gr=Ca/(Fe+Mn+Mg+Ca) in garnet Hed=Fe/(Fe+Mg) in hedenburgite; Aug = Fe/(Fe+Mg) in augite; Woll= Ca/2 in clinopyroxene
An= Ca/(Ca+Na+K) in plagioclase Fs = Fe/(Fe+Mg) in orthopyroxene Ann = Fe/(Fe+Mg) in biotite Cz = (Al-2)/((Al-2)+Fe) and Ep = Fe/((Al-2)+Fe) in epidote

hornblende, plagioclase, quartz, give a pressure estimate of 11–12 kbar for 9455, following the method of Kohn & Spear (1990) and 13.6±3.1 kb, following the average pressure method of (Powell & Holland 1988; Table 4). The average pressure result is improved to 13.8±2.4 kb when the garnet activity is modified after Berman (1990; Table 4). Although this refinement is generally the case for average pressure estimates involving high-P granulite facies, the trend does not hold for the sub-eclogite facies assemblages discussed below. Pressure estimates made using sample 28-141-11, a recrystallised felsic granitoid from the Champ de Mars, and the method of Kohn & Spear (1990), give similar results to those from 9455. The S_3 orthopyroxene–plagioclase symplectites that enclose S_2 garnet in sample 9117 reflect significantly lower pressure conditions of 4–6 kb (see, for example, Harley 1989). Thus, both high-P (9082) and low-P estimates (9117) are obtained for samples taken from Mt Aloysius that are not obviously separated by major faults. Since significant isothermal, syn-S_3 decompression of at least parts of the western Musgrave Block is inferred on the basis of the cordierite+hercynitic spinel coronas on garnet (Clarke & Powell 1991), the simplest explanation involves the orthopyroxene + plagioclase symplectites being an expression of such decompression in the garnet-bearing felsic rocks, and having formed late in D_3. Whereas the cordierite moats on garnet are not abundant and it could be argued that they are not representative of terrane-wide decompression, S_3 is cut by abundant and terrane-wide Type C olivine+plagioclase-bearing mafic dykes that do imply decompression from maximum D_3 pressures (see Green & Ringwood 1967; Banno & Green 1968).

Zones of intense D_6 recrystallisation involved minimum temperatures of 750°C on the basis of garnet–hornblende (Graham & Powell 1984) and garnet–clinopyroxene (Ellis & Green 1979) geothermometry, using recrystallised mafic dykes and felsic gneiss (Table 3). Consistent estimates (2–10°C) obtained using the two methods on individual samples agrees with the textural interpretation that neoblastic grains imply chemical re-equilibration of clinopyroxene in at least some rocks. Pressure estimates for S_6 are 11–15 kb (Tables 3 and 4). The composition of neoblastic clinopyroxene in the dykes, assuming its coexistence with plagioclase and quartz, implies S_6 pressures of 12–13 kb, after Holland (1983), for a temperature of 750°C. Calculations made using the assemblage garnet, hornblende, plagioclase and quartz in sample 9480 and following the method of Kohn & Spear (1990) give results of 12.4–12.7 kb (Table 3); a lower pressure estimate of 11.1 kb is obtained with the assemblage garnet, clinopyroxene, plagioclase and quartz for sample 9480, after Eckert et al. (1991). Average pressure calculations using the assemblage garnet, hornblende, plagioclase, quartz, clinopyroxene and clinozoisite in sample 9480 give a result of 14.1±1.9 kb, which is consistent with the result following the method of Kohn & Spear (1990). The result of the average pressure calculation varies from 13.2 to 15.0 kb for T=700–800°C (Table 4) and the result changes only slightly to 14.4±1.7 kb when garnet end-member activities are corrected following Berman (1990; Table 4). A statistically identical, but more precise, result of 14.0±1.1 kb is obtained for the assemblage garnet, hornblende, plagioclase, kyanite and quartz in sample 9485b and the average pressure method of Powell & Holland (1988). The pressure estimate for this sample ranges from 12.9 to 15.0 kbar for T=700–800°C (Table 4). Changing the garnet activity according to Berman (1990) does not improve the results for average pressure calculations using these sub-eclogite facies assemblages.

Whereas temperature and pressure can be estimated using symplectite assemblages for the less intensely recrystallised dykes (Table 3), they are of questionable significance since they involve complexities of limited diffusion and arrested reaction. Nonetheless, using complex symplectites and analyses from adjacent grains, identical conditions are implied for D_6 conditions on the Bates 1:100 000 sheet area (e.g. sample 9497, Table 3).

Pressure estimates for S_6 overlap with those for S_3. Whereas S_3 assemblages involve haematite, ilmenite, garnet and hornblende, the S_6 assemblages involve rutile, more Na-rich plagioclase, clinozoisite and, commonly, more Ca-rich garnet than S_3 minerals. Such distinctions are consistent with D_6 having occurred at conditions transitional between the granulite and eclogite facies (see Green & Ringwood 1967; Banno & Green 1968) and S_3 under high-T medium-P granulite facies conditions. The persistence of S_6 plagioclase precludes the assemblages from being true eclogites (Carswell 1990). The changes in mineral chemistry are consistent with S_3 conditions having involved lower pressure than those for S_6, but we cannot preclude the possibility that S_3 conditions were simply significantly more oxidising. The distinction between S_6 and S_3 assemblages is not, however, always clear. For example, several rocks from the Champ de Mars contain symplectitic assemblages that are similar to D_6 symplectites in recrystallised dykes from the Bates 1: 100 000 sheet (e.g. samples 27-074-33B (charnockite) and 28-142-15A (mafic granulite), Table 3). The Champ de Mars symplectites imply cooler conditions and lower pressures of 6–8 kb (Table 3) than were obtained from D_6 assemblages from the Bates 1:100 000 sheet. If these symplectites formed during D_6, then the lower pressure estimates are consistent with a shallowing in the structural level with distance south of the Woodroffe Thrust, as suggested by Ballhaus (1992). Alternatively, the assemblages may have

Table 4. Thermocalc output for average pressure calculations made on representative samples from the western Musgrave Block (after Powell & Holland, 1988; Holland & Powell, 1990).

Average pressure calculations for sample 9455, S_3 grt-hbl-hmte-plag-bi-Kf-q gneiss assuming ideal mixing on sites

	gr	py	alm	phl	ann	tr	ftr	hb	parg	ed	an	ab	ksp
Activities (a)	0.0152	8.30e-4	0.204	0.0908	0.0322	8.24e-5	1.86e-4	0.00179	0.00601	0.00155	0.300	0.700	0.900
σ (ln a)	0.50934	0.73879	0.15227	0.29288	0.41844	2.20326	1.01000	0.55030	0.62479	0.79018	0.14700	0.05000	0.05000

Independent reactions	Calculated pressures at T=700°C			
	P(T)	σ (P)	ln K	σ (ln K)
1) 4gr + 2py + 9hb + 3ab = 6tr + 3parg + 12an	18.9	6.06	2.720	14.569
2) 4gr + 2py + 6hb + 3ab = 3tr + 3ed + 12an	14.5	3.50	7.889	8.347
3) 2gr + 12alm + 9east + 3tr + 3ksp = 11py + 12ann + 12an	5.1	5.24	-22.329	12.908
4) 2gr + 7alm + 9east + 3ftr + 3ksp = 6py + 12ann + 12an	3.3	4.32	2.751	9.138
5) 3parg + 3ksp = 2gr + py + 3phl + 3ab	10.4	6.61	-8.075	2.432
6) 4gr + 9alm + 9east + 3tr + 3ab = 7py + 9ann + 3parg + 12an	3.4	4.14	5.370	11.020

T°C	650	675	700	725	750
avP	12.6	13.1	13.6	14.1	14.7
σ	2.7	2.9	3.1	3.3	3.5
σ_{fit}	1.3	1.4	1.4	1.5	1.5

garnet A-X after Berman (1990)

	gr	py	alm	all other end-members have the same activity as above
Activities (a)	0.0187	0.00196	0.237	
σ (ln a)	0.48564	0.68883	0.150	

Independent reactions	Calculated pressures at T=700°C			
	P(T)	σ (P)	ln K	σ (ln K)
1) 4gr + 2py + 6hb + 3ab = 3tr + 3ed + 12an	15.6	3.48	5.342	8.308
2) 4gr + 2py + 3tr + 6parg + 3ab = 9ed + 12an	6.9	4.58	15.681	10.822
3) 2gr + py + 10ann + 9hb + 3ksp = 13phl + 6ftr + 12an	13.7	5.25	8.623	9.890
4) 4gr + 10alm + 9hb + 3ab = 8py + 6ftr + 3parg + 12an	17.7	3.71	-42.894	10.212

T°C	650	675	700	725	750
avP	12.8	13.3	13.8	14.3	14.9
σ	2.1	2.3	2.4	2.6	2.8
σ_{fit}	1.0	1.1	1.1	1.2	1.2

Average pressure calculations for sample 9480, grt-hbl-cpx-ru-plag-q-ep gneiss

	gr	py	alm	di	hed	cz	ftr	hb	parg	ed	an	ab	q
Activities (a)	0.0205	0.0143	0.0902	0.595	0.146	0.622	2.35e-5	0.0653	0.0623	0.0133	0.290	0.710	1.0
σ (ln a)	0.47478	0.51612	0.27376	0.05000	0.22908	0.05000	4.12568	0.33253	0.33786	0.52336	0.25000	0.05000	0

Independent reactions — Calculated pressures at T=750°C

	P(T)	σ (P)	ln K	σ (ln K)
1) 4gr + 3hb + 3an = py + 9di + 6cz	16.6	2.70	15.680	2.392
2) 2gr + 4py + 6cz + 9q = 3hb + 12an	13.1	1.20	4.573	3.905
3) 4gr + 5alm + 6cz + 15q = 3ftr + 18an	15.9	2.81	-23.830	13.380
4) alm + 2hed + 2cz + 3q = ftr + 4an	17.0	4.16	-8.406	4.280
5) 4gr + 5py + 6cz + 3ab = 3di + 3parg + 15an	13.6	1.35	12.210	5.049
6) 8gr + 9py + 3ftr + 3ab = 5alm + 12di + 3ed + 12an	8.3	5.38	56.256	14.245

T°C	700	725	750	775	800
avP	13.2	13.7	14.1	14.6	15.0
σ	1.8	1.8	1.9	2.0	2.1
σ_{fit}	1.7	1.7	1.7	1.7	1.8

Average pressure calculations for sample 9485a, grt-hbl-ky-ru-plag-q gneiss

	gr	py	an	ab	tr	hb	parg	ed	q	ky
Activities (a)	0.00970	0.0300	0.310	0.690	0.00234	0.0733	0.0763	0.0137	1.0	1.0
σ (ln a)	0.55705	0.42759	0.15000	0.05000	4.27350	0.31909	0.31431	0.51937	0	0

Independent reactions — Calculated pressures at T=750°C

	P(T)	σ (P)	ln K	σ (ln K)
1) 4gr + 3tr + 12ky = py + 12an + 3hb	11.3	4.17	11.315	13.178
2) gr + q + 2ky = 3an	14.3	0.98	1.122	0.716
3) 12an + 3tr + 3ed = 4gr + 2py + 3ab + 6hb	19.8	5.91	2.750	13.395
4) 12an + 9ed = 4gr + 2py + 3ab + 3tr + 6parg	11.0	6.27	-7.613	14.097

T°C	700	720	740	750	760	780	800
avP	12.9	13.3	13.7	13.9	14.1	14.6	15.0
σ	1.1	1.1	1.1	1.1	1.1	1.1	1.1
σ_{fit}	1.3	1.2	1.2	1.2	1.1	1.1	1.1

formed during D_3. Without clear timing relationships between the development of these assemblages and S_3 it is not possible to assess the significance of the lower P–T estimates from the Champ de Mars symplectites.

Discussion

Mid-Proterozoic metasedimentary gneisses, felsic and mafic orthogneisses of the Tomkinson Ranges, western Musgrave Block, were affected by several periods of magmatism and deformation that spanned at least 600 million years. Granulite facies metamorphism and D_1-2 deformation at ~1200 Ma occurred under conditions of T>750°C and P=5±1.0 kbar. Such low-P granulite facies metamorphism could be related to an asthenospheric thermal perturbation, which must have been very strong to account for the high geotherm implied by the peak metamorphic conditions (Sandiford et al. 1991). If so, there should be field evidence for an extensive magmatic flux contemporary with peak conditions. The common large, simply twinned and zoned feldspar grains in the layered felsic–mafic granulites suggest that many of these rocks could be derived from recrystallised pre-D_1 mafic sills and/or dykes and felsic intrusions. Moreover, some felsic granulites, including charnockitic gneiss, cut S_1 but are affected by S_2, suggesting that felsic magmatism continued between D_1 and D_2. Any grossly discordant intrusive contacts were destroyed by recrystallisation during D_2. The monotonous nature of the layered felsic–mafic granulites is consistent with much of the exposed rock representing orthogneiss (see also Daniels 1974). However, the common discontinuous quartzite lenses suggest a significant component of metasedimentary gneiss (Gray 1971, 1978).

Large mafic to ultramafic layered intrusions comprising the Hinckley and Michael Hills gabbros are now thought to have been intruded at ~1080 Ma, i.e. near-contemporaneously with the 1080 Ma Tollu Group volcanics (Sun et al. in press). Estimates for confining pressures during intrusion of the Giles Complex centre on 6 kb on the basis of cooling-induced mineral reaction textures (Ballhaus & Berry 1991) and lower pressures in the western intrusions (Ballhaus & Glikson 1995—this issue). The thin nature of rare chilled margins suggests that the country rocks were still at temperatures well above the stable continental geotherm, consistent with intrusion of the Giles Complex into high-temperature host rocks. Intrusion of younger granitic veins and dykes contemporaneously with extensive volcanic activity of the Tollu Group followed at about 1080–1060 Ma (Sun et al. in press), and was associated with the recrystallisation of gabbro to mafic granulites. D_3 resulted in an impersistent, steep southeast-trending S_3 foliation at high-P conditions of T=650–700°C and P≈11 kb. Whereas the Type A mafic dykes show marginal to complete recrystallisation to granulite facies mylonitic S_3 assemblages, in most places the layered intrusions of the Giles Complex were not exposed to hydrous conditions during D_3 and are, therefore, little affected, except along shear zones. However, parts of the Hinckley gabbro and the Michael Hills gabbro were extensively intruded by the ~1060 Ma granite dykes. The introduced volatiles resulted in syn-D_3 recrystallisation of gabbro to mafic granulite (cf. Daniels 1974; Glikson 1990; Stewart & Glikson 1991). The Tollu Group is overlain by the Townsend Quartzite, which forms a likely equivalent of the areally extensive Heavitree Quartzite, located at the base of the Late Proterozoic to Phanerozoic Amadeus Basin (Forman 1965). Significant uplift and exposure of at least part of the currently exposed structural level of the Musgrave Block, i.e. south and west of the Blackstone and Bell Rock ranges, predated D_3, forming a source of sediments whose present location remains unknown.

The 1080–1060 Ma magmatic event is now shown to be the dominant event within the Musgrave Block (Sun et al. in press). Near-isothermal decompression of the western Hinckley Range to conditions of P = 4–5 kb (Clarke & Powell 1991) is inferred to have occurred late in D_3 on the basis of syn-S_3 cordierite coronas on garnet. Given that the cordierite+spinel coronas on garnet imply thermally perturbed conditions (Clarke & Powell 1991), it is tempting to temporally link D_3 with the ~1060 Ma metamorphism. However, whereas sections of the Musgrave Block within the Tomkinson Ranges and Bates 1:100 000 sheet area apparently experienced high-pressure early in D_3 and were being intruded by 1080–1060 Ma mafic and granitic dykes, other sections west of Bell Rock and south of Blackstone were close to the surface at that time—forming a basement for the Tollu Group volcanics. Significant dislocation of the Musgrave Block did occur during D_6 (see below) and it is probable that such tectonism has disrupted any pattern of S_1–3 isograds. Assuming that S_3 and the ~1060 Ma magmatism are related, it is also possible that thermal weakening may have ultimately resulted in extensional tectonism, possibly involving large detachments, resulting in the rapid exhumation of the dense intrusions and surrounding rocks (e.g. Lister & Baldwin 1993). Such a tectonic setting could be appropriate for the syn-S_3 cordierite coronas on garnet.

On the Bates 1:100 000 sheet area, 800 Ma mafic dykes cut S_3, but were recrystallised by a second high-pressure event during the 550 Ma Petermann Orogeny (Forman 1965; Maboko et al. 1992; Camacho & Fanning in press) that exposed crustal levels of the western Musgrave Block formed under T>750° and P=14±1 kb. Corona textures that may perhaps be correlated with this orogeny occur in rocks throughout the western Musgrave Block, but they are not as well developed and cannot be unambiguously constrained as being post-S_3. Similar high-temperature sub-eclogite facies assemblages have been reported from large ultramylonite zones farther east in the Musgrave Block (Ellis & Maboko 1992). Considerable movement is also evident along related thrusts in the Musgrave Ranges in this area (Major 1973), where Late Proterozoic cover rocks of the Amadeus Basin to the north include kyanite ± staurolite + muscovite schists (Forman 1965), and where the granulite facies Musgrave Block was thrust over the amphibolite facies Olia Gneiss terrane (Forman 1965; Maboko et al. 1992). Whereas the earlier cycle of D_{1-3} events and contemporaneous metamorphism required extensive contributions of heat in the form of a magmatic flux, the P–T conditions recorded by the 550 Ma D_6 event are interpreted in terms of tectonic exhumation: large thrust surfaces such as the Woodroffe Thrust, some of which *could* be reactivated late-D_3 detachment faults, resulted in nappe-style stacking of the Musgrave Block and Amadeus Basin sediments to the north. The structural significance of these late faults has been recognised for some time (Forman & Shaw 1973; Bell 1978): for example, the Woodroffe Thrust has been interpreted as the root zone of the Petermann Ranges Nappe at the southwest margin of the Amadeus Basin. Polymictic boulder beds and matrix-supported, poorly sorted conglomeratic sandstones of the Olgas Range are interpreted as thrust-scarp front molasse (Sweet & Crick 1992). The role of high-P shear zones and effects of high-P recrystallisation on post-S_3 mafic dykes has recently been recognised south of the Woodroffe Thrust in the Bates 1:100 000 sheet area (Stewart 1993). In this area, northward overthrusting during D_6 of a crustal section >25 km thick has resulted in the exhumation of granulites on the southern edge of the block. Thus the Woodroffe Thrust formed a crustal suture that controlled the 550 Ma old north–south convergence of the Musgrave Block and the Amadeus Basin. The lateral extent of such crustal overthickening and the extension of the Woodroffe Thrust into the Paterson province in northwestern Australia (Horwitz & Daniels 1966; Myers 1990) remain the subject of further field work in the westernmost Musgrave Block.

Some of the garnet-bearing corona textures within intrusions

of the Giles Complex match very closely those in post-S_3 dykes that were less affected by shearing during the eclogite facies event, and may thus be related only to the 550 Ma eclogite event rather than to post-intrusion cooling. Whereas all of the Giles Complex intrusions in the Tomkinson Ranges pre-date D_3, the levels of crustal emplacement and precise ages of the different intrusions remain a subject for further isotopic and PT investigations.

Acknowledgements

GLC acknowledges support from the Division of Regional Geology and Minerals, Western Musgrave Project (211.14), of the Australian Geological Survey Organisation, and Australian Research Council Grant No. A39230559. ISB acknowledges support from ARC Grant No. A38930485 (to Powell & Wilson, University of Melbourne) and a La Trobe University Research Fellowship. Comments by T. Bell, R.W. White, an anonymous reviewer and S.-S. Sun improved earlier versions of the manuscript. This is a contribution to IGCP 304—Lower Crustal Processes.

References

Ballhaus, C.G., 1992. Petrology of the layered mafic/ultramafic Giles Complex, western Musgrave Block, Western Australia. Australian Geological Survey Organisation, Record 1992/73.

Ballhaus C. & Berry R.F., 1991. Crystallization pressure and cooling history of the Giles layered igneous complex, central Australia. Journal of Petrology, 32, 1–28.

Ballhaus C.G. & Glikson A.J., 1989. Magma mixing and intraplutonic quenching in the Wingellina Hills Intrusion, Giles Complex, central Australia. Journal of Petrology, 30, 1443–1470.

Banno, S. & Green, D.H., 1968. Experimental studies on eclogites: the roles of magnetite and acmite in eclogite assemblages. Chemical Geology, 3, 21–32.

Bell T.H., 1978. Progressive deformation and reorientation of fold axes in a ductile mylonite zone: the Woodroffe thrust. Tectonophysics , 44, 285–320.

Berman, R.G., 1990. Mixing properties of Ca-Mg-Fe-Mn garnets. American Mineralogist, 75, 328–344.

Bohlen, S.R., Wall, V.J. & Boettcher, A.L., 1983. Experimental investigation and application of garnet granulite equilibria. Contributions to Mineralogy and Petrology, 83, 52–61.

Camacho, A. & Fanning, C.M., in press. Some isotopic constraints on the evolution of the granulite and upper amphibolite facies terranes in the eastern Musgrave Block, central Australia. Precambrian Research.

Carswell, D.A., 1990. Eclogites and the eclogite facies: definitions and classification. In: Carswell, D.A. (editor), Eclogite facies rocks. Blackie, London, pp 1–13.

Clarke, G.L., 1992. Field relationships and tectonic history of the Hinckley Gabbro, felsic to mafic granulites and granitoids, west Hinckley Range and Champ de Mars areas, Tomkinson Ranges, Musgrave Block, W.A. Australian Geological Survey Organisation, Record 1992/33.

Clarke, G.L. & Powell R., 1991. Decompressional coronas and symplectites in granulites of the Musgrave Block, central Australia. Journal of Metamorphic Geology, 9, 441–440.

Clarke, G.L., Sun, S.-S. & White, R.W., 1994. Grenville-age belts and associated older terranes in Australia and Antarctica. AGSO Journal of Australian Geology & Geophysics, this issue.

Daniels J.L., 1974. The geology of the Blackstone Region Western Australia. Bulletin of the Geological Survey of Western Australia, 123, 257 pp.

Eckert, J.O., Newton, R.C. & Kleppa, O.J., 1991. The H of reaction and recalibration of garnet-pyroxene-plagioclase-quartz geobarometers in the CMAS system by solution calorimetry. American Mineralogist, 76, 148–160.

Ellis, D.J. & Green, D.H., 1979. An experimental study of the effect of Ca upon garnet-clinopyroxene Fe-Mg exchange equilibria. Contributions to Mineralogy and Petrology, 71, 13–22.

Ellis, D.J. & Maboko, M.A.H., 1992. Precambrian tectonics and the physicochemical evolution of the continental crust. I. The gabbro eclogite transition revisited. Precambrian Research, 55, 491–506.

Evans, B.W., Shaw, D.M., & Houghton, D.R., 1969. Scapolite stoichiometry. Contributions to Mineralogy and Petrology, 24, 293–305.

Forman D.J., 1965. Ayers Rock, Northern Territory, 1:250,000 geological map sheet. Bureau of Mineral Resources, Geology & Geophysics, Canberra.

Forman D.J. & Shaw R.D., 1973. Deformation of the crust and mantle in central Australia. Bureau of Mineral Resources, Australia, Bulletin 144, 20 pp.

Glikson, A.Y., 1990. The Giles Complex, central Australia: new insights into tectonics and metamorphism. BMR Research Newsletter, 12, 18–20

Glikson, A.Y., Ballhaus, C.J., Goleby, B.R. & Shaw, R.D., 1990. Major thrust faults and the vertical zonation of the middle to upper Proterozoic crust in central Australia. In: Salisbury, M.H. & Fountain, D.M. (editors), Exposed cross sections of the continental crust. Kluwer Academic Publishers, pp. 285–304.

Goode A.D.T., 1978. High temperature, high strain rate deformation in the lower crustal Kalka Intrusion, central Australia. Contributions to Mineralogy and Petrology, 66, 137–148.

Goode, A.D.T. & Krieg, G.W., 1967. The geology of the Ewarra intrusion, Giles Complex, central Australia. Journal of the Geological Society of Australia, 14, 185–194.

Goode, A.D.T. & Moore, A.C., 1975. High-pressure crystallization of the Ewarra, Kalka and Gosse Pile intrusions, Giles Complex, central Australia. Contributions to Mineralogy and Petrology, 51.

Graham, C.M. & Powell, R., 1984. A garnet-hornblende geothermometer: calibration, testing, and application to the Pelona Schist, Southern California. Journal of Metamorphic Geology, 2, 13–31.

Gray C.M., 1971. Strontium isotopic studies on granulites. Ph.D. thesis, Australian National University, Canberra (unpublished).

Gray C.M., 1977. The geochemistry of central Australian granulites in relation to the chemical and isotopic effects of granulite facies metamorphism. Contributions to Mineralogy and Petrology, 65, 79–89.

Gray C.M., 1978. Geochronology of granulite facies gneisses in the Western Musgrave Block, central Australia. Journal of the Geological Society of Australia, 25, 403–414.

Green, D.H. & Ringwood, A.E., 1967. An experimental investigation of the gabbro to eclogite transformation and its petrologic application. Geochimica et Cosmochimica Acta, 3, 767–834.

Harley, S.L., 1984. An experimental study of the partitioning of Fe and Mg between garnet and orthopyroxene. Contributions to Mineralogy & Petrology, 86, 359–373.

Harley, S.L., 1989. The origins of granulites: a metamorphic perspective. Geological Magazine, 126, 215–247.

Holland, T.J.B., 1980, The reaction albite = jadeite + quartz determined experimentally in the range 600–1200°C. American Mineralogist, 65, 129–134.

Holland, T.J.B. & Powell, R., 1990. An enlarged and

updated internally consistent dataset with uncertainties and correlations: the system K_2O–Na_2O–CaO–MgO–MnO–FeO–Fe_2O_3–Al_2O_3–TiO_2–SiO_2–C–H_2–O_2. Journal of Metamorphic Geology, 8, 89–124.

Horwitz, R.C. & Daniels, J.D., 1966. A late Precambrain belt of volcanicity in central Australia. Geological Survey of Western Australia, Annual Report, 1966, 50–53.

Hossfeld, P.S. 1954. Stratigraphy and structure of of the Northern Territory. Transactions of the Royal Society of South Australia, 77, 103–161.

Kohn, M.J. & Spear, F.S., 1990. Two new geobarometers for garnet amphibolites, with applications to southeastern Vermont. American Mineralogist, 75, 89–96.

Lister, G.S. & Baldwin, S.L., 1993. Plutonism and the origin of metamorphic core complexes. Geology, 21, 607–610.

Maboko M.A.H., 1988. Metamorphic and geochronological evolution in the Musgrave Ranges, central Australia. Ph.D. thesis, Australian National University, Canberra (unpublished).

Maboko M.A.H., Williams I.S. & Compston W., 1991. Zircon U-Pb chronometry of the pressure and temperature history of granulites in the Musgrave Ranges, central Australia. Journal of Geology, 99, 675–697.

Maboko M.A.H., Williams I.S. & Compston W., 1992. Geochronological evidence for ~530–550 Ma juxtaposition of two Proterozoic metamorphic terranes in the Musgrave Ranges, central Australia. Australian Journal of Earth Sciences, 39, 457–471.

Major R.B. 1973. Woodroofe, South Australia, 1:250,000 geological map sheet. Geological Survey of South Australia, Adelaide.

Moore A.C., 1969. Corona textures in granulites from the Tomkinson Ranges, central Australia. Special Publication of the Geological Society of Australia, 2, 361–366.

Moore A.C. & Goode A.D.T., 1978. Petrography and origin of granulite facies rocks in the western Musgrave Block, central Australia. Journal of the Geological Society of Australia, 25, 341–358.

Moores, E.S., 1991. SWEAT: a hypothesis. Geology, 19, 325–428.

Myers, J.S., 1990. Precambian tectonic evolution of part of Gondwana, southwestern Australia. Geology, 18, 537–540.

Nesbitt R.W. & Kleeman A.W., 1964. Layered intrusions of the Giles Complex, central Australia. Nature, 203, 391–393.

Nesbitt R.W. & Talbot J.L., 1966. The layered basic and ultrabasic intrusives of the Giles Complex, central Australia. Contributions to Mineralogy and Petrology, 13, 1–11.

Nesbitt R.W., Goode A.D.T., Moore A.C. & Hopwood T.P., 1970. The Giles Complex, central Australia: a stratified sequence of mafic and ultramafic intrusions. Geological Society of South Africa, Special Publication, 1, 547–564.

Newton, R.C. & Perkins, D., 1982. Thermodynamic calibration of geobarometers based on the assemblages garnet-plagioclase-orthopyroxene (clinopyroxene)-quartz. American Mineralogist, 67, 203–222.

Perkins, D. & Chipera, S.J., 1985. Garnet-orthopyroxene-plagioclase-quartz barometry: refinement and application to the English River subprovince and the Minnesota River Valley. Contributions to Mineralogy and Petrology, 89, 69–80.

Powell, R. & Holland, T.J.B., 1988. An internally consistent dataset with uncertainties and correlations: 3. Applications to geobarometry, worked examples and a computer program. Journal of Metamorphic Geology, 6, 173–204.

Sandiford M., Martin N., Zhou S. & Fraser G., 1991. Mechanical consequences of granite emplacement during high-T, low-P metamorphism and the origin of "anticlockwise" PT paths. Earth and Planetary Science Letters, 107, 164–172.

Sprigg R.C., & Wilson R.B., 1959. The Musgrave mountain belt in South Australia. Geologische Rundschau, 47, 531–542.

Stewart, A.J., 1993. Extension of the Woodroffe Thrust into Western Australia. Australian Geological Survey Organisation, Research Newsletter, 18, 5–6.

Stewart, A.J., 1995. Resolution of conflicting structures and deformation history of the Mount Aloysius granulite massif, western Musgrave Block, central Australia. AGSO Journal of Australian Geology & Geophysics, 16(1), this issue.

Stewart, A.J., in press. Bates 1:100K geological mapsheet and explanatory notes. Australian Geological Survey Organisation, Canberra.

Stewart, A.J. & Glikson, A.Y., 1991. The felsic metamorphic/igneous core complexes hosting the Giles Complex. BMR Research Newsletter, 14, 6–7.

Sun, S.-S., Gray, C.M., Sheraton, J.W., Glikson, A.Y. & Stewart, A.J., 1994a. Zircon U–Pb chronology and neodymium isotope study of tectonothermal and crust-forming events in the Tomkinson Ranges, western Musgrave Block, central Australia. AGSO Journal of Australian Geology & Geophysics, this issue.

Sun, S.-S. & Sheraton, J., 1992. Zircon U/Pb chronology, tectonothermal and crust-forming events in the Tomkinson Ranges, Musgrave Block, central Australia. AGSO Research Newsletter, 17, 9–10.

Sweet, I.P. & Crick, I.H., 1992. Uluru & Kata Tjuta: a geological history. Australian Geological Survey Organisation, Canberra, 27 pp.

AGSO Journal of Australian Geology & Geophysics, 16 (1/2), 147–153

Western extension of the Woodroffe Thrust, Musgrave Block, central Australia

A.J.Stewart[1]

The Woodroffe Thrust has until now been known in outcrop only in South Australia and the Northern Territory, where it forms part of a system of south-dipping thrust faults that penetrate the continental crust forming the Proterozoic Musgrave Block. Detailed mapping by AGSO in 1991 located new exposures of granite mylonite—previously mapped as sheared porphyry—in Western Australia, at a position predicted from geophysical data some 20 years earlier, and 120 km farther west than the most westerly known previous exposure. The Western Australian exposures of the thrust separate subeclogite facies metamorphic rocks and deformed granite in the south from amphibolite facies deformed granite in the north. The thrust dips gently south, and is marked by isolated exposures of mylonite derived from the granite north of the thrust. Lineations in the mylonite and in the northern and southern terranes are subhorizontal to gently plunging and east-northeast-trending, oblique to the strike of the thrust.

Introduction and geological setting

The Woodroffe Thrust in the Musgrave Block is part of a major system of south-dipping thrust faults that penetrate the continental crust on the southern margin of the Amadeus Basin, central Australia (Fig. 1). A 'mirror-image' counterpart—the north-dipping Redbank Thrust Zone—is present in the Arunta Block north of the basin. Detailed mapping by AGSO in 1991 has shown that the Woodroffe Thrust extends 120 km farther west than previously known.

The Musgrave Block (Fig. 2) consists chiefly of supracrustal metavolcanics and metasediments intruded by layered mafic intrusions (Giles Complex), granites, and mafic dykes. Metamorphic facies ranges from greenschist to subeclogite. The parent volcanics and sediments accumulated between about 1550 and 1330 Ma, and were metamorphosed at about 1200 Ma (Gray 1978; Gray & Compston 1978; Sun & Sheraton 1992). Renewed tectonism—the Petermann Ranges Orogeny—formed major east-striking thrust-faults, ranging from low to high-angle, including the Woodroffe Thrust, at about 550 Ma (Camacho

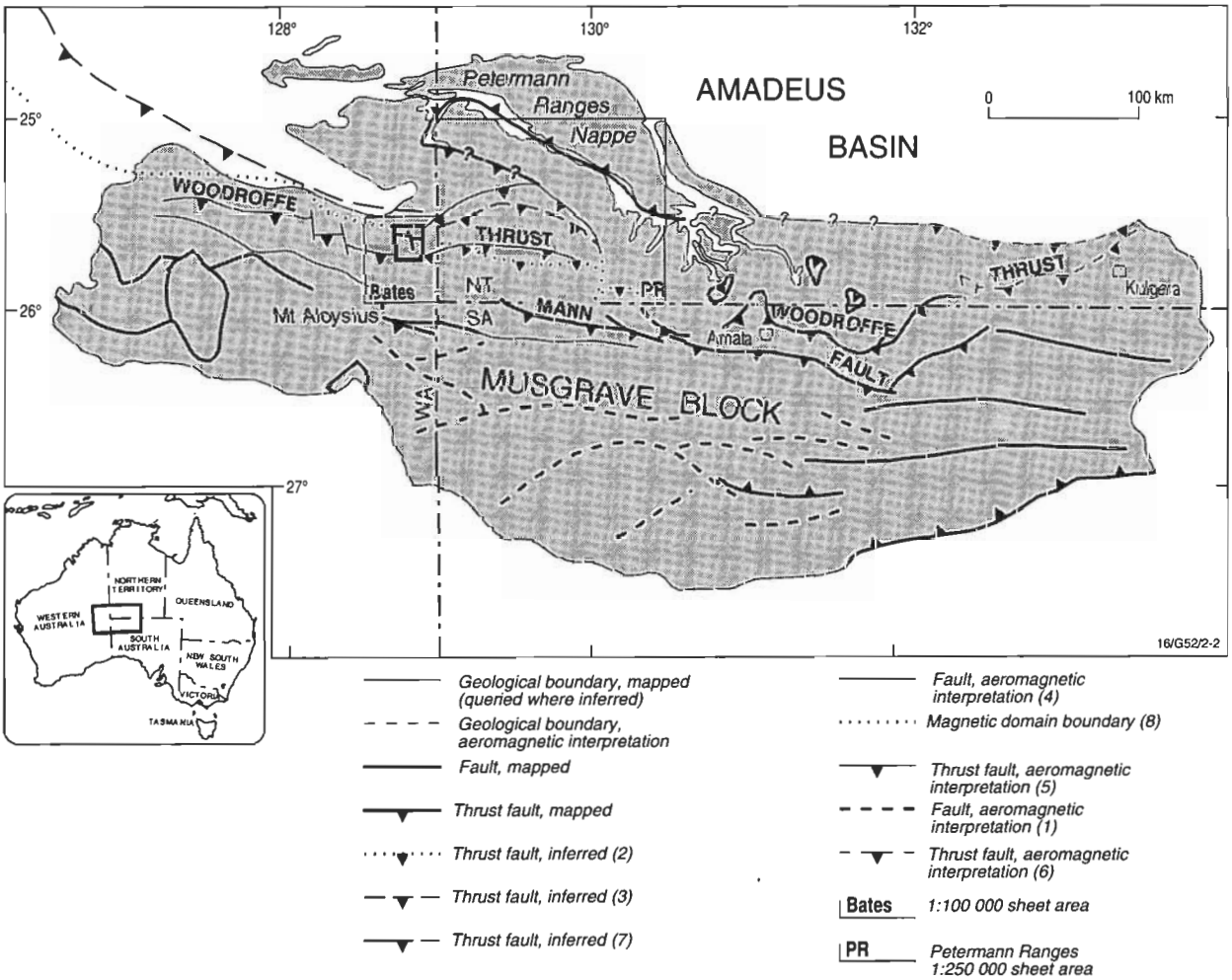

Figure 1. Structural map of Musgrave Block, showing major faults, locations of Petermann Ranges (PR) 1:250 000 and Bates 1:100 000 Sheet areas, and of Figure 4 (bold rectangle). [1]A.J. Stewart, AGSO, unpublished data; [2]Forman 1972; [3]D'Addario et al. 1976; [4,5]Pharaoh 1990; [6]Edgoose et al. 1993; [7]Myers 1990; [8]Shaw in Reeves et al. 1994.

[1] Division of Regional Geology & Minerals, Australian Geological Survey Organisation, GPO Box 378, Canberra, ACT 2601

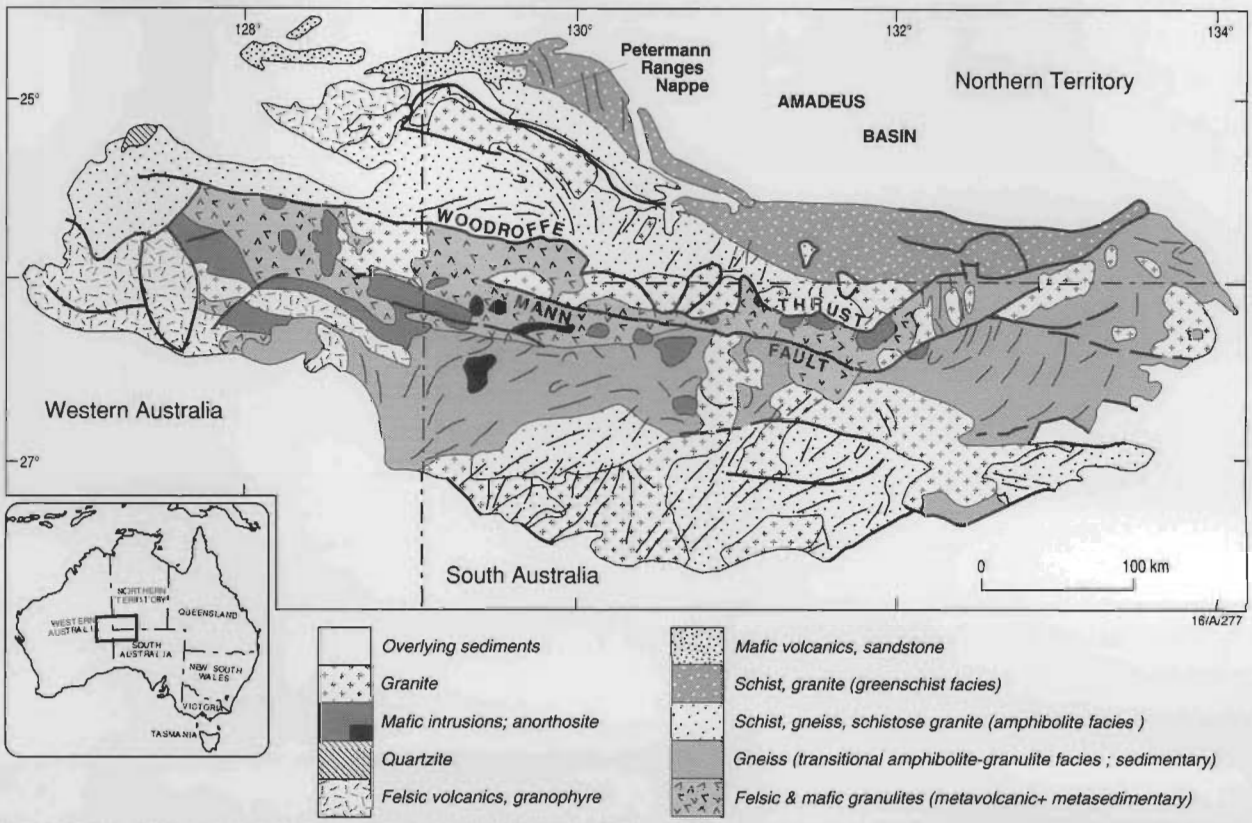

Figure 2. Geological map of Musgrave Block (compiled from Daniels 1974; Stewart 1992; B.P. Thomson, R.C. Mirams, J.E. Johnson, R.B. Major, R.C. Sprigg, B. Wilson, R.P. Coats, J.A. Teluk, G.W. Krieg, P.A. Rogers et al. 1959–1984, Mann, Woodroffe, Alberga, Abminga, Birksgate, Everard & Lindsay 1:250 000 geological maps, Geological Survey of South Australia. Western part of Woodroffe Thrust in the Northern Territory is after Forman (1972); in Western Australia, after this study and Pharaoh (1990).

Figure 3. Largest exposure of Woodroffe Thrust in Bates 100 000 sheet area, grid reference 827632, looking southwest. Entire hill is mylonite, with most intense zone arrowed. Striped rock face at centre is location of Figure 6.

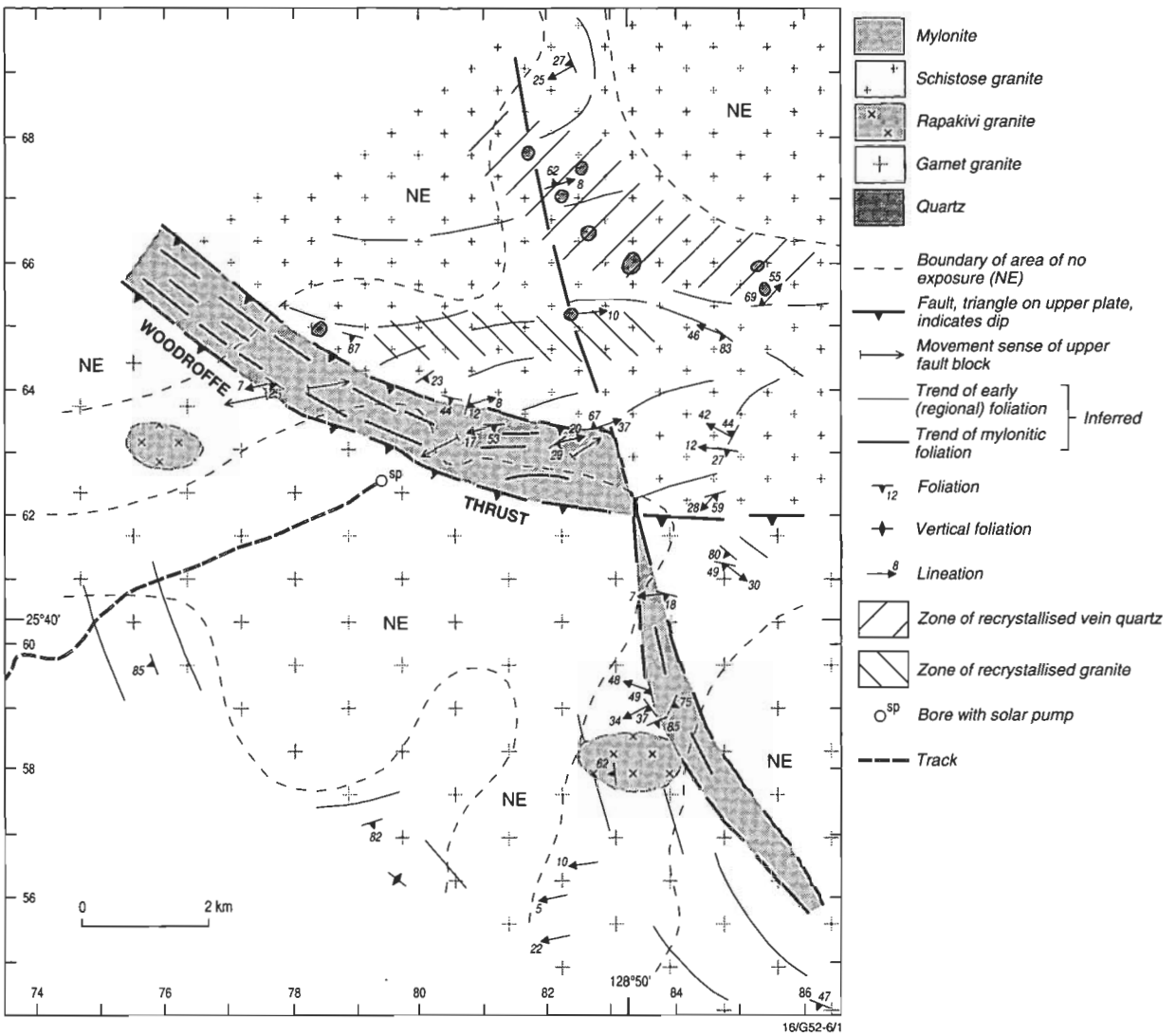

Figure 4. Geological map of mylonite zone, Bates 1:100 000 sheet area, Western Australia. Numbered ticks are 1 km intervals of Australian Map Grid, Zone 52.

1991; Maboko et al. 1992).

The Woodroffe Thrust dips south at 20–30° and separates high-grade metamorphic rocks in the south—the Fregon Subdomain of Major & Conor (1993)—from moderate-grade metamorphics in the north—the Mulga Park Subdomain of Major & Conor. The thrust has been interpreted as the root zone of the Petermann Ranges Nappe at the southwest margin of the Amadeus Basin (Fig. 1). In the Amata area, northeast movement on the thrust is well documented (Collerson et al. 1972; Bell 1978). Both the Woodroffe Thrust and Redbank Thrust Zone (Goleby et al. 1988; Shaw & Black 1991; Lambeck & Burgess 1992), formed in response to north–south compression of the Australian plate, which transmitted stress from the plate margins to the continental interior (Shaw 1991).

Until 1991, the most westerly outcrop of the Woodroffe Thrust had been at latitude 26°00′00″S, longitude 130°01′00″E (Fig. 2), where granulite-facies gneiss containing orthopyroxene–clinopyroxene–plagioclase ± K-feldspar biotite is thrust over amphibolite facies gneiss containing garnet–biotite–hornblende–plagioclase ± quartz ± K-feldspar (Forman & Shaw 1973, Plate 1). The thrust was inferred from aeromagnetic contour data to exist for another 270 km farther west into Western Australia, as far as longitude 127°30′ (Forman & Shaw 1973, Plate 1). Pharaoh (1990, Plate 2) interpreted the thrust from reprocessed aeromagnetic data as far west as longitude 127°12′ (Fig. 1). Myers (1990) depicted the thrust extending northwest to latitude 22°46′S, longitude 125°40′E, where it possibly formed the northeast margin of the Paterson Orogen. Shaw (in Reeves et al. 1994) drew a magnetic compositional domain boundary (marking a change in upper crustal material) which corresponds to the Woodroffe Thrust between Pharaoh's and Myers' locations (Fig. 1), but could not link the domains corrresponding to the Musgrave Block and region affected by the Petermann Ranges Orogeny to the domains corrresponding to the Paterson Province (Shaw et al. 1994). No field exposures of the thrust were known in Western Australia.

Because of the considerable tectonic significance of the Woodroffe Thrust and the question of its existence in Western Australia, detailed mapping was conducted in 1991 in the Bates 1:100 000 sheet area (Fig. 1) as part of the National Geoscience Mapping Accord. The results included the discovery and delineation of a major east-striking mylonite zone (Fig. 3) precisely at the predicted position of the Woodroffe Thrust. The mylonite was previously mapped as sheared porphyry, believed to be flows and sills, by Daniels et al. (1970). Exposures in the area are small, sparse, and separated by distances ranging from half to several kilometres.

The mylonite zone is about 1 km wide (Fig. 4). It separates granulite facies garnet ± orthopyroxene ± clinopyroxene

Figure 5. Schistose mylonitic granite sliced by extensional shear bands, northern margin of Woodroffe Thrust, looking south. Same locality as Figure 10e. Rock consists of small angular porphyroclasts of strained microcline and oligoclase in a groundmass of recrystallised granuloblastic microcline, quartz ribbons, strings of broken hornblende grains, and anastomosing aggregates of small strongly aligned ragged flakes of biotite. Grid reference 812635. Scale in centimetres and millimetres.

Figure 6. Interlayered ultramylonite (dark grey) and mylonite (white) in most intense zone of Woodroffe Thrust (striped rock face at centre of Fig. 3), looking southwest. Mylonitic foliation is displaced by extensional shear bands (top block down to left, i.e. east-northeast), one band 2.5 cm to right of scale, another 9 cm to left of scale. Ultramylonite comprises clasts of fractured and subrounded hornblende, nearly strain-free quartz, subrounded plagioclase, pink fractured garnet, rutile, and titanite in streaky brown groundmass of very fine-grained biotite, opaque grains, and cryptocrystalline quartz and/or feldspar. Grid reference 826630. Scale 15 cm long.

hornblende ± granite patchily recrystallised to subeclogite facies (G. Clarke, University of Sydney, personal communication, January 1993) from amphibolite facies schistose biotite hornblende granite to the north.

Deformation effects near the mylonite zone

Garnet granite south of the mylonite zone has patchily recrystallised to a mosaic of fine-grained quartz, plagioclase, garnet and hornblende, enclosing large relics of K-feldspar. One km south of the mylonite zone, garnet granite is cut by seams of mylonite up to about 1 m thick.

Schistose granite north of the mylonite zone shows effects of the faulting over a much wider area than does the garnet granite south of the mylonite. The schistose granite is generally mylonitic, and consists of lenses and ribbons of highly strained quartz, bent and broken alkali feldspar and plagioclase, and aligned biotite flakes; it is commonly cut by finer grained mylonite seams. In places, it is recrystallised to a fine-grained strain-free mosaic of microcrystalline quartz, microcline and biotite with porphyroclasts of microcline and mosaic quartz. Four kilometres north of the mylonite zone, generally massive, fine-grained, recrystallised vein quartz blows occur throughout a northwest-trending belt 5 km long (Fig. 4). In some places, the quartz veins have a relict mylonitic lineation, but elsewhere are massively brecciated or sheared to quartz augen wrapped by secondary limonite.

The mylonite zone is derived from the schistose granite, and displays a transition in rock type, as follows.

- Along the northern and southern margins of the mylonite zone, the schistose granite is sliced by numerous anastomosing extensional shear bands, which dip gently southwest; these are a few centimetres thick and 10–20 cm apart (Fig. 5) in the north; a few metres thick and several metres apart in the south.
- Near the centre of the zone, fine-grained schistose friable mylonite with small feldspar augen is intensely foliated and lineated.
- In the centre of the mylonite zone, the most intensely deformed rock comprises either thin gently south-dipping alternating layers of black aphanitic ultramylonite and pale mylonitic schistose granite (Fig. 6), or gently folded clasts of mylonitic granite in ultramylonite. Steeply northeast-dipping extensional shear bands of mylonite crosscut the gently-dipping mylonite and schistose granite (Fig. 6).

All the granitic mylonitic rocks consist, in various proportions, of angular bent clasts of K-feldspar, sericitised plagioclase, and hornblende (in some samples), and a streaky groundmass of ribbon quartz and microcrystalline K-feldspar and uniformly oriented biotite aggregates (Fig. 7). A mafic dyke with altered garnet relics in the mylonite zone is metamorphosed to actinolite, bleached biotite, and sericitised plagioclase.

The mylonite zone is cut by a north-striking cross or

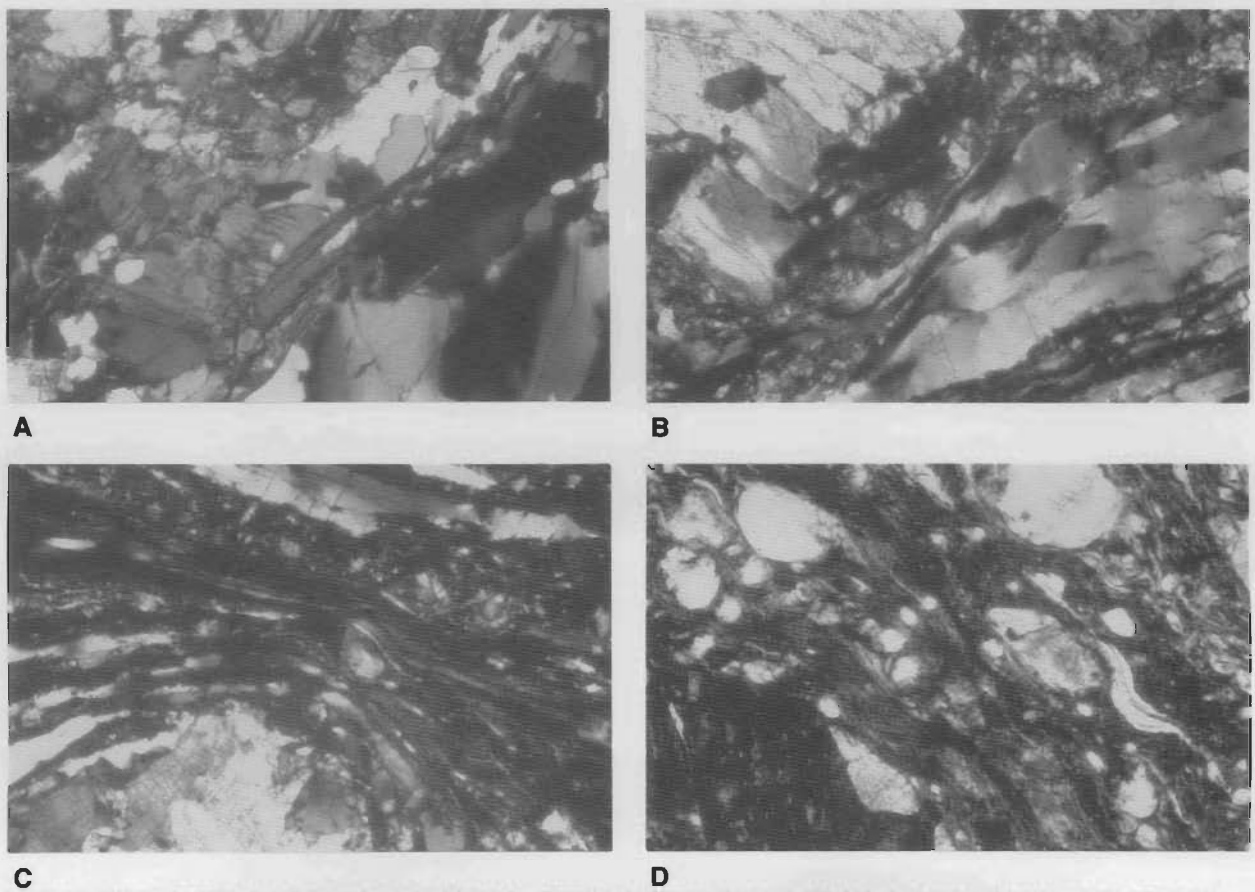

Figure 7. Photomicrographs of granitic mylonitic rocks, Woodroffe Thrust, Bates 1:100 000 sheet area. Longer side of all photos = 2 mm. All with crossed nicols. (a) Tonalite at margin of mylonite zone, showing broken oligoclase (left), strained quartz (three large grains, right), and round titanite grain (centre of top edge); thin section 91989421, grid reference 802643. (b) Granite mylonite at centre of mylonite zone, showing broken microcline clasts (top left), large lenticle of flattened elongate quartz (right), and granulated oligoclase (middle); thin section 91989423A, grid reference 813635. (c) granite mylonite at centre of mylonite zone, showing laminae of recrystallised platy quartz (white, left), extremely flattened unrecrystallised quartz (white, top), unresolvable biotite (black), and granulated microcline and oligoclase bent around large microcline clast (bottom); thin section 91989423A, grid reference 813635. (d) Granite ultramylonite at centre of mylonite zone, comprising round clasts of nearly strain-free quartz (white), subrounded plagioclase (grey, right of centre), and large broken clast of hornblende (bottom left) in dark streaky groundmass of unresolvable biotite and opaque grains, and small, bent, highly flattened lenses of cryptocrystalline quartz and/or feldspar; thin section 91989425E, grid reference 826630.

tear-fault, which also has mylonite along it (Fig. 8), similar in grade to that along the east–west fault, implying that the two faults formed at the same time.

Structure

Foliation (schistosity) trends throughout the northern (Fig. 9a) and southern (Fig. 9b) terranes (interpreted from scattered isolated exposures) appear to be at large angles to the east–west mylonite zone (Fig. 4), which dips gently to moderately south (Fig. 9c). Lineations in the two terranes and in the mylonite zone are subhorizontal to gently plunging and mostly east-northeast-trending (Fig. 9d, e, f), and indicate a west-southwest–east-northeast movement direction. The coincidence of the lineations suggests a common origin, and this is supported by Neoproterozoic to Cambrian isotopic dates on various mineral separates from subeclogitic mylonitic rocks a few kilometres south of the mylonite zone (Clarke et al. 1995—this issue). Kinematic indicators are rare, and were observed in only five exposures at four locations (Fig. 10); three indicate movement of the top block to the east (Fig. 10a, c, d), and two indicate movement of the top block to the west (Fig. 10b, e). The scarcity of shear indicators suggests that the fabric is not markedly asymmetrical, implying that large strain produced almost parallel shearing and flattening planes.

Conclusion

The east-northeast lineation and, hence, movement direction in the mylonite zone are oblique to the general strike of the mylonite zone, and only 30° from the northeast overthrusting direction recorded on the Woodroffe Thrust in the Amata area. In addition, the Bates mylonite zone separates a granulite facies terrane to the south from an amphibolite facies terrane to the north, dips gently south, and is several hundred metres thick. In these respects it resembles, and is interpreted as a continuation of, the Woodroffe Thrust. The observed mylonite zone is located exactly on strike with the position of the thrust shown in the southwest Petermann Ranges 1:250 000 sheet area by Forman (1972). Mapping of the many isolated exposures north of the Mann Range in this sheet area should locate the Woodroffe Thrust there also.

Acknowledgements

I thank R.D.Shaw, P.R.Williams, P.G.Stuart-Smith, and A.Y.Glikson for critical reviews of the manuscript, and AGSO's Cartographic Services Unit for preparing the diagrams.

References

Bell, T.H., 1978. Progressive deformation and reorientation of fold axes in a ductile mylonite zone: the Woodroffe Thrust. Tectonophysics 44, 283–320.

Camacho, A., 1991. Mulga Park 1:100 000 Sheet area data record. Northern Territory Geological Survey Report 91/019.

Clarke,G.L., Buick, I.S., Glikson, A.Y. & Stewart, A.J., 1995. Structural and pressure–temperature evolution of host rocks of the Giles Complex, western Musgrave Block, central Australia: evidence for multiple high-pressure events. AGSO Journal of Australian Geology & Geophysics, this issue.

Collerson, K.D., Oliver, R.L. & Rutland, R.W.R., 1972. An example of structural and metamorphic relationships in the Musgrave orogenic belt, central Australia. Journal of the Geological Society of Australia, 18, 379–393.

D'Addario, G.W. et al., 1976. Geology of the Northern Territory, 1:2 500 000 geological map. Bureau of Mineral Resources, Canberra.

Daniels, J., 1974. Structural sketch map of the Blackstone region, W.A.. Geological Survey of Western Australia

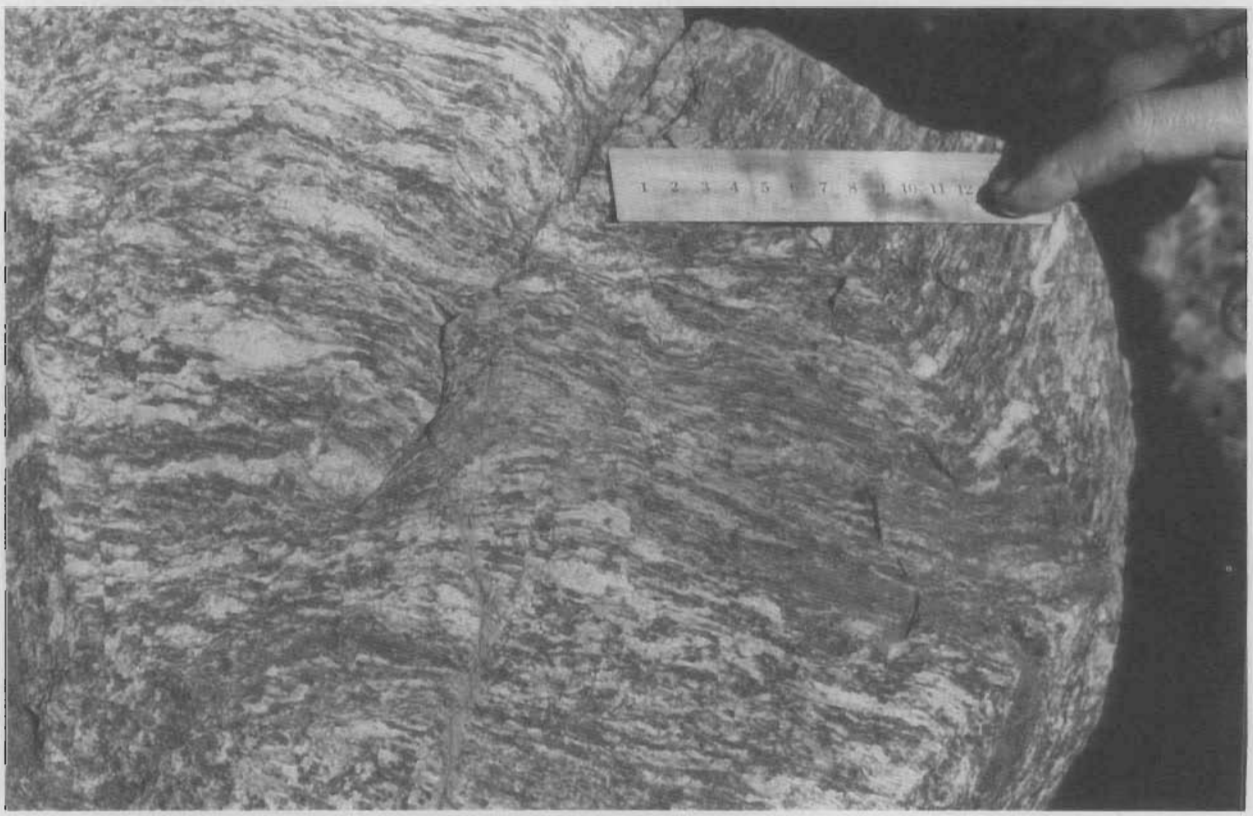

Figure 8. Garnet granite mylonite in tear fault crossing Woodroffe Thrust, Bates 100 000 sheet area. Augen and lenticles of fine-grained recrystallised K-feldspar (white), quartz as deformed and recrystallised lenticles (pale grey), and broken and cracked garnet, in dark grey groundmass of cryptocrystalline quartz, feldspar, garnet microclasts, hornblende grains, opaque grains, and unresolvable microcrystalline biotite. Grid reference 838593. Scale 15 cm long.

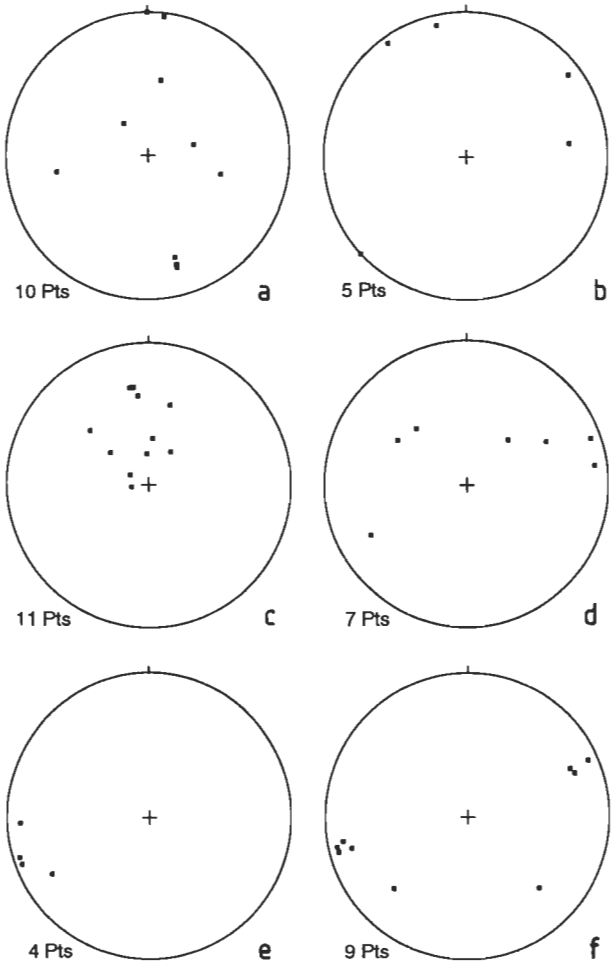

Figure 9. Stereograms of foliations and lineations in and near Woodroffe Thrust. (a) Poles to foliation in schistose granite of northern terrane; (b) poles to foliation in garnet granite of southern terrane; (c) poles to foliation in main and subsidiary mylonite zones; (d) lineations in northern terrane; (e) lineations in southern terrane; (f) lineations in main and subsidiary mylonite zones. Equal-area plots on lower hemisphere. Stereograms plotted using GEORIENT program devised by R.Holcombe, University of Queensland.

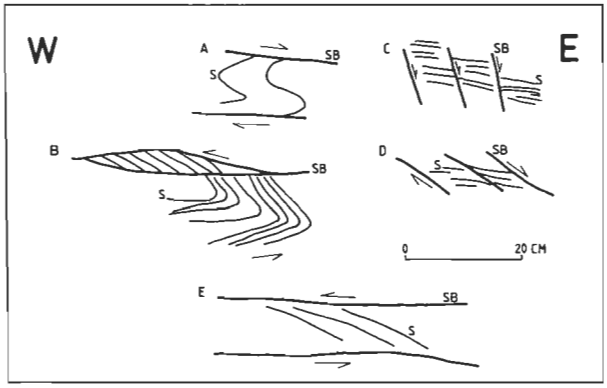

Figure 10. Sketches of shear indicators in granitic mylonite, Woodroffe Thrust, Bates 1:100 000 sheet area. Mylonitic foliation (S), shear bands (SB) interpreted as extensional, because of observed extensional offsets, large angle to foliation, and paucity of bending of foliation near shear bands. (a, b) northern margin of Woodroffe Thrust; (c, d) southern margin of thrust; (e) northern margin of thrust, same locality as Figure 5.

Bulletin 123, Plate 2.

Daniels, J.L., Horwitz, R.C. & Kriewaldt, M., 1970. Scott 1:250 000 Geological Sheet (1st edition) SG52-6. Geological Survey of Western Australia, Perth.

Edgoose, C.J., Camacho, A., Wakelin-King, G.A. & Simons, B.A., 1993. Kulgera 1:250 000 Geological Map (second edition, 1992) and Explanatory Notes SG/53–5. Northern Territory Department of Mines & Energy, Darwin, 46 pp.

Forman, D.J., 1972. Petermann Ranges 1:250 000 Geological Sheet and Explanatory Notes SG/52–7. Bureau of Mineral Resources, Canberra, 17 pp.

Forman, D.J. & Shaw, R.D., 1973. Deformation of the crust and mantle in central Australia. Bureau of Mineral Resources, Australia, Bulletin 144, 20 pp., 1 pl.

Goleby, BR., Wright, C., Collins, C.D.N. & Kennett, B.L.N., 1988. Seismic reflection and refraction profiling across the Arunta Block and the Ngalia and Amadeus Basins. Australian Journal of Earth Sciences, 35, 275–294.

Gray, C.M., 1978. Geochronology of granulite-facies gneisses in the western Musgrave Block, central Australia. Journal of the Geological Society of Australia, 25, 403–414.

Gray, C.M. & Compston, W., 1978. A rubidium-strontium chronology of granulite-facies rocks in the western Musgrave Block, central Australia. Geochimica et Cosmochimica Acta, 42, 1735–1748.

Lambeck, K. & Burgess, G., 1992. Deep crustal structure of the Musgrave Block, central Australia: results from teleseismic travel-time anomalies. Australian Journal of Earth Sciences, 39, 1–19.

Maboko, M.A.H., McDougall, I., Zeitler, P.K. & Williams, I.S., 1992. Geochronological evidence for ~530–550 Ma juxtaposition of two Proterozoic metamorphic terranes in the Musgrave Ranges, central Australia. Australian Journal of Earth Sciences, 39, 457–471.

Myers, J.S., 1990. Geological evolution; Precambrian. In: Geology and mineral resources of Western Australia. Geological Survey of Western Australia, Memoir 3, 737–750.

Pharaoh, T.C., 1990. Aspects of structural geology of the Giles layered basic/ultrabasic complex and associated felsic granulites, Tomkinson Range, Musgrave Block, central Australia. Bureau of Mineral Resources, Australia, Record 1990/5, 28 pp., 2 pl.

Reeves, C., Shaw, R., Wellman, P. & Whitaker, A., 1994. Australian basement elements. 1:5 000 000 preliminary compilation. Australian Geological Survey Organisation, Canberra.

Shaw, R.D. & Black, L.P., 1991. The history and tectonic implications of the Redbank Thrust Zone, central Australia, based on structural, metamorphic and Rb–Sr isotopic evidence. Australian Journal of Earth Sciences, 38, 307–332.

Shaw, R.D., 1991. The tectonic development of the Amadeus Basin, central Australia. Bureau of Mineral Resources, Australia, Bulletin 236, 429–461.

Shaw, R.D., Morse, M.P. & Tarlowski, C., 1994. The geological framework of northwestern Australia from geophysical mapping. Geological Society of Australia, Field Conference on Deformation Processes in the Earth: from Microcracks to Mountain Belts, Jindabyne, 1994, Abstracts 36, 142–143.

Stewart, A.J., 1992. Structural map of the Amadeus Basin, 1:1 000 000. In: Lindsay, J.F. (editor), Geological atlas of the Amadeus Basin. Australian Geological Survey Organisation, Canberra.

Sun, S.-S. & Sheraton, J.W., 1992. Zircon U/Pb chronology, tectono-thermal and crust-forming events in the Tomkinson Ranges, Musgrave Block, central Australia. AGSO Research Newsletter, 17, 9–11.

AGSO Journal of Australian Geology & Geophysics, 16 (1/2), 155–161

A geophysical investigation of the southern margin of the Musgrave Block, South Australia

J.H. Leven[1] & J.F. Lindsay[1]

New geophysical data provide the first clear image of the marginal structure of the southern Musgrave Block and the northern Officer Basin of western South Australia. The data show that the Officer Basin and the Musgrave Block are underlain by a series of pervasive, north-dipping planar structures that predate development of the Officer Basin. Reactivation of these structures formed a wide thrust fault complex and developed a major homocline at the northern margin of the basin.

Introduction

The southern boundary of the Musgrave Block in South Australia is a major arcuate feature, clearly evident in Bouguer gravity and total magnetic intensity (TMI) images of Australia. In the gravity image, the boundary is marked by an abrupt gravity gradient of up to 20 ns^{-2}; in the TMI image, it is marked by a change from a short wavelength ('high frequency') magnetic variation, characteristic of the Musgrave Block, to a relatively subdued ('low frequency') magnetic signature over the Officer Basin. This boundary is important in understanding the structure and evolution of the central Australian region, but, until now, geophysical investigation of the feature has been hampered by logistic and access considerations.

In 1993 the Australian Geological Survey Organisation (AGSO) and Mines & Energy South Australia (MESA; formerly South Australian Department of Mines and Energy) undertook a major reflection seismic survey in the central Officer Basin, recording five regional lines (Fig. 1). Of these, seismic line 93AGS01 traverses from the northern Officer Basin onto the southern Musgrave Block, and provides a clear seismic image of the structure of this boundary.

Geology

The geology of the Musgrave Block is described in Drexel & others (1993) and elsewhere in this issue (see also references in the Preface). The Officer Basin lies south of the Musgrave Block and is one of a series of related broad intracratonic basins which formed on the Australian craton during the Neoproterozoic to Late Palaeozoic (800–360 Ma) (Lindsay et al. 1987). In South Australia, sediments of the Officer Basin thin from up to 7 km in the northern sub-basins to around 3 km in the southern platform area, and are for the most part little deformed, except along the northern margin and in the eastern region, where thrusting has occurred. At least three major compressional events are known to have affected the Officer Basin: the Neoproterozoic to Early Cambrian Petermann Ranges Orogeny, the Late Cambrian Delamerian Orogeny, and the Carboniferous Alice Springs Orogeny (Fig. 2). The geology of the South Australian sector of the Officer Basin has been discussed by Kreig (1969), Drexel et al. (1993), and, more recently, Lindsay (1995).

Previous seismic work

During 1972 to 1974 the then South Australian Department of Mines and Energy acquired and processed a network of reflection seismic lines in the eastern Officer Basin (Milton & Parker 1973). Although results are somewhat inconclusive, interpretation of those seismic lines crossing the northern margin of the Officer Basin suggests the Musgrave Block has overthrust Officer Basin sediments. Seismic line OF74FD, for example, clearly images a 25° north-dipping reflector which extends to a depth of around 6 km.

NGMA Project—AGSO seismic acquisition 1993

As part of the National Geoscience Mapping Accord, AGSO recorded five regional seismic lines (Fig. 1) in the central portion of the Officer Basin during 1993 (Barton et al. 1995). The central Officer Basin is divided, from a logistic point of view, by the Namungarintja Conservation Park, in which seismic acquisition was not permitted. Line 93AGS01 to the north of the Conservation Park investigates the nature of the northern margin of the Officer Basin and its relationship to the Musgrave Block. It is tied to Birksgate-1 well for stratigraphic control. Lines 93AGS04, 93AGS05 and 93AGS06 provide a regional seismic network south of the Conservation Park, designed to investigate the basin's transition onto the Murnaroo Platform. This network is connected by line 93AGS03 to Munta-1 well for stratigraphic control.

Deep reflection seismic image of the southern margin of the Musgrave Block

Deep seismic data from 93AGS01 (Fig. 3) show the structure of the Musgrave Block at its southern margin. These data show a series of pervasive, north-dipping reflection events within the basement, extending from at or near the surface to a two-way-time (TWT) of around 10 seconds (approx. 30 km depth), with a northerly dip of around 30°.

Two hundred kilometres south of this margin, deep seismic data from line 93AGS05 show a similar series of roughly parallel north-dipping structures. These structures, however, terminate at the base of the Officer Basin succession without disrupting the basin sediments, suggesting they were truncated by the erosional event that peneplaned basement before deposition of the regionally extensive Willouran basal units of the Officer Basin (Pindyin Sandstone and Alinya Formation of Fig. 2). These basement events are, therefore, interpreted to have formed as pre-Willouran crustal structures, some of which were truncated by the basal erosional surface of the Officer Basin and subsequently remained inactive, whereas others were reactivated during later orogenic events.

Twenty kilometres north of the Officer Basin margin, line 93AGS01 shows a set of prominent north-dipping basement structures which bifurcate at a branch point around 3 s TWT (approx. 7.5 km depth) beneath CMP 3300 (Fig. 3). The lower branch of this bifurcation forms a basal decollement which soles into the evaporitic Alinya Formation near the base of the sedimentary succession as a blind thrust. The upper branch of this bifurcated thrust flattens at depths less than 2 km. Its surface expression has not been mapped, because of the blanket cover of Pleistocene dunes. However, its surface location corresponds to a significant topographic ridge, with surface elevation decreasing southwards by 40 m over 2.5 km, which can be interpreted as indicating recent thrust-sense movement on this fault zone.

In the vicinity of the northern margin of the Officer Basin

[1] Division of Marine Petroleum & Sedimentary Resources, Australian Geological Survey Organisation, GPO Box 378, Canberra, ACT 2601

these basement features are genetically related to the steep northern margin of the basin. Figure 4 shows that at the present northern margin of the Officer Basin, strata have been folded into a homocline. Farther east in the eastern Officer Basin, foreland basin sediments of Devonian age indicate movement of this fault system during the Alice Springs Orogeny. The margin is thus erosional, and the original northerly extent of the basin unknown. South of this structure (Fig. 4), sediments of the central Officer Basin have suffered relatively little disruption, in spite of their proximity to this major thrust boundary.

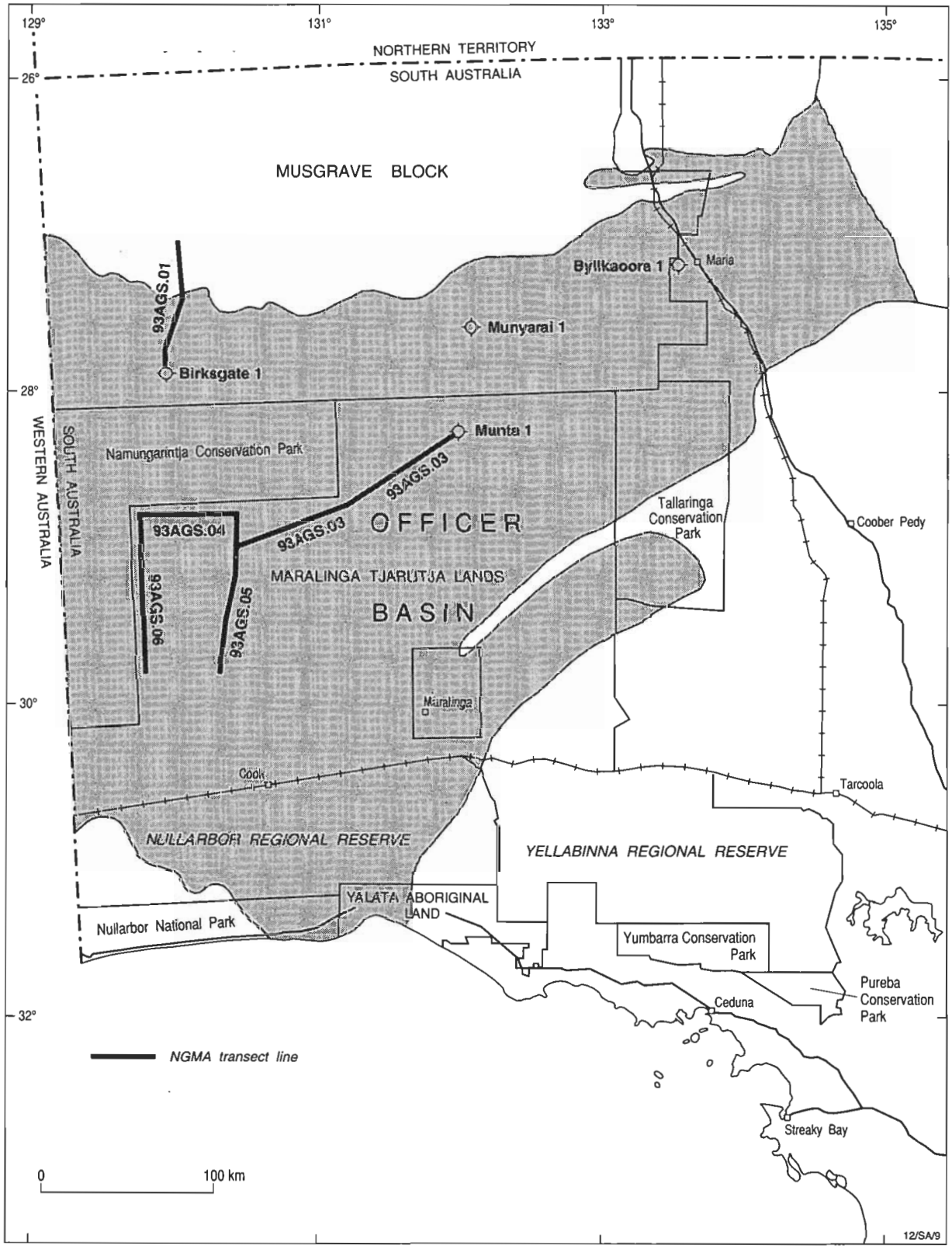

Figure 1. Map of the Musgrave Block and the Officer Basin (shaded grey) and surrounding regions of western South Australia, showing the location of the five NGMA seismic reflection traverses. 93AGS01 images the boundary between the southern Musgrave Block and the northern Officer Basin.

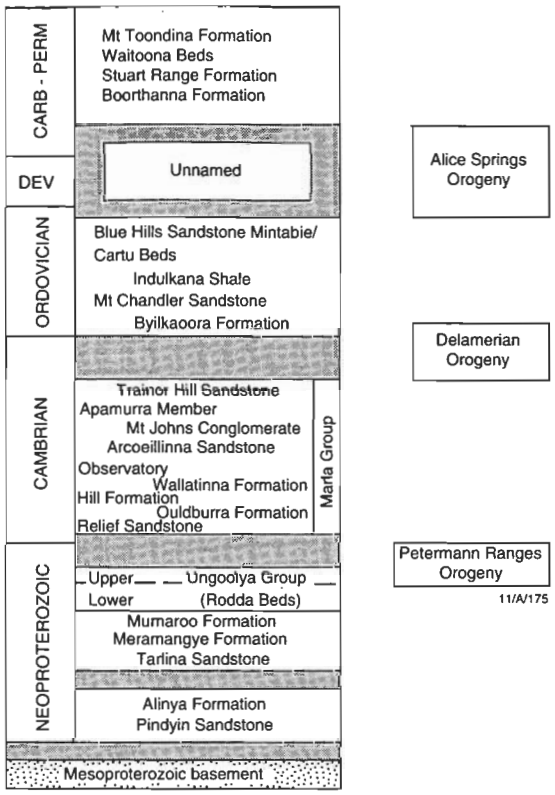

Figure 2. A simplified stratigraphic succession of the central Officer Basin.

Basin response to thrusting: structure in the sediments

Figure 4 shows the detailed structure of the northern margin of the Officer Basin, and the structure of the thrusts in the Musgrave Block. Only the upper succession of the Officer Basin strata has been folded into the homoclinal upturn at this margin. The lower succession, interpreted to include part of the Alinya Formation and the Pindyin Sandstone, has been abruptly truncated beneath CMP 4520. North of this, portions of stratal units with a similar reflection character to this lower succession are evident, suggesting that in this region, rather than being folded into a homoclinal upturn, the lower succession has failed by thrust faulting. A complex set of faults has been interpreted in this disrupted zone beneath the homocline, but these faults do not penetrate into the upper succession.

South of the thrust margin, the lower succession has been compressed into several broad kinks over a distance of 30 km (Fig. 5). These have an amplitude of around 150 m and are unconformable with the more gently folded strata of the upper succession. They represent a net shortening of the lower succession relative to the upper succession, and are interpreted to have formed by flowage within the Alinya Formation (an evaporitic unit) in response to the compression of the Officer Basin sediments during the southward thrusting of the Musgrave Block. As the lower succession is not involved in the homoclinal structure, its shortening has been accommodated by kinking and ductile flow within the evaporitic units south of CMP 4300, and by imbrication and extensive brecciation north of CMP 4300, forming a triangle zone.

In contrast, the clastic upper succession responded to the compression by slippage along a bedding plane separating the two successions, and back-thrusting over the imbricated and brecciated lower succession in the triangle zone (Fig. 6).

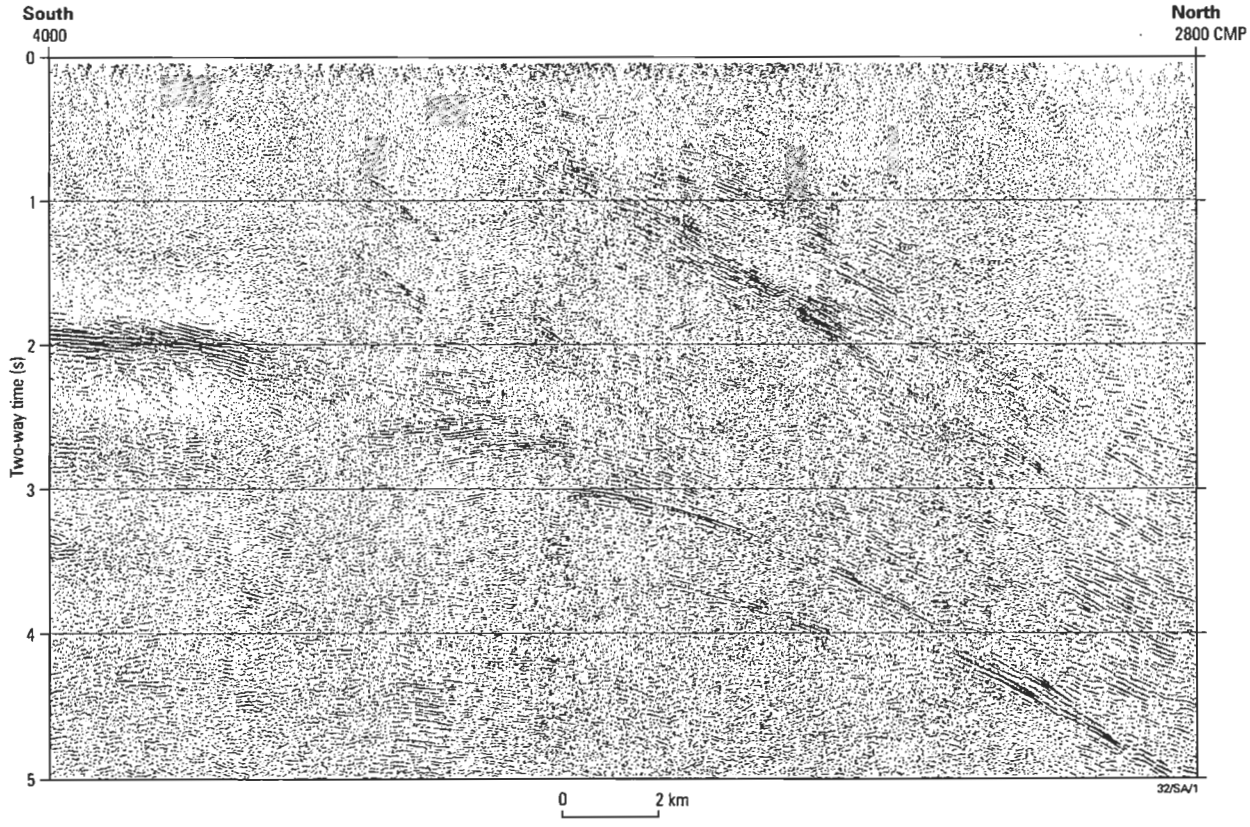

Figure 3. Portion of the seismic traverse 93AGS01 between CMP 2800 and 4000, showing the top 6 s TWT of the upper crustal structure beneath the southern boundary of the Musgrave Block. A prominent series of north-dipping structures is imaged. The lower set of these structures bifurcates around 3 s TWT (approx. 7.5 km depth) beneath CMP 3300. The lower branch flattens and soles into the base of the sedimentary succession farther south (see Fig. 6).

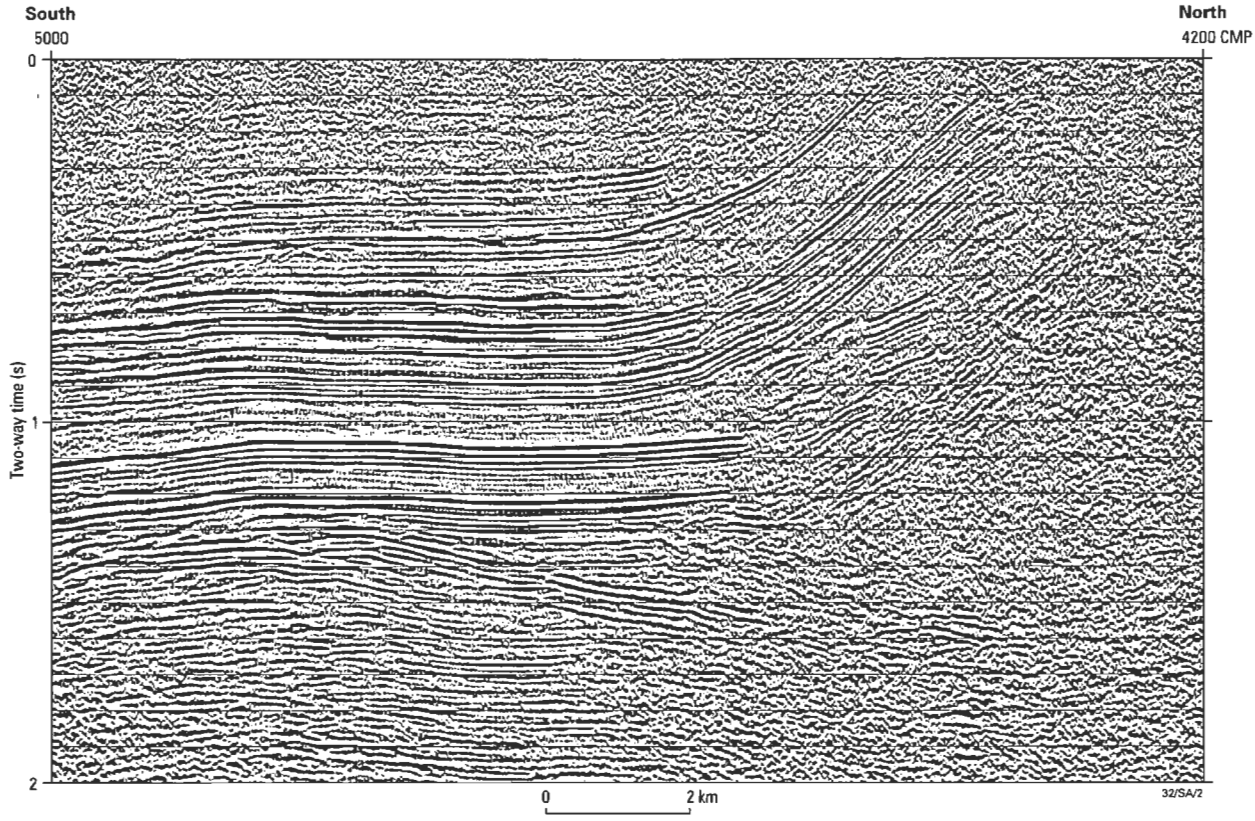

Figure 4. Portion of the seismic traverse 93AGS01 between CMP 4200 and 5000 (2 s TWT), showing the sedimentary structure at the northern margin of the Officer Basin. The sedimentary strata are divided into two packages, the upper succession folded into a homocline, and the lower succession abruptly truncated beneath CMP 4520. A prominent north-dipping structure soles into the base of the sedimentary succession at 1.4 s beneath CMP 4800.

Back-thrusting of the upper succession must postdate formation of the adjacent brecciated lower succession in the triangle zone, as faults in this zone do not penetrate the homocline. We interpret this structure to be the result of bedding-plane slippage on a surface within the Alinya Formation which accommodated different mechanical responses to the compression in these two successions.

Total magnetic intensity data

The total magnetic intensity (TMI) image (Fig. 7) gives a clear picture of the structure of the Musgrave Block and, for the Officer Basin, provides structural information over an area where the geology is generally obscured by Pleistocene sand dunes. The image illustrates the changing nature of the Musgrave Block's southern margin along strike. To the west, the TMI image suggests that this margin is a relatively sharp feature, involving a single thrust fault or a narrow fault zone, whereas to the east of meridian 130° E, the margin gives the appearance of having a stepped structure, suggesting the presence of multiple thrust sheets of basement.

This difference in character along the southern margin of the Musgrave Block corresponds to a change in boundary structure associated with the thrusting. West of 130° E, this boundary appears to have a relatively simple structure, with tectonic disturbance of the basin sediments constrained to a narrow region close to the edge of the Musgrave Block. In this central region, the Musgrave Block appears to have encountered little impediment to its southward thrust-sense movement. In contrast, the structure east of 130° 30′ E in the eastern Officer Basin is relatively complicated, as evidenced by basement-involved thrusting extending a considerable distance southwards into the basin (Lindsay et al. 1995). Here, movement of the Musgrave Block was obstructed by the Gawler Craton to the southeast, and the basin was confined between the Musgrave Block and Gawler Craton.

Aeromagnetic TMI data were collected along the seismic lines subsequent to seismic acquisition. TMI data along line 93AGS01 have a long wavelength character south of CMP 4100, and a short wavelength ('high frequency') response, characteristic of the Musgrave Block, north of this point. Interpretation of the TMI data indicates that the thin edge of the Musgrave Block thrust sheet starts at CMP 4100. Seismic data do not image this portion of the thrust clearly in the top 200 ms, although the upper branch of the bifurcated thrust structure appears to flatten near the surface in agreement with the magnetic interpretation.

Gravity data

Gravity observation were made along the seismic traverses during seismic acquisition, and the reduced Bouguer gravity profile along line 93AGS01 is plotted in Figure 8. Notice that the major inflection in Bouguer gravity does not correspond to the location of the homoclinal fold in basin sediments near CMP 4400, but is displaced to the north. These data require a causative density contrast to be located north of this homoclinal fold. This observation is reconciled in the gravity model by proposing, as required by the TMI data, that the upper branch of the bifurcating thrust is the major thrust zone associated with the southern margin of the Musgrave Block thrust sheet. The triangle zone between the Musgrave Block thrust zone and the homocline is proposed to be a zone of brecciated and disrupted Officer Basin sediments. This trapezoidal volume above the basal décollement therefore has a density appropriate to sediments.

Figure 8 shows a model of the density variation which is consistent with the seismic, TMI, and gravity observations

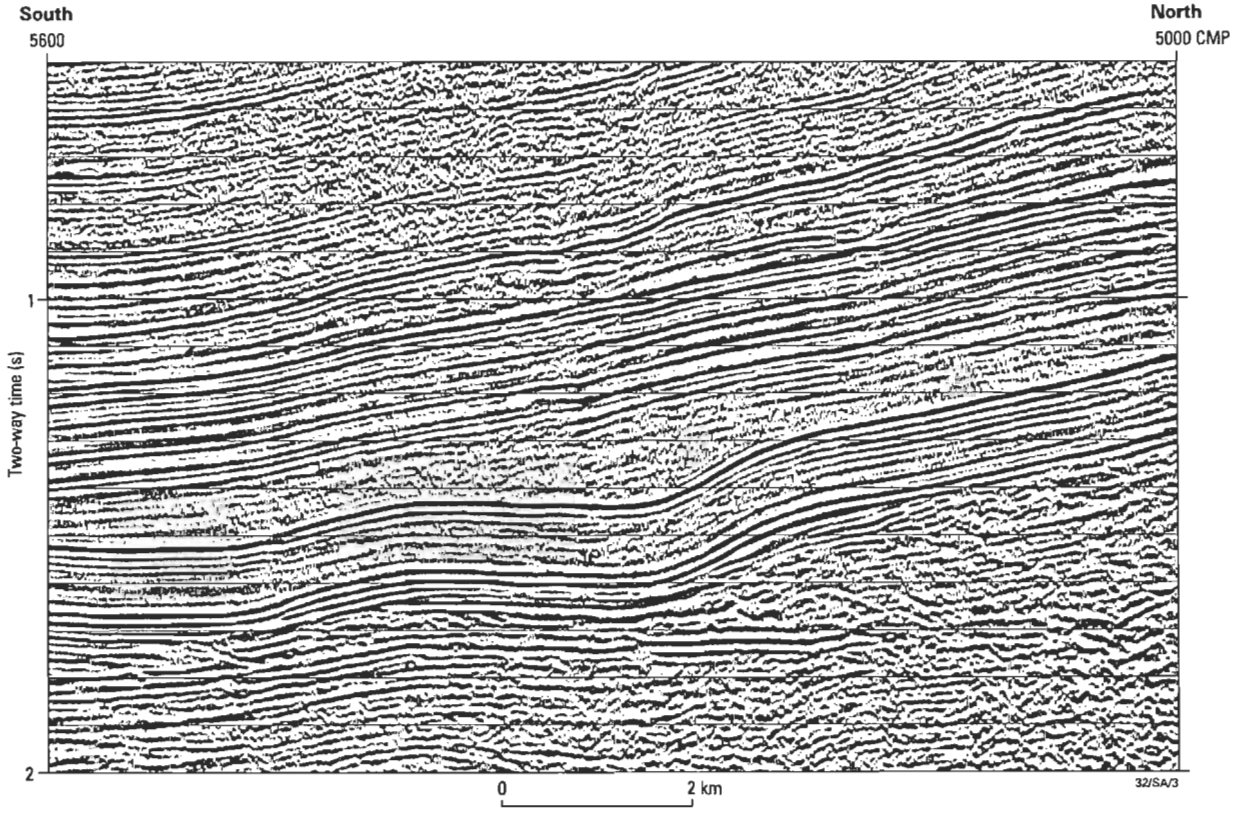

Figure 5. Portion of the seismic traverse 93AGS01 between CMP 5000 and 5600 (2 s TWT), showing the sedimentary structure south of the northern margin of the Officer Basin. The sedimentary strata are divided into two packages, which are unconformable. The upper succession is gently folded, whereas the lower succession has been folded into additional kink structures evident beneath CMP 5500 and 5280.

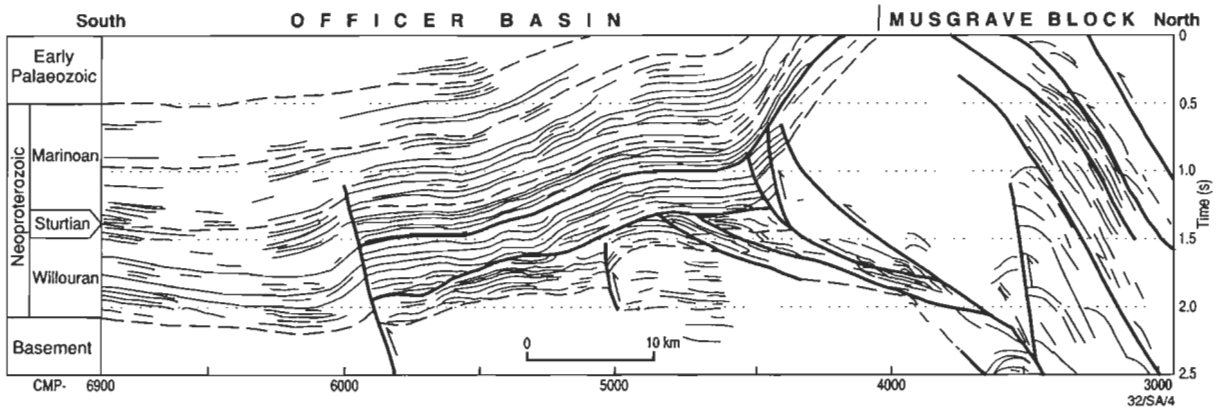

Figure 6. Line diagram of the structure of reflection events from 93AGS01 at the northern margin of the Officer Basin, showing the Officer Basin succession folded and back-thrust over a non-reflective triangle zone which underlies the main thrust zone at the southern margin of the Musgrave Block.

along seismic line 93AGS01. Like the model of Milton & Parker (1973), displacement of the major inflection in the Bouguer gravity profile approximately 20 km north of the homoclinal fold zone can be explained by a wedge of lower density disrupted sediments beneath the basement thrust sheet. The upper succession of Officer Basin sediments which now form the homoclinal structure appears to have been folded by back-thrusting over the brecciated and disrupted sediments in the triangle zone.

Conclusions

Seismic data from the NGMA Officer Basin Project have given the clearest picture yet of the structure of the Officer Basin's northern margin. It consists of a major thrust zone, in which the Musgrave Block to the north has overthrust sediments of the Officer Basin. Interpretation of these data in conjunction with gravity and magnetic data indicate:

- the region is underlaid by a series of pervasive north-dipping structures, which predate basin formation;
- reactivation of some of these older (pre-Willouran) structures developed a major thrust zone, which forms the basin's northern margin;
- the thrust fault zone bifurcates beneath the Musgrave Block;
- the lower branch of the bifurcated thrust zone forms a basal décollement, which soles into the base of the Officer

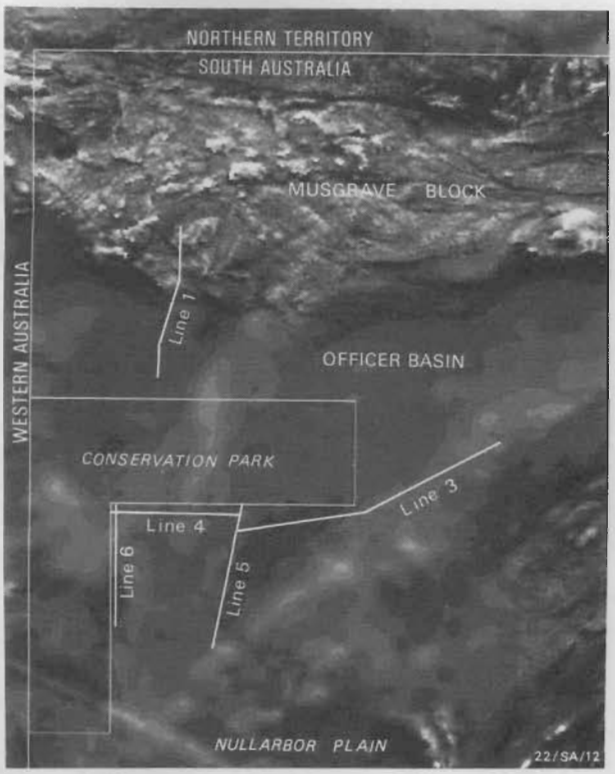

Figure 7. TMI image of the Musgrave Block and the northern Officer Basin, also showing the location of the NMGA seismic traverses.

Basin sedimentary succession;

- the upper branch of the bifurcated thrust zone flattens near the surface;
- a trapezoidal wedge or triangle zone of disrupted sediments has formed in front of the thrust zone;
- an upper portion of the sedimentary section has been excised by this wedge and has back-thrust into a homoclinal fold structure.

Acknowledgments

We wish to thank those involved in the acquisition and processing of the seismic, magnetic and gravity data during the Officer Basin Project. We also wish to thank the traditional Aboriginal landowners, without whose cooperation this project would not have been possible.

References

Barton, T., Owen, A.J., Leven, J.H., Lindsay, J.F., in prep. The 1993 AGSO Officer Basin survey—operations report. Australian Geological Survey Organisation, Record.

Drexel, J.F., Preiss, W.V. & Parker, A.J., 1993. The geology of South Australia. Vol. 1, The Precambrian. South Australia Geological Survey, Bulletin 54.

Krieg, G., 1969. Geological development in the eastern Officer Basin of South Australia. APEA Journ. 6, 8–13.

Lambeck, K. & Burgess, G., 1992. Deep crustal structure of the Musgrave Block, central Australia: Results from teleseismic travel-time anomalies. Australian Journal of Earth Sciences, 39, 1–20.

Lindsay, J.F. (editor), 1995. Geological atlas of the Officer Basin, South Australia. Australian Geological Survey Organisation & Mines and Energy South Australia, 30 plates.

Lindsay, J.F., Korsch, R.J. & Wilford, J.R., 1987. Timing

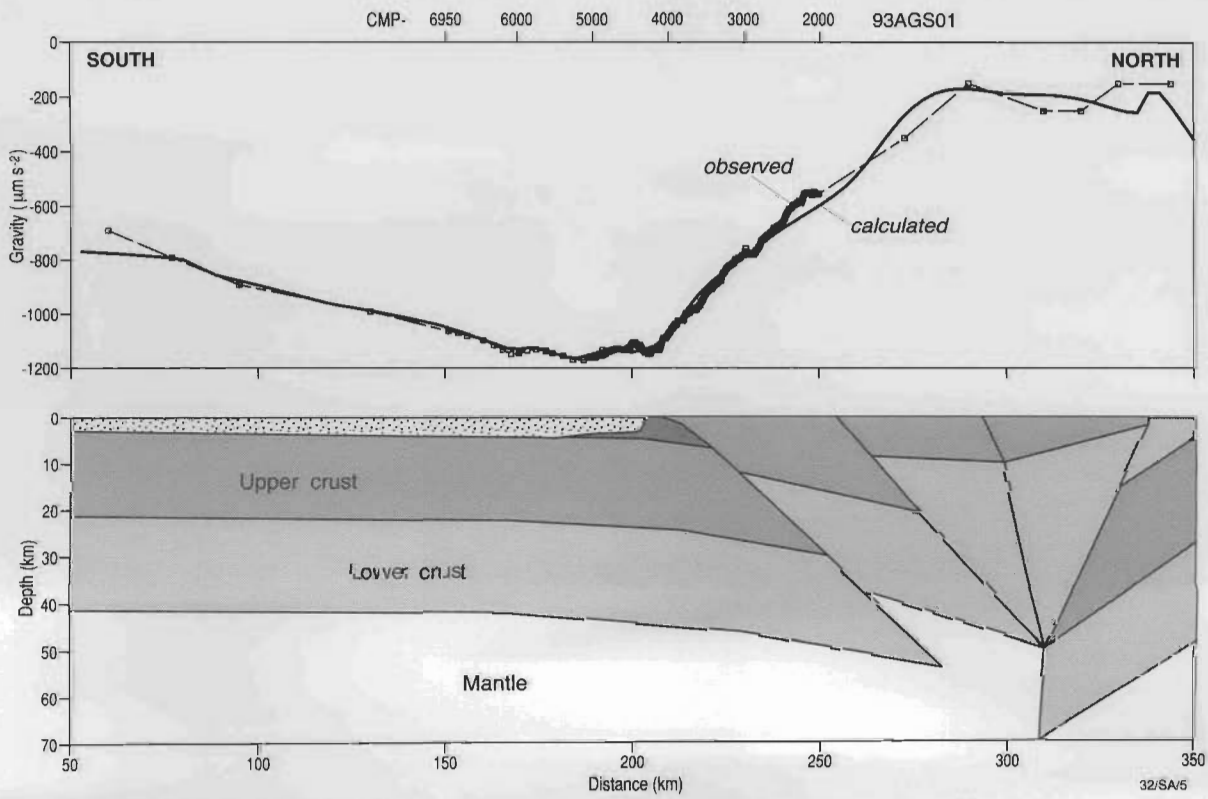

Figure 8. Bouguer gravity data observed with a station spacing of 250 m along seismic traverse 93AGS01 has been extended to the north and south with regional gravity data to produce an observed gravity profile. The modelled gravity profile has been calculated from the proposed gravity model, which is consistent with both the seismic data from 93AGS01.

the breakup of a Proterozoic supercontinent: Evidence from Australian intracratonic basins. Geology, 15, 1061–1064.

Milton, B.E. & Parker A.J., 1973. An interpretation of geophysical observations on the northern margin of the eastern Officer Basin. Quarterly Notes of the South Australia Geological Survey, 46, 10–14.

Shaw, R.D., Korsch, R.J., Wright, C. & Goleby, B.R., 1991. Seismic interpretation and thrust tectonics of the Amadeus Basin, central Australia, along the BMR regional seismic line. In: Korsch, R.J & Kennard, J.M., (editors) Geological and geophysical studies in the Amadeus Basin, central Australia. Bureau of Mineral Resources, Australia, Bulletin 236, 385–408.

AGSO Journal of Australian Geology & Geophysics, 16 (1/2), 163–171

Remote sensing of mafic–ultramafic rocks: examples from Australian Precambrian terranes

L.F. Macias[1]

Mafic and ultramafic rocks of the intrusive Andover Complex and Munni Munni Complex of the West Pilbara, and the Panton Intrusion of the East Kimberley, Western Australia, have been discriminated by Landsat-5 TM imagery. Band-ratioing procedures were used to enhance spectral differences determined from field spectral-reflectance information. For the Andover and Munni Munni Complexes, lithological discrimination is mainly based on the spectral response of different weathering products of the various ultramafic rock types. For the Panton Intrusion, the discrimination represents variations in the weathering products of the plagioclase-rich gabbroic units. Discrimination was hampered by vegetation—spinifex and lichen—and by fireburns.

Introduction

The application of Landsat-5 Thematic Mapper (TM) remote-sensing system to the mapping of the intrusive Andover and Munni Munni Complexes of the West Pilbara, and the Panton Intrusion of the East Kimberley has resulted in the successful discrimination of several types of mafic and ultramafic rocks. The intrusive bodies are located in semi-arid regions, where spinifex is the dominant vegetation. Mapping of mafic and ultramafic rocks can be complicated by the combined effects of weathering, soil, and extensive vegetation cover in the form of spinifex and lichen. During field work, outcrops must be broken to expose fresh surfaces for examination, as mafic and ultramafic rocks often have a ferruginous weathered crust up to 1 cm thick. There appears to be little correlation between geology and vegetation: trees are normally restricted to stream courses, and hills and scree slopes are largely covered by low-growing spinifex species. At Munni Munni, black lichen completely covers most outcrops, masking the spectral response of the rocks and inhibiting their discrimination in processed imagery. At Andover, outcrops are not generally as extensive, and spinifex and lichen are also less. At Panton, lichen is at a minimum on the gabbroic rocks.

Preliminary processed imagery was used for field reconnaissance and to locate areas for the collection of spectral data by portable spectroradiometer. The spectral data were used to develop the image processing methodology. Two wavelength units are used throughout: micrometres (μm) and nanometres (nm) (1 μm = 1000 nm).

Scanner data characteristics

Landsat-5 TM sensor acquires data in seven discrete bands (Table 1) with a ground pixel resolution of 30 m x 30 m.

Table 1. Wavelengths recorded by Landsat-5 TM

Landsat-5 TM			
Band	*nm*	*CL*	
1	450–520	485 }	
2	520–600	560 }	Visible (Vis)
3	630–690	660 }	
4	760–900	835	Near Infrared (NIR)
5	1550–1750	1650 }	Shortwave Infrared (SWIR)
7	2080–2350	2215 }	
6	10 400–12 500	11 450	Thermal

CL: centre line.

General geology

Andover Complex

The Andover Complex (Fig. 1) is 3 km south of Roebourne, in the western part of the Pilbara Block, Western Australia. It covers an area of about 7 km by 20 km, and consists of a layered ultramafic zone, about 1300 m thick, overlain by a mafic zone, about 800 m thick. The ultramafic zone comprises peridotite, orthopyroxenite, clinopyroxenite, olivine websterite, olivine orthopyroxenite, and websterite, with interlayered anorthositic gabbro and anorthosite. The mafic zone consists of gabbro, anorthositic gabbro, and anorthosite. The complex is intruded by dolerite, granitic rocks, and pegmatites. No significant calcrete development was noted at Andover.

Munni Munni Complex

The Munni Munni Complex (Fig. 3) is in the Pinderi Hills, 42 km south of Karratha, Western Australia, and is exposed over an area of 4 km by 9 km. It consists of a basal ultramafic zone, 1850 m thick, comprising rhythmically layered dunite, lherzolite, olivine websterite, clinopyroxenite, and websterite, and an overlying 3600 m thick mafic zone, consisting of a lower subzone, A, of gabbronorite and an upper subzone, B, of anorthositic gabbro. It contains subeconomic platinum group elements (PGEs) in a fairly persistent layer of porphyritic plagioclase websterite, along the contact between the ultramafic and mafic zones (Hoatson & England 1986).

The more erosion-resistant rock types (e.g. pyroxenite) constitute about 30–50% of the total outcrop. Peridotitic rock types are far less-well exposed and form recessive topographic troughs covered by in-situ soils. Extensive sandy-soil-hosted calcrete deposits have developed on the western and north-western sides of the ultramafic zone. Incised drainage shows the calcrete to be at least 1.5 m thick; it appears to have formed by surface and groundwater leaching and evaporative deposition of calcium carbonate, resulting from breakdown of calcic pyroxene in ultramafic rocks.

Gabbronorite of subzone A is well exposed, massive, and generally affected by an iron-oxide-rich weathering crust, whereas rock outcrop in subzone B is poor and affected by carbonate-chlorite alteration (Hoatson et al. 1992).

Panton Intrusion

The Panton Intrusion (Fig. 4) is 55 km north-northeast of Halls Creek, Western Australia. Exposed over an area 11 km long by 3 km wide, it consists of a sequence of cumulates about 1500 m thick, folded into a southwesterly plunging syncline and disrupted by cross-faulting, which has divided it into a number of blocks. The intrusion consists of a basal ultramafic sequence and an overlying gabbroic sequence. The ultramafic sequence forms approximately half the thickness of the sequence, and comprises dunite and olivine-chromite cumulates, with some porphyritic harzburgite along the eastern contact of the northern block. Sulphide-bearing chromitites occur in harzburgite, near the base of the sequence and also as laterally continuous layers in dunite some 150 m below the mafic–ultramafic contact. The gabbroic sequence comprises three zones: a lower zone of layered olivine gabbronorite, gabbronorite, gabbros and norite; a middle zone of olivine gabbro, tractolite and chromite-bearing dunite lenses; and an

[1] Division of Regional Geology & Minerals, Australian Geological Survey Organisation, GPO Box 378, Canberra, ACT 2601

upper zone of anorthosite and ferrogabbro (Hoatson 1993).

Spectral reflectance

Spectral-reflectance measurements of freshly broken, weathered and lichen-covered rocks, and soils were carried out, both in the field and in the laboratory, using the InfraRed Intelligent Spectroradiometer (IRIS; manufactured by Geophysical Environmental Research, USA). Sample measurements are relative to a Halon standard.

Figure 6 shows IRIS spectral curves of representative mafic and ultramafic rocks from the three intrusions described above. The spectral reflectance of fresh ultramafic rocks ranges from 8% to 14% in the 600–900 nm region, dropping to 6% in the 2200–2400 nm region, owing to stronger absorption in the SWIR range. Some of the spectra show absorption features centred at 640–650 nm, 1020–1050 nm, and 2300 nm, indicating clinopyroxene; others have broad absorption features centred at 630 nm and 1030–1050 nm, indicating olivine. Fresh mafic rocks have a higher reflectance than fresh ultramafic rocks, with maxima ranging from 10% to 30% in the 1500–1800 nm region. Although reflectance drops towards the ultraviolet region (400 nm), it shows broad absorption features at 1030 nm, with slight increases in the 600 nm region. Reflectance falls sharply at longer wavelengths; absorption features at 2250 nm and 2332 nm indicate the presence of epidote. Spectra of both weathered mafic and ultramafic rocks (Fig. 6) are strongly influenced by the presence of iron in the 800–1000 nm region, which relates to the surface concentration of iron oxides from weathering.

The analysis of all available IRIS reflectance curves of ultramafic rocks from the three sites (including those in Fig. 6) showed two discrete types: in the first case, reflectance maxima range from 18% to 24% in the 700–1300 nm region, dropping to about 6% towards the ultraviolet, and to about 12% towards the 2300 nm region; in the second case, reflectance maxima range from 24% to 32% (exceptionally to 78%) in the 1200–1800 nm region, dropping to about 20% toward the 900–1100 nm region, where they display broad absorption features, and then to about 6% towards the ultraviolet. Reflectance drops evenly to a 25% average in the 2300 nm region (Macias & Simpson in Hoatson & others, 1992). In weathered gabbros, reflectance has an average maximum of 60% in the 2000–2100 nm region, dropping to about 30%–40% near 2500 nm, and to 5%–10% in the 400 nm region.

The IRIS spectral curves of lichen-covered mafic and ultramafic rocks, show lichen-masking effects on spectral features in the 400–2000 nm region; however, some absorption features deriving from the underlying mineralogy are discernible in the 2100–2400 nm region.

Alteration and weathering products

The IRIS spectral curves for ultramafic rocks show absorption features that indicate the presence of serpentine, actinolite, carbonates, and clays (saponite); and of epidote, chlorite, clays,

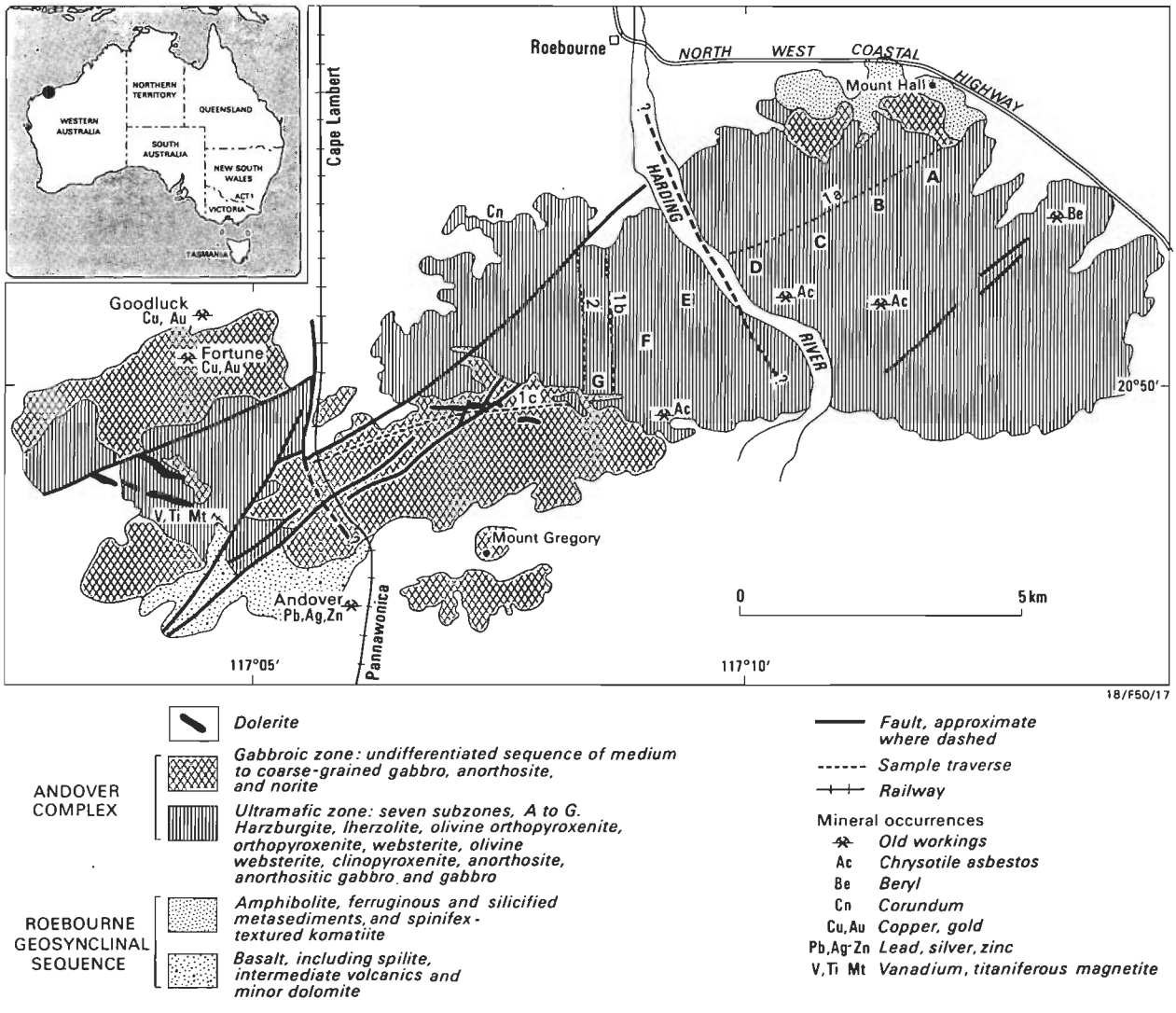

Figure 1. Geological map of the Andover Complex (after Wallace in Hoatson et al. 1992).

and carbonates in gabbroic rocks. Thus, analysis implies there were sufficient mineralogical differences between the products of primary alteration, between secondary weathering products, and between these two groups, to allow discrimination with the TM sensing bands.

The weathering products of the primary minerals are as follows:

olivine → serpentine + magnetite → talc, carbonates, clays (saponite)

clinopyroxene → clinoamphibole, chlorite, epidote, carbonates, saponite

Digital data processing

Initial processing of the Landsat-5 TM data involved the subtraction of dark pixel values from every band, to correct for additive atmospheric scatter. In the case of the Andover and Munni Munni Complexes, the data were then calibrated by the radiance-to-reflectance conversion method of Honey et al. (1974). The logarithmic residuals and principal components image-processing techniques were assessed; however, emphasis was placed on band ratioing to enhance spectral differences determined from field spectral-reflectance information.

Andover Complex

Figure 2 is a TM composite ratio-image of the Andover Complex, with bands 1650 μm/2215 μm (5/7), bands 1650 μm/660 μm (5/3), and bands 2215 μm/835 μm (7/4), displayed, respectively, as red, green, and blue (RGB). The ratios were selected on the basis of the IRIS spectral measurements, to enhance the response of clay/carbonates (5/7) and iron oxides (5/3), and to minimise the response of vegetation in areas of soil. The image provided excellent discrimination of ultramafic rocks (deep-red-brown) and gabbros (green to yellow), adequate discrimination of doleritic dykes (pale-blue), and poor discrimination of volcanics. Field checking confirmed that the discrimination of ultramafic rocks was accurate.

Examination of TM images, focussing on the distribution of ultramafic outcrops in the northeastern half of the complex, combined with patterns indicative of flat-lying lithological units, led to the interpretation that that area of the body is relatively thin and essentially flat-lying.

Munni Munni Complex

For the Munni Munni Complex, a basic TM composite image, with bands 1, 4, and 7 displayed as RGB, respectively, (Fig. 7), offers some discrimination between gabbro (magenta to dark-brown) and ultramafic rocks (light-brown). However, discrimination between these rock types is significantly hindered by the spectral response of vegetation, in particular, by late fireburns (areas of olive-green on the ultramafic rocks and blue on the gabbro). Ground inspection of the burn area on the ultramafic zone, in the northeast of the complex, indicated the presence of dense green spinifex regrowth. This area may represent a somewhat older fireburn than the one affecting the gabbro zone, in the northwest of the complex, where inspection showed scattered, and/or less-dense, regrowth.

Figure 8 is a TM composite ratio-image 5/7, 5/3, 7/4 displayed as RGB. The ratios were selected in order to discriminate and enhance differences between ultramafic rocks, and between gabbro and doleritic rocks. Ultramafic rocks are displayed in red, indicating a predominant response of a clay-carbonate-vegetation mixture (ratio 5/7); the image shows some discrimination of the layering in the ultramafic zone. Carbonate-rich soil to the west and northwest are displayed as brown magenta. The mafic zone is differentiated into three areas: (1) an eastern area, immediately above the contact with the ultramafic zone, displayed as light blue to cyan, indicating

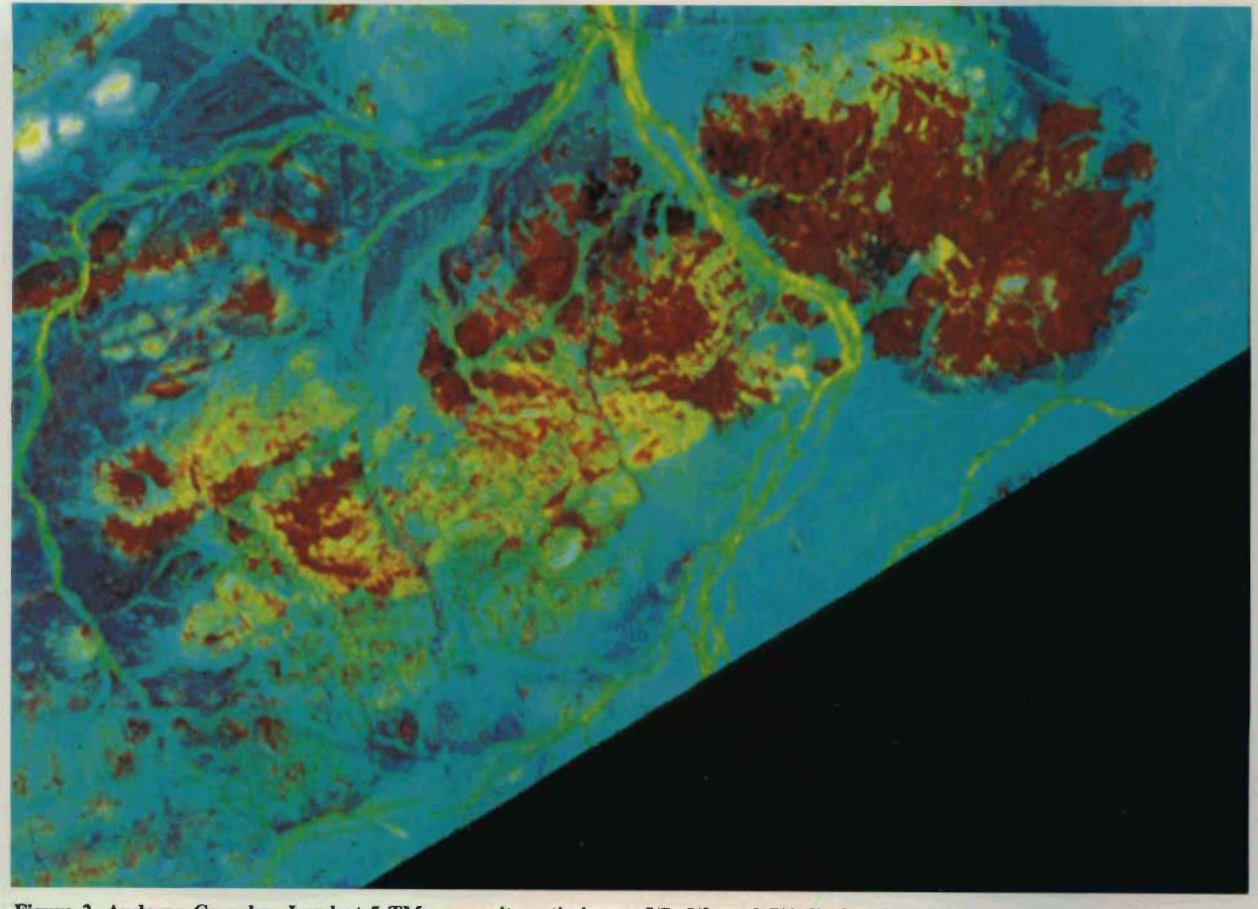

Figure 2. Andover Complex. Landsat-5 TM composite ratio-image 5/7, 5/3, and 7/4 displayed as RGB.

the response of an iron-rich weathering: (2) a central area, covering part of Subzone A (Fig. 3), and displayed as light green to cyan indicating the combined response of an iron-oxide-rich weathering crust on gabbro (ratio 5/3) and soil (ratio 7/4): and (3) a southern area, which partly cover Subzone A and the whole of Subzone B, displayed mainly as blue magenta, indicating the response of soil (ratio 7/4), with minor areas of red and brown. Vegetation along stream is displayed as yellow (ratios 5/7 and 5/3), as well those outcrops densely covered by lichen such as the Pinderi Hills gabbronorite dyke and some areas of both the mafic and ultramafic zones.

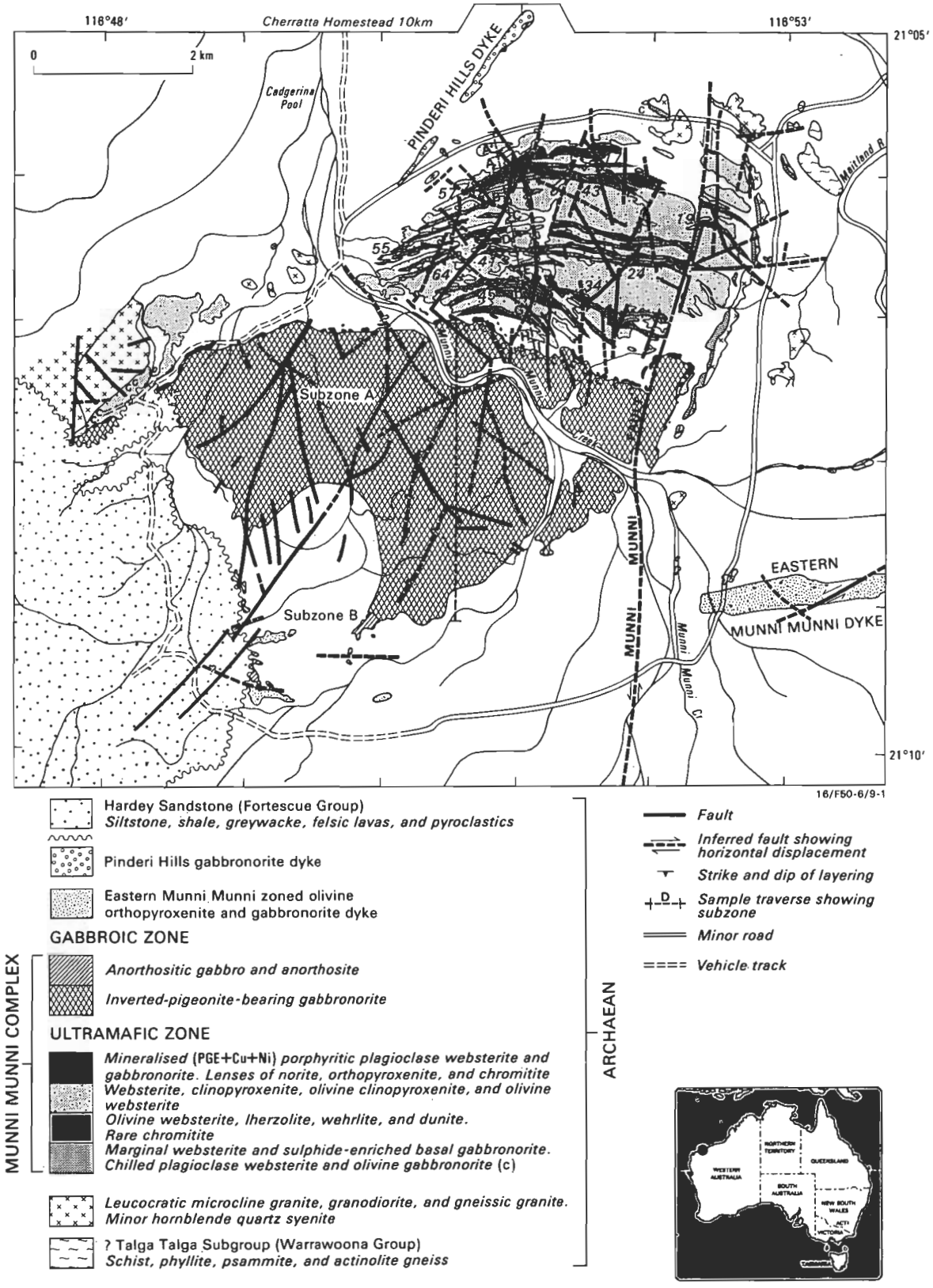

Figure 3. Geological map of the Munni Munni Complex (after Hoatson in Hoatson et al. 1992).

Panton Intrusion

Figure 5 is a TM composite ratio-image of the Panton Intrusion, with 5/7, 5/3, and band 5, displayed, respectively, as RGB. The image allows effective discrimination between ultramafic rocks, displayed as deep-brown magenta, and gabbroic rocks. Three gabbroic zones are discriminated as follows: (1) a lower zone, displayed as red to yellow, indicating the response of clay/carbonates and Fe-oxides: (2) a middle zone, displayed as green-yellow to light-green to cyan, indicating a predominant response from iron-oxides: and (3) an upper zone, consisting of plagioclase-rich anorthosite and ferrogabbro, displayed as red to dark brown, suggesting that the outcrop spectral 'signature' is probably dominated by the vegetation spectral response. Elsewhere in the image, vegetation is displayed as blue (band 5).

Conclusions

Landsat-5 TM can discriminate mafic and ultramafic rocks in the Andover Complex and the Panton Intrusion, and, to a lesser extent, in the Munni Munni Complex. Lithological discrimination in the Andover and Munni Munni Complexes is mainly based on the spectral response of different weathering products of the various ultramafic rock types. In the Panton Intrusion the discrimination represents variations in the weathering products of the plagioclase-rich gabbroic units.

Spinifex vegetation density has a significant influence on ground reflectance. Field measurements in the Munni Munni area show that a density of 30–40% can totally mask the reflectance from underlying soil and/or rock and, thus, severely hamper discrimination of rock types on the imagery. This may arise from a combination of factors relating to scattering from spinifex spines and the growth characteristics of spinifex, e.g. individual plants tend to be uniformly separated on the ground. In those areas where burning has reduced the density of spinifex, interpretation is hampered by regrowth of younger spinifex and patterns of fireburns of different ages (Simpson, 1990). In a similar way, lichen covering even less than half the rock surface can effectively mask most of the spectral response from the rock underneath. Black lichen has similar growth distribution characteristics to spinifex; however, it is destroyed by fire. Both these factors limit effective lithological discrimination by the imagery, although band ratioing assists with rock discrimination and is capable of partly resolving the effect of fireburns on ultramafic rocks.

Discrimination of mafic and ultramafic rocks using the low-spatial resolution TM data was most successful for the Andover Complex; it is significant that Andover has less spinifex and lichen cover than the Munni Munni Complex and the Panton Intrusion.

These problems are significantly lessened by the use of scanner data with higher spectral resolution than the Landsat-5 TM scanner, as reported by Macias et al. (1987) and Macias & Simpson (in Hoatson et al. 1992) in remote sensing studies of the Munni Munni Complex, using data from the experimental scanner, Thematic Mapper Simulator NS001 (aircraft version of the Landsat-5 TM scanner), of the USA National Atmospheric & Space Administration (Huntington & Simpson 1985; Simpson 1986).

Acknowledgments

I am indebted to D. Hoatson for providing the geological information on the Munni Munni Complex and Panton Intrusion, and to D. Wallace for the geological information on the Andover Complex. I thank J. Creasey, P. Bierwith and A. Glikson, whose comments helped to improve the text.

References

Hoatson, D.M., 1993. East Kimberley: Panton Intrusion. AGSO 92: yearbook of the Australian Geological Survey Organisation, Canberra, 78–80.

Hoatson, D.M. & England, R.N., 1986. Platinum group minerals from a layer in the Munni Munni Complex of the Pilbara Block. BMR Research Newsletter, 5, 1–2.

Hoatson, D.M., Wallace, D.A., Sun, S.-S., Macias, L.F., Simpson, C.J. & Keays, R.R., 1992. Petrology and platinum-group-element geochemistry of Archaean layered mafic-ultramafic intrusions, west Pilbara Block, Western Australia. Australian Geological Survey Organisation, Bulletin 242.

Honey, F.R., Prelat, A., & Lyon, R.J.P., 1974. Stansort: Standard Remote Sensing Laboratory pattern recognition and classification system. Proceedings of the 9th International Symposium on Remote Sensing of Environment, 2, 897–905, Environmental Research Institute of Michigan, Ann Arbor, Michigan,

Huntington, J.H. & Simpson, C.J., 1985. Major new Australian US remote sensing initiative. The Australian Geologist, 57, 34–35.

Macias, L.F., Simpson, C.J. & Moore, R.F., 1987. Differentiation of mafic and ultramafic rock types using NS001 and TIMS data. In: Bruce, D. (editor), Proceedings of the 4th International Remote Sensing Conference, 1, 364-370.

Simpson, C.J., 1986. US/Australia Joint Scanner Project. BMR Research Newsletter, 4, 14–15.

Simpson, C.J., 1990. Deep weathering, vegetation & fire burn. Significant obstacles to geoscience remote sensing in Australia. International Journal of Remote Sensing, 11(11), 2019–2034.

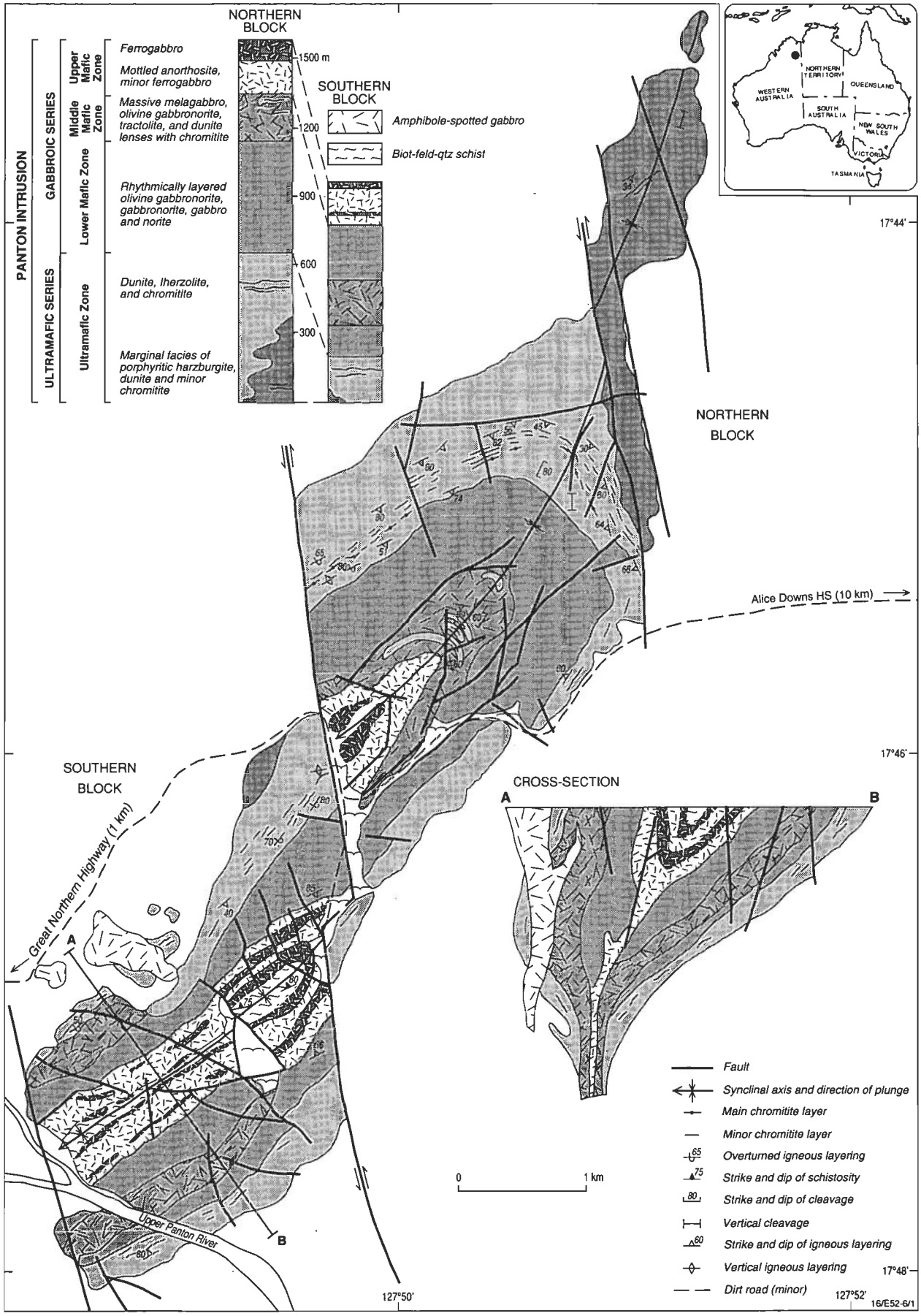

Figure 4. Geology of the Panton Intrusion (after Hoatson 1993).

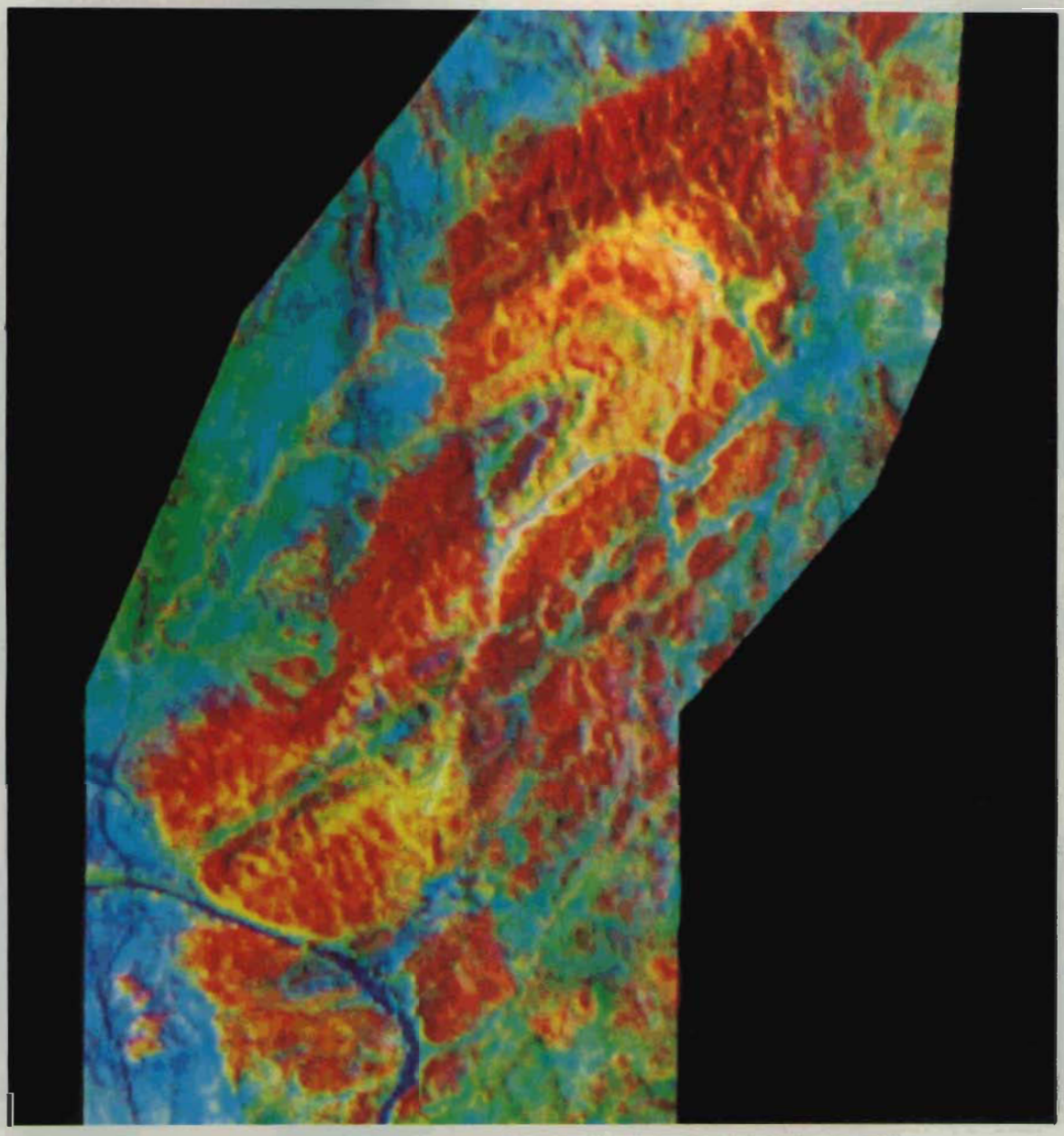

Figure 5. Panton Intrusion. Landsat-5 TM composite ratio-image 5/7, 5/3 and band 5 displayed as RGB.

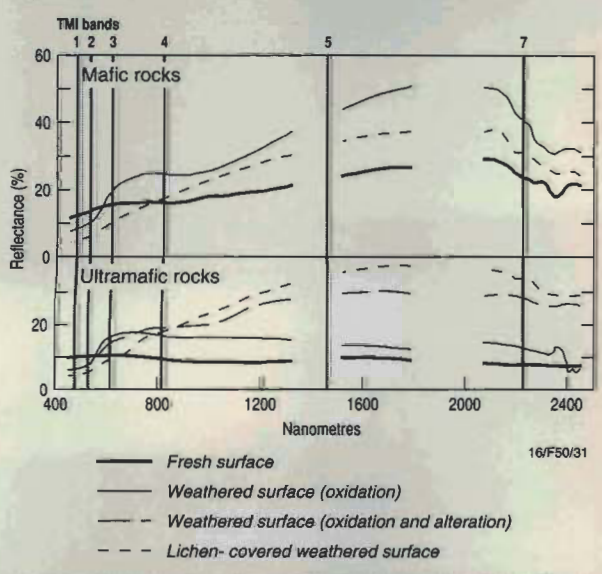

Figure 6. IRIS spectra of representative mafic and ultramafic rocks from Andover, Munni Munni and Panton Intrusions.

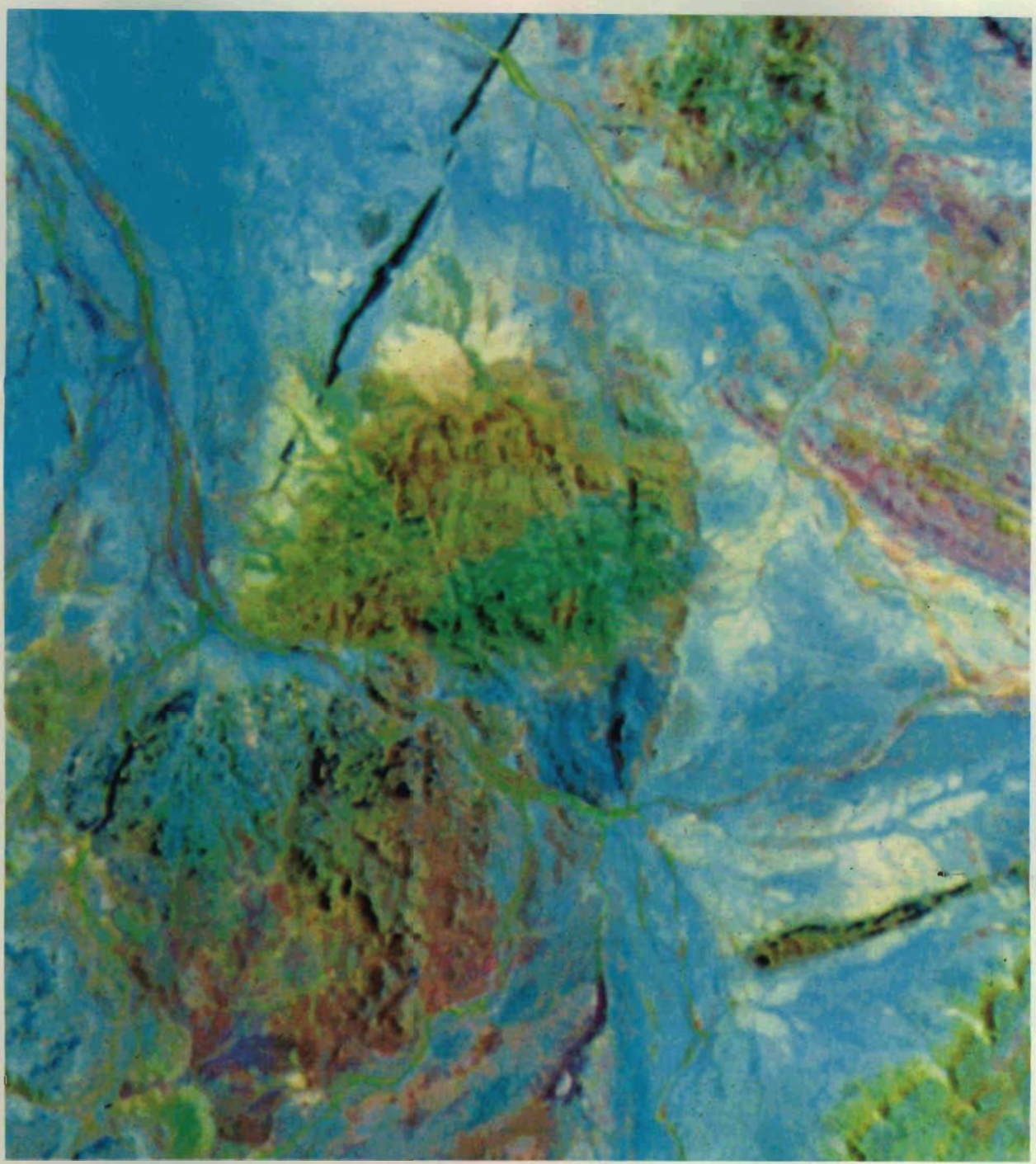

Figure 7. Munni Munni Complex. Landsat-5 TM composite image 1, 4, and 7 displayed as RGB.

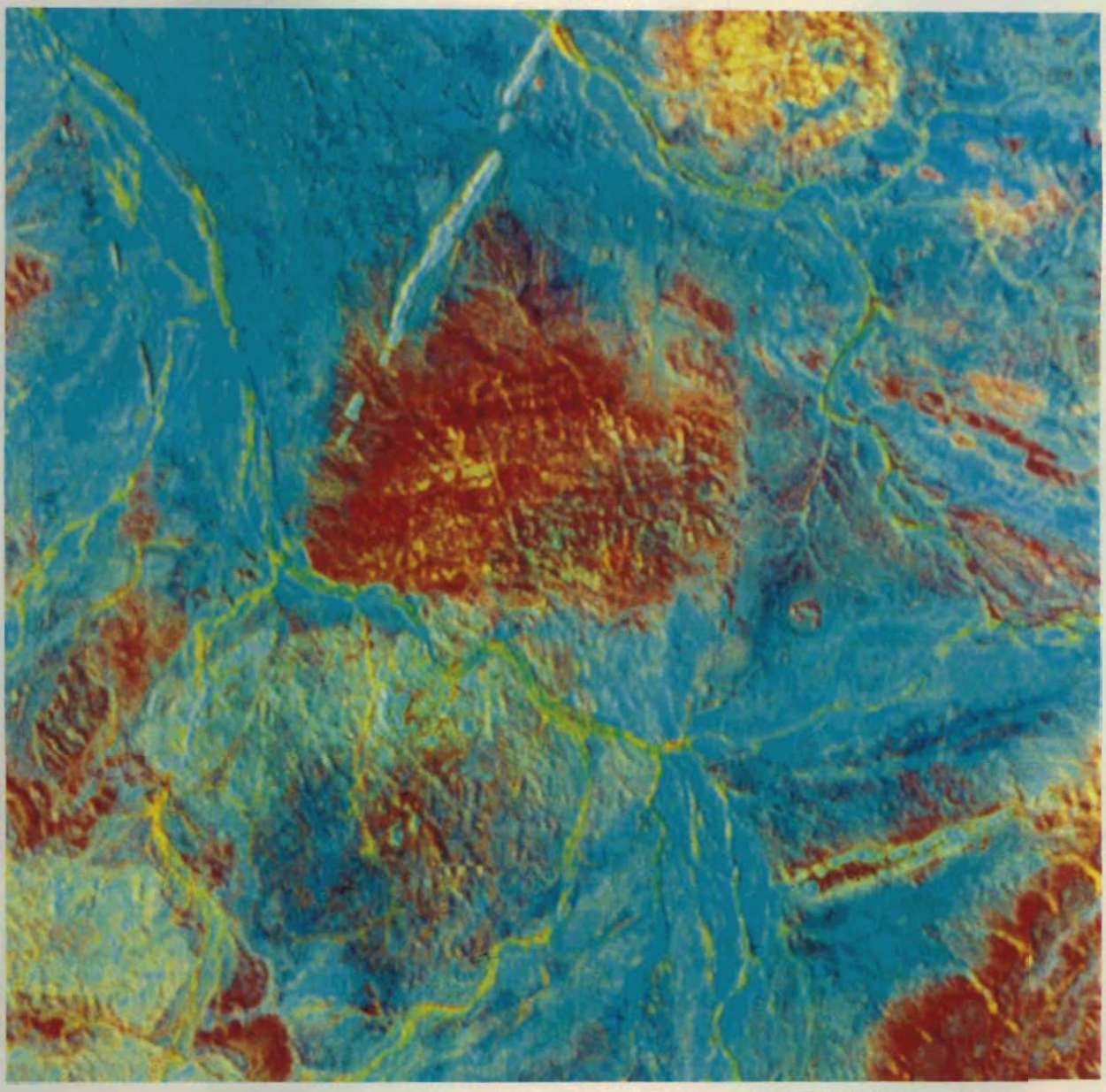

Figure 8. Munni Munni Complex. Landsat-5 TM composite ratio-image 5/7, 5/3, and 7/4 displayed as RGB.

AGSO Journal of Australian Geology & Geophysics, 16 (1/2), 173–193

Application of Landsat-5 TM imagery to mapping of the Giles Complex and associated granulites, Tomkinson Ranges, western Musgrave Block, central Australia

A.Y. Glikson[1] & J.W. Creasey[2]

Application of Landsat-5 Thematic Mapper multispectral scanner data to the detailed mapping of the Tomkinson Ranges–Blackstone–Jameson region, western Musgrave Block, provides a test for spectral–lithological correlations in metamorphic–igneous terranes under the arid conditions of central Australia. The terrane consists of ~1.3–1.5 Ga felsic/intermediate granulites metamorphosed at ~1.2 Ga and intruded by layered ~1.08 Ga mafic–ultramafic bodies of the Giles Complex and near-contemporaneous granites. Significant correlations are observed between Landsat-5 TM spectra, the reflectance patterns of iron oxide and clay–carbonate-dominated weathering surfaces and primary rock types. The weathering surfaces of gabbroic rocks are dominated by clay signatures, and those of felsic granulites, by mixed clay–iron oxide signatures. Iron oxides are well expressed by band ratio 5/4, log residual of bands 5 and 7, inverted log residual of band 1, and the iron oxide end member of pixel-unmixed images. Clay and/or carbonate are identified by high band ratio 5/7 partly masked by dry vegetation, high reflectance in the visible bands, high inverted log residuals of band 7, and the clay end member of pixel-unmixed images, and are effectively distinguished from green vegetation by the second principal component of (pc2[4/3, 5/7]). Discrimination between carbonate and clay in the visible to infrared range is difficult, but calcrete banks along creeks are characterised by higher reflectance than clay. Quartz in weathered felsic rocks is commonly coated by clay and iron oxide, but abraded quartz in alluvial deposits and dunes shows high reflectance in combined bands [1+3+5+7]. As shown by field evidence, the remotely sensed spectra allow discriminations between several lithologic types, including peridotite (commonly covered by calcrete and magnesite weathering crusts), orthopyroxenite (iron oxide-rich weathering), clinopyroxenite (weaker iron oxide signature than orthopyroxene), gabbro (clay [carbonate]-dominated weathering), ferrogabbro (very strong iron oxide-rich weathering signature), anorthosite (strong clay/carbonate signature of weathering crusts), mafic granulites (iron oxide and silica-rich crusts), felsic granulites and granites (clay, iron oxide and silica-bearing weathering crusts), laterite (iron oxide-rich), calcrete (high reflectance, common along creeks), silcrete (very high reflectance), oxidised mafic source-derived alluvium (iron oxide-dominated), felsic source-derived alluvium (quartz and clay-dominated), clay pans and silty, in places ferruginous, dry lake (playa) deposits. The composition of small isolated bedrock outcrops is identified by the spectral signatures of derived detritus. Geologically useful discriminations include (1) separation of thin sills of anorthosite from host felsic granulites; (2) distinction between gabbro and derived mafic granulites (meta-gabbro); (3) distinction between ferrogabbro and gabbro; (4) separation between lateritic deposits and weathered gabbro. Pending field spectrometric measurements, these criteria can be applied in further mapping of the Musgrave Block and other metamorphic and igneous terranes in central Australia.

Introduction

The application of remotely sensed multispectral imagery to regional mapping of unmetamorphosed terranes and to greenschist–amphibolite facies metamorphic terranes utilises the characteristic absorption spectra of hydrosilicates, viz. amphibole, mica, chlorite, and their alteration products—clay minerals, serpentine, carbonates and iron oxides. In these terranes, remotely sensed data in the visible (VIS), near-infrared (NIR) and shortwave infrared (SWIR) can be correlated with a range of surface types, provided weathering, vegetation, and fireburn effects are carefully assessed (Simpson 1978; Simpson et al. 1987). In some instances, recent fireburns provide good windows through to bedrock. By contrast, the scarcity of primary hydrosilicates in igneous and high-grade metamorphic rocks complicates their identification by remote sensing. However, the characteristic weathering crusts on these rocks, including combinations of clay, carbonate, hematite, goethite, etc. in varying proportions, offer potentially diagnostic fingerprints of the primary lithologies.

Systematic geological mapping of high-grade metamorphic terranes in central Australia (Stewart et al. 1984; Warren 1983; Shaw et al. 1984; Glikson 1987; Glikson 1990; Stewart 1991) requires the interpolation and extrapolation of outcrop-scale (mesoscale: ~10 m) data to map-scale (macroscale: >100 m) units, aided by aerial photography, airborne geophysical data, and remotely sensed multispectral data. Penetrative deformation and recrystallisation associated with high-grade metamorphism, partial melting, remobilisation, and anatectic injection of veins, bands, and migmatite, result generally in dismemberment of the original rock units into interdigitated mesoscale, hand specimen-scale and microscopic units, and gradational transitions between all these. For this reason, interpolation of field data and identification and charting of map-scale units generally require numerous field traverses and petrographic examinations.

Thanks to the spectral resolution of sub-pixel components, Landsat-5 TM data allow discrimination of surface types on a scale commensurate with field observations (<30 m), providing a powerful tool for charting the high-grade metamorphic terrane. Thus, whereas the 30 x 30 m pixel size of Landsat-5 TM imagery exceeds the scale of individual outcrops, spectrally distinct materials that occupy parts of pixels (>~30%) can be traced, provided that (1) lithologies are correlated with the field evidence and (2) contiguous lithologic units, such as thin ~10 m thick dykes, sills, or layered units, string along adjacent pixels.

This study refers to the Kalka and Mount Davies mafic intrusions and associated felsic granulites as a type sub-area (Figs 1, 3). It examines single band images (Fig. 4), log residual images (Fig. 5), band ratio images (Fig. 6), and combined band ratios and directed principal component of band ratios (Fig. 7). Results from the last method are compared with the geology of several areas in the Tomkinson Ranges in Figures 9–12.

Morphology and geology of the Tomkinson Ranges

The Tomkinson Ranges straddle the Western Australia–South Australia border, centering about longitude 129°00′ E and latitudes 26°00′–26°23′ S. They form an 80 x 40 km terrane of ridges and inselbergs separated by alluvial plains and dunes. The highest points reach about 1000 m above sea level. Duricrusts may form low rises above valley floors and plains. Major elevated morphological units in the Tomkinson Ranges consist of mafic and, to a lesser extent, ultramafic rock, including the Hinckley Range, Bell Rock Range, Mount Kalka, Mount Davies, Michael Hills, and the southern part of the Mount West massif. Other elevated units consist of felsic

[1] Division of Regional Geology & Minerals, Australian Geological Survey Organisation, GPO Box 378, Canberra, ACT 2601

[2] Information Systems Division, Australian Geological Survey Organisation

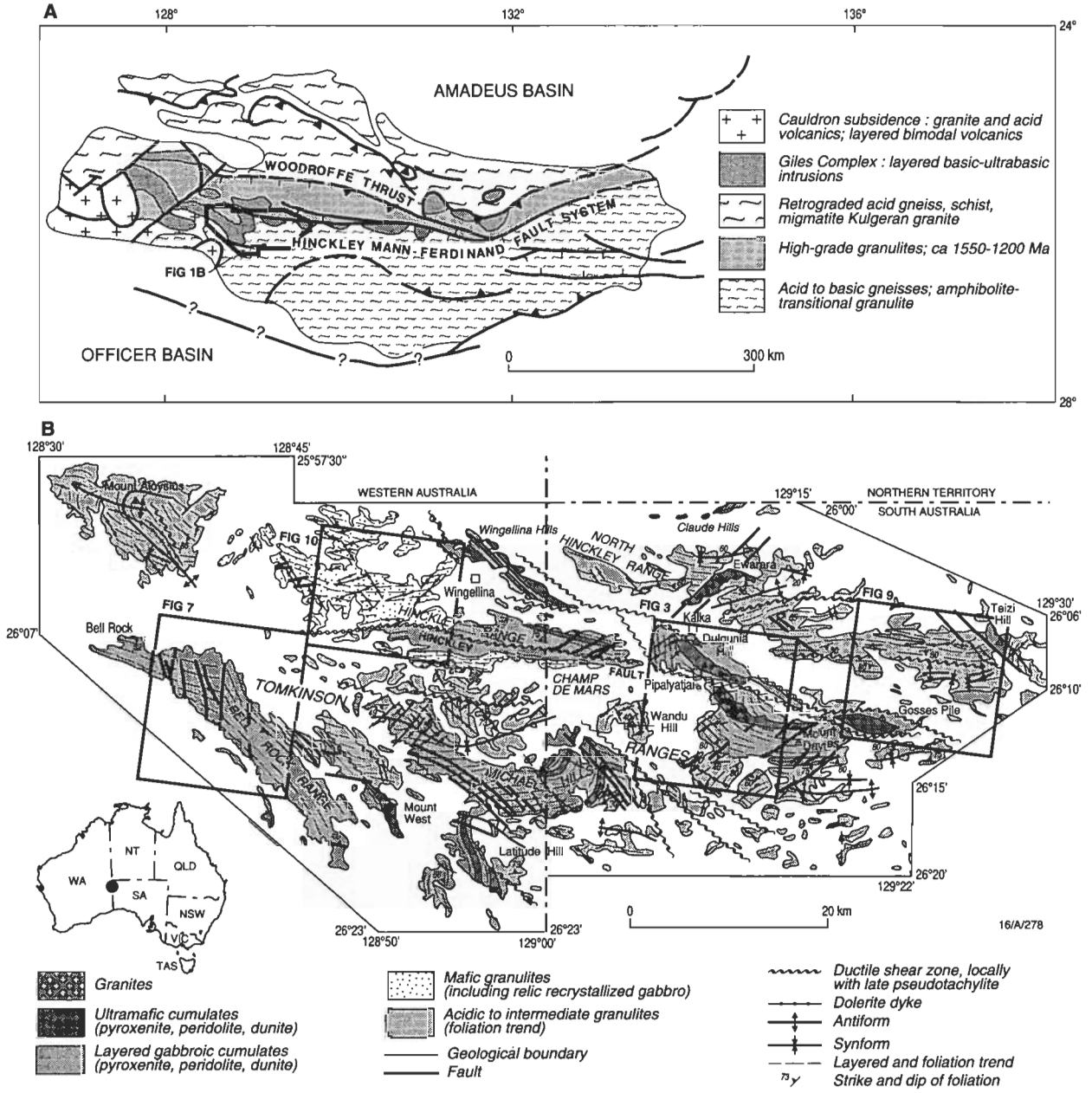

Figure 1. Location and geological sketch map of the Tomkinson Ranges, Western Australia and South Australia. Frames define locations of Figures 3–12.

granulites and granitic gneiss, including Mount Aloysius, Mount West, Ewarara Hills and numerous scattered outcrops. Ridges of gabbro or pyroxenite display jagged skylines and may contain prominent rock piles consisting of slumped subangular boulders several meters across with little soil or vegetation in between. Such boulder piles are common in the Bell Rock Range, where they consist largely of gabbro, and Mount Kalka and Ewarara intrusions, where they consist mainly of pyroxenite. Mafic granulites are, as a rule, less resistant to erosion than the gabbro, and form more subdued morphological features. Mafic dykes form linear depressions within gabbro terranes, but stand out as narrow linear ridges in mafic and felsic granulite and granite terranes.

Vegetation distribution patterns in the Tomkinson Ranges can be correlated with surface deposits (Feeken 1992). The flora is dominated by mulga, spinifex, and annual and perennial grasses. A reciprocal relationship is seen between mulga and spinifex—mulga occurs on alluvial plains, and spinifex on outcrops of Ca-rich rocks and on dunes. Spinifex tussocks dominate mafic and ultramafic outcrops, whereas felsic outcrops may be covered by either spinifex or by grasses. Bunch grasses dominate on the plains and are also important on felsic granulite and granitic outcrops. Corkwood trees of the Hakea family are locally prominent, and often occupy the margins of outcrops, including pediments and alluvial fans. Fireburns are prominent in the region, both on the plains and over outcrops of bedrock.

For a review of the geology of the Tomkinson Ranges and adjoining areas to the west refer to Glikson et al (1995—this issue). The most important geological unit in the Tomkinson Ranges, the Giles Complex, consists of a suite of deformed, partly recrystallised, massive gabbroic to interlayered gabbro–pyroxenite intrusions emplaced in the southern granulite facies block of the upper middle to upper Proterozoic Musgrave Block (Fig. 1). The Giles Complex is emplaced into a suite of felsic granulite facies orthogneiss and paragneiss, is intruded in turn by a suite of porphyritic granites and several sets of mafic dykes, and is considered near-coeval with the 1.08 Ga volcanics of the Tollu Group. For the purposes of the remote sensing investigation, lithologic assemblages are referred to in terms of the following groupings:

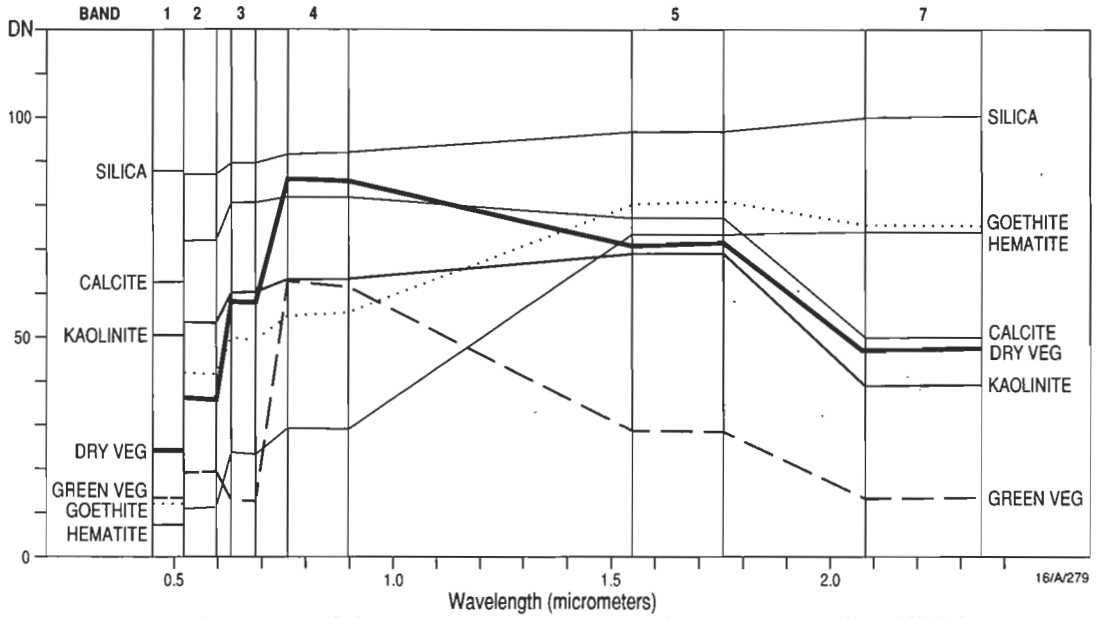

Figure 2. Landsat-5 TM spectra of characteristic mineral and vegetation end members (from MSPECLIB file, P.N. Bierwirth, pers. comm., 1994).

Bedrock

A. banded to massive felsic to intermediate granulites.
B. massive to foliated granitoids associated with felsic granulites.
C. mafic granulites: C1, associated with felsic granulites; C2, representing recrystallised products of gabbro of the Giles Complex.
D. gabbro, gabbronorite and norite of the Giles Complex.
E. anorthosites of the Giles Complex.
F. pyroxenites of the Giles Complex.
G. peridotites of the Giles Complex.
H. mafic/ultramafic plugs.
I. mafic, intermediate and felsic volcanic rocks

Duricrust

K. calcrete and magnesite.
L. ferricrete and laterite.
M. silcrete

Surface deposits

N. colluvium (coarse-grained arenites and conglomerates associated with pediments).
O. alluvium (including plains and creek terrace deposits).
P. clay pans

Regional mapping of the Tomkinson Ranges presents several problems, whose solution purely on the basis of field work may be extremely time consuming or even impossible. These problems include:

1. discrimination between gabbro and ferrogabbro, e.g. in the Bell Rock and Blackstone intrusions (Figs 9,10).
2. discrimination between felsic granulites and calc-silicate and/or anorthosite units interlayered on a small scale, e.g. in the Teizi area (Fig. 11).
3. discrimination between gabbro and gabbro-derived mafic granulites, e.g. in the western part of the Hinckley Range (Fig. 12) and northern Michael Hills.
4. discrimination between interlayered gabbro and pyroxenite, e.g. in the Michael Hills and Kalka (Fig. 7) intrusions.
5. identification of the degree of lateritisation of bedrock types, e.g. of pyroxenite along the northern flank of the Kalka intrusion (Fig. 7).
6. identification of the degree of weathering of felsic rocks to quartz and clay.
7. application of the composition of alluvial surface types as a means for identifying their source terranes.

Image processing methodology

Remotely sensed data available for the Tomkinson Ranges include the Landsat-5 Thematic Mapper 180 x 180 km Cooper scene (path 105 row 78; scanning date 27.10.1986), comprising 7 spectral bands (30 x 30 m pixels for bands 1–5 and 7; 120 x 120 m pixels for band 6). Spectral ranges are listed in Table 1 and Digital Number (DN) values for test pixels are listed in Table 2. Statistical data for the image and sub-image are tabulated in Glikson (1994). The Landsat data are affected by the additive atmospheric radiance (path radiance or multiple atmospheric scatter) and by multiplicative factors (including atmospheric transmittance of solar radiation, solar illumination variations, reflected radiation at specific solar zenith and satellite nadir view angles, and sensor gains), and require calibration, i.e. convertion to pixel reflectance DN values. This involves removal of the atmospheric influences, sensor gains and sensor offsets from the scanned data. Ideally, direct comparisons are performed between the remotely sensed data and field or laboratory spectral measurements. For this purpose, relatively homogeneous pixels are selected, e.g. water, uniform green vegetation cover, open cuts of lithologically uniform material of known composition, and are compared with available mineral or rock spectra. Potential test pixels were examined in the Tomkinson Ranges by Simpson (1987), but no homogeneous pixels consisting of a single component were identified. Chrysoprase open cuts in silcrete near Wingellina and Kalka settlements show high reflectance, as well as spectral features suggestive of contamination with iron oxides and clay (Table 2). A eucalypt and grass-rich patch at the Wingellina school offers a relatively homogeneous green vegetation pixel (Table 2).

Effective correlations can be obtained by the application of the log residuals method. This approach represents both within-pixel spectral relations and the relations between individual pixels and the entire scene. Images produced by this method are less affected by topographic shade component, although shade still affects ratios, especially in the visible range. Consequently, the method is relatively independent from overall atmospheric and gain corrections that apply uniformly to all the pixels of any particular scene.

Log residual (LR) images help to identify the significance of any single within-pixel band DN value relative to the within-pixel bands mean and relative to the entire image pixels mean (Green & Craig 1985). Each LR digital number (DN) in band I represents the radiance value of a particular band

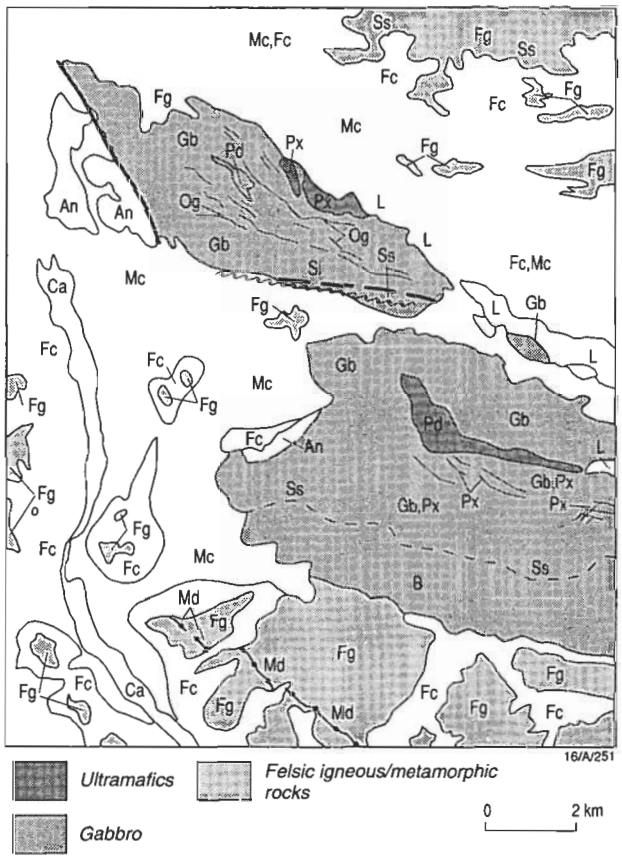

Figure 3. Geological overlay for the Kalka–Mount Davies area (Figs 4–7). Symbols for this overlay and for overlays in Figures 9–12: Pd, peridotite; Px, pyroxenite; Og, olivine gabbro; Gb, gabbro; N, norite; Gf, ferrogabbro; An, anorthosite; Mn, mafic granulite; Md, mafic dyke; V, volcanic rocks; Fg, felsic granulite and granitic gneiss; L, laterite; Ca, calcrete; Si, silcrete; Fc, felsic alluvial collar; Mc, mafic alluvial collar; Dv, dry vegetation; Gv, green vegetation; Ss, southern slopes (normally densely vegetated); B, burnout.

of a single pixel (R_{bp}) divided by the within-band mean value (R_{bmp}), and further divided by the mean of the entire image (R_{mmi}):

$$\text{LR DN(i) value} = R_{bp(i)} / R_{bmp} / R_{mmi}$$

This normalisation procedure cancels out multiplicative effects such as atmospheric absorption, solar illumination and sensor gains, all of which effect all the pixels of a scene scanned at a particular time. The log residual program separates a shadow component, which can be subsequently recombined with LR bands or with dark pixel-corrected radiance bands in any particular image in order to enhance topography and structure. Inverted log residual (ILR) DN values assign high DN values to and, therefore, highlight distinct spectral absorption features.

Lithologic correlations of Landsat-5 TM data

Of the wide range of image processing methods applied in the present study, only the more diagnostic criteria identified are discussed (see summary of correlations in Table 3), the Kalka–Mount Davies area being referred to as the principal example (Figs 3-8).

Spectral characteristics of single Landsat-5 TM bands

Dark pixel-subtracted radiance data and data corrected for atmospheric effects for training areas are presented in Table 2.

The visible range (VIS, bands 1-3): For green vegetation, reflectance in band 2 forms a small peak relative to bands 1 and 3. By contrast, clay minerals reflect strongly, whereas iron oxides absorb in the VIS, allowing a useful distinction between materials with different clay/iron oxide proportions. Silica and free quartz reflect more strongly in all spectral bands than other materials, and can be identified by combination (addition) of bands, e.g. (bands 1 + 3 + 5 + 7 or bands 1 +7)(Fig. 8). Combined quartz and clay-bearing weathering products of felsic rocks have stronger reflectance in the VIS, compared to iron oxide and clay-bearing weathered mafic bedrock surfaces. Iron oxide-rich materials, including laterites, weathering crusts of ferrogabbro and iron-rich pyroxenites and their derived detritus, show low reflectance in the visible range, owing to absorption by iron oxides.

The Near Infrared Range (NIR, band 4): The NIR band 4 is characterised by strong reflectance of green and dry vegetation, carbonate and clay minerals, whereas the iron oxides reflectance is somewhat subdued. Although calibrated reflectances of end members (clay, hematite, carbonate, goethite) are closely grouped in band 4 (Fig. 2), Landsat-5 TM data is capable of distinguishing between high-reflectance felsic granulites, lower reflectance mafic rocks and lowermost reflectance pyroxenites and their derived detritus. The differences between the weathering crusts of mafic rocks and orthopyroxene-rich ultramafics represent the respective proportion of clay and iron oxides in these materials. The reflectance of dry vegetation exceeds that of green vegetation, allowing their separation.

The Short Wave Infrared Range (SWIR, bands 5 and 7): Landsat-5 TM SWIR bands display high reflectance of iron oxides, allowing the effective discrimination of ferruginous materials (laterite and weathering surfaces of ferrogabbro and some pyroxenites) from clay-rich weathering crusts of mafic components of the layered intrusions (gabbro, gabbronorite, norite, anorthosite). Although quartz in felsic rocks is partly coated by clay and iron oxide films, it results in higher reflectance of these rocks in the SWIR relative to mafic rocks, owing to the absorption effect of clay-weathered crusts of the latter. For band 5, the high reflectance of silica and, to a lesser extent, carbonate result in higher albedo of silcrete and calcrete relative to laterites.

The combination of single bands is particularly useful where the more clearly identifiable correlations are displayed. An example is offered by red–green–blue [RGB] 741 images, which emphasise the role of iron oxide in band 7 [R], the role of vegetation in band 4 [G] and the role of clay and/or carbonate in band 1 [B] (Figs 4a,b,c). Consequently, RGB 741 and 541 images display gabbroic rocks in blue/black (kaolinite carbonate-bearing weathering crusts); anorthosite in bright cyan (clay and carbonate-weathered plagioclase in bands 1 and 4); felsic granulites and granites in purple (clay, showing in blue in band 1, combined with contribution of iron oxide detritus derived from mafic dykes, showing in red in band 7); calcrete in light blue (band 1); iron oxide-rich pediments and laterite in red (band 7); vegetated areas in green, and alluvial planes in yellow (representing combined effects of silica, iron oxide [R] and vegetation [G]). The composition of alluvial/pediment collars around or along unidentified bedrock outcrops can be gainfully applied to regional mapping of remote or unaccessible inselbergs. These outcrops may be too small for the identification of their bedrock spectra and the spectral characteristics of their surrounding alluvial shed provides a clue for the source composition. As a rule, mafic outcrops are mostly fringed/surrounded by iron oxide-rich detritus (red collars on RGB 741 images), whereas felsic outcrops are associated with quartz and clay-rich detritus (light cyan collars on RGB 741 images).

Spectral data for dark pixel-corrected images indicate that, in general, orthopyroxene-rich rocks, clinopyroxene-rich rocks, gabbroic rocks and anorthosite display an increasing reflectance in the visible and short-wave infrared bands, in this order, owing to increasing abundance of carbonate/clay weathering crusts with higher abundance of clinopyroxene and plagioclase. Characterisation of the usually altered peridotitic rocks is

complicated, as weathering surfaces may be dominated by carbonate (magnesite), hydrated magnesium silicates and iron oxides. Orthopyroxene-rich (calcium-poor) rocks may have low reflectance DN values in the visible range—a result of absorption by iron oxide coatings, which characterise their weathering surfaces. By contrast, clinopyroxene-bearing websterite shows higher reflectance, owing to higher Ca and Al-rich weathering products. For these reasons mafic igneous rocks—including gabbro, gabbronorite, norite, anorthosite and ferrogabbro—are characterised by generally higher reflectance than pyroxenites (Table 2). Anorthosites show a high reflectance in the lower visible band, owing to high clay and carbonate content of their weathering surfaces, displayed in bright cyan on RGB 741 images, relative to the darker blue

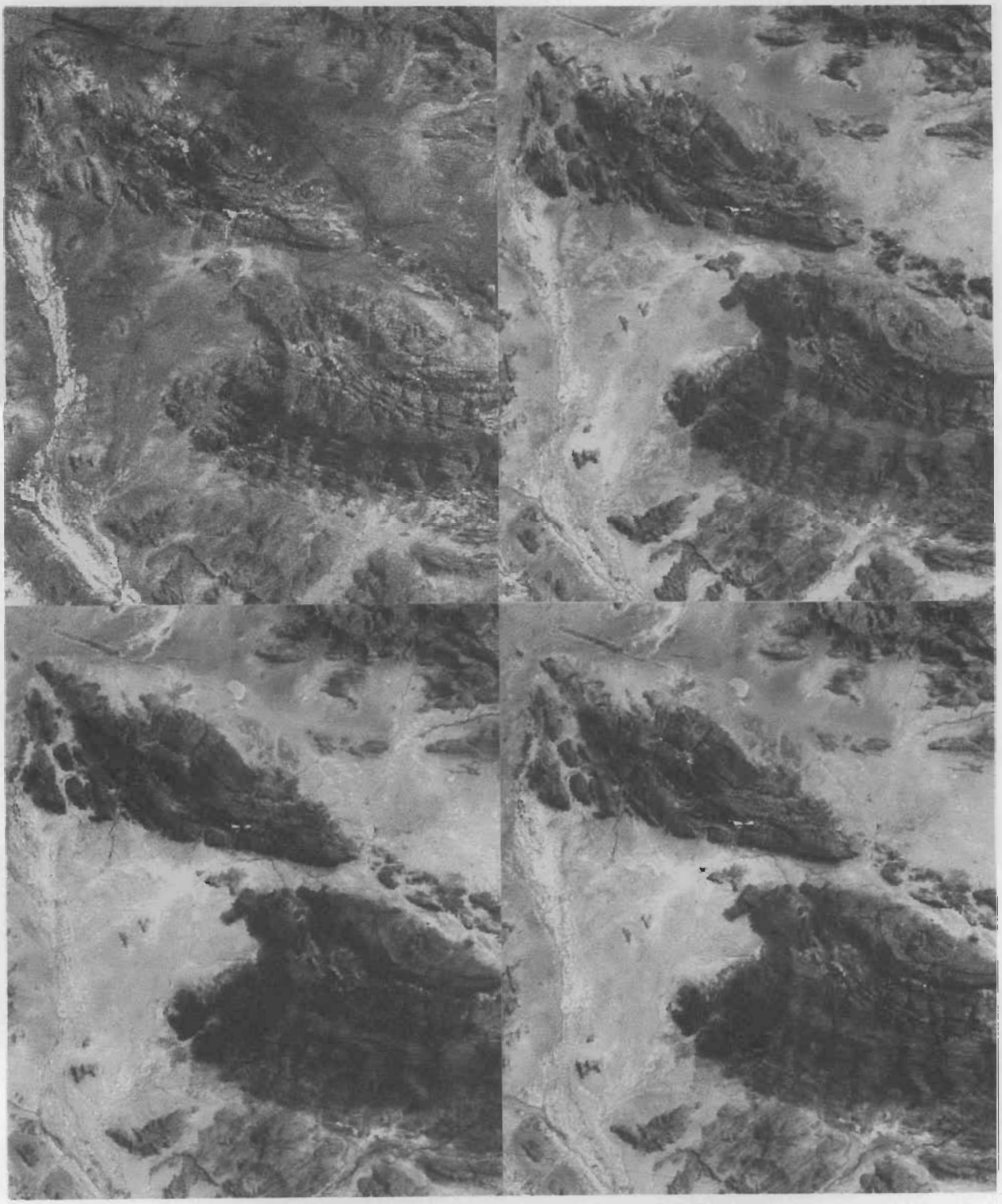

Figure 4. Single and combined band images of the Kalka–Mount Davies area: (A–top left) band 1, showing high reflectance of clay-rich weathering of gabbro, clay-rich alluvial girdles fringing felsic granulites and calcrete along creek; (B–top right) band 4, showing high reflectance of green vegetation along southern slopes, gullies and alluvial plains; (C–bottom left) band 7, showing high reflectance of iron oxide in laterites and alluvial shed from mafic rock outcrops; (D–bottom right) bands (1+3+5+7), showing a combined high reflectance of quartz/silica, mainly quartz-rich alluvial shed from outcrops of felsic metamorphic and igneous rock and a silcrete pit on the south slopes of Mount Kalka. For a geological overlay refer to Figure 3.

of gabbro. Felsic granulites and granitoids, which show higher reflectance than mafic materials in the infrared range, are not readily distinguished from the latter in the visible range.

Log residual images

Examinations of LR and ILR images offer lithologic discriminations that are better pronounced than those shown by single band or band ratio images. For each pixel the log residual program calculates the band mean (average brightness or albedo), which is included in the output as an additional spectral band, allowing the creation of an image representing the topographic and structural characteristics of the area

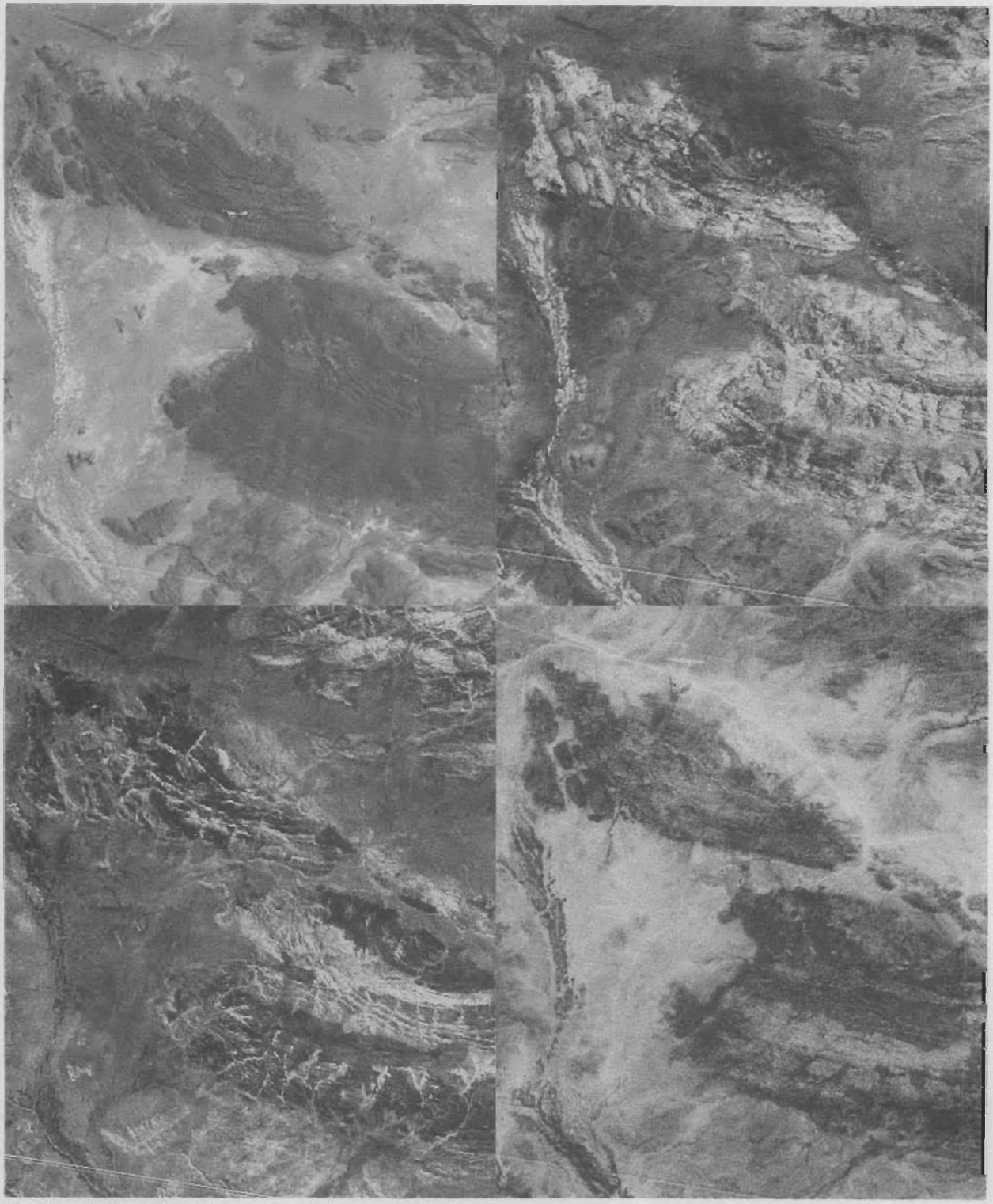

Figure 5. Log residual images of the Kalka–Mount Davies area: (A–top left) log residual band 8, representing the shadow component and thus the topographic features of the terrane; (B–top right) inverted log residuals of band 7, representing the high absorption by clay minerals and carbonates; (C–bottom left) inverted log residuals of band 3, representing absorption by green vegetation; (D–bottom right) inverted log residuals of band 1, representing absorption by iron oxides. Images B, C and D represent dominance of clay-rich weathering of gabbro and anorthosite, occurrence of calcrete along creeks, relative abundance of green vegetation along southern slopes and gullies and on alluvial plains, the iron oxide-rich laterite zones (north of Kalka), and the abundance of iron oxides in alluvial deposits derived from mafic igneous rocks. For a geological overlay refer to Figure 3.

(Fig. 5a). This image can be usefully combined with other LR and ILR images as well as images of any other type. Clays and/or carbonates are represented by either high LR DN values in band 1 or high ILR DN values in band 7 (Fig. 5b). Green vegetation is represented by high LR-4 DN values or by inversion of the band 3 absorption feature, namely high ILR-3 DN values (Fig. 5c). Iron oxides are represented by either high LR-7 DN values or by high ILR-1 DN values. Because laterite and gullies that cut mafic rocks are commonly covered by relatively dense green vegetation, some of the features in Figures 5c and 5d are similar. However, the ILR-1 image is poorly defined, representing inverted absorption features for iron oxides, green and dry vegetation, and includes fireburn zones (particularly along the southern flank of Mount Davies) probably due to dry vegetation (Fig. 5d).

Orthopyroxene-dominated rocks and ferrogabbro display high LR-7 DN values and low LR-4 and LR-3 DN values, compared to norite and gabbro, representing the high iron oxide and low clay components of weathering crusts of these feldspar-poor ultramafic rocks. These variations are clearly

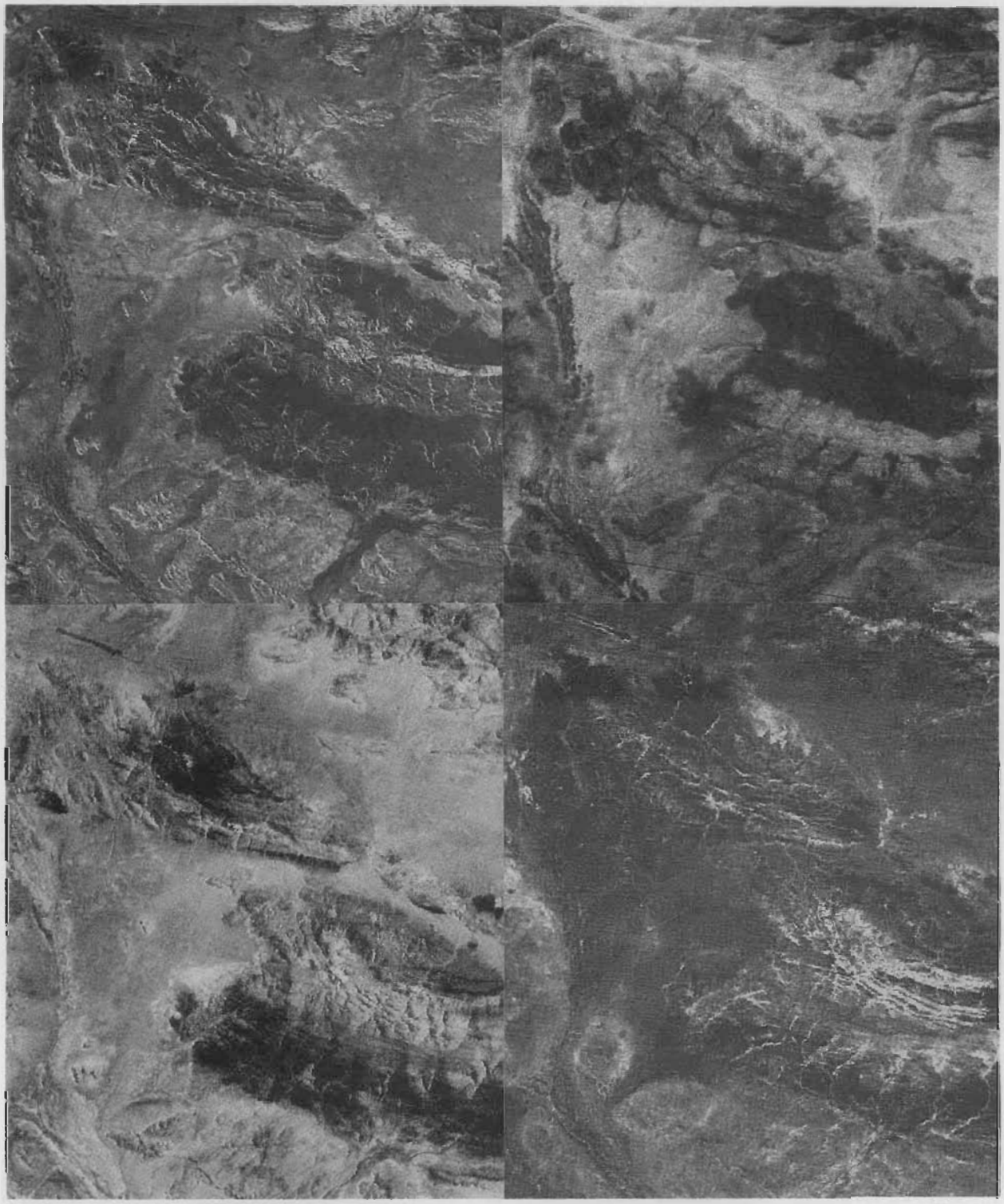

Figure 6. Band ratio images of the Kalka–Mount Davies area: (A–top left) band ratio 5/7 , expressing clay minerals and/or carbonates; (B–top right) band ratio 3/1, expressing a weak signature of iron oxides; (C–bottom left) band ratio 5/4 , expressing a marked signature of iron oxides; (D–bottom right) band ratio 4/3, expressing green vegetation. For a geological overlay refer to Fig. 3.

shown on RGB log residual 741 images by high LR-5 and LR-7 of pyroxenites and ferrogabbro. The signatures of clay (±carbonate)-rich weathering crusts of anorthosites and leucogabbro are broadly similar to those of gabbro, showing high DN values in LR-3 and LR-4 and higher DN values of ILR-7 (Fig. 5b), including clay-rich arkose girdles around outcrops of felsic granulites and calcrete along creeks. Higher abundance of calcic plagioclase and its weathered clay products over anorthosite results in a stronger reflectance in LR-4 and consequent cyan color on RGB LR-741 images. A similar effect is imparted by deep weathering profiles of gabbro, representing combined effects of clay and vegetation. Anorthosites interbanded with felsic granulites are distinguished from the latter by their higher LR-4 and lower LR-7 and ILR-1 DN values. Mafic granulites of the western Hinckley Range show significantly higher LR-5 and LR-7 DN values when compared with gabbro and lower LR-7 DN values relative to iron-rich weathering crusts of pyroxenites and ferrogabbro. This distinction stands out, for example, on RGB LR-741 images (mafic granulite, red; gabbro, cyan), allowing

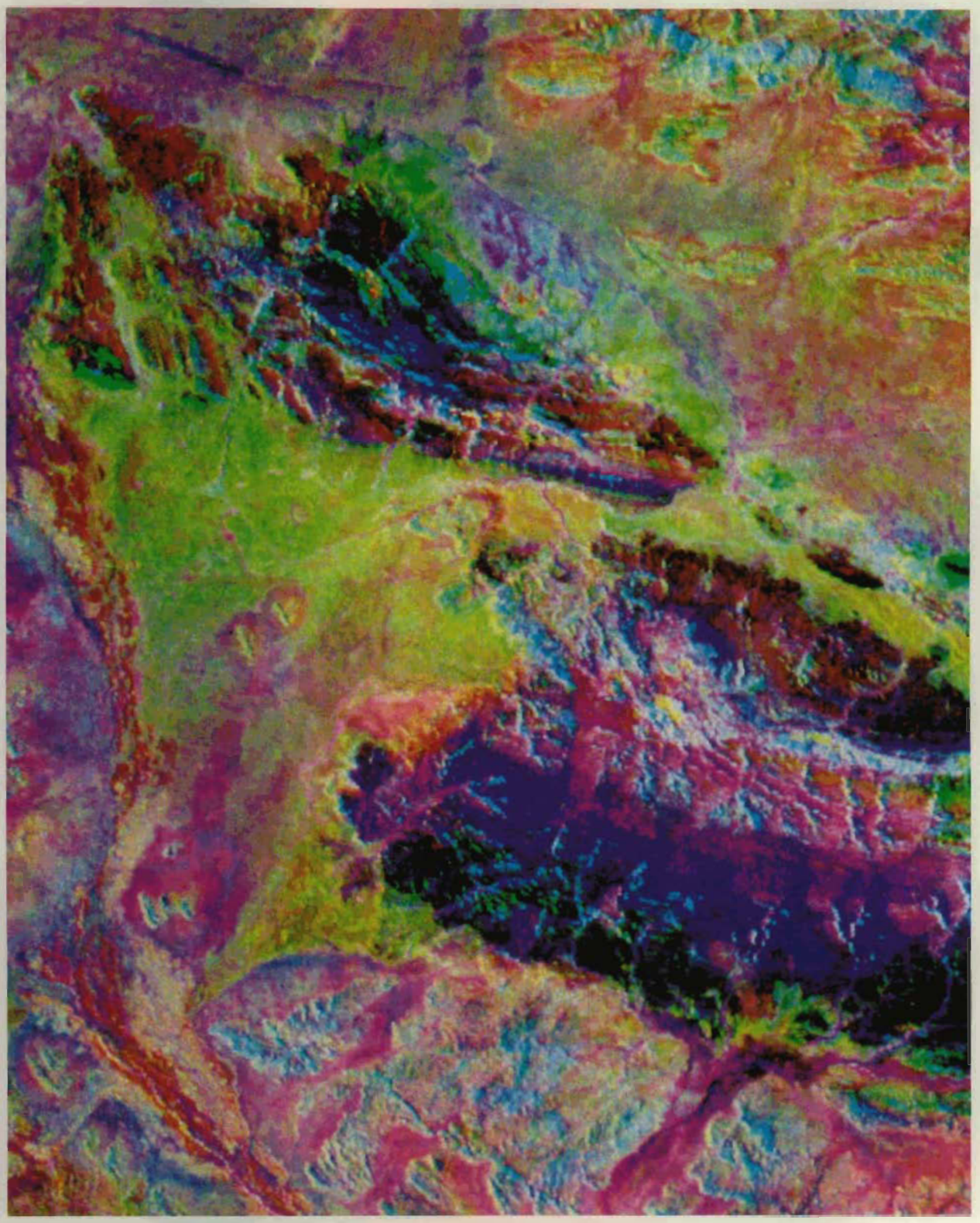

the charting of little-recrystallised relic bodies of gabbro from mafic granulites in the western Hinckley range (Glikson 1994). The spectral difference between gabbro and mafic granulite, which have near-identical mineralogy and chemistry, is attributable to the silica-bearing weathering crusts, which show as films of silica on granulite outcrops and are related to penetrative intrusion by granitic veins. This is contrasted with the clay/carbonate rich weathering crusts on little-recrystallised coarser grained gabbro from which the mafic granulites have been derived by recrystallisation. Another factor contributing to the different spectral characteristics of the gabbro and mafic granulites is the finer grained texture of the latter.

Log residual images allow an effective discrimination between gabbroic rocks and felsic igneous/metamorphic rocks on the basis of differences in LR-5, which displays higher DN values in felsic rocks, owing to a greater abundance of iron oxide in their weathering crusts. Consequently, images such as RGB LR-754 commonly display iron-rich pyroxenites in red [LR-7], felsic materials in shades of green (LR-5), and gabbro in dark blue [LR-4]. Intrusion of mafic dykes into felsic rocks enhances the iron oxide signature of the latter due to scattered mafic detritus. Weathered felsic rocks located at topographically high positions below uplifted early erosion surfaces (peneplain) display higher DN values in LR-3 and LR-4, owing to clay and associated green vegetation, represented on RGB LR-741 images by green (LR-4), e.g. Mount Aloysius, Mount West and Ewarara ridge (Fig. 1). Felsic and mafic granulites have similar DN values in LR-7 and LR-5, and appear in similar colors on RGB LR-754 and LR-741 images. The mafic granulites have somewhat lower DN values than felsic granulites in LR-3 and LR-4 images.

The spectral response of laterites is similar to that of ferrogabbro in LR-7, LR-5 and LR-4, representing the high abundance of iron oxides in these materials. On RGB LR-754 images, the high DN value in LR-5 results in a diagnostic deep apple green color for laterite. Calcrete deposits associated with creeks are distinguished by high DN value in LR-3 and LR-1, similar to anorthosite and gabbro, where clay (±carbonate) coatings may be important. On RGB LR-741 images calcrete shows in cyan blue, but is difficult to discriminate from silcrete, an analogy related to local mixtures of these components.

Alluvial deposits derived from specific bedrock types are closely related to their source composition. Thus, oxidised colluvium and alluvium derived from mafic rocks display higher DN value in LR-7 (iron oxide-dominated) than debris derived from felsic rocks. Alluvial deposits derived from the latter have generally higher DN values in LR-5 and LR-4, the latter representing green vegetation supported by the arkose-rich shed from felsic sources. Such alluvial collars fringe or form rings around outcrops of felsic granulite, as displayed on RGB LR-741 images in cyan (vegetation on clay-rich soil)(Glikson 1994). Alluvial deposits derived from mixed sources display intermediate effects. Dunes show little difference from mixed-source alluvial deposits, and display generally high reflectance related to the effect of abraded free quartz. Some silt/clay deposits display lower DN value in LR-5 and high DN value in LR-3 and LR-1, representing lower iron oxide and higher clay components relative to coarser grained alluvial deposits

Fireburn effects in alluvial and dune areas are manifest by a higher LR-4 DN values, representing young green vegetation, relative to old growth dominated by high LR-7 DN values that represent dry vegetation. On RGB LR-741 images foreruns are displayed in mixtures of bands LR-4 and LR-7 (yellow), whereas old growth areas are displayed by high LR-7 DN values (red). Fireburnt gabbro outcrops reflect more strongly in LR-4 and LR-3 and less in LR-7, as compared to old growth areas dominated by high LR-7 and LR-1 DN values. Consequently, on RGB LR-741 images, mafic fireburn areas show in cyan and old growth in purple.

Log residual images are significantly enhanced by the application of AMSS Geoscan MK-1 images. For example, an RGB LR-941 image of the Wingellina Hills area allows discrimination between weathered gabbro and laterite. The weathered gabbro shows high reflection by clay in band LR-1 and high absorption DN values in ILR-9 and ILR-4, and is consequently displayed in red and green (yellow). By contrast the bush-covered laterite reflects strongly in LR-4 and to a lesser extent LR-9, showing high absorption in bands ILR-1 and to a lesser extent ILR-9, resulting in a purple color (Glikson 1994).

Landsat-5 TM Band ratio images

Given the limited number of bands and the broad wavelength spectrum covered by Landsat-5 TM bands, the identification of surface types is complicated by spectral superposition. Landsat-5 TM spectra allow identification of iron oxide (hematite—high 3/1, 5/4 and 5/3), clay + dry vegetation (high 5/7), green vegetation (high 4/3), and quartz/silica (bands 1+3+5+7). Since band ratios 3/1 is also representative of green vegetation spectra, iron oxides are better discriminated by the

Figure 7. pc2[4/3;5/7]:5/4:4/3 RGB image of the Kalka and Mount Davies layered intrusions. The Kalka layered intrusion consists of a >5000 m thick south-younging sequence, which includes (1) a basal zone of orthopyroxenite and websterite; (2) a thick zone of norite, minor pyroxenite, gabbro, anorthosite, olivine bearing norite and olivine-websterite; (3) a lense of harzburgite occurs within the norite zone, occupying a marked topographic depression; (4) an olivine gabbro zone <600 m thick within the norite zone; (5) an anorthosite zone. The basal pyroxenite units (Px) and the olivine gabbro (Og) display in deep azur green, representing their iron oxide-rich weathering crusts. The norite (N) displays in red, representing clay-dominated weathering crusts covered by dry spinifex vegetation. Anorthosites (An) show in orange, representing clay/carbonate-dominated weathering crusts. The Mount Davies gabbro (Nesbitt & Kleeman 1964) is the second largest layered mafic/ultramafic body of the Giles Complex. It consists of a >7000 m thick south-younging sequence of cumulates, including (1) a lower gabbro zone with pyroxenite intercalations; (2) a central valley-forming serpentinised peridotite unit; (3) a gabbroic zone with numerous pyroxenite intercalations, and (4) a thick upper gabbroic zone which intrudes felsic granulites discordantly through a wide hybrid transition zone. The Mount Davies intrusion is cut by numerous faults, including the near-strike Greenwood fault. The lower gabbroic zone (displaying in red, representing clay-rich weathering and dry vegetation) is overlain by a large depression-forming peridotite lense (Pd) capped by magnesite/calcrete, which shows in mottled yellow/white/red patterns. Pyroxenite intercalations (Px) of sequence 3 form narrow strike valleys showing in green (iron oxide-rich) and blue (green vegetation-rich). Felsic granulites (Fg) intruded by the Mount Davies body show greenish yellow, signifying mixed iron oxide–clay high-albedo (quartz-rich) weathering surfaces, and are cut by NW-trending mafic dykes (Md), which show in blue-green, thanks to their iron oxide-rich weathering surfaces and thicker vegetation. Outcrops of felsic bedrocks are surrounded by red to purple collars (Fc), signifying clay rich alluvial material shed from the felsic rocks. A zone of nickel-bearing laterite (L) east of the Kalka intrusion shows in apple green. Alluvial materials derived from the layered mafic intrusions are dominated by iron oxide (Fg). Thick calcrete (Ca) duricrust along Pidingadinga Creek show in deep orange. The southern slopes (Ss) of Mount Davies bear thick green vegetation (Gv) that show in blue, especially along gullies, and at lower levels feature a major burnout (B) of low dark brown albedo. The southern fault-bounded (Hinckley fault, Hf) escarpment of Kalka and the southern slope of a felsic granulites ridge (Fg) at the northeastern corner of the area also feature strong green vegetation effects. For a geological overlay refer to Figure 3.

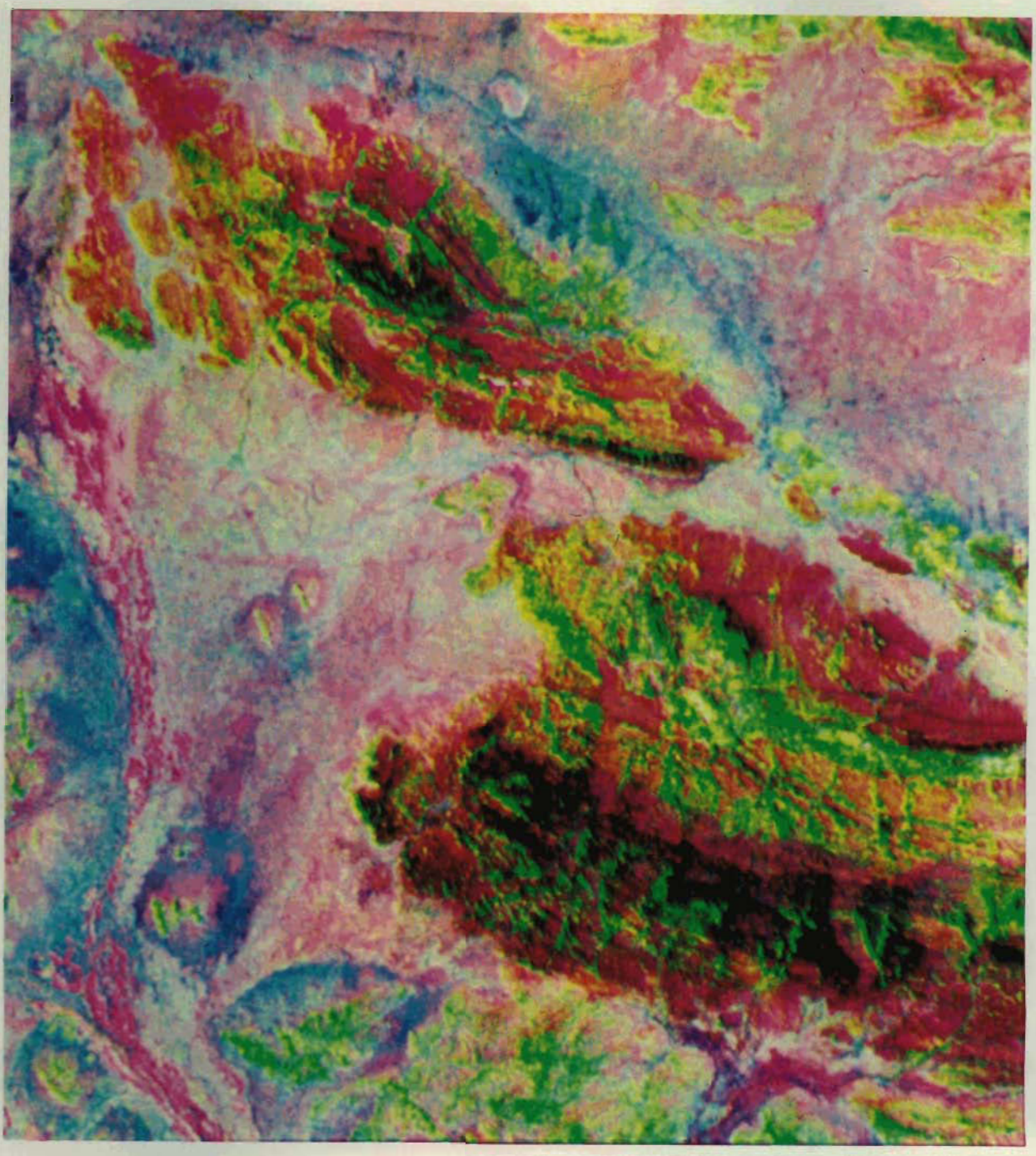

Figure 8. pc2[4/3;5/7]:5/4:[bands 1+3+5+7], RGB image, representing clay/carbonate–iron oxide–quartz/silica relationships in the Kalka–Mount Davies area. Note the concentration of alluvial quartz, showing in blue, around outcrops of felsic granulites and granites. The spectral signature of quartz is not expressed on the weathered surfaces of the felsic rocks, owing to thin coatings of quartz grains by films of clay and iron oxide. For a geological overlay refer to Figure 3.

5/4 and 7/4 band rations. green and dry vegetation spectra, the band ratio 5/4 is better suited for discrimination of iron oxides. Thus, the RGB 5/4:4/3;5/7 image is useful for distinction of iron oxides, green vegetation and clay, respectively. In this image, a partial green vegetation cover over clay/carbonate bedrock displays in cyan, whereas fireburn areas show in dark brownish colour. However, near-spectral overlaps occur, for example: (1) clay and carbonate; (2) the 5/7 ratio of clay and dry vegetation; (3) goethite and hematite (Fig. 2). The effects of histogram stretching, maximising the range of DN values for each of the ratios on RGB images, complicates comparisons between band ratios. Examination of Landsat-5 TM spectral patterns for training areas in the Tomkinson Ranges indicates systematic differences with regard to some of the principal ratios, summarised below (Table 2).

Laterite, characterised by high reflectance in band 7, owing to its iron oxide-rich nature, displays high 5/4 ratio DN values (~2.7) and high 5/1 ratio DN values (~4.6–5.1), but does not display high 3/1 ratios relative to other less-ferruginous materials (Table B). Clay pans and dry lakes (Champ de Mars, Lake Wilson) do not display the high band ratio 5/7 DN values expected for clay, suggesting they may consist principally of silt. The Lake Wilson bed is characterised by high band ratio 5/4 (~2.6), signifying iron oxide-rich detritus. Weathered clay-rich felsic granulites and anorthosites have relatively high 5/7 band ratios DN values (~1.4) due to clay (±carbonate)

enrichments, as does calcrete. The high 5/7 ratios of silcrete suggest silica/carbonate mixtures. The masking effects of dry and green vegetation are partly overcome by calculating the band ratios of devegetated images, using a pixel-unmixing program that subtracts the green vegetation end member from the bands (Bierwirth 1990; Glikson 1994). The results of this analysis indicate consistent lowering of the band ratios 5/7 and 5/4 and increases in the band ratios 3/1 and 5/1 in green vegetation-free images, as compared to mixed mineral/vegetation images. In the following, the characteristics of individual band ratio images are described:

***Band ratio 5/4 image*:** this band ratio is extremely useful for the identification of hematite and goethite, since the other common components—clay, carbonate, silica, green and dry vegetation—have significantly lower ratios. High 5/4 DN values are typical of laterites, iron-rich pyroxenite and oxidised mafic-derived pediment and colluvium deposits (Fig. 6a). By contrast, the band ratio 3/1of hematite and goethite is partly overlapped by the spectral patterns of dry vegetation (Fig. 2), yielding a poorly defined image, which shows only a weak expression of iron oxide-rich units, including dry vegetation patterns corresponding to fireburn patterns (Fig. 6b). Felsic rocks are characterised by higher 5/4 ratios than gabbroic rocks, confirming the higher iron oxide levels in their weathering crusts and shed from mafic dykes. In mafic terranes, fireburn areas show a lower 5/4 ratios than old vegetated areas.

***Band ratio 5/7 images*:** this band ratio is diagnostic of clays and minerals; however, it is overlapped by the band ratio 5/7 of dry vegetation (Fig. 2). Felsic rocks show higher DN values than mafic rocks. Surface types displaying very high band ratio 5/7 DN values in the Kalka–Mount Davies sub-scene include (1) clay-rich alluvial/arkose girdles around isolated outcrops of felsic granulites; (2) carbonate-rich weathering zones overlying peridotitic rocks at the core of the Mount Davies range; (3) calcrete accompanying creeks; (4) very low band ratio 5/7 typical of vegetated shaded southern slopes, i.e. Mount Davies, Kalka, Hinckley fault scarp and ridges southeast of Ewarara. Patchy zones of high band ratio 5/7 DN values also occur over gabbro bedrock surfaces, representing combination of clay-rich areas and dry vegetation patterns (Fig. 6c).

***Band ratio 4/3 images*:** DN values of this ratio representing green vegetation are markedly higher than for areas rich in dry vegetation and/or iron oxides. High band ratio 4/3 DN values occur along gullies, creeks, strike depressions over pyroxenite in Mount Davies, parts of the southern shaded and better vegetated slopes of Mount Davies and the eastern extension of Ewarara ridge (Fig. 6d). High band ratio 4/3 DN value zones may coincide with young regrowth of green vegetation in recent fireburns areas.

Principal components analysis of single bands

The generally high correlation between bands of common materials in natural terranes requires a method of discriminating spectral patterns which depart from the general norm. Principal components (PC) analysis measures the correlation between band reflectance DN values in each pixel and the mean spectral pattern of the total pixel array. The method quantifies the proximity of each reflectance value to best-fit variance axes in N-dimensional space—the number of axes equalling the number of spectral channels. The highest principal component (PC1) represents best correlated band DN values, whereas lower PCs represent increasingly less-correlated spectra of potential interest. Each PC is influenced by all the 6 Landsat-5 TM bands. Particular PCs are influenced by particular surface types, although such correlations may vary within and between images.

Eigen vectors weighing the effect of each of the 6 spectral bands in each of the 6 PCs (based on bands 1,2,3,4,5,7, excluding the thermal band 6) are tabulated in Glikson (1994). In general, the PC analysis of Landsat-5 TM in the Tomkinson Ranges suggests correlations of low-order least-well correlated PCs with vegetation types and fireburn patterns. Thus, whereas RGB images of PCs 1, 2 and 3 outline geological and structural elements, RGB images of PCs 3, 4 and 5 display the distribution of vegetation and fireburn areas. PCs 3 and 4 contain information on the distribution of free quartz in alluvial and dune deposits, as contrasted from weathering-coated quartz in bedrock and from silcrete.

Single principal component images display the following features:

- PC-1 is dominated by bands 2, 3 and 7 (i.e. clay, carbonate, iron oxides). Both mafic and felsic rock types display high DN values. Gabbro and pyroxenite display high to very high DN values, as do felsic granulites/granites. However, whereas mafic source-derived alluvium reflects in intermediate DN values, felsic source-derived alluvium and dune crests have very low DN values. This difference is interpreted in terms of (1) high bands correlation of the clay–carbonate–iron oxide-dominated weathering crusts in a compositionally wide range of bedrock types, and (2) low bands correlations of free quartz-dominated felsic source-derived alluvium and dunes. The relatively low quartz expression in the felsic rocks themselves is attributed to their coating by weathering products such as clay and iron oxides. Calcrete and silcrete show very low band correlations in PC1. Fireburns are displayed by the somewhat higher DN values of old growth. Shade is represented by lower DN values.
- PC-2 shows a strong negative correlation with band 7 (iron oxides), allowing discrimination between iron oxide-rich materials (pyroxenites, ferrogabbro and laterite) of intermediate to high DN and anorthositic to gabbroic rocks of low DN. Felsic granulite/granite displays intermediate to high DN values. Fireburn areas on gabbro show lowering of DN values as compared to old growth. Calcrete and silcrete show may show low DN values and felsic-derived alluvium and dunes show in black—representing the low bands correlation of free quartz. Green vegetation and thereby creeks show as low-DN dark zones.
- PC-3 is influenced by bands 2 and 5 (clay, iron oxides), and appears to be dominated by free quartz, as suggested by very high DN values of felsic-derived alluvial materials and of dunes. The role of quartz is confirmed by the high negative Eigen vector value of the thermal band [6] in the original Landsat-5 TM image (Glikson 1994). Interpretations of band 6 are complicated by its sensitivity to atmospheric conditions. The PC3 image is useful for discrimination of fireburns, thanks to significantly higher DN values in fireburn areas over bedrock and alluvial deposits. Calcrete and silcrete duricrusts show low DN. PC-3 images display little discrimination between other surface types.
- PC-4 shows a strong negative correlation with bands 5 and 3 and displays high DN values for iron oxides and for fireburn areas. The DN values of the latter are in inverse relation to their age, i.e. young fireburns display higher DN values. PC-4 offers a good discrimination between gabbro and mafic granulites, the latter displaying higher DN values. Felsic materials show lower DN values than mafic materials, and free quartz-bearing felsic alluvium as black areas.
- PC-5 shows a negative correlation with band 1 and a positive correlation with band 4 (green vegetation), which occurs mainly along creeks and depressions, in agreement with the high Eigen vectors in band 4. Little contrast is shown between mafic and felsic lithologies.
- PC-6 is dominated by negative correlations in bands 4 and 1. The images are very 'noisy' and show faint outlines which can hardly be correlated with geological features, possibly reflecting old fireburn patterns and dry vegetation patterns.

Directed principal components analysis of band ratios

Application of directed principal component analysis to band ratios allows a discrimination between materials with partly overlapping spectral patterns (Fraser & Green 1987). High 4/3 ratio DN values pertain to both iron oxide and green vegetation, and high 5/7 band ratio DN values pertain to both clay and vegetation. However, iron oxide can be distinguished from vegetation by much lower 5/7 ratio DN values. Likewise, clay can be distinguished from vegetation by much lower 4/3 ratios. These discriminations can be made using principal component analysis of pairs of ratios. For vegetation and clay the difference is expressed by principal components analysis of bands 4/3 and 5/7, namely, pc2(4/3:5/7). The discriminative principal component can be combined with band ratios in

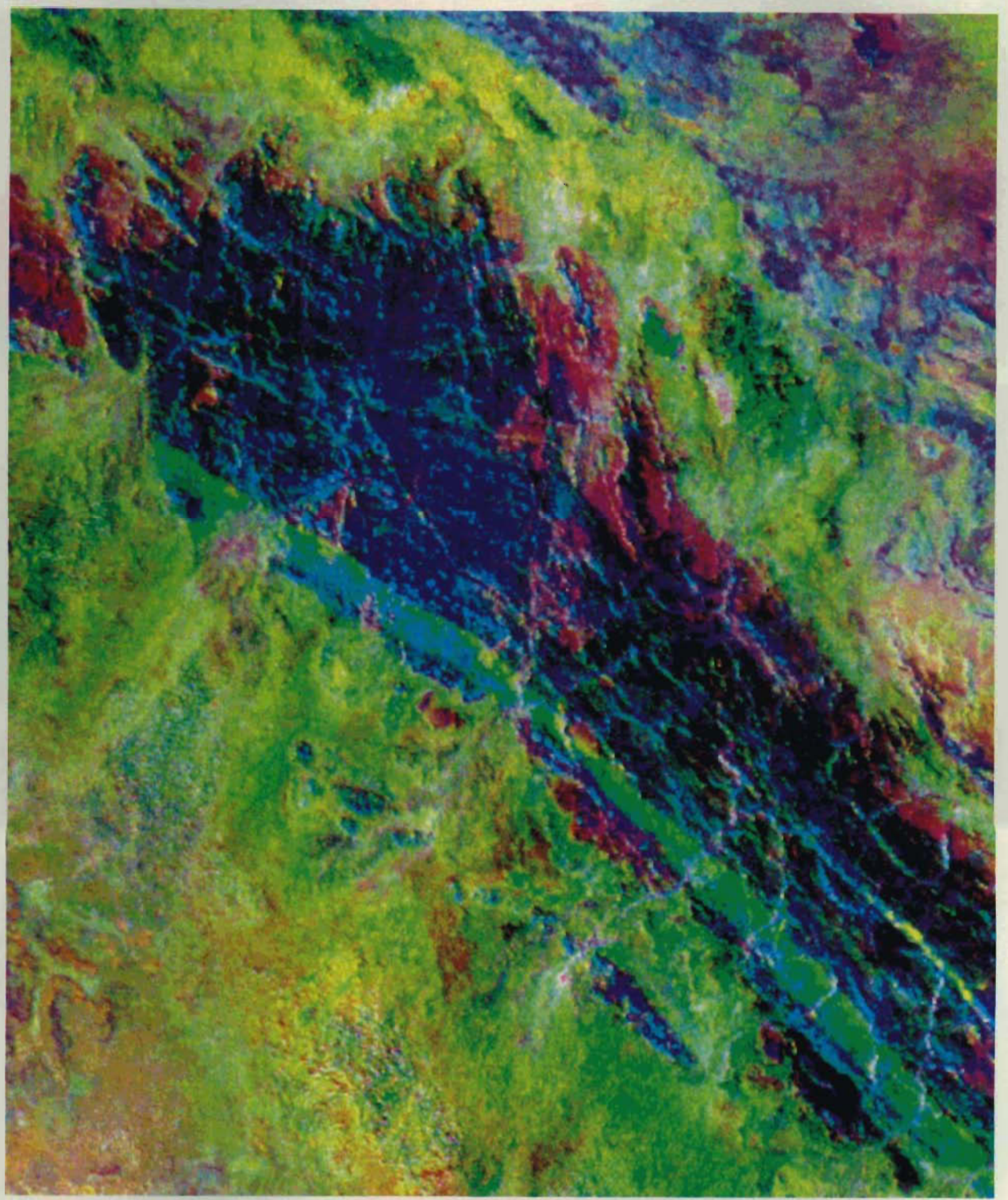

Figure 9. (A, above) pc2[4/3;5/7]:5/4:4/3 RGB image, northwest Bell Rock layered gabbro /troctolite; (B, right) a corresponding geological overlay (for explanation of symbols refer to Fig. 3). Extensive fireburns in the northwestern part of the Bell Rock range result in excellent exposure of the mafic layered rocks. Unburnt areas show in the typical clay-like red reflectance of dry vegetation. Whereas the gabbro (Gb) in burnt areas reflects in low-albedo dark brown color, units of ferrogabbro (Gf) and also mafic dykes, characterised by abundant magnetite and its weathering products, show in bright green. The high resolution of these units and dykes allows their delineation in greater detail than allowed by field and aerial photographs mapping.

RGB images to display a range of clay/iron oxide variations along with a separate vegetation component.

The colour composite image, pc-2(clay-dominated)–5/4 (iron oxide)–4/3 (green vegetation), displayed as RGB, has been found to allow direct comparisons between the ratios of clay/carbonate, iron oxide, and green vegetation (see Figs 7 and 9–12). In this type of image, the visually sensitive red and green colours represent lithologic variations and the visually less-sensitive blue colour represents vegetation. Comparisons between lithologic correlations allowed by this image and correlations suggested by log residual images, band ratio images and pixel-unmixed images suggest superior resolution of surface types, as follows:

- old growth-covered gabbro: red and purple, representing clay/carbonate weathering crusts and dry vegetation, green vegetation being particularly dense in shaded southward slopes that show in deep purple (Fig. 7).
- fireburn over gabbro: dark brown to red, representing low DN values of clay covered weathering surfaces (Figs 7, 9).
- ferrogabbro: bright apple green, representing iron oxide (Fig. 9).
- pyroxenite: green-dominated, commonly ranging to cyan, representing strong effect of iron oxides, i.e. northern Kalka (Fig. 7), Ewarara, Latitude Hill, Gosse Pile (Fig. 11), merging into cyan where vegetation is important, i.e. southern shaded slopes of Gosse Pile.
- felsic granulite and granitic gneiss: mostly yellow (clay/iron oxide red/green mixtures)(Figs 7, 11) covered in places by blue (vegetation on southern slopes) and red where weathered to clay. Strong sub-peneplain clay weathering is conspicuous on high levels of Mount Aloysius (Fig. 1).
- laterite: marked apple-green (iron oxide) to yellow (iron oxide–clay mixture), i.e. east of Kalka (Fig. 7) and Poonawarra, and cyan, where laterite is covered by dense mulga bush, such as around Wingellina (Fig. 1).
- calcrete: orange red, i.e. along creeks (Fig. 7) and locally over peridotite (Fig. 7).

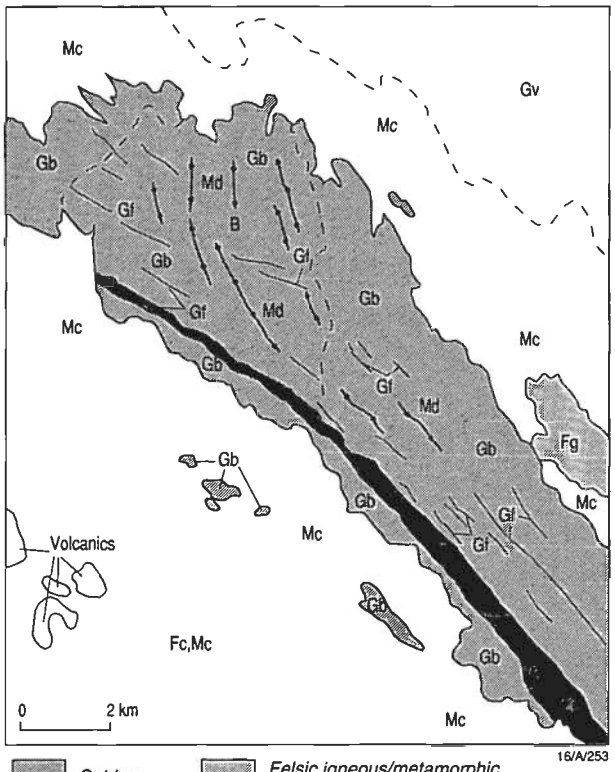

- silcrete: bright red (Fig. 7).
- mafic source-derived alluvium: shows in shades of light green to light orange, representing the importance of iron oxide and clay (Figs 9–11).
- felsic source-derived alluvium: light red to purple, commonly forming collars around outcrops of felsic granulite, representing the importance of clay and vegetation (Figs. 7, 11).
- silt and claypans: light orange to red (Champ de Mars clay pan) and green (Lake Wilson), the latter suggesting suspended iron oxide/clay mixture.

An equally effective RGB image combines pc2(4/3:5/7)[R], band ratio 5/4 [G] and bands (1+3+5+7)[B]—the latter representing the high albedo of free quartz (Fig. 8).

Discussion

The results of the image analysis methods discussed above are summarised here in relation to the identification of specific surface material types (see Table 3):

Iron oxides. Hematite shows a good correlation with the band ratio 5/4 and 7/4 images, thanks to their uniquely high DN values in iron oxides compared to other materials (Fig. 2). Surface types identified in this way include lateritic deposits, iron oxide-impregnated weathering crusts of pyroxenite and ferrogabbro, oxidised mafic debris in strike valleys that overly pyroxenite units and in creeks, and, to a lesser extent, iron oxide-bearing weathering products of felsic granulites transected by mafic dykes (Figs 7, 11). The low band ratio 5/4 DN values of gabbroic rock surfaces represent the dominance of clay in their weathering products. Low band ratios 5/4 of tracks represent the winnowing away of fine iron oxide dust from quartz-rich arenite. A distinction between hematite and goethite may be possible where iron oxide-rich material has low band ratio 5/4 DN values (Fig. 2). Other iron oxide correlations, namely band ratio 3/1, are largely masked by high band ratio 3/1 DN values of dry grass (Fig. 2).

Clay and carbonates. Traditionally, band ratio 5/7 DN values are used as an effective discriminant of clay components, although similar criteria apply to carbonates and dry vegetation (Fig. 2). Band ratio 5/7 DN values in the Kalka–Mount Davies area represent the relative abundance of clay components in the weathering products of gabbroic rocks, carbonate weathering of peridotite, and calcrete deposits, and as are mixed with iron oxide in the weathering products of felsic rocks and their alluvial derivates (Fig. 7). The second principal component of the combined band ratios (4/3;5/7) allows the separation of the clay component from the vegetation component. The inverted ILR-7 image, which represents strong absorption of band 7, owing to clay minerals, indicates clay/carbonate weathering of gabbroic rocks as high DN values, but represents clay components shed from felsic granulite to a lesser extent (Fig. 5b).

Quartz/silica. The uniformly high reflectance of quartz and silica in all bands can be used to separate these components by means of adding the DN values of several spectral bands, e.g. bands [1+3+5+7] or bands [1+7], resulting in high combined reflectance values compared to other materials (Fig. 4d). The identified quartz/silica component can be combined with clay/carbonate and iron oxide, forming a diagnostic three-mineral components RGB image, for example: pc2[4/3;5/7] : 5/4 : [1+3+5+7], representing clay/carbonate–iron oxide–quartz/silica (Fig. 8).

Green vegetation. Band ratio 4/3 DN values effectively discriminate green vegetation (Fig. 2), which under the arid conditions of the Tomkinson Ranges concentrate along creeks, southern slopes, strike valley depressions, alluvial collars around felsic rocks outcrops, vegetation-fringed tracks, and airstrips. In view of the strong absorption by the chlorophyll of green vegetation in band 3, an inverted log residual image

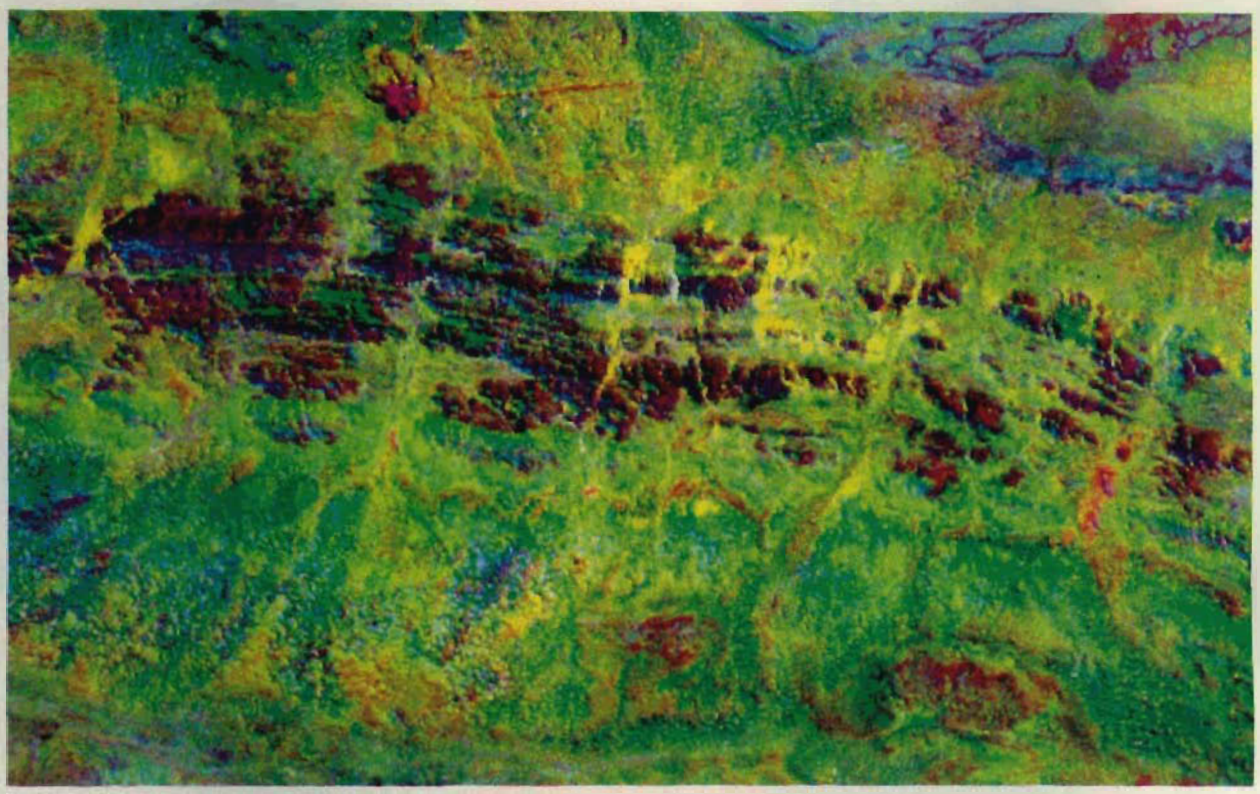

Figure 10. (A, above) pc2[4/3;5/7]:5/4:4/3 image eastern part of the Blackstone layered gabbro/troctolite; (B, below) corresponding geological overlay (for explanation of symbols refer to Fig. 3). The Blackstone intrusion is similar to the Bell Rock intrusion in mineralogy, magmatic stratigraphy, styles of magmatic layering, and degree of fractionation, and is considered its equivalent (Daniels 1974). It consists of a >3600 m thick south-younging sequence of highly fractionated troctolites and magnetite rick gabbro, and minor olivine gabbros, anorthosites (Ballhaus & Glikson 1995—this issue). Along the north the intrusion is recrystallised into phlogopite-bearing mafic granulites. Along its southern contact it is faulted against the Tollu Group volcanics. The Landsat image allows effective delineation of thin magnetite-rich gabbro units (Gf), otherwise difficult to map in the field, and showing as green strike lineaments between the clay-weathered gabbro zones. The iron oxide-rich alluvial shed from the intrusion is deep apple green. Creeks are marked by yellow, namely mixtures of iron oxide and clay.

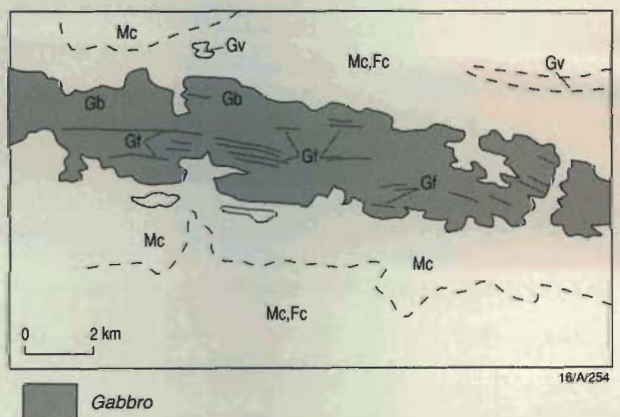

of this band [ILR-3] is also useful in fingerprinting green vegetation, yielding high DN values for green vegetation (Fig. 5c). However, vegetated alluvial collars around felsic rock outcrops are only weakly displayed on this image, possibly owing to variations in the type of plants.

Other image processing methods

***Pixel unmixing and vegetation screening analysis*:** Pixel unmixing analysis (Bierwirth 1990; P.N. Bierwirth pers. comm., 1994) depends on a choice of realistic spectrally distinct end-members identified in the field. Similar spectral patterns are difficult to separate, e.g. distinctions between clay and carbonate and between haematite and goethite are not readily obtained on Landsat-5 TM images. Model end-members can include dry vegetation and green vegetation (higher 4/3 and 2/3 band ratio than dry vegetation). The number of end members can not exceed the number of bands, namely up to six bands in Landsat-5 TM images (excluding the thermal band 6). Modelling of end member abundances by pixel unmixing allows subtraction of the reflectance effect of dry and/or green vegetation end members in each band from the primary (radiance-corrected) Landsat-5 TM band DN value in order to obtain the devegetated images.

In the present study (Glikson 1994) the following field-measured end member spectra were selected: (1) kaolinite; (2) calcite; (3) hematite; (4) goethite; (5) silica; (6) eucalyptus green vegetation; (7) dry vegetation; (8) spinifex vegetation (similar to green vegetation). Comparisons between pixel-unmixed model images and selected band ratio images confirm the unmixing model with regard to (1) the unmixed clay component, correlates with band ratio 5/7 images; (2) the unmixed iron oxide component correlates with band ratio 5/4 images, and (3) the unmixed green vegetation component correlates with band ratio 4/3 images. On the other hand, no discriminations of clay from carbonate, of haematite from goethite and of silica have proven possible: (1) kaolinite, representative of clays in general, is suggested in the weathered surfaces of felsic igneous and metamorphic rocks and derived alluvial materials—the latter forming distinct rings and fringes juxtaposed with felsic igneous and metamorphic outcrops; (2) clay/carbonate mixtures are suggested in the weathering

surfaces of gabbroic igneous rocks; (3) carbonates and carbonate/silica mixtures are represented by calcrete along creeks and by calcrete rises beneath alluvial surfaces; (4) haematite and/or goethite dominate outcrops of orthopyroxenites, ferrogabbro, lateritic deposits and iron oxide-rich alluvial deposits derived from mafic igneous rocks. Attempts to model goethite are unsuccessful, in part due to its spectral overlap with vegetation; (5) silica is not discriminated except as a generally high to very high reflectance, i.e. in silcrete open cuts near Wingellina and Pipalyatjarra; (6) green vegetation is well represented along creeks and in fireburn areas covered by young green spinifex regrowth, allowing discrimination of fireburn outlines. These areas offer geological 'windows' through which the spectral patterns of mineral components are better manifest than in old growth areas covered by the highly reflective dry vegetation.

In view of the near overlap between the band ratio 5/7 of dry vegetation and clay, removal of the dry vegetation component in the unmixing analysis may result in loss of information with regard to the clay component, as indicated by comparisons between the original data and devegetated images with log residual images. Comparisons between single band pixel-unmixed images and band ratio images indicate the following similarities and differences (Glikson 1994): The haematite end member band of the pixel-unmixed image shows important features in common with the 5/4 band ratio image. Both images show very high reflectance for laterite and for oxidised mafic-derived colluvium, intermediate reflectance for felsic granulites and low reflectance for clay/carbonate weathered mafic rocks and for clay and quartz-rich girdles around felsic outcrops. The correlation between the clay end member band of the pixel unmixed image and the band ratio 5/7 image is not as good, although clay/carbonate-rich areas at the centre of Mount Davies and clay/quartz-rich alluvial girdles around felsic granulite outcrops are expressed by high DN values in both types of images. The otherwise poor correlation arises due to superposition of vegetation on the band ratio 5/7, requiring comparisons with devegetated images. A close similarity is shown between the green vegetation end member in the pixel unmixing image and the 4/3 band ratio image. Both images display the greater concentration of green vegetation in creeks, strike-parallel depressions of less resistant lithologies and some southern slopes, i.e. Gosse Pile.

In attempting to produce devegetated images based on the pixel unmixing analysis it is evident that, since field-measured spectra indicate a close coincidence between the 5/7 ratios of dry vegetation and clay, a significant loss of mineral-related data occurs upon subtraction of the dry vegetation end member. For this reason, only green vegetation subtraction was applied to the Tomkinson Ranges scene. The comparison between original (dark pixel-corrected) images and devegetated images (Glikson 1994) shows (1) a consistent reduction in the band ratios 4/5 and 5/7 of the devegetated spectra, consequent on the removal of the positive 5/7 and 5/4 ratios of green vegetation, and (2) a consistent decrease in the band ratio 4/3 of the devegetated spectra, due to the removal of the high band ratio 4/3 of green vegetation; (3) lowering of the band ratios 2/1 and 2/3, which are high in green vegetation. Devegetated images of the Tomkinson Ranges show that, whereas sharpening of the images and good definition of some lithological units are obtained, much of the detail shown in the original images and in log residual images and ratio images is lost. This may indicate that green vegetation concentrations help define surface mineral types.

***Unsupervised classification*:** Unsupervised image classification involves comparisons between nearest-neighbour pixels, calculation of mid points, and migration of means by an iterative process—grouping analogous spectra into a user-specified number of classes. The method differs from supervised classification where specified spectral types are derived from training areas, a process involving *a priori* categorisation of the classes, or subjective selection. Unsupervised classification can be performed either on raw spectral data, corrected spectral data or processed images. On classified images each spectral group is given a separate color, allowing its visual distinction. In this study unsupervised classification images produced on the IIS system, using 20 and 30 class selections allow the following correlations:

- A 20-class image differentiates between the following surface types:
  1. gabbro.
  2. ferrogabbro and pyroxenite.
  3. felsic granulites and granites.
  4. quartz-rich alluvial deposits.
  5. weathered felsic granulites.
  6. vegetated dune areas.
- A 30-class images differentiates between the following surface types:
  1. mafic and ultramafic rocks.
  2. felsic granulites and granites.
  3. quartz-rich alluvium.
  4. vegetated dunes.

The above suggests that an increase in the number of classes may result in subdivisions whose significance in terms of correlation with surface types is unclear. In view of the limited resolution of classified raw data images, unsupervised classification was performed on geologically particularly useful images, for example RGB pc2(4/3:5/7) : 5/4 : 4/3 image. The classification process results in image degradation due to the averaging of pixel arrays, generally diminishing the resolution of individual surface type. Thus, whereas the classified image still allows a discrimination between gabbro, iron oxide-rich ferrogabbro/pyroxenite/laterite, felsic granulite and weathered felsic granulite—its spatial resolution is distinctly inferior as compared to that of the unclassified image.

***AMSS Geoscan MK-I image correlations*:** Two runs of AMSS Geoscan 13-band 10 metre-pixel MK-I imagery flown over the Tomkinson Ranges have been provided by Geoscan, courtesy of Dr J.L. Daniels, for lithological comparisons. The two runs, covering 5 km wide east–west and north–south strips (Fig. 1), allow further discrimination thanks to the smaller pixel size as well as additional information derived from bands in the thermal range. A comparison between the AMSS Geoscan MK-I band intervals and those of Landsat-5 TM are given in Table 1. The data allow correlations with surface type not readily identified by Landsat-5 TM data, as follows (Honey & Daniels, 1986, 1987):

bands 6/7 ratio—highlights kaolin-rich areas.
bands 6/8 ratio—highlights sericite and smectite-rich areas.
bands 6/9 ratio—highlights carbonate-rich areas
bands 7/8 ratio—positive discrimination of smectites.
bands 8/7 ratio—bright areas for high alunite
bands 11/10 ratio—highlights areas of high free silica.

Comparisons between RGB ratio images of the above bands (6/8:6/9:5/4, 6/8:6/9:11/10, 10:11:12) for the Tomkinson Ranges area allow the following observations and correlations:

1. The 6/8 band ratio is manifest in clay/arkose-rich pediments which fringe felsic granulites and granites, as a patchy pattern over weathered clay-bearing outcrops of felsic granulites and over calcrete.
2. The 6/9 band ratio is manifest over outcrops of gabbro of the Giles Complex.
3. The 5/4 band ratio is manifest over gabbro of the Giles Complex and more strongly on oxidised mafic detritus and alluvium derived from mafic sources—representing iron oxide, although the AMSS Geoscan band 5 is different from the Landsat-5-TM band 5 interval.
4. The 11/10 band ratio is manifest over quartz-rich alluvial materials derived from felsic sources and also over silcrete.

AMSS Geoscan MK-I log residual images help to accentuate

lithological distinctions. For example, a RGB log residual 9:4:1 image of the Wingellina area clearly expresses the difference between weathered outcrops of gabbro and laterite. Further processing of AMSS Geoscan MK-I images will be reported elsewhere.

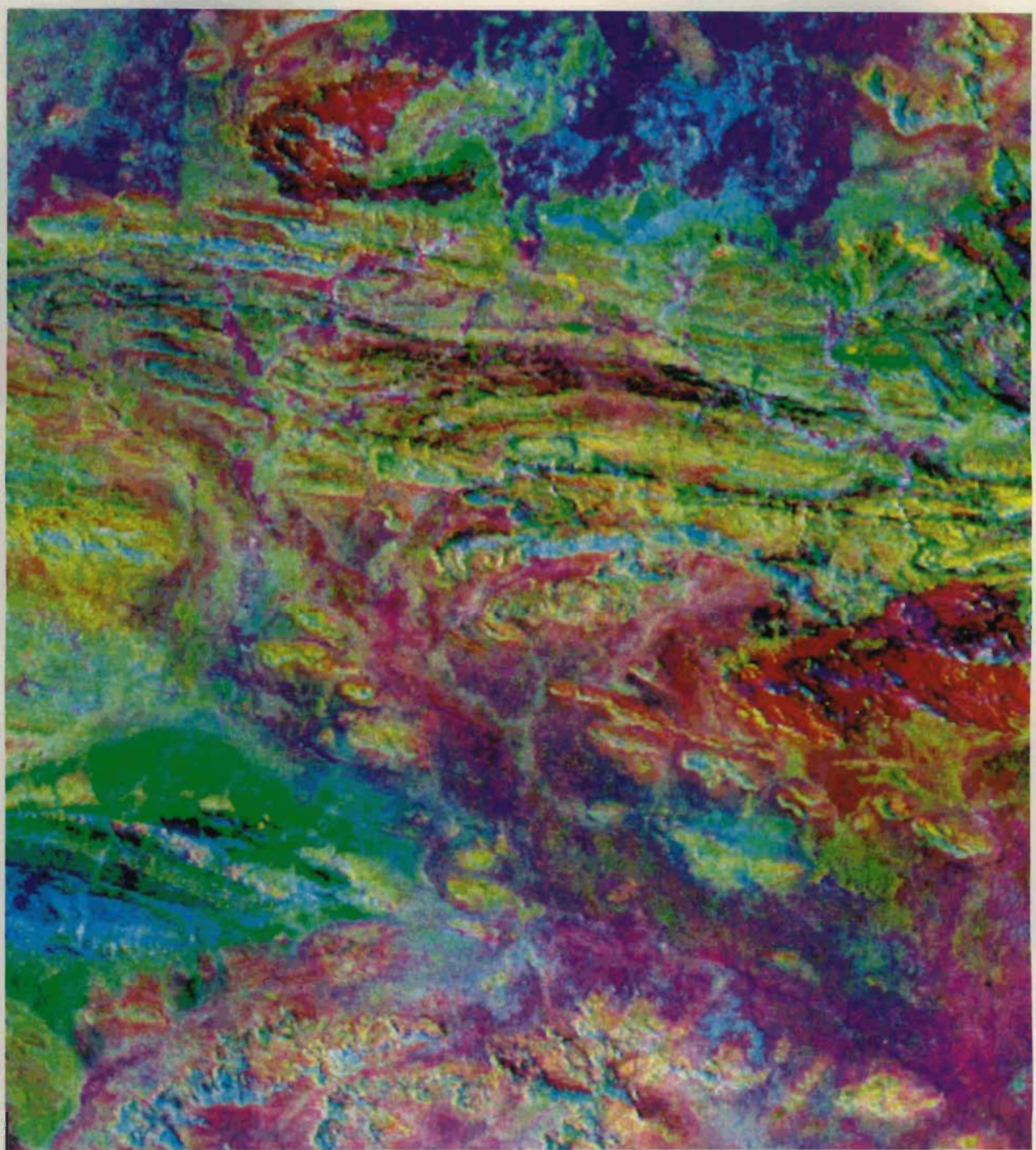

Figure 11. (A) pc2[4/3;5/7]:5/4:4/3 RGB image, Teizi bore area interlayered felsic granulites–anorthosites and Gosse Pile layered intrusion; (B) corresponding geological overlay (for explanation of symbols refer to Fig. 3). The southwestern part of this image includes the Gosse Pile pyroxenite consisting of >2000 m thick south-younging sequence of pyroxene-dominated cumulates separated by a major fault from the Mount Davies intrusion (Moore 1971). Thin noritic intrusives at the base of the body are interdigitated with felsic granulites, and are overlain by a discrete, deeply weathered and valley-forming body of serpentinised peridotite. The overlying layered sequence consists of orthopyroxenite, websterite and norite. The pyroxenites (Px) are dominated by iron oxide-rich weathering crusts, and the different shades of green reflect the importance of this component, i.e. clinopyroxene–plagioclase-rich rocks have higher clay content in the weathering crust and thus a red component resulting in yellow. The peridotite strike depression is characterised by calcrete/magnesite crusts showing in red and white. Shed iron oxide-rich alluvials show in deep apple green (Fg). Shaded southern slopes (Ss) display green vegetation superposed on pyroxenite bedrock, resulting in deep azur blue. The Teizi anorthosite suite (Gray, 1967) includes several massive bodies (An) and numerous thin recrystallised tongues intercalated with felsic granulites (Fg). the anorthosites show in red, representing clay/carbonate-dominated weathering, and the felsic granulites in green and yellow, representing iron oxide/clay mixtures. The Landsat identification of the thin recrystallised anorthosite units allows their effective delineation to a greater extent than time-consuming field work. The sequence is cut by east–west to northwest-striking mafic dykes (Md). Alluvium derived from felsic granulites is typically clay-rich (Fc), showing in red or in purple where sustaining green vegetation.

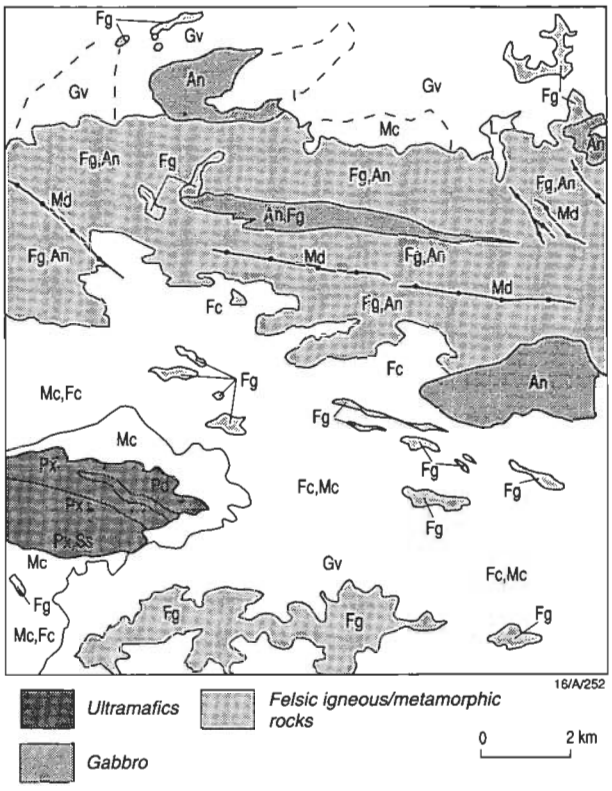

Conclusions

The following observations are allowed by the Landsat-5 TM study of the Tomkinson Ranges:

- Landsat-5 TM images furnish an ideal method for fingerprinting and correlating a range of surface types, under the arid conditions of central Australia, including weathered bedrock, duricrust and alluvial deposits, provided the composition of surface types is ascertained in the field. Once correlations are established, interpolations and extrapolations of the data can be pursued with a high degree of confidence, provided the morphological and structural patterns of the units in question are taken into account.
- Vegetation and fireburn patterns have only a limited masking effect on the mineral-produced reflectance. In the lack of field spectrometric calibration, band ratio images, logarithmic residual images, principal component analysis of vegetation and mineral ratios, and pixel unmixing analysis yield significant correlations with surface types tested in the field.
- Landsat-5 TM and AMSS Geoscan MK-I visible to infrared spectra are capable of characterizing individual components of the layered mafic/ultramafic Giles Complex with differing orthopyroxene:clinopyroxene:plagioclase ratios.
- Identification of iron oxide is best facilitated by the band ratio 5/4; clay, by the band ratio 5/7 and by the 2nd principal component of combined band ratios (4/3;5/7); quartz/silica, by a combination of bands [1+3+5+7]; and green vegetation, by the 4/3 band ratio.
- Separation of hematite from goethite, and clay from carbonate could not be achieved on images from Landsat-5 TM. However, in some instances, these components can be identified from their mode of occurrence, for example calcrete banks along creeks.
- The identification of quartz on weathered rock surfaces is obscured by thin films of clay and iron oxide. Free abraded quartz in alluvial and dune deposits stands up well through addition of Landsat-5 TM bands [1+3+5+7], expressing the combined high reflectance of quartz and silcrete. Geoscan images allow expression of quartz and silica through high band ratio 11/10.
- The composition of isolated bedrock outcrops (inselbergs), which may be too small to identify on Landsat-5 TM images, can be identified from associated wider alluvial haloes. Mafic bedrock sheds iron oxide-rich alluvium and colluvium. whereas felsic bedrock sheds clay and quartz-rich alluvium.
- The present study emphasises the importance of weathered surfaces of characteristic lithologic types. The nature of these is not necessarily controlled by the major mineral composition of the fresh lithologies. For example: (1) the weathering crusts of felsic igneous and metamorphic rocks yield mixed spectral signatures of iron oxide and clay, whereas weathering surfaces of gabbro mainly yield clay/carbonate signatures; (2) felsic vein-intruded mafic granulites display silica-coated and iron oxide-rich weathering surfaces, contrasted with the clay/carbonate dominated weathering surfaces of gabbro, from which the mafic granulites are derived by recrystallisation, whereas the weathered surfaces of gabbro is dominated by clay/carbonate; (3) anorthosite bands and plagioclase-rich felsic granulite bands can be distinguished, owing to the strong clay/carbonate reflectance signature of the former and clay–iron oxide signature of the latter.
- Landsat-5 TM and AMSS Geoscan MK-I images are ideal for discrimination of palaeoweathering surfaces at high topographic levels and representing relicts of an eroded peneplain. The identification of these surfaces is enabled by the deeper weathering on these rocks, represented by clay and richer vegetation.
- Landsat-5 TM and AMSS Geoscan MK-I images can be used effectively to identify calcrete duricrust along creeks and elsewhere in connection with searches for suitable target areas for hydrological purposes.
- Although the present study did not focus on the identification and correlation of vegetation types, it is clear from comparisons between the environmental map of the Tomkinson Range (Feeken 1992) and the imagery, that classification of areas dominated by grasses, bush, mulga and eucalypt habitats can be achieved once the specific spectral differences between these vegetation types are calibrated.
- The lithologic surface type variations displayed on the Landsat-5 TM images and on AMSS Geoscan images provide information which cannot be identified in any other way—including field work—in view of the ability of the reflectance in the infrared range to distinguish surface patterns and variations dependent on cryptic mineralogical/geochemical patterns undetected in the visible range.

Whereas, at present, Landsat-5 TM offers the most efficient imagery for large-scale regional mapping, especially where combined with 10 metre pixel SPOT data, the limits in the number of bands and the wide band widths preclude resolution of a range of components in the NIR and SWIR range. Future application of satellite-mounted multispectral scanners promises to resolve some the outstanding questions discussed above.

Acknowledgements

We thank P.N. Bierwirth for assistance with application of pixel demixing and devegetation programs, and P.N. Chopra, L.F. Macias, M. Peljo, A.J. Whitaker and J.R. Wilford for advice and assistance with the image processing work. Supervision of the Sun computer system by P. Miller and provision of AMSS Geoscan imagery by J.L. Daniels and R. Agar are gratefully acknowledged. We thank L.F. Macias and P.N. Bierwirth for their comments on this paper.

References

Bierwirth, P.N., 1990. Mineral mapping and vegetation removal via data-calibrated pixel unmixing, using mul-

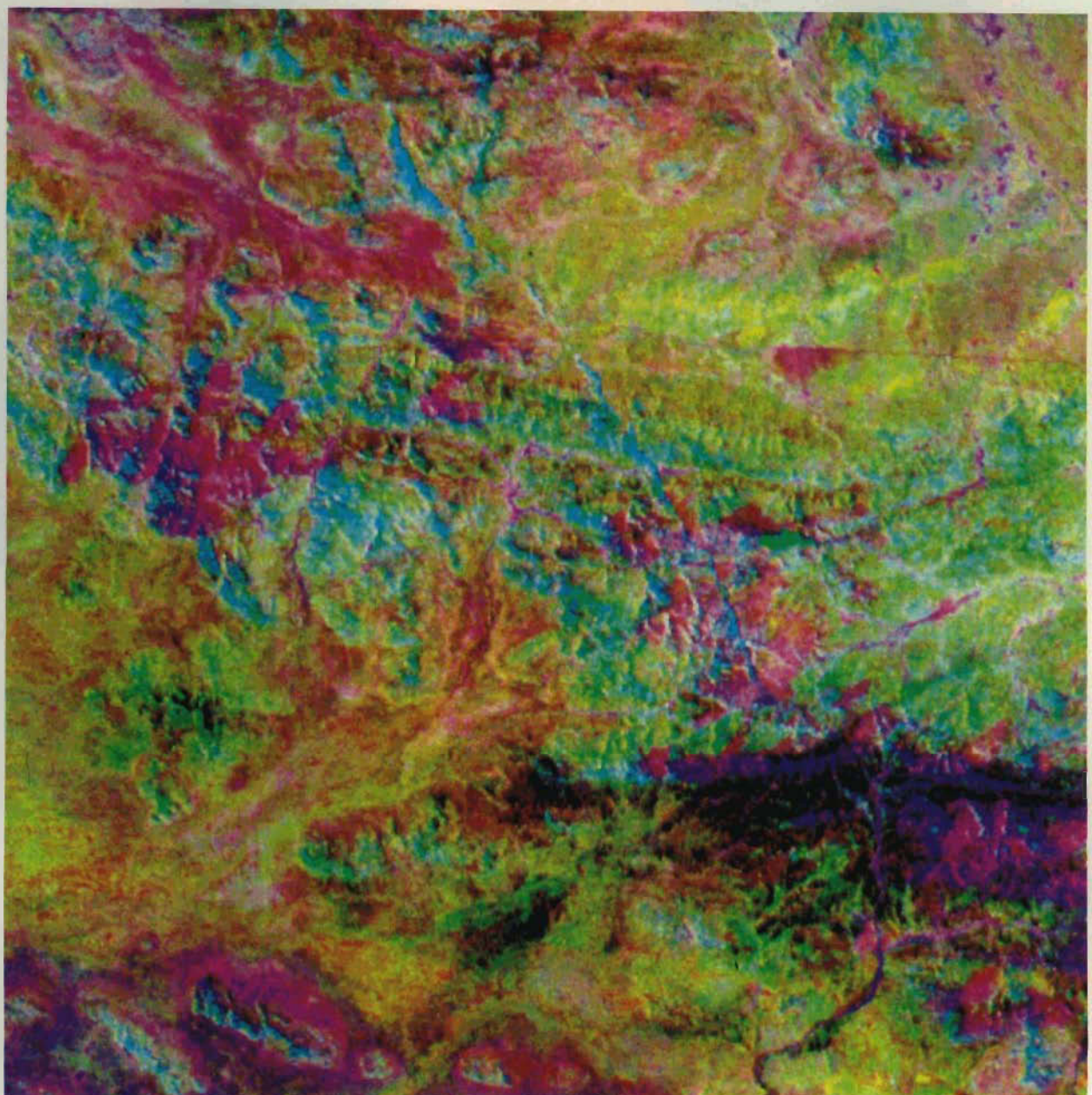

Figure. 12. (A) pc2(4/3;5/7):5/4:4/3 RGB image, western part of the Hinckley gabbro and derived mafic granulites; (B) corresponding geological overlay. For explanation of symbols refer to Figure 3. The Gosse Pile intrusion consists of an approximately 5800 m thick magmatic sequence, which youngs northward. The western and northern parts of the intrusion have been extensively recrystallised into mafic granulites, which contain abundant gabbroic relics. The mafic granulites are intruded by numerous granite/aplite veins. The layered sequence is cut by several generations of basaltic dykes. Effective mapping of the gabbro from the mafic granulite in the field is complicated by their irregular dimensions and borders, and is facilitated by Landsat imagery, where the clay-weathered gabbro relics (Gb) shown in red are readily discriminated from the mafic granulites (Mn), which show in yellow to green, thanks to the iron oxide and silica-rich weathering crusts of the latter. The silica is formed by thin evaporative crusts on the bedrock and its enrichment in the rocks is related to the numerous granite and felsite veins associated with the mafic granulites. Thus, despite the overall similarities between the chemistry and mineralogy of the gabbro and the mafic granulites, the reflectance characteristics of the latter is more akin to that of felsic granulites.

tispectral images. International Journal of Remote Sensing, 11, 1999–2017.

Daniels, J.L., 1974. The Geology of the Blackstone Region, Western Australia. Geological Survey of Western Australia, Bulletin 123.

Feeken, E., 1992. Notes on the 1:100 000 environmental map of the Tomkinson Ranges, Western Musgrave Block, central Australia. Australian Geological Survey Organisation, Record 1992/34.

Fraser, S.J. & Green, A.A., 1987. A software defoliant for geological analysis of band ratios. International Journal of Remote Sensing, 8, 525–532.

Glikson, A.Y., 1987. An upthrusted early Proterozoic mafic granulite–anorthosite suite and anatectic gneisses, southwestern Arunta Block, central Australia: evidence on the nature of the lower crust. Transactions of the Geological Society of South Africa, 89, 263–283.

Glikson, A.Y., 1990. The Giles Complex, central Australia: new insights into tectonics and metamorphism. BMR Research Newsletter, 12, 18–20.

Glikson, A.Y., 1994. Landsat-5 thematic mapper correlation: application to NGMA mapping of the Western

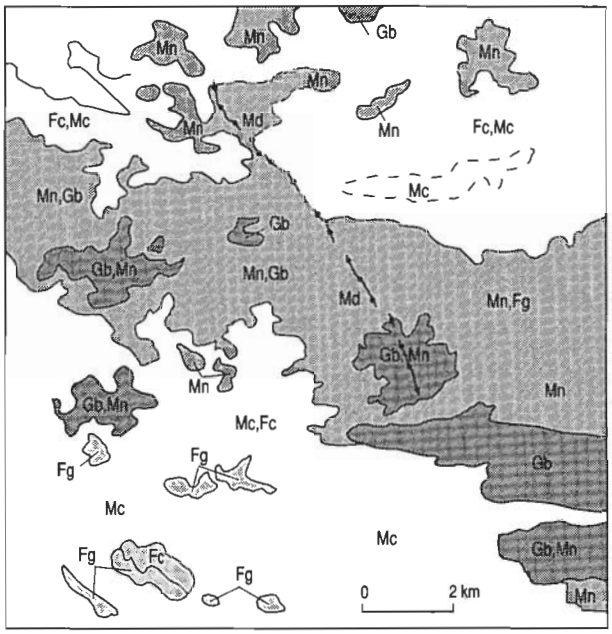

Musgrave Block, central Australia. Australian Geological Survey Organisation, Record 1994/17.

Glikson, A.Y., Stewart, A.J. Ballhaus, C.G., Clarke, G.L., Sheraton, J.W. & Sun, S.S., 1995. Geological framework and crustal evolution of the Giles Complex and environs, western Musgrave Block, central Australia. AGSO Journal of Australian Geology & Geophysics, this issue.

Gray, C.M., 1967. The geology, petrology and geochemistry of the Teizi anorthosite. B.Sc. Honors thesis, University of Adelaide (unpublished)

Green, A.A. & Craig, M.D., 1985. Analysis of aircraft spectrometer data with logarithmic residuals. Jet Propulsion Laboratory Publication, 85-41, 111–119.

Honey, F.R. & Daniels, J.L., 1986. Rock discrimination and alteration mapping for mineral exploration using the Carr Boyd/Geoscan airborne multispectral scanner. In: 5th Thematic Conference on Remote Sensing for Exploration Geology, Reno, Nevada.

Honey, F.R. & Daniels, J.L., 1987. Application of Carr Boyd Minerals Limited airborne multispectral scanner to spectral discrimination of hydrothermally altered areas. In: 4th Thematic Conference on Remote Sensing for Exploration Geology, San Francisco, California.

Moore, A.C., 1971. Some aspects of the geology of the Gosse Pile ultramafic intrusion, central Australia. Journal Geological Society Australia, 18, 69–80.

Nesbitt, R.W. & Kleeman, A.W., 1964. Layered intrusions of the Giles Complex, Central Australia. Nature, 203, 391–393.

Shaw, R.D., Stewart, A.J. & Black, L.P., 1984. The Arunta inlier: a complex ensialic mobile belt in central Australia. Part 2: Tectonic history. Australian Journal of Earth Science, 31, 457–484.

Simpson, C.J., 1978. LANDSAT-5: developing techniques and applications in mineral and petroleum exploration. BMR Journal of Australian Geology & Geophysics, 3, 181–191.

Simpson, C.J., Macias, L.F. & Moore, R.F., 1987. Differentiation of mafic and ultramafic rock types using NS001 and TIMS data (unpublished).

Stewart, A.J., Shaw, R.D. & Black, L.P., 1984. The Arunta inlier: a complex ensialic mobile belt in central Australia. Part I: Stratigraphy, correlations and origin. Australian Journal of Earth Science, 31, 445–455.

Stewart, A.J. & Glikson, A.Y., 1991. The felsic metamorphic/igneous core complexes hosting the Giles Complex. BMR Research Newsletter, 14, 6–7.

Warren, R.G., 1983. Metamorphic and tectonic evolution of granulites, Arunta Block, central Australia. Nature, 305, 300–303.

Table 1. Spectral bands of Landsat-5 TM data correlated with AMSS Geoscan MK-I airborne scanner data.

Landsat-5 TM band	*spectral channel (micrometer)*	*AMSS Geoscan MK-I band*	*spectral channel (micrometer)*
1	0.45–0.52	1 vis (blue)	0.45–0.5
2	0.52–0.60	2 vis (green)	0.55–0.6
3	0.63–0.69	3 vis (red)	0.65–0.7
4	0.76–0.90	4 near-infrared	0.83–0.87
		5 near-infrared	0.93–0.97
5	1.55–1.75	6 sw-infrared	1.98–2.08
7	2.08–2.35		
		7 sw-infrared	2.16–2.19
		8 sw-infrared	2.205–2.235
		9 sw-infrared	2.3–2.4
		10 thermal infrared	8.5–8.9
		11 thermal infrared	9.7–10.1
6	10.4–12.5		
		12 thermal infrared	10.8–11.2
		13 thermal infrared	11.5–12.0

Table 2. Landsat-5 TM mean radiance DN values for training areas (consisting of relatively homogeneous surface types) in the Tomkinson Ranges.
Values on the left, dark pixel-corrected mean radiance values. Values on the right, mean reflectance corrected for atmospheric effects.

Landsat-5 TM band	*1*	*2*	*3*	*4*	*5*	*7*
1. igneous and metamorphic rocks						
opx-rich rocks, GP	13 / 12	10 / 18	16 / 21	20 / 34	40 / 43	38 /62
cpx-rich rocks, EW	15 / 14	13 / 24	27 / 33	29 / 48	66 / 68	57 / 91
gabbro, BR	20 / 18	18 / 30	35 / 42	38 / 62	69 / 71	59 / 94
ferrogabbro, BR	22 / 14	18 / 23	35 / 32	39 / 44	78 / 72	62 / 95
gabbro, HG	23 / 20	19 / 33	33 / 40	36 / 59	47 / 50	42 / 68
weather.ed gabbro, HG	17 / 15	17 / 30	35 / 42	38 / 63	56 / 59	47 / 75
mafic granulite, HG	21 / 19	16 / 27	27 / 33	30 / 51	69 / 71	54 / 86
norite, KA	23 / 21	22 / 37	42 / 51	41 / 68	64 / 67	57 / 91
leucogabbro, KA	24 / 21	21 / 36	38 / 46	39 / 64	72 / 74	57 / 91
anorthosite, TEIZI	27 / 23	27 / 45	52 / 63	54 / 87	89 / 91	65 / 104
gabbro, MH, fireburn	20 / 18	18 / 30	33 / 40	36 / 59	57 / 60	46 / 74
gabbro, MH, old veg	21 / 19	16 / 28	26 / 32	28 / 46	51 / 54	42 / 69
felsic granulites	22 / 20	20 / 34	39 / 47	45 / 73	93 / 95	69 / 109
granite gneiss	19 / 17	16 / 28	30 / 37	35 / 57	76 / 78	58 / 93
weathered felsic granulites	18 / 16	17 / 29	34 / 42	41 / 66	74 / 76	53 / 85
2. duricrust						
laterite, WIN	17 / 16	13 / 24	25 / 31	30 / 50	78 / 80	59 / 95
laterite, KA	17 / 16	14 / 23	30 / 31	33 / 46	88 / 76	67 / 96
calcrete, PID	44 / 37	36 / 58	62 / 74	68 / 108	125 / 127	86 / 136
calcrete, CDM	27 / 24	25 / 42	52 / 62	57 / 911	16 / 118	87 / 137
silcrete, WIN	51 / 43	41 / 67	65 / 77	65 / 104	120 / 122	81 / 129
silcrete, KA	55 / 46	43 / 69	63 / 75	67 / 107	139 / 141	87 / 138
3. alluvial deposits						
alluvium, basic source	23 / 20	19 / 33	35 / 45	37 / 64	75 / 83	62 / 106
alluvium, felsic source	19 / 17	20 / 34	51 / 61	56 / 90	119 / 121	86 / 136
silt and clay, CDM	22 / 19	22 / 37	50 / 59	52 / 84	95 / 97	77 / 122
silt and clay, LW	31 / 27	24 / 40	38 / 46	38 / 63	98 / 100	82 / 129
dunes, fireburn	21 / 19	18 / 31	45 / 54	52 / 84	102 / 104	78 / 123
dunes, old growth	24 / 21	18 / 31	35 / 43	40 / 65	91 / 93	67 / 108

BR, Bell Rock range; CDM, Champ de Mars valley; EW, Ewarara Range; GP, Gosse Pile; HG, Hinckley Range; KA, Kalka Hill; LW, Lake Wilson; MH, Michael Hills; PID, Pidingadinga Creek; TEIZI, Teizi bore area; WIN, Wingellina.

Table 3. Spectral classifications of surface types in the western Musgrave Block, from Landsat-5 TM images. Note, only the more diagnostic criteria identified in the present study are listed.
image [1]—RGB pc2[4/3;5/7]:5/4:4/3 (clay/carbonate : iron oxide : green vegetation).
image [2]—RGB log residuals 543 (iron oxide : green vegetation: clay/carbonate).
image [3]—RGB log residuals 741 (iron oxide : green vegetation: clay/carbonate).
image [4]—RGB 741
image [5]—RGB pc2[4/3;5/7]:5/4:[1+3+5+7] (clay : iron oxide : quartz/silica)

I. Layered mafic–ultramafic intrusions	
peridotite: commonly coated by laterite, carbonate and silcrete	image [1] patchy combination of red, green and white; image [5] [blue] - where silcrete weathering occurs.
orthopyroxenite: iron oxide-rich weathering crusts:	image [1] green to cyan; image [2] yellowish red to orange; image [3] purplish red
clinopyroxenite/websterite: iron oxide & clay/carbonate weathering crusts	image [1] green with red dots. image [3] purplish red.
gabbro/norite: clay/carbonate–iron oxide-bearing weathering crusts	image [1] mainly red; blue where covered by. green vegetation; yellowish to red where covered by dense old dry vegetation (spinifex); brown where fireburnt. image [2] purple (iron oxide, clay and carbonate). image [3] cyan (clay/carbonate + vegetation); image [4] purple.
ferrogabbro: iron oxide-rich weathering crusts:	image [1] apple green to yellowish green. image [2] orange to yellowish red. image [3] brilliant pink
anorthosite: carbonate/clay weathering crusts	image [1] orange red. image [3] cyan. image [4] cyan (higher reflectance than gabbro)
II. Metamorphic rocks	
mafic granulites: clay, iron oxide and quartz-bearing weathering crusts, commonly cut by iron oxide-rich mafic dykes	Image [1] yellow (red/green), cut by green/blue mafic dykes. image [3] purplish red (iron oxide + clay) with relict cyan patches (gabbro).
felsic granulites: clay, iron oxide, quartz-bearing weathering crusts, cut by iron oxide-rich mafic dykes.	image [1] felsic granulites, yellow (red/green); mafic dykes, apple green; clay-rich weathering zones, red; shaded/vegetated southern slopes display in cyan. image [2] felsic granulites: yellowish green, cut by orange red mafic dykes. image [3] purplish red (iron oxide shed by mafic dykes) and cyan (clay+vegetation) weathering surfaces; image [4] purple.
III. Felsic igneous rocks	image [1] yellow (red/green), as for felsic granulites, or in places purple (vegetated clay-rich exfoliated outcrops); image [4] purple
IV. Volcanic rocks	
mafic/andesitic volcanics	image [1] yellow (red/green); image [3] purplish red
felsic volcanics	image [1] red (clay weathering); image [3] blue
V. Duricrusts	
laterite	image [1] apple green, cyan where covered by dense bush; image [2] apple green to yellow, representing iron oxide and thick vegetation; image [3] orange red; image [4] red
calcrete	image [1] orange zones along creeks; image [2] blue to purple; image [3] cyan to blue; image [4] cyan
silcrete	image [4] high reflectance in all bands (white) image [5](blue)
VI. Alluvial deposits	
felsic source-derived pediment	image [1] pink rings (clay-rich arkose) around felsic granulite outcrops; image [3] apple green to bluish green; image [4] cyan (vegetation on clay); image [5] (blue) where abraded/washed quartz abounds.
mafic source-derived pediment	image [1] green to yellow/green colluvium; in places reddish clay-rich alluvial zones; image [4] red
mixed alluvial deposits	image [1] yellow/red/blue alluvial plains
dunes	image [1] dune crests: thickly vegetated, purple; dune valleys: clay/iron oxide-rich, yellow (red/green); heavily vegetated dunes, blue with white lineaments (quartz-rich crests); image [5](blue) free quartz.
silt and clay pans	image [1] orange/brown areas; green where iron oxide-rich clay occurs
green vegetation	image [1] cyan; image [4] green; image [2] yellowish green; image [3] apple green.

Burst, J.F., 1965. Subaqueously formed shrinkage cracks in clay. Journal of Sedimentary Petrology, 35, 348–353.

Davies, G.R., 1970. Algal-laminated sediments, Gladstone Embayment, Shark Bay, Western Australia. In: Logan, B.W., Davies, G.R., Read, J.F. & Cebulski, D.E. (editors), Carbonate sedimentation and environments, Shark Bay, Western Australia. American Association of Petroleum Geologists, Memoir 13, 169–205.

Friedman, G.M. & Sanders, J.E., 1978. Principles of sedimentology. Wiley, New York.

Wellman, P. & McDougall, I., 1974. Cainozoic igneous activity in Eastern Australia. Tectonophysics, 23, 49–65.

Illustrations

Line diagrams or maps should be professionally drafted. (AGSO can provide a full professional drafting service to *Journal* standards at competitive rates. See advertisement below.) Figures should be designed for reproduction at either single column (80 mm) or double column (165 mm) width. Final versions of line drawings should be supplied as high-contrast photographic prints, but photocopies of draft figures may be submitted initially (see **Submissions** above).

All illustrations, both line drawings and photographs, are referred to as figures.

Figures should be numbered consecutively, in the order in which they are referred to in the text, with parts of an individual figure identified, if necessary, by upper case letter.

Do not draft figure titles on the figure. Captions are typeset and should be listed on a separate sheet.

Photographs should be good quality glossy prints. Scale in photographs should be indicated by either a recognisable object or a plain bar scale whose length is given in the figure caption.

Figures are reproduced in black and white unless special arrangements for use of colour have been made with the editor.

Tables

Tables should be set out on separate sheets. When preparing tables, if possible, please use the Tables function of your wordprocessor rather than use tabs to align columns.

Providing a disk version

When your manuscript has been accepted, you will be asked to provide a copy on disk.

The disk can be either 3.5 or 5.25 inch MS-DOS or Apple Macintosh format. The *Journal* is edited using WordPerfect 5.2 for Windows, which can convert from most other word-processing programs. If you are using WordPerfect for DOS version 6, please save your file as WordPerfect 5.1/5.2. Please check with the editor if you have any doubts, and send an ASCII file as backup.

Proofs

Authors will receive one proof of their manuscript, in its final formatted version, but without illustrations, to check before it goes for printing. Authors may be charged for the cost of major changes.

Reprints

The author(s) will receive a total of 50 free reprints of their paper.

Authors may buy extra reprints, which should be ordered when proofs are returned. The cost for 50 additional reprints is $100; special rates apply if more are required.

Please address all correspondence to

The Editor,
AGSO Journal of Australian Geology & Geophysics
Australian Geological Survey Organisation
GPO Box 378
ACT 2601

Tel. (06) 249 9760
Fax (06) 249 9987

AGSO
AUSTRALIAN GEOLOGICAL SURVEY ORGANISATION

AGSO Journal of Australian Geology & Geophysics

Volume 16, Numbers 1 & 2, 1995

The Giles mafic–ultramafic complex and environs, western Musgrave Block, central Australia
Guest associate editor: Andrew Glikson

CONTENTS